NOTICE

The quality of this microform is heavily dependent upon the quality of the original thesis submitted for microfilming. Every effort has been made to ensure the highest quality of reproduction possible.

If pages are missing, contact the university which granted the degree.

Some pages may have indistinct print especially if the original pages were typed with a poor typewriter ribbon or if the university sent us an inferior photocopy.

Reproduction in full or in part of this microform is governed by the Canadian Copyright Act, R.S.C. 1970, c. C-30, and subsequent amendments.

AVIS

La qualité de cette microforme dépend grandement de la qualité de la thèse soumise au microfilmage. Nous avons tout fait pour assurer une qualité supérieure de reproduction.

S'il manque des pages, veuillez communiquer avec l'université qui a conféré le grade.

La qualité d'impression de certaines pages peut laisser à désirer, surtout si les pages originales ont été dactylographiées à l'aide d'un ruban usé ou si l'université nous a fait parvenir une photocopie de qualité inférieure.

La reproduction, même partielle, de cette microforme est soumise à la Loi canadienne sur le droit d'auteur, SRC 1970, c. C-30, et ses amendements subséquents.

THE EFFECTS OF CURVATURE ON SHEARED TURBULENCE

by

ARTHUR GORDON LAWRENCE HOLLOWAY

A Thesis

presented to the University of Ottawa

October, 1989

in partial fulfillment of the

requirements for the degree of

DOCTOR of PHILOSOPHY

in

MECHANICAL ENGINEERING

Ottawa-Carleton Institute for

Mechanical and Aeronautical Engineering

ISBN 0-315-60043-8

UNIVERSITÉ D'OTTAWA
UNIVERSITY OF OTTAWA

Abstract

The present experiment is an attempt to study the effect of curvature on sheared turbulence in relative isolation from wall and entrainment effects. The flow is an extension of previous studies on nearly homogeneous, parallel, shear flows. Uniformly sheared turbulence is allowed to reach a state of transverse statistical homogeneity in a straight rectangular duct, it is then passed into a curved duct, also of rectangular cross-section. The near homogeneity of the turbulence and the near uniformity of the shear are preserved.

The present experiments span a range of $S = U_c/AR_c$, from -.49 to .65, (U_c is the centerline velocity, $A = \frac{dU}{dn}$ is the mean shear rate and R_c is the radius of curvature at the centerline of the duct), using two curved tunnels with R_c=2m and 5m respectively as well as shear generators producing several values of A.

Measurements indicate that the growth of the turbulent stresses and length scales is enhanced for $S < 0$ and suppressed for $S > 0$. For $S > .05$, the stresses decay. In cases where sufficiently large total strain was achieved, the stresses seem to grow or decay exponentially and to develop in a self-preserving manner. The magnitude of the dimensionless shear stress, $K_{uv} = \frac{\overline{uv}}{q^2}$, decreases monotonically with increasing S. The effect of curvature on shear stress is more pronounced in the low wave number range.

Acknowledgements

I express gratitude to Professor Stavros Tavoularis for suggesting the topic of my research and for always being available to discuss the latest result with helpful doses of scepticism and encouragement. Professor Tavoularis has taught me detachment, objectivity and intellectual honesty. His example has enriched my life, his values will remain with me throughout my career.

My time at the University of Ottawa was enjoyable because of my friends, especially Umesh Karnik with whom I had many enjoyable discussions on social values, religion and turbulence.

I must thank my wife Patti for putting aside her own ambitions so that I could pursue what she felt was important to me.

Financial support was provided by the Natural Sciences and Engineering Research Council of Canada through a post graduate scholarship and operating grant funds.

Contents

List of Figures

List of Tables

Nomenclature

A	mean shear rate
B_{uu}, B_{vv}, etc.	components of the space correlation tensor
C_{ab}	the covariance of a and b
$\mathbf{D}$	the strain tensor
$\mathbf{e_s}$	unit vector in the streamwise direction
$\mathbf{e_n}$	unit vector in the transverse direction
$\mathbf{e_z}$	unit vector in the spanwise direction
E	the anemometer bridge voltage
$E = \frac{\epsilon}{Aq^2}$	the dimensionless viscous dissipation
f_a	probability density function of the random variable a
f_{ab}	joint probability density function of a and b
F_{uu}, F_{vv}, etc.	components of the streamwise spectrum
h	ratio of the turbulent length scale to centerline radius
h_s	the height of the straight wind tunnel section
h_c	the height of the curved wind tunnel section
$\mathbf{k}$	the wave vector
K_{uu}, K_{vv}, etc.	components of the structural tensor
L_{uu}, L_{vv}, etc.	the integral length scales
n	the transverse coordinate
p	the fluctuating pressure
P	the mean pressure

$\frac{1}{2}q^2$	the kinetic energy of turbulence per unit mass
R_c	centerline radius
R_{uu}, R_{vv}, etc.	components of the autocorrelation function
s	the streamwise position
S	the curvature parameter $\frac{U_c}{AR_c}$
t	time
u	the fluctuating velocity in the streamwise direction
v	the fluctuating velocity in the transverse direction
w	the fluctuating velocity in the spanwise direction
U	the mean velocity in the streamwise direction
U_{eff}	the effective cooling velocity for the hot wires
V	the mean velocity in the transverse direction
W	the mean velocity in the spanwise direction
z	spanwise position
$\mathbf{z}$	position vector

Greek Symbols

α wave number in the s direction

β wave number in the n direction

γ wave number in the z direction

ϵ viscous dissipation

λ the Taylor microscale

Λ the integral time scale

μ dynamic fluid viscosity

ν kinematic fluid viscosity

κ_q the exponent of growth of q^2

κ_L the exponent of growth of L_{uu}

ρ fluid density

ω the vorticity vector

$\mathbf{\Omega}$ the rotation tensor

Others

$\Re$ Reynolds number

$\aleph$ metric scale factor $= \frac{1}{1+\frac{y}{R_c}}$

Subscripts

$(.)_o$ value at the time origin

$\overline{(.)}$ average value

$\widehat{(.)}$ the Fourier coefficient of a function

$\widetilde{(.)}$ instantaneous value of a stochastic process

$(.)'$ root mean square value

Chapter 1

INTRODUCTION

1.1 Motivation and Objective

Turbulent motions predominate in enviromental and technological flows and for this reason fluid turbulence has been studied extensively under a myriad of conditions. However, it is within the shear layers that the turbulent motions are the most active, transporting momentum at rates which are orders of magnitude higher than is possible by molecular motions in laminar flow.

The instantaneous streamlines of all such turbulent motions are highly curved but the term "curved shear layer" is reserved for those flows in which the mean streamlines are curved. With few exceptions all shear layers have some degree of streamline curvature.

The importance of curvature effects varies widely from one flow to another. For example, the curvature of the mean streamlines for the boundary layer along

a flat plate is so slight that the effects of curvature are essentially unoticable, while in some vortex flows the turbulence is dominated by curvature effects. Among the technologically important examples of curved shear flows would be those on the curved surfaces of airplanes and ships or the internal passages of turbo-machinery such as turbines and pumps.

Curvature can have a stabilizing or destabilizing effect on the fluid motion depending on the direction of the mean shear with respect to the curvature.

The quasi-periodic motions associated with the transition to turbulence and the fully turbulent motions are very sensitive to curvature. Even when a boundary layer thickness is only a small fraction of the radius of curvature, curvature causes significant changes in skin friction. With stronger curvature, longitudinal vorticity can develop.

A better understanding of the interaction between streamline curvature and shear may provide insight into drag reduction and perhaps lead to better design of vehicles and fluid machinery.

Significant efforts have been made to study the effect of curvature on boundary layers and free shear layers. Such studies have provided useful information but the interpretation of these results is complicated by the simultaneous action of different turbulent mechanisms such as entrainment of irrotational flow, viscous wall layers and the inevitable inhomogeneity of the mean shear.

An ideal flow in which one could study the generic interaction of shear and curvature would be one where turbulence, curvature and shear are homogeneous. While an exactly homogeneous curvature seems difficult to materialize,

the present experimental work is an attempt to generate a flow which has approximately homogeneous turbulence, shear and curvature.

Uniformly sheared turbulence is allowed to reach a state of transverse statistical homogeneity in a straight rectangular duct, it is then passed into a curved duct, also of rectangular cross-section. The near homogeneity of the turbulence and the near-uniformity of the shear are preserved along radial lines in the curved tunnel.

Therefore, away from the tunnel walls, the curvature effects on the turbulence structure can be studied in relative isolation.

1.2 Literature Review

The effect of streamline curvature on shear flow stability was recognized by Reynolds as early as in 1884. Most analyses of curved shear flows have been concerned with the stability of basic motions, i.e. "simple" solutions of the governing equations. Rayleigh (1916) and Synge (1933) studied inviscid flow and found it unstable in cases where the angular momentum decreased with radius. Taylor (1923) and Synge (1938) studied viscous flow between rotating cylinders. Görtler (1940) examined the stability of curved boundary layers and Dean (1928) the stability of Poiseuille flow in curved circular pipes. All of these studies show that the instability has the form of longitudinal vortices. Summaries of centrifugal instability can be found in books by Lin (1955), Chandrasekhar (1961) and Stuart (1963), and more recently in the review by

DiPrima and Swinney (1981). Such analyses have questionable relevance to fully turbulent flows, nevertheless, results of linear analysis currently provide the only mathematical and physical basis for understanding curved turbulent flows.

Rayleigh (1916) suggested that centrifugal instability and buoyant instability were analogous. Jeffreys (1928) showed that there is an analogy between buoyant flow instability between parallel planes and centrifugal instability between concentric cylinders in the limiting case of a small gap. The analogy is such that temperature corresponds to angular momentum. In the case of unstable curved shear flow the region away from the walls would be expected to have a constant mean angular momentum, due to diffusion; similarily the flow between heated parallel plates would have a nearly constant mean temperature (Townsend, 1976).

The earliest attempt to model turbulence in curved flows was that of Prandtl (1929) who balanced the production of kinetic and potential energies of turbulence for small inviscid disturbances, using the analogy between curved and buoyant flows, and proposed a modified mixing length, which was a linear function of the difference between these production rates. This analogy between buoyant turbulent shear flow and curved turbulent shear flow has been further discussed by Bradshaw (1969,1973), who showed that Prandtl's modification of the mixing length was too small by an order of magnitude and proposed alternatives.

Buoyant shear flow data and models have been used cautiously in the pre-

diction of curved shear flows (Bradshaw 1969).

Recent modelling efforts have extended Prandtl's (1929) analysis by accounting for viscous dissipation, inhomogeneities and finite disturbances with various degrees of sophistication. So (1975) has applied a model similar to the Reynolds stress models developed for plane shear layers (for example see Launder, Reece and Rodi 1975) to curved boundary layer flows under the assumption that the turbulence is in local equilibrium. Irwin and Smith (1975) applied the Reynolds stress model to curved boundary layers. Gibson (1978) applied to curved flows an algebraic stress model, where the Reynolds stress model is simplified under the assumption that all components of the Reynolds stress and heat flux are transported at the same rate as the turbulent kinetic energy. In contrast to these approaches, Launder, Pridden and Sharma (1977) have proposed a modification of the k-ϵ model (for example, see Launder and Spalding, 1974), where the dissipation equation is a function of the Richardson number. The full Reynolds stress model has been applied by Gibson and Rodi (1981) to a curved mixing layer, by Gibson, Jones and Younis (1981) to curved boundary layers, by Gibson and Younis (1981) to a curved wall jet and by Launder, Tselepidakis and Younis (1987) to a rotating channel flow. Pouagare and Lakshminarayana (1983) have applied an algebraic stress model to a rotating channel flow.

A review of the performance of several k-ϵ and algebraic stress turbulence models in curved shear flows has been made by Rodi and Scheuerer (1983). One of the few critical discussions of the Reynolds stress models with respect to curved shear flows has been given by Gibson (1984).

The consensus among modelists appears to be that the effects of curvature can be predicted by standard Reynolds stress models. Most of the less complicated k-ϵ models display qualitatively correct behavior and possess sufficient flexibility to reproduce the average velocity and turbulent kinetic energy of a given experiment. The performance of these models seems, to the author, poorly understood in plane shear flows and less so in curved flows. Little attempt has been made to evaluate the various assumptions with respect to curved flow structure.

Most available experimental studies of two-dimensional turbulent curved shear flows can be classified as a) flow between rotating cylinders b) boundary layers on convex and concave surfaces c) curved free shear flows d) curved duct flows and e) rotating flows.

Experiments in turbulent flow between rotating cylinders have been performed by Wendt (1933), Taylor (1936), MacPhail (1941), Pai (1943) and Smith and Townsend (1982). Only the latter authors report turbulence statistics.

Experiments on convex boundary layers have been performed by Wilcken (1930), Schmidbauer (1936), So and Mellor (1973), Meroney and Bradshaw (1975), Ellis and Joubert (1974), Mayle, Blair and Kopper (1979), Smits, Young and Bradshaw (1979), Gibson, Verriopoulos and Nagano (1982), Ramaprian and Shivaprasad (1977, 1978a, 1978b ,1982), Gillis and Johnston (1983), Gibson, Verriopoulos and Vlachos (1984), Gibson and Verriopoulos (1984) and Muck, Hoffman and Bradshaw (1985). With the exception of the experiments by So and Mellor (1973), these are cases of relatively mild curvature.

Experiments on concave boundary layers have been performed by Wilcken (1930), Tani (1962), Ellis and Joubert (1974), Meroney and Bradshaw (1975), So and Mellor (1975), Mayle, Blair and Kopper (1979), Smits, Young and Bradshaw (1979), Gibson and Servat-Djoo (1981), Nakano, Takahashi, Shizawa and Honami (1981), Ramaprian and Shivaprasad (1978,1982), Shizawa and Honami (1983,1985), Barlow and Johnston (1985) and Hoffman, Muck and Bradshaw (1985). Tani(1962) and So and Mellor (1975) used strong curvature and observed longitudinal vortices in the mean flow.

The measurements of Ramaprian and Shivaprasad (1978, 1982) provide the most comprehensive study of flow structure in curved boundary layer flows.

The boundary layer experiments of Mayle, Blair and Kopper (1979) and Gibson, Verriopoulos and Nagano (1982) also contained heat transfer studies.

The experiment of Nakano, Takahashi, Shizawa and Honami (1981) is directly related to the present study. To study the effect of free stream turbulence on a concave boundary layer a flow with an approximately linear shear was generated at the entrance to the curved tunnel. The Reynolds stresses were measured within two boundary thicknesses (where U=.99U_∞) of the concave wall. While the turbulence was not uniform it did grow for the case where velocity decreased away from the center of curvature and did not grow where the velocity increased away from the center of curvature.

Experiments on curved free shear flows have been performed in strongly curved mixing layers by Margolis and Lumley (1965), Wyngaard, Tennnekes, Lumley and Margolis (1968), Castro and Bradshaw (1976) and Townsend

(1983). Curved wake flows have been examined by Savill (1983) and Koyama (1985). A curved free jet flow has been studied by Pelfrey and Liburdy (1986). The measurements of Townsend (1983) and Savill (1983) include multiple point hot-wire statistics.

Experiments in curved circular ducts are extensive. The earliest experiments were performed by Eustice (1911), who observed secondary flow patterns by dye injection. For a recent review see Ito (1987). Experiments in fully developed curved rectangular duct flow have been done by Wattendorf (1935), Eskinazi and Yeh (1956), and Hunt and Joubert (1979). Humphrey, Whitelaw and Yee (1981) studied a developing flow. The direct numerical simulation of low Reynolds number (Re=2990) turbulent curved rectangular channel flow by Moser and Moin (1987) can also be used for comparison with experimental results.

The experimental results have consistently demonstrated the enhancement of turbulent mixing in cases where the velocity decreases with radius of curvature and the suppression of turbulent mixing where the velocity increases with radius of curvature, in agreement with the results of linear inviscid theory.

Steady longitudinal vortices have been seen by some investigators in cases of extremely strong concave curvature but no counterpart seems to exist for convex curvature.

Among the references mentioned above, the experiments of Ramaprian and Shivaprasad (1978b) on convex and concave boundary layers have been chosen as containing experimental results representative of inhomogeneous curved

shear flows. These experiments will be used for comparison to the present flow.

An important parameter in curved flows which is used widely in the literature is the curvature parameter $S = U_c/AR_c$, where U_c is the streamwise velocity on the windtunnel centerline, A is the shear rate and R_c is the centerline radius. S represents the ratio of strain rate due to the turning of the flow to the strain rate due to shearing of the flow. For an unsheared flow, $S \rightarrow \pm\infty$; for a flow in pure rotation, S=1; for a straight shear flow, S=0; and for irrotational flow, S=-1.

Chapter 2

ANALYTICAL PRELIMINARIES

2.1 Curvilinear Coordinates and the ∇ Operator

A curvilinear orthogonal system of coordinates denoted by s, n and z is shown in Figure 2.1. The s coordinate is the arc length of a circle coincident with the tunnel centerline and having radius R_c. The point s=0 is located at the entrance to the curved tunnel. The n coordinate runs normal to s, is zero on the tunnel centerline and is positive outward from the center of curvature. The z coordinate is normal to s and n and forms a right- handed system. This cooordinate system is related to a x_1, x_2, x_3 cartesian system by the transformation

$$x_1 = (R_c + n)\sin\frac{s}{R_c} \tag{2.1}$$

$$x_2 = (R_c + n)\cos\frac{s}{R_c} \tag{2.2}$$

$$x_3 = z \tag{2.3}$$

The scale factors (Karamcheti, 1966, p.140) of the s, n, z system are

$$h_1 = 1 + \frac{n}{R_c} \tag{2.4}$$

$$h_2 = 1 \tag{2.5}$$

$$h_3 = 1 \tag{2.6}$$

The unit vectors tangent to s, n and z are related to the $\mathbf{e}_1, \mathbf{e}_2, \mathbf{e}_3$ unit vectors by the transform (see Figure 2.1)

$$\mathbf{e}_s = \cos\frac{s}{R_c}\mathbf{e}_1 - \sin\frac{s}{R_c}\mathbf{e}_2 \tag{2.7}$$

$$\mathbf{e}_n = \sin\frac{s}{R_c}\mathbf{e}_1 + \cos\frac{s}{R_c}\mathbf{e}_2 \tag{2.8}$$

$$\mathbf{e}_z = \mathbf{e}_3 \tag{2.9}$$

The velocity vector will be represented by $\mathbf{u}$ with components defined by

$$\mathbf{u} = u\mathbf{e}_s + v\mathbf{e}_n + w\mathbf{e}_z \tag{2.10}$$

To obtain the equations for fluid flow in the s, n, z, system, the ∇ operator can be expressed in s, n, z coordinates and substituted in the vector equations for fluid flow which are independent of the coordinate system. The del operator in curvilinear orthogonal coordinates is (Karamcheti, 1966, p. 145)

$$\nabla = \mathbf{e}_1\frac{1}{h_1}\frac{\partial}{\partial q_1} + \mathbf{e}_2\frac{1}{h_2}\frac{\partial}{\partial q_2} + \mathbf{e}_3\frac{1}{h_3}\frac{\partial}{\partial q_3} \tag{2.11}$$

where $\mathbf{e}_1, \mathbf{e}_2, \mathbf{e}_3$ are the unit vectors tangent to the orthogonal coordinates q_1, q_2, q_3. For $s = q_1, n = q_2$, and $z = q_3$, equation (2.12) becomes

$$\nabla = \mathbf{e}_s\frac{\partial}{\partial s} + \mathbf{e}_n\frac{\partial}{\partial n} + \mathbf{e}_z\frac{\partial}{\partial z} \tag{2.12}$$

where $\aleph = (1 + n/R_c)^{-1}$. From equation (2.12) the gradient of a scalar ϕ is

$$\nabla\phi = \mathbf{e}_s\aleph\frac{\partial\phi}{\partial s} + \mathbf{e}_n\frac{\partial\phi}{\partial n} + \mathbf{e}_z\frac{\partial\phi}{\partial z} \tag{2.13}$$

The gradient of a vector in orthogonal curvilinear coordinates (Karamcheti, 1966, p. 103) can be expressed as

$$\nabla\mathbf{a} = \mathbf{e}_s(\nabla a_s + \chi_s) + \mathbf{e}_n(\nabla a_n + \chi_n) + \mathbf{e}_z(\nabla a_z + \chi_z) \tag{2.14}$$

where a_s, a_n and a_z are the $\mathbf{e}_s, \mathbf{e}_n$ and $\mathbf{e}_z$ components of a and χ_s, χ_n and χ_z are vectors which are functions of a_s, a_n, a_z and the derivatives of the unit vectors. The only non-zero derivatives of the unit vectors (see equations (2.7) to (2.9)) are

$$\aleph\frac{\partial\mathbf{e}_s}{\partial s} = -\frac{\aleph}{R_c}\mathbf{e}_n \tag{2.15}$$

$$\aleph\frac{\partial\mathbf{e}_s}{\partial s} = \frac{\aleph}{R_c}\mathbf{e}_s \tag{2.16}$$

Evaluating χ_s, χ_n and χ_z with equation (2.15) and (2.16) and substituting into (2.14) gives

$$\nabla\mathbf{a} = \mathbf{e}_s(\nabla a_s + \frac{\aleph}{R_c}a_n\mathbf{e}_s) + \mathbf{e}_n(\nabla a_n - \frac{\aleph}{R_c}a_s\mathbf{e}_s) + \mathbf{e}_z\nabla a_z \tag{2.17}$$

Equation (2.17) may be expanded to give

$$\begin{aligned}\nabla\mathbf{a} = {} & \mathbf{e}_s\mathbf{e}_s(\aleph\frac{\partial a_s}{\partial s} + \aleph\frac{a_n}{R_c}) + \mathbf{e}_s\mathbf{e}_n\frac{\partial a_s}{\partial n} + \mathbf{e}_s\mathbf{e}_z\frac{\partial a_s}{\partial z} + \\ & \mathbf{e}_n\mathbf{e}_s(\aleph\frac{\partial a_n}{\partial s} - \aleph\frac{a_s}{R_c}) + \mathbf{e}_n\mathbf{e}_n\frac{\partial a_n}{\partial n} + \mathbf{e}_n\mathbf{e}_z\frac{\partial a_n}{\partial z} + \\ & \mathbf{e}_z\mathbf{e}_s\aleph\frac{\partial a_z}{\partial s} + \mathbf{e}_z\mathbf{e}_n\frac{\partial a_z}{\partial n} + \mathbf{e}_z\mathbf{e}_z\frac{\partial a_z}{\partial z}\end{aligned} \tag{2.18}$$

The strain tensor (Karamcheti, 1966, p. 106) is

$$\mathbf{D} = \frac{1}{2}[\nabla\mathbf{a} + (\nabla\mathbf{a})^T] \tag{2.19}$$

$$
\begin{aligned}
= \; & \aleph(\frac{\partial a_s}{\partial s} + \frac{a_n}{R_c})\mathbf{e}_s\mathbf{e}_s + \frac{1}{2}(\frac{\partial a_s}{\partial n} + \aleph(\frac{\partial a_n}{\partial s} - \frac{a_s}{R_c}))(\mathbf{e}_s\mathbf{e}_n + \mathbf{e}_n\mathbf{e}_s) + \\
& \frac{1}{2}(\frac{\partial a_s}{\partial z} + \aleph\frac{\partial a_z}{\partial s})(\mathbf{e}_s\mathbf{e}_z + \mathbf{e}_z\mathbf{e}_s) + \frac{\partial a_n}{\partial n}\mathbf{e}_n\mathbf{e}_n + \\
& \frac{1}{2}(\frac{\partial a_z}{\partial n} + \frac{\partial a_n}{\partial z})(\mathbf{e}_n\mathbf{e}_z + \mathbf{e}_z\mathbf{e}_n) + \frac{\partial a_z}{\partial z}\mathbf{e}_z\mathbf{e}_z
\end{aligned}
$$

where $(.)^T$ indicates the transpose of the tensor. The rotation tensor (Karamcheti, 1966, p. 106) is

$$
\begin{aligned}
\Omega &= \frac{1}{2}[\nabla\mathbf{a} - (\nabla\mathbf{a})^T] \qquad (2.20) \\
&= \frac{1}{2}(\frac{\partial a_s}{\partial n} - \aleph(\frac{\partial a_n}{\partial s} - \frac{a_s}{R_c}))(\mathbf{e}_s\mathbf{e}_n - \mathbf{e}_n\mathbf{e}_s) + \\
&\quad \frac{1}{2}(\frac{\partial a_s}{\partial z} - \aleph\frac{\partial a_z}{\partial s})(\mathbf{e}_s\mathbf{e}_z - \mathbf{e}_z\mathbf{e}_s) + \\
&\quad \frac{1}{2}(\frac{\partial a_n}{\partial z} - \frac{\partial a_z}{\partial n})(\mathbf{e}_n\mathbf{e}_z - \mathbf{e}_z\mathbf{e}_n)
\end{aligned}
$$

The axial vector associated with the rotation tensor,i.e. the vorticity, (Karamcheti, 1966, p.106) is

$$\omega = \nabla\times\mathbf{a} = (\frac{\partial a_n}{\partial z} - \frac{\partial a_z}{\partial n})\mathbf{e}_s + (\frac{\partial a_s}{\partial z} - \aleph\frac{\partial a_z}{\partial s})\mathbf{e}_n + (\frac{\partial a_s}{\partial n} - \aleph(\frac{\partial a_n}{\partial s} - \frac{a_s}{R_c}))\mathbf{e}_z \quad (2.21)$$

Using equation (2.13) the divergence of a vector (Karamcheti, 1966, p.106) may be calculated from

$$\nabla\cdot\mathbf{a} = \aleph\frac{\partial a_s}{\partial s} + \aleph\frac{\partial}{\partial n}\frac{a_n}{\aleph} + \frac{\partial a_z}{\partial z} \qquad (2.22)$$

The Laplacian of a scalar (Karamcheti, 1966, p.145) may be calculated using equations (2.12), (2.13) and (2.22)

$$\nabla^2\phi = \nabla\cdot(\nabla\phi) = \aleph^2\frac{\partial^2\phi}{\partial s^2} + \aleph\frac{\partial}{\partial n}\frac{1}{\aleph}\frac{\partial\phi}{\partial n} + \frac{\partial^2\phi}{\partial z^2} \qquad (2.23)$$

The vector Laplacian (Karamcheti, 1966, p.134) may be written as

$$\nabla^2\mathbf{a} = \nabla(\nabla\cdot\mathbf{a}) - \nabla\times(\nabla\times\mathbf{a}) \qquad (2.24)$$

Using equations (2.12), (2.21) and (2.22) the vector Laplacian is

$$\nabla^2\mathbf{a} = [\nabla^2 a_s + 2\frac{\aleph^2}{R_c}\frac{\partial a_n}{\partial s} - \frac{\aleph^2}{R_c^2}a_s]\mathbf{e}_s + [\nabla^2 a_n - 2\frac{\aleph^2}{R_c}\frac{\partial a_s}{\partial s} - \frac{\aleph^2}{R_c^2}a_n]\mathbf{e}_n + \nabla^2 a_z \mathbf{e}_z \quad (2.25)$$

For a vector field without divergence, such as the velocity of an incompressible fluid, the vector Laplacian may also be written as

$$\begin{aligned}
\nabla^2\mathbf{a} &= -\nabla\times(\nabla\times\mathbf{a}) \qquad (2.26)\\
&= [\frac{\partial^2 a_s}{\partial n^2} + \frac{\partial^2 a_s}{\partial z^2} + \frac{\aleph^2}{R_c}\frac{\partial a_n}{\partial s} + \frac{\aleph}{R_c}\frac{\partial a_s}{\partial n} - \aleph\frac{\partial^2 a_z}{\partial s\partial z} - \aleph\frac{\partial^2 a_n}{\partial s\partial n} - \frac{\aleph^2}{R_c^2}a_s]\mathbf{e}_s +\\
&\quad [\aleph^2\frac{\partial^2 a_n}{\partial s^2} + \frac{\partial^2 a_n}{\partial z^2} - \aleph\frac{\partial^2 a_s}{\partial s\partial n} - \frac{\aleph^2}{R_c}\frac{\partial a_s}{\partial s} - \frac{\partial^2 a_z}{\partial z\partial n}]\mathbf{e}_n +\\
&\quad [\aleph^2\frac{\partial^2 a_z}{\partial s^2} + \frac{\partial^2 a_z}{\partial n^2} + \frac{\aleph}{R_c}\frac{\partial a_z}{\partial n} - \frac{\partial^2 a_n}{\partial n\partial z} - \aleph\frac{\partial^2 a_s}{\partial s\partial z} - \frac{\aleph}{R_c}\frac{\partial a_n}{\partial z}]\mathbf{e}_z
\end{aligned}$$

2.2 Statistical Definitions

2.2.1 Probabilities

The first order distribution function for a stochastic process $\tilde{y}(\mathbf{z},t)$ (where the tilde denotes the instantaneous value) is defined as (Papoulis,1984,p.206)

$$F(\mathcal{Y};\mathbf{z},t) = \mathcal{P}(\tilde{y}(\mathbf{z},t) \le \mathcal{Y}) \qquad (2.27)$$

where $\mathcal{P}(A)$ is the probability of the event A. The corresponding first order probability density function is given by

$$f(\mathcal{Y};\mathbf{z},t) = f_y(\mathbf{z},t) = \frac{\partial}{\partial\mathcal{Y}}F(\mathcal{Y};\mathbf{z},t) \qquad (2.28)$$

Equation (2.28) may be used to derive the n^{th} moment of the stochastic process $\tilde{y}(\mathbf{z},t)$

$$\overline{y^n}(\mathbf{z},t) = \int_{-\infty}^{\infty} \mathcal{Y}^n f(\mathcal{Y};\mathbf{z},t)d\mathcal{Y} \tag{2.29}$$

The second order distribution and probability density functions for the stochastic process $\tilde{y}(\mathbf{z},t)$ at times t_1 and t_2 are (Papoulis,1984,p207)

$$F(\mathcal{Y}_1,\mathcal{Y}_2;\mathbf{z},t_1,t_2) = \mathcal{P}(\tilde{y}(\mathbf{z},t_1) \leq \mathcal{Y}_1, \tilde{y}(\mathbf{z},t_2) \leq \mathcal{Y}_2) \tag{2.30}$$

$$f(\mathcal{Y}_1,\mathcal{Y}_2;\mathbf{z},t_1,t_2) = f_{\mathcal{Y}_1\mathcal{Y}_2}(\mathbf{z},t_1,t_2) = \frac{\partial^2}{\partial\mathcal{Y}_1\partial\mathcal{Y}_2}F(\mathcal{Y}_1,\mathcal{Y}_2;\mathbf{z},t_1,t_2) \tag{2.31}$$

Equation (2.31) may be used to derive the autocorrelation in the following way

$$R(\mathbf{z},t_1,t_2) = \int_{-\infty}^{\infty}\int_{-\infty}^{\infty} \mathcal{Y}_1\mathcal{Y}_2 f(\mathcal{Y}_1,\mathcal{Y}_2;\mathbf{z},t_1,t_2)d\mathcal{Y}_1 d\mathcal{Y}_2 \tag{2.32}$$

In a similar way the joint distribution and probabilty density functions for the two stochastic processes $\tilde{x}(\mathbf{z},t)$ and $\tilde{y}(\mathbf{z},t)$ are defined as

$$F(\mathcal{X},\mathcal{Y};\mathbf{z},t) = \mathcal{P}(\tilde{x}(\mathbf{z},t) \leq \mathcal{X}, \tilde{y}(\mathbf{z},t) \leq \mathcal{Y}) \tag{2.33}$$

$$f(\mathcal{X},\mathcal{Y};\mathbf{z},t) = f_{\mathcal{X}\mathcal{Y}}(\mathbf{z},t) = \frac{\partial^2}{\partial\mathcal{X}\partial\mathcal{Y}}F(\mathcal{X},\mathcal{Y};\mathbf{z},t) \tag{2.34}$$

Equation (2.34) may be used to derive the joint moments of the stochastic processes $\tilde{x}(\mathbf{z},t)$ and $\tilde{y}(\mathbf{z},t)$ as

$$\overline{x^m y^n} = \int_{-\infty}^{\infty}\int_{-\infty}^{\infty} \mathcal{X}^m\mathcal{Y}^n f_{\mathcal{X}\mathcal{Y}}(\mathbf{z},t)d\mathcal{X}d\mathcal{Y} \tag{2.35}$$

While the statistical moments of a random process are defined in terms of the probability density function for that particular process, in practice the statistical moments can be estimated from the experimental observations as the ensemble

average of different realizations of a stochastic process $\tilde{y}$ as (Papoulis, 1984, p.245)

$$\overline{y}(\mathbf{z},t) = \lim_{N\to\infty} \frac{1}{N} \sum_{m=0}^{N} \tilde{y}_m(\mathbf{z},t) \tag{2.36}$$

where the subscript m denotes the particular realization of the experiment. In cases where $\tilde{y}_m$ is a stationary function of time, the ensemble average defined by equation (2.28) is equal to the time average (Papoulis, 1984, p.245)

$$\overline{y}(\mathbf{z}) = \lim_{T\to\infty} \frac{1}{2T} \int_{-T}^{T} \tilde{y}(\mathbf{z},t)dt \tag{2.37}$$

In the case where $\tilde{y}$ is spatially homogeneous, the ensemble average may be replaced by the space average (Batchelor, 1953, p.15)

$$\overline{y}(t) = \lim_{\forall\to\infty} \frac{1}{\forall} \int_{\forall} \tilde{y}(\mathbf{z}',t)d\forall' \tag{2.38}$$

A stationary discrete time series is defined as

$$\tilde{y}_j(\mathbf{z}) = \tilde{y}(j\Delta t,\mathbf{z}) \tag{2.39}$$

where Δt is the time interval between points and N is the number of points. In cases where the time interval is large enough that successive points are statistically independent, the average may be written using equation (2.28)

$$\overline{y}(\mathbf{z}) = \lim_{N\to\infty} \frac{1}{N} \sum_{j=0}^{N} \tilde{y}_j(\mathbf{z}) \tag{2.40}$$

2.2.2 Space and Time Averages

The instantaneous variables $\tilde{U}, \tilde{V}, \tilde{W}$ and $\tilde{P}$ have been decomposed into mean and fluctuating parts

$$\tilde{U} = U + u \tag{2.41}$$

$$\tilde{V} = V + v \tag{2.42}$$

$$\tilde{W} = W + w \tag{2.43}$$

$$\tilde{P} = P + p \tag{2.44}$$

where the average of the fluctuation is by definition equal to zero. An $\overline{(.)}$ will indicate the average of a composite expression.

The covariance of two random variables at different points in space or time is (Papoulis, 1984, p.209)

$$C_{ab}(\mathbf{z}_1, t_1; \mathbf{z}_2, t_2) = \overline{a(\mathbf{z}_1, t_1) b(\mathbf{z}, t_2)} \tag{2.45}$$

The Reynolds stresses are covariances in the limiting case where point 1 and point 2 coincide. The nine components of the Reynolds stress tensor are (Townsend, 1976)

$$\begin{pmatrix} \overline{uu} & \overline{uv} & \overline{uw} \\ \overline{uv} & \overline{vv} & \overline{vw} \\ \overline{uw} & \overline{vw} & \overline{ww} \end{pmatrix}$$

Due to symmetry only six of these components are independent. A measure of the structure of the turbulent stress tensor is provided by dividing Reynolds stresses by twice the kinetic energy (per unit mass) of the turbulence

$$\begin{pmatrix} \overline{uu}/q^2 & \overline{uv}/q^2 & \overline{uw}/q^2 \\ \overline{uv}/q^2 & \overline{vv}/q^2 & \overline{vw}/q^2 \\ \overline{uw}/q^2 & \overline{vw}/q^2 & \overline{ww}/q^2 \end{pmatrix}$$

where $q^2 = (\overline{u^2} + \overline{v^2} + \overline{w^2})$. This tensor is referred to as the structural tensor and its elements are denoted by K_{uu}, K_{uv}, K_{uw} etc. Another important covariance

is the "time correlation" (Hinze, 1975, p.57)

$$R_{uu}(\mathbf{z},\tau) = \frac{\overline{u(\mathbf{z},t)u(\mathbf{z},t+\tau)}}{\overline{u^2(\mathbf{z},t)}} \tag{2.46}$$

of a stationary function. R_{vv}, R_{ww}, R_{uv} and R_{uw} are defined similarily. Two measures of the time correlation are the micro-scale (Hinze, 1975, p.57)

$$\lambda_{u\tau}^{-2} = (\frac{\partial^2 R_{uu}(\mathbf{z},\tau)}{\partial \tau^2})_{\tau=0} \tag{2.47}$$

and the integral scale (Hinze, 1975, p.57)

$$\Lambda_{uu} = \int_0^\infty R_{uu}(\mathbf{z},\tau)d\tau \tag{2.48}$$

In a similar way one can define a "space correlation" for a homogeneous turbulence as

$$B_{uu}(\mathbf{r},t) = \frac{\overline{u(\mathbf{z},t)u(\mathbf{z}+\mathbf{r},t)}}{\overline{u^2(\mathbf{z},t)}} \tag{2.49}$$

B_{vv}, B_{ww}, B_{uv} and B_{uw} are defined similarily. The associated micro-scale

$$\lambda_{ur}^{-2} = (\frac{\partial^2 B_{uu}(\mathbf{z},t)}{\partial r^2})_{r=0} \tag{2.50}$$

and the integral scale

$$L_{uu,r} = \int_0^\infty B_{uu}(\mathbf{r},t)d\mathbf{r} \tag{2.51}$$

$L_{vv,r}$, $L_{ww,r}$, $L_{uv,r}$ and $L_{uw,r}$ are defined similarily.

The "space correlation" of the kinetic energy could be defined as

$$B_{qq}(\mathbf{r},t) = \frac{\overline{\mathbf{v}(\mathbf{z},t)\cdot\mathbf{v}(\mathbf{z}+\mathbf{r},t)}}{\overline{q^2(\mathbf{z},t)}} \tag{2.52}$$

where $\mathbf{v}$ is the velocity vector. The integral scale for this space correlation is

$$L_{qq,r} = \int_0^\infty B_{qq}(\mathbf{r},t)d\mathbf{r} \tag{2.53}$$

$L_{qq,r}$ is related to $L_{uu,r}$, $L_{vv,r}$ and $L_{ww,r}$ as

$$L_{qq,r} = L_{uu,r}K_{uu} + L_{vv,r}K_{vv} + L_{ww,r}K_{ww} \tag{2.54}$$

In the following only space correlations which are separated in the streamwise direction, s, will be considered and for convience the s subscript will be dropped with the understanding that all length scales and the microscales are for streamwise separations and derivatives unless stated otherwise.

The space correlation for streamwise separations can be approximated when the turbulence intensity is low, from the time correlation using Taylor's "Frozen Flow" hypothesis (Tavoularis, 1986). For example

$$B_{uu}(s,t) \approx R_{uu}(\mathbf{z}, U\tau) \tag{2.55}$$

from which follows the approximate relations for the integral scales and microscales

$$L_{uu,s} \approx U\Lambda_{uu} \tag{2.56}$$

$$\lambda_{us} \approx U\lambda_{u\tau} \tag{2.57}$$

2.2.3 Spectra

The Fourier transform (or spectrum) of a covariance may be formed where the covariance is spatially homogeneous or stationary in time. For a spatially homogeneous covariance the Fourier transform is (Hinze, 1975, p.334)

$$\widehat{C_{ab}}(\mathbf{k},t) = \frac{1}{8\pi^3}\int_{-\infty}^{\infty}\int_{-\infty}^{\infty}\int_{-\infty}^{\infty} C_{ab}(\mathbf{r},t)e^{-i(\mathbf{r}\cdot\mathbf{k})}dr_1dr_2dr_3 \tag{2.58}$$

where $\mathbf{r} = \mathbf{z}_1 - \mathbf{z}_2$ and k is the position vector in wavespace and has the components

$$\mathbf{k} = \alpha \mathbf{e}_s + \beta \mathbf{e}_n + \gamma \mathbf{e}_z \tag{2.59}$$

A one dimensional streamwise spectra can be defined as

$$F_{ab}(\alpha, t) = \frac{1}{2\pi} \int_{-\infty}^{\infty} C_{ab}(\mathbf{r}, t) e^{-i(s\alpha)} ds \tag{2.60}$$

It is also possible to form the Fourier transform of the covariance from the average of the product of the Fourier transforms of finite records of the random variables themselves (Yeh and Van Atta, 1973) as

$$\widehat{C_{ab}}(\mathbf{k}, t) = \overline{\hat{a}(\mathbf{k}, t) \hat{b}^{\spadesuit}(\mathbf{k}, t)} \tag{2.61}$$

where

$$\hat{a}(\mathbf{k}, t) = \frac{1}{8\pi^3} \int_{-\infty}^{\infty} \int_{-\infty}^{\infty} \int_{-\infty}^{\infty} a(\mathbf{r}, t) e^{-i(\mathbf{r}\cdot\mathbf{k})} dr_1 dr_2 dr_3 \tag{2.62}$$

$$\hat{b}(\mathbf{k}, t) = \frac{1}{8\pi^3} \int_{-\infty}^{\infty} \int_{-\infty}^{\infty} \int_{-\infty}^{\infty} b(\mathbf{r}, t) e^{-i(\mathbf{r}\cdot\mathbf{k})} dr_1 dr_2 dr_3 \tag{2.63}$$

and the spade superscript denotes a complex conjugate.

The Fourier transform of the components of the velocity covariance may be written for spatially homogeneous or a temporally stationary turbulence as

$$\begin{pmatrix} \overline{\hat{u}\hat{u}^{\spadesuit}} & \overline{\hat{u}\hat{v}^{\spadesuit}} & \overline{\hat{u}\hat{w}^{\spadesuit}} \\ \overline{\hat{v}\hat{u}^{\spadesuit}} & \overline{\hat{v}\hat{v}^{\spadesuit}} & \overline{\hat{v}\hat{w}^{\spadesuit}} \\ \overline{\hat{w}\hat{u}^{\spadesuit}} & \overline{\hat{w}\hat{v}^{\spadesuit}} & \overline{\hat{w}\hat{w}^{\spadesuit}} \end{pmatrix}$$

and will be denoted by $\hat{C}_{uu}, \hat{C}_{uv}, \hat{C}_{uw}$ etc. This tensor is Hermitian since it equals the conjugate of its transpose.

For a temporally stationary time correlation the Fourier transform is (Hinze, 1975, p.64)

$$\hat{R}_{ab}(\mathbf{z},\omega) = \frac{1}{2\pi}\int_{-\infty}^{\infty} R_{ab}(\mathbf{z},\tau)\exp^{-\iota\omega\tau}\,d\tau \tag{2.64}$$

or directly in terms of the transforms of the finite time series

$$\widehat{R_{ab}}(\mathbf{z},\omega) = \overline{\hat{a}(\mathbf{z},\omega)\hat{b}^{\spadesuit}(\mathbf{z},\omega)} \tag{2.65}$$

where

$$\hat{a}(\mathbf{z},\omega) = \frac{1}{2\pi}\int_{-\infty}^{\infty} a(\mathbf{z},t)e^{-i(\omega t)}dt \tag{2.66}$$

$$\hat{b}(\mathbf{z},\omega) = \frac{1}{2\pi}\int_{-\infty}^{\infty} a(\mathbf{z},t)e^{-i(\omega t)}dt \tag{2.67}$$

As with the time and space correlations the one dimensional streamwise spectra and the power spectrum can be related approximately using Taylor's "frozen flow" approximation as

$$F_{ab}(\alpha,t) = \hat{R}_{ab}(\mathbf{z},\frac{\omega}{U})\overline{ab} \tag{2.68}$$

where U is the mean streamwise velocity.

The discrete Fourier transform of a stationary discrete time series

$$\hat{y}_k(\mathbf{z}) = \hat{y}(k\Delta\omega,\mathbf{z}) \tag{2.69}$$

where $k = -\frac{N}{2}...\frac{N}{2}$ and $\Delta\omega = \frac{1}{N\Delta t}$ is the frequency interval may be calculated from the relation (Papoulis,1978)

$$\hat{y}_k(\mathbf{z}) \approx \frac{1}{N}\Sigma_{j=-\frac{N}{2}}^{\frac{N}{2}}\tilde{y}_j(\mathbf{z})e^{-\iota\frac{kj}{N}} \tag{2.70}$$

2.3 Governing Equations

The motion of a incompressible, constant viscosity fluid is customarily described by the Navier Stokes equations and the continuity equation which in vector form are (Slattery, 1981, p.58)

$$\frac{\partial \tilde{\mathbf{U}}}{\partial t} + \tilde{\mathbf{u}} \cdot \nabla \tilde{\mathbf{U}} = -\nabla \frac{\tilde{P}}{\rho} + \nu \nabla \cdot (\nabla \tilde{\mathbf{U}}) \tag{2.71}$$

$$\nabla \cdot \tilde{\mathbf{U}} = \mathbf{0} \tag{2.72}$$

On substituting the various operators expressed in s, n, z coordinates from section (2.1), the components of equation (2.71) are

$$\frac{\partial \tilde{U}}{\partial t} + \aleph \tilde{U} \frac{\partial \tilde{U}}{\partial s} + \tilde{V} \frac{\partial \tilde{U}}{\partial n} + \tilde{W} \frac{\partial \tilde{U}}{\partial z} + \frac{\aleph \tilde{U} \tilde{V}}{R_c} = -\aleph \frac{\partial}{\partial s} \frac{\tilde{P}}{\rho} + \nu(\nabla^2 \tilde{U} + 2\frac{\aleph^2}{R_c} \frac{\partial \tilde{V}}{\partial s} - \frac{\aleph^2}{R_c^2} \tilde{U}) \tag{2.73}$$

$$\frac{\partial \tilde{V}}{\partial t} + \aleph \tilde{U} \frac{\partial \tilde{V}}{\partial s} + \tilde{V} \frac{\partial \tilde{V}}{\partial n} + \tilde{W} \frac{\partial \tilde{V}}{\partial z} - \frac{\aleph \tilde{U} \tilde{U}}{R_c} = -\frac{\partial}{\partial n} \frac{\tilde{P}}{\rho} + \nu(\nabla^2 \tilde{V} - 2\frac{\aleph^2}{R_c} \frac{\partial \tilde{U}}{\partial s} - \frac{\aleph^2}{R_c^2} \tilde{V}) \tag{2.74}$$

$$\frac{\partial \tilde{W}}{\partial t} + \aleph \tilde{U} \frac{\partial \tilde{W}}{\partial s} + \tilde{V} \frac{\partial \tilde{W}}{\partial n} + \tilde{W} \frac{\partial \tilde{W}}{\partial z} = -\frac{\partial}{\partial z} \frac{\tilde{P}}{\rho} + \nu \nabla^2 \tilde{W} \tag{2.75}$$

The continuity equation is

$$\aleph \frac{\partial \tilde{U}}{\partial s} + \aleph \frac{\partial}{\partial n} \frac{\tilde{V}}{\aleph} + \frac{\partial \tilde{W}}{\partial z} = 0 \tag{2.76}$$

If one decomposes the instantaneous velocity and pressure into mean and fluctuating parts and average equations (2.73) to (2.76), one gets the equations for the mean motion

$$\frac{DU}{Dt} + \aleph \frac{UV}{R_c} = -\aleph \frac{\partial}{\partial s} \frac{P}{\rho} - (\aleph \frac{\partial \overline{u^2}}{\partial s} + \aleph \frac{\partial}{\partial n} \frac{\overline{uv}}{\aleph} + \frac{\partial \overline{uw}}{\partial z} + \frac{\aleph \overline{uv}}{R_c}) + \nu(\nabla^2 U + 2\frac{\aleph^2}{R_c} \frac{\partial V}{\partial s} - \frac{\aleph^2}{R_c^2} U) \tag{2.77}$$

$$\frac{DV}{Dt} - \aleph\frac{U^2}{R_c} = -\frac{\partial}{\partial n}\frac{P}{\rho} - (\aleph\frac{\partial\overline{uv}}{\partial s} + \aleph\frac{\partial}{\partial n}\frac{\overline{v^2}}{\aleph} + \frac{\partial\overline{vw}}{\partial z} - \frac{\aleph\overline{u^2}}{R_c}) \quad (2.78)$$
$$+\nu(\nabla^2 V - 2\frac{\aleph^2}{R_c}\frac{\partial U}{\partial s} - \frac{\aleph^2}{R_c^2}V)$$

$$\frac{DW}{Dt} = -\frac{\partial}{\partial z}\frac{P}{\rho} - (\aleph\frac{\partial\overline{uw}}{\partial s} + \aleph\frac{\partial}{\partial n}\frac{\overline{vw}}{\aleph} + \frac{\partial\overline{w^2}}{\partial z}) + \nu\nabla^2 W \quad (2.79)$$

$$0 = \aleph\frac{\partial U}{\partial s} + \aleph\frac{\partial}{\partial n}\frac{V}{\aleph} + \frac{\partial W}{\partial z} \quad (2.80)$$

where $\frac{D}{Dt} = \frac{\partial}{\partial t} + \aleph U\frac{\partial}{\partial s} + V\frac{\partial}{\partial n} + W\frac{\partial}{\partial z}$. Equations for the fluctuating velocity and pressure may be derived by subtracting equations (2.77) to (2.80) from equations (2.73) to (2.76) respectively. The resulting equations for the fluctuating velocity and pressure are

$$\frac{Du}{Dt} = -[\aleph u\frac{\partial U}{\partial s} + v\frac{\partial U}{\partial n} + w\frac{\partial U}{\partial z} + \frac{\aleph}{R_c}(vU + uV)] \quad (2.81)$$
$$-\aleph\frac{\partial}{\partial s}\frac{p}{\rho} + \nu[\nabla^2 u + 2\frac{\aleph^2}{R_c}\frac{\partial v}{\partial s} - \frac{\aleph^2}{R_c^2}u]$$
$$-[\aleph\frac{\partial}{\partial s}(u^2 - \overline{u^2}) + \aleph\frac{\partial}{\partial n}\frac{1}{\aleph}(uv - \overline{uv}) + \frac{\partial}{\partial z}(uw - \overline{uw}) + \frac{\aleph}{R_c}(uv - \overline{uv})]$$

$$\frac{Dv}{Dt} = -[\aleph u\frac{\partial V}{\partial s} + v\frac{\partial V}{\partial n} + w\frac{\partial V}{\partial z} - 2\frac{\aleph}{R_c}Uu] \quad (2.82)$$
$$-\frac{\partial}{\partial n}\frac{p}{\rho} + \nu[\nabla^2 v - 2\frac{\aleph^2}{R_c}\frac{\partial u}{\partial s} - \frac{\aleph^2}{R_c^2}v]$$
$$-[\aleph\frac{\partial}{\partial s}(uv - \overline{uv}) + \aleph\frac{\partial}{\partial n}\frac{1}{\aleph}(v^2 - \overline{v^2}) + \frac{\partial}{\partial z}(vw - \overline{vw}) - \frac{\aleph}{R_c}(u^2 - \overline{u^2})]$$

$$\frac{Dw}{Dt} = -[\aleph u\frac{\partial W}{\partial s} + v\frac{\partial W}{\partial n} + w\frac{\partial W}{\partial z}] - \frac{\partial}{\partial z}\frac{p}{\rho} + \nu\nabla^2 w \quad (2.83)$$
$$-[\aleph\frac{\partial}{\partial s}(uw - \overline{uw}) + \aleph\frac{\partial}{\partial n}\frac{1}{\aleph}(vw - \overline{vw}) + \frac{\partial}{\partial z}(w^2 - \overline{w^2})]$$

$$0 = \aleph\frac{\partial u}{\partial s} + \aleph\frac{\partial}{\partial n}\frac{v}{\aleph} + \frac{\partial w}{\partial z} \quad (2.84)$$

The last terms in equations (2.81) to (2.83) are not linear.

It is possible to form equations for the Reynolds stresses which appear in equations (2.77) to (2.79). For example the $\overline{uv}$ equation can be formed by multiplying equation (2.77) by v, equation (2.78) by u, adding the two equations and averaging. The equations for $\overline{u^2}, \overline{v^2}, \overline{w^2}, \overline{uw}$ and $\overline{vw}$ may be derived similarily.

The equations for the Reynolds stresses in s, n, z coordinates are

$$\frac{D}{Dt}\frac{\overline{u^2}}{2} = -[\aleph\overline{u^2}\frac{\partial U}{\partial s} + \overline{uv}\frac{\partial U}{\partial n} + \overline{uw}\frac{\partial U}{\partial z} + \frac{\aleph}{R_c}(\overline{uv}U + \overline{u^2}V)] + \tag{2.85}$$
$$\aleph\overline{\frac{p}{\rho}\frac{\partial u}{\partial s}} - [\aleph\frac{\partial}{\partial s}(\frac{\overline{pu}}{\rho} + \frac{\overline{u^3}}{2}) + \aleph\frac{\partial}{\partial n}\frac{\overline{u^2v}}{2\aleph} + \frac{\partial}{\partial z}\frac{\overline{u^2w}}{2} + \frac{\aleph}{R_c}\overline{u^2v}] +$$
$$\nu\nabla^2\frac{\overline{u^2}}{2} - \nu\overline{[(\frac{\partial u}{\partial n})^2 + \aleph^2(\frac{\partial u}{\partial s})^2 + (\frac{\partial u}{\partial z})^2 - 2\frac{\aleph^2}{R_c}u\frac{\partial v}{\partial s} - \frac{\aleph^2}{R_c^2}u^2]}$$

$$\frac{D}{Dt}\frac{\overline{v^2}}{2} = -[\aleph\overline{uv}\frac{\partial V}{\partial s} + \overline{v^2}\frac{\partial V}{\partial n} + \overline{vw}\frac{\partial V}{\partial z} - 2\frac{\aleph}{R_c}\overline{uv}U] + \tag{2.86}$$
$$\aleph\overline{\frac{p}{\rho}\frac{\partial}{\partial n}\frac{v}{\aleph}} - [\aleph\frac{\partial}{\partial s}\frac{\overline{uv^2}}{2} + \aleph\frac{\partial}{\partial n}(\frac{\overline{pv}}{\rho\aleph} + \frac{\overline{v^3}}{2\aleph}) + \frac{\partial}{\partial z}\frac{\overline{v^2w}}{2} - \frac{\aleph}{R_c}\overline{u^2v}] +$$
$$\nu\nabla^2\frac{\overline{v^2}}{2} - \nu\overline{[(\frac{\partial v}{\partial n})^2 + \aleph^2(\frac{\partial v}{\partial s})^2 + (\frac{\partial v}{\partial z})^2 + 2\frac{\aleph^2}{R_c}v\frac{\partial u}{\partial s} + \frac{\aleph^2}{R_c^2}v^2]}$$

$$\frac{D}{Dt}\frac{\overline{w^2}}{2} = -[\aleph\overline{uw}\frac{\partial W}{\partial s} + \overline{vw}\frac{\partial W}{\partial n} + \overline{w^2}\frac{\partial W}{\partial z}] + \tag{2.87}$$
$$\aleph\overline{\frac{p}{\rho}\frac{\partial w}{\partial z}} - [\aleph\frac{\partial}{\partial s}\frac{\overline{uw^2}}{2} + \aleph\frac{\partial}{\partial n}\frac{\overline{vw^2}}{2\aleph} + \frac{\partial}{\partial z}(\frac{\overline{pw}}{\rho} + \frac{\overline{w^3}}{2})] +$$
$$\nu\nabla^2\frac{\overline{w^2}}{2} - \nu\overline{[(\frac{\partial w}{\partial n})^2 + \aleph^2(\frac{\partial w}{\partial s})^2 + (\frac{\partial w}{\partial z})^2]}$$

$$\frac{D}{Dt}\overline{uv} = -[\aleph\overline{u^2}\frac{\partial V}{\partial s} + \aleph\overline{uv}\frac{\partial U}{\partial s} + \overline{uv}\frac{\partial V}{\partial n} + \tag{2.88}$$
$$\overline{v^2}\frac{\partial U}{\partial n} + \overline{uw}\frac{\partial V}{\partial z} + \overline{vw}\frac{\partial U}{\partial z} - \frac{\aleph}{R_c}(U(2\overline{u^2} - \overline{v^2}) + \overline{uv}V)] +$$
$$\aleph\overline{\frac{p}{\rho}(\frac{\partial v}{\partial s} + \aleph\frac{\partial}{\partial n}\frac{u}{\aleph})} - [\aleph\frac{\partial}{\partial s}(\frac{\overline{pv}}{\rho} + \overline{u^2v}) +$$
$$\aleph\frac{\partial}{\partial n}(\frac{\overline{pu}}{\rho\aleph} + \frac{\overline{uv^2}}{\aleph}) + \frac{\partial}{\partial z}\overline{uvw} + \frac{\aleph}{R_c}(\overline{uv^2} - \overline{u^3})] +$$
$$\nu\nabla^2\overline{uv} - 2\nu\overline{[(\frac{\partial u}{\partial n}\frac{\partial v}{\partial n}) + \aleph^2(\frac{\partial u}{\partial s}\frac{\partial v}{\partial s}) + (\frac{\partial u}{\partial z}\frac{\partial v}{\partial z}) + 2\frac{\aleph^2}{R_c}(u\frac{\partial u}{\partial s} - v\frac{\partial v}{\partial s}) + 2\frac{\aleph^2}{R_c^2}uv]}$$

$$\frac{D}{Dt}\overline{uw} = -[\aleph\overline{uw}\frac{\partial U}{\partial s} + \aleph\overline{u^2}\frac{\partial W}{\partial s} + \overline{vw}\frac{\partial U}{\partial n} + \tag{2.89}$$
$$\overline{uv}\frac{\partial W}{\partial n} + \overline{w^2}\frac{\partial U}{\partial z} + \overline{uw}\frac{\partial W}{\partial z} + \frac{\aleph}{R_c}(U\overline{vw} + \overline{uw}V)] +$$
$$\overline{\frac{p}{\rho}(\aleph\frac{\partial w}{\partial s} + \frac{\partial u}{\partial z})} - [\aleph\frac{\partial}{\partial s}(\frac{\overline{pw}}{\rho} + \overline{u^2w}) +$$
$$\aleph\frac{\partial}{\partial n}\frac{uvw}{\aleph} + \frac{\partial}{\partial z}(\frac{\overline{pu}}{\rho} + \overline{uw^2}) + \frac{\aleph}{R_c}\overline{uvw}] +$$
$$\nu\nabla^2\overline{uw} - 2\nu\overline{[(\frac{\partial u}{\partial n}\frac{\partial w}{\partial n}) + \aleph^2(\frac{\partial u}{\partial s}\frac{\partial w}{\partial s}) + (\frac{\partial u}{\partial z}\frac{\partial w}{\partial z}) + \frac{\aleph^2}{R_c}w\frac{\partial v}{\partial s} + \frac{\aleph^2}{R_c^2}uw]}$$

$$\frac{D}{Dt}\overline{vw} = -[\aleph\overline{uv}\frac{\partial W}{\partial s} + \aleph\overline{uw}\frac{\partial V}{\partial s} + \overline{vw}\frac{\partial V}{\partial n} + \tag{2.90}$$

$$\overline{v^2}\frac{\partial W}{\partial n} + \overline{w^2}\frac{\partial V}{\partial z} + \overline{vw}\frac{\partial W}{\partial z} - 2\frac{\aleph}{R_c}U\overline{uw}] +$$
$$\overline{\frac{p}{\rho}(\aleph\frac{\partial}{\partial n}\frac{w}{\aleph} + \frac{\partial v}{\partial z})} - [\aleph\frac{\partial \overline{uvw}}{\partial s} +$$
$$\aleph\frac{\partial}{\partial n}(\frac{\overline{v^2w}}{\aleph} + \frac{\overline{pw}}{\rho\aleph}) + \frac{\partial}{\partial z}(\frac{\overline{pv}}{\rho} + \overline{vw^2}) - \frac{\aleph}{R_c}\overline{u^2w}] +$$
$$\overline{\nu\nabla^2\overline{vw} - 2\nu[(\frac{\partial v}{\partial n}\frac{\partial w}{\partial n}) + \aleph^2(\frac{\partial v}{\partial s}\frac{\partial w}{\partial s}) + (\frac{\partial v}{\partial z}\frac{\partial w}{\partial z}) + \frac{\aleph^2}{R_c}w\frac{\partial u}{\partial s} + \frac{\aleph^2}{R_c^2}vw]}$$

Equations (2.85), (2.86) and (2.87) may be added to form the equation for the kinetic energy of the turbulence

$$\begin{aligned}
\frac{D}{Dt}\frac{\overline{q^2}}{2} &= -[\aleph\overline{u^2}\frac{\partial U}{\partial s} + \overline{uv}\frac{\partial U}{\partial n} + \overline{uw}\frac{\partial U}{\partial z} + \\
&\quad \aleph\overline{uv}\frac{\partial V}{\partial s} + \overline{v^2}\frac{\partial V}{\partial n} + \overline{vw}\frac{\partial V}{\partial z} + \\
&\quad \aleph\overline{uw}\frac{\partial W}{\partial s} + \overline{vw}\frac{\partial W}{\partial n} + \overline{w^2}\frac{\partial W}{\partial z} - \frac{\aleph}{R_c}(\overline{uv}U - \overline{u^2}V)] \\
&\quad -[\aleph\frac{\partial}{\partial s}(\frac{\overline{pu}}{\rho} + \frac{\overline{uq^2}}{2}) + \aleph\frac{\partial}{\partial n}(\frac{\overline{pv}}{\rho\aleph} + \frac{\overline{vq^2}}{2\aleph}) + \frac{\partial}{\partial z}(\frac{\overline{pw}}{\rho} + \frac{\overline{wq^2}}{2})] + \\
&\quad \overline{\nu\nabla^2\frac{\overline{q^2}}{2} - \nu[(\frac{\partial u}{\partial n})^2 + \aleph^2(\frac{\partial u}{\partial s})^2 + (\frac{\partial u}{\partial z})^2 + (\frac{\partial v}{\partial n})^2 + \aleph^2(\frac{\partial v}{\partial s})^2 + (\frac{\partial v}{\partial z})^2 +} \\
&\quad \overline{(\frac{\partial w}{\partial n})^2 + \aleph^2(\frac{\partial w}{\partial s})^2 + (\frac{\partial w}{\partial z})^2 + \frac{\aleph^2}{R_c}(v\frac{\partial u}{\partial s} - u\frac{\partial v}{\partial s}) + \frac{\aleph^2}{R_c^2}(u^2 + v^2)]}
\end{aligned} \tag{2.91}$$

Chapter 3

HOMOGENEOUS CURVED SHEAR FLOW

3.1 An Introduction

Shear plays an important role in the initiation and maintenance of turbulence. As an idealization of a shear flow, von Karman (1937) introduced the concept of a "homogeneous shear flow", in which spatially homogeneous turbulence is uniformly sheared. The turbulent shear stress works against the mean distortion of the fluid to provide energy to the turbulence but the shear also has a role in determining the turbulence structure (see the numerical simulations of Rogallo, 1981). The homogeneous shear flow is suitable for scrutinizing the interaction of turbulence and shear in relative isolation from other features of turbulent flows such as intermittency, viscous wall layers and inhomogeneity.

In a curved shear flow the energy provided to the turbulence comes from the mean straining of the fluid as in rectilinear flow. The strain is a function of the curvature but unlike buoyancy, for example, the flow curvature does not provide energy to the turbulence directly but may alter the turbulence structure from what one would expect to evolve due to shear alone. Changing the turbulence structure affects the efficiency of the energy transfer from the mean flow to the turbulence.

As an extension of the study of homogeneous shear flow one might consider a flow with mean streamlines which are not parallel but which form concentric rings (see Figure 3.1). The shear could be uniform in the radial direction but the fluid would move along a curved path. In general it is not possible to have a homogeneous turbulence under these conditions because of the spatial variation of the curvature and strain. The concept of a homogeneous curved shear flow might, however, be a limiting case.

Consider a finite volume of space which is large in comparison with the scales of the turbulence but is located far enough from the center of curvature for the curvature to be nearly constant within the volume. Under these circumstances the turbulence in the volume, which is assumed to be initially homogeneous, might for some time remain independent of remote turbulent motions having different structure, due to the different local curvature.

To formally establish the homogeneous curved shear flow we reduce equations (2.81) to (2.84) for the fluctuating velocities for the case where the mean

velocity is of the form

$$U = U_c + An \tag{3.1}$$

$$V = 0 \tag{3.2}$$

$$W = 0 \tag{3.3}$$

(A is assumed constant) and non- dimensionalize these equations in the following way

$$\tau = tA \quad s^* = \frac{s}{l} \quad n^* = \frac{n}{l} \qquad z = \frac{z}{l}$$

$$u^* = \frac{u}{\mathcal{V}} \quad v^* = \frac{v}{\mathcal{V}} \quad w^* = \frac{w}{\mathcal{V}} \quad p^* = \frac{p}{\rho A l \mathcal{V}}$$

$$\Re = \frac{\mathcal{V}l}{\nu}$$

where l and $\mathcal{V}$ are length and velocity scales and ν is the kinematic viscosity of the fluid. In following we will take $\mathcal{V} = Al$. The result is

$$\begin{aligned}
\frac{D^*u^*}{D\tau} + (1 + \aleph^* S + \aleph^* h n^*)v^* &= -\aleph \frac{\partial p^*}{\partial s^*} + \frac{1}{\Re}(\nabla^2 u^* + 2\aleph^2 h \frac{\partial v^*}{\partial s^*} - \aleph h^2 u^*) \qquad (3.4)\\
&\quad -[\aleph \frac{\partial}{\partial s^*}(u^{*2} - \overline{u^{*2}}) + \aleph \frac{\partial}{\partial n^*}\frac{u^*v^* - \overline{u^*v^*}}{\aleph}\\
&\quad + \frac{\partial}{\partial z^*}(u^*w^* - \overline{u^*w^*}) + h(u^*v^* - \overline{u^*v^*})]\\
\frac{D^*v^*}{D\tau} - 2\aleph^*(S + hn^*)u^* &= -\frac{\partial p^*}{\partial n^*} + \frac{1}{\Re}(\nabla^2 v^* - 2\aleph^2 h \frac{\partial u^*}{\partial s^*} - \aleph h^2 v^*) \qquad (3.5)\\
&\quad -[\aleph \frac{\partial}{\partial s^*}(u^*v^* - \overline{u^*v^*}) + \aleph \frac{\partial}{\partial n^*}\frac{v^{*2} - \overline{v^{*2}}}{\aleph}\\
&\quad + \frac{\partial}{\partial z^*}(v^*w^* - \overline{v^*w^*}) + h(u^{*2} - \overline{u^{*2}})]\\
\frac{D^*w^*}{D\tau} &= -\frac{\partial p^*}{\partial z^*} + \frac{1}{\Re}\nabla^2 w^* \qquad (3.6)\\
&\quad -[\aleph \frac{\partial}{\partial s^*}(u^*w^* - \overline{u^*w^*}) + \aleph \frac{\partial}{\partial n^*}\frac{v^*w^* - \overline{v^*w^*}}{\aleph}\\
&\quad + \frac{\partial}{\partial z^*}(w^{*2} - \overline{w^{*2}})\\
\aleph \frac{\partial u^*}{\partial s^*} + \aleph \frac{\partial v^*}{\partial n}\frac{v^*}{\aleph} + \frac{\partial w^*}{\partial z^*} &= 0 \qquad (3.7)
\end{aligned}$$

where $\frac{D^*}{D\tau} = \frac{\partial}{\partial t^*} + \aleph^*(Sh^{-1} + (1 - S)n^*)\frac{\partial}{\partial s^*}, h = \frac{l}{R_c}, \aleph^* = (1 + hn^*)^{-1}$ and $S = \frac{U_c}{AR_c}$. The variable S will play an important role in the following discussion.

It represents a relative measure of the curvature effects with respect to the shear effects.

Expanding $\aleph$ in powers of n^* about the point $n^* = 0$, one gets

$$\aleph^* = 1 - hn^* + h^2 n^{*2} + ... \tag{3.8}$$

Substituting this expression into equations (3.4), (3.5), (3.6) and (3.7) and taking h small enough that terms of order h^2 may be neglected gives

$$\begin{aligned}
\frac{D^*u^*}{D\tau} + (1+S)v^* &\approx -\frac{\partial p^*}{\partial s^*} + \frac{1}{\Re}\nabla^2 u^* \qquad (3.9)\\
&\quad -[\frac{\partial}{\partial s^*}(u^{*2} - \overline{u^{*2}}) + \frac{\partial}{\partial n^*}(u^*v^* - \overline{u^*v^*}) + \frac{\partial}{\partial z^*}(u^*w^* - \overline{u^*w^*})\\
\frac{D^*v^*}{D\tau} - 2Sv^* &\approx -\frac{\partial p^*}{\partial n^*} + \frac{1}{\Re}\nabla^2 v^* \qquad (3.10)\\
&\quad -[\frac{\partial}{\partial s^*}(u^*v^* - \overline{u^*v^*}) + \frac{\partial}{\partial n^*}(v^{*2} - \overline{v^{*2}}) + \frac{\partial}{\partial z^*}(v^*w^* - \overline{v^*w^*})\\
\frac{D^*w^*}{D\tau} &\approx -\frac{\partial p^*}{\partial z^*} + \frac{1}{\Re}\nabla^2 w^* \qquad (3.11)\\
&\quad -[\frac{\partial}{\partial s^*}(u^*w^* - \overline{u^*w^*}) + \frac{\partial}{\partial n^*}(v^*w^* - \overline{v^*w^*}) + \frac{\partial}{\partial z^*}(w^{*2} - \overline{w^{*2}})\\
\frac{\partial u^*}{\partial s^*} + \frac{\partial v^*}{\partial n^*} + \frac{\partial w^*}{\partial z^*} &\approx 0 \qquad (3.12)
\end{aligned}$$

where $\frac{D^*}{D\tau} = \frac{\partial}{\partial \tau^*} + (Sh^{-1} + (1-S)n^*)\frac{\partial}{\partial s^*}$. In the following the asterisks will be omitted with the understanding that all variables are dimensionless.

3.2 Equations for the Reynolds Stresses

Equations for Reynolds stresses in a curved shear flow for the limiting case where $h^2 \to 0$ can be derived using equations (3.9) to (3.12) in a manner similar to the derivation of equations (2.85) to (2.90). If we further restrict the discussion to a homogeneous turbulence we can neglect spatial gradients of the statistics

to give

$$\frac{\partial}{\partial\tau}\frac{\overline{u^2}}{2} = -\overline{uv}(1+S) + p\overline{\frac{\partial u}{\partial s}} - \frac{1}{\Re}\overline{[(\frac{\partial u}{\partial n})^2 + (\frac{\partial u}{\partial s})^2 + (\frac{\partial u}{\partial z})^2)]} \tag{3.13}$$

$$\frac{\partial}{\partial\tau}\frac{\overline{v^2}}{2} = 2\overline{uv}S + p\overline{\frac{\partial v}{\partial n}} - \frac{1}{\Re}\overline{[(\frac{\partial v}{\partial s})^2 + (\frac{\partial v}{\partial n})^2 + (\frac{\partial v}{\partial z})^2]} \tag{3.14}$$

$$\frac{\partial}{\partial\tau}\frac{\overline{w^2}}{2} = p\overline{\frac{\partial w}{\partial z}} - \frac{1}{\Re}\overline{[(\frac{\partial w}{\partial s})^2 + (\frac{\partial w}{\partial n})^2 + (\frac{\partial w}{\partial z})^2]} \tag{3.15}$$

$$\frac{\partial}{\partial\tau}\overline{uv} = -\overline{v^2}(1+S) + 2\overline{u^2}S + \overline{p(\frac{\partial u}{\partial n} + \frac{\partial v}{\partial s})} \tag{3.16}$$

$$-2\frac{1}{\Re}\overline{[(\frac{\partial u}{\partial s}\frac{\partial v}{\partial s}) + (\frac{\partial u}{\partial n}\frac{\partial v}{\partial n}) + (\frac{\partial u}{\partial z}\frac{\partial v}{\partial z})]}$$

$$\frac{\partial}{\partial\tau}\frac{\overline{q^2}}{2} = -\overline{uv}(1-S) - \frac{1}{\Re}\overline{[(\frac{\partial u}{\partial s})^2 + (\frac{\partial u}{\partial n})^2 + (\frac{\partial u}{\partial z})^2 +} \tag{3.17}$$

$$\overline{(\frac{\partial v}{\partial s})^2 + (\frac{\partial v}{\partial n})^2 + (\frac{\partial v}{\partial z})^2 + (\frac{\partial w}{\partial s})^2 + (\frac{\partial w}{\partial n})^2 + (\frac{\partial w}{\partial z})^2]}$$

The shear correlations $\overline{uw}$ and $\overline{vw}$ have been omitted under the assumption that we consider only homogeneous turbulence having symmetry about the s-n planes.

The above analysis shows that the curvature appears explicitly in the equations for the streamwise and transverse components of kinetic energy and for the shear stress. Leaving aside, for a moment, the effects of curvature on the pressure strain covariance and dissipation rate the curvature appears to act as follows: when $S < 0, \overline{uv} > 0$ the growth rate of $\overline{v^2}$ is increased; when $\overline{v^2}$ increases, the growth rates of $\overline{uv}$ and $\overline{u^2}$ increase; conversely when $S > 0, \overline{uv} < 0$ the growth rate of $\overline{v^2}$ is decreased, which causes a decrease in the growth rates of $\overline{uv}$ and $\overline{u^2}$.

In contrast, in a straight shear flow ($S = 0$), direct energy production from the mean flow appears only in the equation for the streamwise component of the turbulence energy and shear stress (Champagne, Harris and Corrsin (1970)).

3.3 Linearized Dynamic Equations for the Velocity Spectra

The dynamic equations for the velocity spectra can be derived from equations for the two point velocity covariances by taking their Fourier transforms (Hinze, 1975). A simpler method which is mathematically equivalent will be used here. The fluctuating velocities in equations (3.9) to (3.12) are replaced by their Fourier series representation and equations for the Fourier coefficients are deduced (Townsend, 1976).

The resulting nonlinear equations for the Fourier coefficients of the fluctuating velocity have not been solved for any case although there have been several empirical and theoretical models of the nonlinear terms in isotropic turbulence (Hinze, 1975). In the following analysis only linear terms will be retained. Champagne, Harris and Corrsin (1970) have suggested that this approximation may be inconsistent, because the pressure fluctuations which are of the order of $\mathcal{V}^2$ are retained. Nevertheless, linear analyses have been performed for uniformly sheared homogeneous straight shear flows by Pearson (1959), Deissler (1961,1975) and Townsend (1976). The results of Deissler (1975) show good agreement between the predicted development of one- and two-point velocity covariances and the observations of Champagne, Harris and Corrsin (1970). The most serious error of the linear approximation is, presumably, the neglect of the direct transfer of energy between various wavelengths of the turbulence.

Excluding the nonlinear terms from equations (3.9) to (3.11) one gets

$$\frac{Du}{D\tau} = -v(1+S) - \frac{\partial p}{\partial s} + \frac{1}{\Re}\nabla^2 u \tag{3.18}$$

$$\frac{Dv}{D\tau} = 2Su - \frac{\partial p}{\partial n} + \frac{1}{\Re}\nabla^2 v \tag{3.19}$$

$$\frac{Dw}{D\tau} = -\frac{\partial p}{\partial z} + \frac{1}{\Re}\nabla^2 w \tag{3.20}$$

$$0 = \frac{\partial u}{\partial s} + \frac{\partial v}{\partial n} + \frac{\partial w}{\partial z} \tag{3.21}$$

where $\frac{D}{D\tau} = \frac{\partial}{\partial \tau} + (Sh^{-1} + (1-S)n)\frac{\partial}{\partial s}$. These equations also appear in linear stability theory of circular Couette flow (for example see Chandrasekhar, 1961).

It is useful in the following to construct an equation for the pressure fluctuation by differentiating equation (3.18) by s, differentiating equation (3.19) by n, differentiating equation (3.20) by z and adding these four equations to get

$$\nabla^2 p = 2(\frac{\partial v}{\partial s} - S\frac{\partial u}{\partial n}) \tag{3.22}$$

Equations (3.18), (3.19), (3.20) and (3.22) form a set of equations for studying small fluctuations of velocity and pressure, however, they still contain a variable coefficient in the convection term. Townsend (1976) has shown that this problem may be treated by transforming to mean material coodinates. The equations for the mean particle trajectories are

$$\frac{\partial s}{\partial \tau} = (Sh^{-1} + (1-S)n) \tag{3.23}$$

$$\frac{\partial n}{\partial \tau} = 0 \tag{3.24}$$

$$\frac{\partial z}{\partial \tau} = 0 \tag{3.25}$$

Intergrating equations (3.23) to (3.25) gives

$$s = s_o + (Sh^{-1} + (1-S)n_o)\tau \tag{3.26}$$

$$n = n_o \tag{3.27}$$

$$z = z_o \tag{3.28}$$

where x_o, s_o and z_o are the material coordinates in the reference configuration at $\tau = 0$. The motion of these material lines is illustrated in Figure 3.2. Transforming equations (3.18) to (3.20) and (3.22) to mean material coordinates gives

$$\frac{\partial u}{\partial \tau} + (1+S)v = -\frac{\partial p}{\partial s_o} + \frac{1}{\Re}\nabla_o^2 u \tag{3.29}$$

$$\frac{\partial v}{\partial \tau} - 2Su = -\frac{\partial p}{\partial n_o} - (1-S)t\frac{\partial p}{\partial s_o} + \frac{1}{\Re}\nabla_o^2 v \tag{3.30}$$

$$\frac{\partial w}{\partial \tau} = -\frac{\partial p}{\partial z_o} + \frac{1}{\Re}\nabla_o^2 \tag{3.31}$$

$$-\nabla_o^2 p = 2(\frac{\partial v}{\partial s_o} - S(\frac{\partial u}{\partial n_o} - (1-S)\tau\frac{\partial u}{\partial s_o})) \tag{3.32}$$

where $\nabla_o^2 = (\frac{\partial^2}{\partial s_o^2} + \frac{\partial^2}{\partial n_o^2} + \frac{\partial^2}{\partial z_o^2} + (1-S)^2\tau^2\frac{\partial^2}{\partial s_o^2} - 2(1-S)\tau\frac{\partial^2}{\partial n_o \partial s_o})$. A solution of these equations is the following

$$u(\mathbf{z_o}, \tau) = \hat{u}(\mathbf{k_o}, \tau)\exp\iota(\alpha_o s_o + \beta_o n_o + \gamma_o z_o) \tag{3.33}$$

$$v(\mathbf{z_o}, \tau) = \hat{v}(\mathbf{k_o}, \tau)\exp\iota(\alpha_o s_o + \beta_o n_o + \gamma_o z_o) \tag{3.34}$$

$$w(\mathbf{z_o}, \tau) = \hat{w}(\mathbf{k_o}, \tau)\exp\iota(\alpha_o s_o + \beta_o n_o + \gamma_o z_o) \tag{3.35}$$

$$p(\mathbf{z_o}, \tau) = \hat{p}(\mathbf{k_o}, \tau)\exp\iota(\alpha_o s_o + \beta_o n_o + \gamma_o z_o) \tag{3.36}$$

where α_o, β_o and γ_o represent the wavenumbers of the fluctuations in the reference configuration at time τ =0 and $\iota = \sqrt{-1}$. Substitution of equations (3.33) to (3.36) into equations (3.29) to (3.32) gives

$$\frac{\partial \hat{u}}{\partial \tau} + (1+S)\hat{v} = -\iota\alpha\hat{p} + \frac{k^2}{\Re}\hat{u} \tag{3.37}$$

$$\frac{\partial \hat{v}}{\partial \tau} - 2S\hat{u} = -\iota\beta\hat{p} + \frac{k^2}{\Re}\hat{v} \tag{3.38}$$

$$\frac{\partial \hat{w}}{\partial \tau} = -\iota\gamma\hat{p} + \frac{k^2}{\Re}\hat{w} \tag{3.39}$$

$$\hat{p} = \frac{2\iota}{k^2}(\alpha\hat{v} - S\beta\hat{u}) \tag{3.40}$$

where

$$\alpha = \alpha_o \tag{3.41}$$

$$\beta = \beta_o - \alpha_o(1-S)\tau \tag{3.42}$$

$$\gamma = \gamma_o \tag{3.43}$$

$$k^2 = \alpha_o^2 + \beta_o^2 + \gamma_o^2 + \alpha_o^2(1-S)^2\tau^2 - 2\alpha_o\beta_o(1-S)\tau \tag{3.44}$$

Eliminating the pressure spectrum from equations (3.37) to (3.39) using equation (3.40) gives

$$\frac{\partial \hat{u}}{\partial \tau} + (1 + S - 2\frac{\alpha^2}{k^2})\hat{v} + 2S\frac{\alpha\beta}{k^2}\hat{u} - \frac{k^2}{\Re}\hat{u} = 0 \tag{3.45}$$

$$\frac{\partial \hat{v}}{\partial \tau} - 2S(1 - \frac{\beta^2}{k^2})\hat{u} - 2\frac{\alpha\beta}{k^2}\hat{v} - \frac{k^2}{\Re}\hat{v} = 0 \tag{3.46}$$

$$\frac{\partial \hat{w}}{\partial \tau} - 2\frac{\alpha\gamma}{k^2}\hat{v} + 2S\frac{\gamma\beta}{k^2}\hat{u} - \frac{k^2}{\Re}\hat{w} = 0 \tag{3.47}$$

A general solution to equations (3.45) to (3.47) for all values of S has not yet been found. There are, however, two values of S for which closed form solutions are known, $S = 0$ and 1. First, in the case of plane shear flow, where $S = 0$, equations (3.45) to (3.47) reduce with the neglect of the viscous terms to

$$\frac{\partial \hat{u}}{\partial \tau} + (1 - 2\frac{\alpha^2}{k^2})\hat{v} = 0 \tag{3.48}$$

$$\frac{\partial \hat{v}}{\partial \tau} - 2\frac{\alpha\beta}{k^2}\hat{v} = 0 \tag{3.49}$$

$$\frac{\partial \hat{w}}{\partial \tau} - 2\frac{\alpha\gamma}{k^2}\hat{v} = 0 \tag{3.50}$$

These are the equations for the "Rapid Distortion" of turbulence in a straight parallel shear flow which have been solved by Townsend (1976). The solutions

to equations (3.48) to (3.50) are

$$\hat{u} = \hat{u}_o + \frac{\beta_o^{\clubsuit 2}}{k^{\clubsuit 2}}(1-\beta_o^{\clubsuit}\beta^{\clubsuit}))\hat{v}_o - \frac{k_o^{\clubsuit 2}\gamma_o^{\clubsuit 2}}{\alpha_o^{\clubsuit}} \arctan \frac{\alpha_o^{\clubsuit}\tau}{1+\beta_o^{\clubsuit}\beta^{\clubsuit}}\hat{v}_o \quad (3.51)$$

$$\hat{v} = \frac{k_o^{\clubsuit 2}}{k^{\clubsuit 2}}\hat{v}_o \quad (3.52)$$

$$\hat{w} = \hat{w}_o + \gamma_o^{\clubsuit} k_o^{\clubsuit 2} \arctan \frac{\alpha_o^{\clubsuit}\tau}{1+\beta_o^{\clubsuit}\beta^{\clubsuit}}\hat{v}_o + \frac{\alpha_o^{\clubsuit}\gamma_o^{\clubsuit}}{k^{\clubsuit 2}}(1-\beta_o^{\clubsuit}\beta^{\clubsuit})\hat{v}_o \quad (3.53)$$

where the supercript $\clubsuit$ indicates that the variable has been normalized by $(\alpha_o^2+\gamma_o^2)^{\frac{1}{2}}$.

For the second case, $S = 1$, equations (3.45) to (3.47) neglecting viscous effects, become

$$\frac{\partial \hat{u}}{\partial \tau} + 2(1-\frac{\alpha^2}{k^2})\hat{v} + 2\frac{\alpha\beta}{k^2} = 0 \quad (3.54)$$

$$\frac{\partial \hat{v}}{\partial \tau} - 2(1-\frac{\beta^2}{k^2})\hat{u} - 2\frac{\alpha\beta}{k^2}\hat{v} = 0 \quad (3.55)$$

$$\frac{\partial \hat{w}}{\partial \tau} + 2\frac{\gamma\beta}{k^2}\hat{u} - 2\frac{\alpha\gamma}{k^2}\hat{v} = 0 \quad (3.56)$$

where $\alpha = \alpha_o$, $\beta = \beta_o$ and $\gamma = \gamma_o$. Equations (3.54) to (3.56) may be integrated to give

$$\hat{u} = \hat{u}_o(\cos 2\omega\tau - \frac{\alpha\beta}{k^2\omega}\sin 2\omega\tau) - \hat{v}_o\frac{k^2-\alpha^2}{k^2\omega}\sin 2\omega\tau \quad (3.57)$$

$$\hat{v} = \hat{u}_o\frac{k^2-\beta^2}{k^2\omega}\sin 2\omega\tau + \hat{v}_o(\cos 2\omega\tau + \frac{\alpha\beta}{k^2\omega}\sin 2\omega\tau) \quad (3.58)$$

$$\hat{w} = \hat{u}_o\frac{\gamma}{k^2\omega}(-\alpha\cos 2\omega\tau - \beta\sin 2\omega\tau) + \hat{v}_o\frac{\gamma}{k^2\omega}(-\beta\cos 2\omega\tau \quad (3.59)$$

$$+\alpha\sin 2\omega\tau)$$

where $\omega = \sqrt{2-\frac{\gamma^2}{k^2}}$. These solutions suggest a harmonic modulation of the turbulence.

The solutions of equations (3.45) to (3.47), if found, may be used to form the spectra of the velocity covariance, or with use of equation (3.40) the spectra

of the pressure-velocity and pressure- strain rate covariances. Alternatively, equations for the spectra may be formed from equations (3.45) to (3.47) directly. To apply either of these methods the initial values of the spectra must be known.

3.4 The Relevance of Uniformly Sheared, Nearly Homogeneous Turbulence

3.4.1 General Discussion

Homogeneous turbulence is difficult to generate and maintain experimentally. Laboratory approximations to homogeneous flow are generally stationary in the laboratory frame but are inhomogeneous in the streamwise direction. A laboratory flow of this type studied in the convected frame may have some similarities to a homogeneous flow provided that the streamwise inhomogeneity is small (Corrsin, 1963). Examples include grid generated turbulence as an approximation to isotropic turbulence (Comte-Bellot and Corrsin, 1971) and the uniformly sheared turbulence (Champagne, Harris and Corrsin , 1970) as an approximation to homogeneous shear flow.

As an approximation to the present problem of homogeneous curved shear flow we will extend the study of the uniformly sheared turbulence.

3.4.2 The Mean Flow

Equations (2.77) to (2.80) for the components of mean velocity may be reduced under the assumptions that the flow is stationary in the laboratory frame and symmetric about s,n planes and V=0. The result is

$$\aleph\frac{\partial}{\partial s}(U^2+\frac{P}{\rho}+\overline{u^2}) = +\aleph\frac{\partial}{\partial n}\frac{\overline{uv}}{\aleph}+\frac{\aleph\overline{uv}}{R_c} \qquad (3.60)$$
$$+\nu(\nabla^2 U-\frac{\aleph^2}{R_c^2}U)$$

$$\frac{\partial}{\partial n}\frac{P}{\rho}-\aleph\frac{U^2}{R_c} = -(\aleph\frac{\partial\overline{uv}}{\partial s}+\aleph\frac{\partial}{\partial n}\frac{\overline{v^2}}{\aleph}-\frac{\aleph\overline{u^2}}{R_c}) \qquad (3.61)$$
$$-2\nu\frac{\aleph^2}{R_c}\frac{\partial U}{\partial s}$$

$$0 = \frac{\partial U}{\partial s} \qquad (3.62)$$

It would appear from equation (3.62) that if V=W=0 then U cannot be a function of s, in which case equation (3.60) suggests that as the turbulence grows the pressure must decrease to conserve mechanical energy. Another possibility suggested by Hinze (1975) is that the pressure is independent of s and the growth of turbulence kinetic energy is balanced by a streamwise decrease in the mean kinetic energy. Any combination of these two mechanisms is also possible but if the growth of the kinetic energy of the turbulence is small then any decline in pressure or change in U may be neglected.

Equation (3.61) shows that there must be a transverse gradient of mean pressure to turn the flow, a feature of curved flows only.

The uniformly sheared flow, for which $U = U_c + An$, is compatible with equations (3.60) to (3.62).

3.4.3 The Reynolds Stresses

In this section it will be assumed that, in addition to stationaity and spanwise symmetry of the statistics, the mean velocity is of the form $(U, V, W) = (U_c + An, 0, 0)$, such that the only component of the shear is $\frac{\partial U}{\partial n} = A$. Under these conditions, equations (2.85) to (2.91) reduce to

$$
\begin{aligned}
(U_c + An)\frac{\partial}{\partial s}\frac{\overline{u^2}}{2} &= -[\overline{uv}A + \frac{\aleph}{R_c}\overline{uv}(U_c + An)] + \\
&\quad \aleph\overline{\frac{p}{\rho}\frac{\partial u}{\partial s}} - [\aleph\frac{\partial}{\partial s}(\frac{\overline{pu}}{\rho} + \frac{\overline{u^3}}{2}) + \aleph\frac{\partial}{\partial n}\frac{\overline{u^2v}}{2\aleph} + \frac{\aleph}{R_c}\overline{u^2v}] + \\
&\quad \nu\nabla^2\frac{\overline{u^2}}{2} - \nu\overline{[(\frac{\partial u}{\partial n})^2 + \aleph^2(\frac{\partial u}{\partial s})^2 + (\frac{\partial u}{\partial z})^2 - 2\frac{\aleph^2}{R_c}u\frac{\partial v}{\partial s} - \frac{\aleph^2}{R_c^2}u^2]}
\end{aligned} \tag{3.63}
$$

$$
\begin{aligned}
(U_c + An)\frac{\partial}{\partial s}\frac{\overline{v^2}}{2} &= -2\frac{\aleph}{R_c}\overline{uv}(U_c + An)] + \\
&\quad \aleph\overline{\frac{p}{\rho}\frac{\partial}{\partial n}\frac{v}{\aleph}} - [\aleph\frac{\partial}{\partial s}\frac{\overline{uv^2}}{2} + \aleph\frac{\partial}{\partial n}(\frac{\overline{pv}}{\rho\aleph} + \frac{\overline{v^3}}{2\aleph}) + \frac{\aleph}{R_c}\overline{u^2v}] + \\
&\quad \nu\nabla^2\frac{\overline{v^2}}{2} - \nu\overline{[(\frac{\partial v}{\partial n})^2 + \aleph^2(\frac{\partial v}{\partial s})^2 + (\frac{\partial v}{\partial z})^2 + 2\frac{\aleph^2}{R_c}v\frac{\partial u}{\partial s} + \frac{\aleph^2}{R_c^2}v^2]}
\end{aligned} \tag{3.64}
$$

$$
\begin{aligned}
(U_c + An)\frac{\partial}{\partial s}\frac{\overline{w^2}}{2} &= +\aleph\overline{\frac{p}{\rho}\frac{\partial w}{\partial z}} - [\aleph\frac{\partial}{\partial s}\frac{\overline{uw^2}}{2} + \aleph\frac{\partial}{\partial n}\frac{\overline{vw^2}}{2\aleph} +] + \\
&\quad \nu\nabla^2\frac{\overline{w^2}}{2} - \nu\overline{[(\frac{\partial w}{\partial n})^2 + \aleph^2(\frac{\partial w}{\partial s})^2 + (\frac{\partial w}{\partial z})^2]}
\end{aligned}
$$

$$
\begin{aligned}
(U_c + An)\frac{\partial}{\partial s}\overline{uv} &= -[\overline{v^2}A - \frac{\aleph}{R_c}((U_c + An)(2\overline{u^2} - \overline{v^2})] + \\
&\quad \aleph\overline{\frac{p}{\rho}(\frac{\partial v}{\partial s} + \aleph\frac{\partial}{\partial n}\frac{u}{\aleph})} - [\aleph\frac{\partial}{\partial s}(\frac{\overline{pv}}{\rho} + \overline{u^2v}) + \aleph\frac{\partial}{\partial n}(\frac{\overline{pu}}{\rho\aleph} + \frac{\overline{uv^2}}{\aleph}) + \frac{\aleph}{R_c}(\overline{uv^2} - \overline{u^3})] + \\
&\quad \nu\nabla^2\overline{uv} - 2\nu\overline{[(\frac{\partial u}{\partial n}\frac{\partial v}{\partial n}) + \aleph^2(\frac{\partial u}{\partial s}\frac{\partial v}{\partial s}) + (\frac{\partial u}{\partial z}\frac{\partial v}{\partial z}) + 2\frac{\aleph^2}{R_c}(u\frac{\partial u}{\partial s} - v\frac{\partial v}{\partial s}) + 2\frac{\aleph^2}{R_c^2}uv]}
\end{aligned} \tag{3.65}
$$

$$
\begin{aligned}
(U_c + An)\frac{\partial}{\partial s}\frac{\overline{q^2}}{2} &= -\overline{uv}A - \frac{\aleph}{R_c}\overline{uv}(U_c + An) - [\aleph\frac{\partial}{\partial s}(\frac{\overline{pu}}{\rho} + \frac{\overline{uq^2}}{2}) + \aleph\frac{\partial}{\partial n}(\frac{\overline{pv}}{\rho\aleph} + \frac{\overline{vq^2}}{2\aleph})] + \\
&\quad \nu\nabla^2\frac{\overline{q^2}}{2} - \nu\overline{[(\frac{\partial u}{\partial n})^2 + \aleph^2(\frac{\partial u}{\partial s})^2 + (\frac{\partial u}{\partial z})^2 + (\frac{\partial v}{\partial n})^2 + \aleph^2(\frac{\partial v}{\partial s})^2 + (\frac{\partial v}{\partial z})^2 + \\
&\quad (\frac{\partial w}{\partial n})^2 + \aleph^2(\frac{\partial w}{\partial s})^2 + (\frac{\partial w}{\partial z})^2 + \frac{\aleph^2}{R_c}(v\frac{\partial u}{\partial s} - u\frac{\partial v}{\partial s}) + \frac{\aleph^2}{R_c^2}(u^2 + v^2)]}
\end{aligned} \tag{3.66}
$$

It is easy to see that equations (3.63) to (3.66) for the Reynolds stresses

and the kinetic energy of turbulence are incompatible with exact transverse homogeneity because n would still appear explicitly in both the convection and curvature terms. The equations have a solution only if the turbulence is streamwise homogeneous and the curvature effects negligible but this would require that the production and dissipation of the turbulence exactly balance, a singular condition which is not generally valid, and that the flow be straight. A similar problem has been pointed out by Champagne, Harris and Corrsin (1970) for the straight uniformly sheared flow (for which $S = 0$). They concluded that if the flow is inhomogeneous in the streamwise direction then it must be transversely inhomogeneous also. It is therefore only in a limited way that the uniformly sheared laboratory flow may be considered relevant to the problem of homogeneous curved shear flow. The shear must be weak, the streamwise and transverse inhomogeneities and curvature effects small.

Chapter 4

EXPERIMENTAL APPARATUS AND INSTRUMENTATION

4.1 The Existing Facility

The existing wind tunnel at the University of Ottawa is illustrated in Figure 4.1. It is described in detail by Karnik (1983). The tunnel has a shear generator comprising 12 separate parallel channels, each 25.4 mm high, and a flow separator which tends to make the larger scales of the flow uniform on the transverse plane. The shear generator has been adjusted to produce a nearly linear shear, for which $k_s = \frac{A}{U_c} \approx 6.2m^{-1}$ for centerline speeds ranging from 5 to 15 m/s (Karnik and Tavoularis, 1987). The shear generator can be inverted to generate a shear of the opposite sign but nearly equal magnitude.

After leaving the flow separator, the flow passes through a straight rectangular section that is 305 mm high, 457 mm wide and 1372 mm long, near the exit of which the turbulent stresses become nearly uniform in the transverse plane and grow exponentially in the streamwise direction (Tavoularis and Karnik, 1988). The flow then passes to another straight section, 1828 mm long, initially of the same cross section but with side walls which diverge slightly to accomodate boundary layer growth.

The first of these straight sections allows grids of parallel rods and woven screens to be inserted normal to the flow. These uniform obstructions reduce the rate of shear and preserve the linearity of the mean velocity (Karnik, 1987).

4.2 Design of the Curved Wind Tunnel Sections

The objective of the curved section design was to introduce two distinct degrees of curvature. A "mild" curvature which would, presumably, introduce a small perturbation to the straight shear flow structure and a "strong" curvature which would create more pronounced effects.

Boundary layers are considered to have mild curvature when $\delta/R_c \leq .01$ (Bradshaw, 1973) where δ is a thickness defined such that $U \leq .99U_\infty$. For the present study of a homogeneous shear flow there is no counterpart to the boundary layer thickness. As mentioned earlier, however, a representative measure of curvature is the parameter $S = \frac{U_c}{AR_c}$. This would, generally, vary across

a boundary layer. As typical cases with mild curvature one may consider the convex boundary layer studied by Hoffman, Muck and Bradshaw (1985); where $\frac{\delta}{R_c} \approx .01$ which had $S = -.08$ at $\frac{y}{\delta} = .5$ and the convex boundary layer studied by Muck, Hoffman and Bradshaw (1985); $\frac{\delta}{R_c} \approx .01$ which at $\frac{y}{\delta} = .5$ had $S = .02$.

In the present experiments the maximum shear generated by the existing facility is restricted to $k_s \leq 6.2$ m. As mild curvature for this flow, a centerline radius of 5 m was chosen, giving a minimum value of $S = \pm.03$.

Smaller values of k_s and, hence, S are possible by placing obstructions in the flow (Karnik and Tavoularis, 1987). Nevertheless, because it is uncertain whether all features of the flow depend solely on S, it was decided another curved section with a smaller radius of curvature should be built.

For the strong curvature case, a tunnel section with a 2 m centerline radius was constructed, giving a minimum value of $S = \pm.08$. Higher values of S can be obtained by decreasing k_s using flow obstructions. With this design, it is possible to perform experiments in the two tunnels with overlapping ranges of S.

The length of the curved sections was chosen with the hope that it would allow full development of the turbulence should such a condition exist. In the unobstructed straight shear flow where $k_s = 6.2m^{-1}$, the turbulence becomes self preserving within 2 m of the flow separator. By analogy, the length of the curved sections was chosen to be 2 m.

The height, H, and width of the curved sections were made 75 mm and 50 mm smaller than the height and width of the existing straight windtunnel so

that the boundary layers would be bled at the entrance of the curved sections. The curved sections are shown in Figure 4.2.

Each curved section was placed 4 m downstream of the flow generator with its centerline tangent (see Figure 4.3) at the entrance to the centerline of the straight section. The tangency of the tunnel was roughly evaluated by measuring the height of the end of the curved section above the horizontal plane of the straight tunnel and comparing this to a calculation based on the ideal circular geometry. However, due to imperfections in construction and warpage and sagging of the tunnel the alignment could not be more precise than $\approx 5°$. To evaluate the sensitivity of the flow to this alignment the altitude of the curved tunnel was adjusted by $\pm$2cm while measuring the turbulent shear stress and checking for flow seperation at the entrance of the curved tunnel. The flow appeared to be insensitive within the accuracy of the alignment proceedure.

Measuring probes were inserted in the curved section from the top through a full-width spanwise slot 10 mm wide (see Figure 4.4). The probes were mounted on a slide (Unislide, model A2000) which allows continuous motion in the n and z directions with a resolution of .01 mm. This slide is mounted on another slide (Unislide, model A4000) which allows continuous motion in the z direction. For streamwise traverse, the top of the curved section was made of 10 removable curved plates, each 197 mm wide. To change the streamwise position of the probe, one of these plates was removed and replaced by the probe traversing system. This limited measurements to 10 streamwise locations.

To locate the tip of the probe in the s, n plane, the two side walls of the

tunnel were engraved with a polar coordinate system. The probe tip was aligned using the corresponding lines on the two tunnel walls.

4.3 Instrumentation and Accuracies

4.3.1 The Hot Wire Anemometer

All present experiments were conducted in air flows for which the hot wire anemometer is known to be a suitable velocity transducer with a fast time response (up to 100 KHz) and a good spatial resolution (as small as 1 mm in length).

All measurements in the present study were performed with a custom-made cross wire array (TSI model 124SBJTI5). The sensing elements were made of tungsten and had a diameter of 5 μm and a length of 1.2 mm. They were separated by .5 mm and had a nominal inclination of 45° with respect to the axis of the probe body . The wires were powered by constant temperature bridges (TSI model 1050A with a TSI 1051 2-D monitor and power supply).

The output from the constant temperature bridge is related to the voltage across the wire by the relation

$$\tilde{E} = \tilde{i}(R_w + R_p + R_c) \tag{4.1}$$

where $\tilde{i}$ is the current in the wire, R_w is the wire resistance, R_p is the resistance of the prongs and lead wires in the probe body and R_c is the resistance of the coaxial cables connecting the hot wire probe to the constant temperature

bridges. Typically R_p = .95Ω, R_c = .3Ω, and R_w = 6Ω at 20°. The wires were operated such that R_w was 1.5 times its resistance at 20°C.

The bridge voltage, E, across a hot wire in a laminar stream with velocity, U, normal to the wire axis can be represented by the modified King's Law (Tavoularis, 1986)

$$E^2 = A + BU^n \tag{4.2}$$

where A, B and n are constants to be adjusted by least squares fitting to the calibration data. Hot wires in turbulent flows, as in the case of an X array, are generally sensitive to cooling by all three components of velocity (see Figure 4.5). The equation (4.2) should be replaced by the expressions

$$\tilde{E}_1^2 = A_1 + B_1 \tilde{U}_{eff1}^{n_1} \tag{4.3}$$

$$\tilde{E}_2^2 = A_2 + B_2 \tilde{U}_{eff2}^{n_2} \tag{4.4}$$

where the effective cooling velocity, $\tilde{U}_{eff}$, is by definiton, the hypothetical flow velocity normal to the wire that would produce the same cooling as the actual flow velocity. Assuming that the velocity component normal to the wire provides all of the cooling, one can derive an expression for the effective cooling velocity as (Perry,1982,p. 112)

$$\tilde{U}_{eff1} = \sqrt{(\tilde{U}\sin\theta_1 - \tilde{V}\cos\theta_1)^2 + \tilde{W}^2} \tag{4.5}$$

$$\tilde{U}_{eff2} = \sqrt{(\tilde{U}\sin\theta_2 + \tilde{V}\cos\theta_2)^2 + \tilde{W}^2} \tag{4.6}$$

when the wires lie in the s,n plane and θ_1 and θ_2 are the angles between the respective wires and the s axis. A similar expression exists when the wires are in the s,z plane.

Even though θ_1 and θ_2 are nominally 45° for X-wire probes, their precise values may vary slightly and, for this reason, they were evaluated empirically. The probe was suspended from a swivelling mechanism so that it could be positioned at any desired angle with respect to the axis of a calibration jet (Karnik, 1988). First, the wires were calibrated in the jet stream with the axis of the probe body vertical. In this case the effective cooling velocities (neglecting tangential cooling) would be

$$U_{eff1} = U_j \sin\theta_1 \tag{4.7}$$

$$U_{eff2} = U_j \sin\theta_2 \tag{4.8}$$

where U_j is the velocity of the jet stream. Because θ_1 and θ_2 are not known *apriori* the bridge voltage was calibrated directly with U_j as

$$E_1^2 = A_1 + (B_1 \sin^{n_1}\theta_1) U_j^{n_1} \tag{4.9}$$

$$E_2^2 = A_2 + B_2 \sin^{n_2}\theta_2) U_j^{n_2} \tag{4.10}$$

so that rather than having B_1, for example, from the calibration we get $B_1 \sin^{n_1}\theta_1$. The wires were then pitched with respect to the vertical by the angle ψ (see Figure 4.6). The effective cooling velocity in this situation would be

$$U_{eff1} = U_j \sin(\theta_1 + \psi) \tag{4.11}$$

$$U_{eff2} = U_j \sin(\theta_2 - \psi) \tag{4.12}$$

which would give the bridge voltages

$$E_1^2 = A_1 + (B_1 \sin^{n_1}\theta_1)(\frac{\sin(\theta_1+\psi)}{\sin\theta_1})^{n_1} U_j^{n_1} \tag{4.13}$$

$$E_2^2 = A_2 + (B_2 \sin^{n_2}\theta_2)(\frac{\sin(\theta_2-\psi)}{\sin\theta_2})^{n_2} U_j^{n_2} \tag{4.14}$$

which allows θ_1 and θ_2 to be calculated for each value fo ψ by rearranging equation (4.13) and (4.14) to the form

$$\theta_1 = \arctan \frac{\sin \psi}{F_1 - \cos \psi} \tag{4.15}$$

$$\theta_2 = \arctan \frac{-\sin \psi}{F_2 - \cos \psi} \tag{4.16}$$

where

$$F_1 = \left(\frac{E_1^2 - A_1}{B_1 \sin^{n_1} \theta_1 U_j^{n_1}}\right)^{\frac{1}{n_1}} \tag{4.17}$$

$$F_2 = \left(\frac{E_2^2 - A_2}{B_2 \sin^{n_2} \theta_2 U_j^{n_2}}\right)^{\frac{1}{n_2}} \tag{4.18}$$

For a range of ψ values ($\pm 14°$) the bridge voltage and U_j (F_1 and F_2 are plotted versus ψ in Figure 4.7) were recorded and values of θ_1 and θ_2 calculated using equations (4.15) and (4.16). Average values of θ_1 and θ_2 are 46.2° and 44.4° respectively.

To test the cooling effect of the component of velocity normal to the plane of the wires the probe was rotated about its axis so that the wires would be normal to the plane of motion of the probe support. The wires were then pitched by the angle ϕ. see Figure 4.6. For this case the effective cooling velocity is given by

$$U_{eff1} = U_j \sqrt{\sin^2 \theta_1 + \sin^2 \phi} \tag{4.19}$$

$$U_{eff2} = U_j \sqrt{\sin^2 \theta_2 + \sin^2 \phi} \tag{4.20}$$

For a range of ϕ ($\pm 20°$) the bridge voltage and U_j were recorded and the effective cooling velocity calculated. The ratio $\frac{U_{eff}}{U_j}$, plotted in Figure 4.8 versus ϕ appears insensitive to ϕ for $\phi < \pm 10°$ and hence the contribution to the cooling from the component of the velocity out of the plane of the wires is negligible.

For the present data the contribution of the component of velocity normal to the plane of the wires to the cooling was neglected, and θ_1 and θ_2 were taken equal to 45° so that the U and V components of the velocity could be calculated from equations (4.5) and (4.6) as

$$\tilde{U} = \frac{1}{2}(U_{eff1} + U_{eff2}) \tag{4.21}$$

$$\tilde{V} = \frac{1}{2}(U_{eff1} - U_{eff2}) \tag{4.22}$$

when the wires are in the s, n plane. Similar expressions can be formed for when the wires are in the s,z plane.

Typically, the hot wires were calibrated in the windtunnel, with all flow obstructions removed to provide a low turbulence airstream ($\frac{u'}{U} \approx .005$). To simplify the calibration proceedure the pressure drop in the contraction of the windtunnel was calibrated against a pitot tube placed in the windtunnel at the position where the hot wires were to be calibrated. The hot wires were then calibrated against the pressure drop in the windtunnel contraction. A typical calibration curve between the bridge voltage, E, and the windtunnel velocity, U, is shown in Figure 4.9.

4.3.2 Signal Proccessing

The hot wire anemometer generates a random electrical signal with a broad frequency bandwidth and a relatively wide range of average and r.m.s. values. To condition the analog signals for digitization, the electronic circuit shown in Figure 4.10 was used. It offsets the input signal by a DC voltage between +6 volts and -6 V, it amplifies it by a gain of .5, 1., 2., 5., 10., 20. or 50. , and low

pass filters the amplified signal with cut-off frequencies selectable from 1, 3, or 10 KHz.

All signals were digitized by a Data Translation DT 2828 board mounted in a System 1800 (IBM AT compatible) micro computer with a 1 Mb random access memory (RAM), 20 Mb hard disk drive and a 11 MHz clock. The digitized samples were transferred to the hard disk drive periodically to make further RAM available for storage, thus allowing real time operation. The hard disk data files were transferred for long term storage to 60 mega byte magnetic cassette tapes using an Everex tape drive.

The DT 2828 is a 12-bit analog to digital converter (ADC) with a ± 10 V range giving a nominal resolution of 5 mV. It can sample 4 signals simultaneously and digitize them consecutively. Sampling frequencies range from .5 KHz to 40 KHz in the continuous operation for one channel. For more channels the sampling rates are reduced in proportion. Higher sampling rates, up to 100 KHz for 1 channel, preclude continuous operation and an entire record must be stored in RAM which limits the total sample size to 64 Kb.

4.3.3 Resolution

Spatial

Air turbulence contains structures which have a wide range of length scales and it is necessary to choose a probe of the appropriate size or apply corrections to the measurements. The order of magnitude of the structures in the present

flow can be estimated from previous studies in uniformly sheared turbulence (Tavoularis and Karnik, 1989) and some preliminary measurements performed in the present flow.

Structures of the order of the Kolmolgorov scale are generally considered to be the smallest which are relevant to the study of turbulence (Corrsin, 1963). The Kolmolgorov scale for the present flow is estimated to be

$$\eta_K = (\frac{\nu^3}{\epsilon})^{\frac{1}{4}} \approx .3mm \tag{4.23}$$

Another scale, associated with the dissipation of the kinetic energy of turbulence and important to the calculation of the statistics of the velocity derivatives, is the Taylor microscale (Tavoularis, 1986), which has a typical value of

$$\lambda = (\frac{\overline{(\frac{\partial u}{\partial \tau})^2}}{\overline{u^2}})^{\frac{1}{2}} \approx 5mm \tag{4.24}$$

The integral scale, generally associated with the energetic structures of the flow (Tavoularis, 1986), is estimated to be

$$L_{uu} = \int_0^\infty R_{uu}(\tau)d\tau \approx 40mm \tag{4.25}$$

The hot wires used in the present study have a length of 1.2 mm which would be too large for accurate measurements of the events described by Kolmolgorov scales and may cause significant errors in the measurements of Taylor's microscales. The spatial resolution of the integral scales should be adequate.

An quantitative estimate of the error due to wire length was made using the analysis of Wyngaard (1968). The estimated error in the measured wave amplitude was less than 5% for wavelengths greater than twice the wire length.

the errors in the measurements of the Taylor microscales due to wire length are expected to be negligible.

Temporal

The local rate of change of the fluctuating velocity as viewed from the laboratory frame, in which the probe is fixed, can be estimated as the time required for the various strutures introduced in the previous section to be convected past the probe (Corrsin, 1963). Making use of Taylor's "Frozen Turbulence Hypothesis" (Tavoularis, 1986) we can make the following estimates

$$\tau_K \approx \frac{\eta_K}{U_c} \approx 30\mu s \tag{4.26}$$

$$\tau_\lambda \approx \frac{\lambda}{U_c} \approx 500\mu s \tag{4.27}$$

$$\tau_L \approx \frac{L}{U_c} \approx 4000\mu s \tag{4.28}$$

where the convective velocity is U=10 m/s. The constant temperature bridge controlling the hot wire temperature seems adequate because it has a flat frequency response up to 100 KHz. However, it takes time for these structures to pass the sensing element of the hot wire probe (X array) which might be estimated as (Corrsin, 1963)

$$\tau_c \approx \frac{l\cos\theta}{U} \approx 350.\mu s$$

where l is the wire length and θ the angle between the wire and the mean flow direction.

Furthermore, the laminar boundary layer on the wire has its own time constant (Corrsin, 1963) for transfering momentum

$$\tau_\nu \approx \frac{d^2}{\nu} \approx 1.7\mu s \tag{4.29}$$

and heat

$$\tau_\alpha \approx \frac{d^2}{\alpha} \approx 1.1\mu s \tag{4.30}$$

where ν and α are the kinematic viscosity and thermal diffusivity of air. The time required for radial conduction in the wire must also be considered and could be estimated as (Corrsin, 1963)

$$\tau_w \approx \frac{d^2}{\alpha_w} \approx 1.25\mu s \tag{4.31}$$

where α_w is the thermal diffusivity of the tungsten wire. From the above discussion it appears that the hot wire is adequate to resolve the smallest time scales of the turbulence.

On the other hand, the digitization rate is a factor limiting the temporal resolution. To resolve events described by the Komolgorov microscale would require a minimum sampling rate of

$$\frac{2.5}{\tau_K} \approx 83kHz \tag{4.32}$$

according to the Nyquist criterion (Papoulis, 1978). This would be beyond the speed of the DT2828 ADC for two channel operation. To resolve the velocity derivatives would require a digitization rate of

$$\frac{2.5}{\tau_\lambda} \approx 5kHz \tag{4.33}$$

To test the effect of sampling rate on the temporal microscale, τ_λ, the conditioned signal was sampled at rates ranging from 1 kHz to 50 kHz and the τ_λ calculated from each sample. The results are shown in Figure 4.11.

Frequencies as low as 10 Hz contain a considerable fraction of total energy of the signal and to properly resolve these low frequencies the data records must be at least .1 s long. To test the effect of the record length on the Reynolds stresses 50 samples of 4096 points seperated by 40 μs were taken and the stresses were calculated from various length pieces of each of the 50 samples.The results, shown in Figure 4.12, suggests that a record of at least 164 ms is necessary to provide a accurate estimate of the Reynolds stresses.

A high sampling rate is required to resolve the small scales and a long record length is required to resolve the large scales. However, the length of the record is related to the sampling rate as $T = N/f_s$ where N is the number of points per record and f_s is the sampling rate. Records with high sampling rates are limited in length by the computer storage.

As a compromise of these conflicting criteria the following proceedure was adopted: signals were

1. low pass filtered to 10 kHz.
2. 4096 points were taken 40 μs apart
3. 4096 points were taken 500 μs apart
4. the process paused for 1 s
5. steps 2, 3 and 4 were repeated 50 times.

The high speed samples were used to estimate the micro-scales and derivative statistics and the low speed samples to calculate the mean velocities, Reynolds stresses, and integral scales.

Amplitude

Signal noise due to the electronics, residual turbulence of the fans and settling chamber and disturbances due the turbulent boundary layers on the walls of the windtunnel limit the signal resolution. To estimate the noise in the turbulent signal the hot wires were placed on the wind tunnel centerline and the shear generator and screens were removed. The signal energy in the unobstructed flow was $< .1\%$ of the energy of a typical shear flow. The power spectrum of the noise is shown in Figure 4.13.

The velocities in the shear flow range from 5 m/s to 15 m/s and if the entire range of velocity is to be accomodated within the ± 10 V range of the ADC the sensitivity of the amplified signal from the anemometer bridge is limited to a maximum of 2 $\frac{V}{m/s}$. The rms velocity in the shear flows is of the order of 1 m/s, which at this sensitivity would correspond to an rms signal of 2 V. The ADC had a nominal resolution of 5 mV, however, tests indicated that the resolution was limited to ± 10 mV which gives about 200 voltage steps rms. However, the rms velocity is not representative of the amplitude of the higher frequencies which are smaller and may be as low as the Kolmolgorov velocity

$$v_K = (\nu\epsilon)^{\frac{1}{4}} \approx .1 m/s \tag{4.34}$$

for which there would be only 20 voltage steps.

In practice, with an overheat ratio, $\frac{R_w}{R_{20^\circ}} = 1.5$, the hot wire had a sensitivity of 58 $\frac{mV}{m/s}$ which was amplified by a gain of 20 to give an overall sensitivity of 1.16 $\frac{V}{m/s}$.

4.3.4 Precision in Probe Positioning

The traversing systems, both transverse and spanwise had an accuracy of .1 mm, while the accuracy of the streamwise position was about 2 or 3 mm. The inclination of the axis of the probe body was aligned by eye at each streamwise location using coodinate lines engraved on the walls of the tunnel. The precision of this alignment is $\approx 1^\circ$ in the s,n plane and $\approx 3^\circ$ in the s,z plane.

The velocity statistics are nearly homogeneous but strongly anisotropic, which makes the measurements somewhat insensitive to probe translation but very sensitive to pitching of the probe.

To study the effect of probe pitch on the mean velocity and the Reynolds stress tensor, consider a rotation of the coordinates through an angle γ, see Figure 4.14. The transformation to the rotated coodinates for small γ gives

$$U^* = U + V\gamma \tag{4.35}$$

$$V^* = V - U\gamma \tag{4.36}$$

$$\overline{u^{*2}} = \overline{u^2} + 2\overline{uv}\gamma \tag{4.37}$$

$$\overline{u^*v^*} = \overline{uv} - (\overline{u^2} - \overline{v^2})\gamma \tag{4.38}$$

$$\overline{v^{*2}} = \overline{v^2} - 2\overline{uv}\gamma \tag{4.39}$$

Equations (4.36) to (4.40) suggest that V^* and $\overline{u^*v^*}$ will be the most sensitive

to error in alignment. An empirical study in which the probe was pitched in the s,n plane, see Figure 4.15, suggests that a 1° error in alignment would lead to 1% error in $\overline{u^2}$, a 2% error in $\overline{v^2}$ and a 5% error in $\overline{uv}$. U is not significantly affected but the error in V could exceed 100 %.

Chapter 5

THE MEASUREMENTS

5.1 Shear Flow in the Straight Section

5.1.1 Generation of the Shear

To meet the objective of the present research, curved sheared flows with different values of the curvature parameter, $S = \frac{U_c}{AR_c}$, must be generated. The shear generator presently available produces flows with a nearly constant $k_s = \frac{A}{U_c}$ within the range of U_c of interest here (Karnik and Tavoularis, 1987; Tavoularis and Karnik, 1989). Flows with different values of k_s can be produced by inserting a number of screens and/or grids normal to the flow downstream of the shear generator (Figure 4.1). In order to facilitate comparisons of the results, the combinations of inserted screens and/or grids were selected such that, at the entrance to the curved section, all flows would have comparable values of the turbulent intensities and length scales. While the solidity of these obstructions

determines k_s the intensity and lengthscales of the turbulence are also influenced by the mesh size and the positioning of the obstructions. Three woven screens and one grid of parallel rods were combined to produce five flows (see Table 5.1 and 5.2) with $6.25 < k_s < .53$. These flows will be referred to as cases A, B, C, D and E. Flows with roughly the same magnitude but opposite direction of shear were achieved by inverting the shear generator. Therefore a total of ten flows were generated, these will be referred to as NA, NB, NC, ND, NE, PA, PB, PC, PD and PE respectively (N stands for "negative" and P stands for "positive"). In the straight tunnel the orientation of the shear is unimportant and any difference in the measured development of the turbulence between, for example, cases NA and PA can be attributed to assymetries in the shear generator, screens, windtunnel or instrumentation. In the curved flow, however, the orientation of the curvature with respect to the shear is an important factor that determines the development of turbulence.

Cartesian coordinates x_1, x_2 and x_3 (see Figure 4.1) will be used to describe the straight shear flow.

5.1.2 The Mean Velocity

The centerline velocity, U_c, was found to be uniform along the windtunnel centerline (see Figure 5.1) with $V, W < .01U_c$. Transverse profiles of U for the flows with negative shear (cases NA, NB, NC, ND and NE) and positive shear (cases PA, PB, PC, PD and PE) are shown in Figures 5.2 and 5.3 respectively. In all cases U appears fairly linear over the central core of the tunnel. A

summary of shear rates and centerline velocities (obtained by linear regression) is provided in Table 5.3.

5.1.3 The Reynolds Stresses

Transverse profiles of $\frac{u'}{U_c}$, $\frac{v'}{U_c}$ and $\frac{w'}{U_c}$ are shown in Figures 5.4 to 5.9. The degree of transverse variation is comparable to that in earlier studies (for example see Tavoularis and Karnik, 1989).

To evaluate whether the shear flows approach a "self-preserving state", as described by Tavoularis and Karnik (1989) the development of $\overline{u^2}$, $\overline{v^2}$, $\overline{w^2}$, $\overline{uv}$ and q^2 along the windtunnel centerline has been plotted versus the non-dimensional straining time, $\tau = k_s(x_1 - x_1^*)$ (x_1^* is the position of the last screen) in semi-logarithmic (Figures 5.10 to 5.19). In cases NA, NB, NC, PA, PB and PC all the stresses appear to grow exponentially and at comparable rates. In cases ND, NE, PD and PE the stresses do not exhibit a tendency to grow even at the end of the straight section. This could be attributed to the insufficient development time, namely small τ-values for these cases (see Table 5.3).

The dominant components of the structural tensor, K_{uu}, K_{vv}, K_{ww} and K_{uv}, have been plotted versus τ in Figures 5.20 to 5.21. In cases NA, NB, NC, ND, PA, PB, PC and PD the values of these components appear to reach nearly constant asymptotes, comparable to the ones in the experiments of Tavoularis and Karnik (1989). In contrast, in cases NE and PE the three normal components are not very different from each other although the cross-component is not small, indicating an anisotropic flow.

The values of the dimensionless stresses, velocity scales and the exponents of growth of the stresses, κ_q, defined by

$$q^2 = q_o^2 e^{\kappa_q \tau} \tag{5.1}$$

are provided in Table 5.4. Notice that, in the notation of Tavoularis and Karnik (1989) $\kappa_q = \frac{k}{\epsilon}$.

5.1.4 Integral Length Scales and Taylor Microscales

The integral length scales were calculated by integrating the autocorrelation coefficient up to its first zero and applying Taylor's "frozen turbulence" approximation (Tavoularis and Corrsin, 1981), as, for example,

$$L_{uu} = U \int_0^{\tau_o} R_{uu}(\tau) d\tau \tag{5.2}$$

where τ_o is the first zero of R_{uu}. L_{vv} and L_{ww} are defined similarily. The development of L_{uu}, L_{vv} and L_{uv} along the windtunnel centerline has been plotted on semi-logarithmic axes versus τ in Figures 5.22 to 5.27. Although the initial magnitudes of the integral scales are different for each flow, they all grow with distance from the origin. This is consistant with previous studies of nearly homogeneous sheared turbulence (Tavoularis and Karnik, 1989). In cases NA, NB, NC, PA, PB and PC the exponents of growth of L_{uu},κ_L, defined as

$$L_{uu} = L_{uuo} e^{\kappa_L \tau} \tag{5.3}$$

($\kappa_L = \frac{k_L}{\epsilon}$ in the notation of Tavoularis and Karnik, 1989) are not very different (see Table 5.5). For comparison the linear growth rates of L_{uu}, computed by

plotting L_{uu} versus $\frac{x_1}{H}$ and τ on linear axes, are provided in Table 5.5 as m_{x1} and m_τ, respectively. These slopes are defined as

$$L_{uu} = m_{x1}\frac{x_1}{h_s} + L_{xuo} \tag{5.4}$$

$$L_{uu} = m_\tau \tau + L_{uuo} \tag{5.5}$$

In cases ND, NE, PD and PE, which use the grid of parallel rods as an obstruction to reduce the shear, the linear rates of growth of the integral scales are considerably larger than those in the other cases. These differences persist not only with respect to the total strain, τ, but also with respect to the streamwise distance $\frac{x_1}{h}$.

The microscales were calculated using the variance of the temporal velocity derivative and Taylor's "frozen turbulence" approximation (see Section 2.2.2). Development of λ_u along the wind tunnel centerline is shown in Figures 5.28 and 5.29. With the execption of cases NE and PE, the microscales are nearly constant away from the obstructions. The magnitudes of the microscales in each case are different and appear to be related to the particular flow generator.

Typical values of integral length scales and microscales for the straight shear flows are provided in Table 5.5.

5.2 Shear Flow in the Curved Sections

5.2.1 Mean Velocity

Mildly Curved Section ($R_c = 5m$)

Figure 5.30 shows the variation of U_c along the wind tunnel centerline. Typically, V, W $< .01U_c$.

Spanwise profiles of U were measured in cases NA and PA (see Figure 5.31). In the case PA U shows a reasonable uniformity but in case NA U becomes distorted in a manner which does not appear to be related to the boundary layer.

Transverse profiles of U are shown in Figures 5.32, 5.33, 5.34 and 5.35. In cases PA, PB, PC, PD, PE, NB, NC and NE the shear are conserved within the measuring section but in cases NA and ND they decline significantly beyond a certain location. It is not clear whether this decline occurs suddenly or gradually over the length of the tunnel.

A summary of shear rates and centerline velocities is provided in Table 5.6.

Strongly Curved Section ($R_c = 2m$)

The streamwise variation of U_c is shown in Figure 5.36. This variation in most cases is less than 10% with the majority of this change occurring beyond $\frac{s}{H}$=3.88. Spanwise profiles of U at two streamwise locations for the cases NA and PA are shown in Figures 5.37 and 5.38. In the case NA U deteriorates in a

similar manner although more dramatically than in the case of mild curvature. Transverse profiles of U at two streamwise locations are shown in Figures 5.39, 5.40, 5.41 and 5.42. For cases PA, PB, PC, PD, PE, NB, NC and NE the shear magnitudes are conserved but in cases NA and ND they decline significantly by $\frac{s}{H}$= 4.74.

A summary of the shear rates and centerline velocities is provided in Table 5.7.

5.2.2 The Reynolds Stresses

Mildly Curved Section ($R_c = 5m$)

Spanwise profiles of $\frac{u'}{U_c}$, $\frac{v'}{U_c}$ and $\frac{\overline{uv}}{u'v'}$ are shown in Figures 5.43 to 5.45. The spanwise inhomogeneity of the positively sheared turbulence is comparable to that in the straight section (see also Tavoularis and Karnik, 1989), however, the negatively sheared turbulence has developed a more pronounced inhomogeneity, which does not appear to be associated with the boundary layers. This inhomogeneity in the turbulence level could be attributed to the spanwise non-uniformity of the mean velocity or it could be due to secondary flows in a negatively sheared curved flow.

Transverse profiles of $\frac{u'}{U_c}$ $\frac{v'}{U_c}$ and $\frac{\overline{uv}}{u'v'}$ at two streamwise locations are shown in Figures 5.46 to 5.57. Their variation is comparable to that in the straight shear flow.

The development of $\overline{u^2}$, $\overline{v^2}$, $\overline{w^2}$, $\overline{uv}$ and q^2 along the tunnel centerline is

shown in Figures 5.58 to 5.67. For the negatively sheared flows the stresses are growing while for the positively sheared flows they remain constant or decay. It is reminded that in the straight section upstream of the curvature the stresses grew monotonically for both positively and negatively sheared flows A, B and C.

Strongly Curved Section ($R_c = 2m$)

Spanwise profiles of $\frac{u'}{U_c}$ $\frac{v'}{U_c}$ and $\frac{\overline{uv}}{u'v'}$ at two streamwise locations are shown in Figures 5.68 and 5.73. The turbulence in case PA is only mildly inhomogeneous, while the turbulence in case NA develops a more visible inhomogeneity in a similar fashion as was observed in the mildly curved section.

Transverse profiles of $\frac{u'}{U_c}$ $\frac{v'}{U_c}$ and $\frac{\overline{uv}}{u'v'}$ at two streamwise locations are shown in Figures 5.74 to 5.85. The positively sheared turbulence displays small inhomogeneity, however, the turbulence in cases NA, NB and NC develops significant inhomogeneity, perhaps due its high intensity.

The development of $\overline{u^2}$, $\overline{v^2}$, $\overline{w^2}$, $\overline{uv}$ and q^2 along the tunnel centerline is shown in Figures 5.86 to 5.95. In the negatively sheared cases the stresses grow while in the positively sheared cases they decay. This result is consistant with the measurements in the mildly curved shear flow but in contrast with the measurements in the straight shear flow where q^2 increased monotonically in both positively and negatively sheared flows.

5.2.3 Integral Length Scales and Taylor Microscales

Mildly Curved Section ($R_c = 5m$)

The development of L_{uu}, L_{vv} and L_{uw} along the windtunnel centerline is shown in Figures 5.96 to 5.98. In cases NA, NB, NC, ND and NE the length scales grow at different rates. In cases PA, PB, PC, PD and PE the length scales generally decline. In all cases the length scales were growing upstream of the curved section.

Development of λ_u along the windtunnel centerline is shown in Figure 5.99. In all cases λ_u is nearly constant, a feature typical of self preserving uniformly sheared flows (Tavoularis, 1985).

Strongly Curved Section ($R_c = 2m$)

Spanwise profiles of L_{uu} and L_{vv} are shown in Figure 5.100 and 5.101 for cases NA and PA. In case PA L_{uu} shows moderate variation while in case NA L_{uu} develops an inhomogeneity similar to that in the measurements of $\frac{u'}{U_c}$. L_{vv} appears to show little variation.

Transverse profiles of L_{uu} and L_{vv} are shown in Figures 5.102 to 5.103 for cases NA and PA. Their variation is comparable to that in the straight section.

Development of L_{uu}, L_{vv} and L_{uw} along the tunnel centerline is shown in Figures 5.104 to 5.106. In cases NA, NB, NC, ND and NE the integral scales grow at different rates. In cases PA, PB, PC and PD the integral scales approach nearly constant values. In case PD the development of L_{uu} and L_{vv} has a

somewhat erratic behavior, first decreasing and then increasing in a way which cannot be solely attributed to measurement error. whether this feature is a genuine feature of curved flow or an artifact of the present facility is not yet clear.

The spanwise and transverse variation of λ_u is shown in Figures 5.107 and 5.108 for cases NA and PA. Development of λ_{uu} along the windtunnel centerline is shown in Figure 5.109. In cases NA, NB, NC, ND, PA, PB, PC and PD λ_u is nearly constant while in cases NE and PE λ_u shows some moderate decay or growth respectively.

5.3 Auto-Correlations and Cross-Correlations

All auto-correlations and cross-correlations were obtained from the ensemble average of 50 discrete time series, each consisting of 4096 points sampled with a time separation of .5 ms.

Typical auto-correlations and cross-correlations observed in straight shear flow and curved shear flows with both positive and negative shear have been plotted in Figures 5.110 to 5.112. The auto-correlations in the curved flows are similar to those of nearly homogeneous straight shear flow (see also Tavoularis and Corrsin, 1981), so that curvature seems to have little qualitative effect on these quantities. The cross-correlations are affected in a similar way to the 1 point velocity covariances. For the case of positive shearing, u and v are less correlated at all time delays than those in the straight shear flow. For the case

of negative shearing u and v are better correlated at all time delays than those in a straight shear flow.

5.4 Powerspectra and Cross-Spectra

All power spectra and cross spectra were derived by ensemble averaging discrete records of the signals consisting of 1024 points each. These were selected from records of 4096 points, such that the first point of each 1024-point record coincided with the ninth point of the previous record. While successive records were not statistically independent, this proceedure resulted in smoother spectra than those computed using a smaller number of statistically independent records alone. Ensemble averaging of spectra corresponding to 50 statistically independent records of 4096 points was used to reduce the bias of the estimates. Time series with two sampling rates, Δt=.5 ms and .04 ms, were used to improve the frequency resolution of the procedure. Both time series were obtained by the descretization of a continuous signal which was low pass filtered at 10 KHz. The spectra from the fast and slow samples overlapped, however, only the spectral coefficients for the range 2 to 500 Hz were retained from the 2kHz sample and the spectral coefficients from 24Hz to 6250 Hz were retained from the 25kHz sample to reduce aliasing errors and noise contamination.

Typical power and cross spectral densities; F_{uu}, F_{vv}, F_{uw} and F_{uv} for the straight and curved flows ($S = \pm.10$) are shown in Figures 5.113 to 5.115.

The power spectra shape does not appear to be affected by the curvature.

The cross-spectrum for $S = .10$, however, is strongly suppressed in the range between 2Hz to 50 Hz, compared to the negatively sheared curved flow or the straight shear flow.

5.5 Probabilities and Higher-Order Moments

All probabilities were obtained from the ensemble average of 50 statisitically independent discrete records of 200 000 points separated by .5 ms. Typical probability density functions for the u,v and w components of velocity in the curved shear flow are shown in Figures 5.116 to 5.118. They are nearly Gaussian.

Joint probability density functions for the shear stresses for u and v and u and w are shown in Figures 5.119 to 5.121 for straight shear flow and curved shear flow with $S = \pm.10$. All cases appear to be jointly Gaussian.

Some typical higher moments of the fluctuating velocity components are summarized in Table 5.8. In all cases the skewness is near zero and the flatness is near the Gaussian value of 3.

Chapter 6

ANALYSIS AND DISCUSSION OF THE RESULTS

6.1 Definitions of Scales for the Evolution of the Turbulence

As discussed in section 3.4 a uniformly sheared flow in a wind tunnel cannot be homogeneous. A precise analysis, taking inhomogeneity into account would be difficult and would perhaps place too much emphasis on effects which are believed to be of secondary importance. However, some understanding of the main effects of curvature may follow from consideration of the idealized curved homogeneous shear flow which was introduced in Chapter 3. The following discussion would also be relevant to the present experimental flows considered in a coordinate frame convected at the mean speed U_c.

If we take the ratio $\frac{p}{\rho}$ as a dependent variable then all the variables of interest in the present flows can be nondimensionalized using appropriate time and length scales which are inherent to the flow. Nondimensionalization by such scales permits the elimination of two variables, and thus a compact description of the flow.

In a straight homogeneous shear flow, the inverse of the mean strain rate, A^{-1}, represents a "natural" time scale. The dimensionless time

$$\tau = tA \tag{6.1}$$

(Harris, Graham and Corrsin, 1977) is equal to the total mean strain of a fluid element and, hence, is proportional to the energy transfered from the mean flow to the turbulence. In the curved flow the fluid strain rate (see section 2.2) is

$$D = A(1 - S) \tag{6.2}$$

and the total mean strain during the time t is

$$Dt = \tau(1 - S) \tag{6.3}$$

In the case of $S = 0$ (straight shear flow) the strain reduces to τ and in the case of $S = 1$ (rigid body rotation) there is no straining of the fluid.

In a straight homogeneous shear flow there is no length scale associated with the mean field. A velocity scale would be equivalent to a length scale since it could be combined with A^{-1} to yield a length scale but because a coordinate transformation to the convected frame should be Galilean (see the discussion in Harris, Graham and Corrsin, 1977) the mean velocity cannot be used as a velocity scale. Therefore, a velocity scale (or length scale) must be defined from

consideration of the turbulence field. A convenient choice is the r.m.s. speed of the turbulent fluctuations, q, which when combined with the time scale A^{-1} yields the length scale

$$\mathcal{L} = \frac{q}{A} \tag{6.4}$$

In curved homogeneous shear flow the radius of curvature of the mean flow, R_c, represents an obvious length scale. Unlike the straight flow a frame fixed with the curved mean flow is not inertial and the mean convection speed, U_c, could represent a velocity scale, because mean convection could affect the dynamics of the turbulent motions. In the present flows, R_c is very large in comparison with the scales of the turbulence and it is unlikely that turbulent motions would scale with it. Besides, a perfectly homogeneous flow should be independent of any external length scale. Then, it is possible that U_c and R_c could be combined to provide another time scale for the flow, in addition to A^{-1}. The equations for the Reynolds stresses (see section 3.2) lend some support to this hypothesis, because in the limit of $\frac{1}{R_c} \to 0$ all explicit appearances of R_c vanish, leaving only the ratio R_c/U_c which could be considered as a period of rotation of the flow. This is precisely so in the case of pure rotating flow where $S = 1$ and $U_c/R_c = A = \Omega$. Note that, when $S = 1$, τ is an appropriate scale since it is equal to the angle of rotation.

If the above argument is correct, then once again no length scale or velocity scale can be associated with the mean flow but they must be defined from the turbulence field. As in the straight shear flow, one may use

$$\mathcal{L} = \frac{q}{A} \tag{6.5}$$

In conclusion, the above discussion implies that all turbulence statistics in a curved homogeneous shear flow, made dimensionless using A^{-1} and $\mathcal{L}$, should depend only on the dimensionless time, τ, and the ratio, S, of the time scales of the mean field.

6.2 Self-Preservation of the Turbulence Structure

In what is an assertion concerning the physics of the flow Tavoularis (1985) has suggested that the sheared homogeneous turbulence evolves asymptotically to a self preserving state for which the dimensionless statistics are independent of τ. Tavoularis and Karnik (1989) have discussed the evidence concerning whether such dimensionless statistics are independent of the starting conditions, i.e. the facility in which the flow was generated, and hence would have universal values in all such flows.

Using the equation for the turbulent kinetic energy Tavoularis (1985) has shown that, if the dimensionless turbulence statistics are independent of τ, then the velocity scale q and hence the length scale $\mathcal{L} = \frac{q}{A}$ must grow exponentially. The equation for the kinetic energy in straight homogeneous shear flow is

$$\frac{1}{q^2}\frac{\partial q^2}{\partial \tau} = -K_{uv} - E \tag{6.6}$$

where $E = \frac{\epsilon}{Aq^2}$. If the right hand side were independent of τ, then q ought to grow exponentially, the rate of growth depending on the asymptotic values of K_{uv} and E. This argument can easily be extended to curved homogeneous

shear flow using the corresponding equation (3.17) for the kinetic energy of the turbulence in a curved homogeneous shear flow

$$\frac{1}{q^2}\frac{\partial q^2}{\partial \tau} = -K_{uv}(1-S) - E \tag{6.7}$$

Once again if K_{uv} and E are independent of τ then q^2 must grow exponentially.

6.3 An Evaluation of Self-Preservation for the Straight Shear Flows

The five straight shear flows used presently (flows with "positive" and "negative" shear are considered identical in this context) could perhaps be divided into what have previously been referred to as "high shear" and "low shear" flows (Harris, Graham and Corrsin, 1977). Cases A, B and C would be considered as "high shear" flows with growing stresses and integral scales; Cases D and E could be considered as "low shear" flows with constant or decaying stresses and growing integral scales; they are comparable to the experiments of Champagne, Harris and Corrsin (1970) and cases O and P of Tavoularis and Karnik (1989).

Figures 5.20 and 5.21 show the development of K_{uu}, K_{vv}, K_{ww} and K_{uv} with τ for cases A, B, C, D and E. While there appears to be some consistancy in the development of the various flows, only cases A, B and C could safely be considered as having achieved dimensionless stresses which are independent of τ. For cases D and E the dimensionless stresses are still changing at the end of the test section and therefore the flow does not reach a self-preserving state, an observation consistent with the fact that q^2 is not growing.

Another test of self-preservation is that the integral length scales, when normalized with $\mathcal{L}$ should become independent of τ. Dimensionless statistics of this type have been investigated by Harris, Graham and Corrsin (1977) who plotted the development of $\frac{q^2}{A^2 L_{uu}^2}$ versus τ for their own experiments and those of Champagne, Harris and Corrsin (1970) and by Tavoularis and Karnik (1989), who evaluated the turbulence Reynolds number, $R_T = \frac{A^2 L_{uu}^2}{K_{uv} q^2}$, for all published data from homogeneous shear flows and found that R_T grows slowly with τ and that, for the available measurements, its values ranged between 25 and 60. Figures 6.1 to 6.2 show the development of $\frac{L_{uu}}{\mathcal{L}}$, $\frac{L_{vv}}{\mathcal{L}}$ and $\frac{L_{ww}}{\mathcal{L}}$ versus τ. In cases A, B and C the ratios are at most changing slowly compared to either q^2 or the length scales. They are ordered as $\frac{L_{uu}}{\mathcal{L}} > \frac{L_{ww}}{\mathcal{L}} > \frac{L_{vv}}{\mathcal{L}}$ as observed by others in "high shear" flows. In cases D and E the ratios are changing slowly but with $\frac{L_{ww}}{\mathcal{L}} \approx \frac{L_{vv}}{\mathcal{L}}$.

The constancy of the dimensionless integral scales is a necessary condition for self-preservation. A physical explanation of this constancy and an order of magnitude estimate of this ratio could be provided by the following mixing length-type argument. A particle traveling with the local mean velocity U would on average be displaced, by the turbulent mixing, the distance $L_{uu,n}$ which is the integral length scale for the stress $\overline{u^2}$ in the direction of mean shear. Assuming that the particle preserves its momentum, at the new position it would have a velocity, U_a, different from the local mean velocity U_b. Then, the local velocity fluctuation due to this particle would, on average, be

$$u' = U_b - U_a \tag{6.8}$$

For a uniform mean shear this would be

$$u' = \frac{\partial U}{\partial n} L_{uu,n} = A L_{uu,n} \tag{6.9}$$

which can be written as

$$\frac{A L_{uu,n}}{u'} = 1 \tag{6.10}$$

In the present flow $L_{uu,n}$ was not measured but at least for straight flow it could be estimated from the experiments of Tavoularis and Corrsin (1981a) as

$$L_{uu,n} \approx .30 L_{uu,s} \tag{6.11}$$

On the basis of this estimate, one would expect that

$$\frac{A L_{uu,s}}{u'} \approx 3.3 \tag{6.12}$$

or, with the typical value $u' \approx .70q$, that

$$\frac{A L_{uu,s}}{q} = \frac{L_{uu,s}}{\mathcal{L}} \approx 2.4 \tag{6.13}$$

Values of the ratio $\frac{A L_{uu,s}}{u'}$ in previous flows, summarized by Tavoularis and Karnik (1989) (τ_c/τ_s in their notation) indicate that this ratio has a value of about 3, which is close to the above estimate.

Measurements of the kinetic energy dissipation rate, ϵ, estimated from the balance of the production and convection terms in the kinetic energy equation and nondimensionalized as

$$E = \frac{\epsilon}{A q^2} \tag{6.14}$$

have been collected in Table 2 of Tavoularis and Karnik (1989), in the notation τ_s/τ_c. For the present purpose of evaluating the development of E the

dissipation rate could also be estimated from the isotropic relation

$$\epsilon \approx 30\nu \frac{\overline{u^2}}{\lambda_u^2} \tag{6.15}$$

which gives the dimensionless expression

$$E \approx 30\nu \frac{K_{uu}}{A\lambda_{us}^2} \tag{6.16}$$

Note that, for constant λ_u and A, this estimate of E is proportional to K_{uu}. The development of E versus τ is shown in Figures 6.3 and 6.4 for cases A, B, C, D and E. Cases A, B, C and D show nearly constant values while case E shows significant change within the range of measurement.

Among those flows which demonstrate a self-preserving character, the above dimensionless statistics span a relatively narrow range of values, while shear rates differ much more substantially (see Table 6.1). The same was also observed for other experiments in uniformly sheared flows by Tavoularis and Karnik (1989). Because of similarities in the way in which these flows were generated, it is not possible to conclude with certainty whether or not these dimensional statistics approach values which are universal and inherent to uniformly sheared turbulence.

6.4 Evaluating the Effect of Curvature on Homogeneous Shear Flow

6.4.1 General Comments

The straight shear flows in Cases A, B and C have length scales and velocity scales with comparable magnitudes and rates of growth. The structures of these flows are effectively identical as indicated by the fact that the ratios of turbulent stresses and of lengthscales approach comparable asymptotic values. The relatively small variation in the rates of growth and in the asymptotic values of the dimensionless statistics (see Table 5.4) is of rather secondary significance in comparison to the effects of curvature. The main parameter expected to produce an effect in the structure of the curved flows is $S = \frac{U_r}{R_c A}$. The effects of curvature will be judged by direct comparison of the turbulence development in cases A, B and C.

The flows in cases D and E show considerably different growth rates of the stresses and integral scales from the other cases, which may be due to insufficient development of their structure. Furthermore, it appears that certain structural aspects of these flows are still developing under the effect of shear at the entrance to the curved section. Therefore, caution is necessary when comparing results from these two cases with results in the other three. On the other hand, cases D and E do produce the highest values of S (due to their low shear rates) and may provide some insight into the stronger effects of curvature, not provided by the flows with the higher shear rates.

One might expect that at least for small values of S, the scaling which has been found suitable for the straight shear flows may also provide some insight into the curved shear flow results. The curved shear flows can be separated into two distinct classes, those with $S < 0$, where the scales of the turbulence grow, and those with $S > 0$, where the scales of the turbulence do not grow. The classes will be considered separatly in the following discussion.

6.4.2 The "High Shear" Flows

The "Destabilized" Flows ($S < 0$)

The growths of $\overline{u^2}$, $\overline{v^2}$, $\overline{w^2}$, $\overline{uv}$ and q^2 in both the mildly and strongly curved flows have been plotted on semi-logarithmic coordinates against the dimensionless time τ in Figures 6.5 to 6.9; the development of the stresses in the straight tunnel has also been included for comparison. In all cases the rate of growth is enhanced by the curvature. The enhancement for a given shear rate is greatest in the more strongly curved tunnel. This growth can be fitted rather well with a exponential function of the form

$$q^2 = q_o^2 e^{\kappa_q \tau} \tag{6.17}$$

where κ_q was evaluated for each flow using linear regression on the semi - logarithmic axes. These values of κ_q are presented in Table 6.3, they appear to increase monotonically with increasingly negative S.

The integral length scales, L_{uu}, L_{vv} and L_{ww} have been plotted on semi-logarithmic axes versus τ in Figures 6.10 to 6.12. The rate of growth of the

integral scales is enhanced in all cases. The growth of L_{uu} can be fitted by the exponential function

$$L_{uu} = L_{uuo} e^{\kappa_L \tau} \tag{6.18}$$

where κ_L was evaluated using linear regression on semi-logarithmic axes (Tables 6.5 and 6.6).

The exponential growth of q^2 suggests that dimensionless stresses would have asymptotic values independent of τ. K_{uu}, K_{vv}, K_{ww} and K_{uv} are plotted versus τ in Figure 6.13. The structure becomes practically independent of τ near the last measurement location with K_{uu} and K_{ww} showing the most change from the straight tunnel values, although this change has no clear trend. K_{uv} shows a modest but consistent increase with increasingly negative S. The asymptotic values of dimensionless stresses are provided in Tables 6.3 and 6.4.

The ratios $\frac{L_{uu}}{\mathcal{L}}$, $\frac{L_{vv}}{\mathcal{L}}$ and $\frac{L_{www}}{\mathcal{L}}$ are plotted versus τ in Figure 6.14. While they show some adjustment to the curvature, they appear to approach constant values. Typical ratios of the integral scales are summarized in Table 6.5 and 6.6. The most notable effect t of curvature is to rearrange the magnitudes of the scales such that $\frac{L_{vv}}{\mathcal{L}} > \frac{L_{www}}{\mathcal{L}}$.

The dimensionless dissipation E is plotted versus τ in Figure 6.15. There is an overall decline of E in all cases although there does not appear to be any systematic trend with S. This decline would contribute to the enhanced growth rate of q^2 in the destabilized flows.

In summary, the destabilized curved shear flows seem to satisfy the conditions of self-preservation, with the velocity and lengthscales growing expo-

nentially and dimensionless statistics approaching asymptotic values which are independent of τ but dependent on S.

The "Stabilized" Flows ($S > 0$)

The development of $\overline{u^2}$, $\overline{v^2}$, $\overline{w^2}$, $\overline{uv}$ and q^2 has been plotted versus τ on semi-logarithmic axes in Figures 6.16 to 6.20. The curvature reduces the growth of q^2 and, for the larger values of S, causes a decay of the stresses. For a given shear rate the effects are strongest in the more strongly curved flow where the value of S is larger. It is difficult to establish whether the decay is exponential because of the small change of q^2 in the tunnel in these cases. Nevertheless, an exponential curve can be fitted by linear regression with satisfactory confidence. The exponents of growth are summarized in Table 6.3 and 6.4.

The development of L_{uu}, L_{vv} and L_{ww} versus τ is presented on semi-logarithmic axes in Figures 6.21 to 6.23. Curvature arrests the growth of the length scales which was established in the straight tunnel. L_{uu} does not resume its growth but L_{vv} and L_{ww} recover modest growth rates before the end of the tunnel. In a exponential fit of the L_{uu}, $\kappa_L \approx 0$ for all the flows although this would seem to over-simplify the data.

The development of K_{uu}, K_{vv}, K_{ww} and K_{uv} has been plotted versus τ in Figure 6.24. K_{uu} and K_{vv} show some scatter but their average values do not seem to be affected by the curvature by more than 10%. K_{vv} shows the least variation of the diagonal components. In contrast the shear component K_{uv} shows a more systematic decline with increasing S. Asymptotic values of K_{uv}

have been summarized in Tables 6.3 and 6.4.

While, as a first approximation, one could possibly assume that K_{uu}, K_{vv} and K_{ww} were independent of τ and more crudely, even independent of S (at least for small values of S), a closer examination seems to suggest that what appears to be scatter may be a systematic behavior involving K_{uu} and K_{ww}. Curiously the sum $K_{uu}+K_{ww}$, plotted versus τ in Figure 6.25, shows the elimination of almost all the apparant scatter in Figure 6.24. Because instrumentation and wind tunnel artifacts cannot be ruled out as possibl explanations of this behavior, a search for a physical expanation may be premature without further investigation. For example, it must be established whether such behavior would persist indefinitely with increasing τ or whether it is the response of the turbulence to the start of curvature and will eventually dampen down.

The development of $\frac{L_{uu_k}}{\mathcal{L}}$, $\frac{L_{vv}}{\mathcal{L}}$ and $\frac{L_{www}}{\mathcal{L}}$ is plotted versus τ in Figure 6.26. For $S = .03$ and .04, $\frac{L_{vv}}{\mathcal{L}}$ and $\frac{L_{www}}{\mathcal{L}}$ are practically independent of τ and S while $\frac{L_{uu}}{\mathcal{L}}$ shows significant adjustment to lower values. When $S = .07$, .12 and .31, all the dimensionless integral scales show accelerating growth rates and, although their total change is small relative to changes in q^2 or the length scales, they do not appear to be approaching asymptotic values. This behavior is a direct result of the decaying energy and the resumed growth of the integral scales. Where appropriate, typical ratios of the integral scales are provided in Tables 6.5 and 6.6.

The development of E versus τ is shown in Figure 6.27. For $S = .03$ and .04, E is independent of τ and S. For S =.07, .18 and .64 E seems to increase

and then decrease, which is probably a result of the approximation used for E (see equation 6.16) which gives $E \sim K_{uu}$.

In summary, some statistics of the stabilized shear flow appear to be self-preserving while others appear to depend on τ. For example, K_{uv} and E are independent of τ, for small S, and q^2 develops exponentially, however, K_{uu}, K_{ww} and the dimensionless integral length scales appear to show some significant dependence on τ. Perhaps a classification less restrictive than complete self preservation is appropriate for these flows.

Consolidation of the Results

The relation between κ_q and S for the "high shear" flows has been plotted in Figure 6.28. κ_q shows a monotonic decrease with increasing S. A least squares fit to the data gives

$$\kappa_q = .084(1 - 17.6S)(1 - S) \tag{6.19}$$

where $-.15 \leq S \leq .18$.

The relation between K_{uv} and S for the "high shear" flow results has been plotted in Figure 6.29. K_{uv} shows a monotonic decrease with increasing S. A least squares fit to the data gives

$$K_{uv} = .14(1 - 2.8S) \tag{6.20}$$

for $-.15 \leq S \leq .18$.

6.4.3 The "Low Shear" Flows

Of the four cases ND, NE, PD and PE, case ND is the closest to full development when it enters the curved wind tunnel. It reaches a strain of nearly 4 by the end of the curved tunnel and its structure is somewhat similar to that in the other cases. Comparing the effects of curvature on case ND in the mildly curved tunnel to those on NB in the strongly curved tunnel which has a comparable value of S we see that the exponent of growth of q^2 in case ND is substantially lower. Similar growth rates might have been expected for cases A,B and C when there were overlapping values of S. In fact the exponent of growth of case ND in either tunnel is lower than the flows which had even lower values of S. On the basis of this discrepancy a quantitative comparison of flows D and E with flows A, B and C does not seem appropriate.

The "Destabilized" Flows, ($S < 0$)

The development of $\overline{u^2}$, $\overline{v^2}$, $\overline{w^2}$, $\overline{uv}$ and q^2 is plotted against τ in Figures 6.30 to 6.34. Although at the entrance of the curved section the growth rates of these quantities could be positive, zero or negative, their development is always enhanced positively. Exponents of growth of q^2 are summarized in Tables 6.3 and 6.4.

The development of L_{uu}, L_{vv} and L_{ww} is plotted against τ in Figures 6.35 to 6.37. In the straight tunnel only L_{uu} showed some growth while after the start of curvature the growth rates of L_{vv} and L_{ww} surpass that of L_{uu}.

The development of K_{uu}, K_{vv}, K_{ww} and K_{uv} is plotted versus τ in Figure

6.38. Case ND in both the mildly and strongly curved tunnels shows some reordering of K_{uu}, K_{vv} and K_{ww} which had not been observed in the other flows. It is difficult to judge if this trend is also occuring in the flow PE because of the near equality of these three diagonal components at the start of curvature. The shear component K_{uv} rises to values above .2 in both flows.

The development of the dimensionless integral scales, shown in Figure 6.39, is consistant with but more pronounced than that in the "high shear" flows. $\frac{L_{uu}}{\mathcal{L}}$ is unaffected while $\frac{L_{vv}}{\mathcal{L}}$ and $\frac{L_{ww}}{\mathcal{L}}$ show a some growth, which is sustained up to the last measurement location. For case E the dimensionless integral scales are widely scattered and show no clear trend.

The normalized dissipation, E, is plotted versus τ in Figure 6.40. Case ND shows some decline in E which is comparable to what was observed in the high shear flows. For case NE E is declining rapidly as it was before the start of curvature.

The "Stabilized" Flows, ($S > 0$)

The development of $\overline{u^2}$, $\overline{v^2}$, $\overline{w^2}$, $\overline{uv}$, and q^2 is plotted against τ in Figures 6.41 to 6.45. Most of the stresses decay after the start of curvature, with the notable exception of $\overline{v^2}$, which first decays and then begins to grow for $S \doteq .65$. The most significant new phenomenon is the change in sign of $\overline{uv}$ such that it has the same sign as the shear. Such reversal in shear stress sign has only, so far, been observed in strongly inhomogeous flows. This feature appears for S=.64, .65 and 1.

The development of L_{uu} is plotted against τ in Figures 6.46 to 6.48. For $S = .49$ all the integral scales decline after the start of curvature. For the higher values of S, L_{uu} and L_{vv}, but not L_{ww}, show an erratic wave-like behaviour.

The development of $\breve{K}_{uu}$, $\breve{K}_{vv}$, $\breve{K}_{ww}$ and $\breve{K}_{uv}$ is shown in Figure 6.49. Case PD in the mildly curved tunnel has $S = .2$ and shows behavior similar to that in other cases of comparable S. In the strongly curved tunnel there is a significant change in the magnitude of the diagonal components, even stronger than the one observed at lower values of S. What is more remarkable is that $\breve{K}_{uv}$ changes sign at $\tau = .8$ from the start of curvature and becomes positive such that the shear and shear stress have the same sense. Similar trends are observed for case PE.

The development of the dimensionless integral lengthscales is shown in Figure 6.51. $\frac{L_{uu}}{\mathcal{L}}$ and $\frac{L_{vv}}{\mathcal{L}}$ demonstrate the same oscillatory pattern as was observed in the integral scales themselves up to the last measurement.

The development of E versus τ is shown in Figure 6.52. For $S = .18$, E is practically unaffected by the curvature and is independent of τ; for $S = .64$, E adjusts to a higher value, .35; for $S = .65$ E demonstrates an initial increase followed by a drop as was observed in the "high shear" flows.

Closure

For the cases of destabilized flow, the "low shear" flows develop in a way that is qualitatively consistent with the "high shear" flows. It is possible that, given sufficient development time, these flows would become self-preserving.

The stabilized "low shear" flows have a range of S approaching that in rigid-body rotation. These flows exhibit some distinct features, such as a change of sign of the shear stress and an apparently wave-like pattern of length scales.

6.5 An Estimate of the Pressure-Strain Covariance Tensor in Curved Shear Flow

The pressure strain covariances which appear in the Reynolds stress equation are believed to play an important role in the partition of turbulent energy and the development of the shear stress. Direct measurements of the pressure-strain covariances do not exist but, as demonstrated by Champagne, Harris and Corrsin (1970), Harris, Graham and Corrsin (1977) and Tavoularis and Karnik (1989), the pressure strain covariance can be estimated from the Reynolds stress equation in a homogeneous flow by balancing it against the measurements of the other terms. The present flow offers an opportunity to extend this analysis to include the effects of curvature.

The Reynolds stress equations for curved homogeneous shear flow may be written in the following way (see section 3.2)

$$\phi_{uu} = q^{-2}\frac{\partial \overline{u^2}}{\partial \tau} + 2K_{uv}(1+S) + 2E_{uu} \tag{6.21}$$

$$\phi_{vv} = q^{-2}\frac{\partial \overline{v^2}}{\partial \tau} - 4K_{uv}S + 2E_{vv} \tag{6.22}$$

$$\phi_{ww} = q^{-2}\frac{\partial \overline{w^2}}{\partial \tau} + 2E_{ww} \tag{6.23}$$

$$\phi_{uv} = q^{-2}\frac{\partial \overline{uv}}{\partial \tau} + K_{vv}(1+S) - 2K_{uu}S + E_{uv} \tag{6.24}$$

where, for example, $o_{uu} = \frac{2}{Aq^2}\overline{p\frac{\partial u}{\partial s}}$ and $E_{uu} = \frac{\epsilon_{uu}}{Aq^2}$. The only non-mesurable terms on the right-hand sides of the above equations are the three components of the dissipation. These can be roughly estimated from the present measurements, using the temporal derivatives of the fluctuating velocity (Tavoularis and Corrsin, 1981b). Alternatively the total dissipation, ϵ, can be estimated as the balance of measured terms in the equation for the kinetic energy of turbulence

$$\epsilon = -\frac{\partial q^2}{\partial t} - \overline{uv}(1-S)A \tag{6.25}$$

or, in a normalized form, as

$$E = -q^{-2}\frac{\partial q^2}{\partial \tau} - K_{uv}(1-S) \tag{6.26}$$

Using the latter approach one must estimate the partition of the dissipation into its components E_{uu}, E_{vv}, E_{ww} and E_{uv}. Two plausible assumptions to this effect are

1. The dissipation is isotropic, i.e.

$$\epsilon_{uu} = \frac{\epsilon}{3} \tag{6.27}$$

$$\epsilon_{vv} = \frac{\epsilon}{3} \tag{6.28}$$

$$\epsilon_{ww} = \frac{\epsilon}{3} \tag{6.29}$$

$$\epsilon_{uv} = 0.0 \tag{6.30}$$

2. The dissipation is anisotropic, but its anisotropy is equal to the anisotropy of the kinetic energy, i.e.

$$\epsilon_{uu} = K_{uu}\epsilon \tag{6.31}$$

$$\epsilon_{vv} = K_{vv}\epsilon \tag{6.32}$$

$$\epsilon_{ww} = K_{ww}\epsilon \tag{6.33}$$

$$\epsilon_{uv} = K_{uv}\epsilon \tag{6.34}$$

The first hypothesis was used, among others, by Champagne, Harris and Corrsin (1970) and is based on the assumption that motions corresponding to high wavenumbers are responsible for the dissipation and would be isotropic at high Reynolds numbers (for a thorough discussion see Hinze, 1975). The second hypothesis was introduced by Tavoularis and Karnik (1989) and assumes that the anisotropy imposed by the mean strain and most noticable at the low wave numbers persists even at the higher wave numbers which are responsible for the dissipation. The implications of both hypotheses will be deduced with the hope that the actual anisotropy of the dissipation tensor would be bounded by the two cases presented above.

The transport terms in the Reynolds stress equations can be calculated from the present measurements even if the stresses are varying at different rates as during the period of development or adjustment to curvature. However, under such circumstances the resulting estimates of the pressure strain would depend on τ, S and the initial conditions of all the stresses. A simpler relation which would depend only on S would be more desirable. Following Tavoularis and Karnik (1989) we assume that K_{uu}, K_{vv}, K_{ww} and K_{uv} have constant asymptotic values and that the kinetic energy grows exponentially as $q^2 = q_o^2 e^{\kappa_q \tau}$.

For an isotropic dissipation, equations (6.21) to (6.24) become

$$\phi_{uu} = (K_{uu} - \frac{1}{3})\kappa_q + \frac{4}{3}K_{uv}(1 + 2S) \tag{6.35}$$

$$\phi_{vv} = (K_{vv} - \frac{1}{3})\kappa_q + \frac{2}{3}K_{uv}(1 + 5S) \tag{6.36}$$

$$\phi_{ww} = (K_{ww} - \frac{1}{3})\kappa_q - \frac{2}{3}K_{uv}(1 - S) \tag{6.37}$$

$$\phi_{uv} = K_{uv}\kappa_q + K_{vv}(1 + S) - 2K_{uu}S \tag{6.38}$$

For an anisotropic dissipation, equations (6.21) to (6.24) become

$$\phi_{uu} = 2K_{uv}(1 + S) - 2K_{uu}K_{uv}(1 - S) \tag{6.39}$$

$$\phi_{vv} = -4K_{uv}S - 2K_{vv}K_{uv}(1 - S) \tag{6.40}$$

$$\phi_{ww} = -2K_{ww}K_{uv}(1 - S) \tag{6.41}$$

$$\phi_{uv} = K_{vv}(1 + S) - 2K_{uu}S - K_{uv}^2(1 - S) \tag{6.42}$$

Equations (6.39) to (6.42) are independent of κ_q.

Equations (6.35) to (6.42) provide expressions for the pressure-strain covariance which depends on S. Using the values of K_{uu}, K_{vv}, K_{ww} and K_{uv} from Tables 6.3 and 6.4, the dependence of ϕ_{uu}, ϕ_{vv}, ϕ_{ww} and ϕ_{uv} on S has been calculated for both isotropic and anisotropic dissipation and is illustrated in Figure 6.53 and 6.54.

It is interesting to note that, when normalized by the production of q^2, as

$$\phi_{uu}^* = \frac{-2\overline{p\frac{\partial u}{\partial s}}}{-\overline{uv}A(1 - S)} \tag{6.43}$$

equations (6.39) to (6.42) take the following simple forms

$$\phi_{uu}^* = 2\frac{1 + S}{1 - S} - 2K_{uu} \tag{6.44}$$

$$\phi_{vv}^* = -4\frac{S}{1 - S} - 2K_{vv} \tag{6.45}$$

$$\phi_{ww}^* = -2K_{ww} \tag{6.46}$$

$$\phi_{uv}^* = \frac{K_{vv}(1 + S)}{K_{uv}(1 - S)} - 2\frac{K_{uu}S}{K_{uv}(1 - S)} - K_{uv} \tag{6.47}$$

While for the destabilized flows the assumption that the dimensionless stresses are independent of τ for the stabilized cases only K_{vv} and K_{uv} show such behavior while K_{uu} and K_{ww} are changing at least as quickly as q^2. However, as illustrated in Figure 6.25 the sum $K_{uu} + K_{ww}$ is more independent of τ and for the stabalized flows it may be more appropriate to limit the estimation of ϕ_{uu} and ϕ_{ww} to their sum $\phi_{uu} + \phi_{ww}$.

6.6 The Stability of Curved Shear Flow

The present experiments include cases for which the energy of turbulence grows and decays exponentially. Figure 6.28 suggests that, for $S < .05$, q^2 will grow while for, $S > .05$, q^2 will decay. Stability analyses of curved shear flows such as circular Couette flow have also predicted exponential growth or decay of the energy of introduced disturbances.

The simplest and most easily applied criterion for instability is that of Rayleigh (1921), which gives the necessary and sufficient condition for the instability of the base motion in inviscid flow as

$$\frac{\partial}{\partial n}(Ur)^2 < 0 \tag{6.48}$$

Equation (6.48) says that, in unstable flow the square of the angular momentum (or in cases where the fluid flows only in one direction the angular momentum itself) of the base motion must decrease outward from the center of curvature. Since this condition is necessary for instability it follows that flows for which

$$\frac{\partial}{\partial n}(Ur)^2 > 0 \tag{6.49}$$

are unconditionally stable.

We can evaluate the implications of equation (6.48) for the present flow by substituting in it the expression for the mean velocity

$$U = U_c + An \tag{6.50}$$

Then the neccesary and sufficient condition for instability on the the wind tunnel centerline ($n = 0$) is

$$S < -1 \tag{6.51}$$

which corresponds to irrotational motion (a potential vortex). Rayleigh's critereon does not describe, even approximately, the growth or decay of the turbulence in the present type of flows.

6.7 The Effect of Curvature on the Specta

The turbulent shear stress is more sensitive to flow curvature than the normal stresses. The cross-spectra in Figures 5.113-5.115 suggest that the contributions of large-scale motions to the shear stress is the most strongly affected. To examine these effects more closely, the cross-spectra for S =-.10, 0. and .10 have been plotted in Figure 6.55. The wave number α and the specta have been normalized with the Kolmolgorov scales, η_K and v_K. Although the spectra at all wavenumbers show effects of the curvature, the low wavenumber range is by far the most affected.

The spectral density of the normal stresses are shown in Figures 6.56, 6.57 and 6.58. When scaled using Kolmolgorov variables the spectra appear to col-

lapse at the higer wavenumbers. The difference between the spectra at the lower wavenumbers may be explained by the difference in the integral length scales between the three flows.

6.8 Comparison to Curved Boundary Layers

Uniformly sheared flows in straight sections are known to have properties comparable to those in the outer regions of turbulent boundary layers (Tavoularis and Corrsin, 1981a). It is therefore worthwhile to examine whether the effects of curvature on homogeneous flows would be similar to the effects of curvature on inhomogeneous flows, particularly on boundary layers. A quantitative comparison between the homogeneous flows and curved boundary layer flows is difficult because the curvature parameter S varies strongly across the boundary layer. For this reason comparisons will be made qualitatively. Typically the strength of the curvature in boundary layer flows is characterized by the ratio $\frac{\delta}{R}$, where δ is the boundary layer thickness and R is the radius of curvature of the surface. In the present context, $\frac{\delta}{R} \sim O(S)$, if we make the crude estimate $A \sim O(U_\infty/\delta)$. For the mildly curved boundary layers studied by Ramaprian and Shivaprasad (1978b), $\frac{\delta}{R} \approx .013$, which suggests milder curvature than that in the present studies.

For the concave boundary layer ($S < 0$) the measurements of Ramaprian and Shivaprasad (1978b) give $K_{uv} \approx .2$ across most of the boundary layer. This is significantly higher than that measured on a flat plate where $K_{uv} \approx .16$. For the convex boundary layer ($S > 0$), $K_{uv} \approx .11$ across most of the boundary layer,

which is significantly less than that measured in a flat plate boundary layer. These observations agree with the results observed in the present homogeneous flows. Cross-spectra measured by Ramaprian and Shivaprasad (1978b) show that these effects of curvature on the shear stress are confined to the lower wavenumber range, in conformity with the present results (Figure 6.55).

The integral length scales are larger in the concave boundary layer than in a comparable flat plate boundary layer and in the convex boundary layer they are smaller than in a comparable flat plate boundary layer.

The Taylor microscales are mostly unaffected by curvature in a boundary layer as well as in the present homogeneous flows.

Chapter 7

CONCLUSIONS

The conclusions of the present study can be summarized as follows:

1. It is possible to generate a curved uniformly sheared flow with approximately homogeneous turbulence.

2. When the mean velocity increases away from the center of curvature the growth of the Reynolds stresses and the integral scales is suppressed.

3. When the mean velocity decreases away from the center of curvature the growth of the Reynolds stresses and integral scales is enhanced.

4. The development of the kinetic energy of turbulence, q^2, can be represented by an exponential function $q^2 = q_o^2 e^{\kappa_q \tau}$. Empirically $\kappa_q = .084(1 - 17.6S)(1 - S)$ for $-.15 < S < .18$.

5. The dimensionless shear stress, K_{uv}, appears to acquire asymptotic values which depend on the curvature parameter S. Empirically $K_{uv} = .14(1 -$

2.8S) for $-.15 < S < .18$. Curvature affects mostly the low wavenumber range of the shear stress spectrum.

6. Effects of curvature on homogeneous shear flow are comparable to those on turbulent boundary layers.

References

Barlow, R.S. and Johnston, J.P. (1985)"Roll-cell structure in a concave turbulent boundary layer", AIAA paper no. 85-0297.

Barlow, R.S. and Johnston, J.P.(1985)"Velocity spectra for turbulent boundary layers on a concave surface", Fifth Symp. on Turbulent Shear Flows, Ithaca, New York, U.S.A.

Batchelor, G.K.(1953)"The Theory of Homogeneous Turbulence", Cambridge University Press, Cambridge.

Bradshaw,P.(1969)"The analogy between streamline curvature and buoyancy in turbulent shear flow", J. Fluid Mech., vol. 36, pp. 177-191.

Bradshaw,P.(1973)"Effects of Streamline Curvature on Turbulent Flow" , AGARDograph No.169, NATO.

Castro, I.P. and Bradshaw, P.(1976)"The turbulence structure of a highly curved mixing layer", J. of Fluid Mech., vol.73, pp.265-304.

Champagne, F.H., Harris, V.G. and Corrsin, S. (1970)"Experiments on nearly homogeneous turbulent shear flow", J. Fluid Mech., vol.41, pp. 81-139.

Chandrasekhar, S.(1961)"Hydrodynamic and Hydromagnetic Stability" , Oxford University Press.

Corrsin, S.(1959) "Outline of some topics in homogeneous turbulent flow", J. Geophys. Res., vol.64, pp.2134-2150.

Corrsin, S.(1963)"Turbulence: Experimental Methods", Handbuch der Physik, vol.8, pp.523-590.

Comte-Bellot, G. and Corrsin, S.(1966)"The use of a contraction to improve the isotropy of grid-generated turbulence", J. Fluid Mech., vol. 25, pp. 657-682.

Dean, W.R.(1928)"Fluid motion in a curved channel", Proc. Roy. Soc. Lond., A121, pp.402-420.

Deissler, R.G.(1961)"Effects of inhomogeneity and of shear flow in weak turbulent fields", Phys. Fluids, vol.4, pp.1187-1198.

Deissler, R.G. (1975)"Comparison of theory and experiment for homogeneous turbulence with shear", Phys. Fluids, vol.18, pp.1237-1240.

DiPrima, R.C. and Swinney, H.L.(1981)"Instabilities and transition in flow between concentric rotating cylinders", IN Hydrodynamic Instabilities and Transition to Turbulence, ed. H.L. Swinney and J.P. Gollub, pp.139-180, Springer.

Dryden, H.L. and Kuethe, A.M.(1929) "The measurement of fluctuations of air speed by the hot wire anemometer", NACA Tech. Report 320.

Ellis, L.B. and Joubert, P.N.(1974)"Turbulent shear flow in a curved duct", J. Fluid Mech., vol. 62. pp.65-84.

Eustice, J.(1911)"Experiments on streamline motion in curved pipes" , Proc. Roy. Soc. Lond., A85, pp.119-130.

Eskinazi S. and Yeh H.(1956)"Fully developed turbulent flow in a curved channel",J. of Aeronaut. Sci., vol.23, pp.23-35.

Gibson, M.M.(1978)"An algebraic stress and heat flux model for turbulent shear flow with streamline curvature", Int. J. Heat Mass Transfer, vol.21, pp.1609-1617.

Gibson, M.M.(1984)"Effects of streamline curvature on turbulence", in Frontiers in Fluid Mech., Ed. S. H. Davies and J. L. Lumley, Springer-Verlag, Berlin.

Gibson, M.M. and Servat-Djoo, K.(1981)"Measurements in the heated turbulent boundary layer on a mildly curved concave surface", Fith Symp. on Turbulent Shear Flows, Ithaca, New York, U.S.A.

Gibson, M.M. and Rodi, W.(1981)"A Reynolds-Stress closure model of turbu lence applied to the calculation of a highly curved mixing layer",J. of Fluid Mech., vol.103, pp.161-182.

Gibson, M.M.and Verriopoulos, C.A.(1984)"Turbulent boundary layer on a mildly curved convex surface:Part 2, Temperature field measurements", Exp. Fluids, vol.2, pp.73-80.

Gibson, M.M., Verriopoulos, C.A. and Vlachos, N.S.(1984)"Turbulent boundary layer on a mildly curved convex surface:Part 1. Mean flow and turbulence measurements", Exp. Fluids, vol.2, pp.17-24.

Gibson, M.M., Jones, W.P. and Younis, B.A.(1981"Calculation of turbulent boundary layers on curved surfaces", Phys. Fluids, vol.24, pp.386-395.

Gibson, M.M. and Younis, B.A.(1981)"Calculation of a turbulent wall jet on a curved wall with a Reynolds stress model of turbulence", Third Symp. on Turbulent Shear Flows, Davis, California, U.S.A.

Gillis, J.C. and Johnston, J.P.(1983)"Turbulent boundary layer flow and structure in a convex wall and its redevelopment on a flat wall", J. Fluid Mech., vol.135, pp.123-153.

Görtler, H.(1940)"Uber eine dreidimensionale instabilitat laminarer grenzschichten an konkaven wanden", Nachr. Ges. Gottingen, Math.-Phys. Kl., vol.2.

Harris, V.G., Graham, J.A.H. and Corrsin, S.(1977)"Further experiments in nearly homogeneous turbulent shear flow", J. Fluid Mech., vol. 81, pp. 657-687.

Hinze, J.O.(1975)"Turbulence", Second Edition, McGraw Hill, New York.

Hoffman, P.H.; Muck, K.C. and Bradshaw, P. (1985)"The effect of concave surface curvature on turbulent boundary layers",J. of Fluid Mech., vol.161, pp.371-403.

Humphrey, J.A.C., Whitelaw, J.H. and Yee, G.(1981)"Turbulent flow in a square duct with strong curvature", J. Fluid Mech., vol. 103, pp.443 -463.

Hunt, I.A. and Joubert P.N.(1979)"Effects of small streamline curvature on turbulent duct flow", J. of Fluid Mechanics, vol.91, pp.633-659.

Irwin, H.P.A.H. and Smith, P.A.(1975)"Prediction of the effect of streamline curvature on turbulence", Phys. Fluids, vol.18, pp.624-630.

Ito, H.(1987)"Flow in curved pipes", JSME, vol.30, no.262, pp.543-552.

Jeffreys, H.(1928)"Some cases of instability in fluid motion", Proc. Roy. Soc. Lond., vol.118, pp.195-208.

Johnston, J.P., Halleen, R.M. and Lezius, D.K. (1972)"Effects of spanwise rotation on the structure of two-dimensional fully developed turbulent channel flow",J. Fluid Mech., vol.56, pp.533-557.

Karamcheti, K.(1966)"Priciples of Ideal Fluid Aerodynamics", John Wiley and Sons, New York.

von Karman, Th.(1937)" ",J. Aero. Sci., vol. 4. p.131.

Karnik (1988) "Experiments on the Structure of Turbulence and the Diffusion of Heat From a Line Source in Uniformly Sheared Flows", Phd Thesis, Department of Mechanical Engineering, University of Ottawa, Ottawa, Canada.

Karnik U. and Tavoularis S. (1987) "Generation and Manipulation of uniform shear with the use of screens",Experiments in Fluids, vol.5, pp.247-254.

Koyama, H.S.(1981)"Turbulent shear flows behind cylinder and sphere in curved channals", Third Symp. on Turbulent Shear Flows, Davis, California, U.S.A.

Koyama, H., Masuda, S., Ariga, I. and Watanabe, I.(1979)"Stabilizing and destabilizing effects of Coriolis force on two-dimensional laminar and turbulent boundary layers", J. Eng. Power, vol.101, pp.23-31.

Koyama, H.S. and Ohuchi, M.(1985)"Effects of coriolis force on boundary layer development", Fifth Symp. on Turbulent Shear Flows, Ithaca, New York, U.S.A.

Launder, B.E., Pridden, C.H. and Sharma, B.I.(1977)"The calculation of turbulent boundary layers on spinning and curved surfaces", J. Fluids Eng., March, pp.232-239.

Launder, B.E., Reece, G.J. and Rodi, W.(1976)"Progress in the development of a Rynolds stress turbulence closure", J. Fluid Mech., vol.68, pp.537- 566.

Launder, B.E. and Spalding, D.B.(1974)"Numerical computation of turbulent flows", Comp. Meth. in Appl. Mech. and Eng., pp.269-289.

Launder, B.E., Tselepidakis, D.P. and Younis, B.A.(1987)"A second- moment closure study of rotating channel flow", J. Fluid Mech., vol. 183, pp.63-75.

Lin, C.C.(1955)"The Theory of Hydrodynamic Stability", Cambridge University Press, Cambridge.

MacPhail, D.C.(1941)"Turbulence in a Distorted Passage and Between Rotating Cylinders", PhD dissertation, University of Cambridge.

Margolis, D.P. and Lumley, J.L. (1965)"Curved turbulent mixing layer", Phys. Fluids, vol.8 , pp.1775-1785.

Mayle, R.E., Blair, M.F. and Kopper, F.C.(1979)"Turbulent boundary layer

heat transfer on curved surfaces", ASME J. Heat Transfer, vol. 101, pp.521-525.

Meroney, R.N. and Bradshaw, P.(1975)"Turbulent boundary layer growth over a longitudinally curved surface", AIAA J., vol.13, pp.1448-1453.

Moser, R.D. and Moin, P.(1987)"The effects of curvature in wall bounded turbulent flows", J. Fluid Mech., vol.175, pp.479-510.

Muck, K.C.; Hoffman, P.H. and Bradshaw, P.(1985)"The effect of convex surfaces curvature on turbulent boundary layers", J. Fluid Mech., vol.161, pp.347-369.

Nakano, S., Tadahashi, A., Shizawa, T. and Honami, S.(1981)"Effects of stable and unstable free streams on a turbulent flow over a concave surface", Third Symp. on Turbulent Shear Flows, Davis, California, U.S.A.

Pai, S.I.(1943)"Turbulent Flow Between Rotating Cylinders", NACA Tech. Note 892.

Pearson, J.R.A.(1959)"The effect of uniform distortion on weak homogeneous turbulence", J. Fluid Mech., vol.5, pp.274-288.

Pelfrey, J.R.R. and Liburdy, J.A.(1986)"Effect of curvature on the turbulence of a two-dimensional jet", Exp. Fluids, vol.4, pp.143-149.

Perry, A.E.(1982)"Hot Wire Anemometry", Clarendon Press, Oxford.

Pouagare, M. and Lakshminarayama, B. (1983)"Computation and turbulence closur models for shear flows in rotating curved bodies", Fourth Symp. on Turbulent Shear Flows, Karlsruhe, Germany.

Prandtl, L. (1929)"Effect of Stabilizing Forces on Turbulence", NACA Tech. Mem. 625.

Rogallo, R.S.(1981)"Numerical Experiments in Homogeneous Turbulence", NASA Tech. Memo. 81315.

Ramaprian, B.R. and Shivaprasad, B.G.(1977)"Mean flow measurements in turbulent boundary layers along mildly curved surfaces", AIAA J., vol. 15, pp.189-196.

Ramaprian, B.R. and Shivaprasad, B.G.(1978a)"Turbulence measurements in boundary layers along mildly curved surfaces", J. Fluids Eng., vol. 100, pp.37-46.

Ramaprian, B.R. and Shivaprasad, B.G.(1978b)"The structure of turbulent boundary layers along mildly curved surfaces", J. Fluid Mech., vol. 85, pp.273-303.

Ramaprian, B.R. and Shivaprasad, B.G.(1982)"The instantaneous structure of mildly curved turbulent boundary layers", J. Fluid Mech., vol.115, pp.39-58.

Rayleigh, Lord (1917)"On the dynamics of revolving fluids", Scientific Papers, vol.6, pp.447-453.

Reynolds, O.(1883) Phil. Trans. Royal Society of London, vol. 174, p.935.

Rodi, W. and Scheuerer, G.(1983)"Calculation of curved shear layers with two-equation turbulence models", Phys. Fluids, vol.26, pp.1422-1436.

Savill, A.M.(1982)"The turbulence structure of a highly curved two-dimensional wake", Structure of Complex Turbulent Shear Flow, IUTAM Sym-

posium Marseille', Eds. R. Dumas, L. Fulachier, Springer, New York.

Schmidbauer, H.(1936)"Turbulent Friction Layer on Convex Surfaces", NASA Tech. Memo. 791.

Shizawa, T. and Honami, S.(1983)"Experiment on turbulent boundary layers over a concave surface-Effects of introduction of curvature", Fourth Symp. on Turbulent Shear Flows, Karlsruhe, Germany.

Shizawa, T. and Honami, S.(1985)"Experiments on turbulent boundary layers over a concave surface-Response of turbulence to curvature", Fifth Symp. on Turbulent Shear Flows, Ithaca, New York, U.S.A.

Slattery, J.C. (1981)"Momentum, Energy, and Mass Transfer in Continua", Second Edition, Robert E. Krieger Publishing Company, Huntington, New York.

Smits, A.J., Young, S.T.P and Bradshaw, P.(1979)"The effect of short regions of high surface curvature on turbulent boundary layers", J. Fluid Mech., vol.94, pp.209-242.

Smith, G.P. and Townsend, A.A.(1982)"Turbulent couette flow between concentric cylinders at large Taylor numbers", J. Fluid Mech., vol.123, pp.187-217.

Stuart, J.T.(1963)"Hydrodynamic Stability", in Laminar Boundary Layers, ed. L. Rosenhead, Oxford University Press.

So, R.M.C.(1975)"A turbulence velocity scale for curved shear flows", J. Fluid Mech., vol.70, pp.37-57.

So, R.M.C and Mellor, G.L.(1973)"Experiment on convex curvature effects

in turbulent boundary layers", J. Fluid Mech., vol.60, pp.43-62.

Synge, J.L.(1933)"The stability of heterogeneous liquids", Trans. Roy. Soc. Canada, vol.27, series 3, section 3, pp.1-18.

Synge, J.L.(1938)"On the stability of a viscous liquid between rotating coaxial cylinders", Proc. Roy. Soc. Lon., vol.167, pp.250-256.

Tani, I.(1962)"Production of longitudinal vortices in the boundary layer along a concave wall", J. Geophys. Res., vol.67, pp.3075-3080.

Tavoularis, S. (1978)"A circuit for the measurement of instantaneous temperature in heated turbulent flows", J. Phys. E.; Sci. Instrum., vol.11, pp.21-23.

Tavoularis, S.(1983)"Simple corrections for the temperature sensitivity of hot wires", Rev. Sci. Instrum., vol.54, pp.741-743.

Tavoularis, S.(1986)"Techniques for turbulence measurement", Encyclopedia of Fluid Mechanics, Vol. 1, ch. 36, N.P. Cheremisinoff (Editor), Gulf Publishing Company, Houston.

Tavoularis, S. and Corrsin, S.(1981a)"Experiments in nearly homogeous turbulent shear flow with a uniform mean temperature gradient: Part 1", J. Fluid Mech., vol.104, pp.311-347.

Tavoularis, S. and Corrsin, S.(1981b)"Experiments in nearly homogeous turbulent shear flow with a uniform mean temperature gradient: Part 2 The fine structure.", J. Fluid Mech., vol.104, pp.349-358.

Tavoularis, S. and Karnik U.(1989)"Further experiments on the evolution of turbulent stresses and scales in uniformly sheared turbulence", J. Fluid Mech.,

vol. 204, pp. 457-478.

Taylor, G.I. (1923)"Stability of a viscous liquid between two rotating cylinders",Phil. Trans. Roy. Soc. Lond., A223, pp.289-343.

Taylor, G.I.(1936)"Fluid friction between rotating cylinders", Proc. Roy. Soc. Lond., vol. A157, pp.546-578.

Townsend, A.A.(1976) "The Structure of Turbulent Shear Flow", ear Flow, Cambridge University Press, Cambridge.

Townsend, A.A.(1982)"Turbulent flow and the effects of curvature ", Structure of Complex Turbulent Shear Flow IUTAM Symp. Marseille, ed. R. Dumas and L. Fulachier, Springer, New York.

Watmuff, J.H., Witt, H.T. and Joubert, P.N.(1985)"Developing turbulent boundary layers with system rotation", J. Fluid Mech., vol. 157, pp.405 -448.

Wattendorf, F.L.(1935)"A study of the effect of curvature on fully developed turbulent flow", Proc. Roy. Soc. Lond., A148, pp.565-598.

Wendt, F.(1933)"Turbulente Stromungen Zwischen Zwei Rotierenden Konaxial Zylindren, Ing-Arch., vol. 4, pp.577-595.

Wilcken, H.(1930)"Effect of Curved Surfaces on Turbulent Boundary Layers", NASA TTF-11421.

Witt, H.T. and Joubert, P.N.(1985)"Effect of rotation on a turbulent wake", Fifth Symp. on Turbulent Shear Flows, Ithaca, New York, U.S.A.

Wyngaard, J.C., Tennekes,H., Lumley,J.L. and Margolis, D.P.(1968) "Struc-

ture of turbulence in a curved mixing layer", Phys. Fluids, vol.11, pp.1251-1253.

Wyngaard, J.C.(1968)"Measurement of small scale turbulence structure with hot wires", J. Sci. Instr., vol.1.

Yeh, T.T. and Van Atta, C.W. (1973)"Spectral transfer of scalar and velocity fields in heated-grid turbulence", J. Fluid Mech., vol.58, pp.233-261.

symbol	type	σ	M (mm)	d (mm)
G	parallel grid	.378	25.4	9.75
S1	woven screen	.26	12.7	1.76
S2	woven screen	.294	3.18	.70
S3	woven screen	.294	3.18	.70

Table 5.1: Specifications for the grid and screens used in the present study.

	$\frac{x_1}{h_s}$			
case	0.0	1.05	2.50	4.50
A	—	—	—	—
B	S2	—	—	—
C	S1	S2	—	—
D	G	S1	S2	—
E	G	S1	S2	S3

Table 5.2: Positioning of various grid/screen combinations used to produce the shear flows

case	symbol	U_c (m/s)	A (s^{-1})	k_s (m^{-1})	τ_{max}
NA	□	10.3	-64.	6.25	20.0
NB	○	9.8	-50.	5.00	16.0
NC	△	10.0	-30.	3.00	8.6
ND	◇	9.9	-15.	1.51	3.7
NE	⊠	9.4	-5.3	.56	1.0
PA	■	9.7	65.0	6.67	21.4
PB	●	9.6	53.0	5.56	17.8
PC	▽	9.8	29.0	3.00	8.6
PD	◆	9.7	13.0	1.33	3.2
PE	⊞	9.4	4.9	.526	.96

Table 5.3: The mean flow conditions for the straight section.

case	τ	K_{uu}	K_{vv}	K_{uuu}	K_{uv}	q^2 ($\frac{m^2}{s^2}$)	κ_q
NA	18.9	.50	.20	.30	.143	1.244	.083
NB	15.1	.48	.21	.31	.150	.5588	.073
NC	8.05	.46	.20	.33	.147	.1603	.113
ND	3.42	.50	.21	.29	.156	.5588	.069
NE	.92	.37	.28	.35	.168	.1023	—
PA	20.1	.50	.20	.30	-.135	1.454	.098
PB	16.8	.47	.21	.32	-.133	.6124	.072
PC	8.1	.46	.22	.32	-.133	.1670	.137
PD	3.0	.45	.23	.31	-.140	.4766	.083
PE	.87	.34	.31	.35	-.134	.1113	—

Table 5.4: The dimensionless Reynolds stresses in the straight section at $\frac{x_1}{h_s}$=9.91.

case	τ	L_{uu} (mm)	$\frac{L_{xx}}{L_{uu}}$	$\frac{L_{yy,w}}{L_{uu}}$	m_s (mm)	m_τ (mm)	κ_L	λ_u (mm)	$\frac{\lambda_x}{\lambda_u}$	$\frac{\lambda_{y,w}}{\lambda_u}$
NA	18.9	37.	.32	.38	.0429	.0021	.071	5.4	.52	.59
NB	15.1	29.	.32	.38	.0275	.0017	.074	5.6	.52	.59
NC	8.05	23.	.40	.42	.0138	.0013	.068	7.0	.56	.61
ND	3.42	82.	.34	.34	.0449	.0071	.112	9.9	.50	.56
NE	.92	73.	.56	.38	.106	.0321	1.15	10.3	.64	.71
PA	20.1	40.	.30	.36	.0452	.0022	.068	5.4	.52	.57
PB	16.8	27.	.32	.40	.0243	.0015	.061	5.3	.53	.60
PC	8.05	23.	.39	.42	.0118	.0013	.059	6.7	.57	.60
PD	3.01	80.	.36	.37	.0518	.0206	.1734	9.4	.53	.60
PE	.868	52.	.59	.52	.0406	.7937	.5207	9.9	.70	.74

Table 5.5: The integral lengthscales and Taylor microscales for the straight section at $\frac{z_1}{h_s}$=9.9.

	$\frac{z}{h_c}$=.417					$\frac{z}{h_c}$=5.42			
case	U_c (m/s)	A (s^{-1})	k_s (m^{-1})	S		U_c (m/s)	A (s^{-1})	k_s (m^{-1})	S
NA	10.2	-61.	6.67	-.03		10.6	-51.	5.00	-.04
NB	9.8	-50.	5.00	-.04		9.8	-46.	5.00	-.04
NC	9.9	-30.	2.86	-.07		10.0	-26.	2.5	-.08
ND	9.8	-16.	1.67	-.12		9.7	-11.	1.11	-.18
NE	9.5	-6.1	.625	-.31		9.5	-6.2	.67	-.30
PA	10.1	64.	6.67	.03		10.1	61.	6.67	.03
PB	10.3	52.	5.00	.04		10.3	50.	5.00	.04
PC	10.3	27.	2.86	.07		10.3	26.	2.50	.08
PD	10.4	11.	1.11	.18		10.5	9.5	.91	.22
PE	9.6	3.0	.312	.64		9.9	1.6	.167	1.2

Table 5.6: The mean flow conditions in the mildly curved section, R_c=5 m.

	$\frac{s}{h_c}$=.417					$\frac{s}{h_c}$=4.74			
case	U_c (m/s)	A (s^{-1})	k_s (m^{-1})	S		U_c (m/s)	A (s^{-1})	k_s (m^{-1})	S
NA	10.1	-64.	6.25	-.08		11.4	-60.	5.00	-.10
NB	9.7	-52.	5.55	-.09		10.0	-54.	5.55	-.09
NC	9.6	-31.	3.33	-.15		10.3	-31.	3.12	-.16
ND	9.6	-19.	1.92	-.26		10.4	-17.	1.67	-.30
NE	9.1	-9.3	1.02	-.49		9.7	-9.1	.91	-.53
PA	10.2	65.	6.25	.08		10.5	64.	6.25	.08
PB	10.6	53.	5.00	.10		10.8	52.	5.00	.10
PC	11.0	30.	.36	.18		11.0	30.	2.79	.18
PD	10.2	7.8	1.3	.65		11.2	9.0	.83	.62
PE	9.6	.15	64.	32.		10.4	.15	.50	35.

Table 5.7: The mean flow conditions in the strongly curved section, R_c=2 m.

S	ρ	$\frac{u^3}{u'^3}$	$\frac{v^3}{v'^3}$	$\frac{w^3}{w'^3}$	$\frac{u^2v}{u'^2v'}$	$\frac{uv^2}{u'v'^2}$	$\frac{u^2w}{u'^2w'}$	$\frac{uw^2}{u'w'^2}$		
-.10	.50	-.141	-.063	-.100	-.051	-.061	.016	.001		
.10	-.30	-.051	.053	-.003	.037	-.037	.002	-.021		
Gaussian	—	0	0	0	0	0	0	0		
S	ρ	$\frac{u^4}{u'^4}$	$\frac{v^4}{v'^4}$	$\frac{w^4}{w'^4}$	$\frac{u^3v}{u'^3v'}$	$\frac{u^2v^2}{u'^2v'^2}$	$\frac{uv^3}{u'v'^3}$	$\frac{u^3w}{u'^3w'}$	$\frac{u^2w^2}{u'^2w'^2}$	$\frac{uw^3}{u'w'^3}$
-.10	.50	2.94	3.14	3.13	1.42	1.49	1.44	-.168	1.03	-.176
Gaussian	—	3	3	3	1.5	1.5	1.5	0	1.0	0
.10	-.30	2.99	3.28	3.17	-.911	1.22	-.945	-.128	.999	-.128
Gaussian	—	3	3	3	-.9	1.18	-.9	0	1.0	0.0

Table 5.8: Typical values of the higher order moments in the curved shear flow; Case B, $\frac{s}{h_c}$=3.01, n=0, z=0, R_c=2m.

case	straight flow symbol	S	symbol	S	symbol
NA		-.03		-.08	
NB		-.04		-.09	
NC		-.07		-.15	
ND		-.12		-.26	
NE		-.31		-.49	
PA		.03		.08	
PB		.04		.10	
PC		.07		.18	
PD		.18		.65	
PE		.64		1.	

Table 6.1: Symbols for the Figures of Chapter 6.

case	R_L	$\frac{u'}{AL_{uu}}$	R_λ	$\frac{\epsilon}{Aq^2}^*$	$\frac{\epsilon}{-\overline{uv}A(1-S)}^+$
NA	1920.	.33	280.	.12	.70
NB	990.	.36	190.	.14	.76
NC	410.	.39	130.	.14	.62
ND	2800.	.41	340.	.15	.78
NE	980.	.51	140.	.30	1.0
PA	2260.	.33	310.	.12	.65
PB	970.	.38	190.	.14	.72
PC	430.	.42	130.	.16	.47
PD	2520.	.45	300.	.18	.89
PE	700.	.78	130.	.32	1.0

Table 6.2: Some dimensionless parameters for straight shear flow. * ϵ estimated from the measurements of λ_u and the isotropic relation for dissipation, + ϵ from balance of the kinetic energy equation.

case	S	K_{uu}	K_{vv}	K_{ww}	K_{uv}	$\frac{q^2}{\frac{m^2}{s^2}}$	κ_q
NA	-.03	.51	.20	.30	.153	3.2704	.118
NB	-.04	.51	.21	.28	.154	1.1706	.139
NC	-.07	.47	.23	.31	.167	.2793	.198
ND	-.12	.47	.26	.27	.204	.6602	.137
NE	-.31	.37	.33	.30	.218	.1096	.270
PA	.03	.49	.20	.31	-.119	1.8179	.014
PB	.04	.48	.21	.31	-.118	.6665	.004
PC	.07	.47	.21	.31	-.102	.1716	-.018
PD	.18	.50	.21	.29	-.073	.3790	-.268
PE	.64	.40	.26	.34	-.085	.0892	-.7911

Table 6.3: The Reynolds stresses in the mildly curved section, R_c=5 m, $\frac{s}{H}$=4.58

case	S	K_{uu}	K_{vv}	K_{ww}	K_{uv}	$\frac{q^2}{\frac{m^2}{s^2}}$	κ_q
NA	-.08	.49	.22	.29	.164	3.4481	.204
NB	-.09	.50	.23	.28	.167	1.3830	.251
NC	-.15	.42	.25	.33	.185	.2991	.332
ND	-.26	.41	.30	.29	.219	.8185	.344
NE	-.49	.31	.37	.32	.208	.1313	.531
PA	.08	.48	.20	.31	-.108	1.3773	-.054
PB	.10	.48	.21	.31	-.096	.5356	-.076
PC	.18	.47	.20	.32	-.064	.2038	-.126
PD	.65	.51	.20	.29	-.009	.4003	-.379
PE	32.	.42	.24	.34	-.048	.0927	-.457

Table 6.4: The Reynolds stresses in the strongly curved section, R_c=2 m, $\frac{s}{H}$=3.01

case	S	L_{uu} (mm)	$\frac{L_{vvv}}{L_{uu}}$	$\frac{L_{www}}{L_{uu}}$	m_s (mm)	m_r (mm)	κ_L	λ_u (mm)	$\frac{\lambda_v}{\lambda_u}$	$\frac{\lambda_w}{\lambda_u}$
NA	-.03	68.	.38	.30	6.54	4.08	.069	5.7	.53	.61
NB	-.04	54.	.34	.30	5.67	.472	.109	6.0	.50	.57
NC	-.07	33.	.44	.37	2.47	3.60	.120	6.6	.56	.62
ND	-.12	110.	.52	.30	4.95	12.3	.114	9.3	.56	.58
NE	-.31	88.	.70	.37	3.26	21.7	.254	10.3	.73	.71
PA	.03	35.	.34	.50	—	—	—	5.3	.51	.60
PB	.04	25.	.33	.51	—	—	—	5.3	.51	.60
PC	.07	19.	.37	.52	—	—	—	6.1	.54	.61
PD	.18	50.	.33	.51	—	—	—	8.8	.49	.57
PE	.64	46.	.45	.57	—	—	—	10.0	.60	.67

Table 6.5: The integral and micro scales for mildly curved section, R_c=5 m. $\frac{s}{H}$=4.58

case	S	L_{uu} (mm)	$\frac{L_{vvv}}{L_{uu}}$	$\frac{L_{www}}{L_{uu}}$	m_s (mm)	m_r (mm)	κ_L	λ_u (mm)	$\frac{\lambda_v}{\lambda_u}$	$\frac{\lambda_w}{\lambda_u}$
NA	-.08	71.	.51	.31	10.9	7.25	.103	5.7	.54	.63
NE	-.09	53.	.47	.32	10.8	8.14	.148	6.1	.52	.59
NC	-.15	33.	.59	.39	4.66	5.83	.162	6.7	6.3	.66
ND	-.26	111.	.64	.35	8.65	18.8	.164	9.5	.64	.62
NE	-.49	83.	.69	.42	6.13	25.04	.299	10.9	.82	.78
PA	.08	27.	.37	.57	—	—	—	5.0	.52	.62
PB	.10	20.	.35	.58	—	—	—	5.1	.51	.61
PC	.18	19.	.36	.54	—	—	—	5.9	.52	.63
PD	.65	56.	.29	.46	—	—	—	8.8	.48	.57
PE	32.	41.	.43	.58	—	—	—	10.0	.56	.66

Table 6.6: The integral and micro scales for strongly curved section, R_c=2 m, $\frac{s}{H}$=3.01

S	$\frac{L_{xx}}{\mathcal{L}}$	E^*	$\frac{\epsilon}{-\overline{uv}A(1-S)}^+$		S	$\frac{L_{xx}}{\mathcal{L}}$	E^*	$\frac{\epsilon}{-\overline{uv}A(1-S)}^+$
-.03	2.31	.12	.64		.03	1.66	.12	.94
-.04	2.50	.13	.55		.04	1.59	.15	1.00
-.07	1.87	.13	.55		.07	1.24	.21	1.10
-.08	2.44	.11	.41		.08	1.5	.13	1.27
-.09	2.36	.12	.32		.10	1.45	.16	1.42
-.12	2.17	.15	.69		.18	1.26	.20	2.28
-.15	1.87	.14	.24		.18	.89	.26	3.33
-.26	2.33	.11	.38		.64	.46	.60	14.7
-.31	1.63	.15	.69		.65	.69	.38	55.
-.49	2.13	.17	.15		1.0	20.2	12.6	—

Table 6.7: Some dimensionless parameters for curved shear flow. * ϵ estimated from the measurements of λ_u and the isotropic relation for dissipation, + ϵ from balance of the kinetic energy equation.

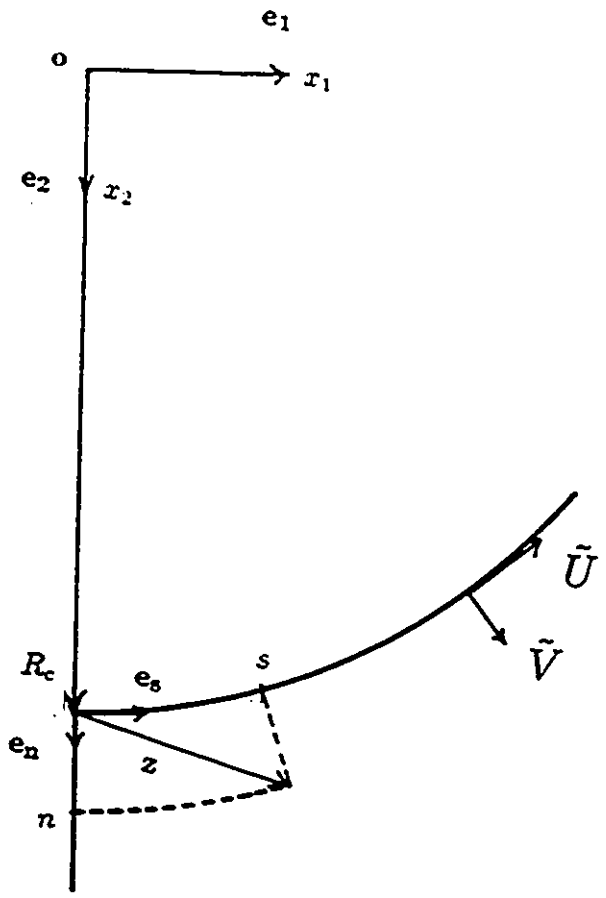

Figure 2.1: The curvilinear coordinate system.

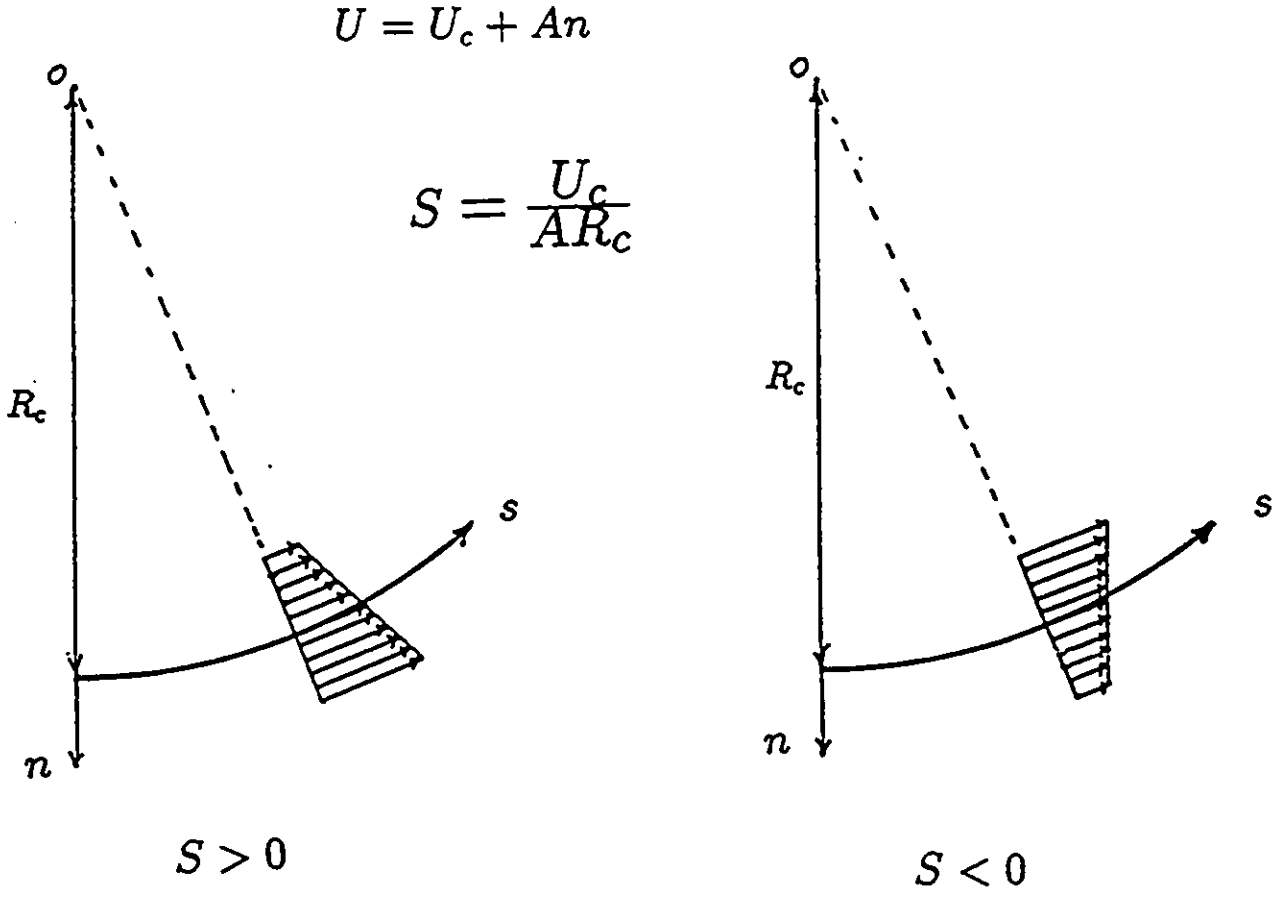

Figure 3.1: The simple curved shear flow a) positive shear b) negative shear.

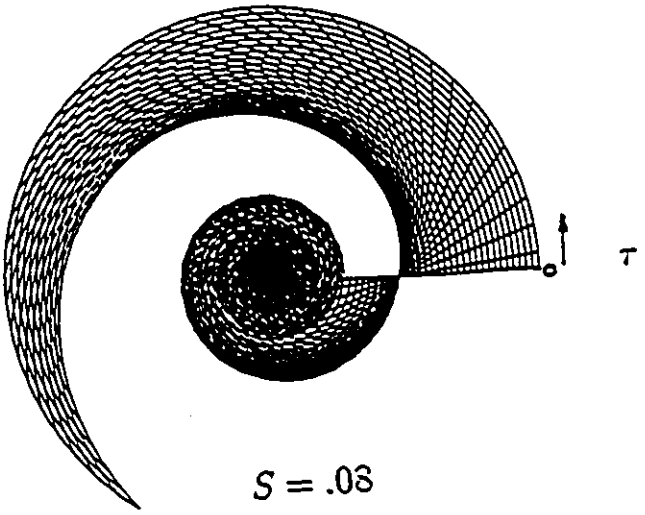

a)

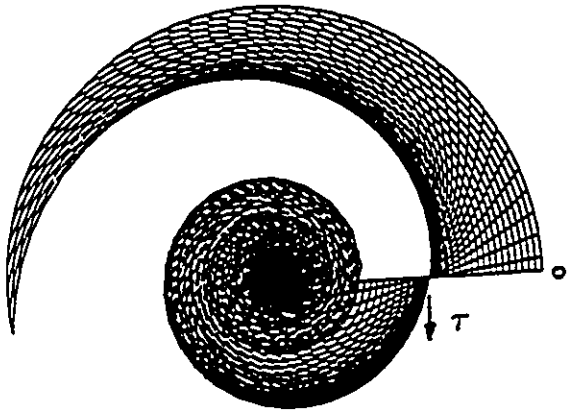

b)

Figure 3.2: Successive positions of material lines in curved shear flow a) positive shear b) negative shear.

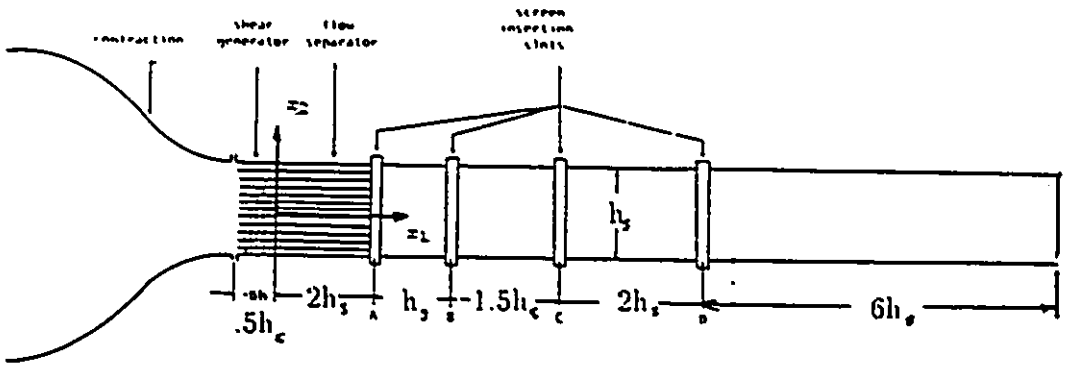

Figure 4.1: The existing wind tunnel facility (after Karnik, 1983),h_s =30 mm.

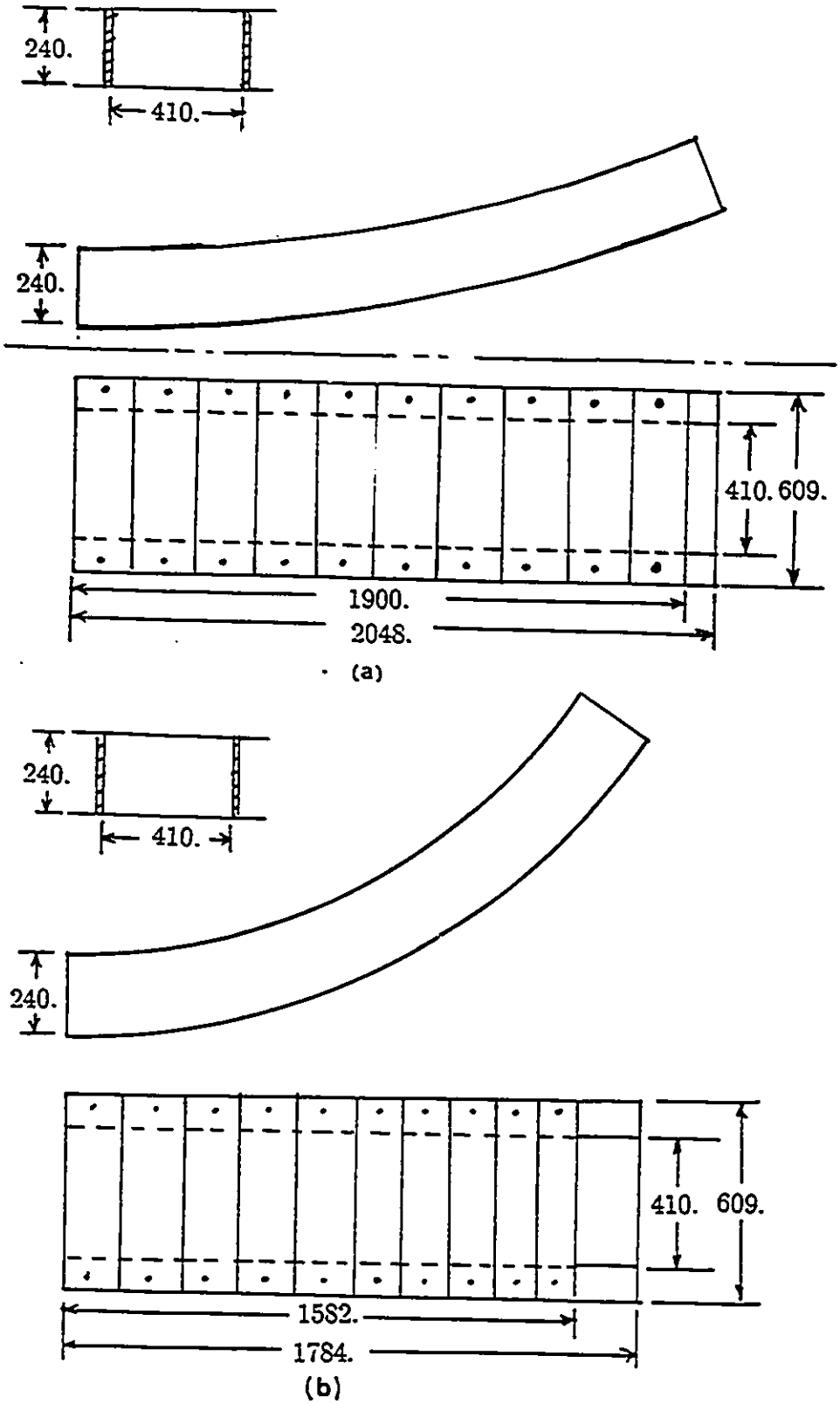

Figure 4.2: The curved test sections a) mild curvature, R_c=5 m b) strong curvature, R_c =2 m.

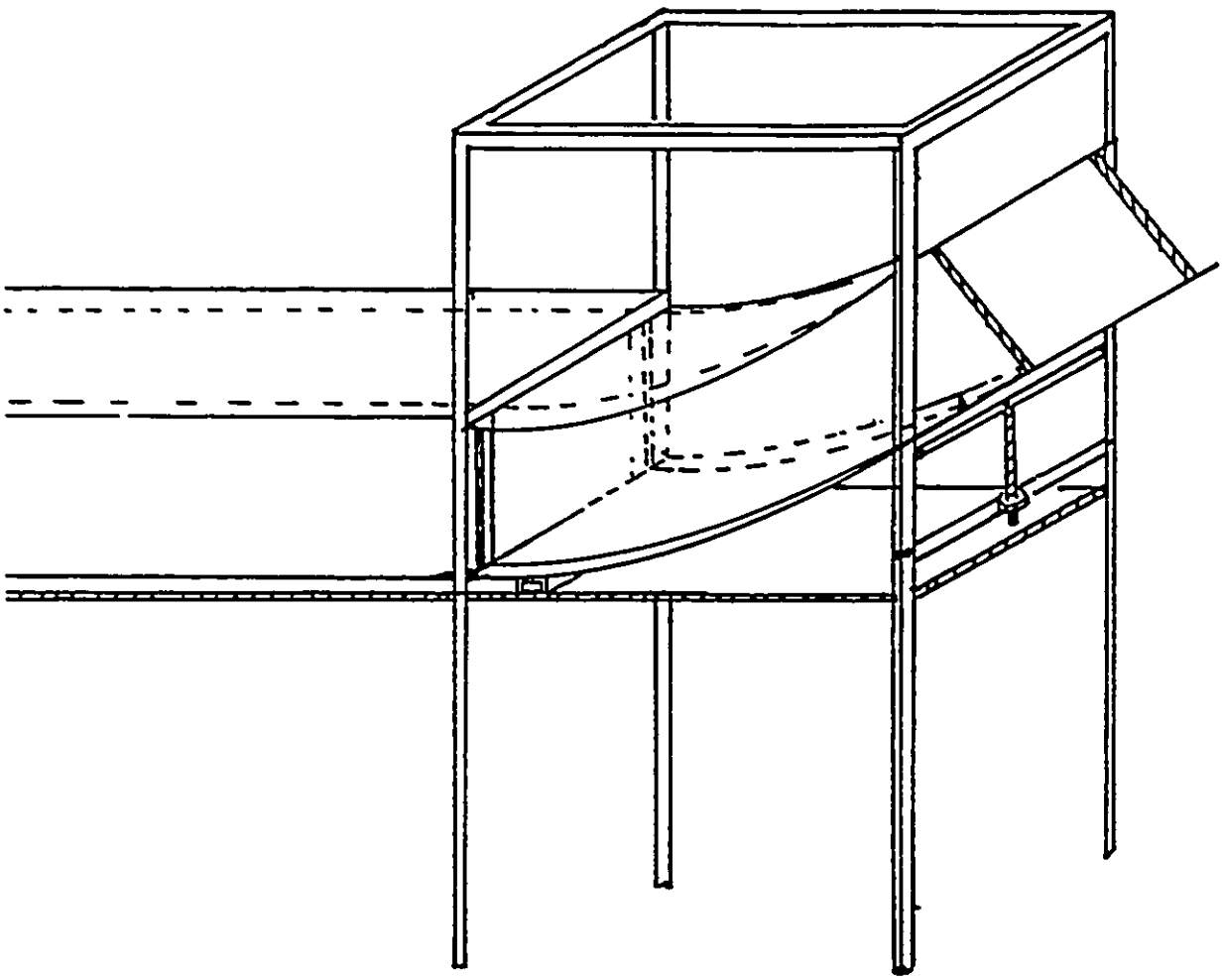

Figure 4.3: The connection between the straight and curved test sections.

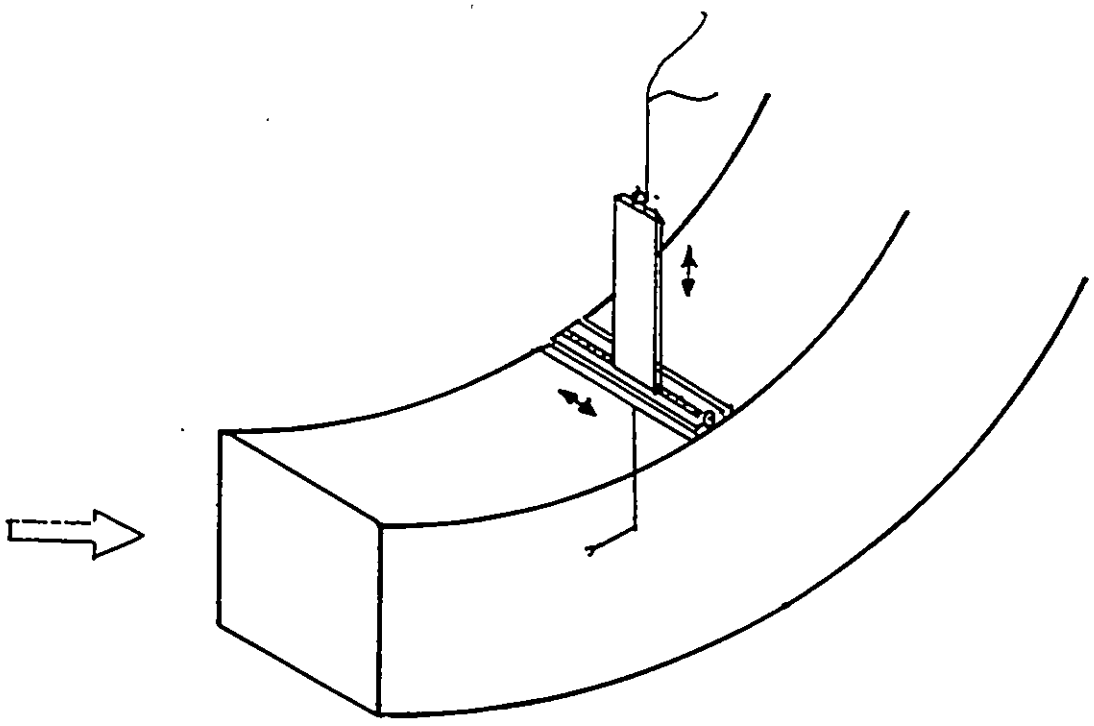

Figure 4.4: Probe support and traversing mechanism.

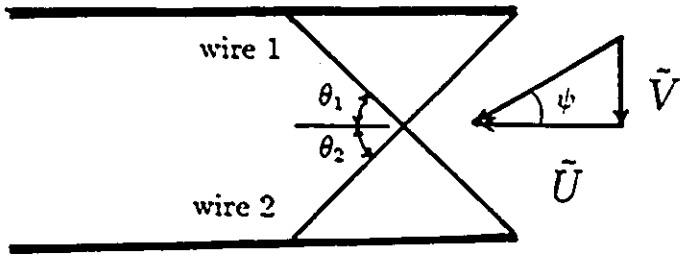

(a)

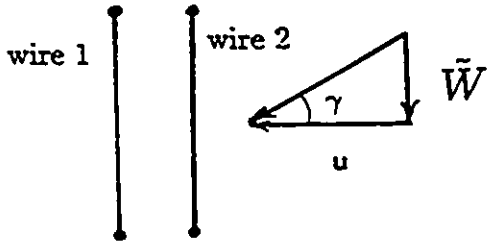

(b)

Figure 4.5: The relationship between the cross wire geometry and the air velocity a) the s, n plane b) the n, z plane.

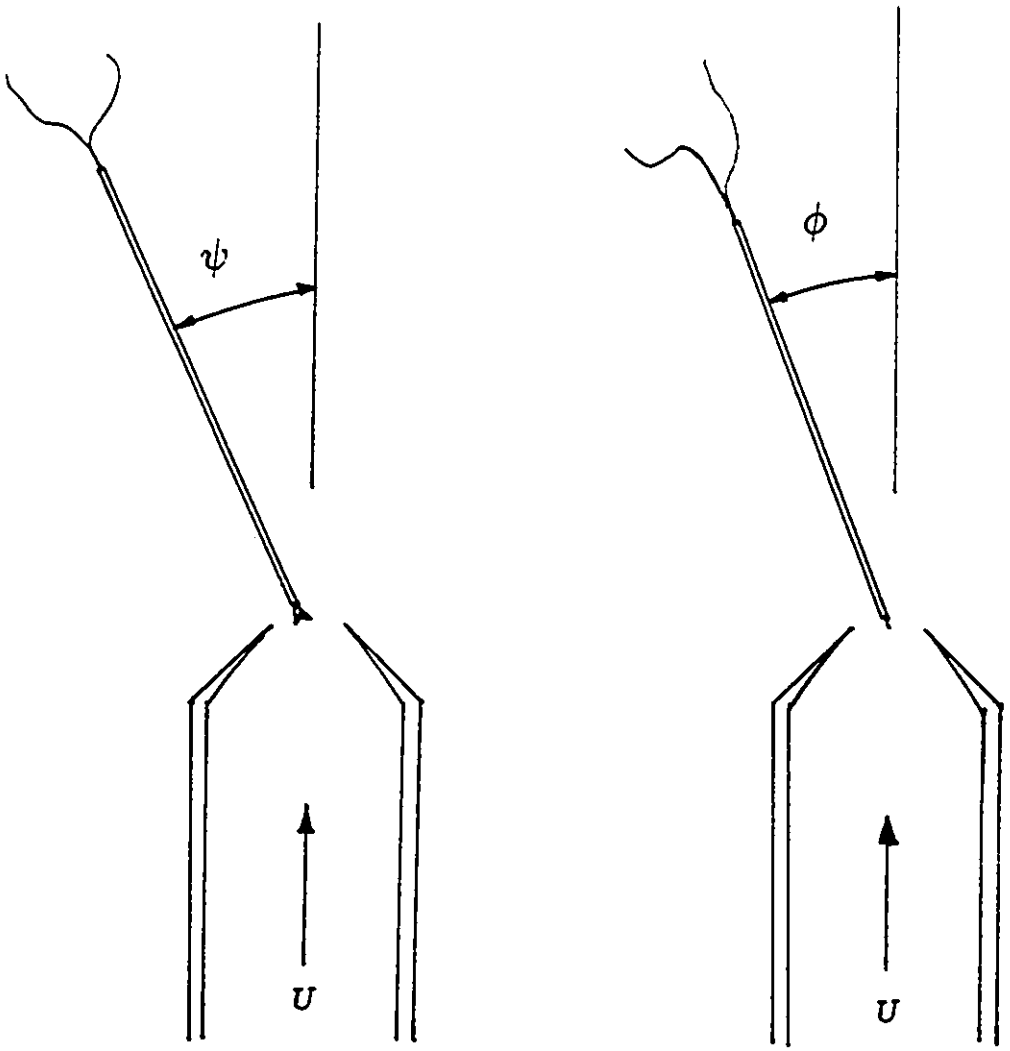

Figure 4.6: The arrangement for testing the directional sensitivity of the cross-wire array a) pitching the probe b) yawing the probe.

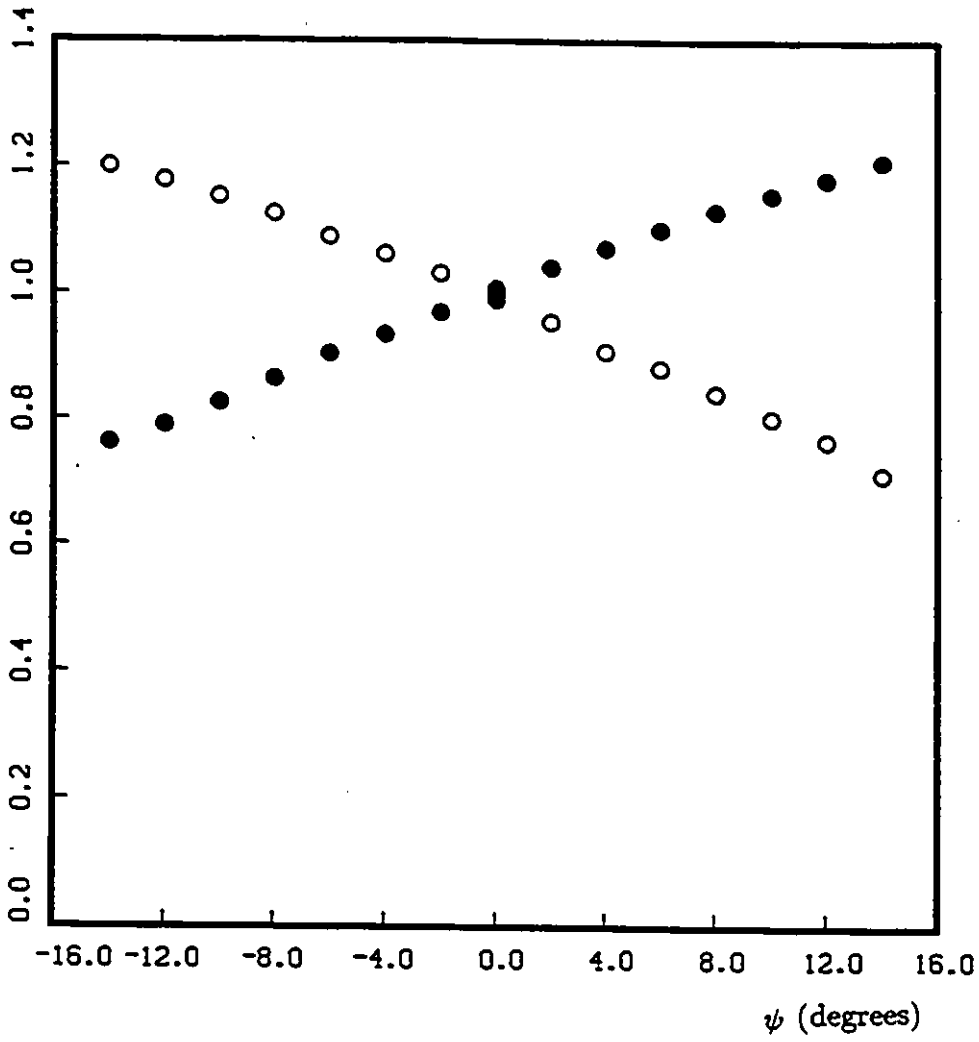

Figure 4.7: The effect of pitch angle on the effective cooling velocity for the cross wire array; o F_1, • F_2.

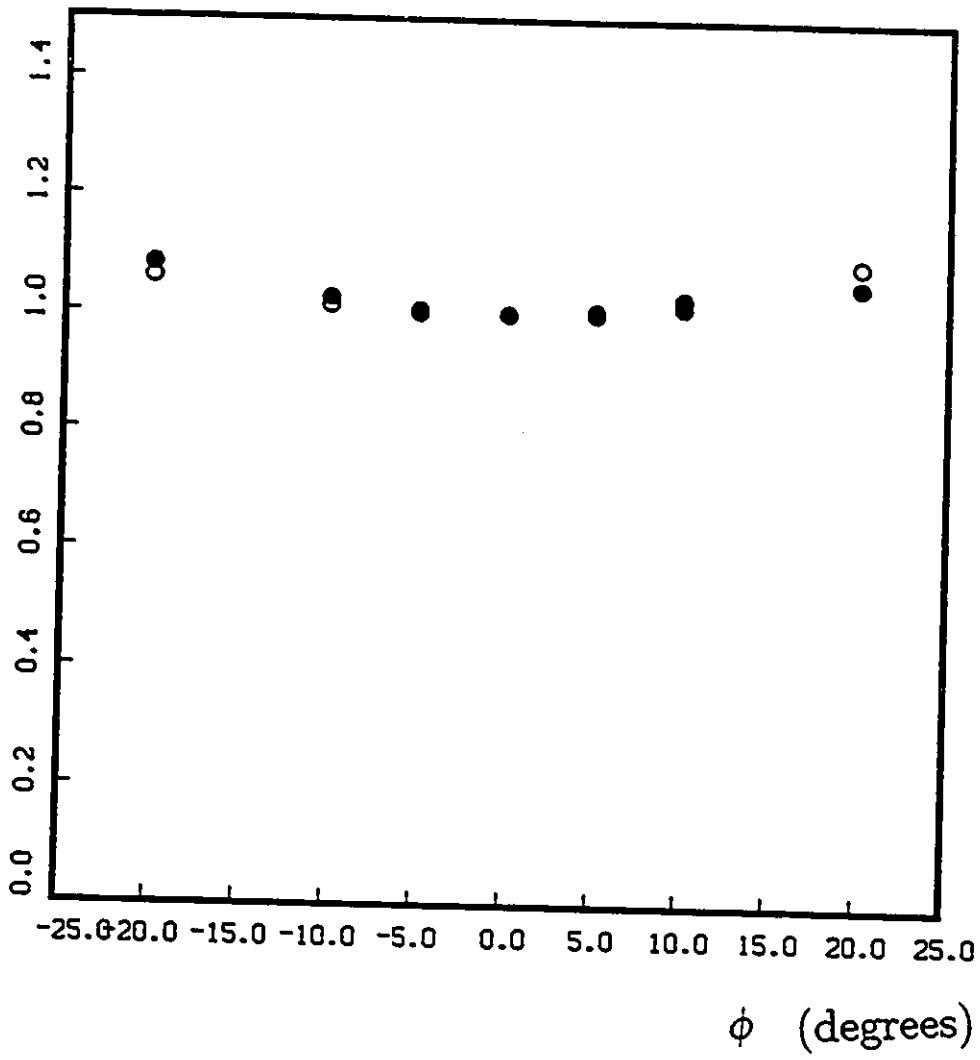

Figure 4.8: The effect of yaw angle on the effective cooling velocity for the cross wire array; o $\frac{U_{eff1}}{U_j}$, • $\frac{U_{eff2}}{U_j}$.

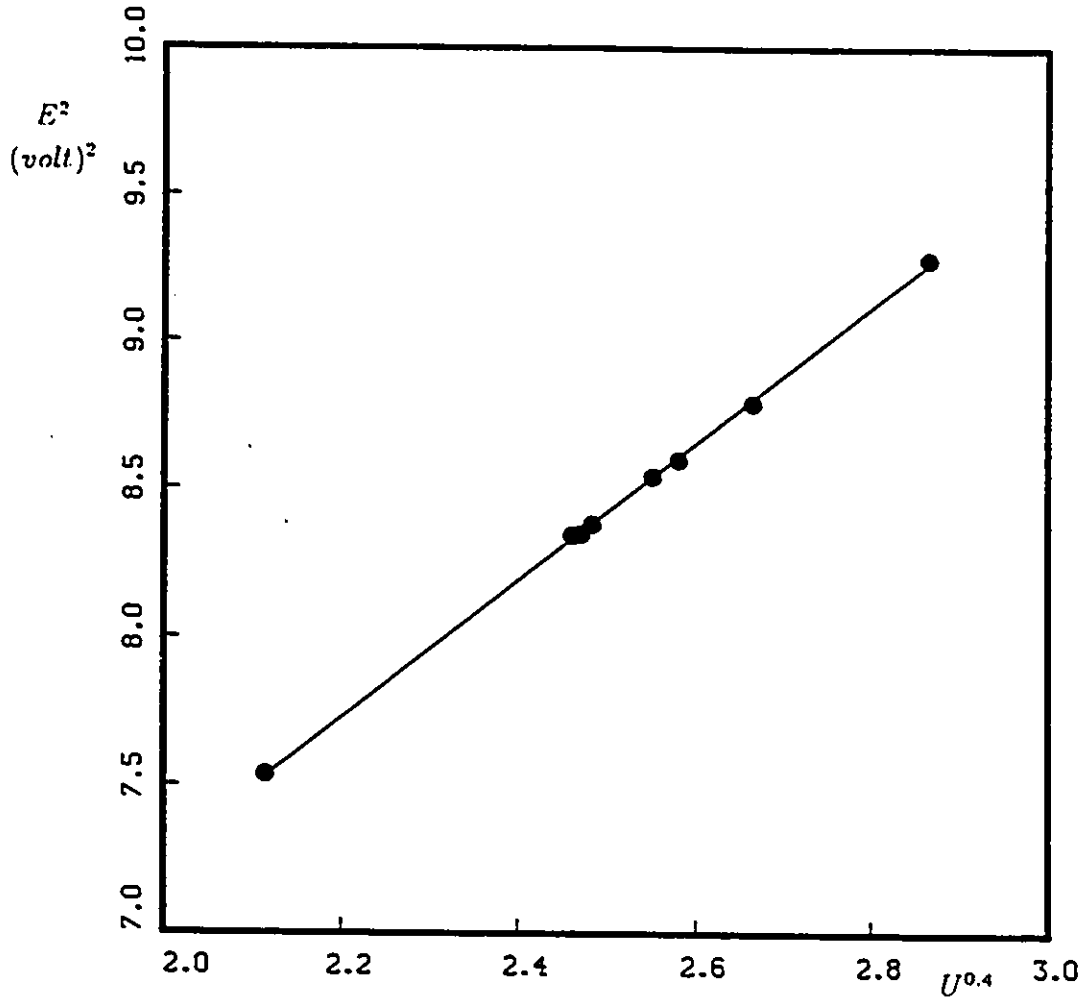

Figure 4.9: A typical calibration curve for the hot wire anemometer, solid line is a least squares fit of the data.

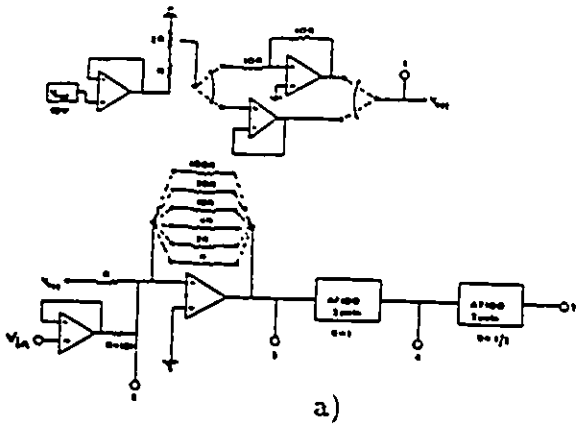

a)

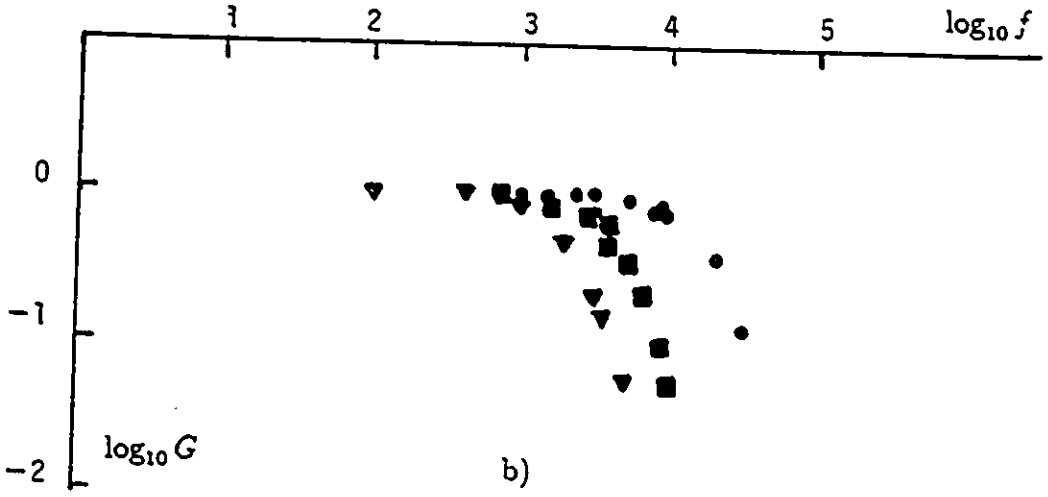

b)

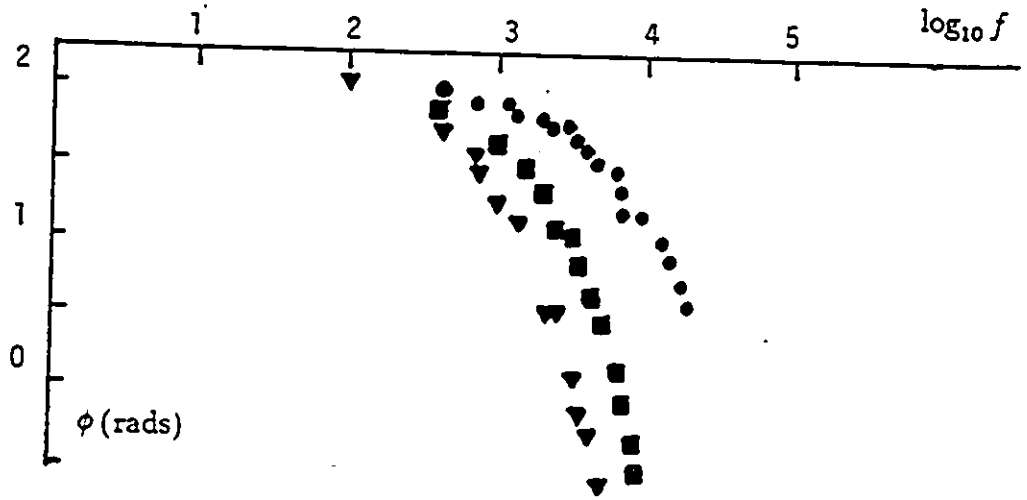

c)

Figure 4.10: The electronic circuit for signal conditioning.

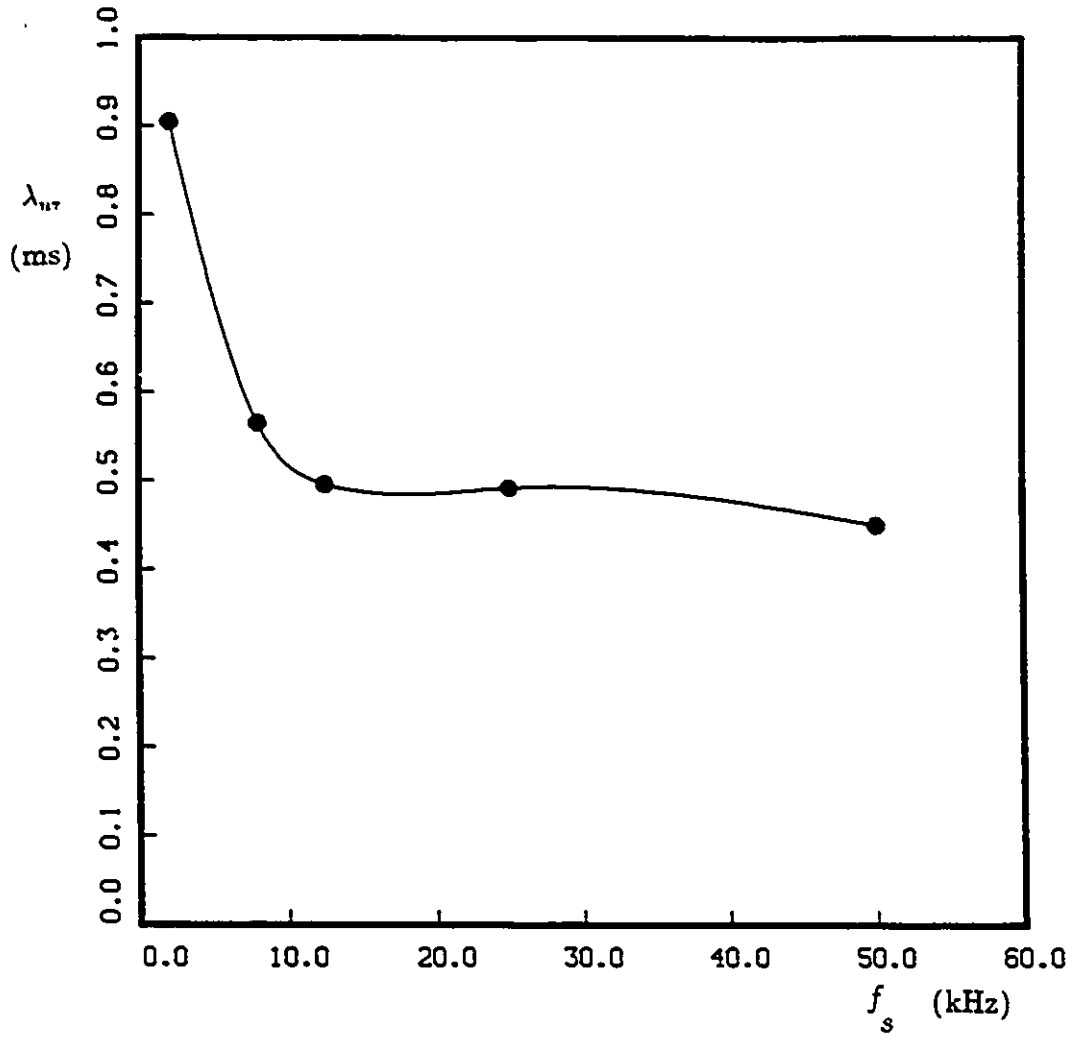

Figure 4.11: The effect of sampling frequency on the measured value of Taylor's microscale; the signal has been low pass filtered to 10kHz.

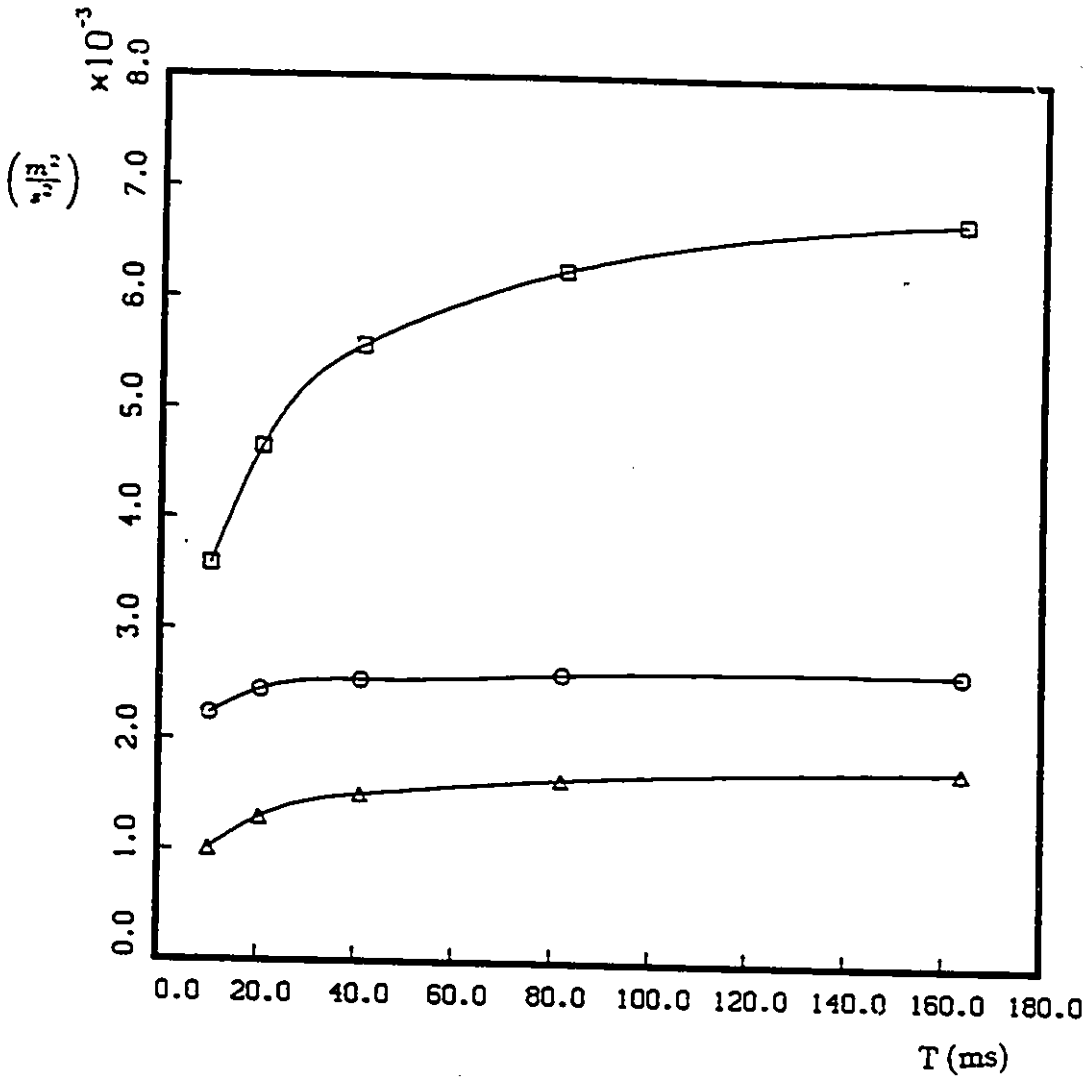

Figure 4.12: The effect of record length onthe measured value of the stresses; the signal has been low-pass filtered to 10kHz and the sampling frequency was 25 kHz. □ $\overline{u^2}$, o $\overline{v^2}$, △ $\overline{uv}$.

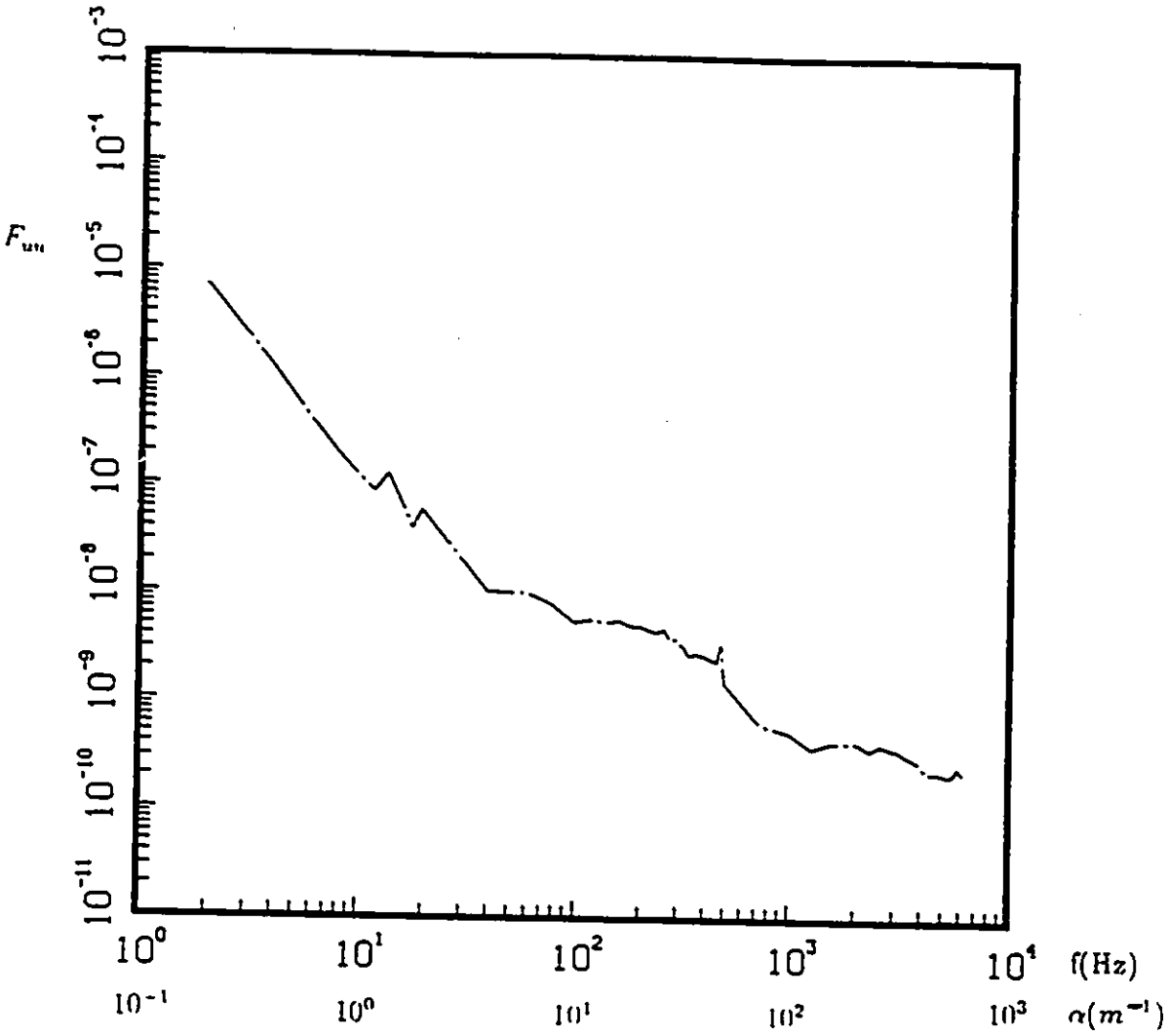

Figure 4.13: The power spectral density of the "noise" in the free stream.

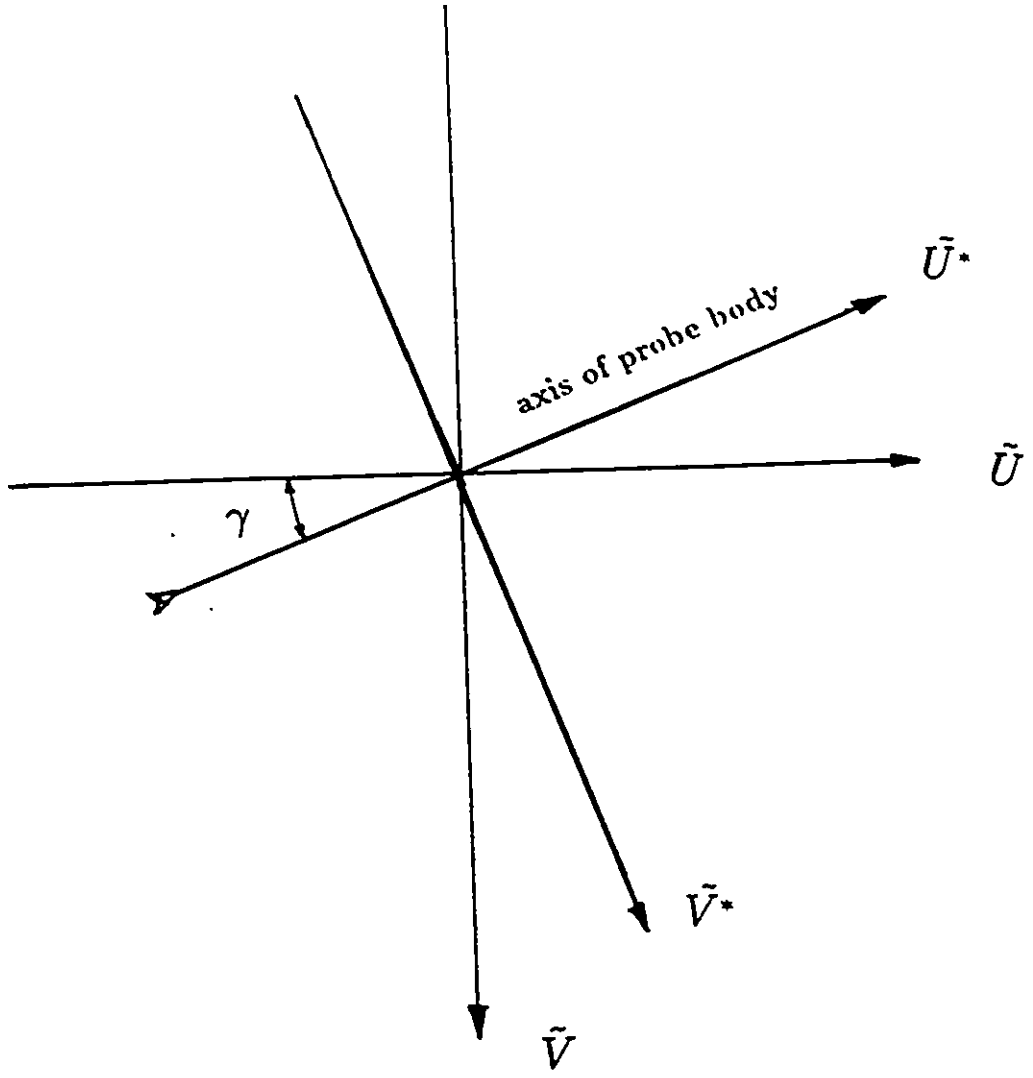

Figure 4.14: Rotation of the s,n plane.

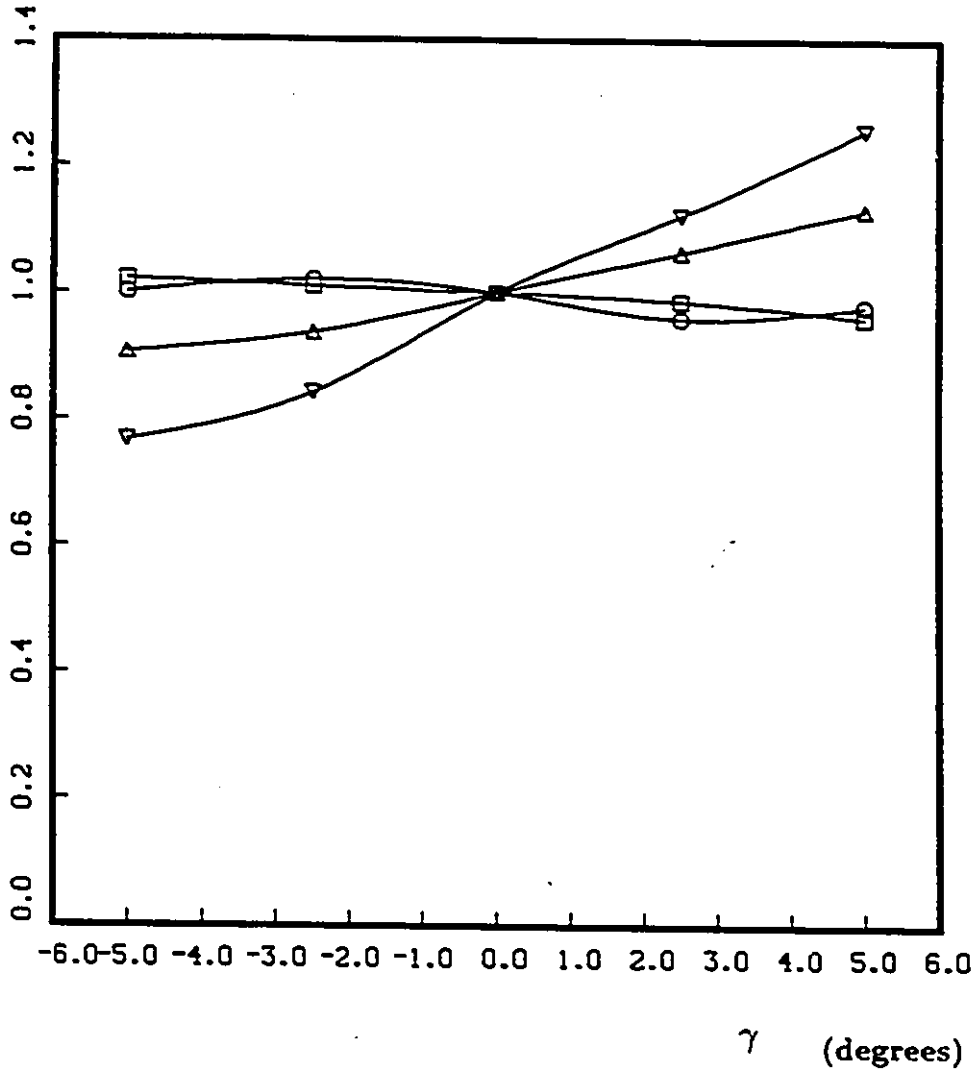

Figure 4.15: The effect of pitching the cross wire array on the mean velocity and Reynolds stresses in curved shear flow. □ U, o $\overline{u^2}$, △ $\overline{v^2}$, ▽ $\overline{uv}$.

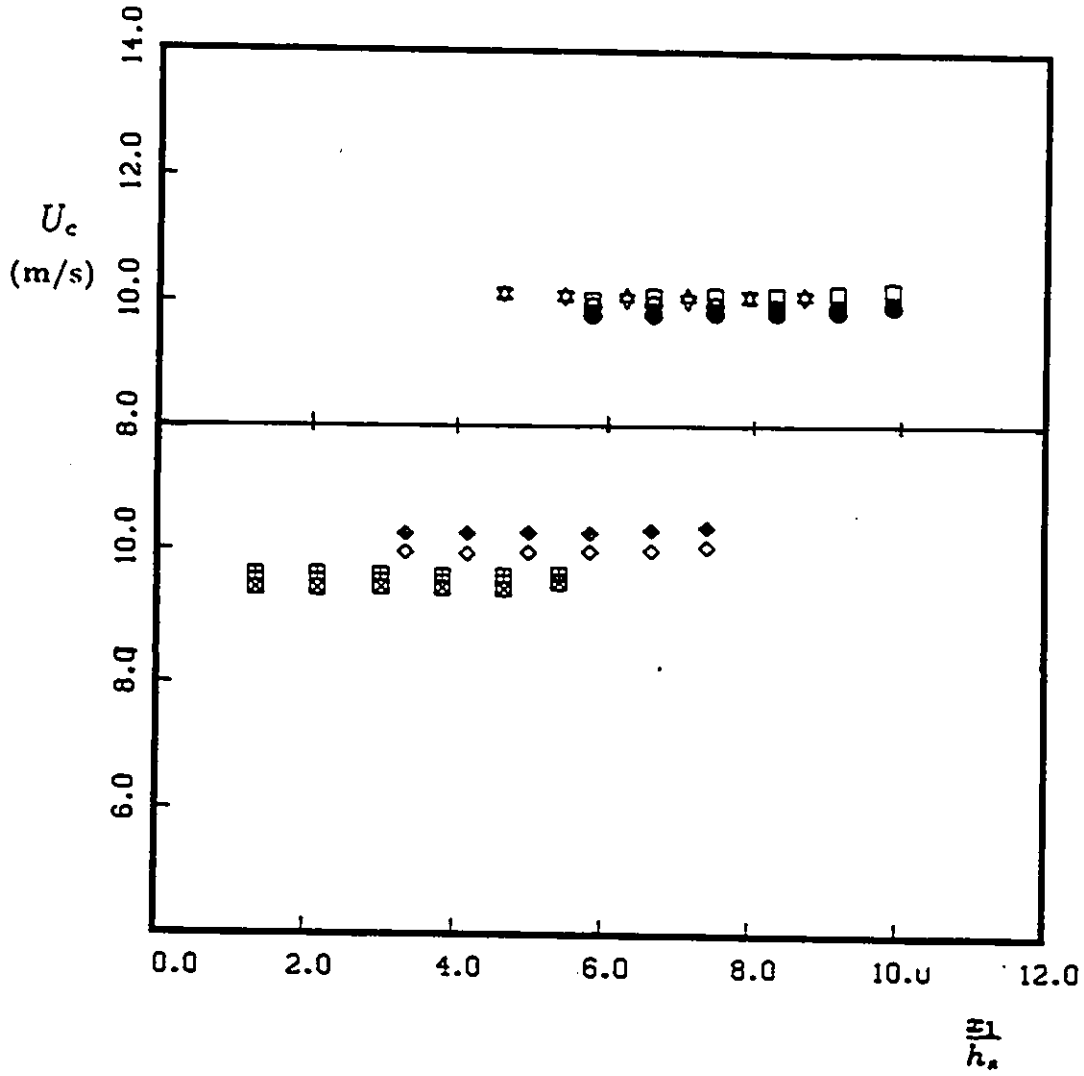

Figure 5.1: Streamwise development of U_c in the straight section, Symbols as in Table 5.3.

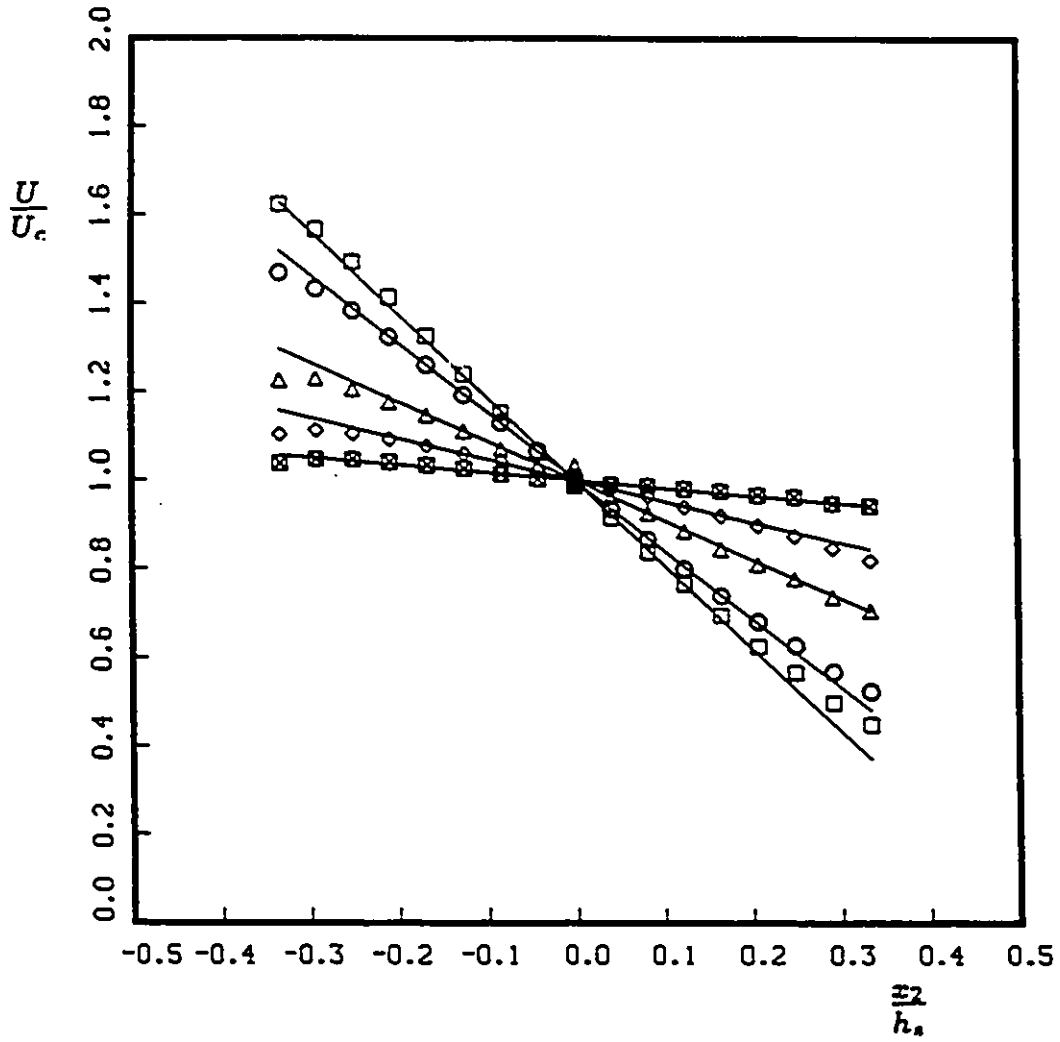

Figure 5.2: Transverse profiles of $\frac{U}{U_c}$ in the straight section; $\frac{x_1}{h_s}$=9.9, x_3=0. Symbols as in Table 5.3.

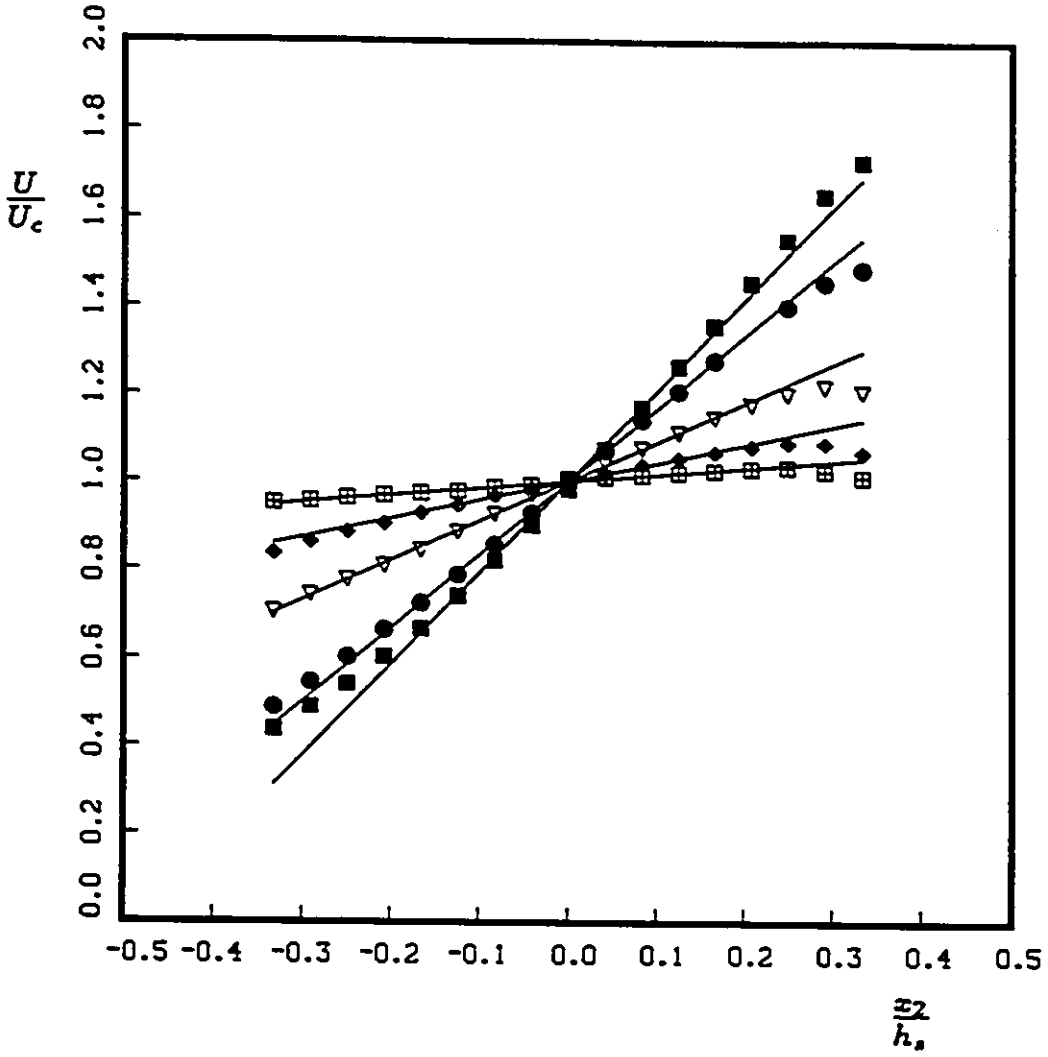

Figure 5.3: Transverse profiles of $\frac{U}{U_c}$ in the straight section; $\frac{x_1}{h_s}$=9.9, x_3=0. Symbols as in Table 5.3.

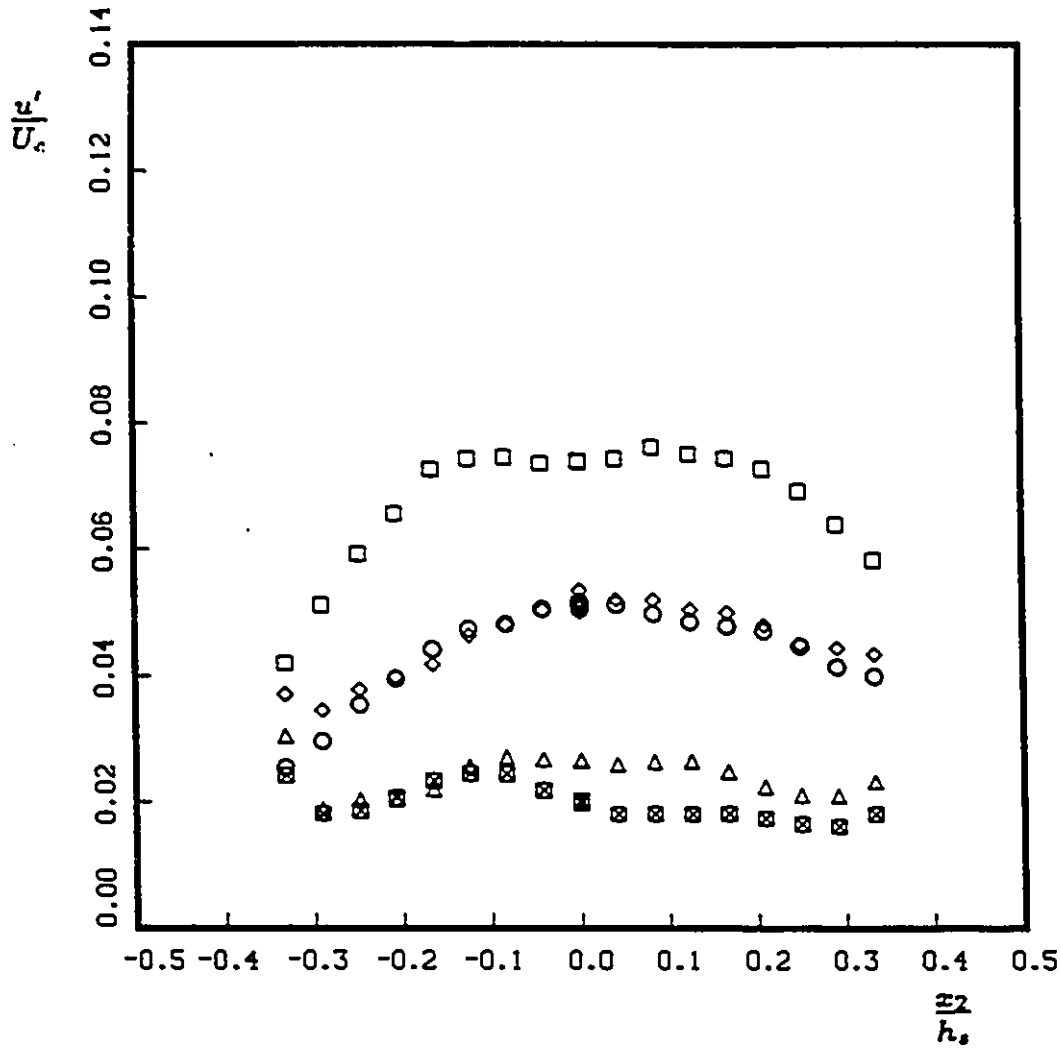

Figure 5.4: Transverse variation of $\frac{u'}{U_c}$ in the straight section, negative shear; $\frac{x_1}{h_s}$=9.9, x_3=0. Symbols as in Table 5.3.

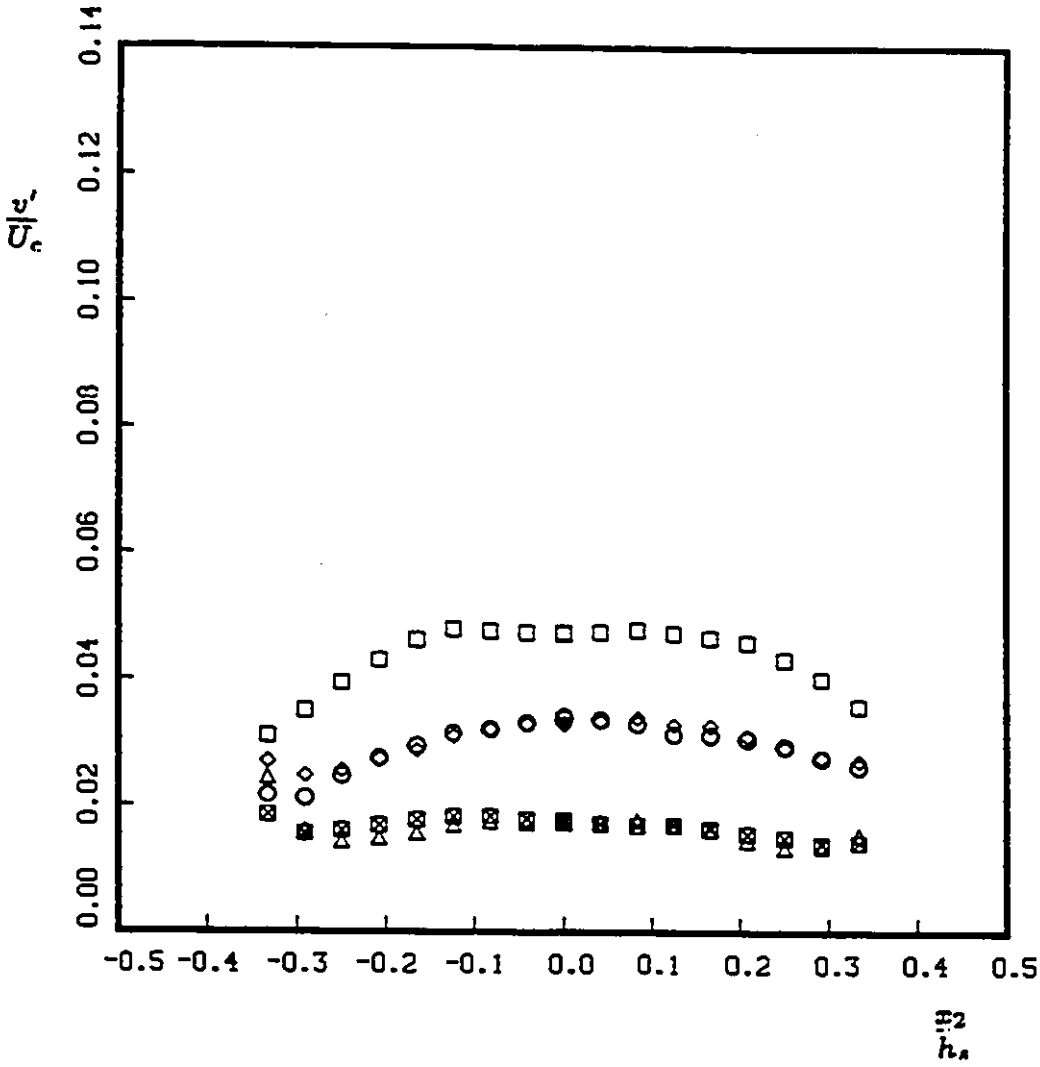

Figure 5.5: Transverse variation of $\frac{v'}{U_c}$ in the straight section, negative shear; $\frac{x_1}{h_s}$=9.9, x_3=0. Symbols as in Table 5.3.

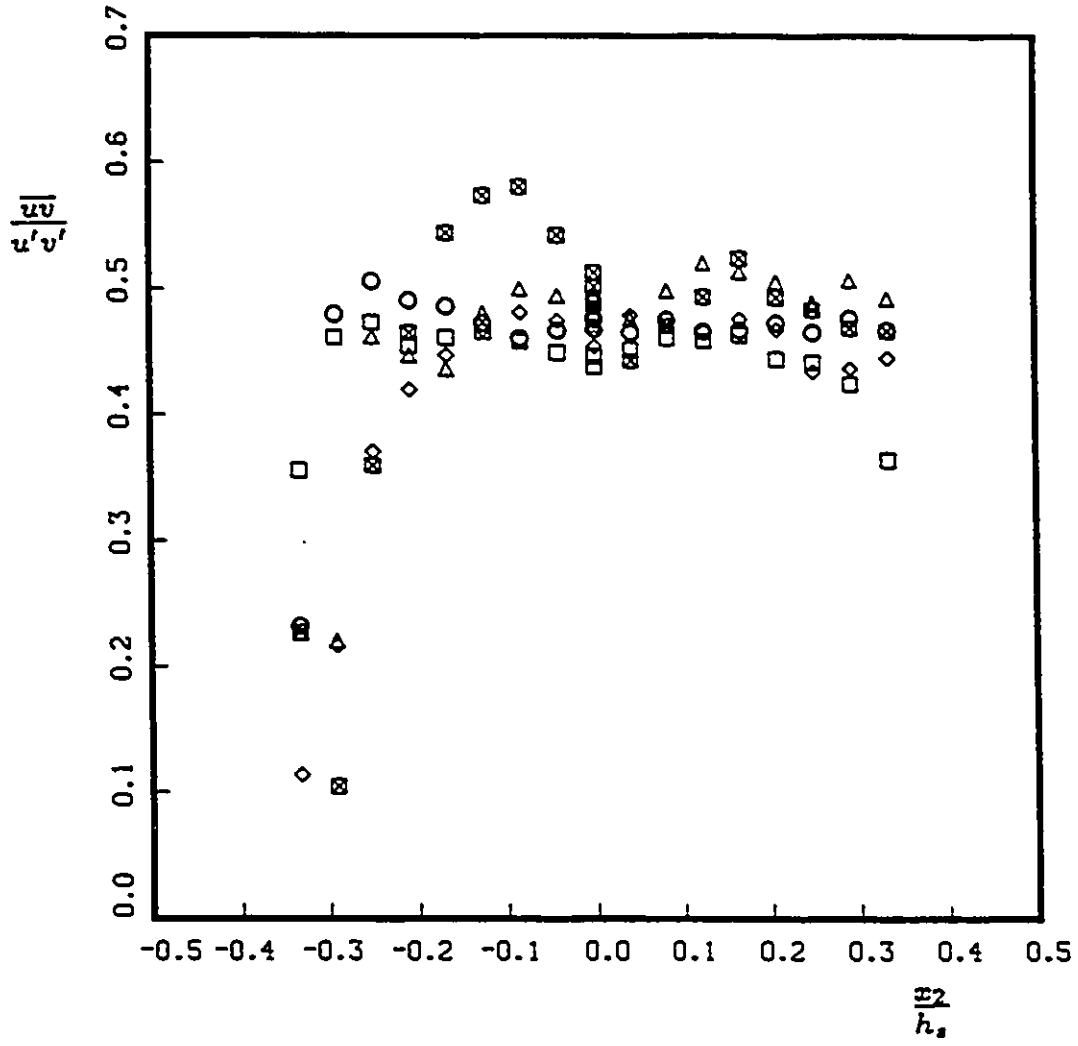

Figure 5.6: Transverse variation of $\frac{\overline{uv}}{u'v'}$ in the straight section, negative shear; $\frac{x_1}{h_s}$=9.9, x_3=0. Symbols as in Table 5.3.

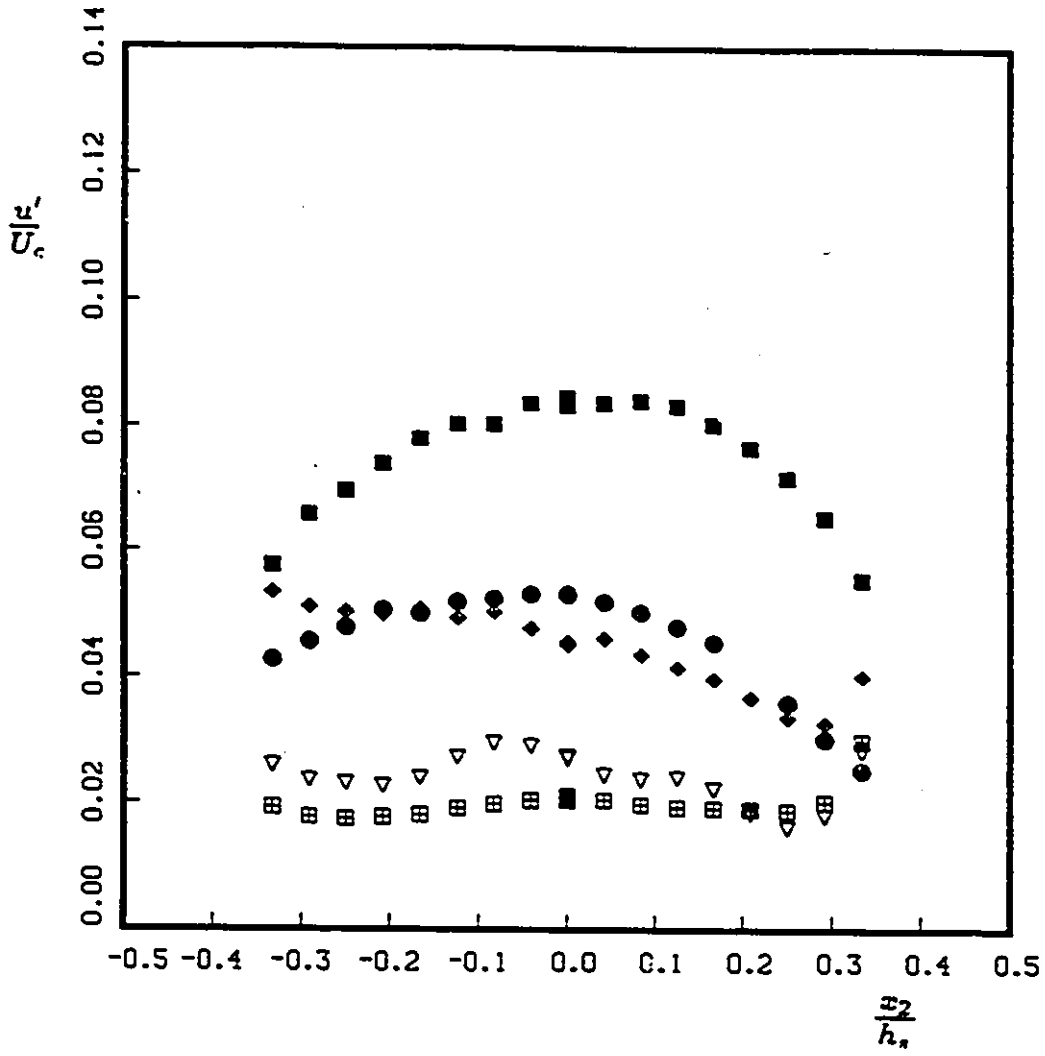

Figure 5.7: Transverse variation of $\frac{u'}{U_c}$ in the straight section, positive shear; $\frac{x_1}{h_s}$=9.9, x_3=0. Symbols as in Table 5.3.

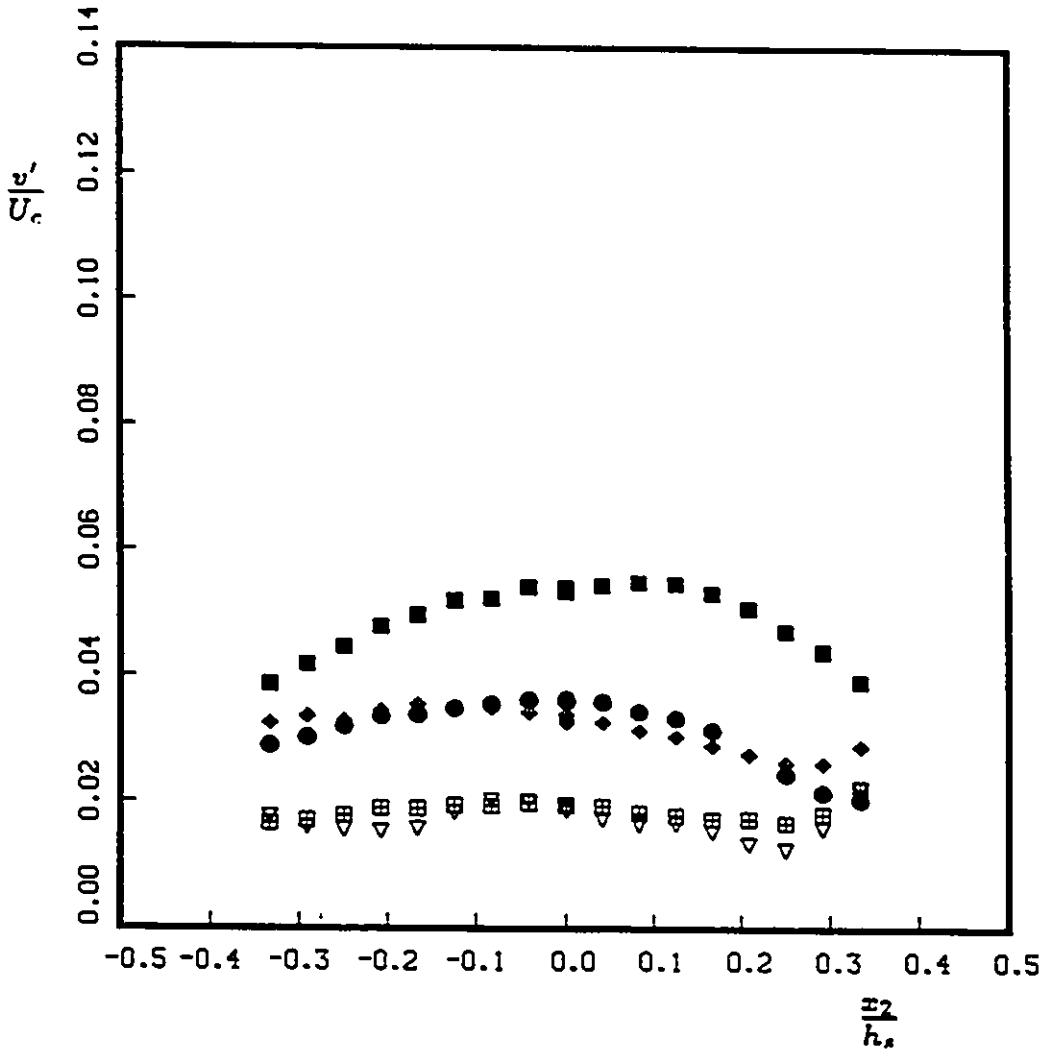

Figure 5.8: Transverse variation of $\frac{v'}{U_c}$ in the straight section, positive shear; $\frac{x_1}{h_s}$=9.9, x_3=0. Symbols as in Table 5.3.

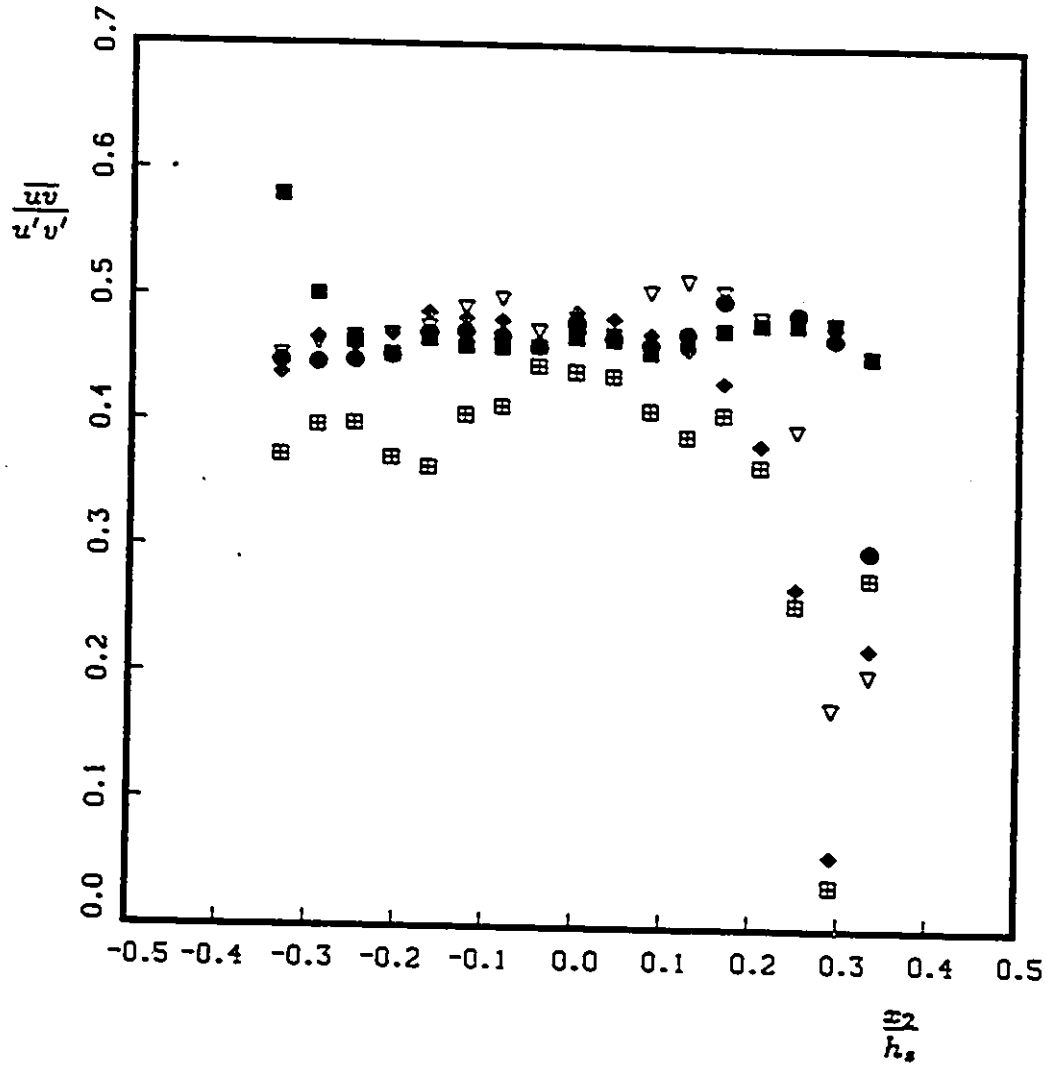

Figure 5.9: Transverse variation of $\frac{\overline{uv}}{u'v'}$ in the straight section, positive shear; $\frac{x_1}{h_s}$=9.9, x_3=0. Symbols as in Table 5.3.

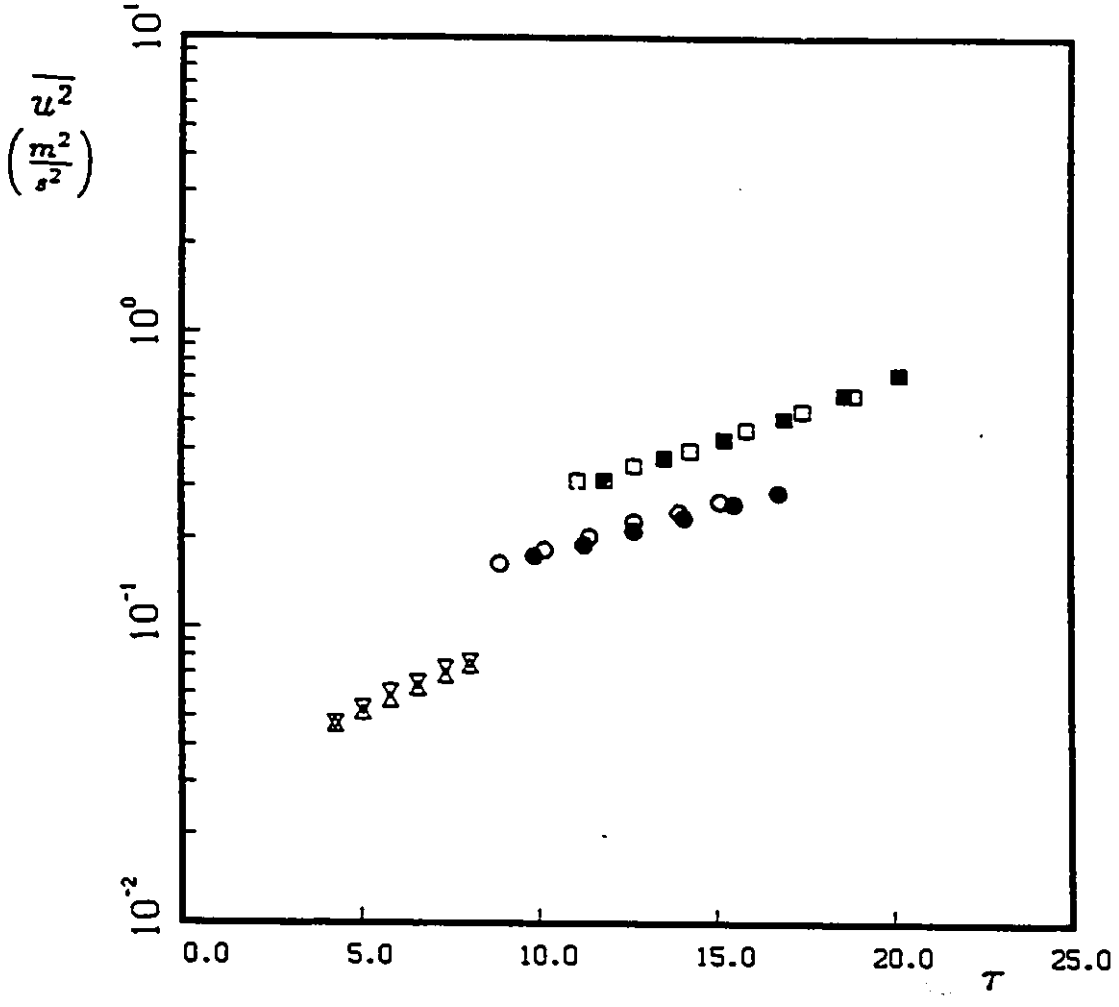

Figure 5.10: Development of $\overline{u^2}$ along the wind tunnel centerline in the straight section, Cases A, B and C. Symbols as in Table 5.3.

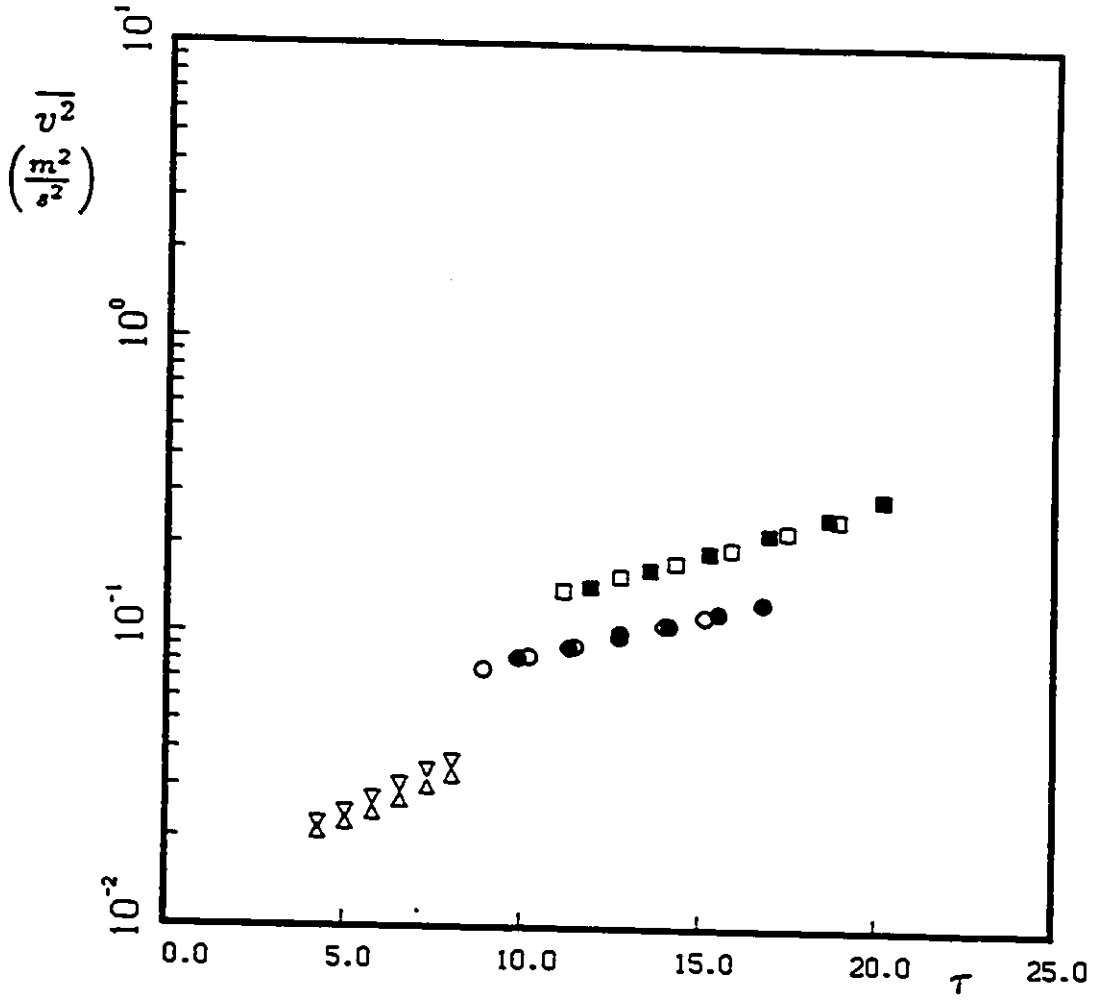

Figure 5.11: Development of $\overline{v^2}$ along the wind tunnel centerline in the straight section, Cases A, B and C. Symbols as in Table 5.3.

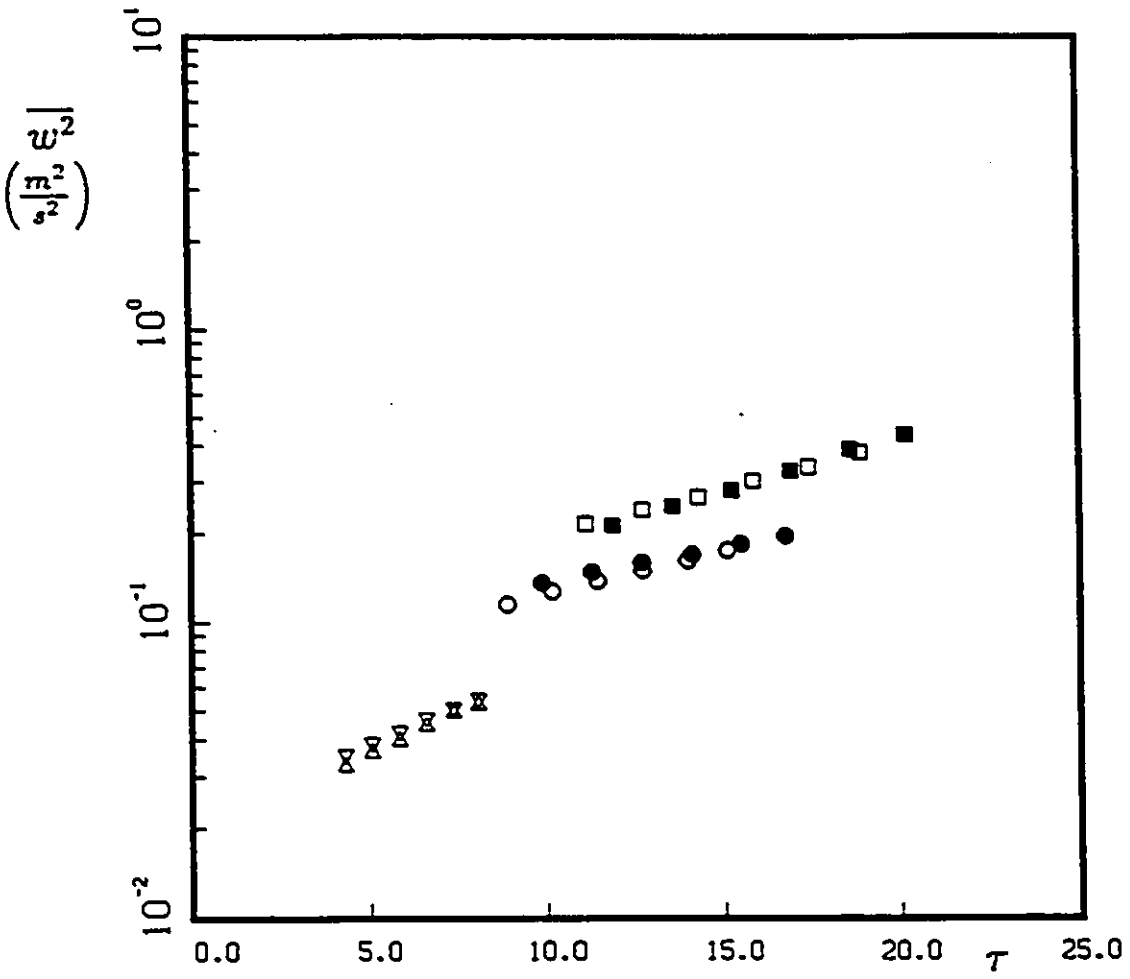

Figure 5.12: Development of $\overline{w^2}$ along the wind tunnel centerline in the straight section, Cases A, B and C. Symbols as in Table 5.3.

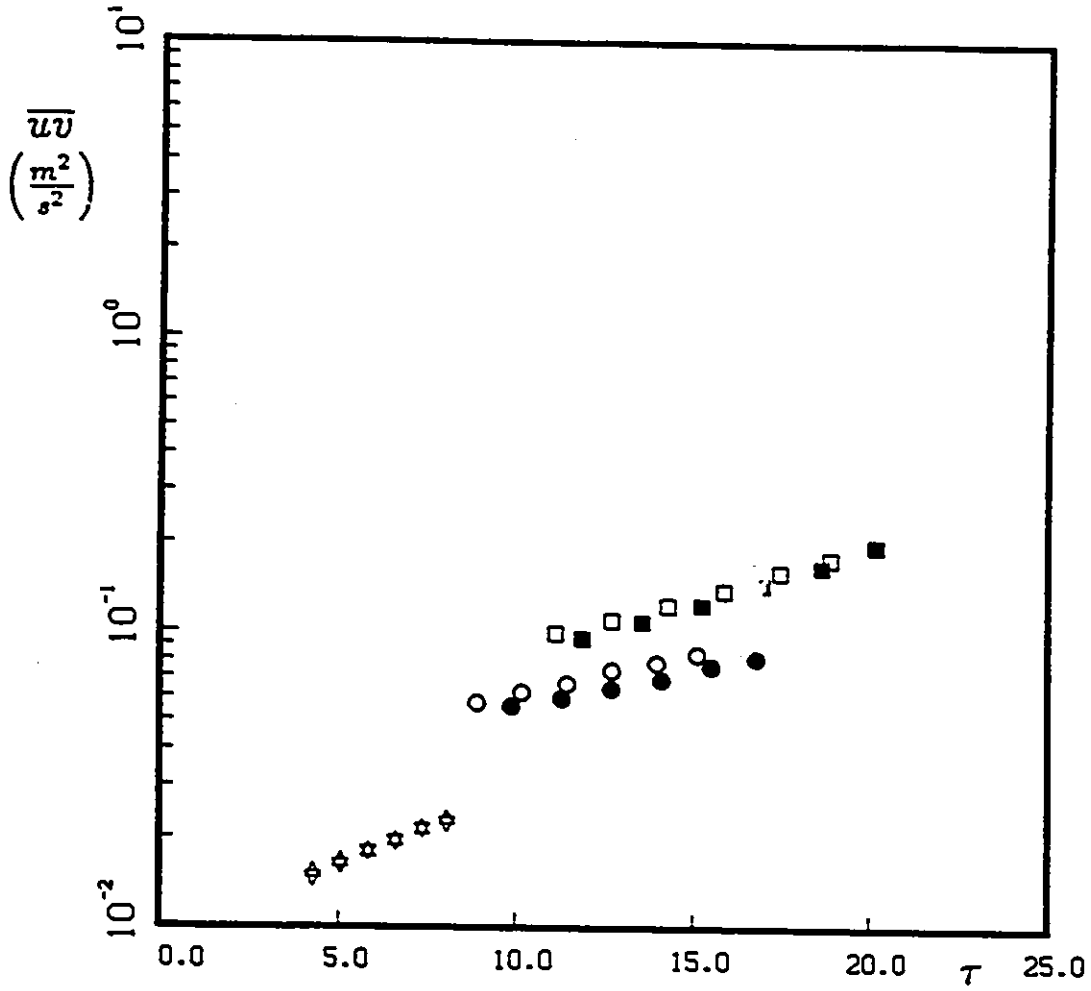

Figure 5.13: Development of $\overline{uv}$ along the wind tunnel centerline in the straight section, Cases A, B and C. Symbols as in Table 5.3.

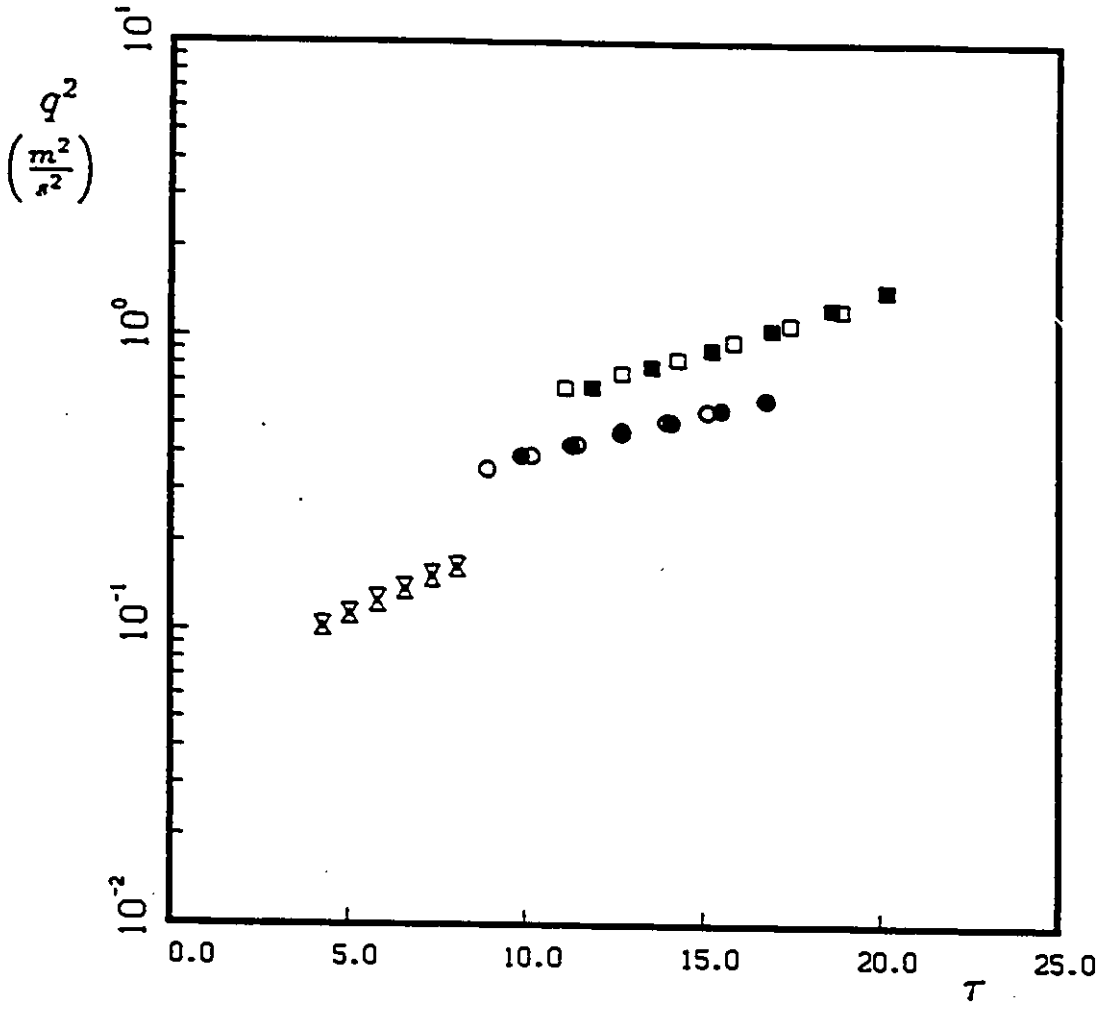

Figure 5.14: Development of q^2 along the wind tunnel centerline in the straight section, Cases A, B and C. Symbols as in Table 5.3.

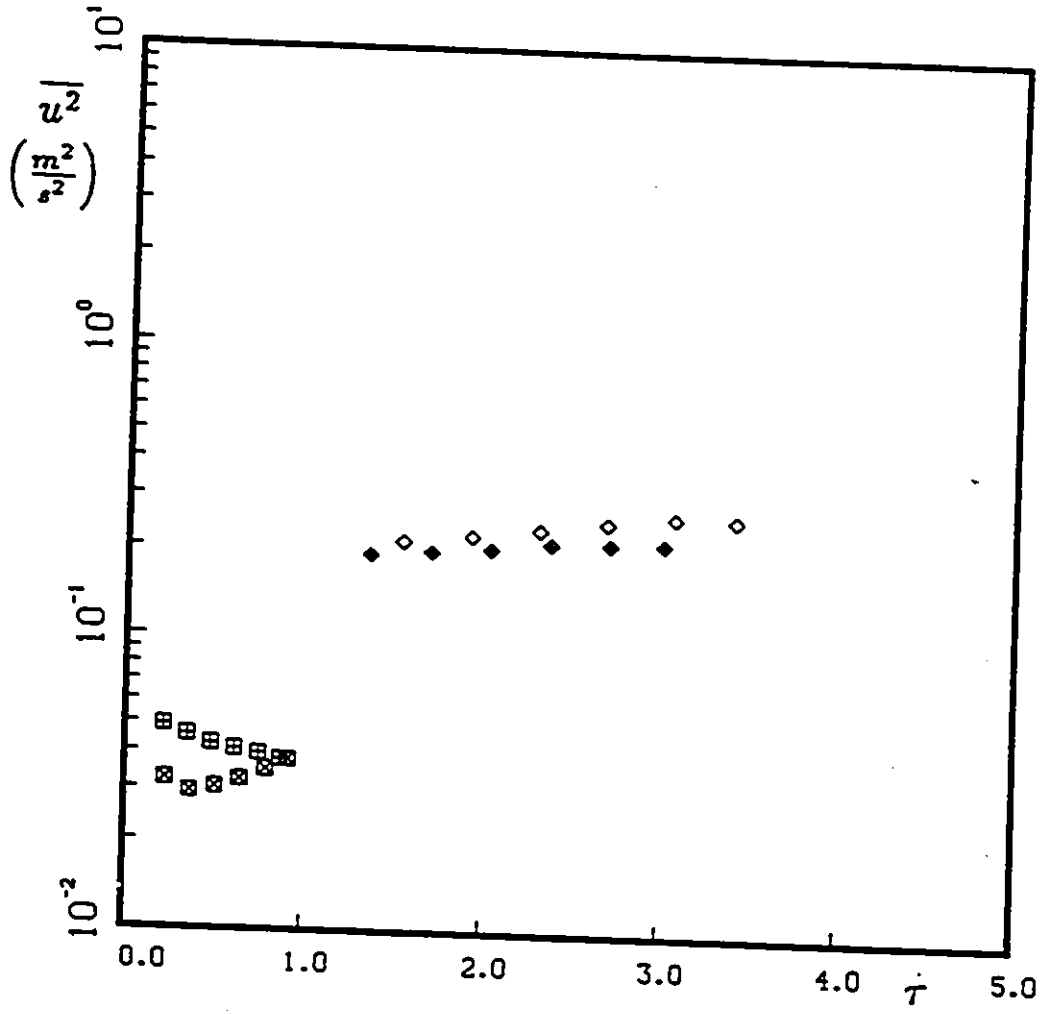

Figure 5.15: Development of $\overline{u^2}$ along the wind tunnel centerline in the straight section, Cases D and E. Symbols as in Table 5.3.

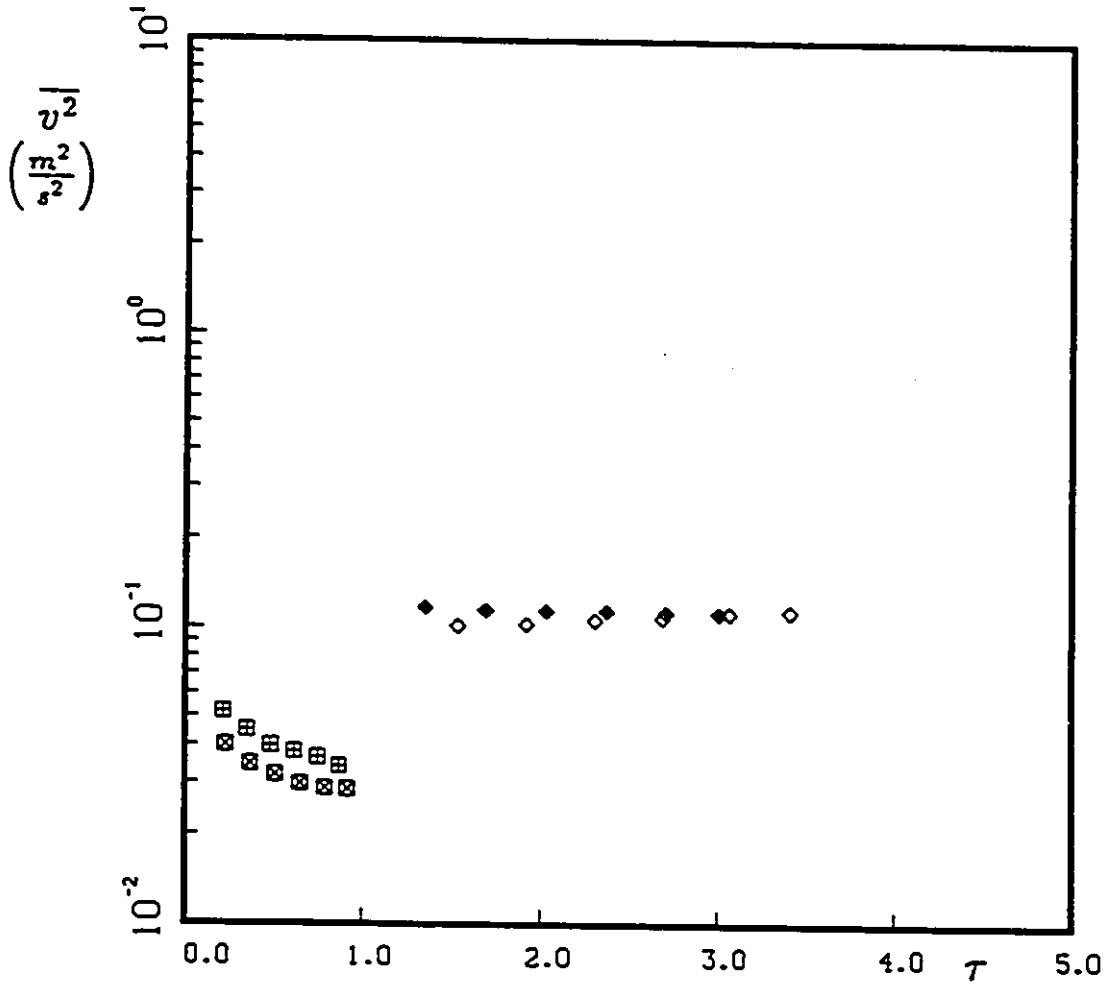

Figure 5.16: Development of $\overline{v^2}$ along the wind tunnel centerline in the straight section, Cases D and E. Symbols as in Table 5.3.

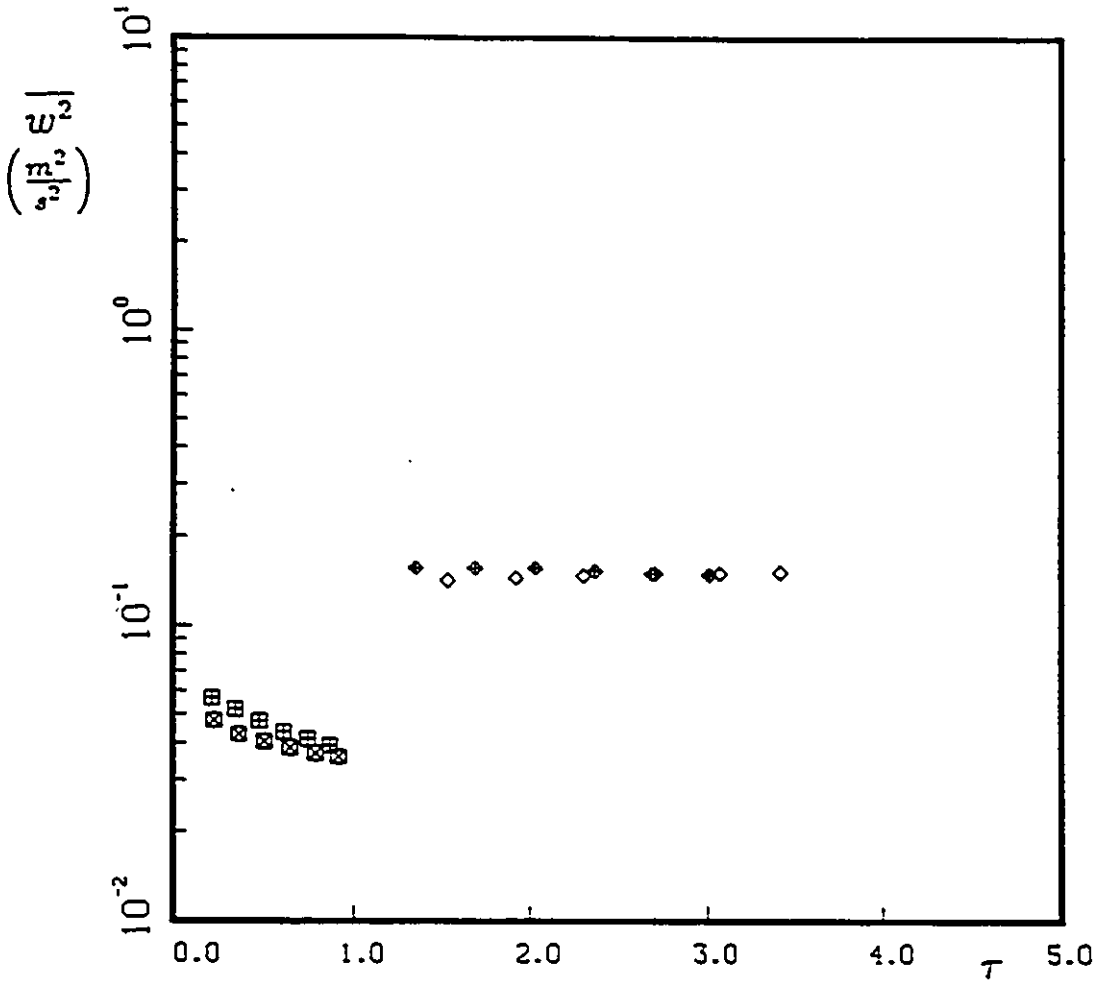

Figure 5.17: Development of $\overline{w^2}$ along the wind tunnel centerline in the straight section. Cases D and E. Symbols as in Table 5.3.

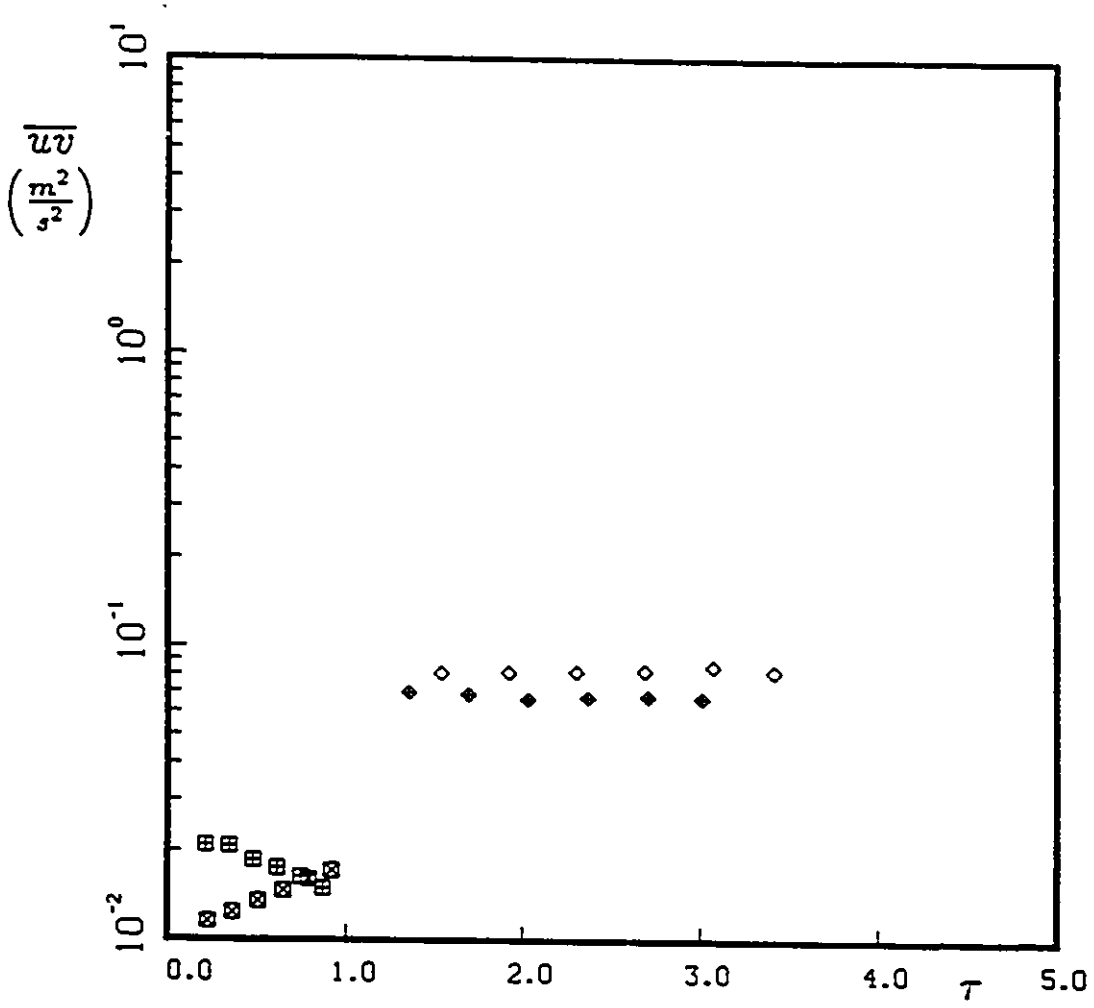

Figure 5.18: Development of $\overline{uv}$ along the wind tunnel centerline in the straight section, Cases D and E. Symbols as in Table 5.3.

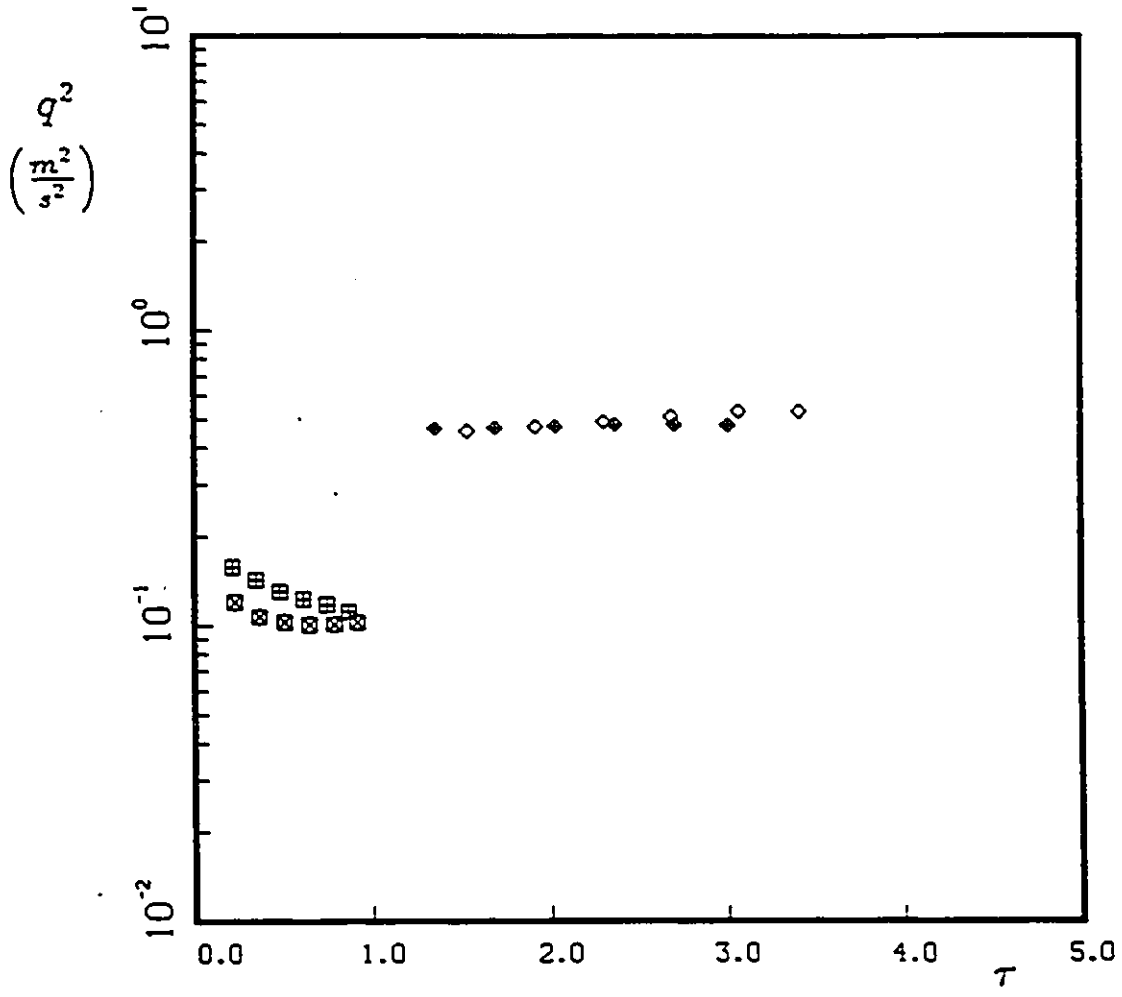

Figure 5.19: Development of q^2 along the wind tunnel centerline in the straight section, Cases D and E. Symbols as in Table 5.3.

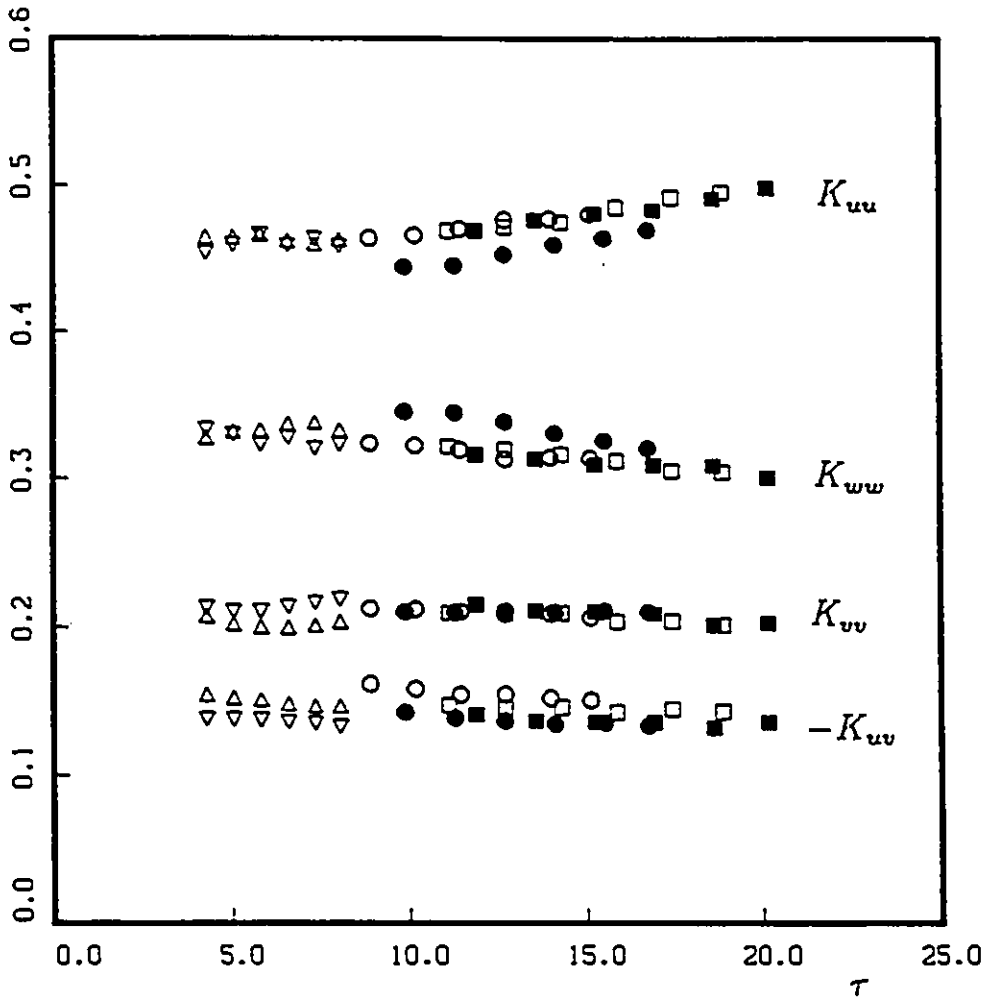

Figure 5.20: Development of K_{uu}, K_{vv}, K_{ww} and K_{uv} along the wind tunnel centerline in the straight section, Cases A, B and C. Symbols as in Table 5.3.

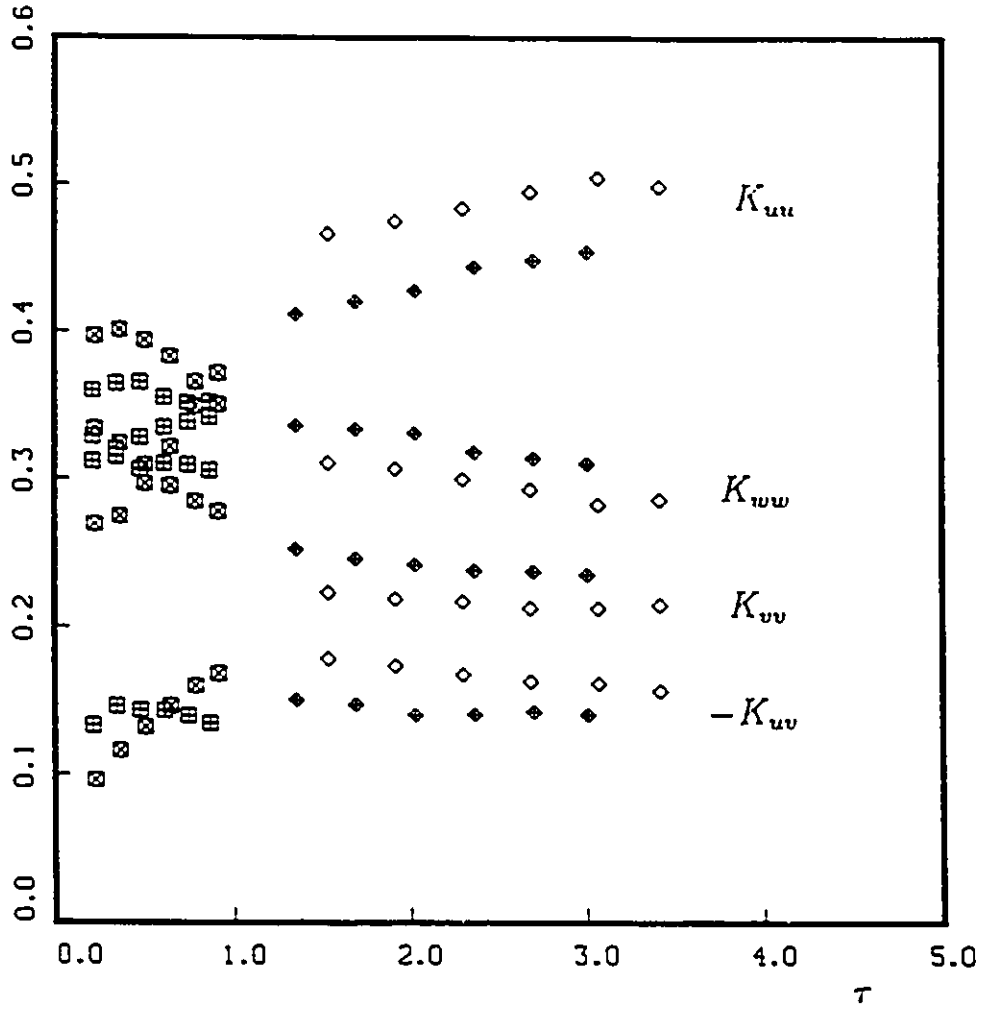

Figure 5.21: Development of K_{uu}, K_{vv}, K_{ww} and K_{uv} along the wind tunnel centerline in the straight section, Cases D and E. Symbols as in Table 5.3.

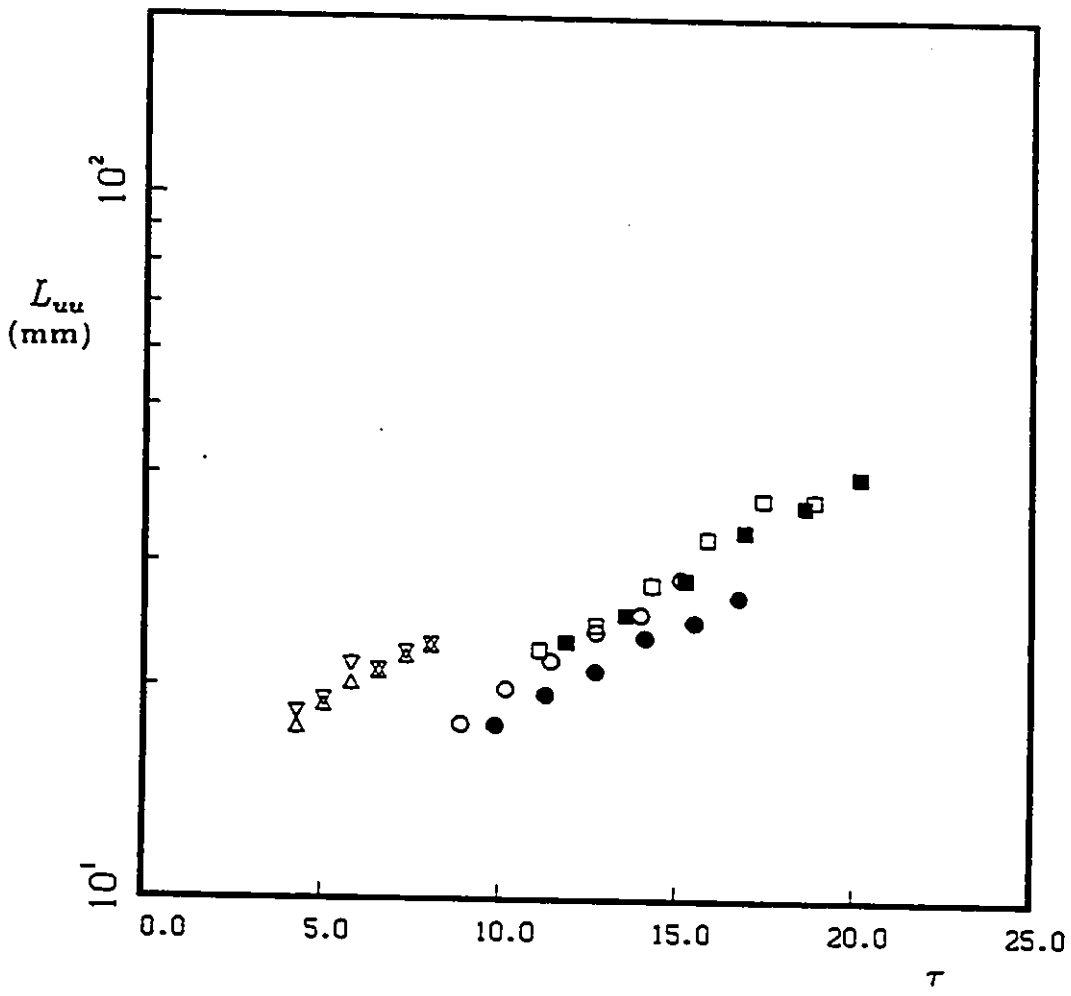

Figure 5.22: Development of L_{uu} along the wind tunnel centerline in the straight section, Cases A, B and C. Symbols as in Table 5.3.

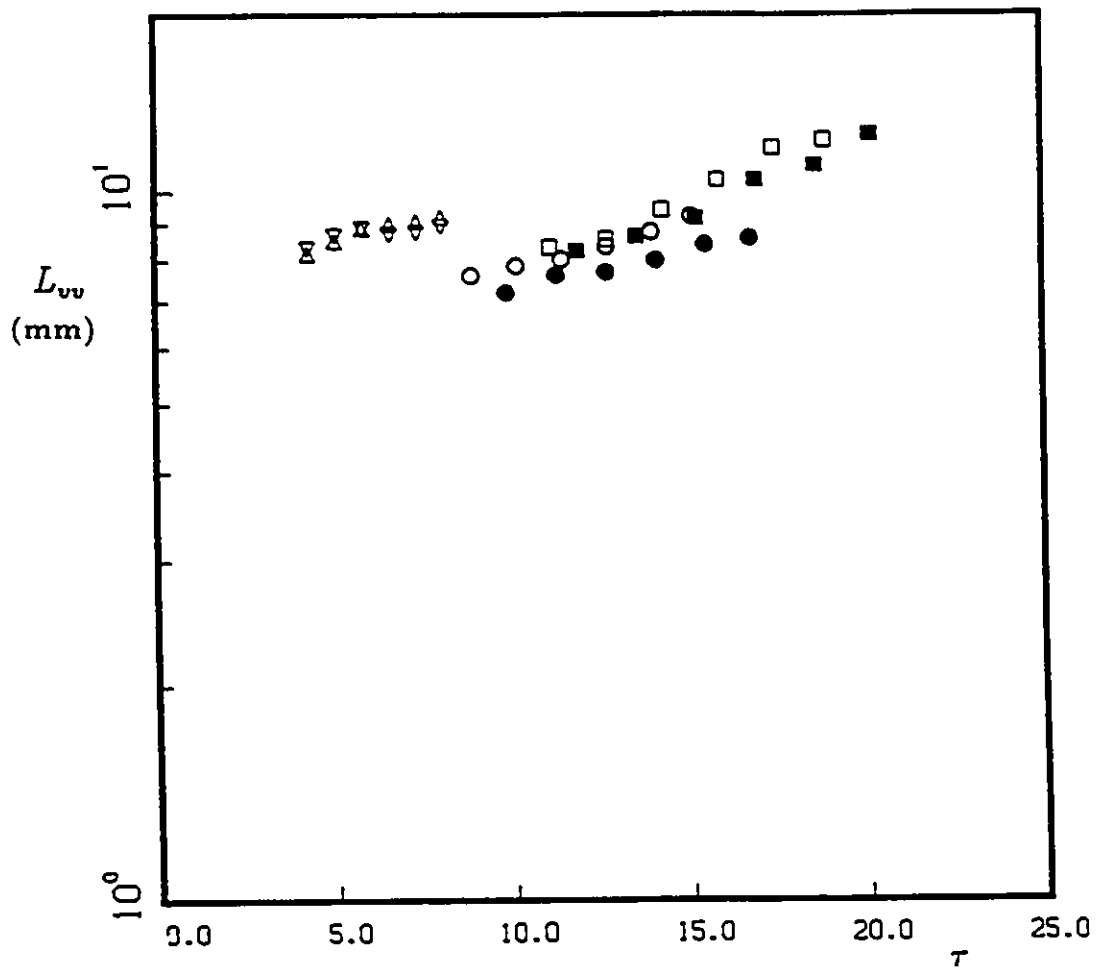

Figure 5.23: Development of L_{vv} along the wind tunnel centerline in the straight section, Cases A, B and C. Symbols as in Table 5.3.

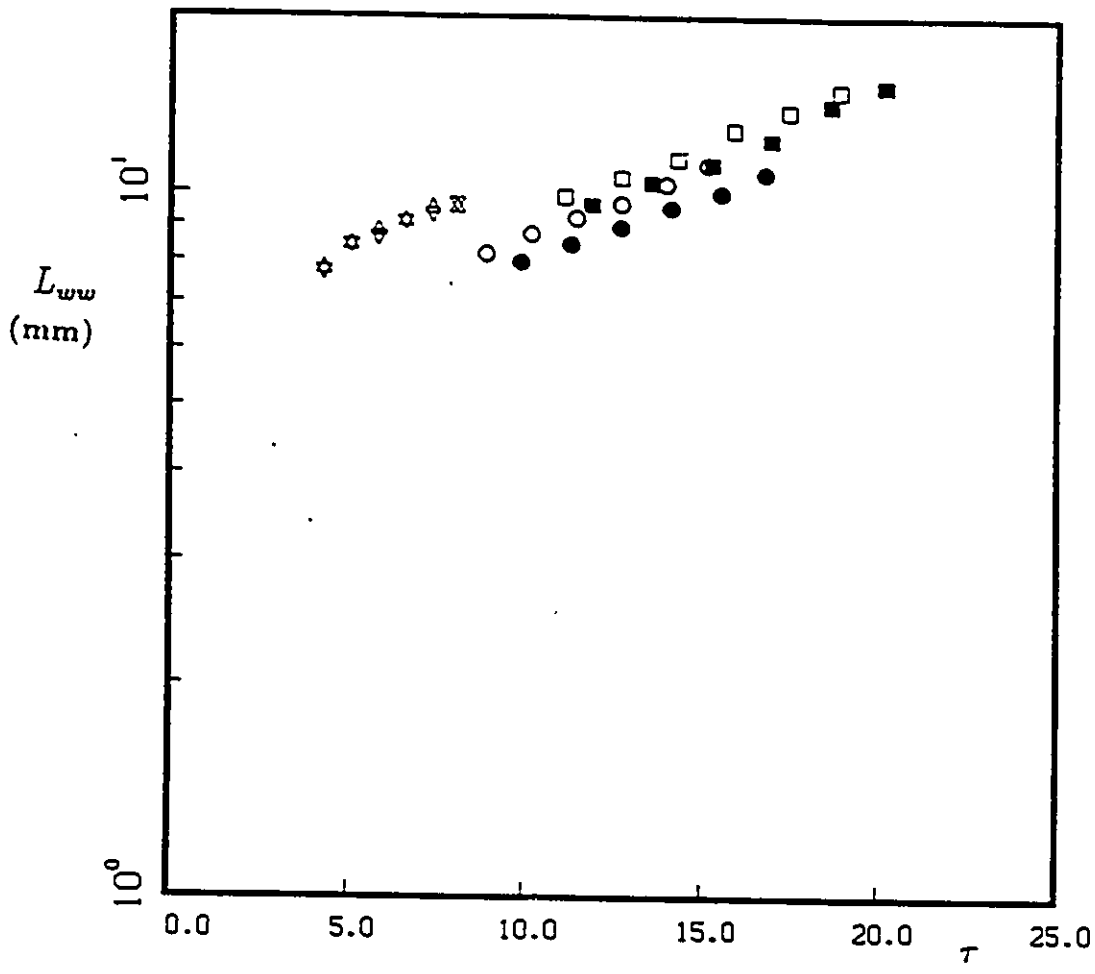

Figure 5.24: Development of L_{ww} along the wind tunnel centerline in the straight section, Cases A, B and C. Symbols as in Table 5.3.

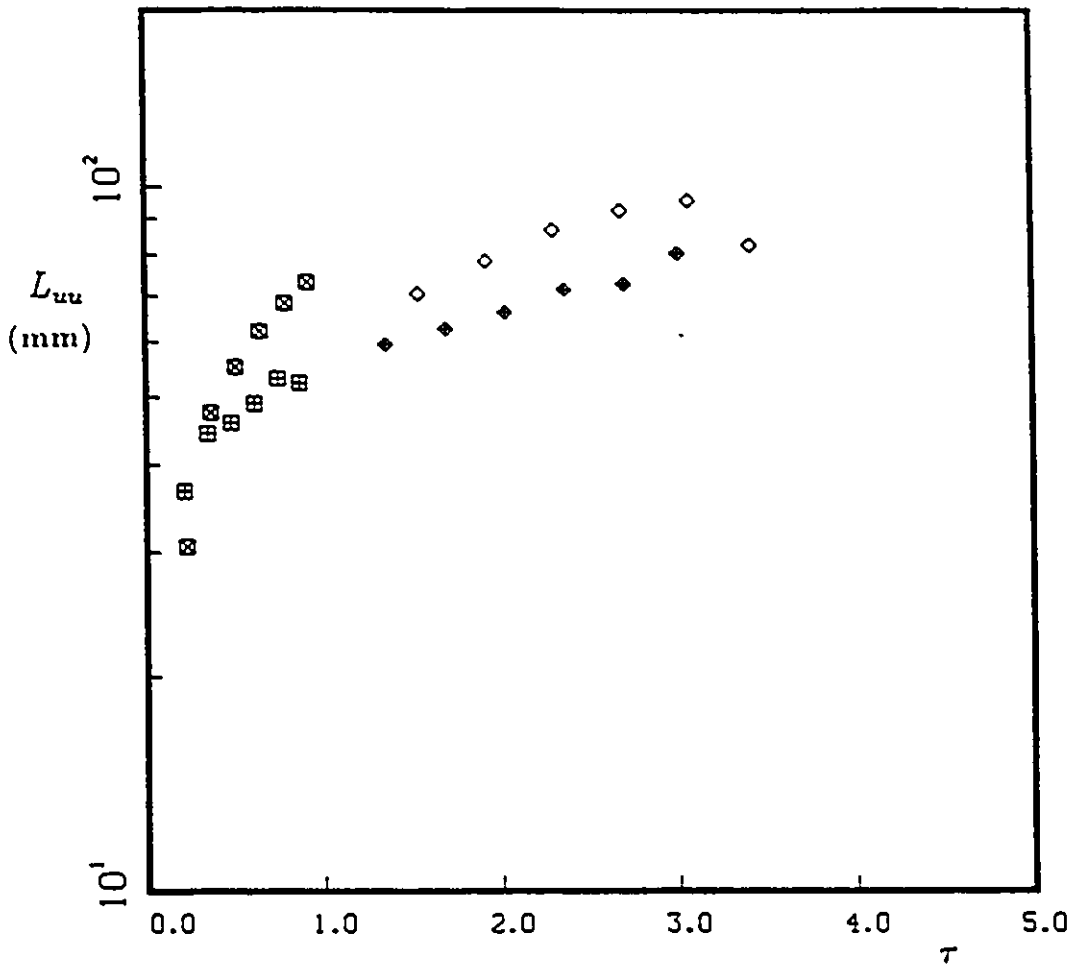

Figure 5.25: Development of L_{uu} along the wind tunnel centerline in the straight section, Cases D and E. Symbols as in Table 5.3.

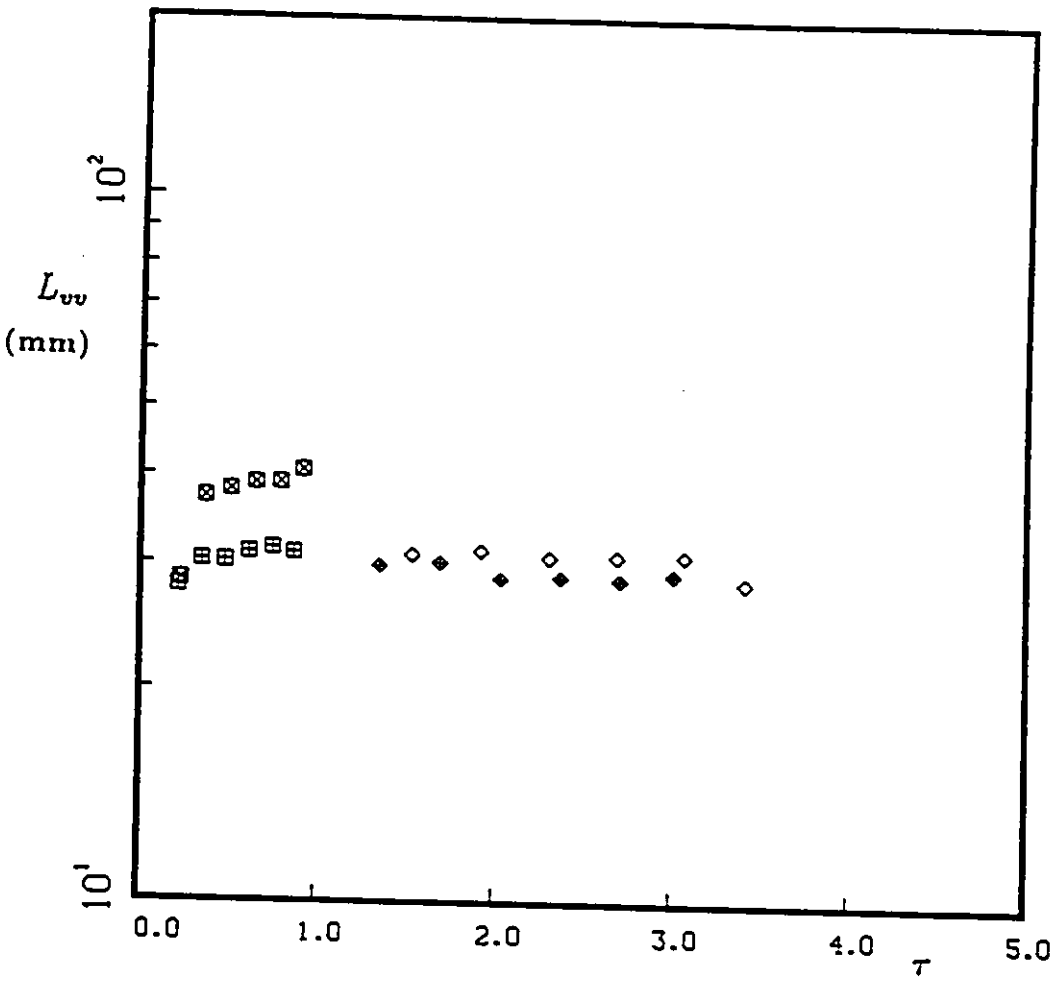

Figure 5.26: Development of L_{vv} along the wind tunnel centerline in the straight section, Cases D and E. Symbols as in Table 5.3.

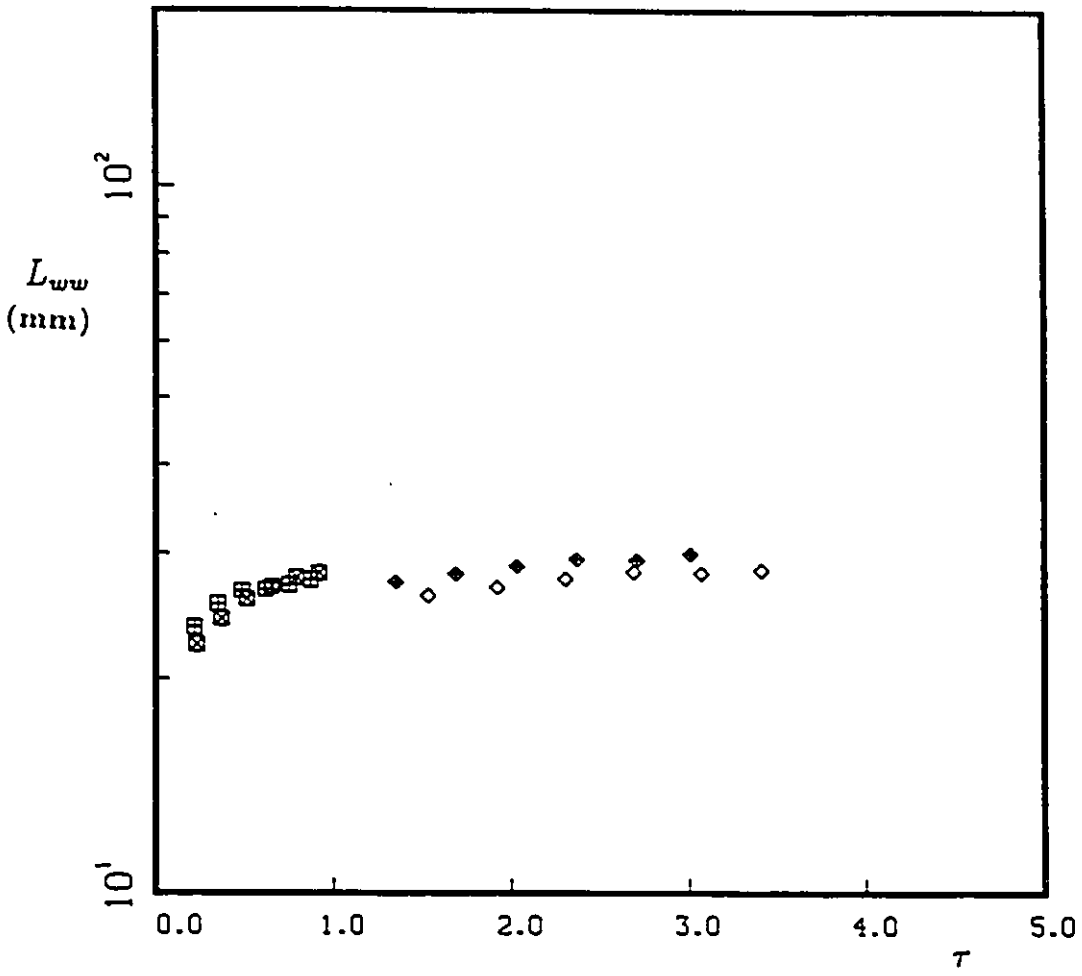

Figure 5.27: Development of L_{ww} along the wind tunnel centerline in the straight section, Cases D and E. Symbols as in Table 5.3.

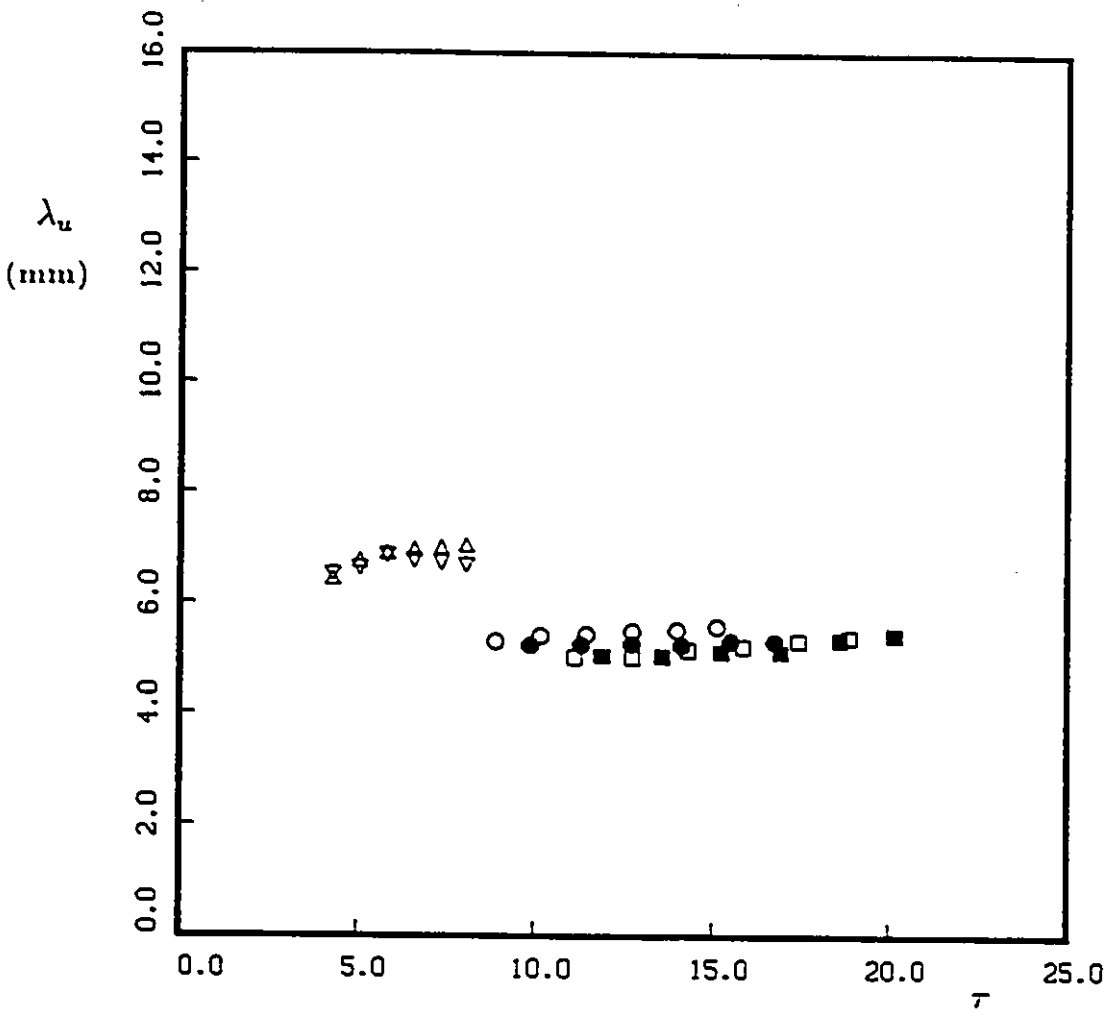

Figure 5.28: Development of λ_u along the wind tunnel centerline in the straight section, Cases A, B and C. Symbols as in Table 5.3.

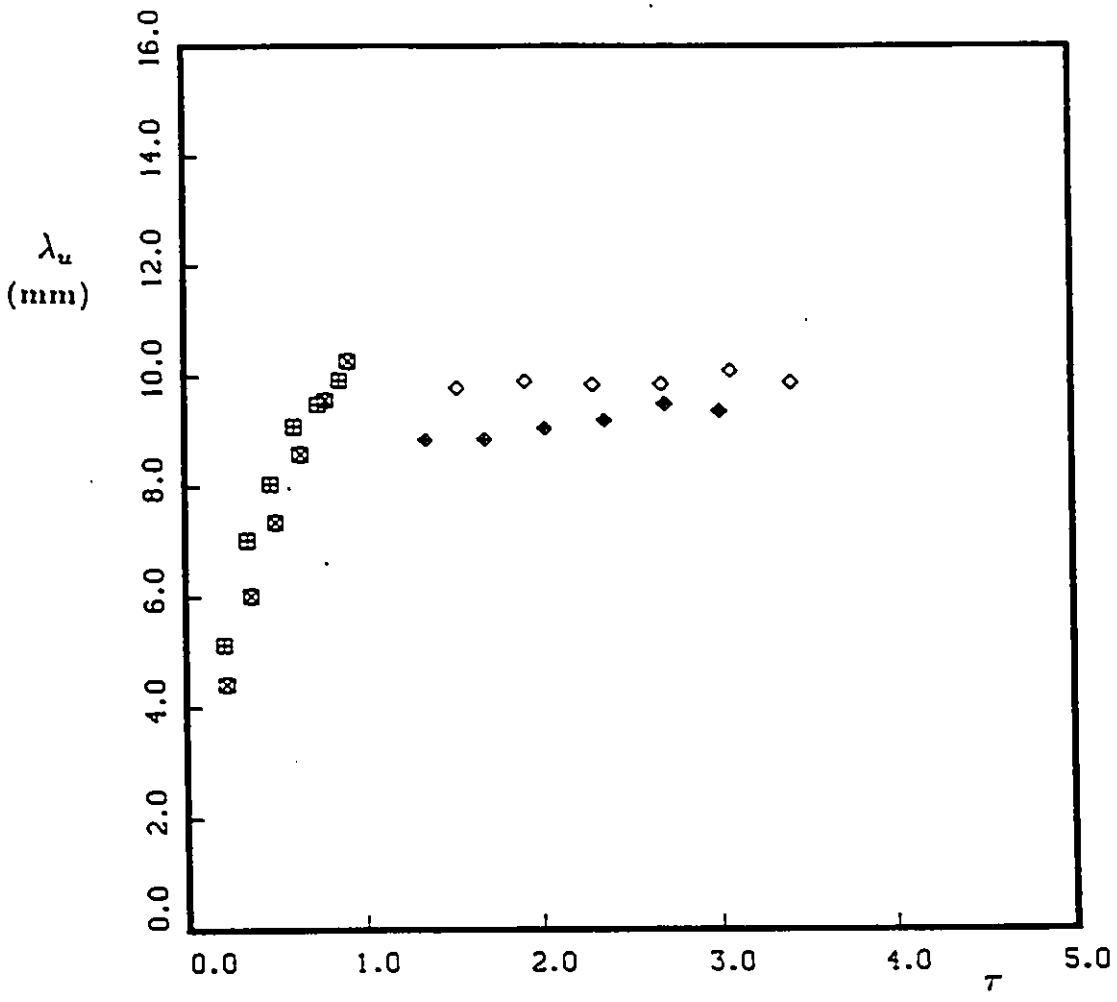

Figure 5.29: Development of λ_u along the wind tunnel centerline in the straight section, Cases D and E. Symbols as in Table 5.3.

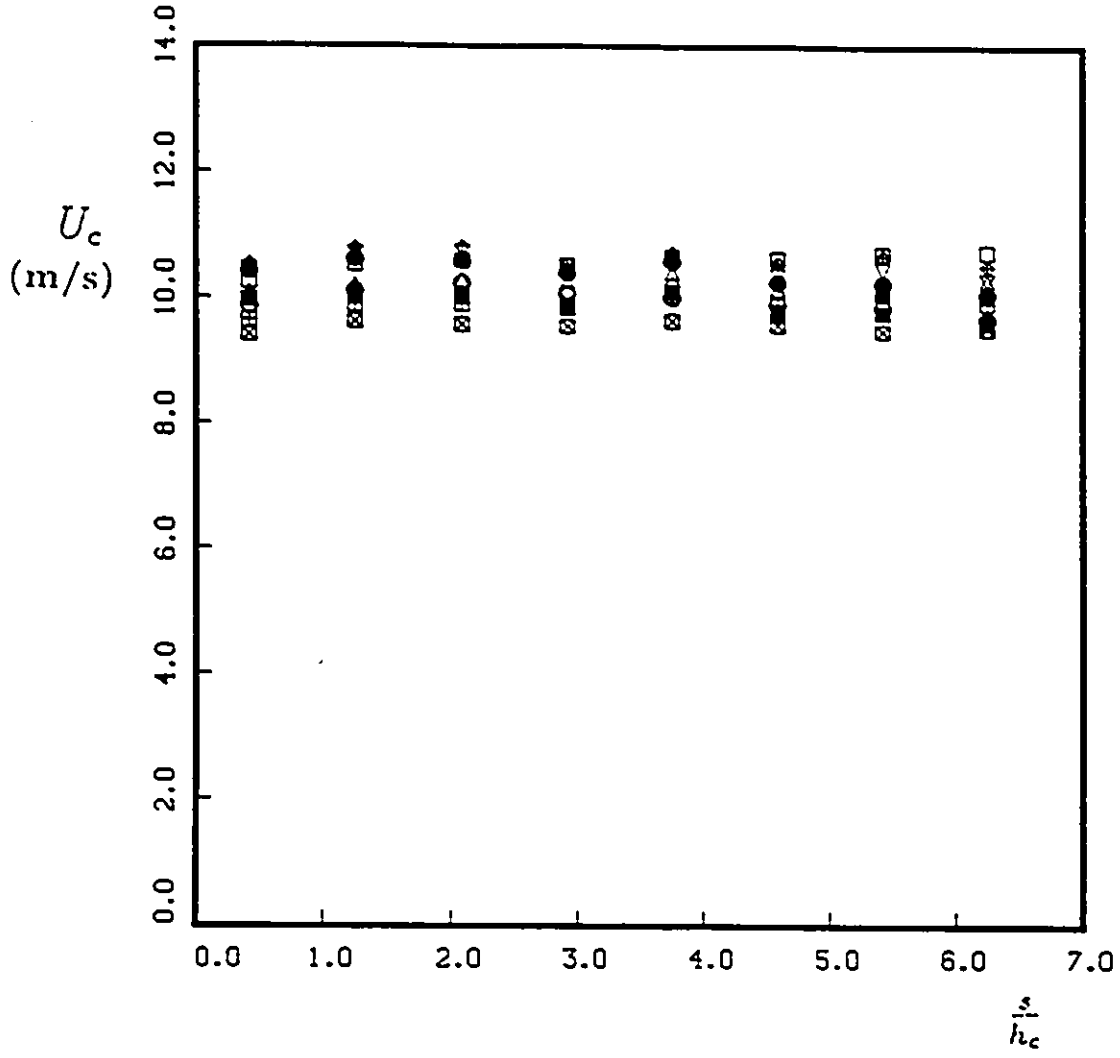

Figure 5.30: Streamwise development of U_c in the mildly curved section, symbols as in Table 5.3.

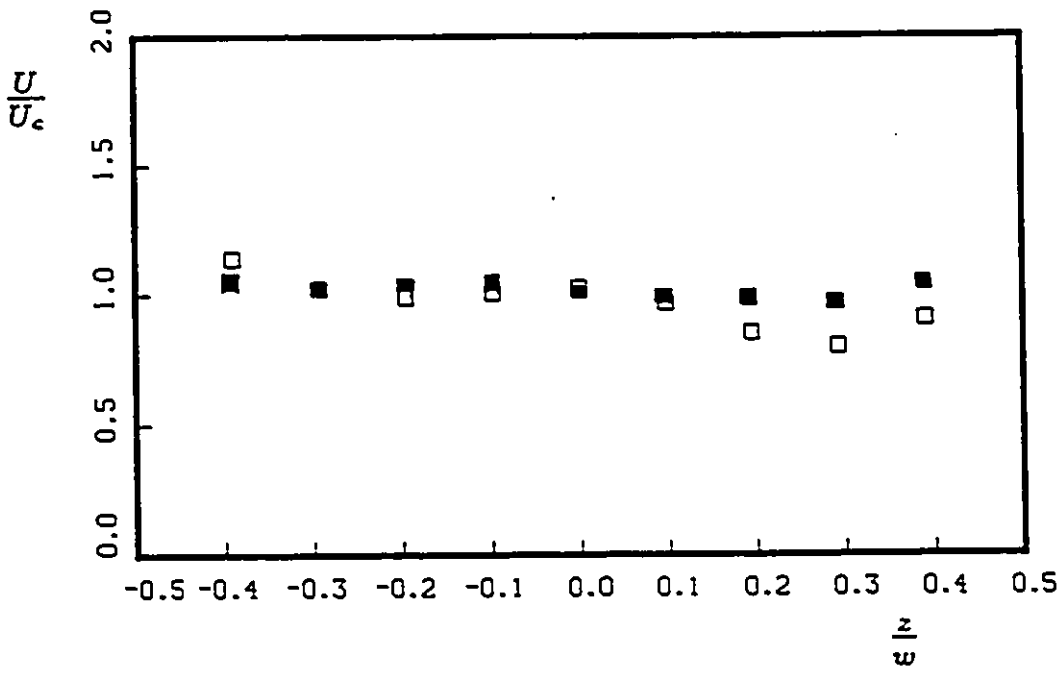

Figure 5.31: Spanwise variation of $\frac{U}{U_e}$ in the mildly curved section; $\frac{s}{h_c}$=5.4, n=0. Symbols as in Table 5.3.

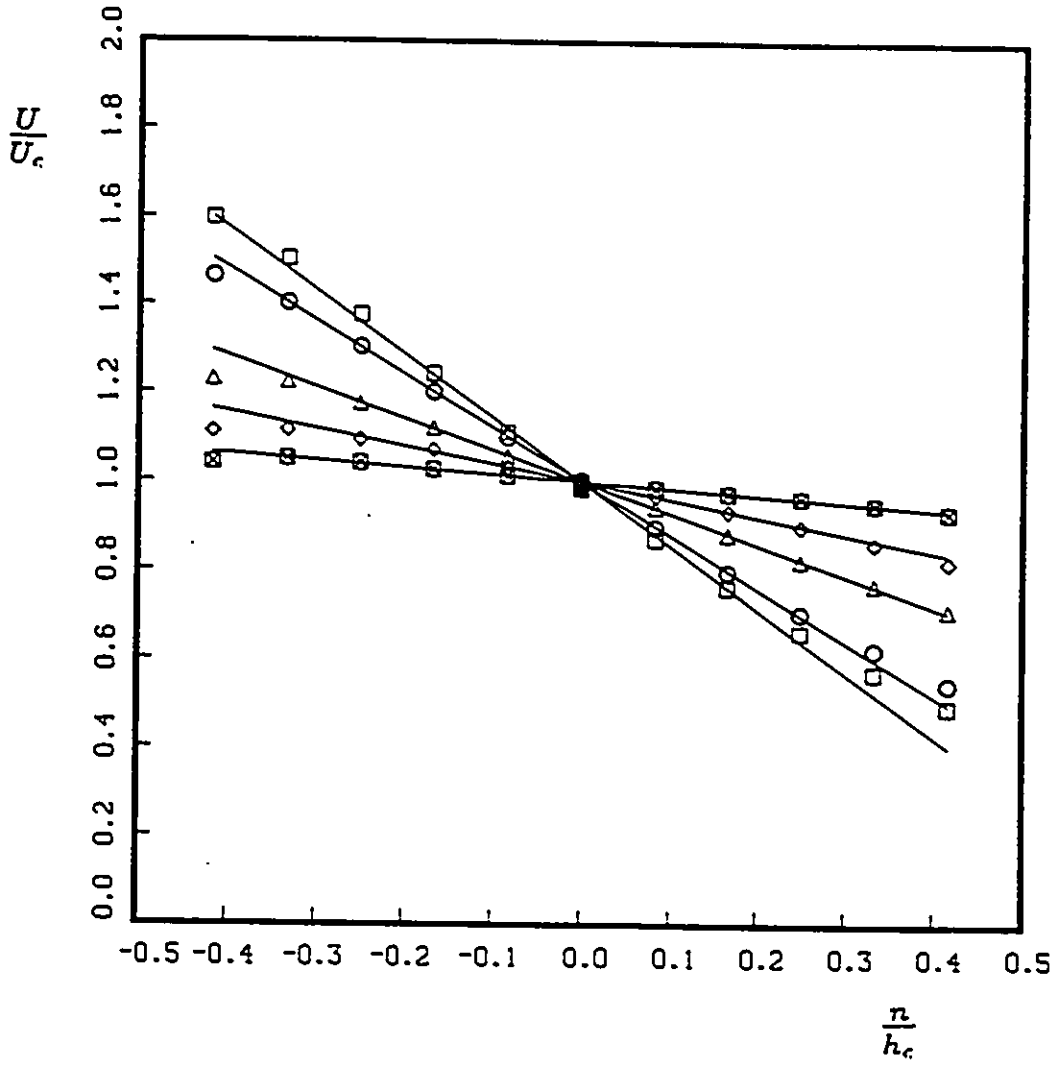

Figure 5.32: Transverse profiles of $\frac{U}{U_c}$ in the mildly curved section, negative shear; $\frac{s}{h_c}$=.42, z=0. Symbols as in Table 5.3.

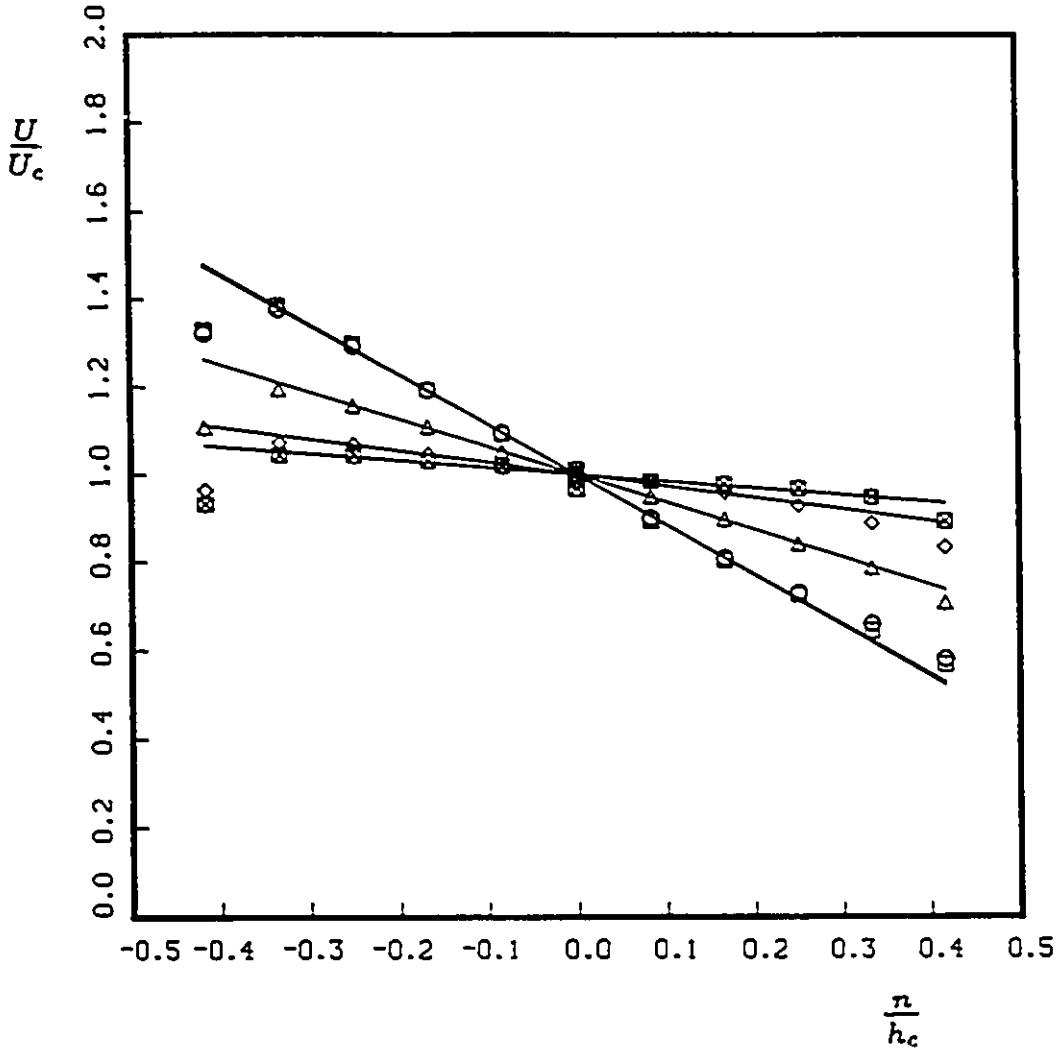

Figure 5.33: Transverse profiles of $\frac{U}{U_c}$ in the mildly curved section, negative shear; $\frac{s}{h_c}$=5.42, z=0. Symbols as in Table 5.3.

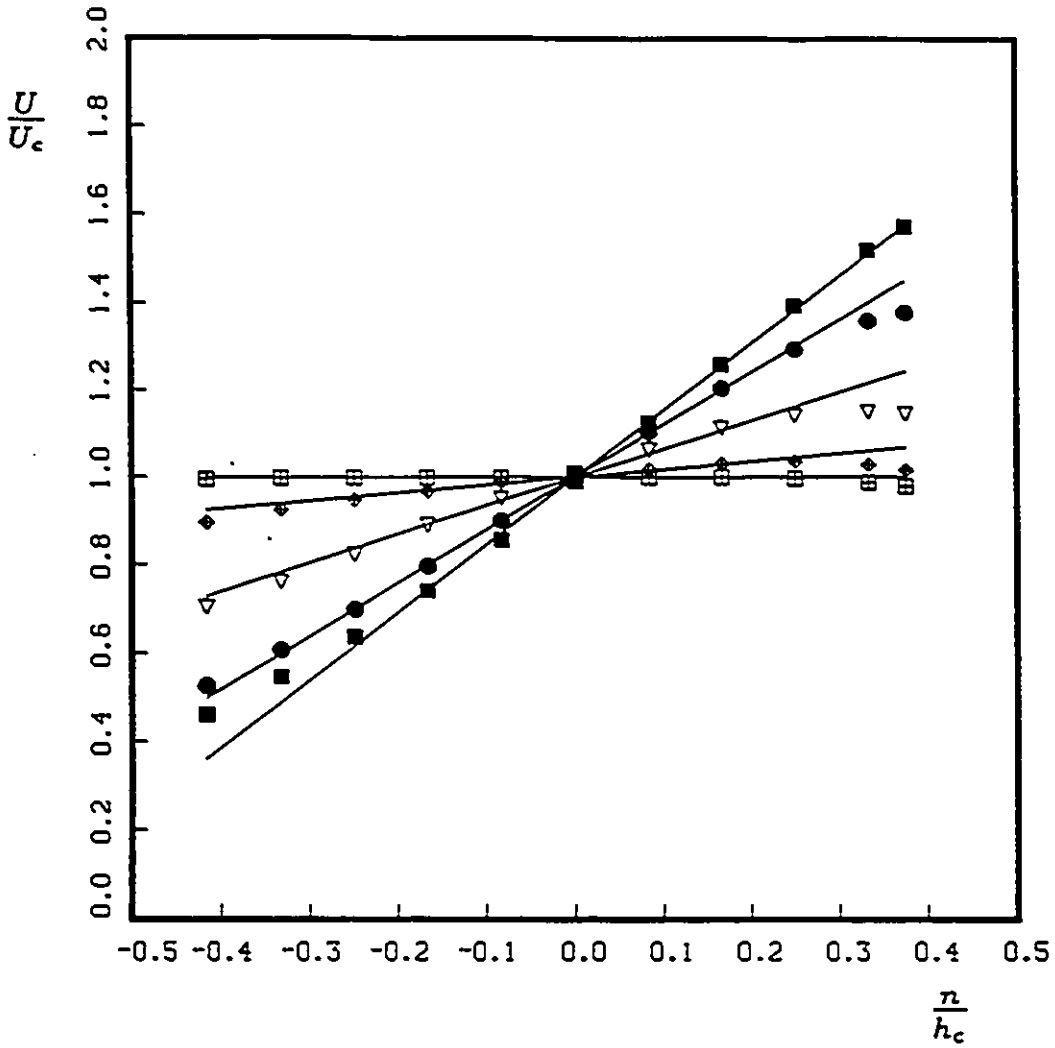

Figure 5.34: Transverse profiles of $\frac{U}{U_c}$ in the mildly curved section, positive shear; $\frac{s}{h_c}$=.42, z=0. Symbols as in Table 5.3.

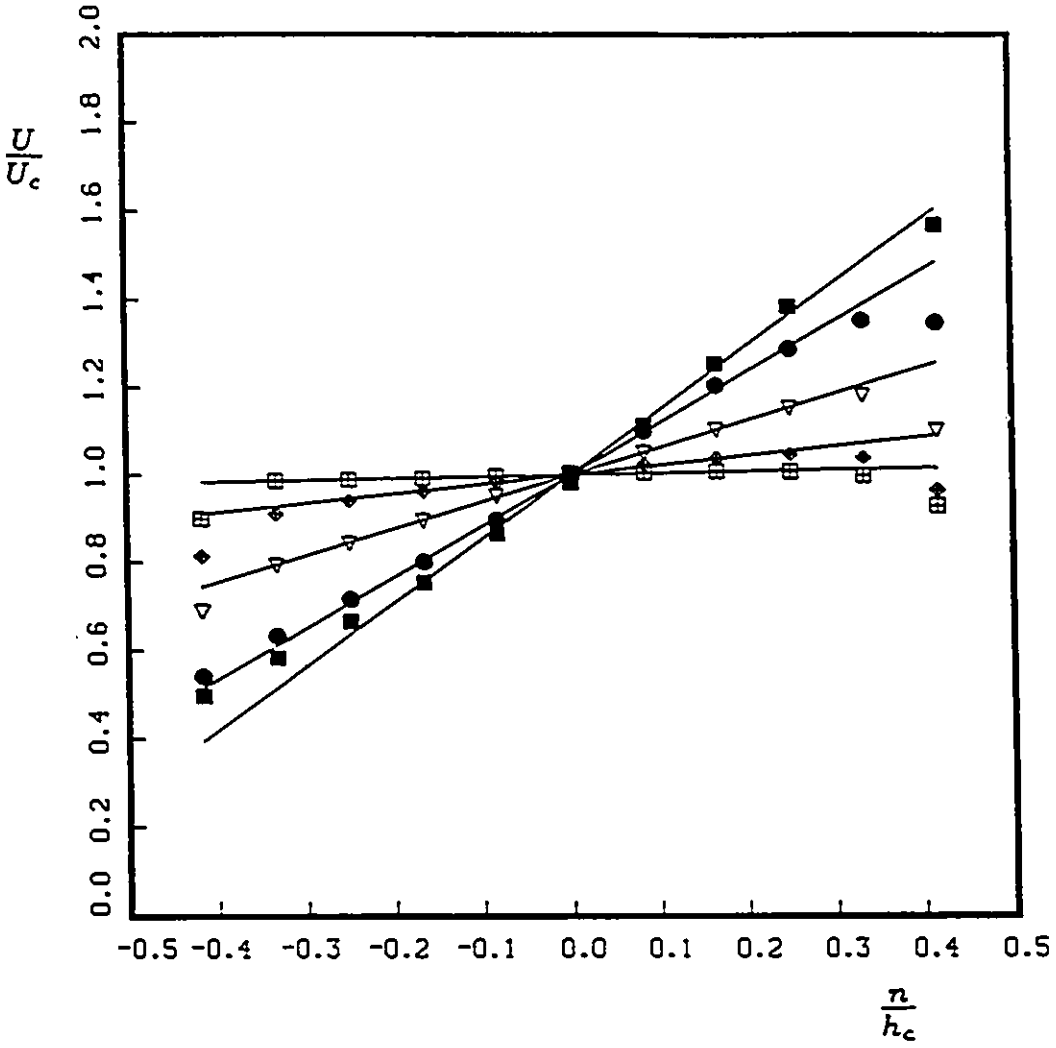

Figure 5.35: Transverse profiles of $\frac{U}{U_c}$ in the mildly curved section, positive shear; $\frac{s}{h_c}$=5.42, z=0. Symbols as in Table 5.3.

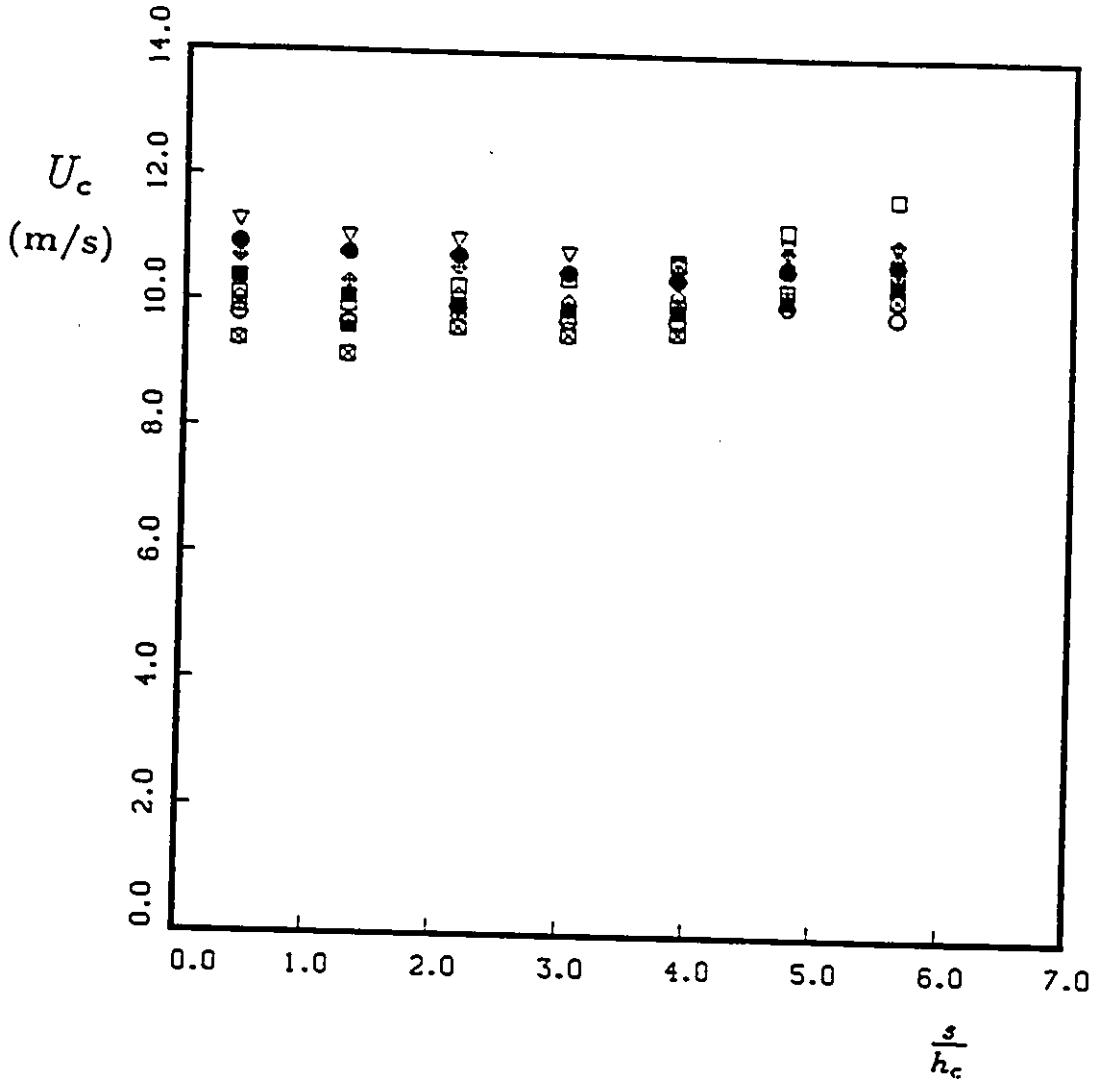

Figure 5.36: Streamwise development of U_c in the strongly curved section; symbols as in Table 5.3.

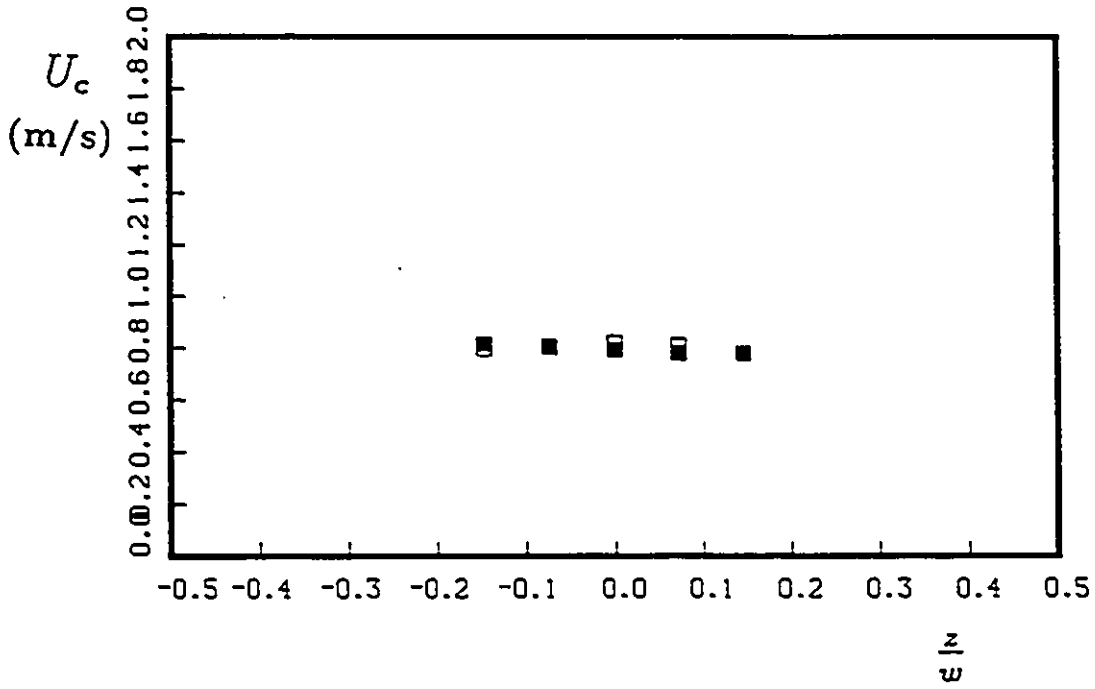

Figure 5.37: Spanwise variation of $\frac{U}{U_c}$ in the strongly curved section: $\frac{s}{h_c}$=2.2. n=0. Symbols as in Table 5.3.

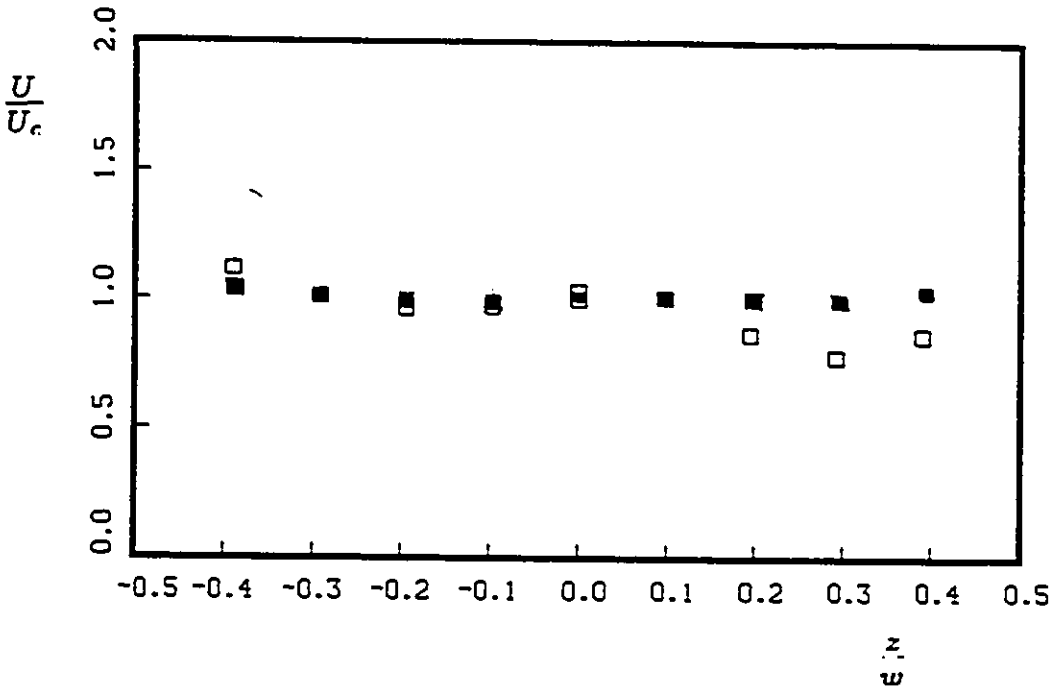

Figure 5.38: Spanwise variation of $\frac{U}{U_c}$ in the strongly curved section; $\frac{s}{h_c}$=4.7. n=0. Symbols as in Table 5.3.

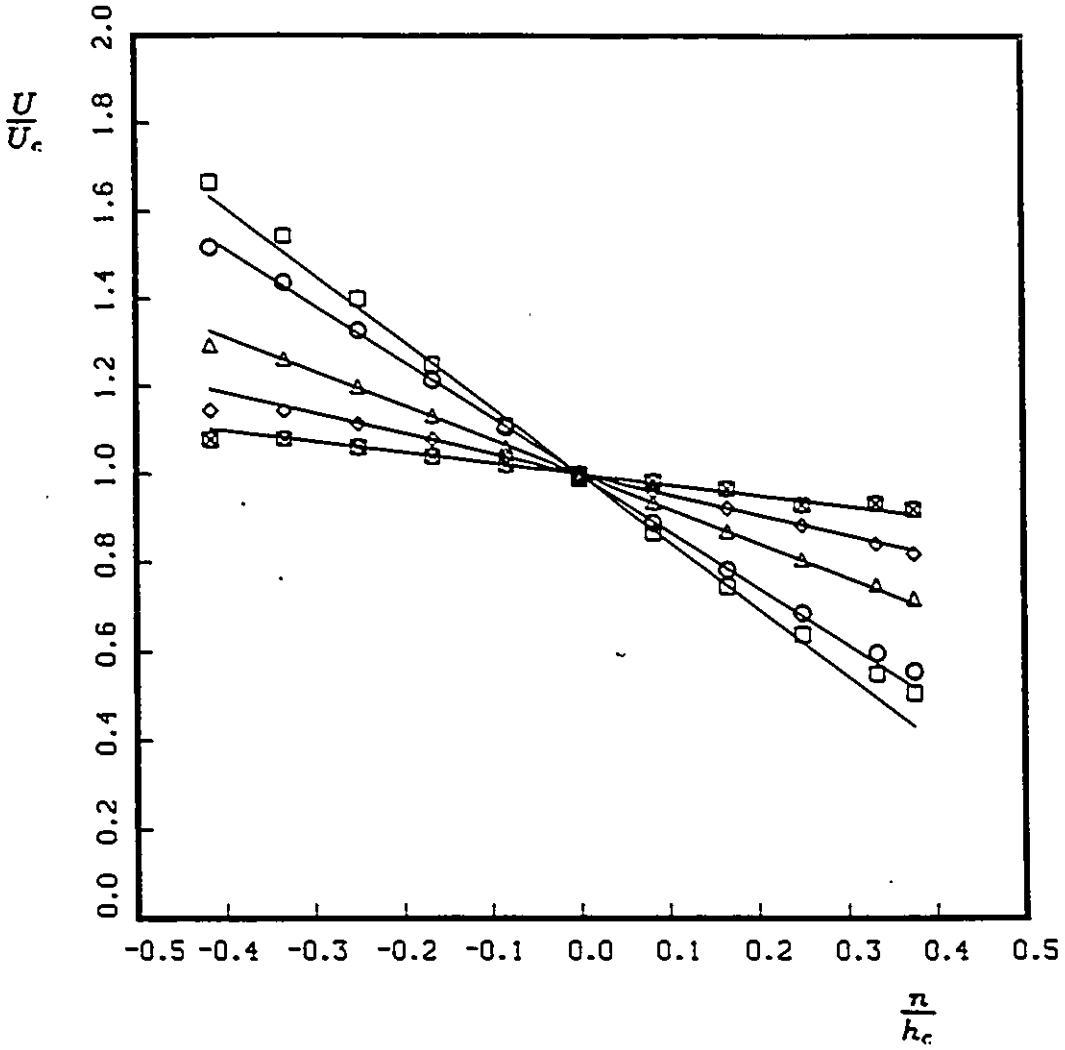

Figure 5.39: Transverse profiles of $\frac{U}{U_c}$ in the strongly curved section, negative shear; $\frac{s}{h_c}$=.42, z=0. Symbols as in Table 5.3.

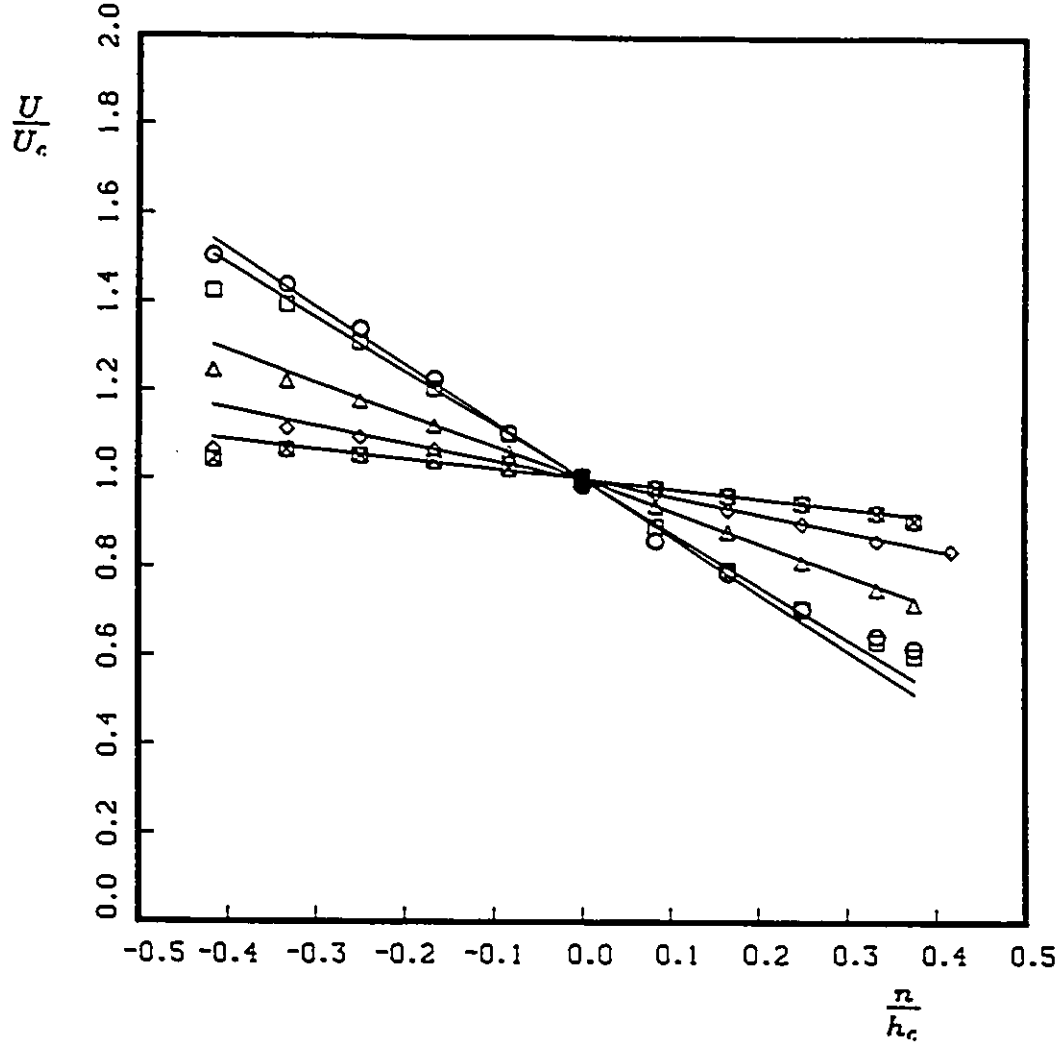

Figure 5.40: Transverse profiles of $\frac{U}{U_c}$ in the strongly curved section, negative shear; $\frac{s}{h_c}$=4.74, z=0. Symbols as in Table 5.3.

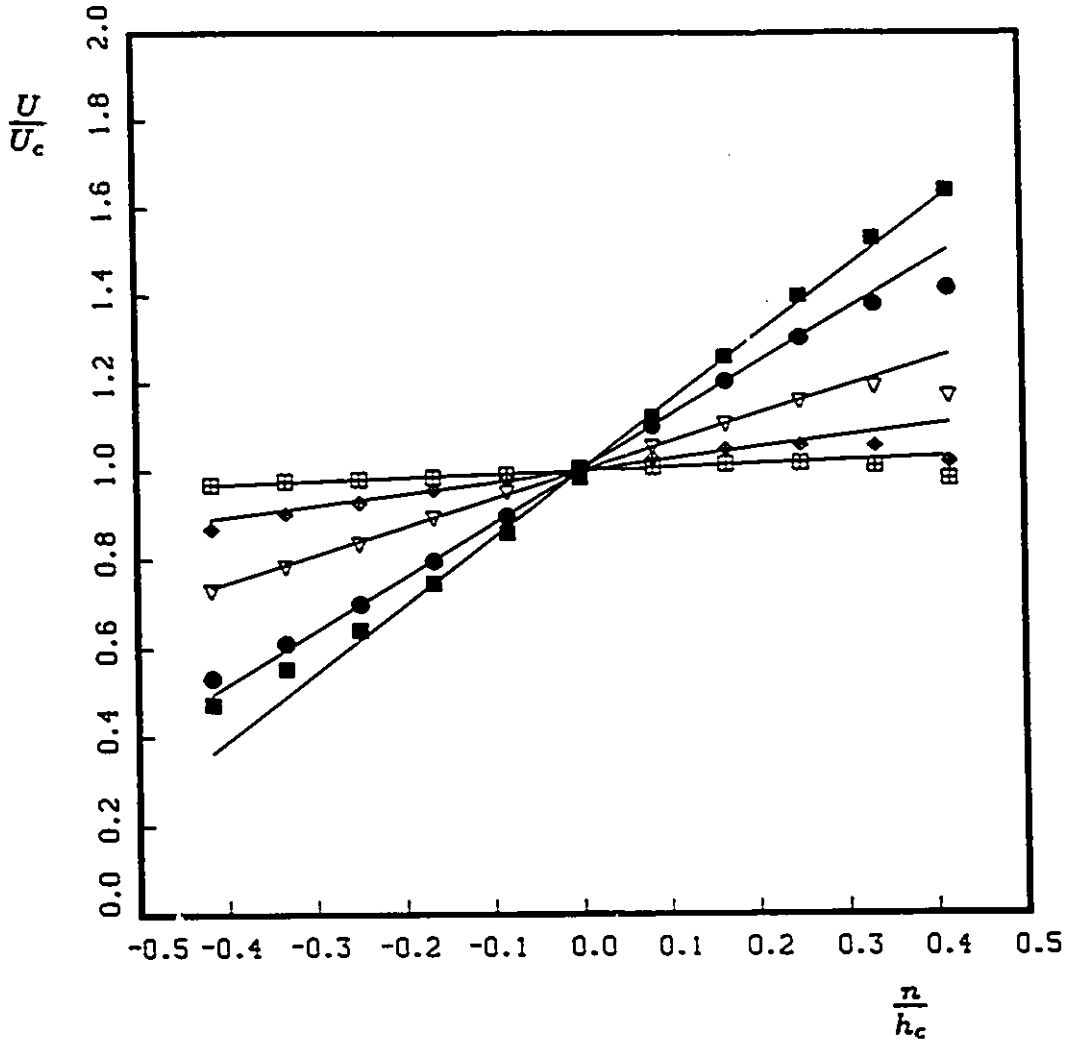

Figure 5.41: Transverse profiles of $\frac{U}{U_c}$ in the strongly curved section, positive shear; $\frac{s}{h_c}$=.42, z=0. Symbols as in Table 5.3.

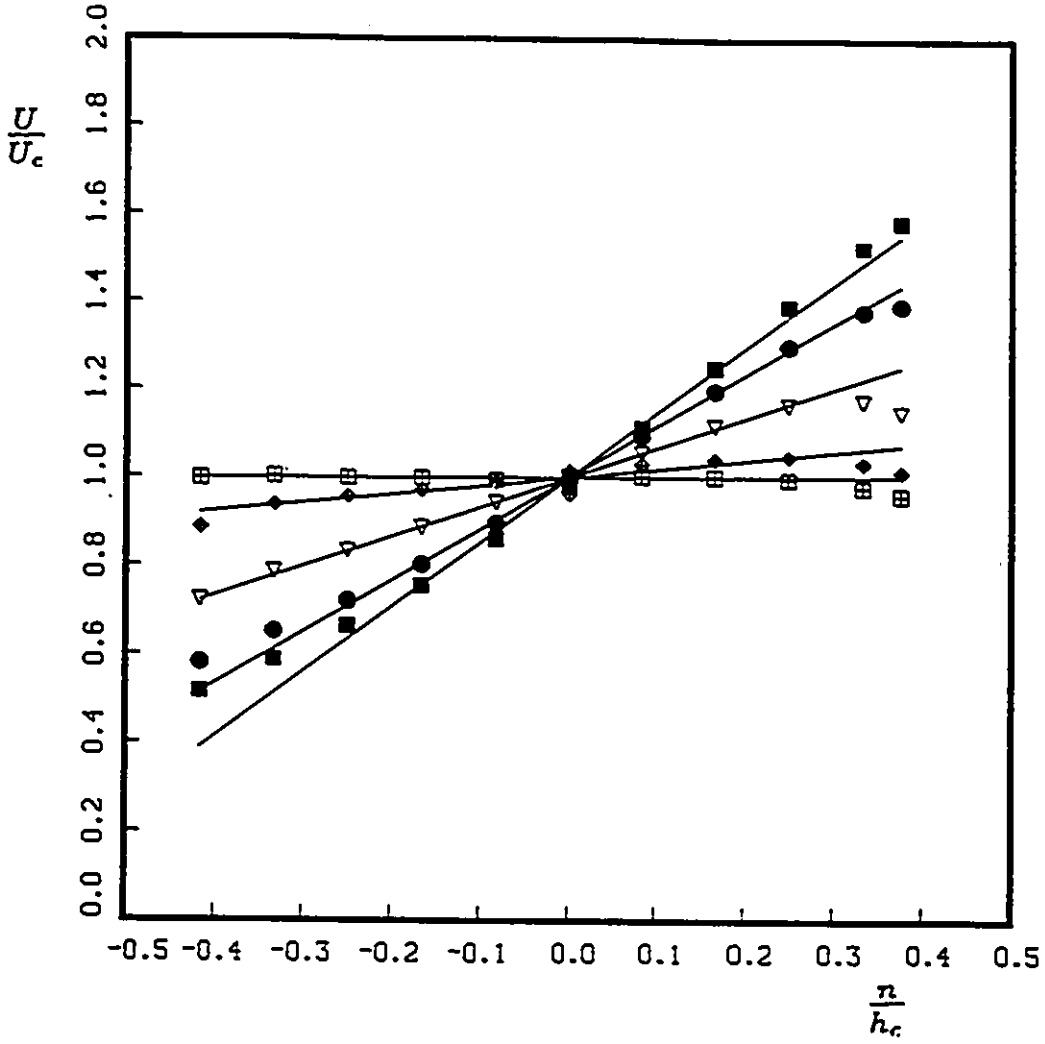

Figure 5.42: Transverse profiles of $\frac{U}{U_c}$ in the strongly curved section, positive shear; $\frac{s}{h_c}$=4.74, z=0. Symbols as in Table 5.3.

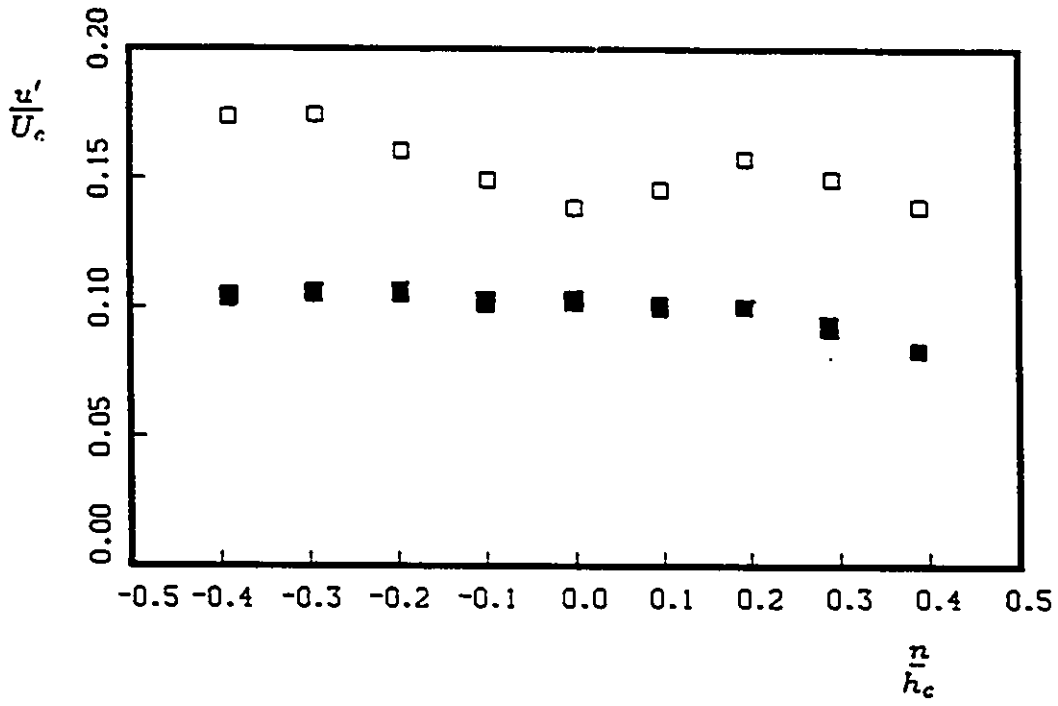

Figure 5.43: Spanwise variation of $\frac{u'}{U_c}$ in the mildly curved section; $\frac{s}{h_c}$=5.42, n=0. Symbols as in Table 5.3.

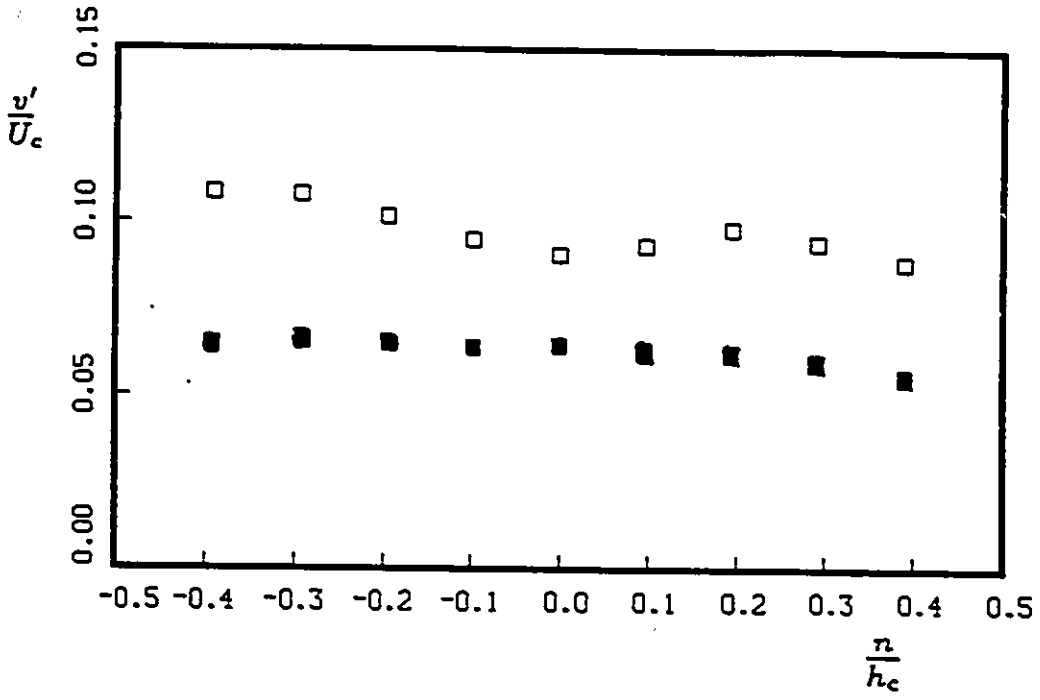

Figure 5.44: Spanwise variation of $\frac{v'}{U_c}$ in the mildly curved section; $\frac{s}{h_c}$=5.42, n=0. Symbols as in Table 5.3.

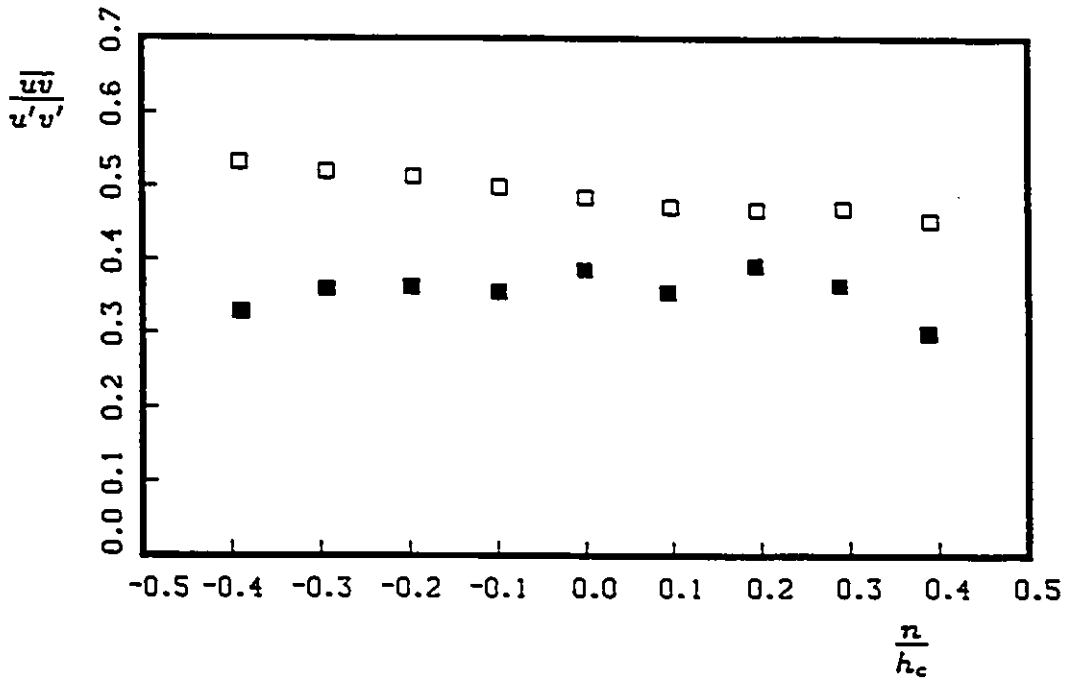

Figure 5.45: Spanwise variation of $\frac{\overline{uv}}{u'v'}$ in the mildly curved section; $\frac{s}{h_c}$=5.42, n=0. Symbols as in Table 5.3.

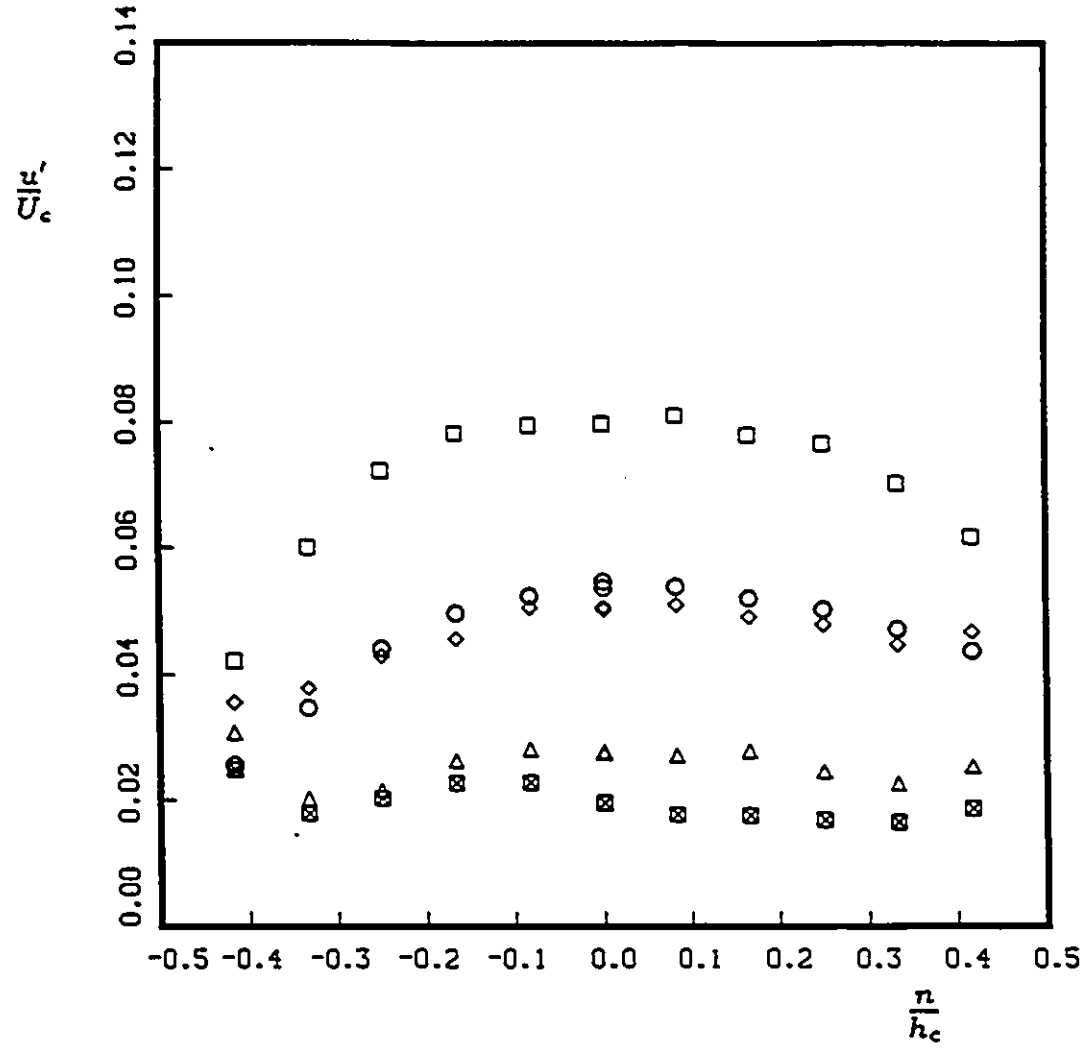

Figure 5.46: Transverse variation of $\frac{u'}{U_c}$ in the mildly curved section, negative shear; $\frac{s}{h_c}$=.42, z=0. Symbols as in Table 5.3.

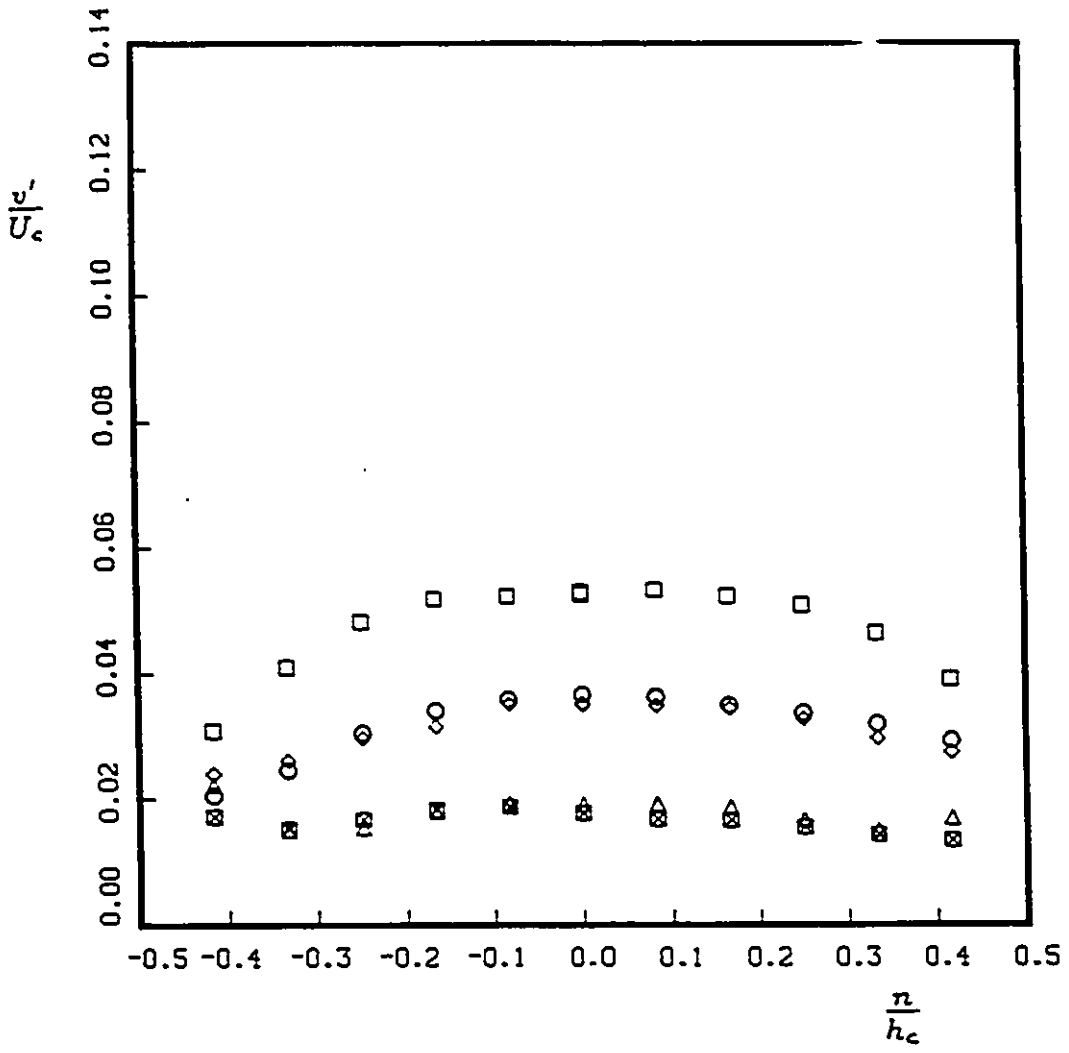

Figure 5.47: Transverse variation of $\frac{v'}{U_c}$ in the mildly curved section, negative shear; $\frac{s}{h_c}$=.42, z=0. Symbols as in Table 5.3.

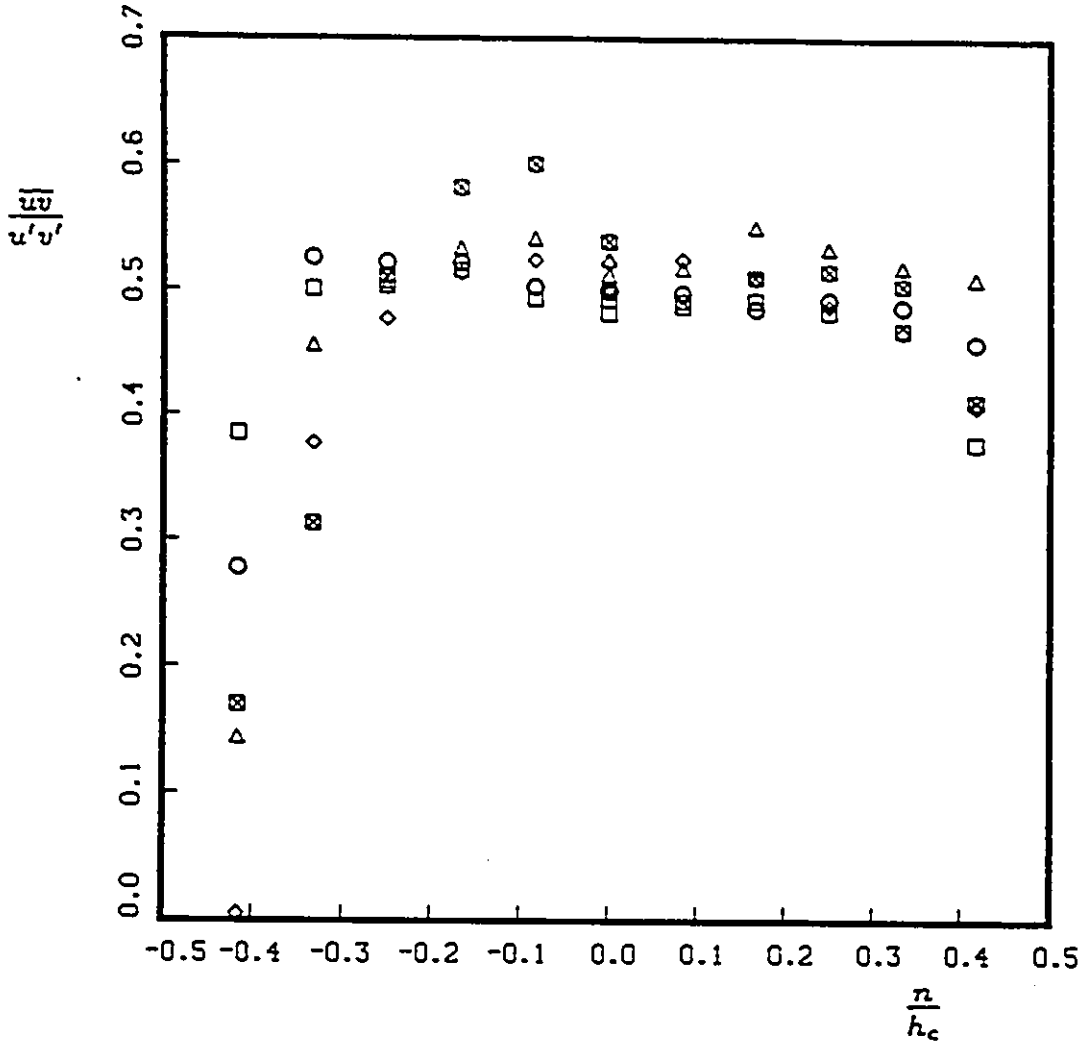

Figure 5.48: Transverse variation of $\frac{\overline{uv}}{u'v'}$ in the mildly curved section, negative shear; $\frac{s}{h_c}$=.42, z=0. Symbols as in Table 5.3.

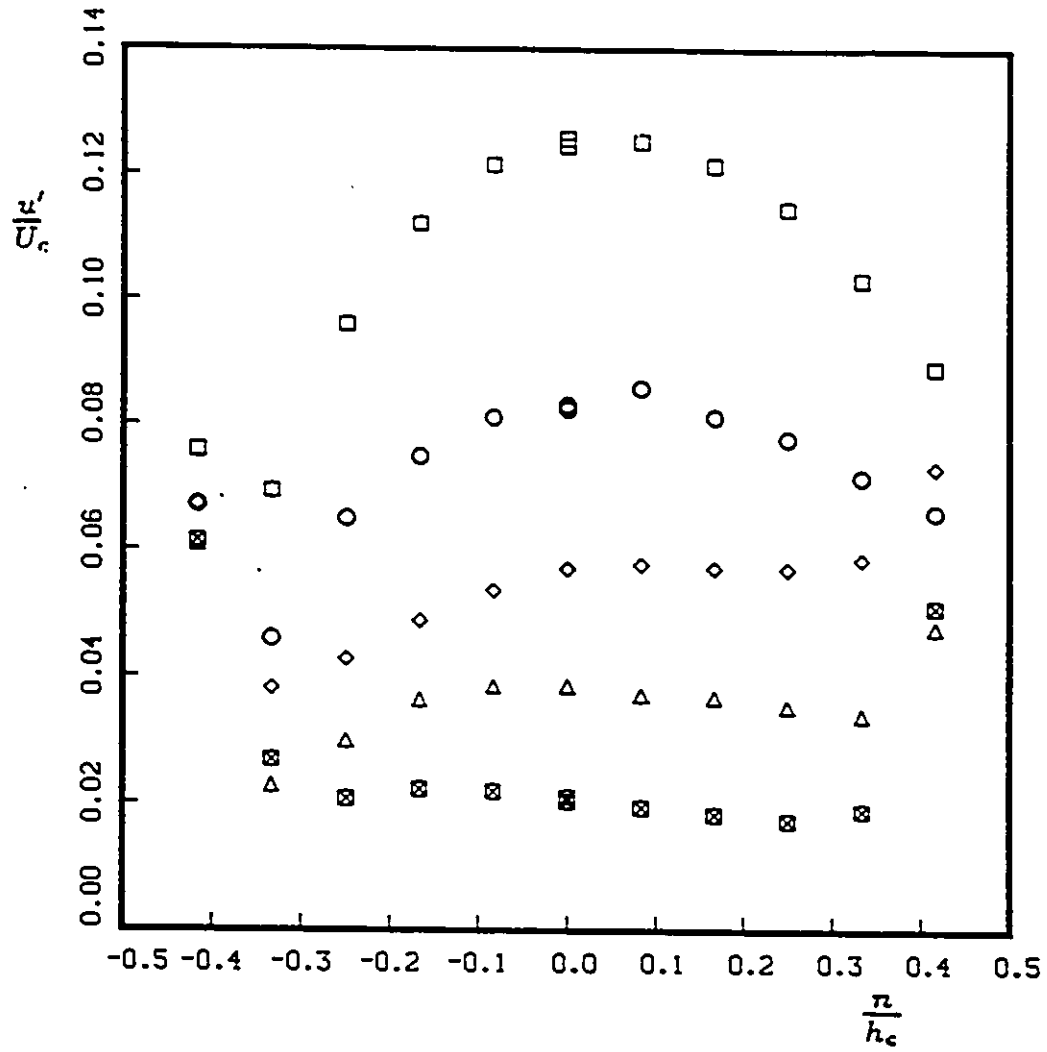

Figure 5.49: Transverse variation of $\frac{u'}{U_c}$ in the mildly curved section, negative shear; $\frac{s}{h_c}$=5.42, z=0. Symbols as in Table 5.3.

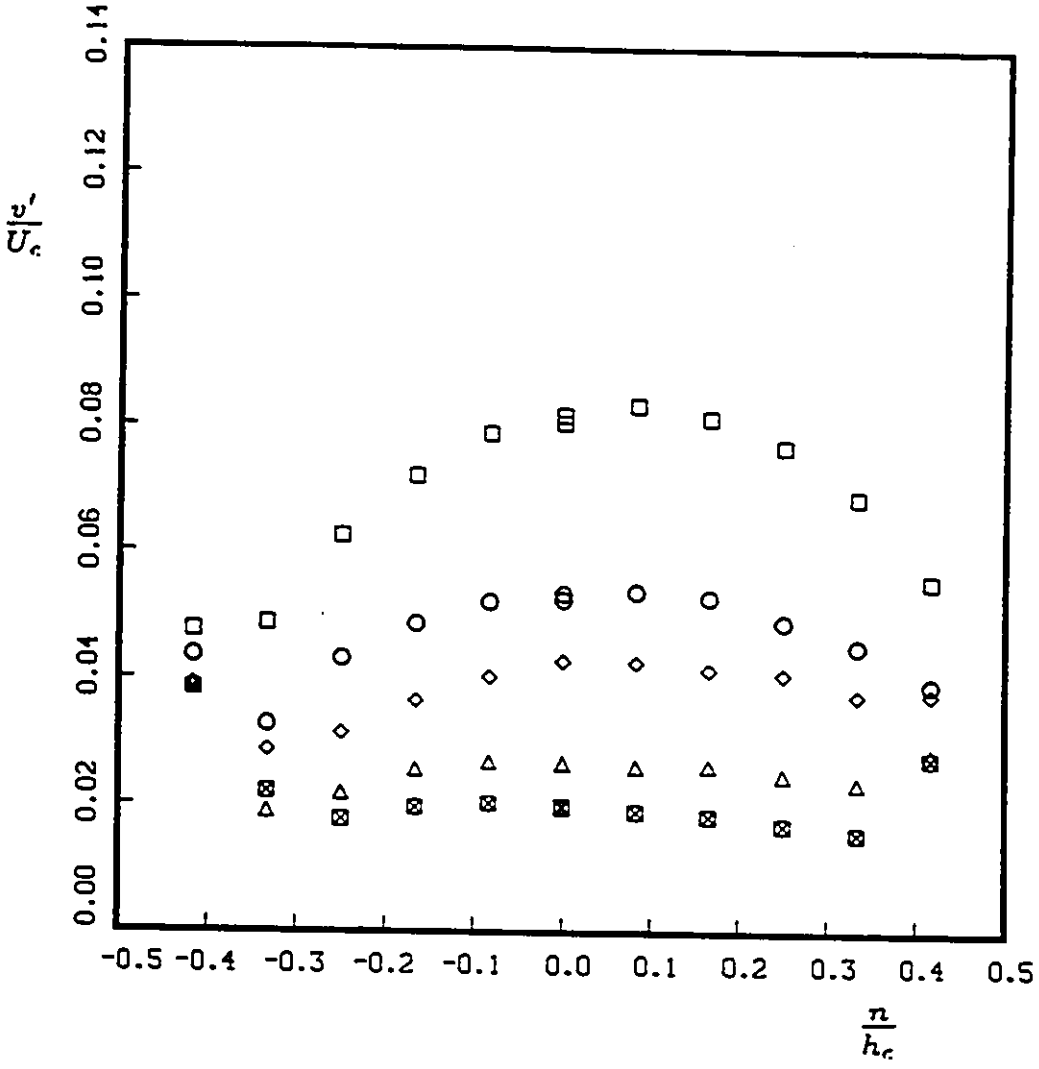

Figure 5.50: Transverse variation of $\frac{v'}{U_c}$ in the mildly curved section, negative shear; $\frac{s}{h_c}$=5.42, z=0. Symbols as in Table 5.3.

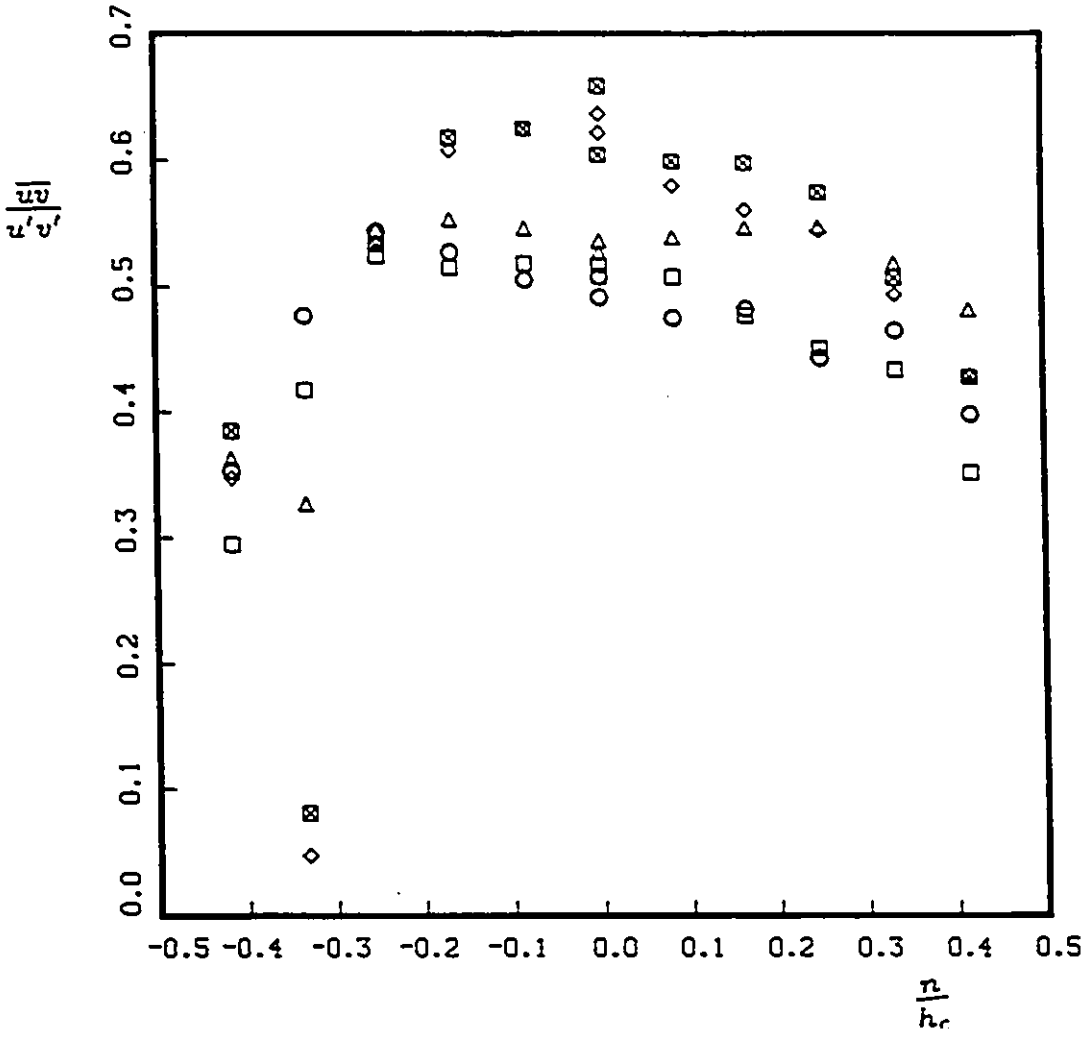

Figure 5.51: Transverse variation of $\frac{\overline{uv}}{u'v'}$ in the mildly curved section, negative shear; $\frac{s}{h_c}$=5.42, z=0. Symbols as in Table 5.3.

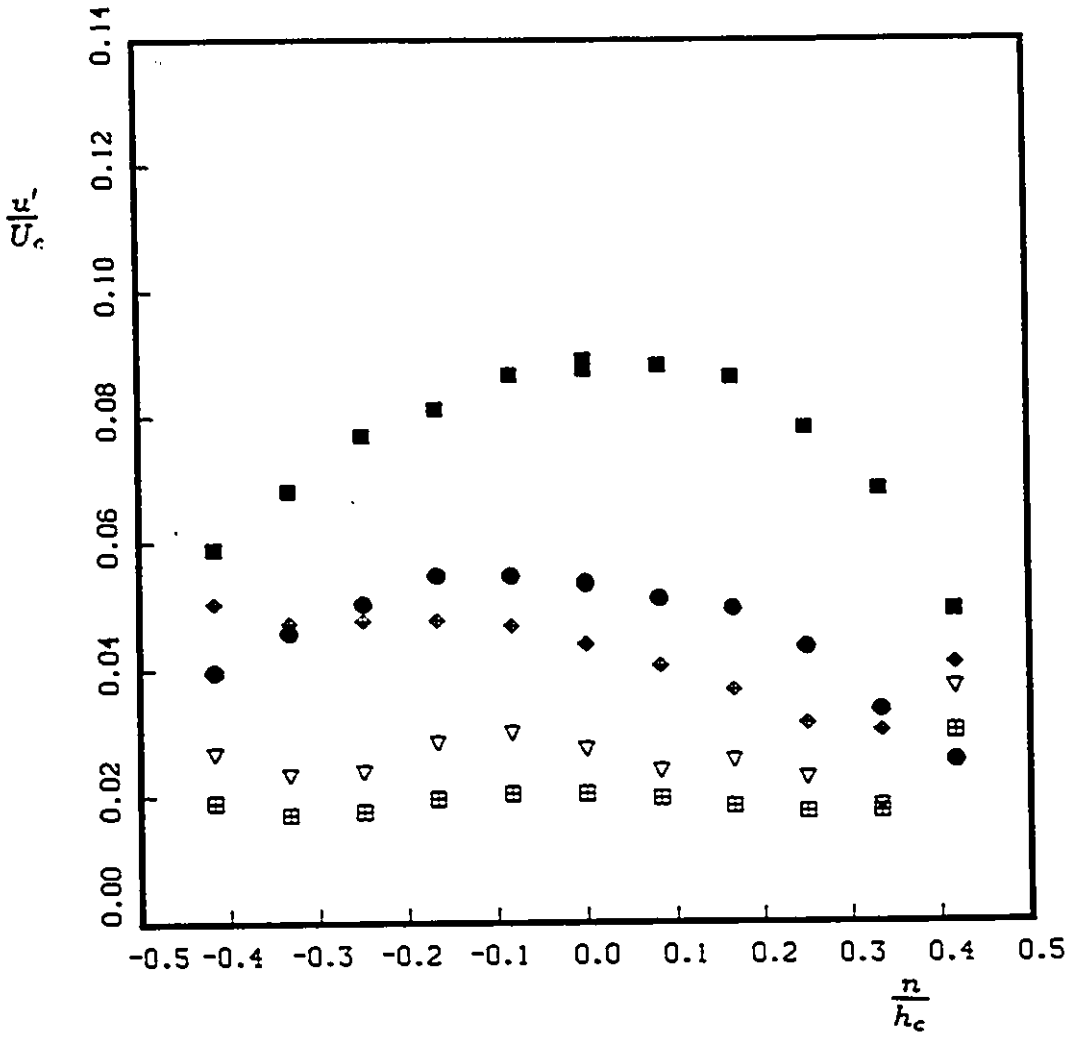

Figure 5.52: Transverse variation of $\frac{u'}{U_c}$ in the mildly curved section, positive shear; $\frac{s}{h_c}$=.42, z=0. Symbols as in Table 5.3.

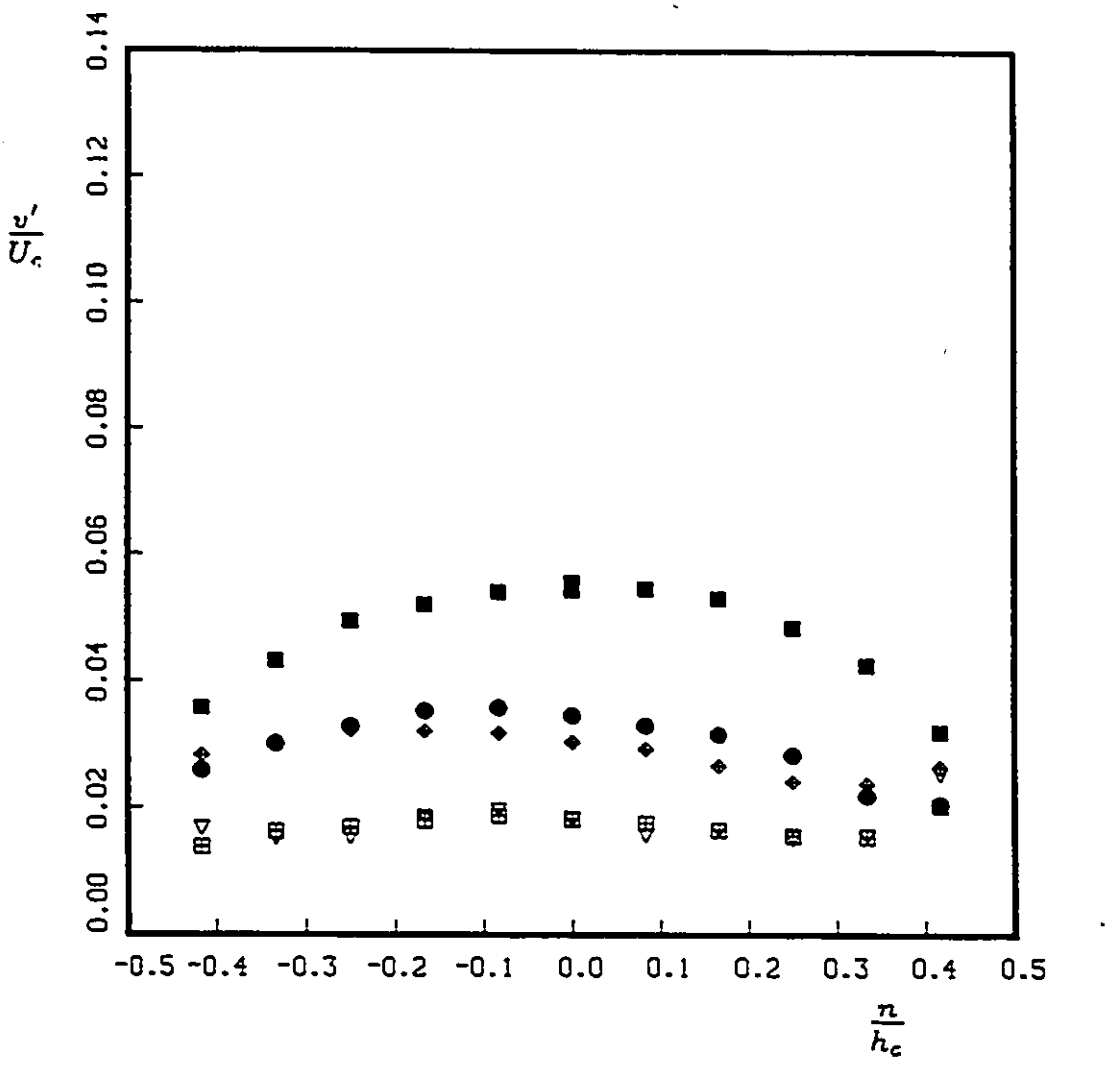

Figure 5.53: Transverse variation of $\frac{v'}{U_c}$ in the mildly curved section, positive shear; $\frac{s}{h_c}$=.42, z=0. Symbols as in Table 5.3.

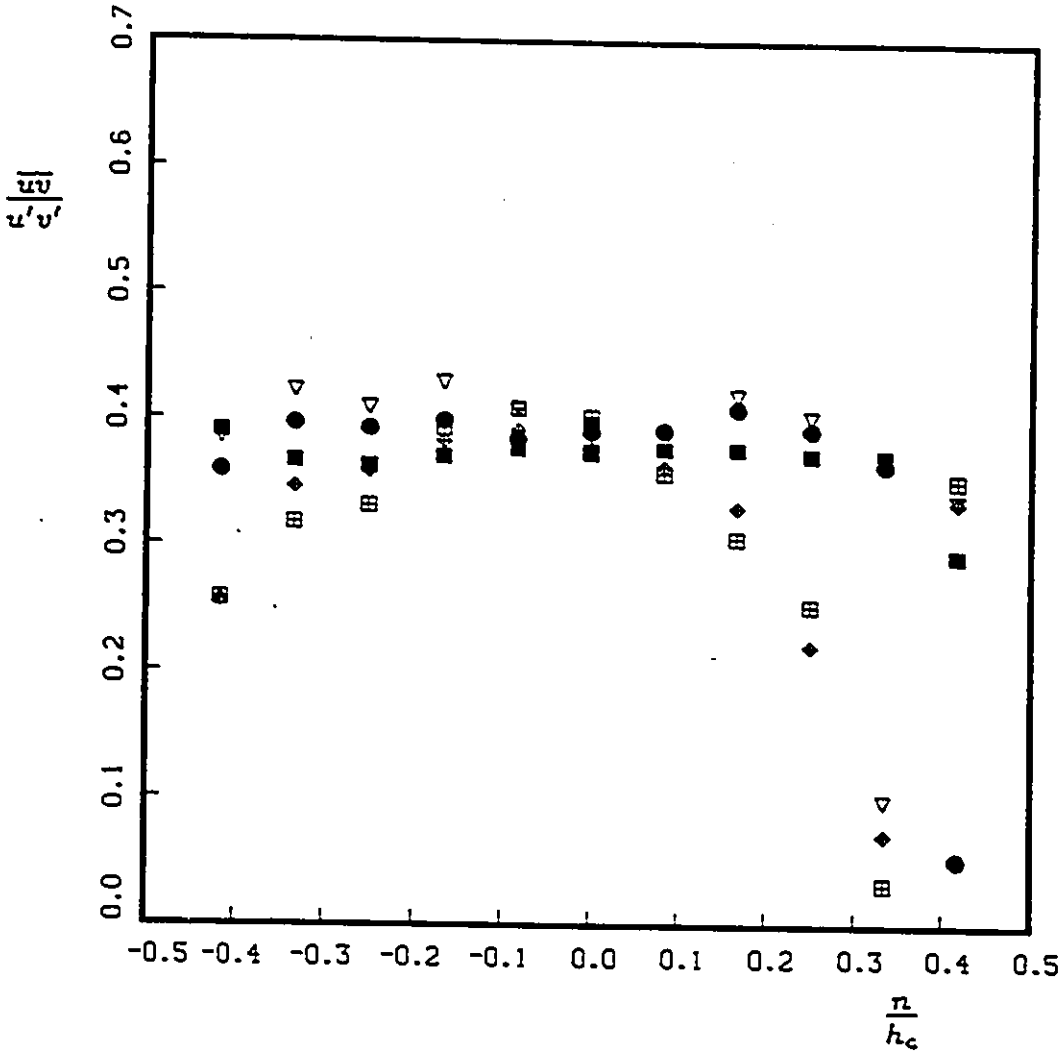

Figure 5.54: Transverse variation of $\frac{\overline{uv}}{u'v'}$ in the mildly curved section, positive shear; $\frac{s}{h_c}$=.42, z=0. Symbols as in Table 5.3.

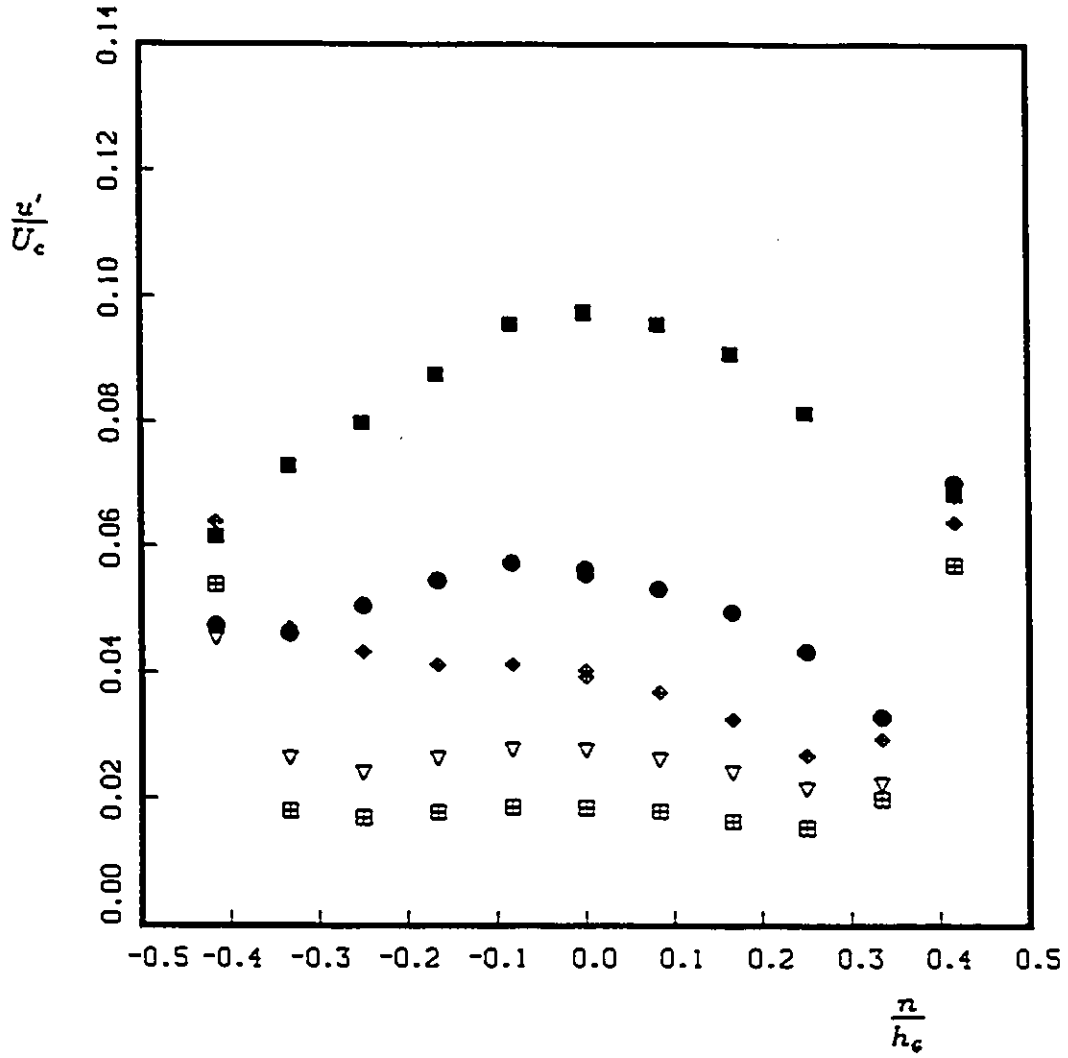

Figure 5.55: Transverse variation of $\frac{u'}{U_c}$ in the mildly curved section, positive shear; $\frac{s}{h_c}$=5.42, z=0. Symbols as in Table 5.3.

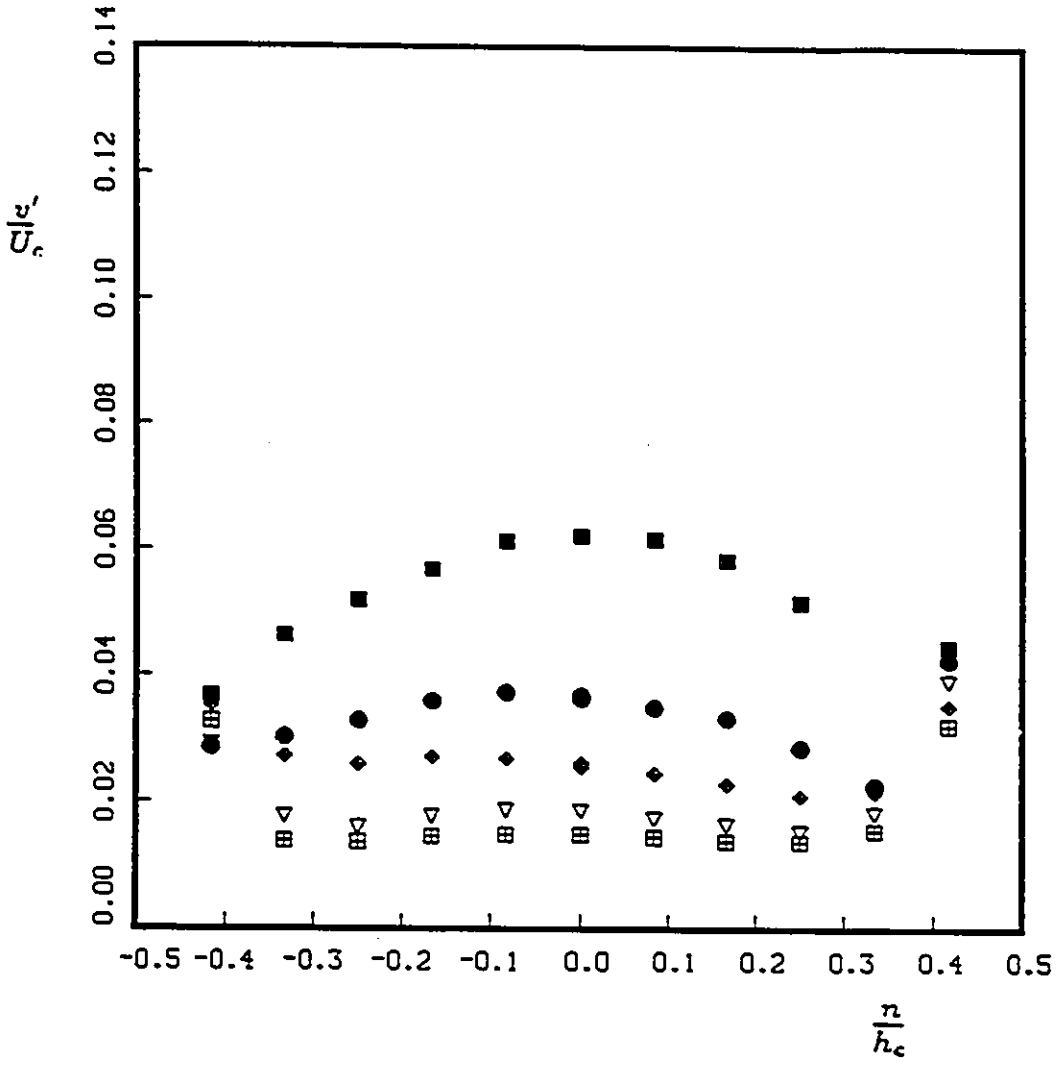

Figure 5.56: Transverse variation of $\frac{v'}{U_c}$ in the mildly curved section, positive shear: $\frac{s}{h_c}$=5.42, z=0. Symbols as in Table 5.3.

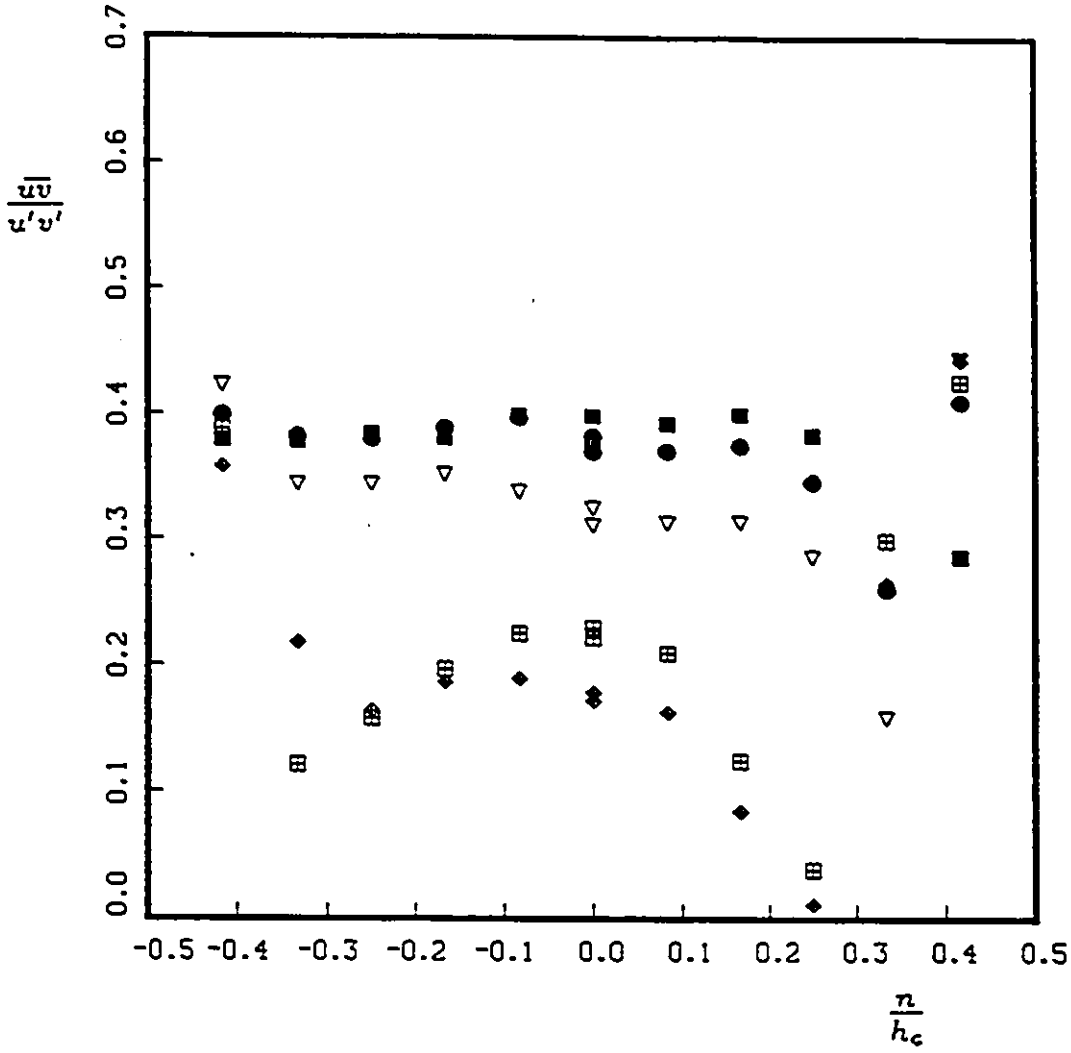

Figure 5.57: Transverse variation of $\frac{\overline{uv}}{u'v'}$ in the mildly curved section, positive shear; $\frac{s}{h_c}$=5.42, z=0. Symbols as in Table 5.3.

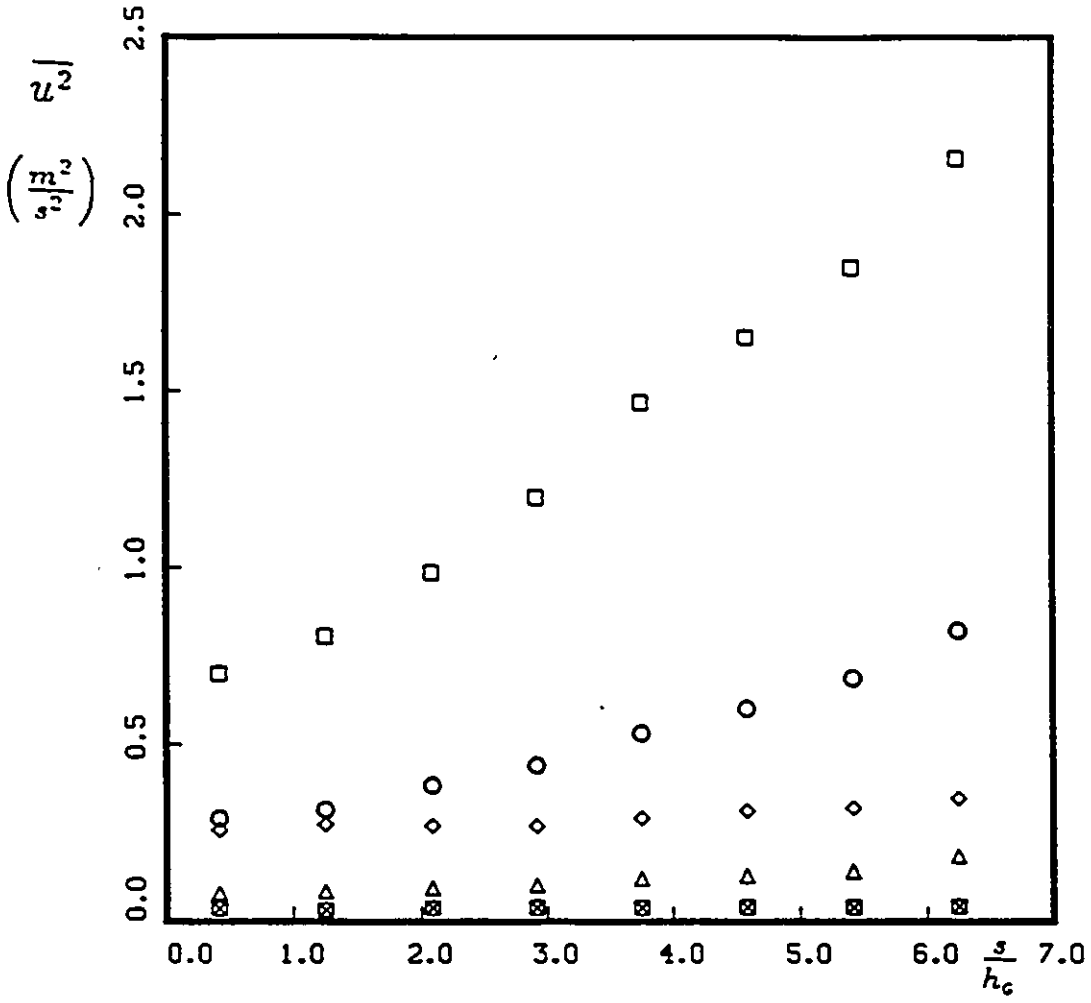

Figure 5.58: Development of $\overline{u^2}$ along the wind tunnel centerline in the mildly curved section; negative shear. Symbols as in Table 5.3.

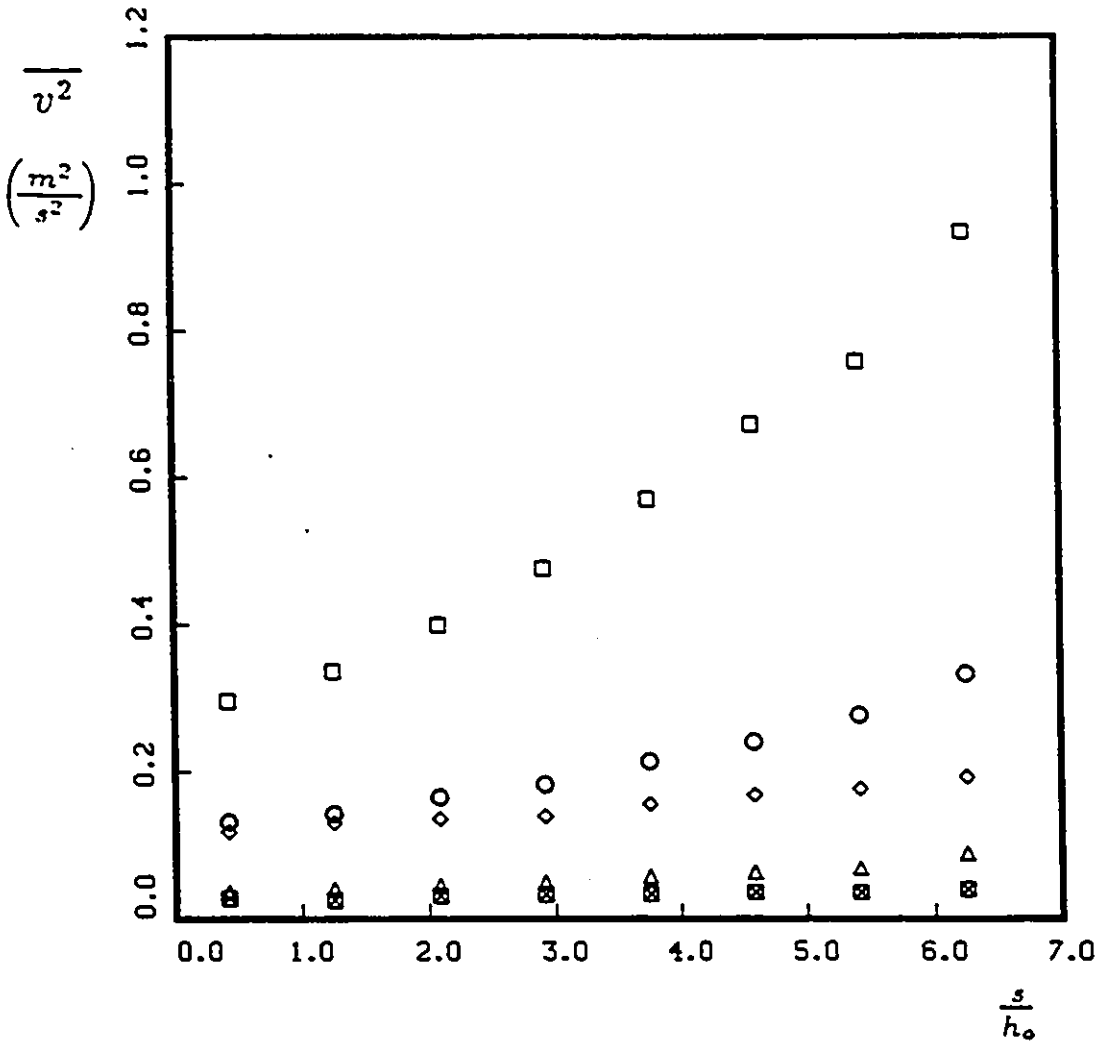

Figure 5.59: Development of $\overline{v^2}$ along the wind tunnel centerline in the mildly curved section; negative shear. Symbols as in Table 5.3.

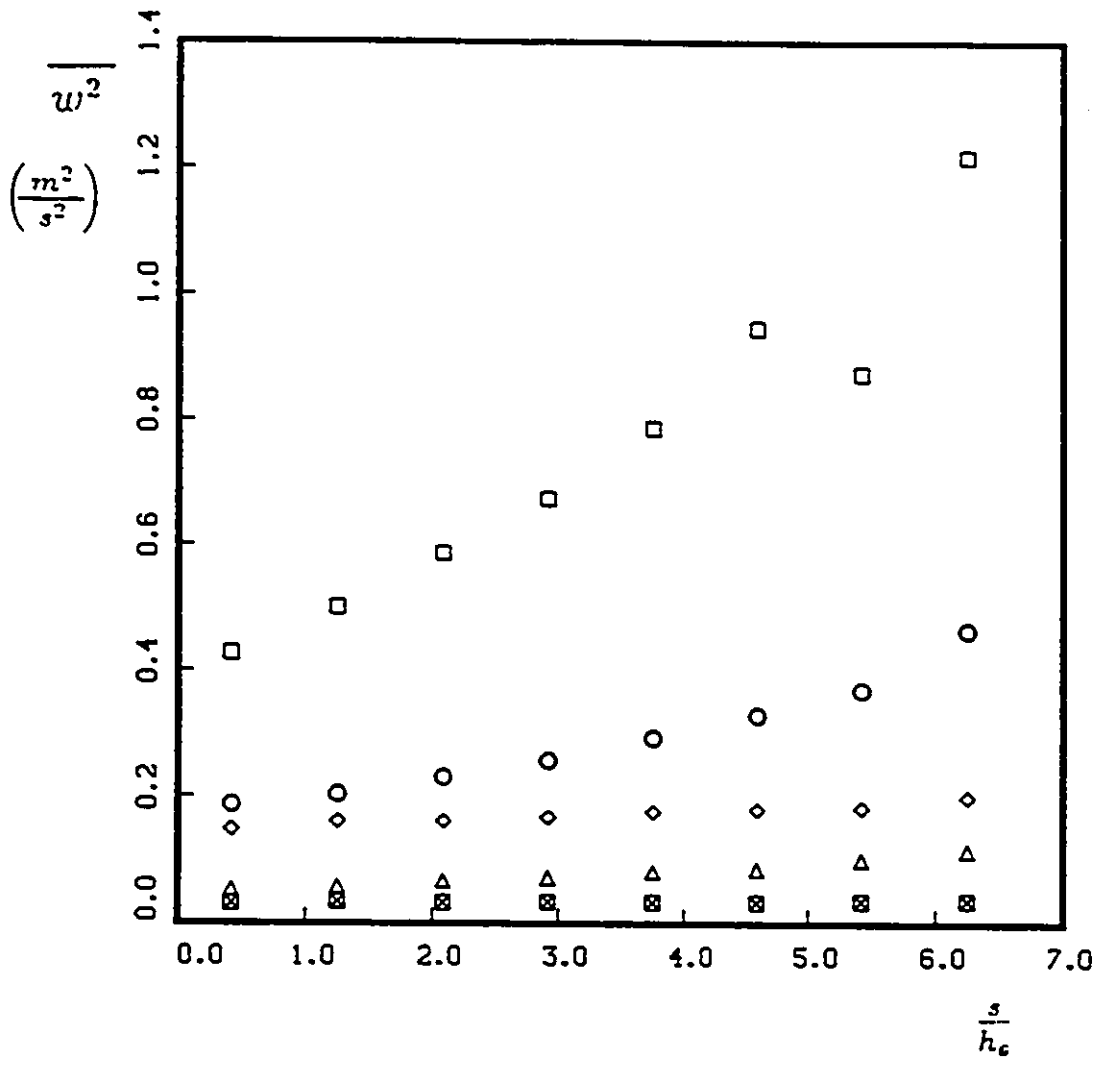

Figure 5.60: Development of $\overline{w^2}$ along the wind tunnel centerline in the mildly curved section; negative shear. Symbols as in Table 5.3.

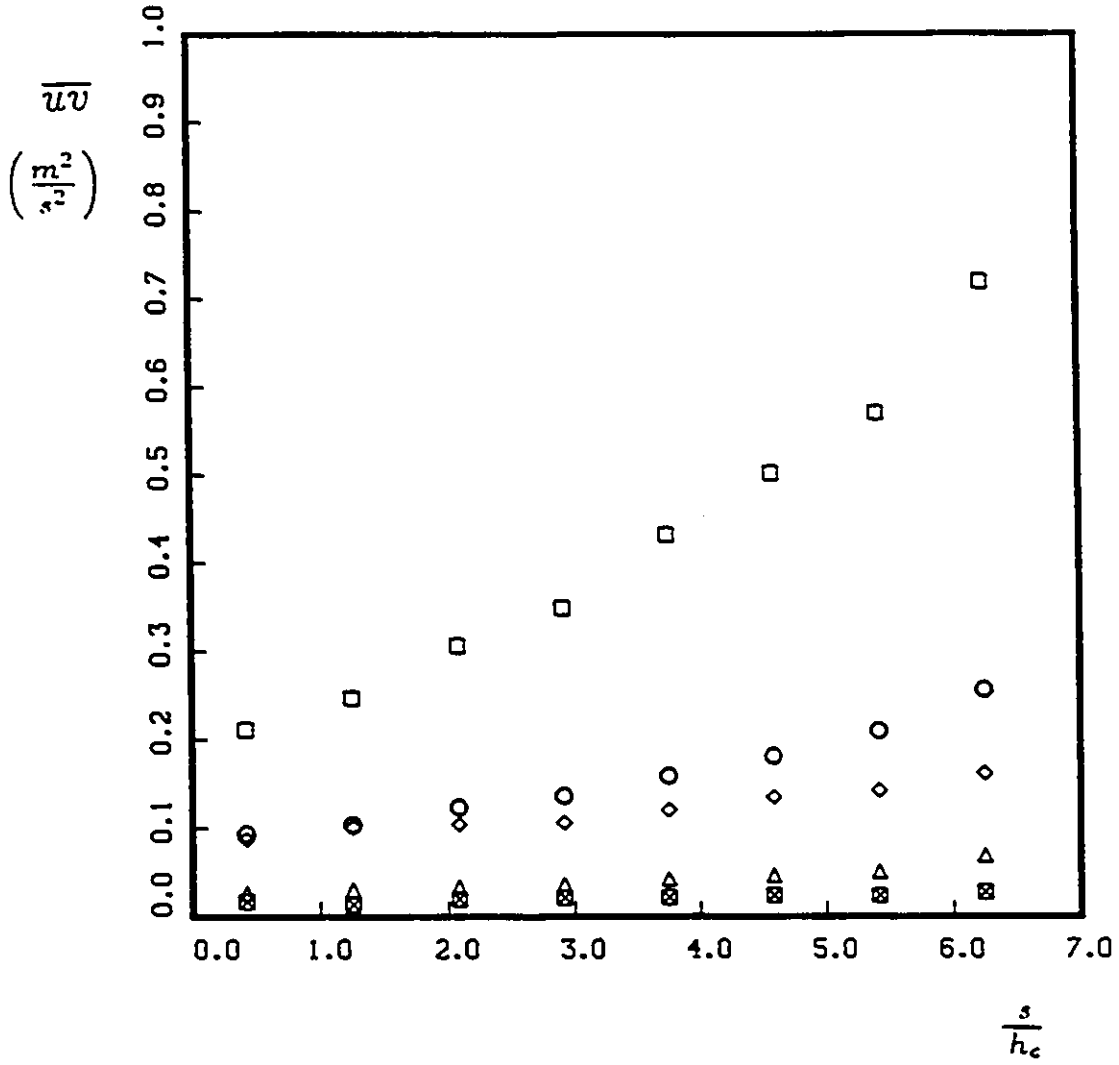

Figure 5.61: Development of $\overline{uv}$ along the wind tunnel centerline in the mildly curved section; negative shear. Symbols as in Table 5.3.

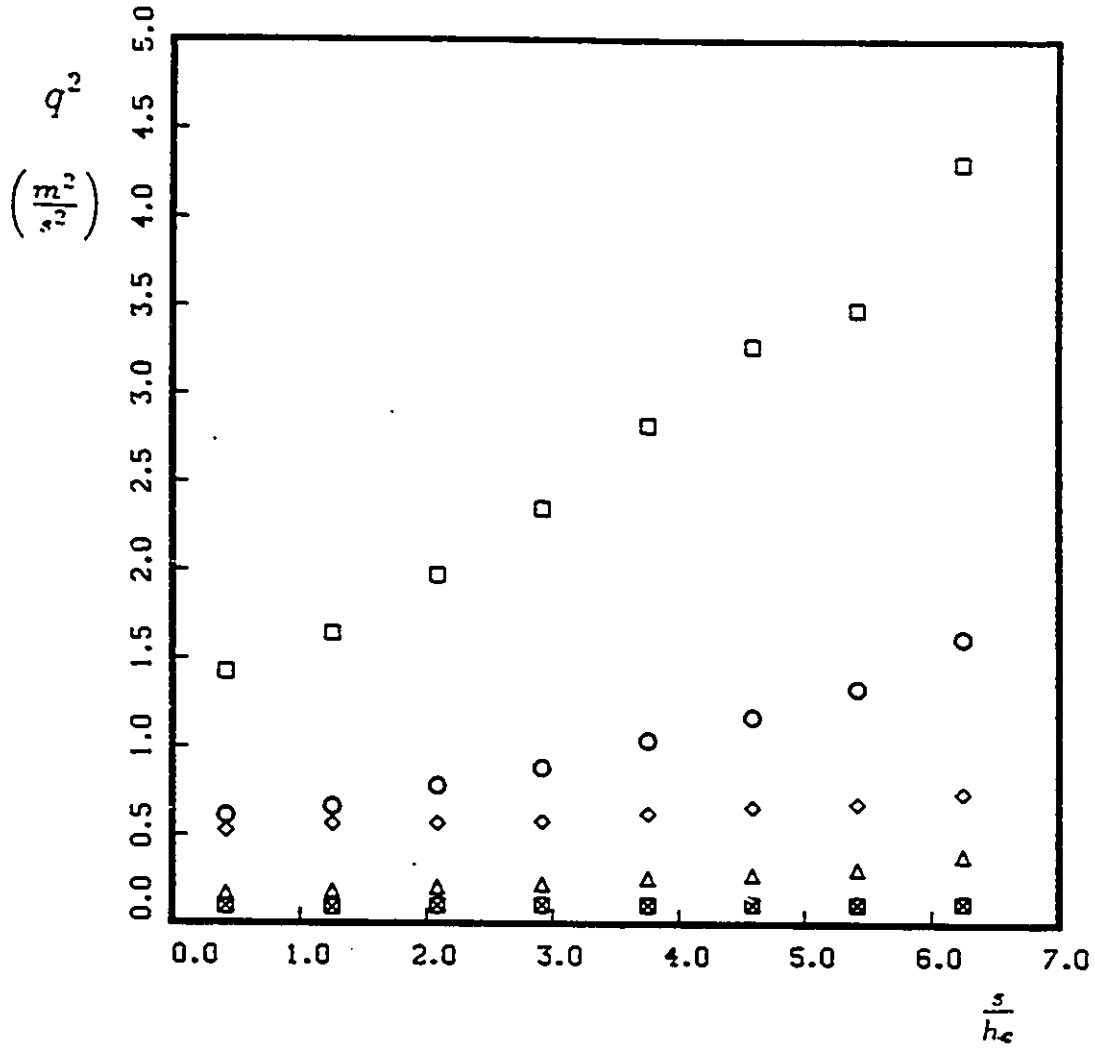

Figure 5.62: Development of q^2 along the wind tunnel centerline in the mildly curved section; negative shear. Symbols as in Table 5.3.

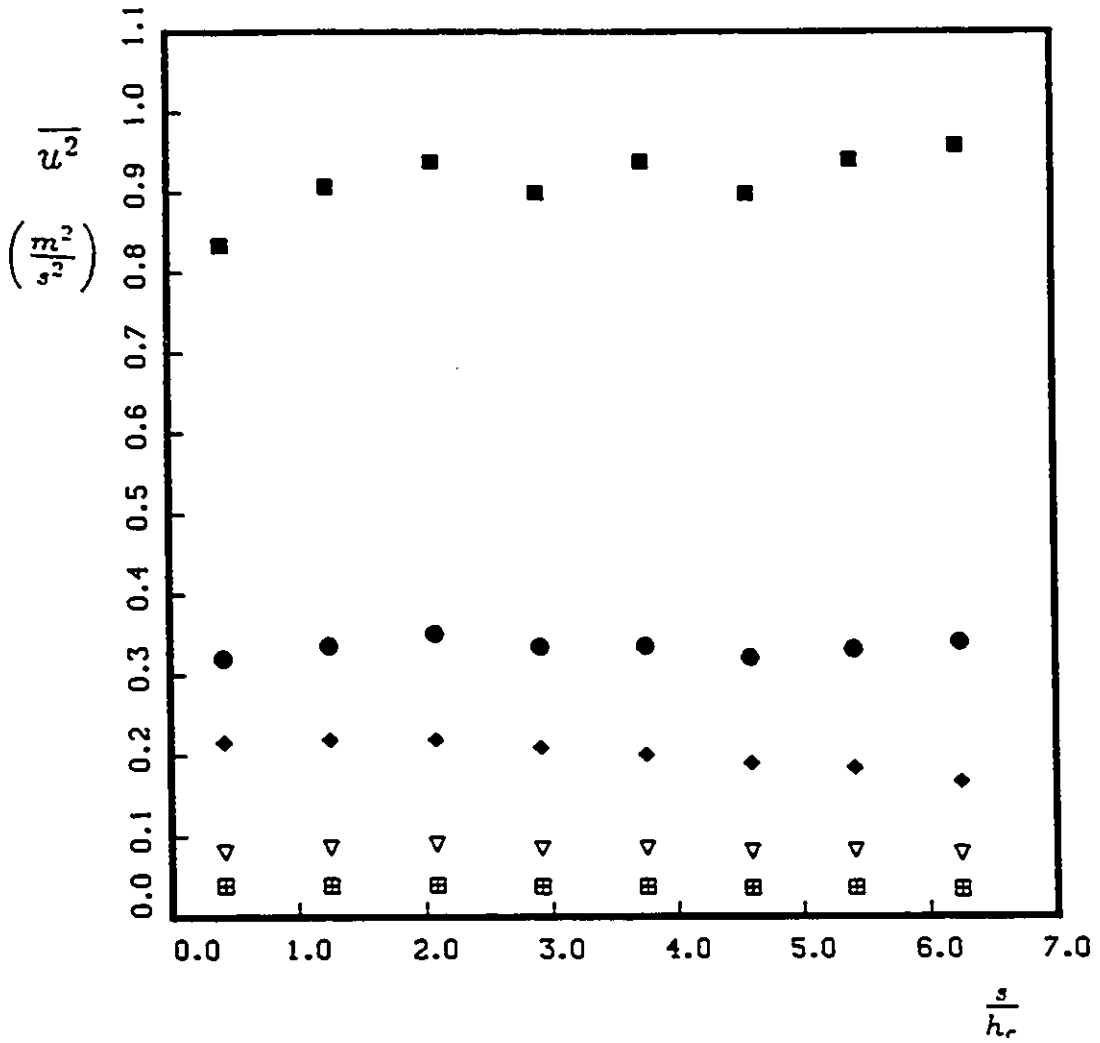

Figure 5.63: Development of $\overline{u^2}$ along the wind tunnel centerline in the mildly curved section; positive shear. Symbols as in Table 5.3.

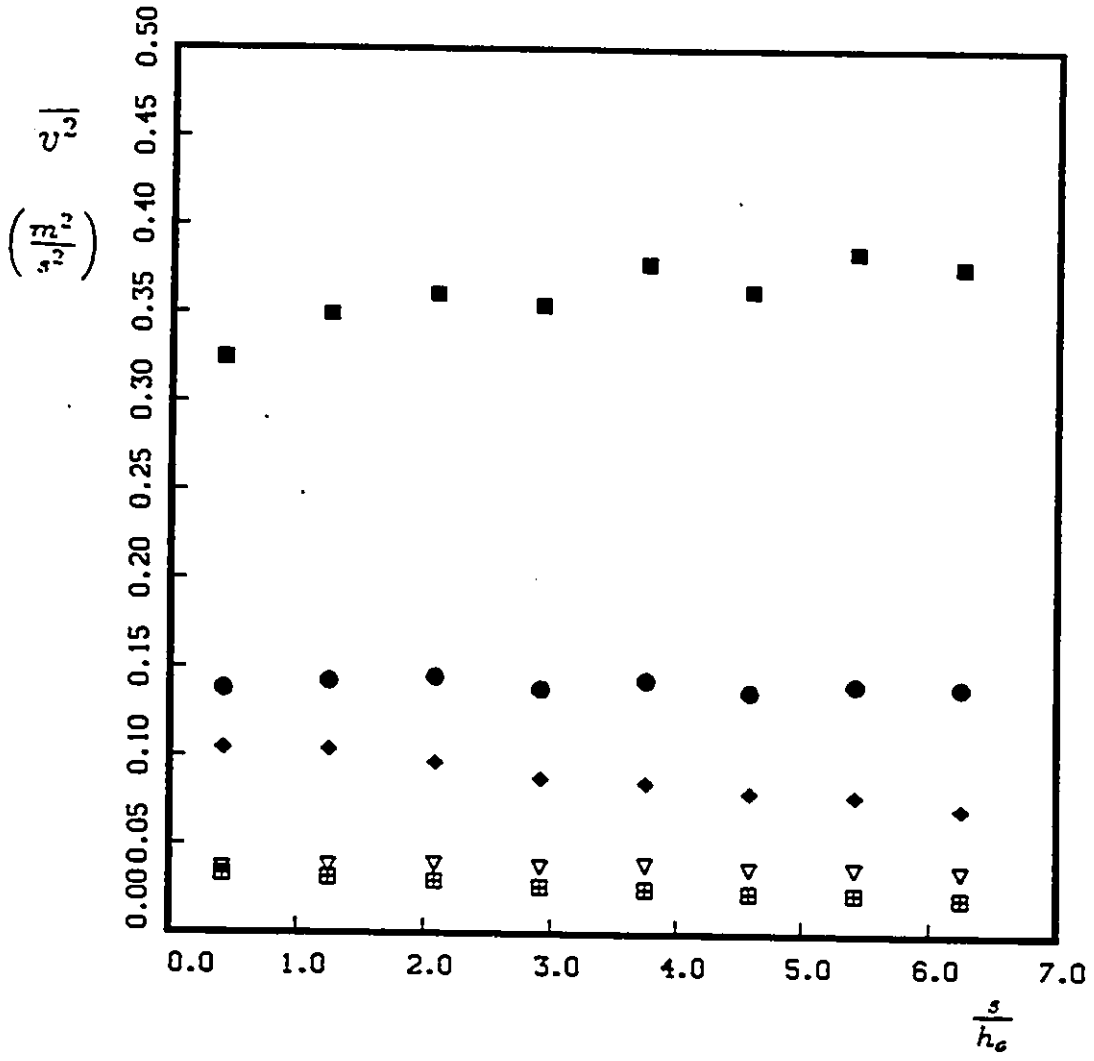

Figure 5.64: Development of $\overline{v^2}$ along the wind tunnel centerline in the mildly curved section; positive shear. Symbols as in Table 5.3.

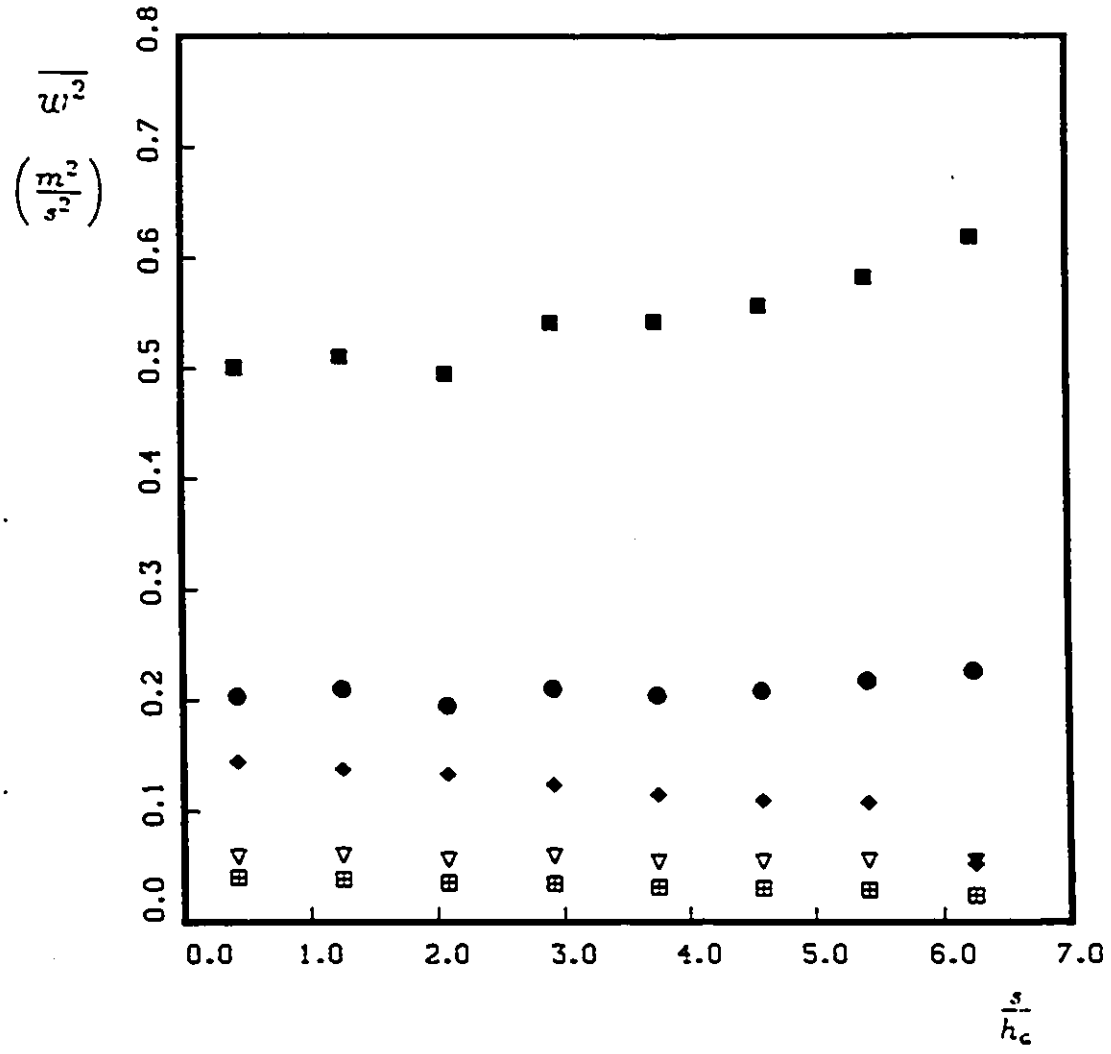

Figure 5.65: Development of $\overline{w^2}$ along the wind tunnel centerline in the mildly curved section: positive shear. Symbols as in Table 5.3.

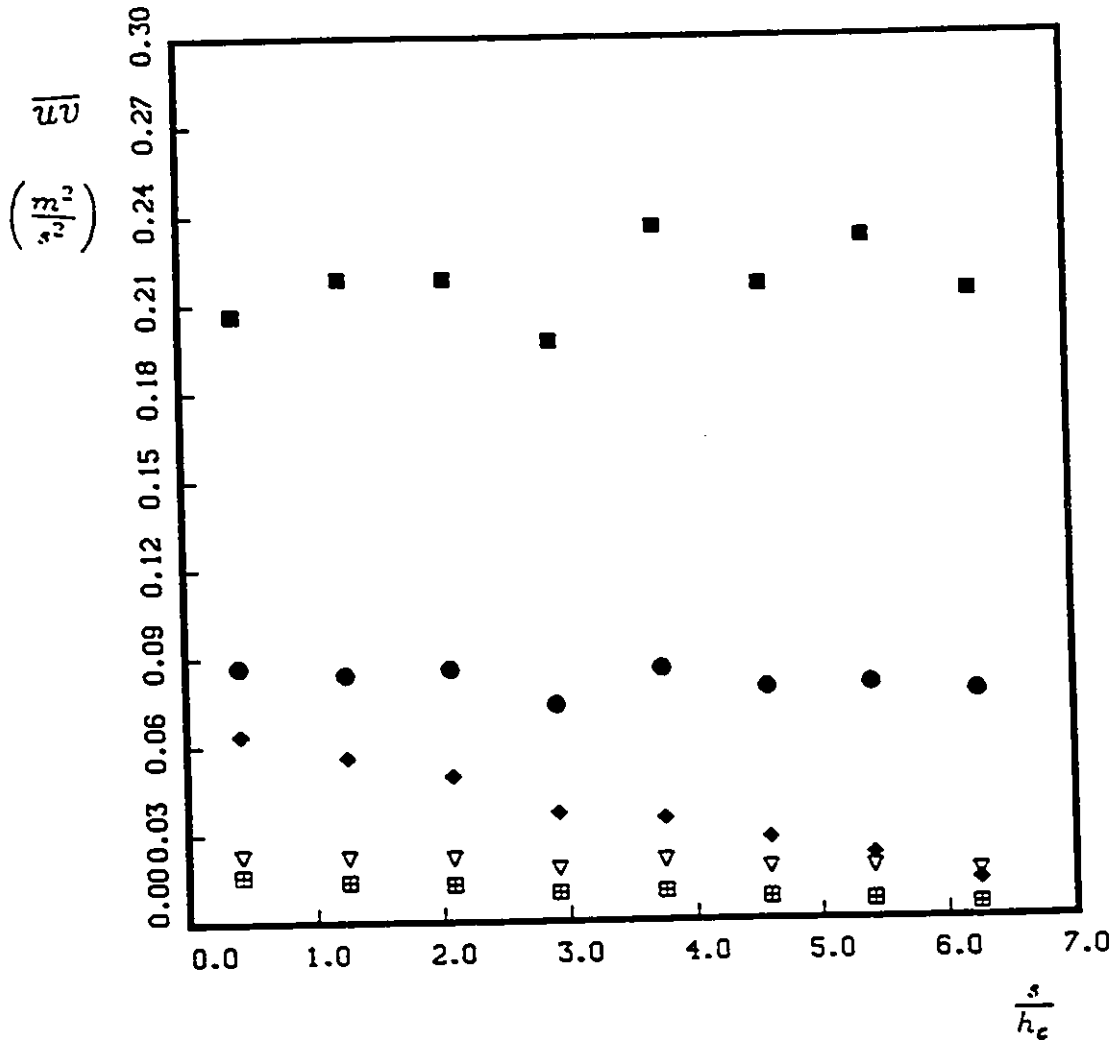

Figure 5.66: Development of $\overline{uv}$ along the wind tunnel centerline in the mildly curved section; positive shear. Symbols as in Table 5.3.

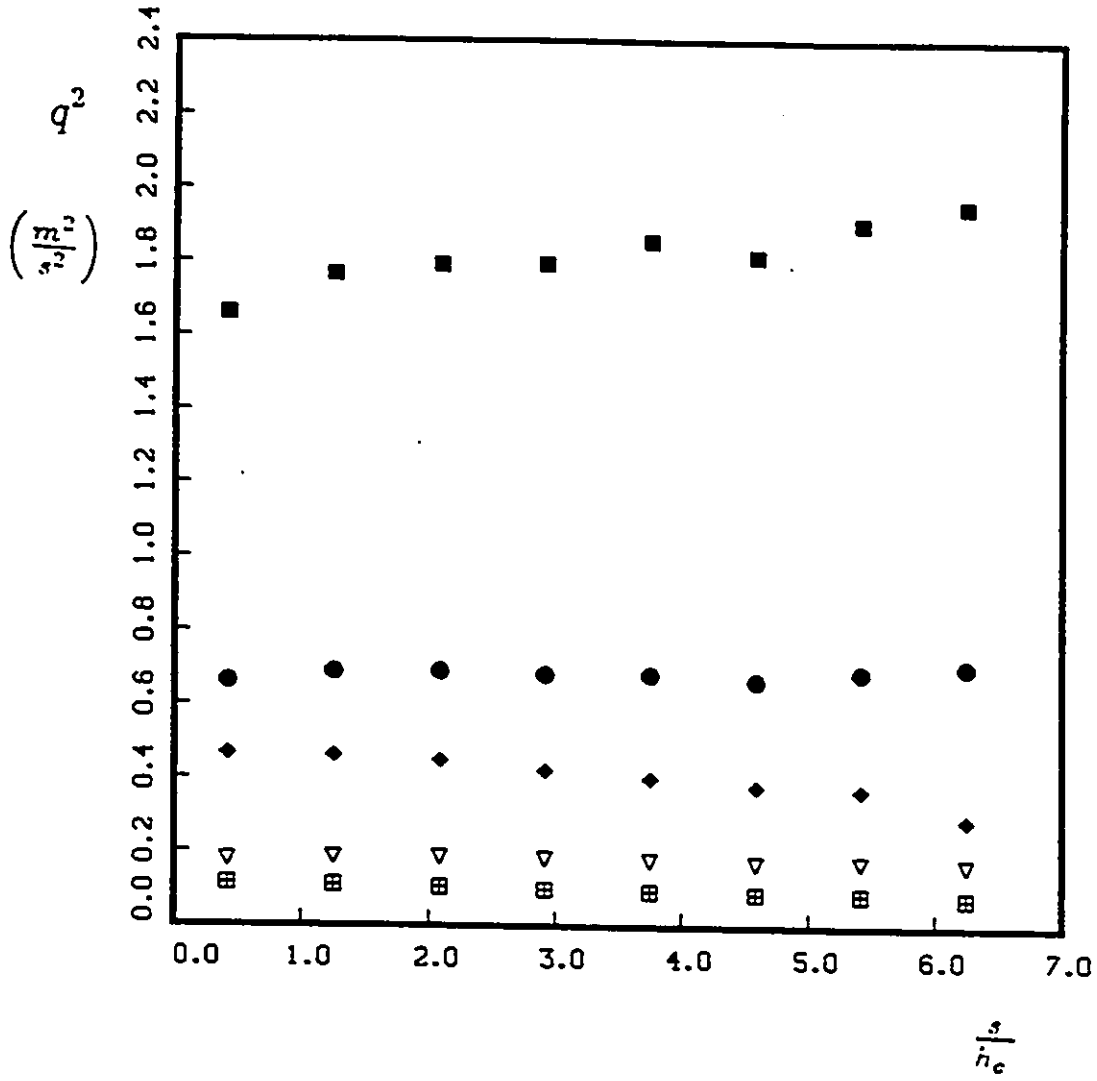

Figure 5.67: Development of q^2 along the wind tunnel centerline in the mildly curved section; positive shear. Symbols as in Table 5.3.

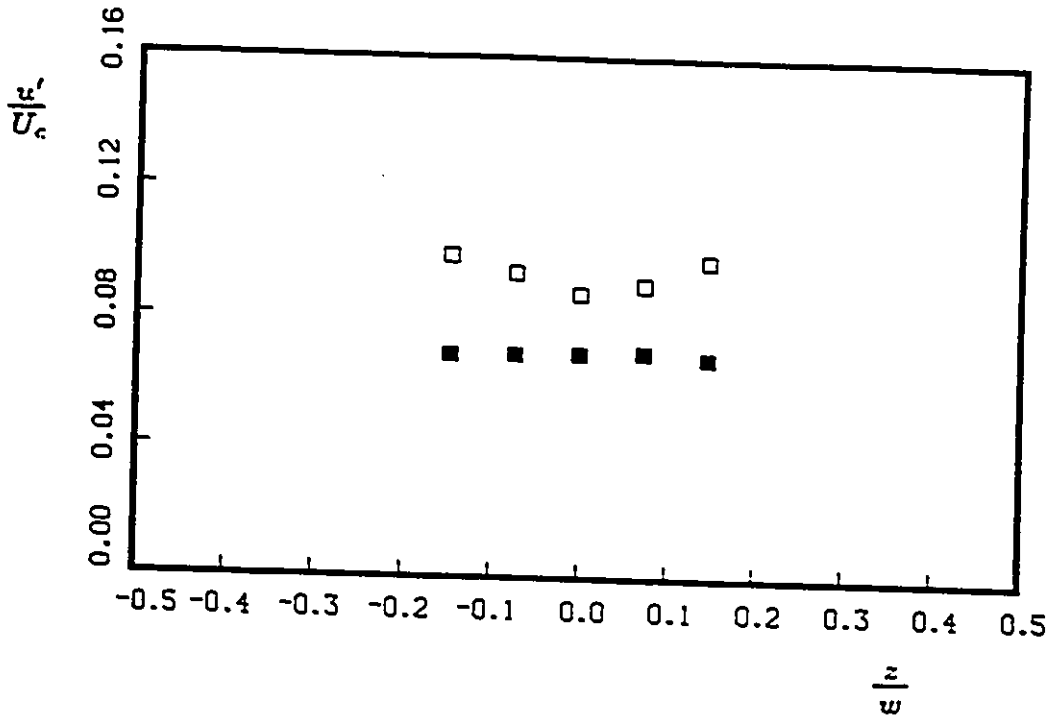

Figure 5.68: Spanwise variation of $\frac{u'}{U_c}$ in the strongly curved section; $\frac{s}{h_c}$=2.15, n=0. Symbols as in Table 5.3.

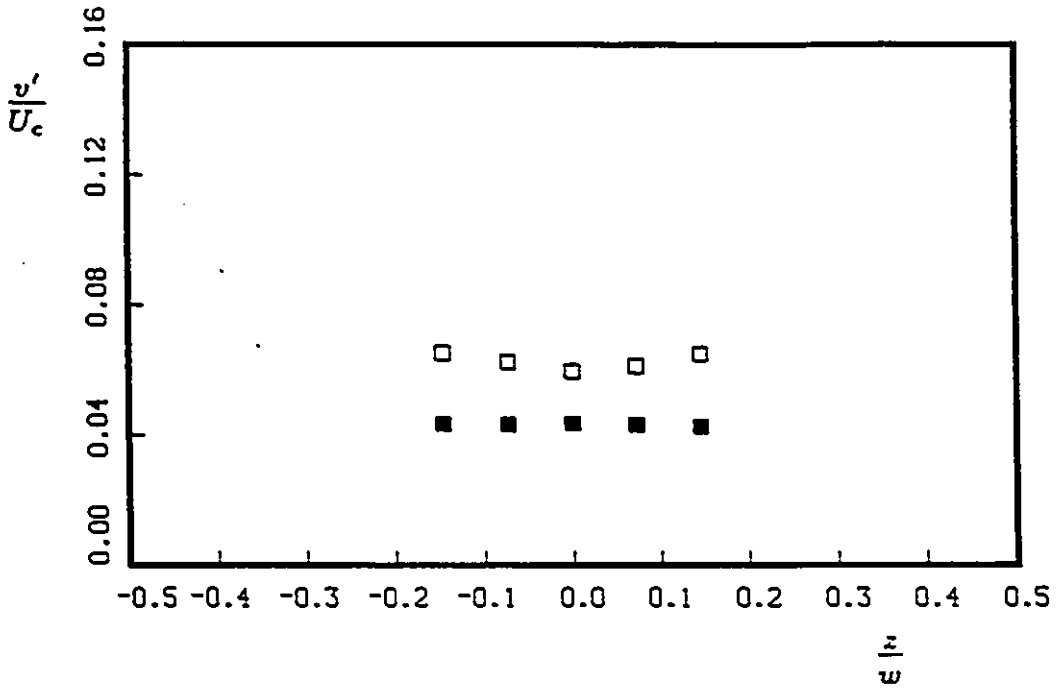

Figure 5.69: Spanwise variation of $\frac{v'}{U_e}$ in the strongly curved section; $\frac{s}{h_e}$=2.15, n=0. Symbols as in Table 5.3.

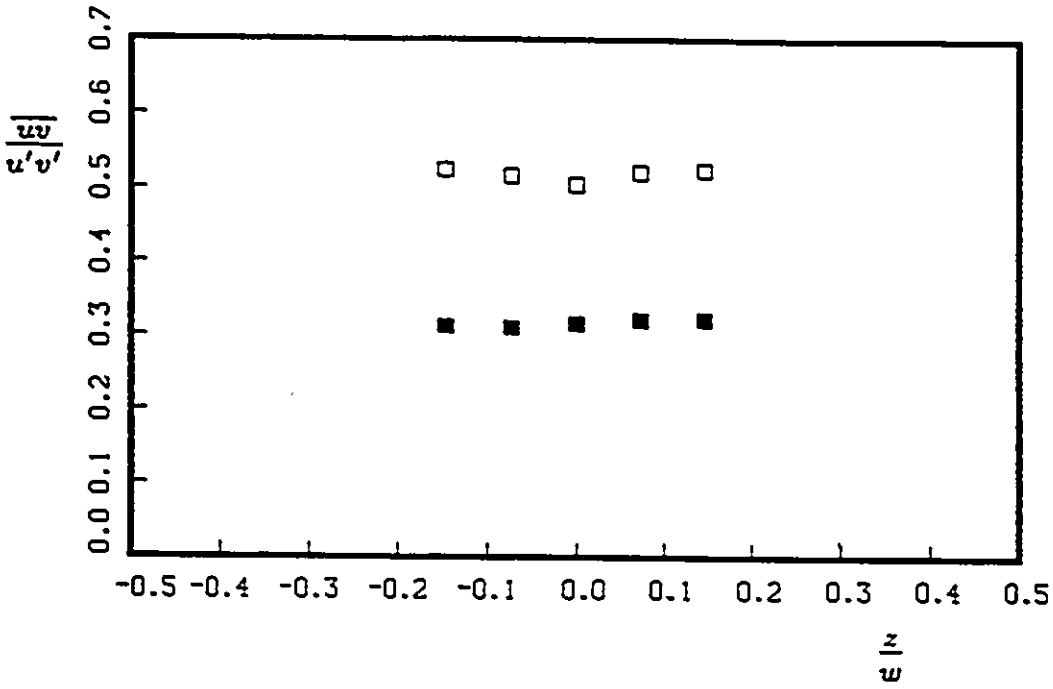

Figure 5.70: Spanwise variation of $\frac{\overline{uv}}{u'v'}$ in the strongly curved section; $\frac{s}{h_c}$=2.15, n=0. Symbols as in Table 5.3.

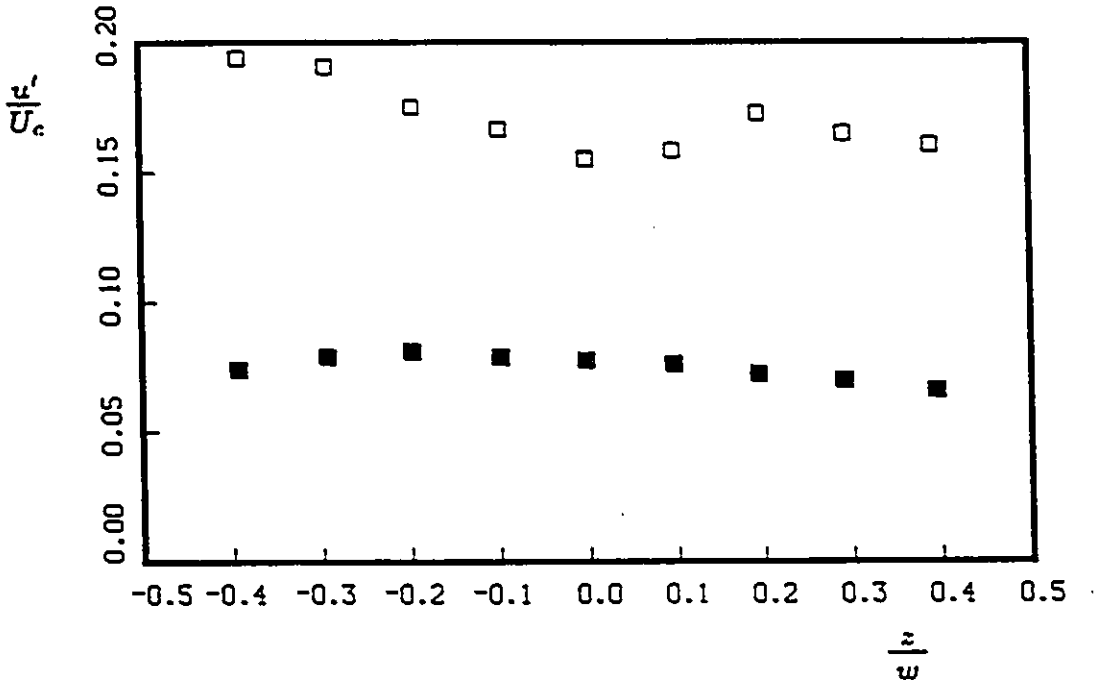

Figure 5.71: Spanwise variation of $\frac{u'}{U_c}$ in the strongly curved section; $\frac{s}{h_c}$=4.74, n=0. Symbols as in Table 5.3.

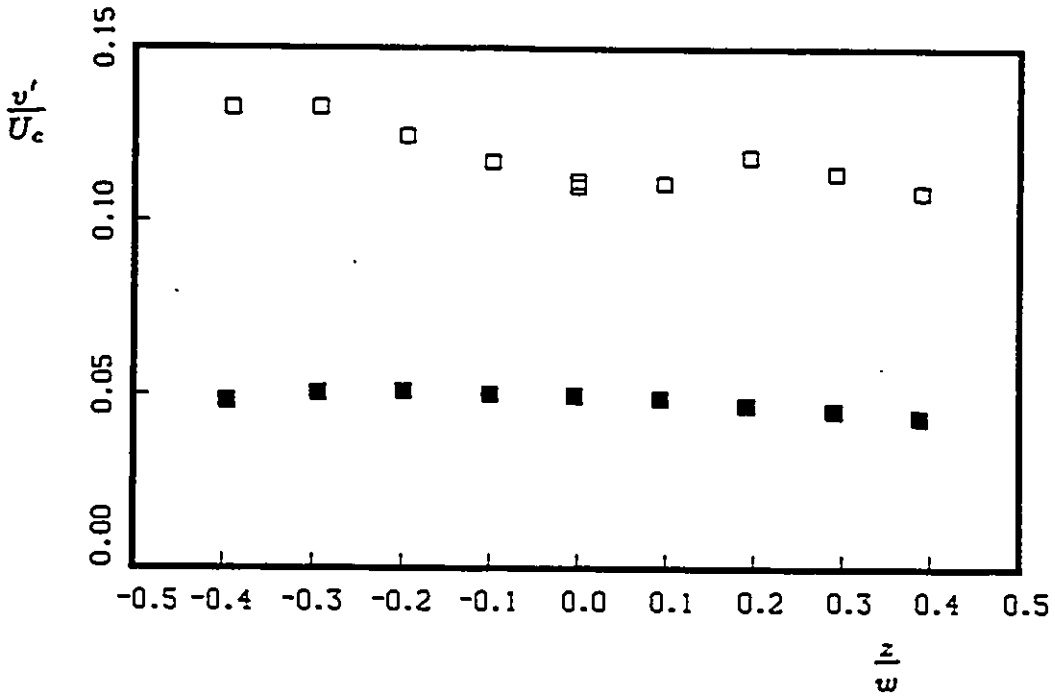

Figure 5.72: Spanwise variation of $\frac{v'}{U_c}$ in the strongly curved section; $\frac{s}{h_c}$=4.74, n=0. Symbols as in Table 5.3.

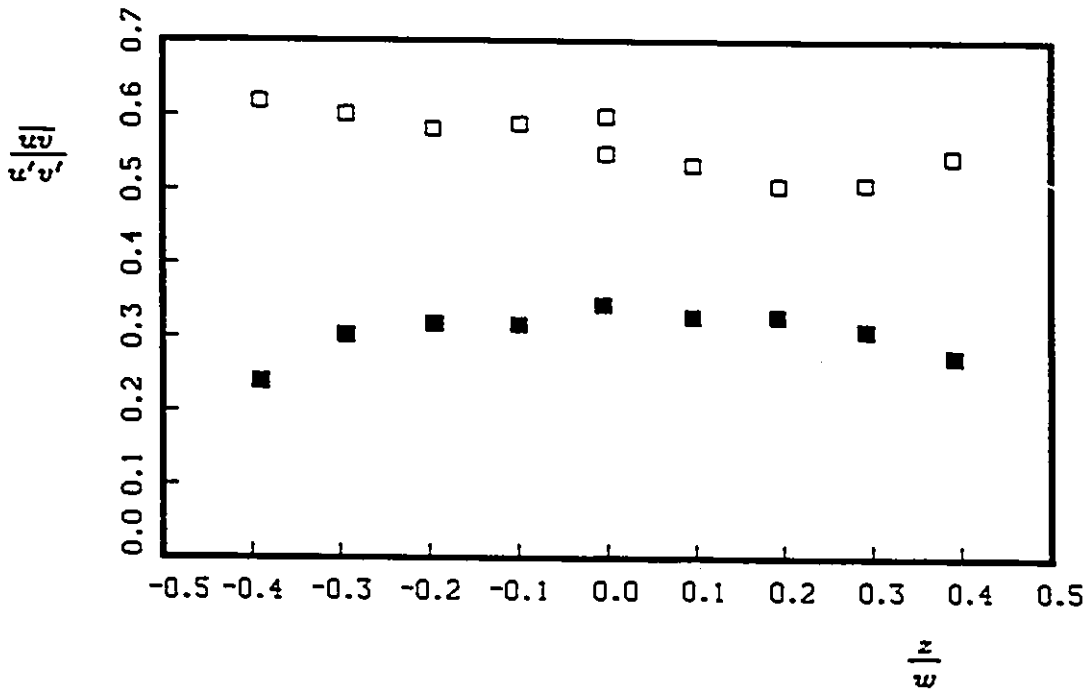

Figure 5.73: Spanwise variation of $\frac{\overline{uv}}{u'v'}$ in the strongly curved section; $\frac{s}{h_c}$=4.74, n=0. Symbols as in Table 5.3.

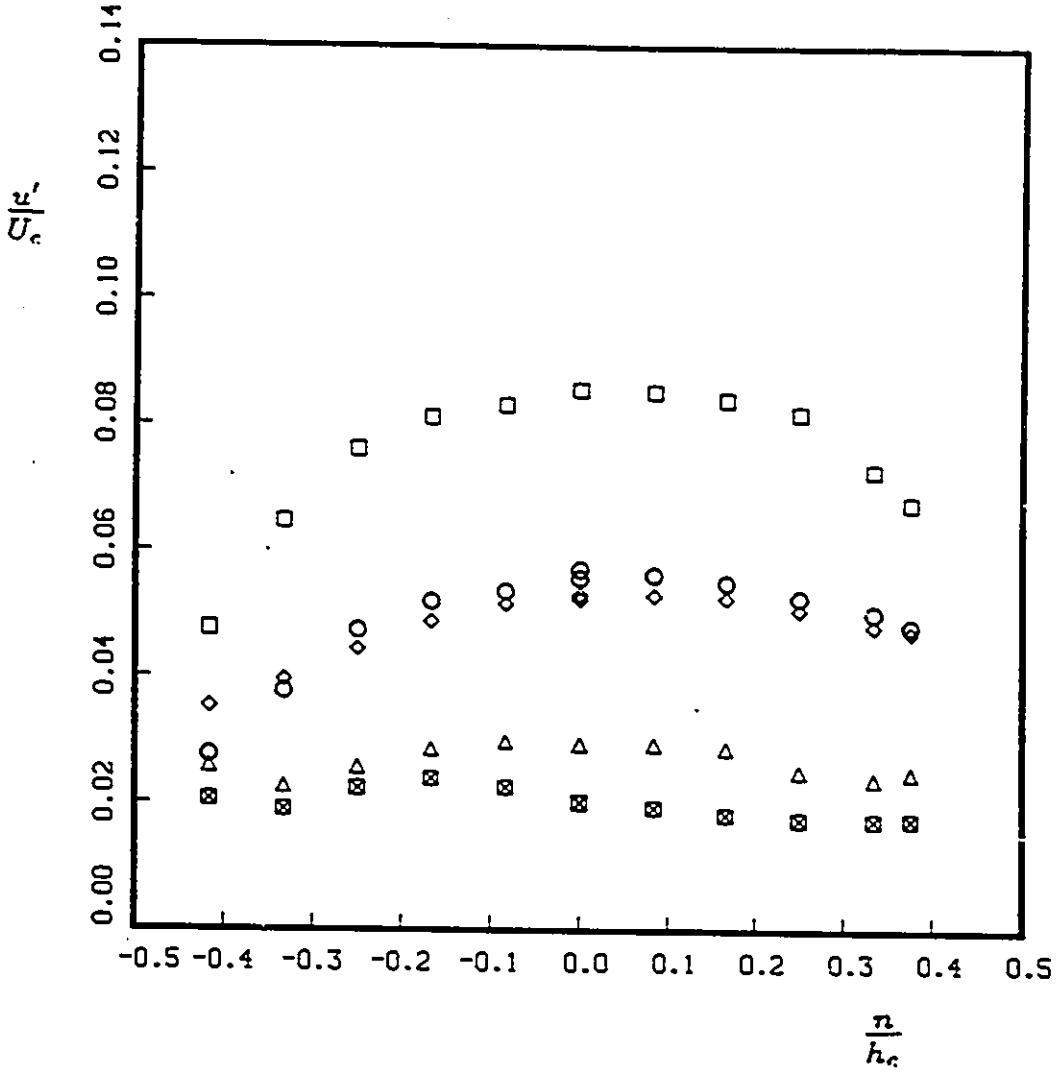

Figure 5.74: Transverse variation of $\frac{u'}{U_c}$ in the strongly curved section, negative shear; $\frac{s}{h_c}$=.42, z=0. Symbols as in Table 5.3.

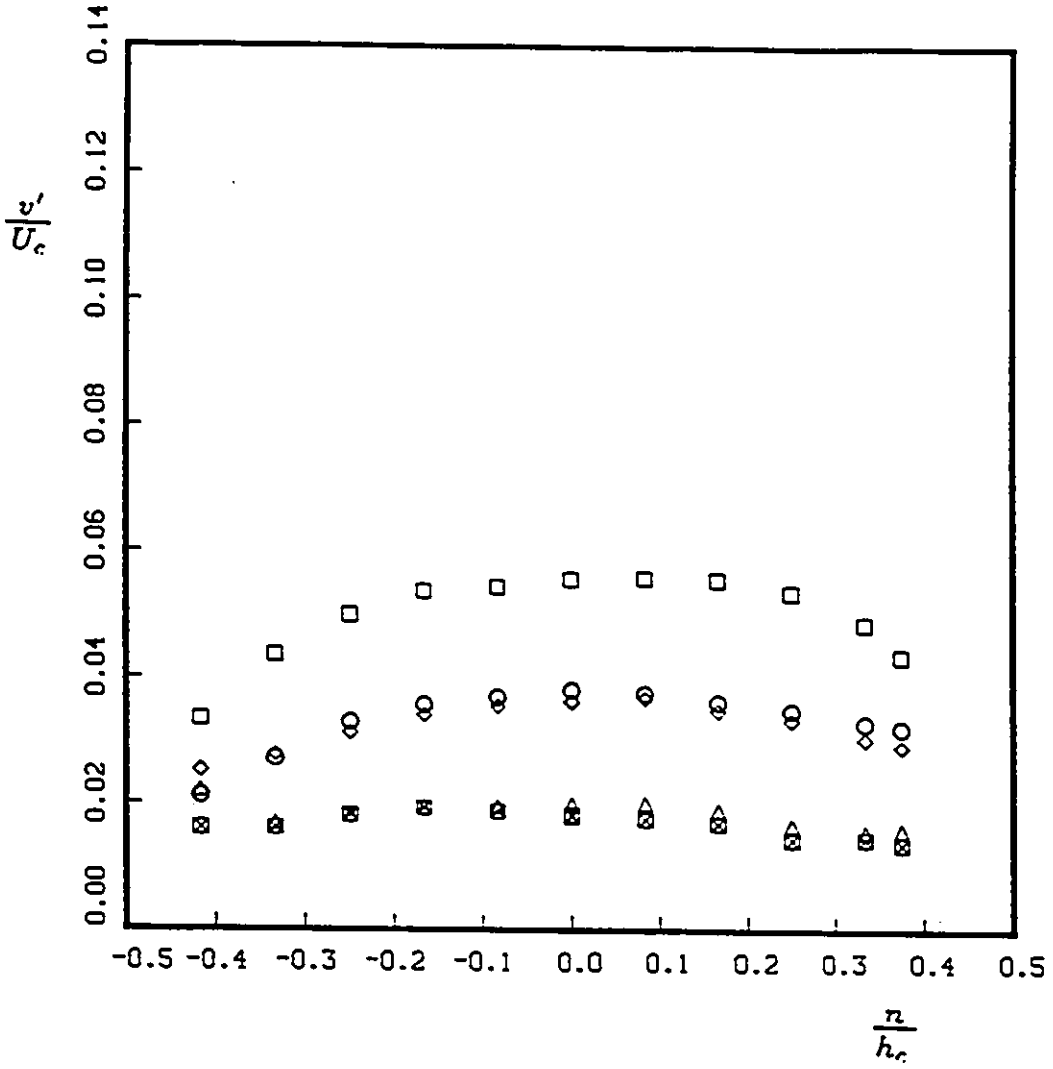

Figure 5.75: Transverse variation of $\frac{v'}{U_c}$ in the strongly curved section, negative shear; $\frac{s}{h_c}$=.42, z=0. Symbols as in Table 5.3.

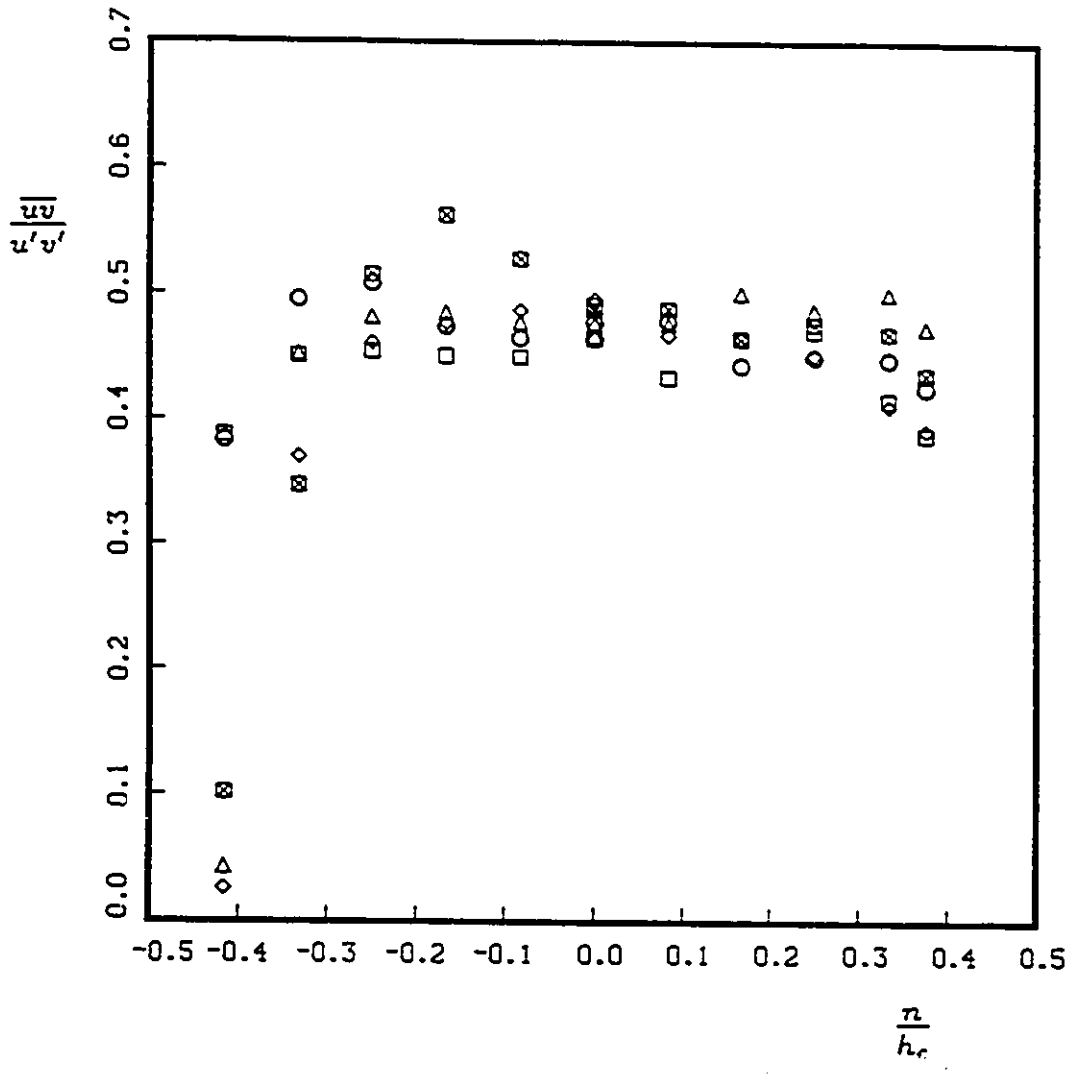

Figure 5.76: Transverse variation of $\frac{\overline{uv}}{u'v'}$ in the strongly curved section, negative shear; $\frac{s}{h_c}$=.42, z=0. Symbols as in Table 5.3.

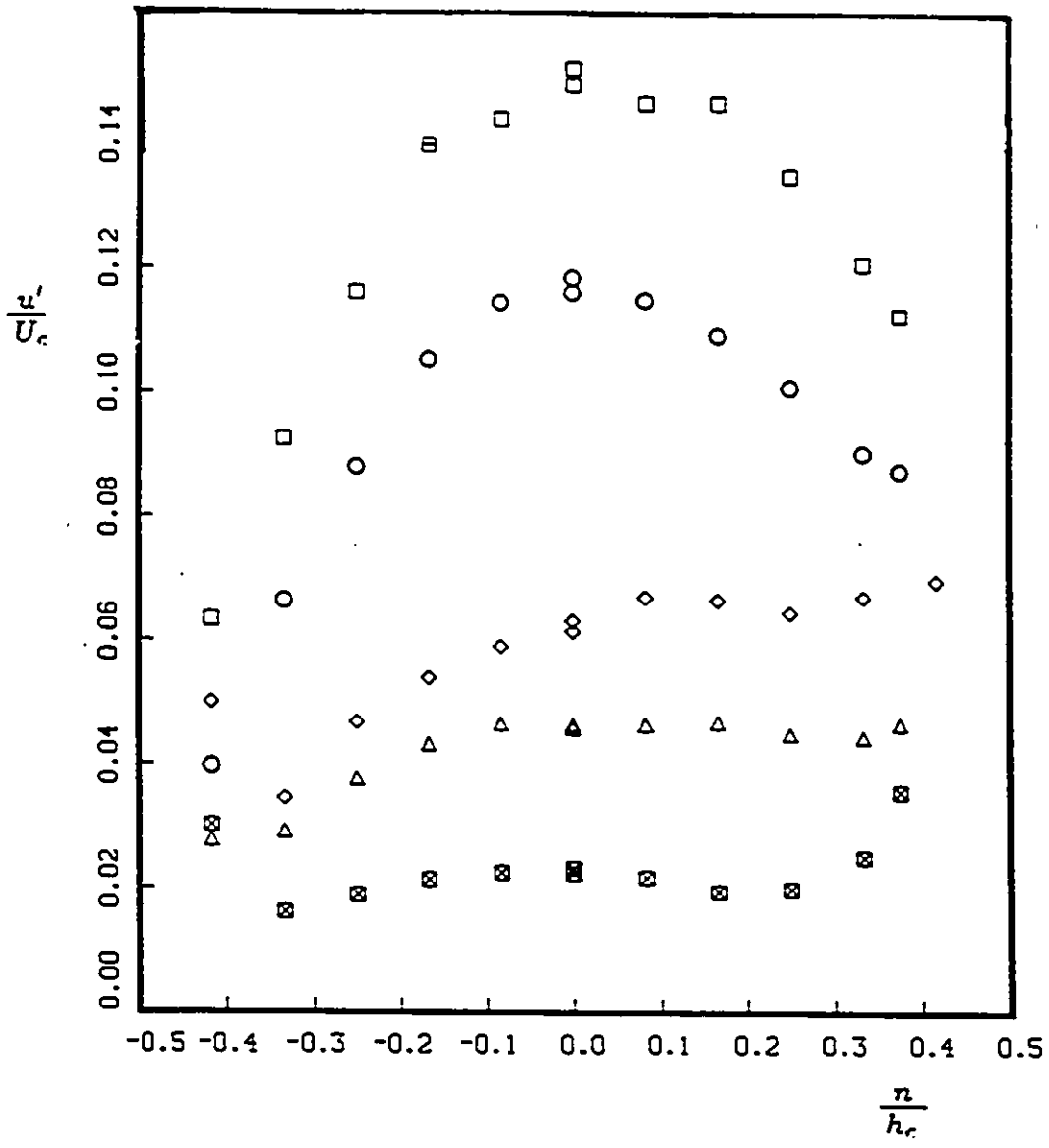

Figure 5.77: Transverse variation of $\frac{u'}{U_c}$ in the strongly curved section, negative shear; $\frac{s}{h_c}$=4.74, z=0. Symbols as in Table 5.3.

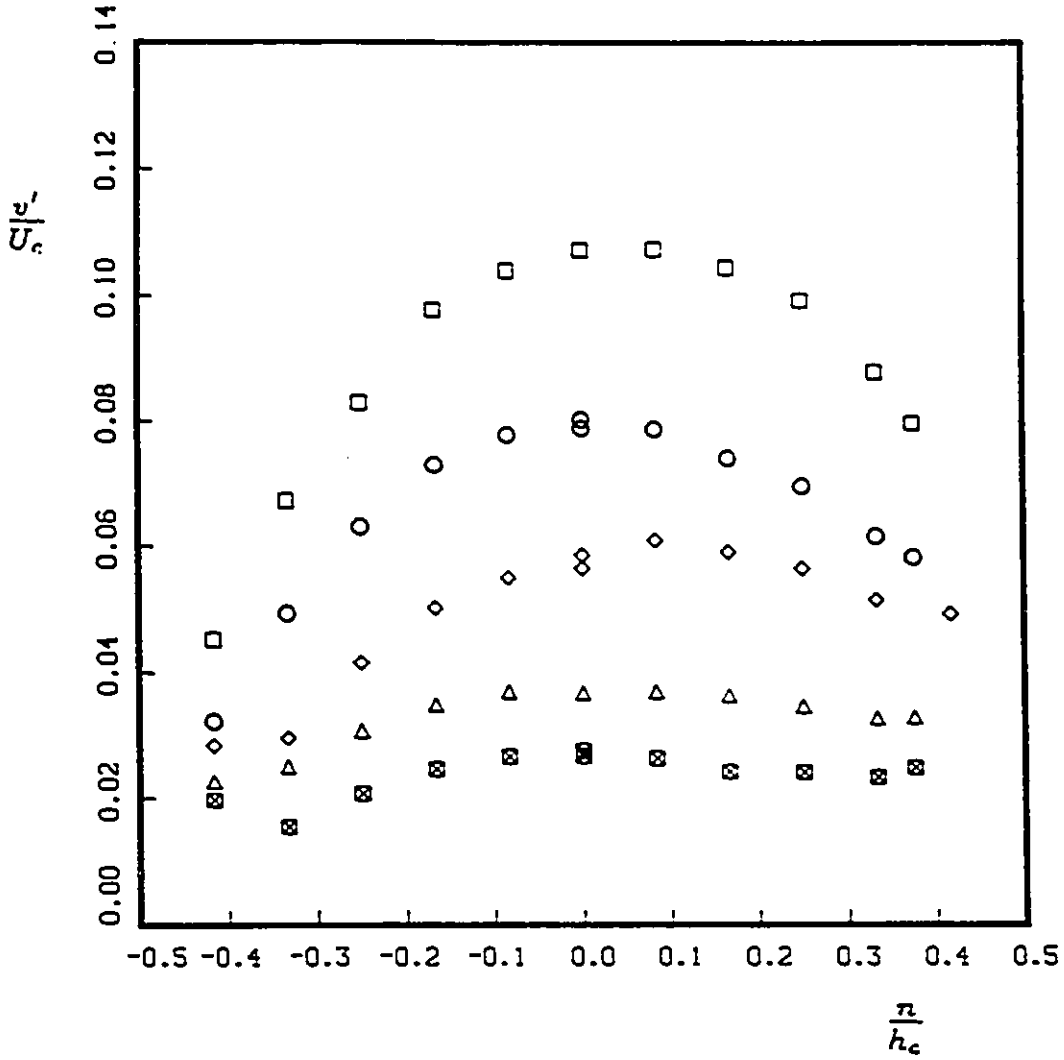

Figure 5.78: Transverse variation of $\frac{v'}{U_c}$ in the strongly curved section, negative shear; $\frac{s}{h_c}$=4.74, z=0. Symbols as in Table 5.3.

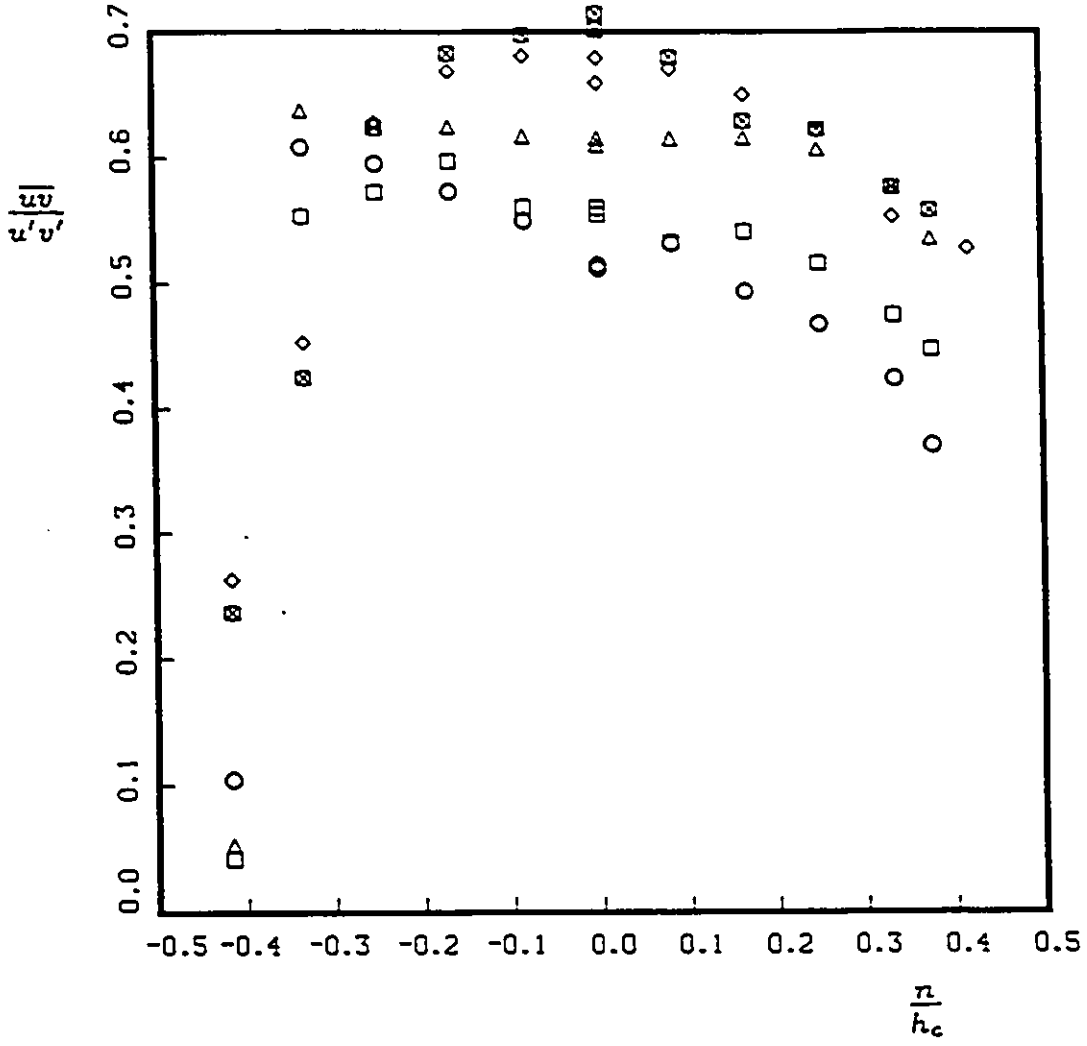

Figure 5.79: Transverse variation of $\frac{\overline{uv}}{u'v'}$ in the strongly curved section, negative shear; $\frac{s}{h_c}$=4.74, z=0. Symbols as in Table 5.3.

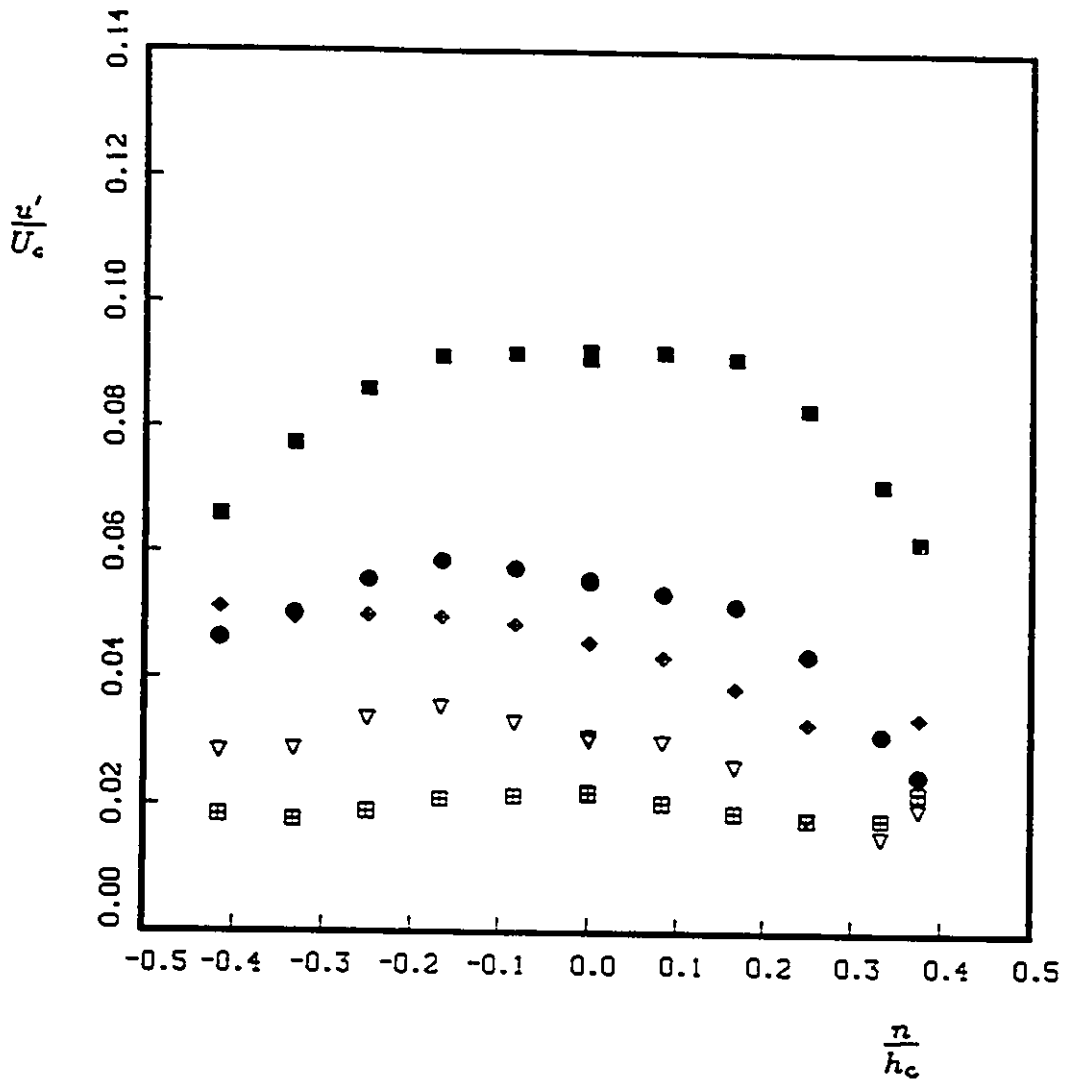

Figure 5.80: Transverse variation of $\frac{u'}{U_c}$ in the strongly curved section, positive shear; $\frac{s}{h_c}$=.42, z=0. Symbols as in Table 5.3.

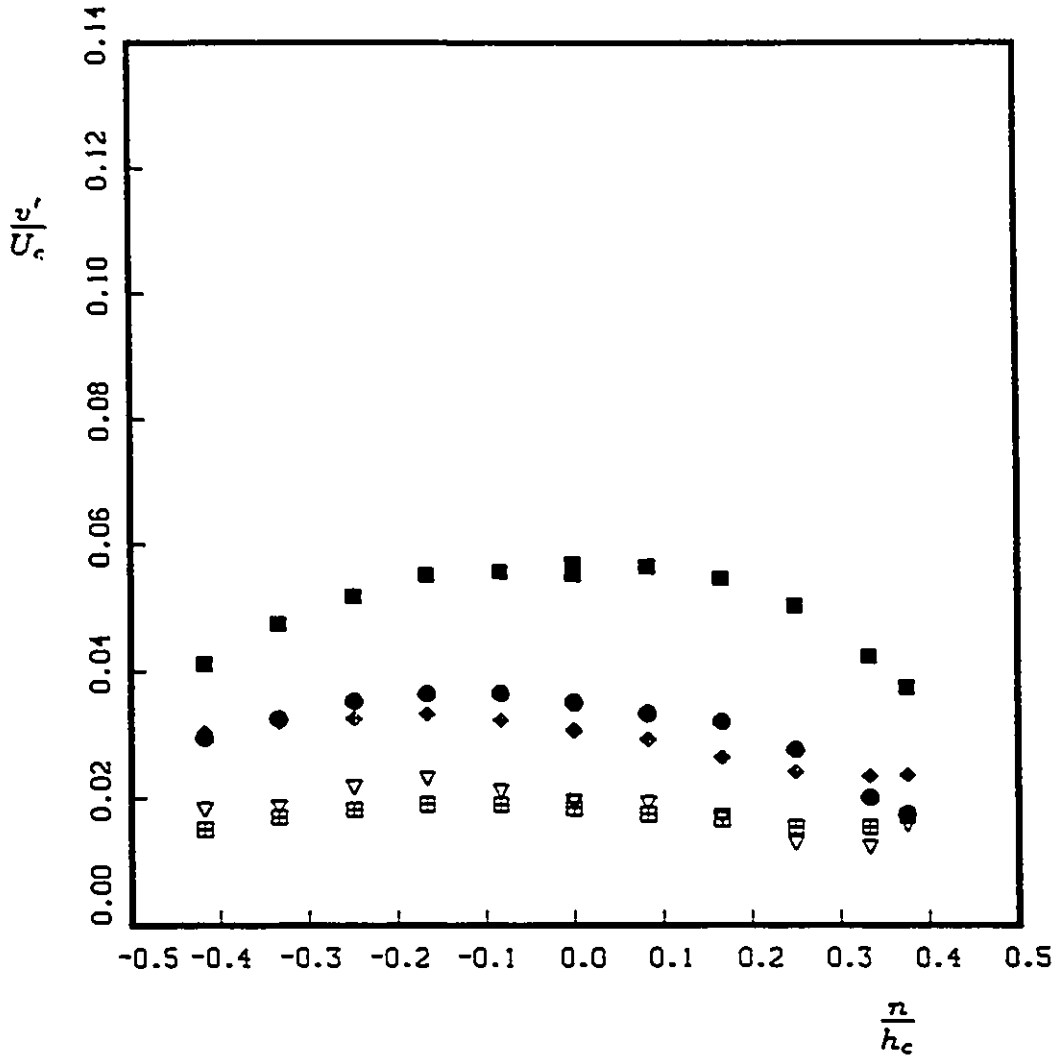

Figure 5.81: Transverse variation of $\frac{v'}{U_c}$ in the strongly curved section, positive shear; $\frac{s}{h_c}$=.42, z=0. Symbols as in Table 5.3.

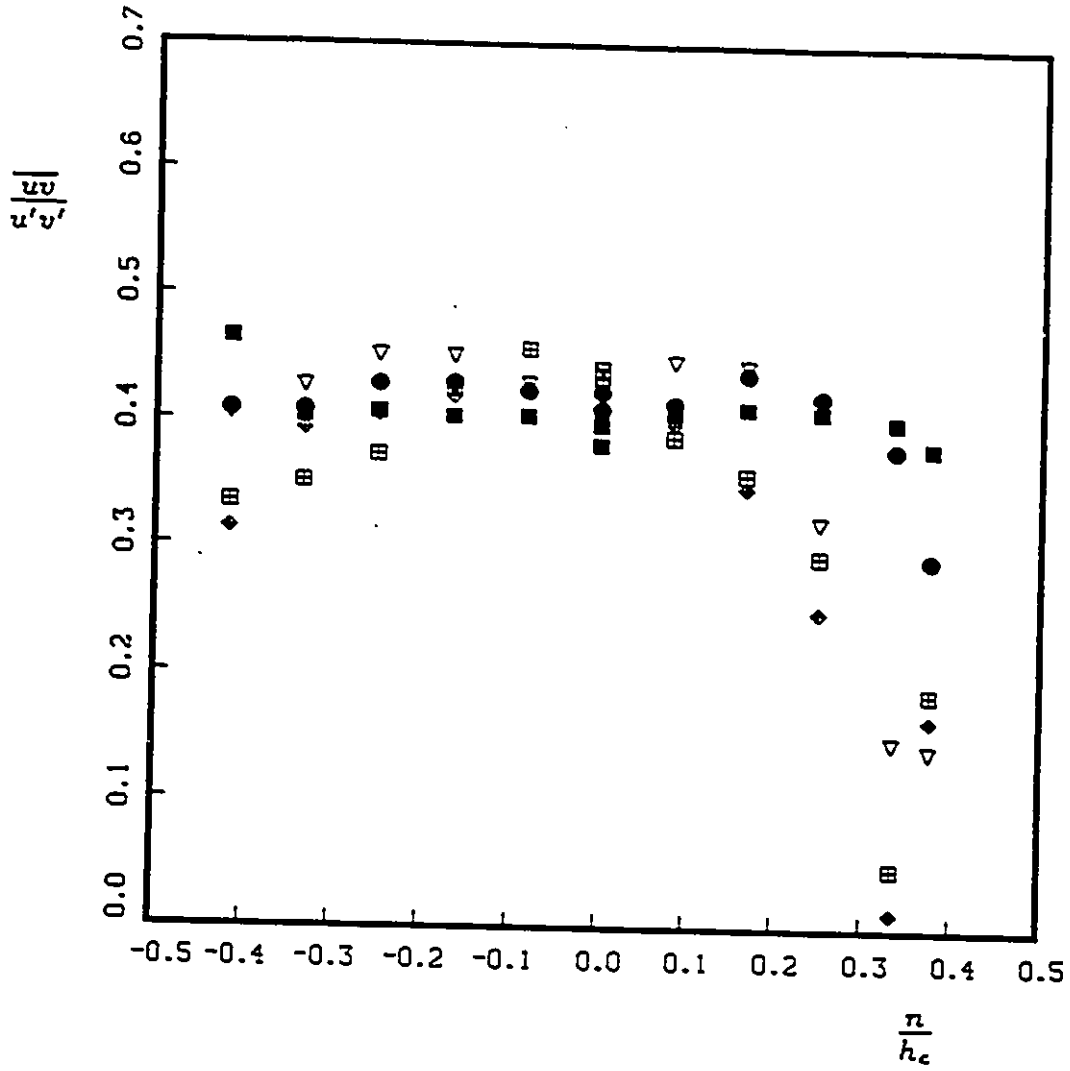

Figure 5.82: Transverse variation of $\frac{\overline{uv}}{u'v'}$ in the strongly curved section, positive shear; $\frac{s}{h_c}$=.42, z=0. Symbols as in Table 5.3.

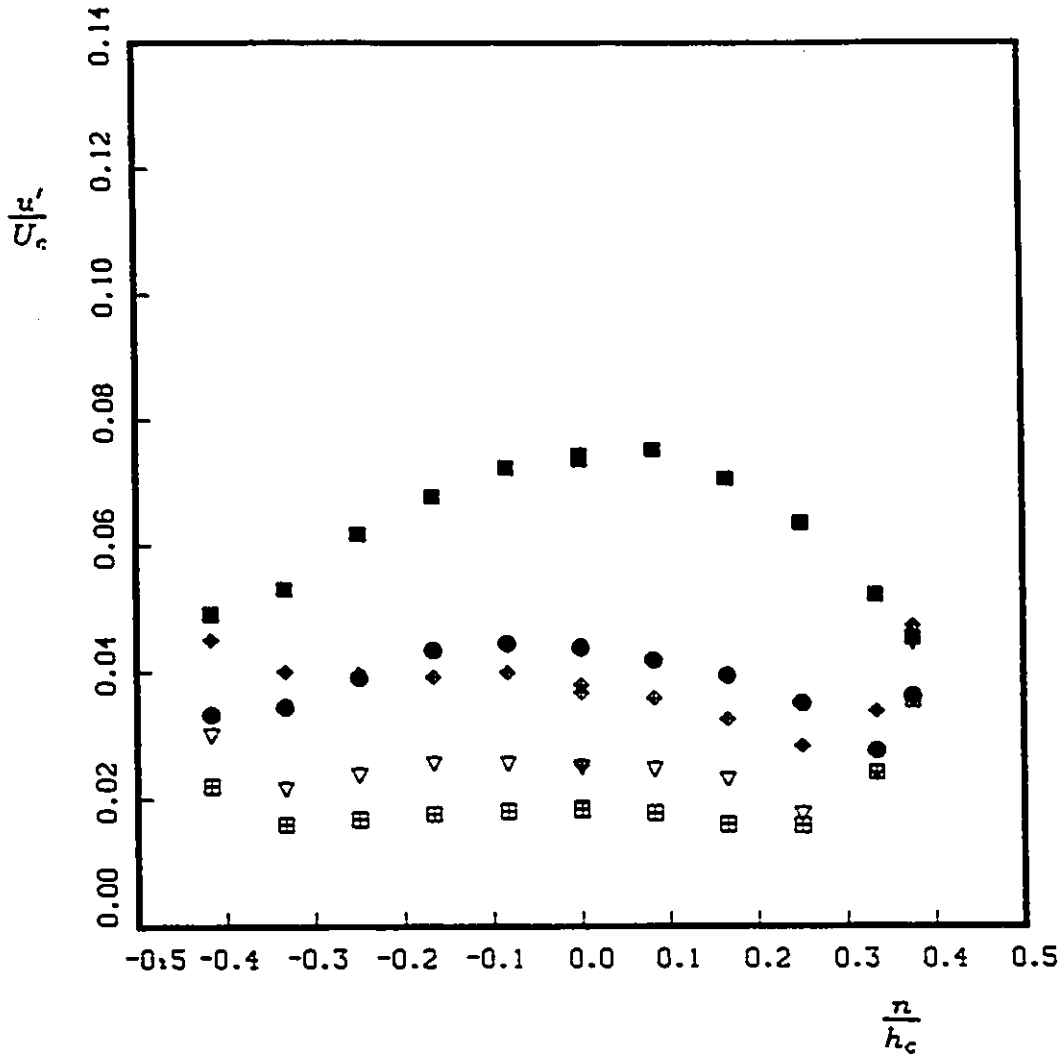

Figure 5.83: Transverse variation of $\frac{u'}{U_c}$ in the strongly curved section, positive shear; $\frac{s}{h_c}$=4.74, z=0. Symbols as in Table 5.3.

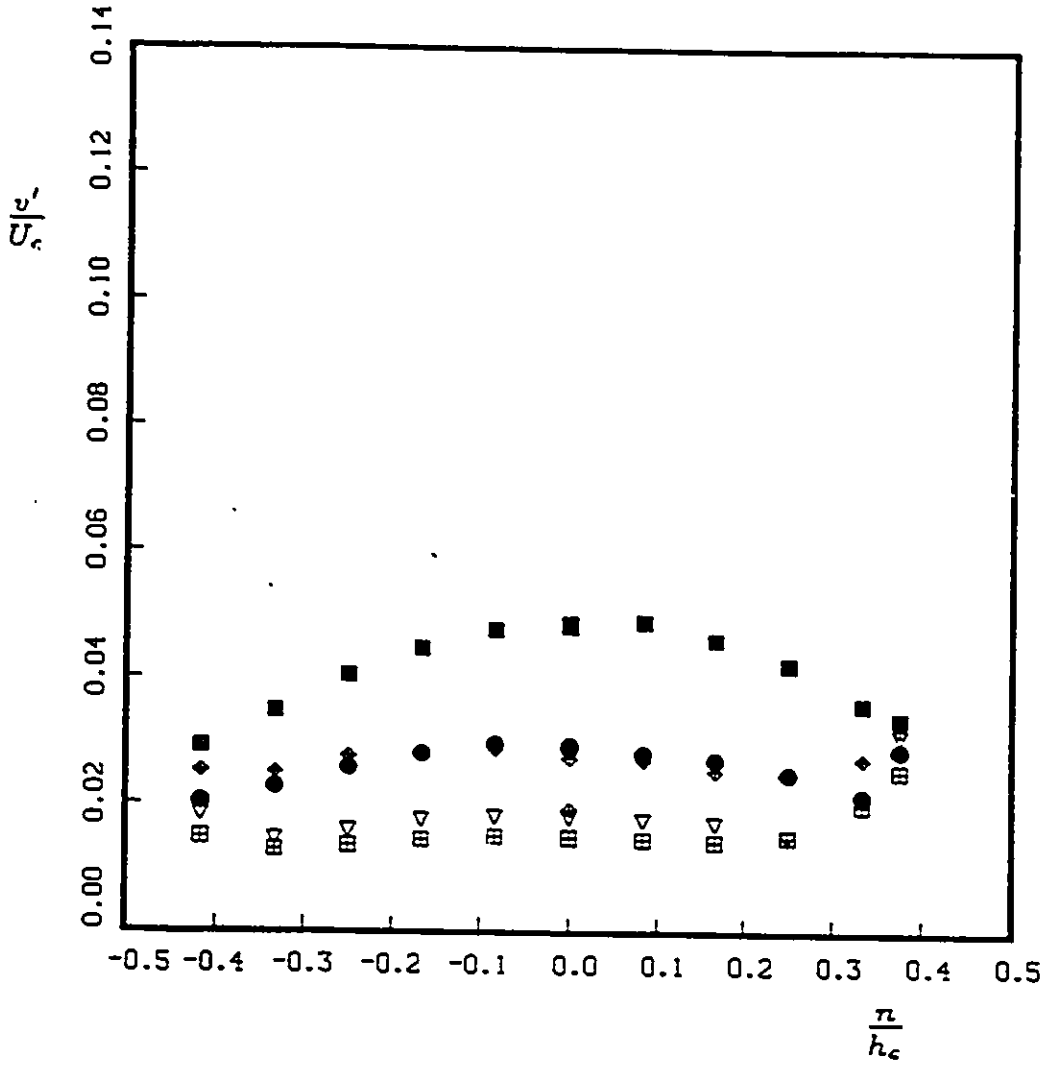

Figure 5.84: Transverse variation of $\frac{v'}{U_c}$ in the strongly curved section, positive shear; $\frac{s}{h_c}$=4.74, z=0. Symbols as in Table 5.3.

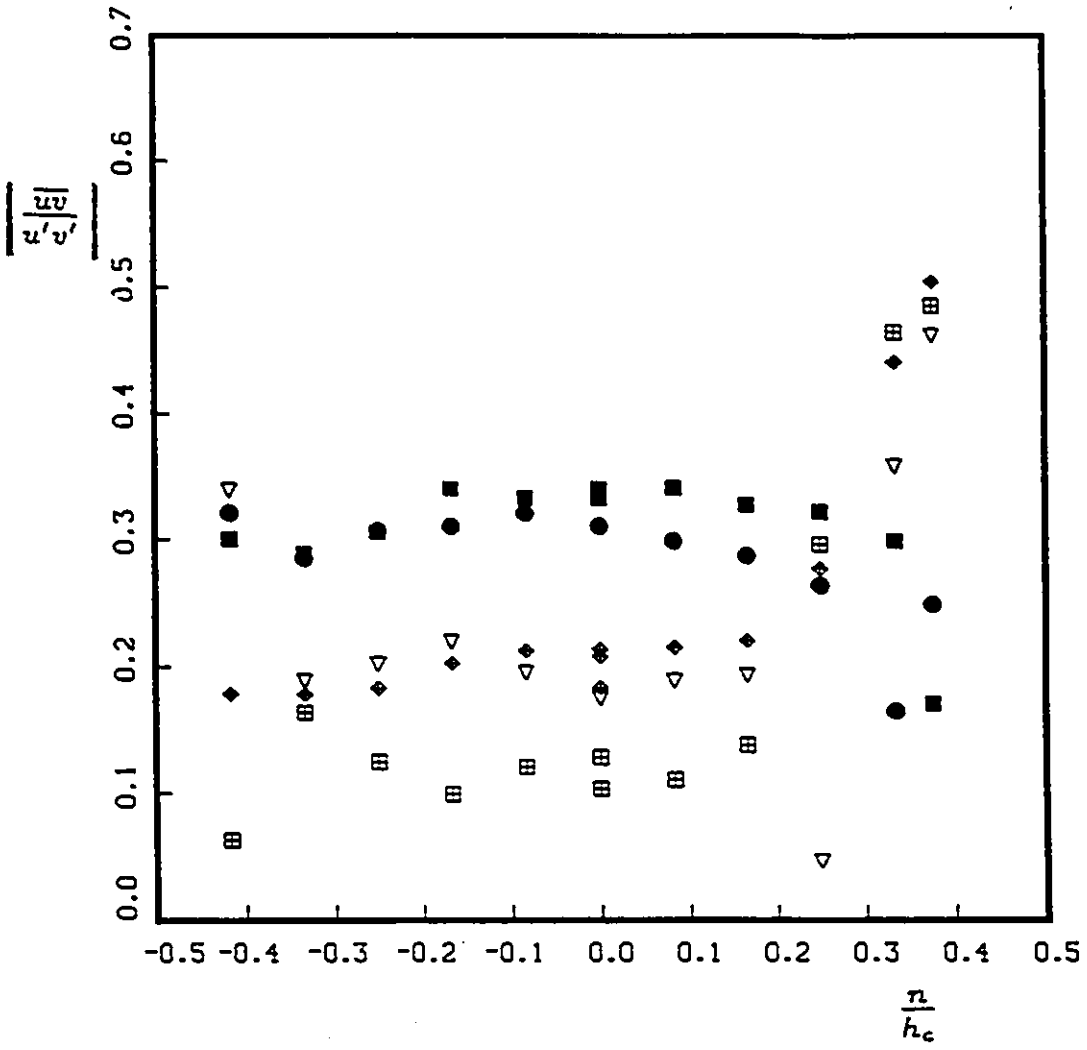

Figure 5.85: Transverse variation of $\frac{\overline{uv}}{u'v'}$ in the strongly curved section, positive shear; $\frac{s}{h_c}$=4.74, z=0. Symbols as in Table 5.3.

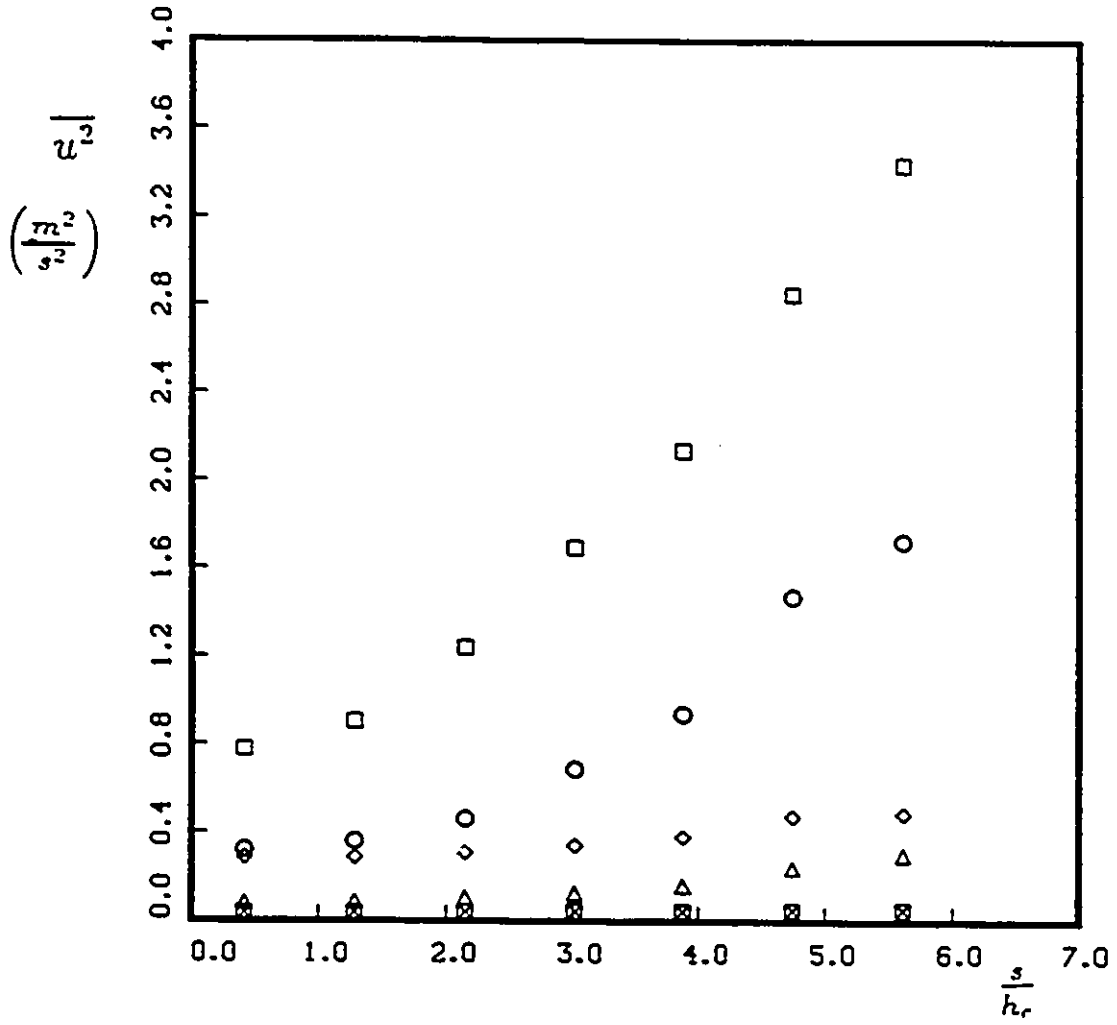

Figure 5.86: Development of $\overline{u^2}$ along the wind tunnel centerline in the strongly curved section; negative shear. Symbols as in Table 5.3.

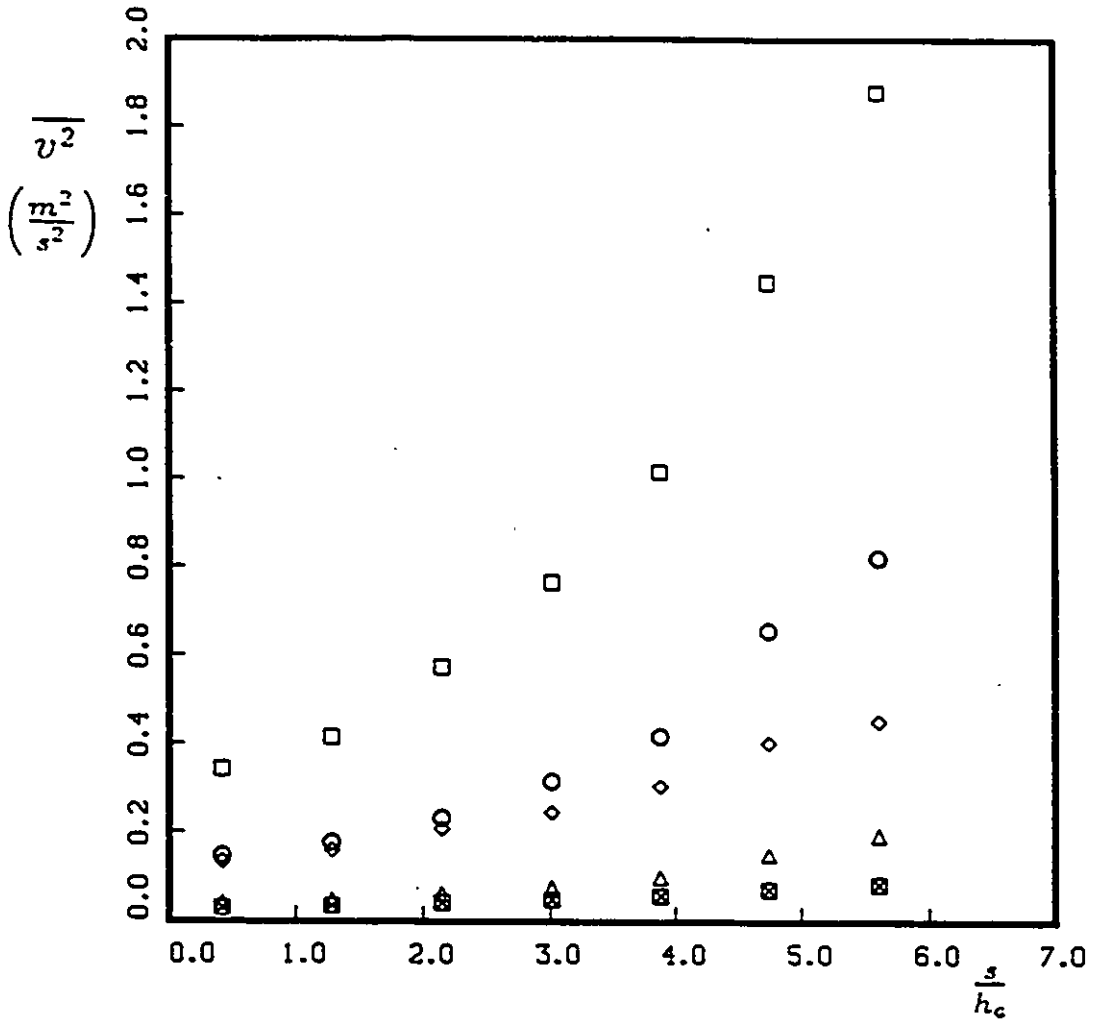

Figure 5.87: Development of $\overline{v^2}$ along the wind tunnel centerline in the strongly curved section; negative shear. Symbols as in Table 5.3.

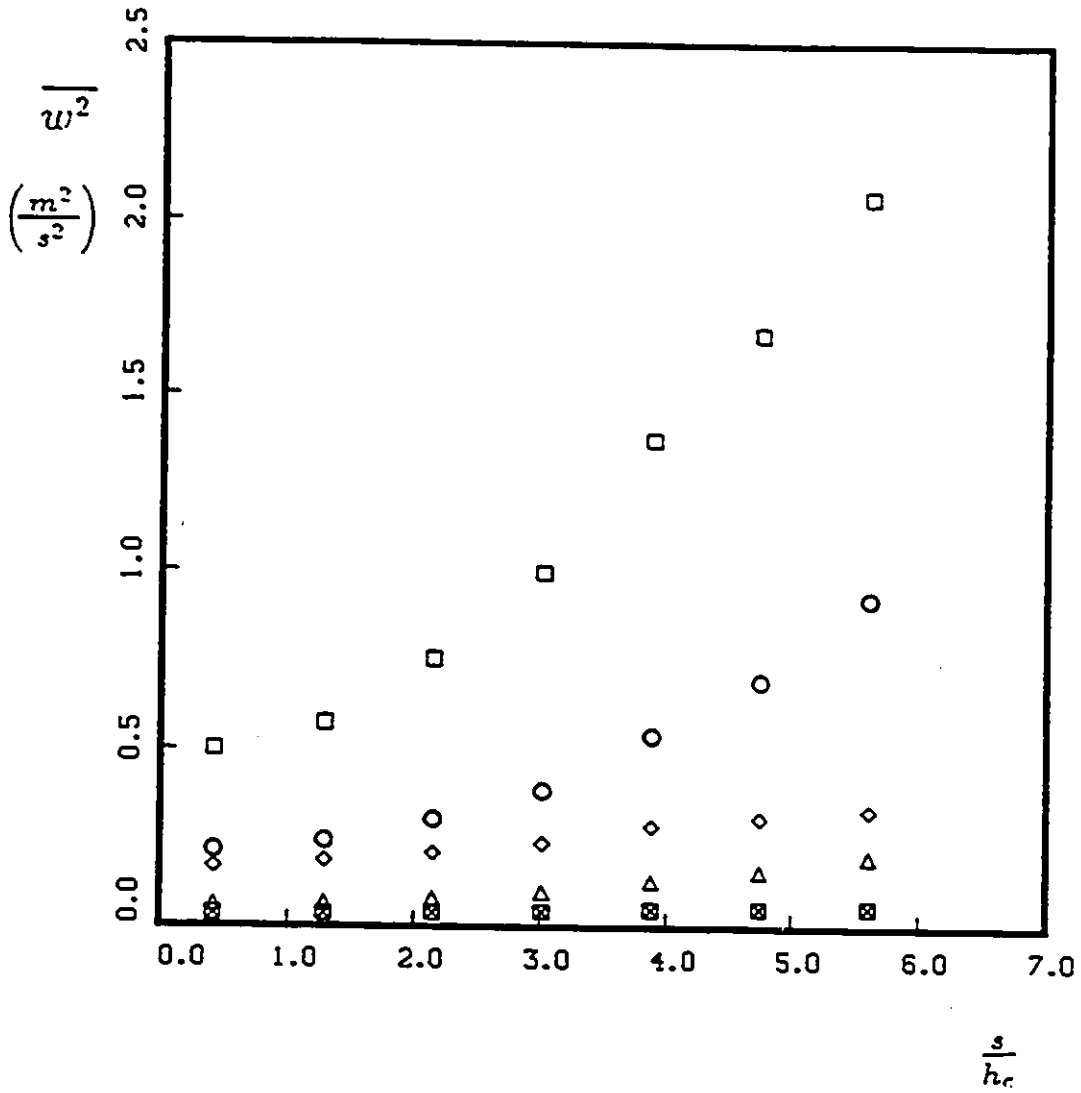

Figure 5.88: Development of $\overline{w^2}$ along the wind tunnel centerline in the strongly curved section; negative shear. Symbols as in Table 5.3.

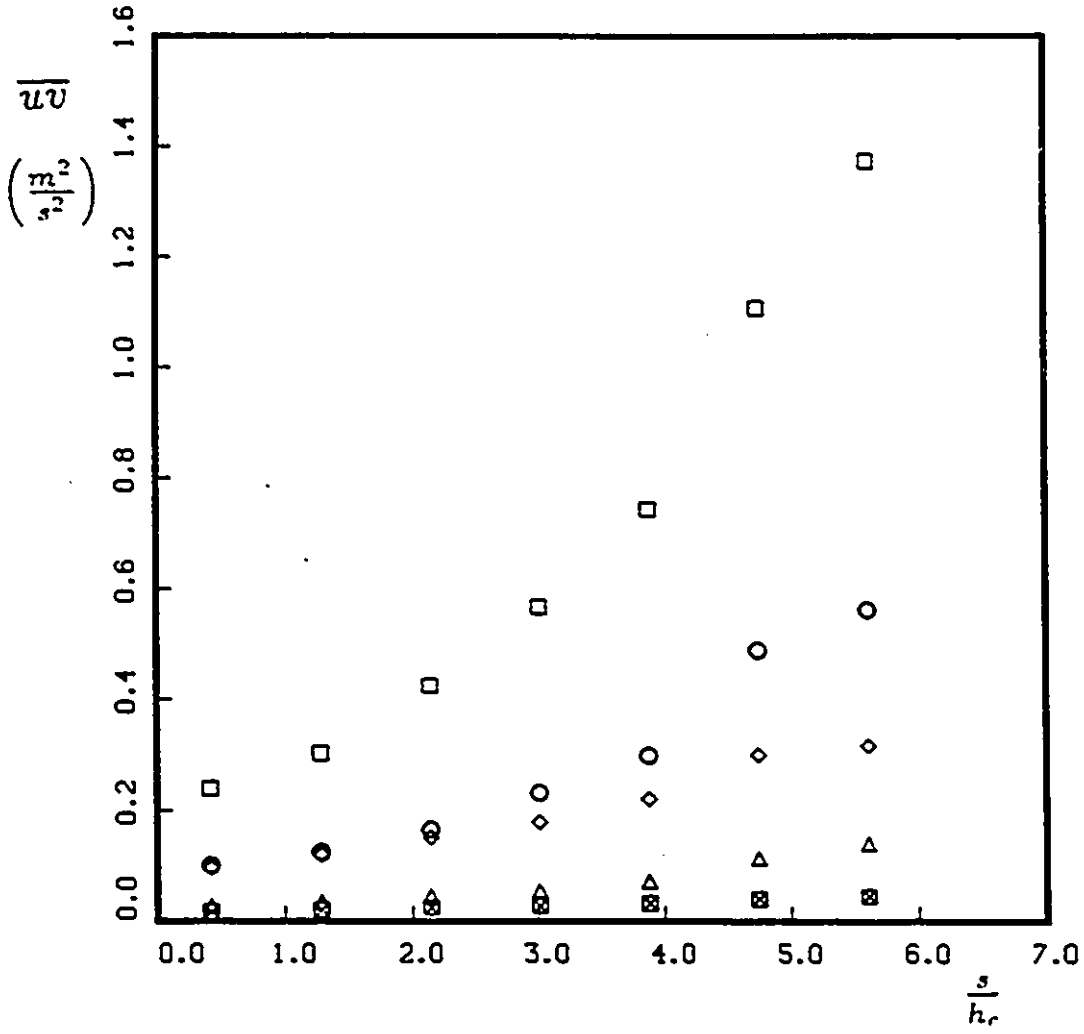

Figure 5.89: Development of $\overline{uv}$ along the wind tunnel centerline in the strongly curved section; negative shear. Symbols as in Table 5.3.

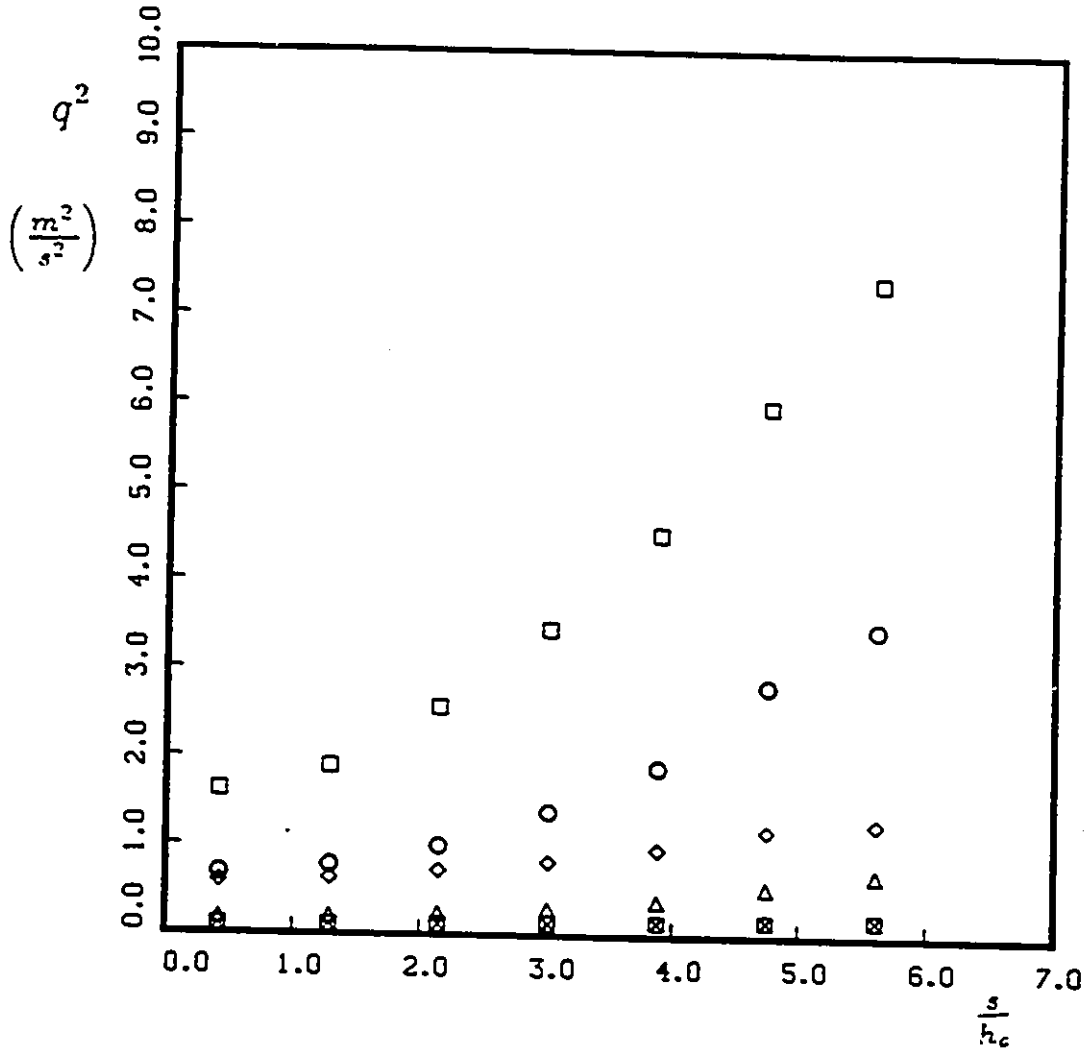

Figure 5.90: Development of q^2 along the wind tunnel centerline in the strongly curved section; negative shear. Symbols as in Table 5.3.

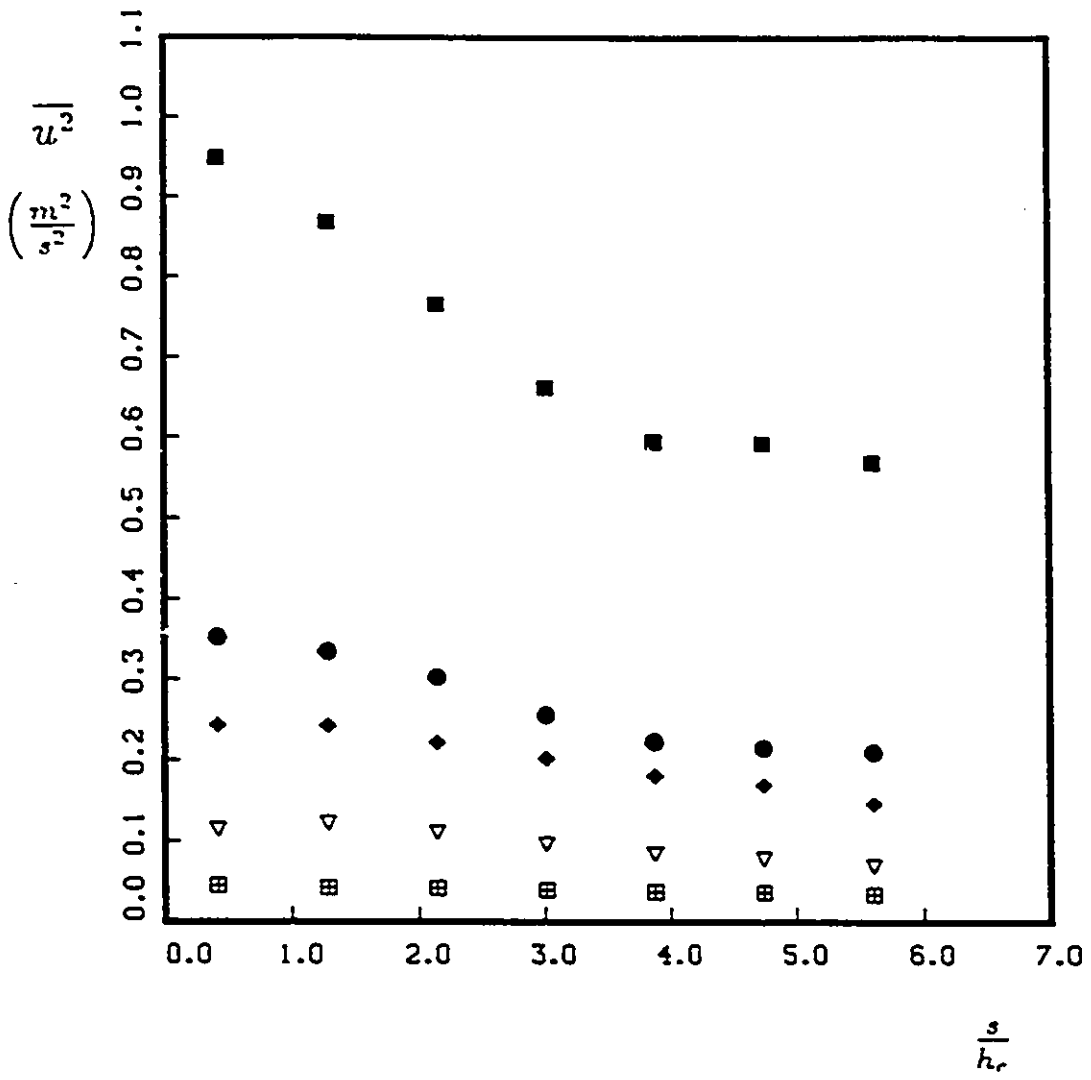

Figure 5.91: Development of $\overline{u^2}$ along the wind tunnel centerline in the strongly curved section: positive shear. Symbols as in Table 5.3.

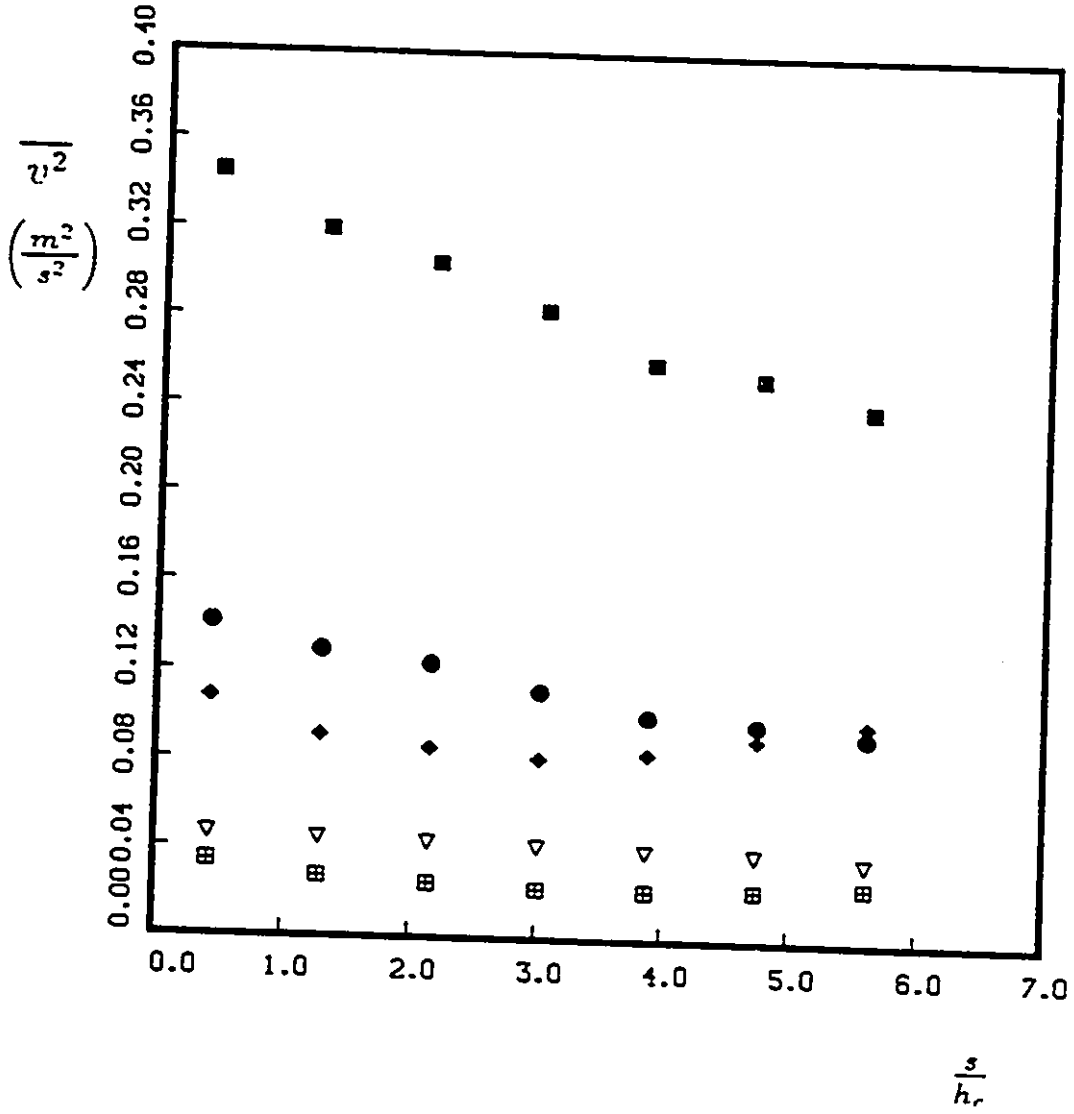

Figure 5.92: Development of $\overline{v^2}$ along the wind tunnel centerline in the strongly curved section: positive shear. Symbols as in Table 5.3.

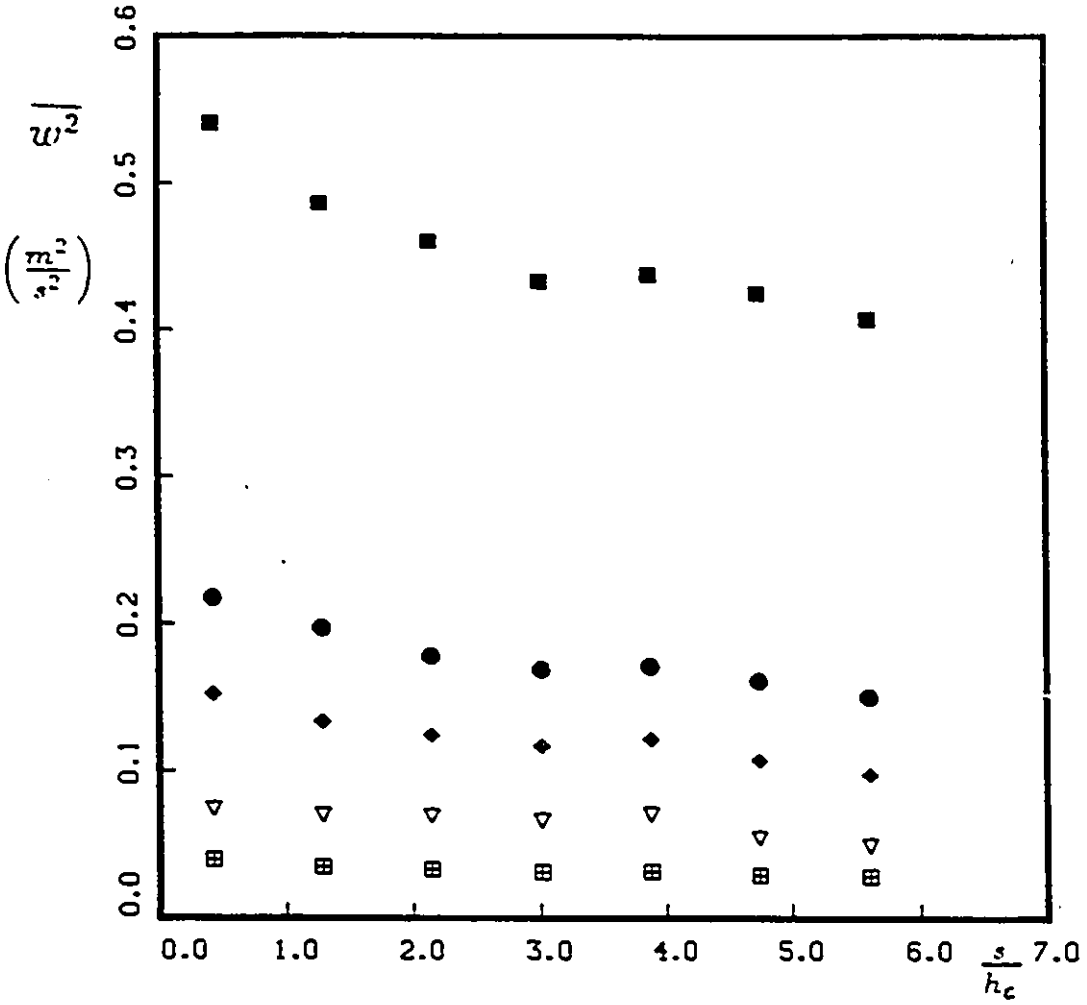

Figure 5.93: Development of $\overline{w^2}$ along the wind tunnel centerline in the strongly curved section; positive shear. Symbols as in Table 5.3.

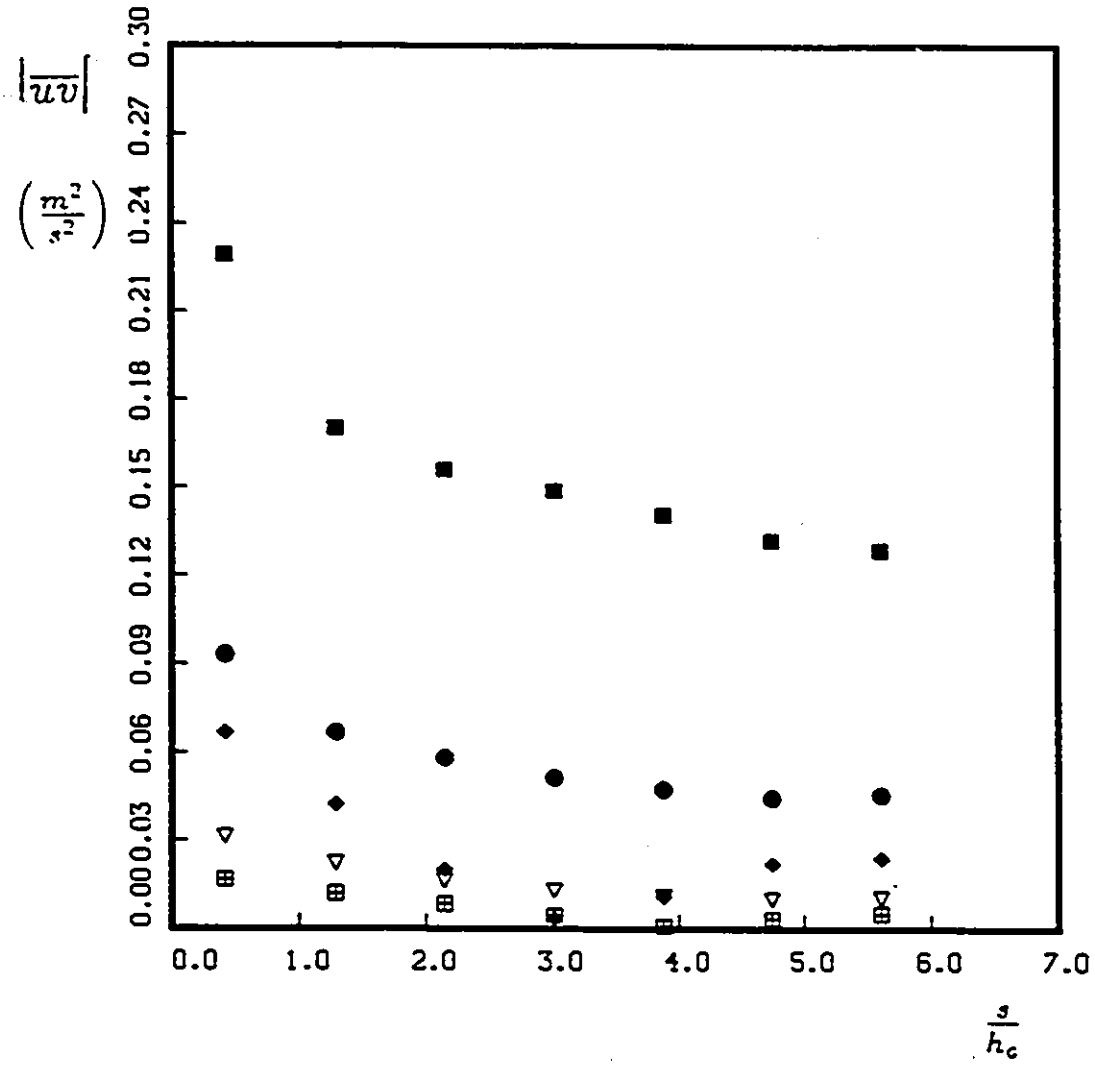

Figure 5.94: Development of $\overline{uv}$ along the wind tunnel centerline in the strongly curved section; positive shear. Symbols as in Table 5.3.

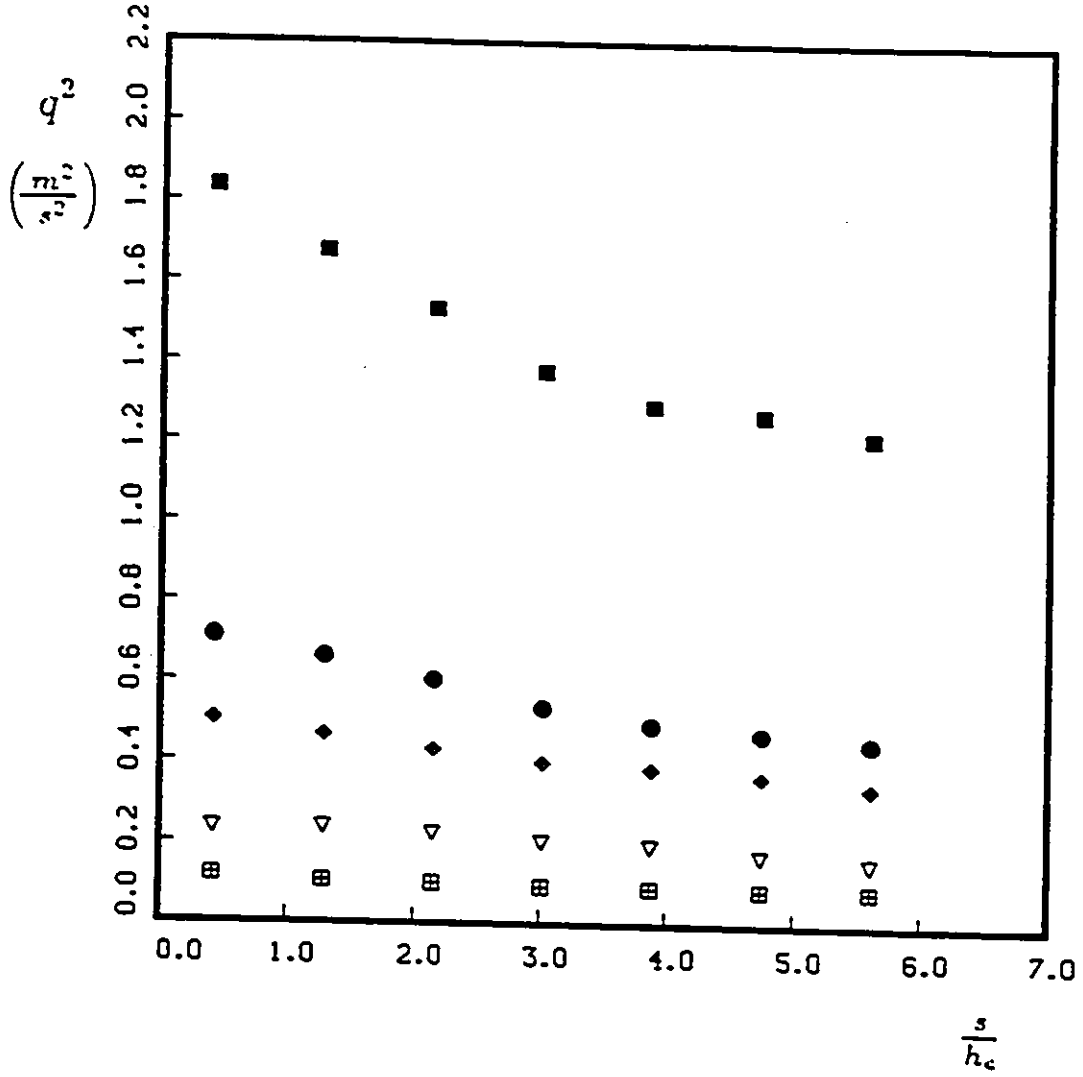

Figure 5.95: Development of q^2 along the wind tunnel centerline in the strongly curved section; positive shear. Symbols as in Table 5.3.

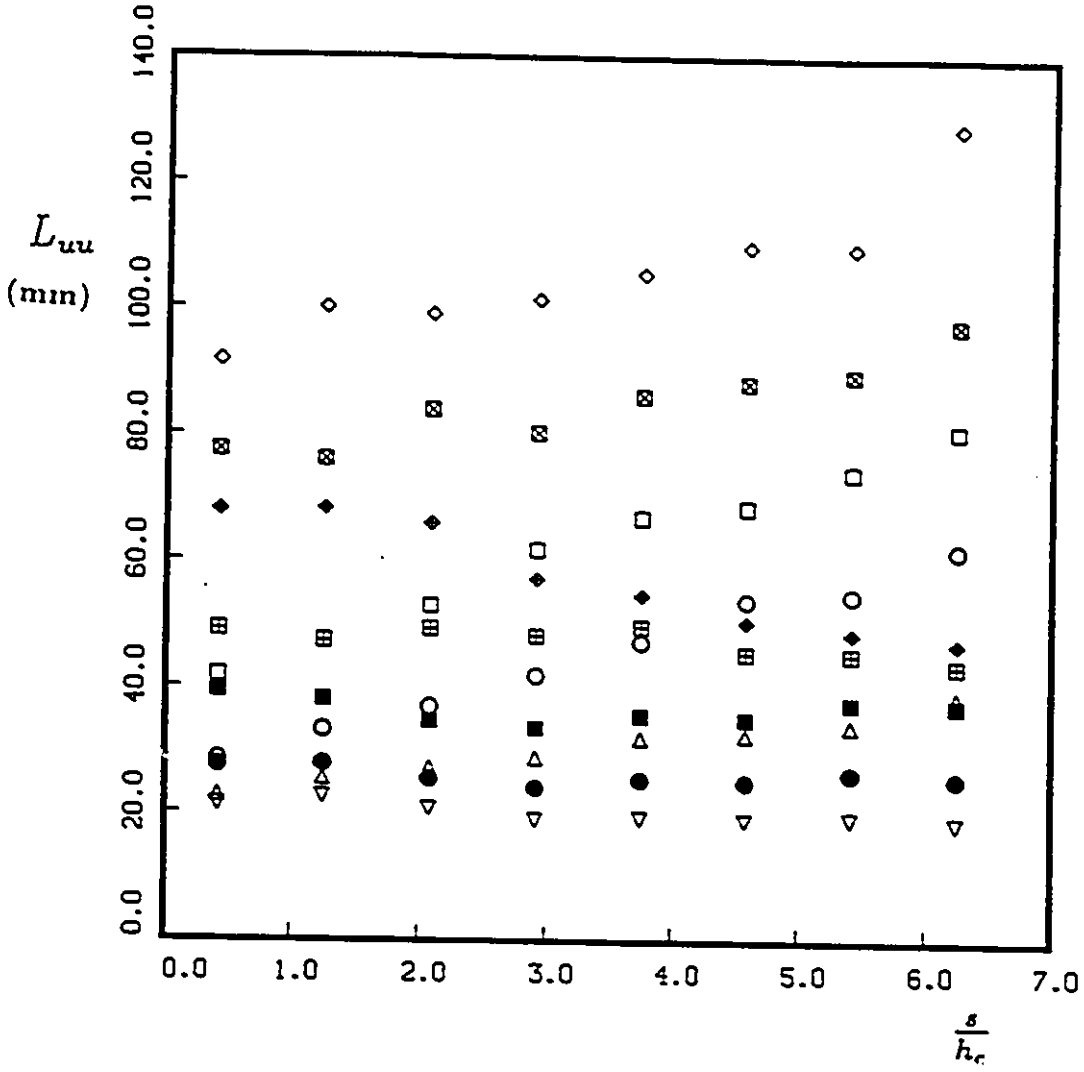

Figure 5.96: Development of L_{uu} along the wind tunnel centerline in the mildly curved section. Symbols as in Table 5.3.

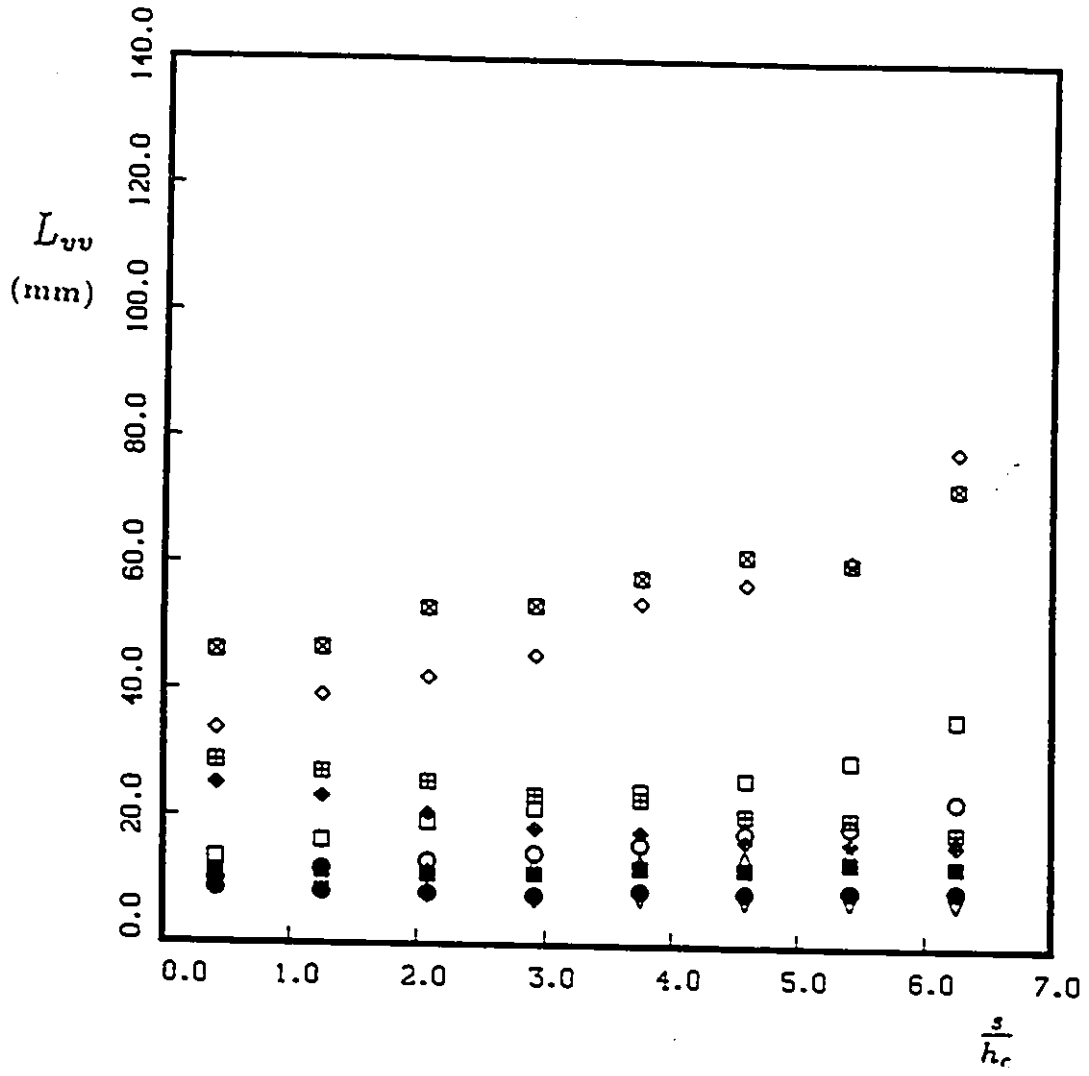

Figure 5.97: Development of L_{vv} along the wind tunnel centerline in the mildly curved section. Symbols as in Table 5.3.

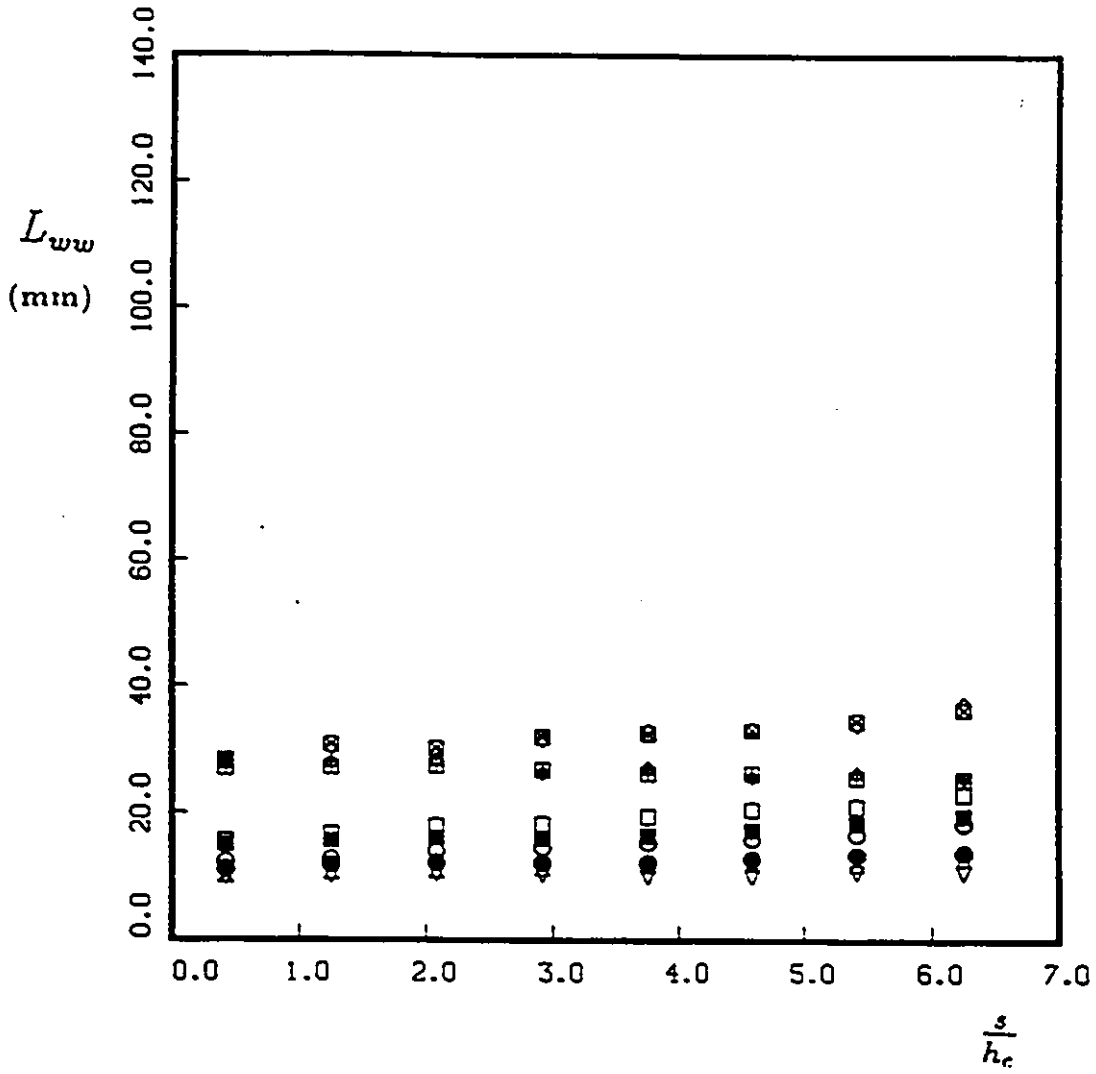

Figure 5.98: Development of L_{ww} along the wind tunnel centerline in the mildly curved section. Symbols as in Table 5.3.

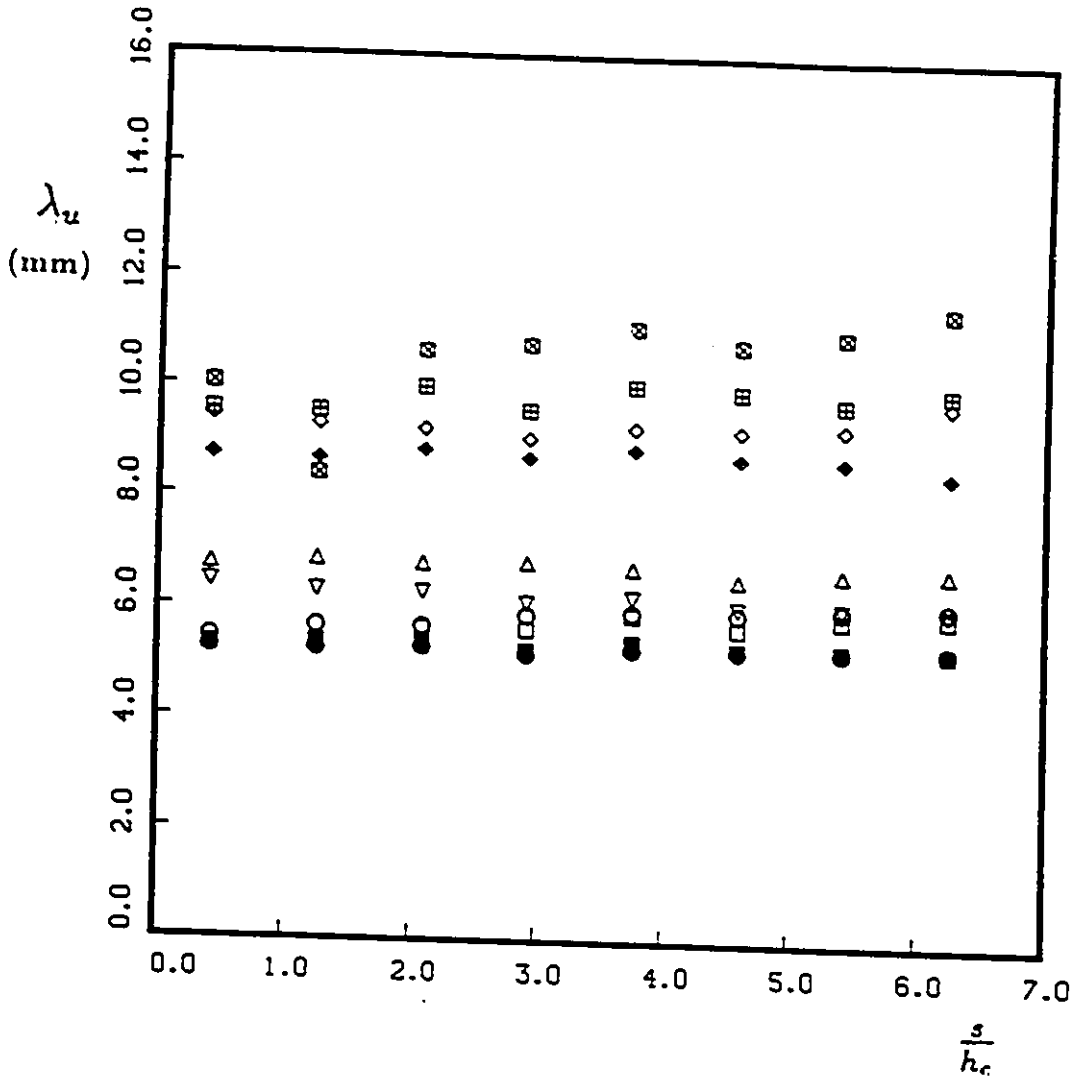

Figure 5.99: Development of λ_u along the wind tunnel centerline in the mildly curved section. Symbols as in Table 5.3.

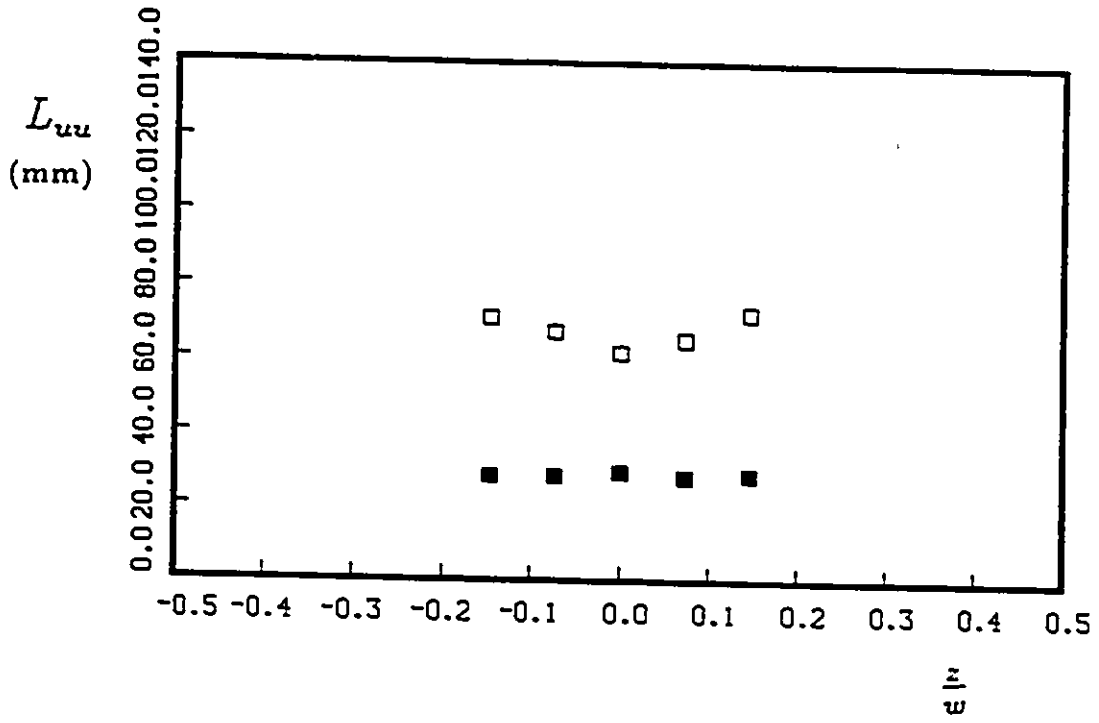

Figure 5.100: Spanwise variation of L_{uu} in the strongly curved section; $\frac{s}{h_c}$=2.15, n=0. Symbols as in Table 5.3.

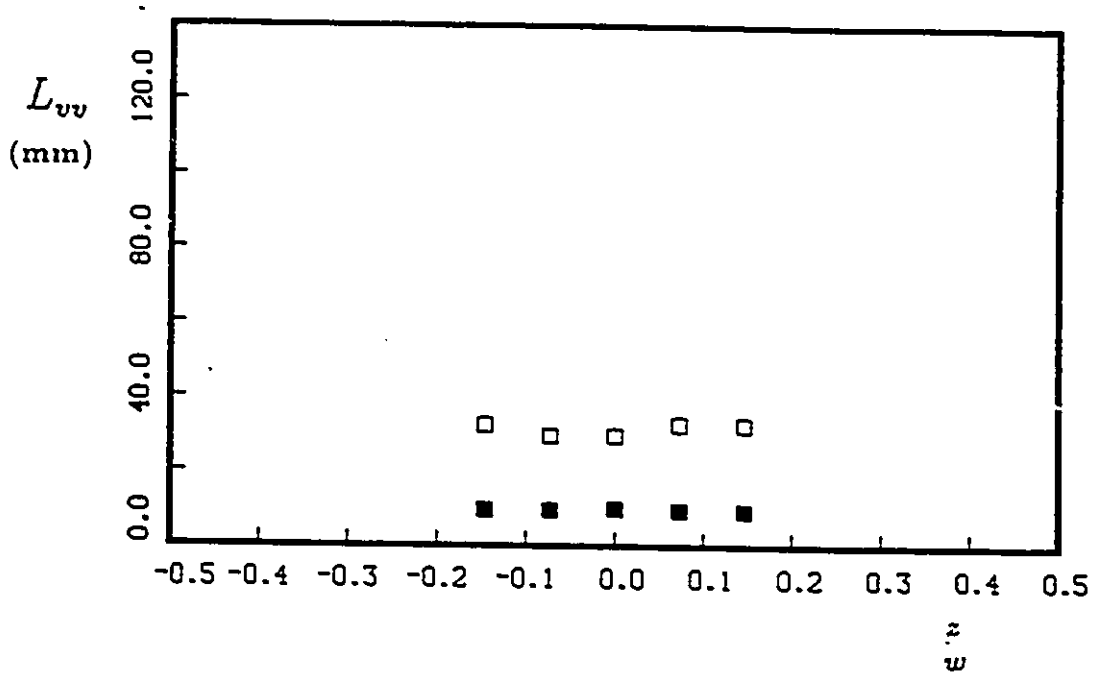

Figure 5.101: Spanwise variation of L_{vv} in the strongly curved section; $\frac{s}{h_c}$=2.15, n=0. Symbols as in Table 5.3.

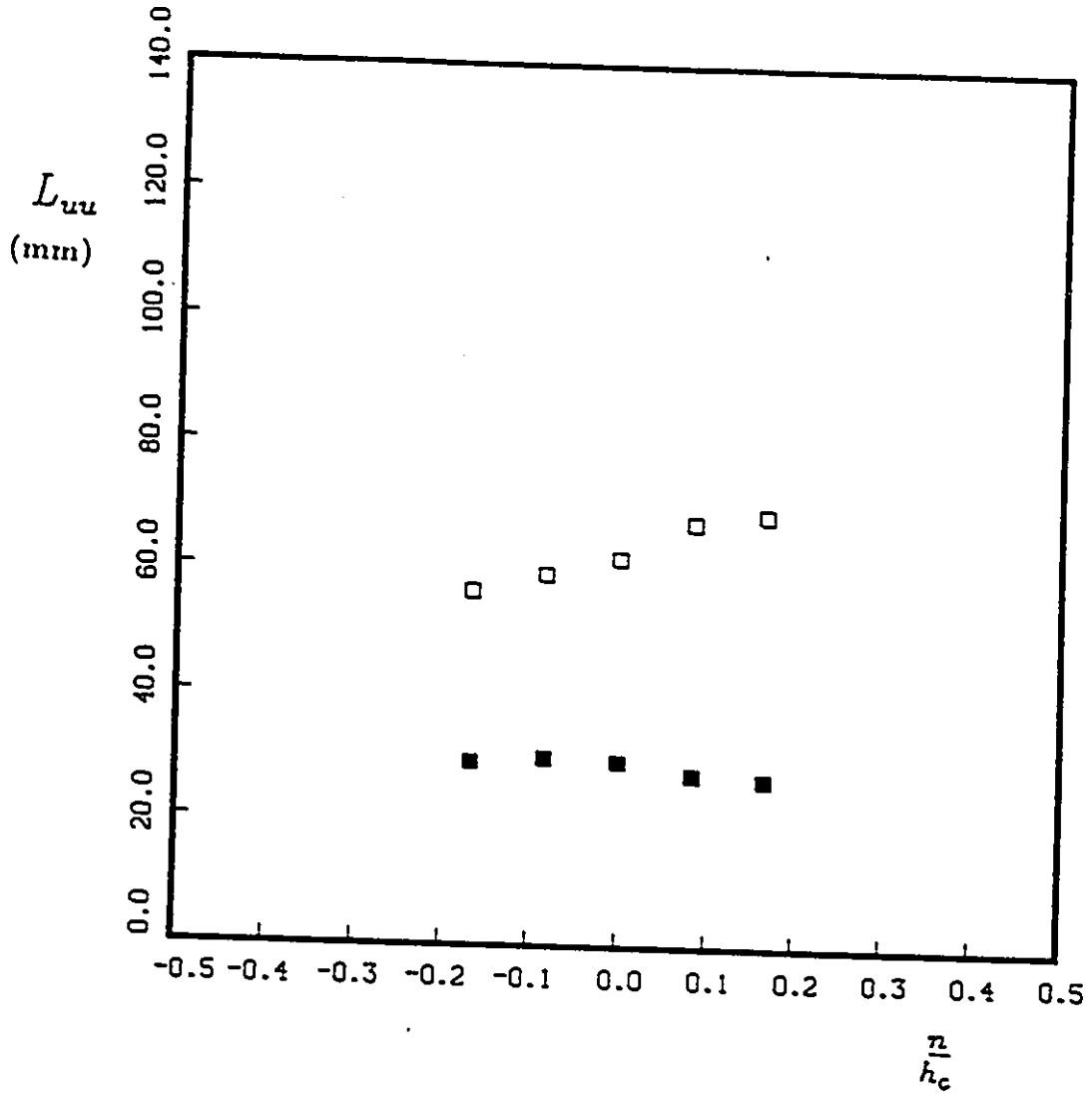

Figure 5.102: Transverse variation of L_{uu} in the strongly curved section; $\frac{s}{h_c}$=2.15, z=0. Symbols as in Table 5.3.

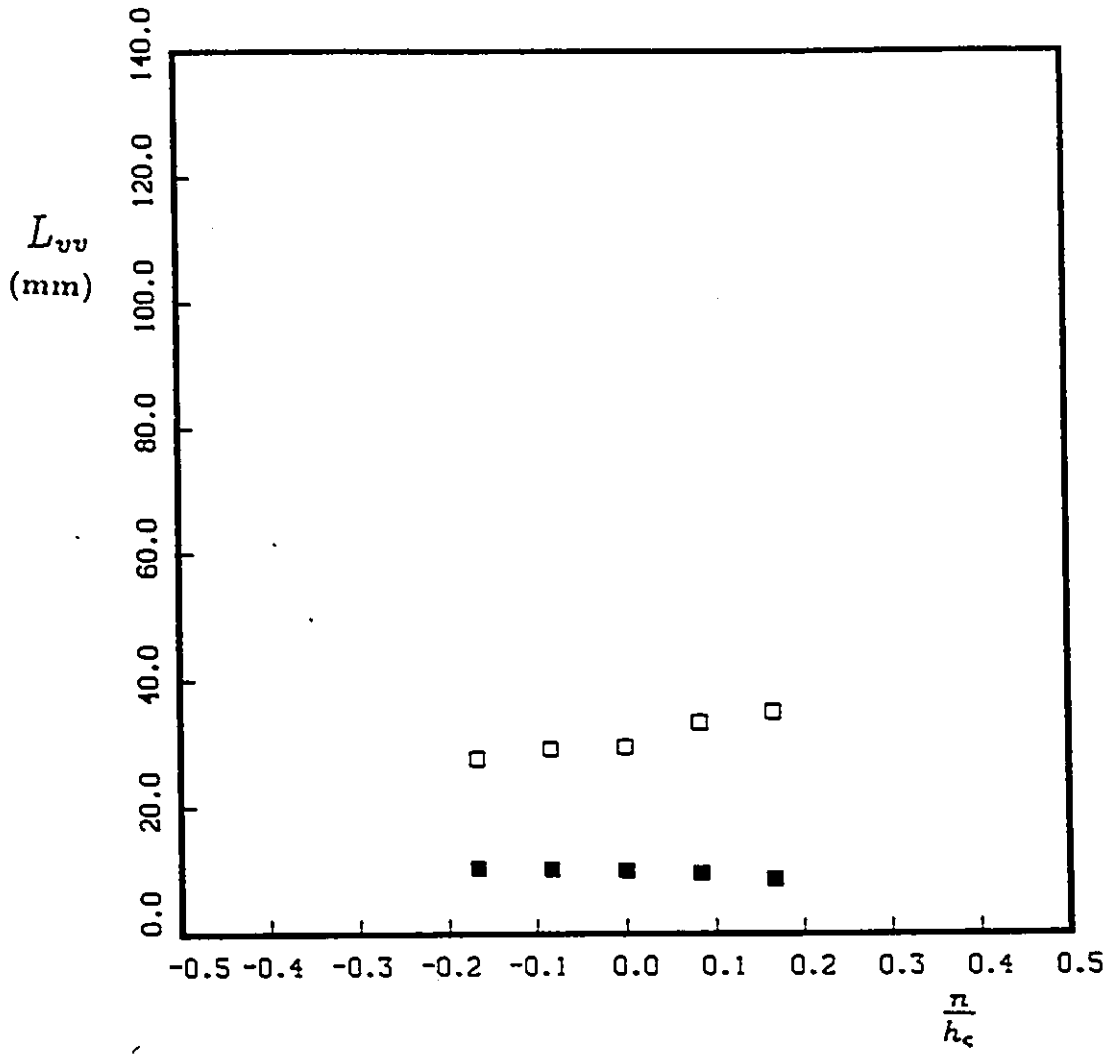

Figure 5.103: Transverse variation of L_{vv} in the strongly curved section; $\frac{s}{h_c}$=2.15, z=0. Symbols as in Table 5.3.

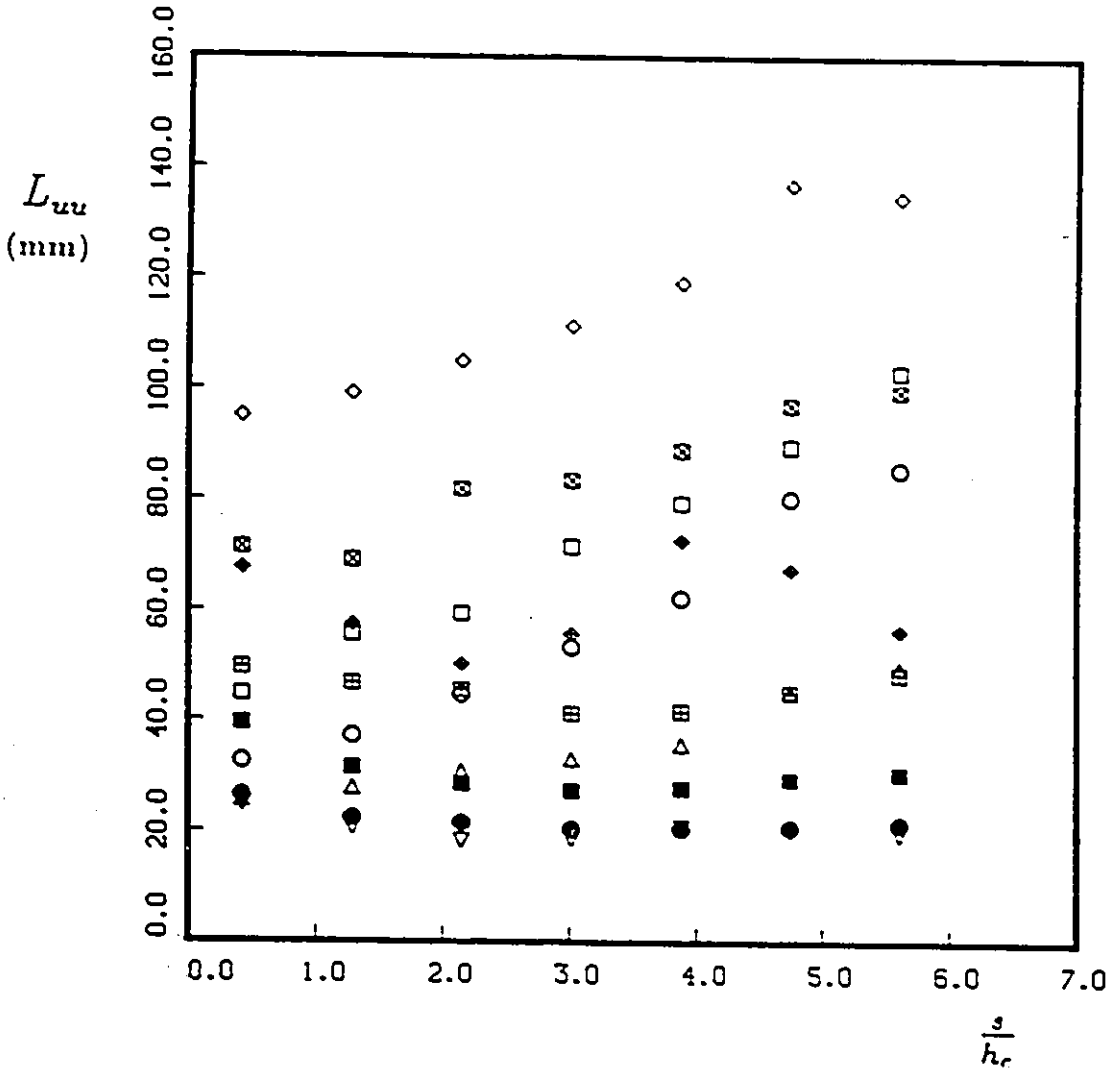

Figure 5.104: Development of L_{uu} along the wind tunnel centerline in the strongly curved section. Symbols as in Table 5.3.

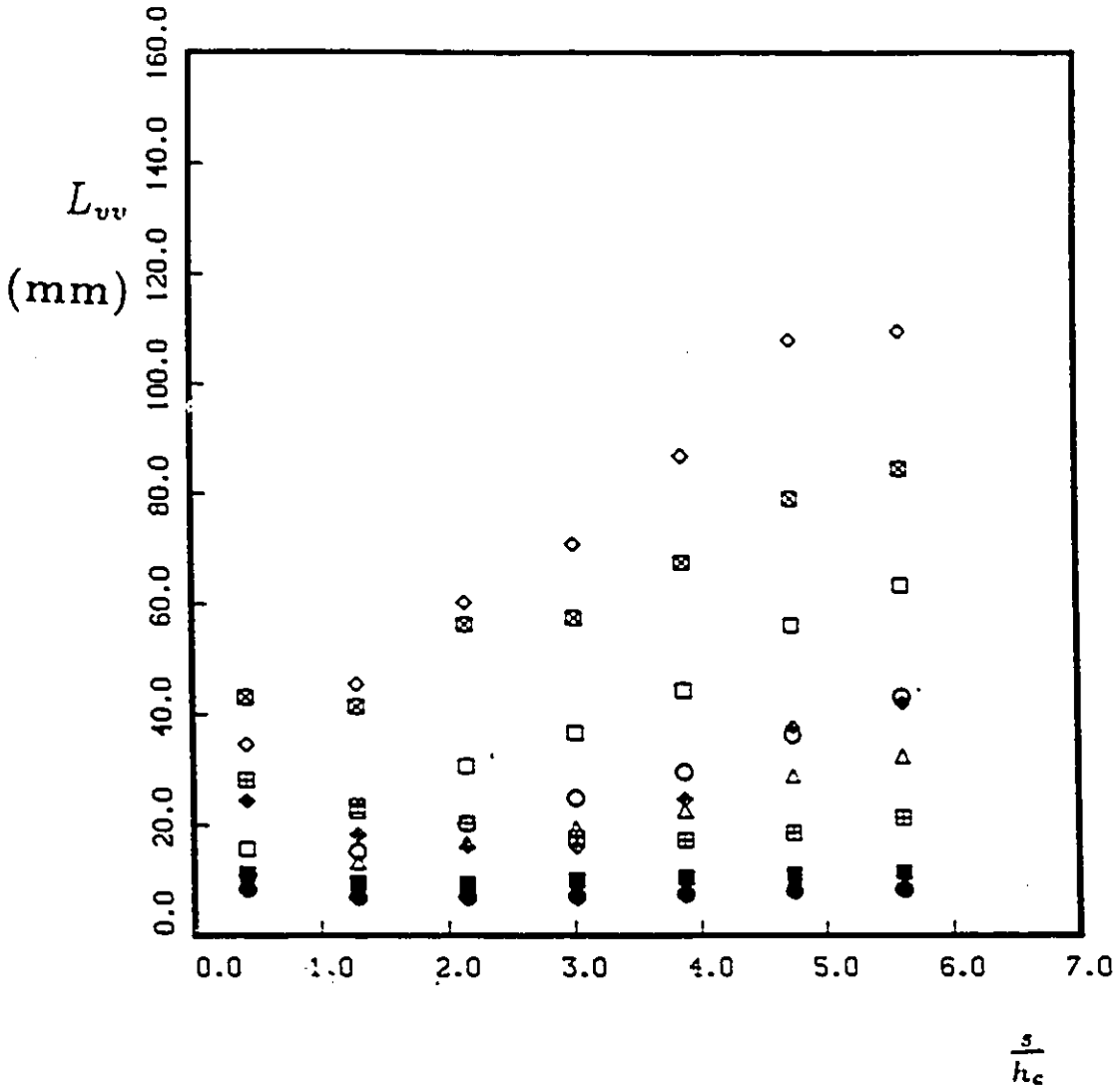

Figure 5.105: Development of L_{vv} along the wind tunnel centerline in the strongly curved section. Symbols as in Table 5.3.

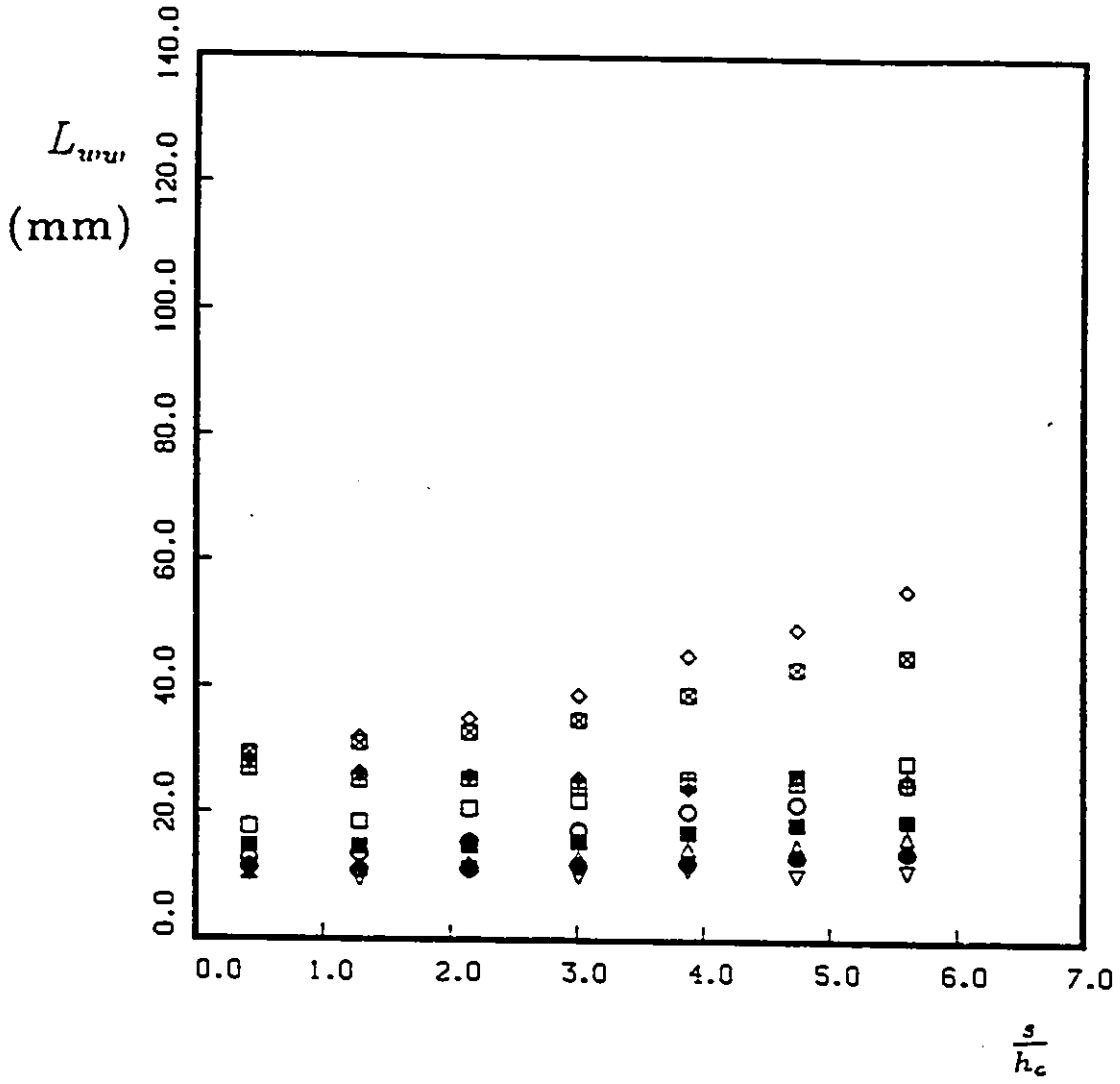

Figure 5.106: Development of L_{uw} along the wind tunnel centerline in the strongly curved section. Symbols as in Table 5.3.

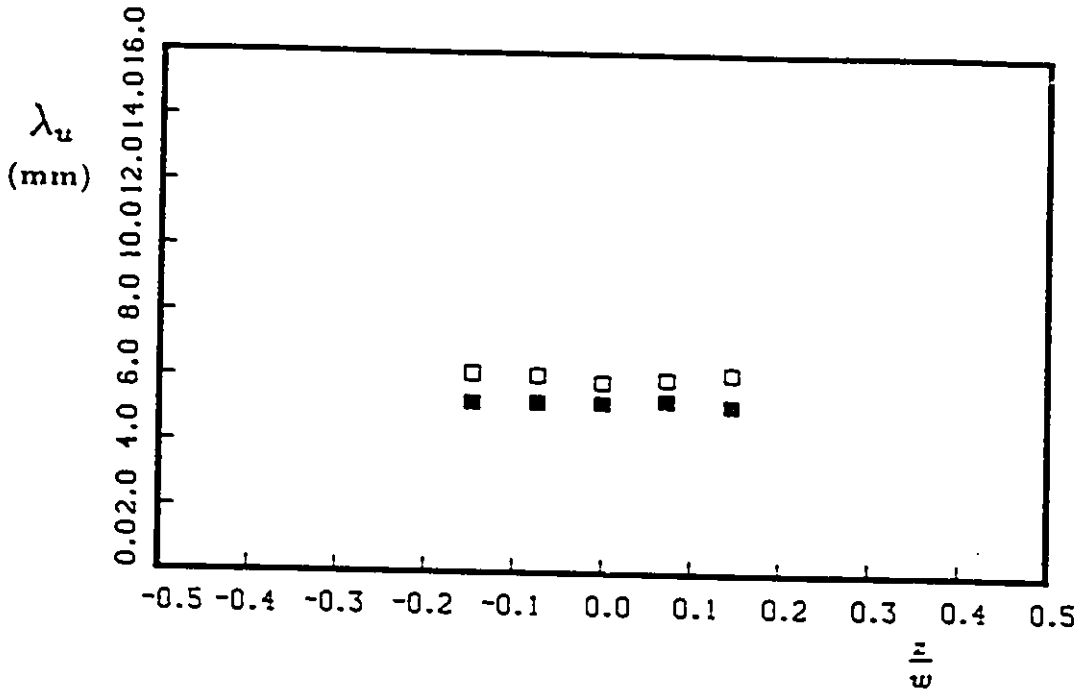

Figure 5.107: Spanwise variation of λ_u in the strongly curved section; $\frac{s}{h_r}$=2.15, n=0. Symbols as in Table 5.3.

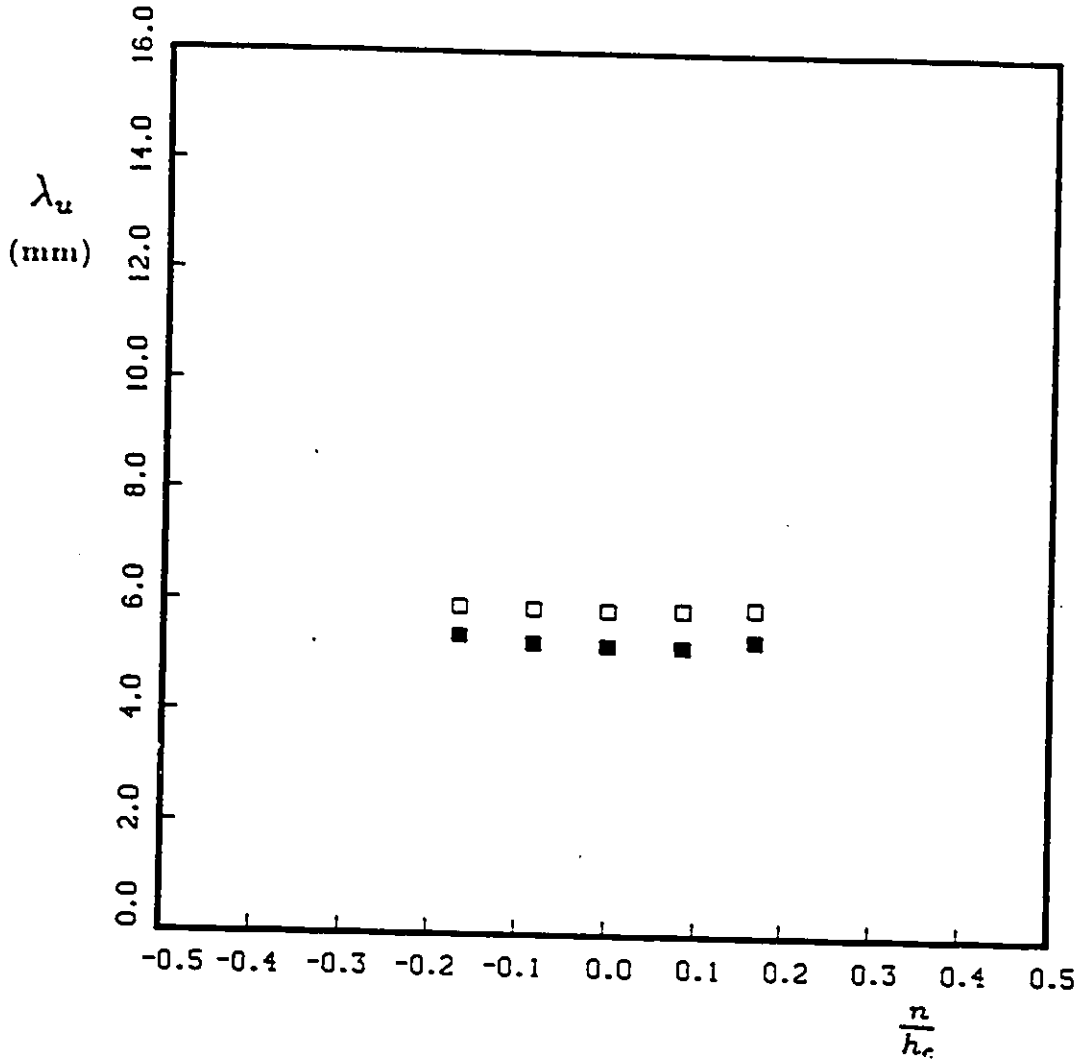

Figure 5.108: Transverse variation of λ_u in the strongly curved section; $\frac{s}{h_c}$=2.15, z=0. Symbols as in Table 5.3.

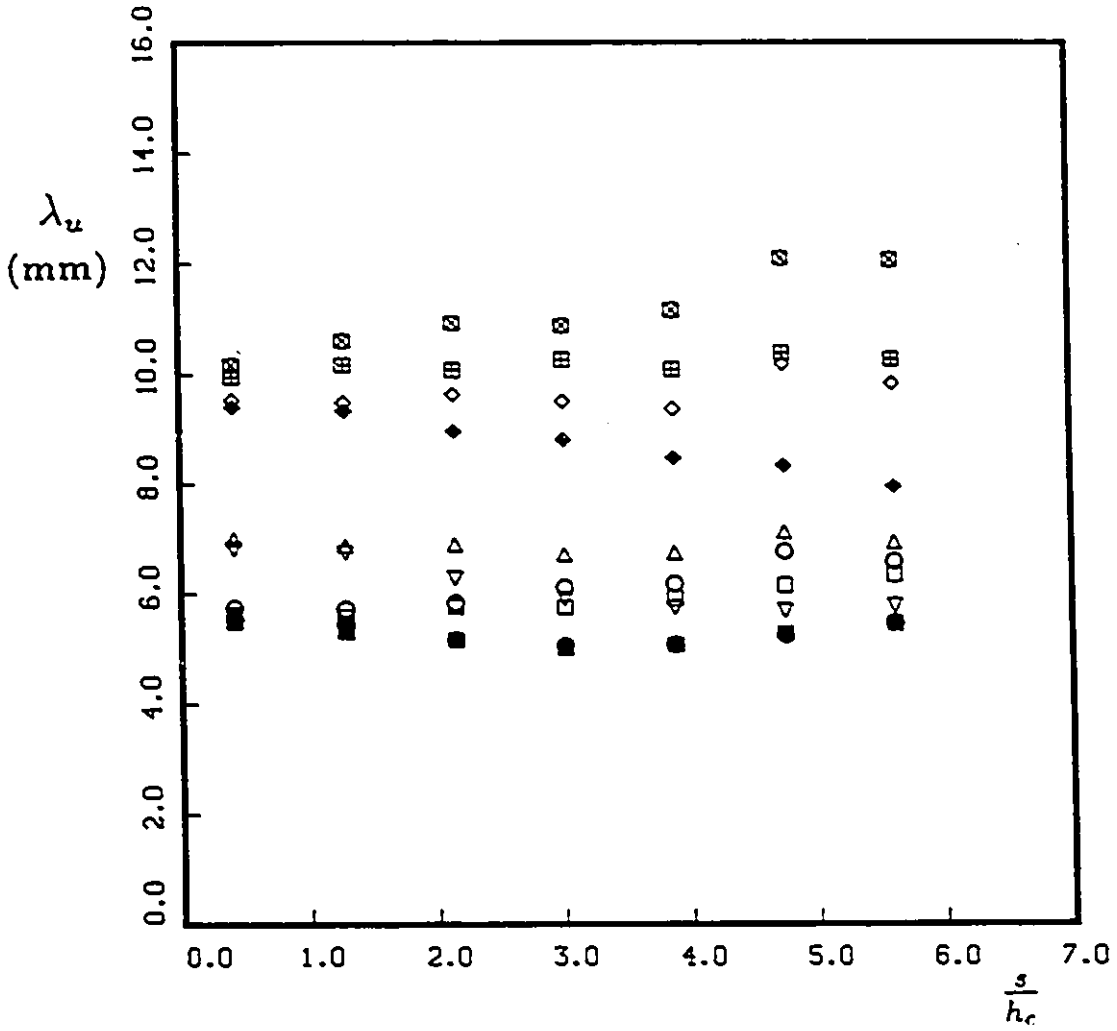

Figure 5.109: Development of λ_u along the wind tunnel centerline in the strongly curved section. Symbols as in Table 5.3.

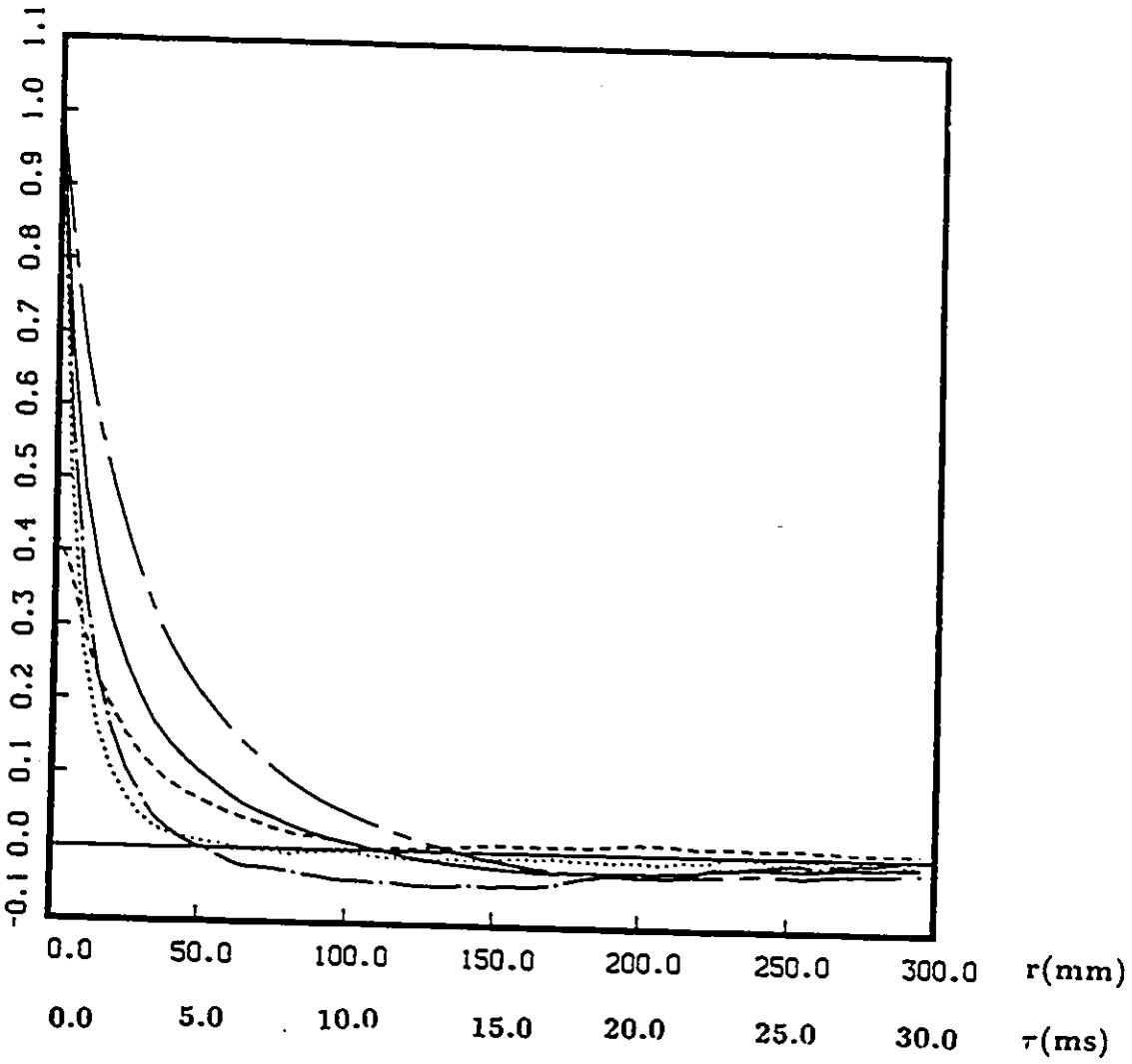

Figure 5.110: Components of the streamwise space-correlation in the straight section, Case NB; — - — B_{uu}, · · · · · B_{vv}, — · — · — B_{ww}, - - - - - B_{uv}, —— B_{qq}; $\frac{x_1}{h_s}$=9.9, x_2=0, x_3=0.

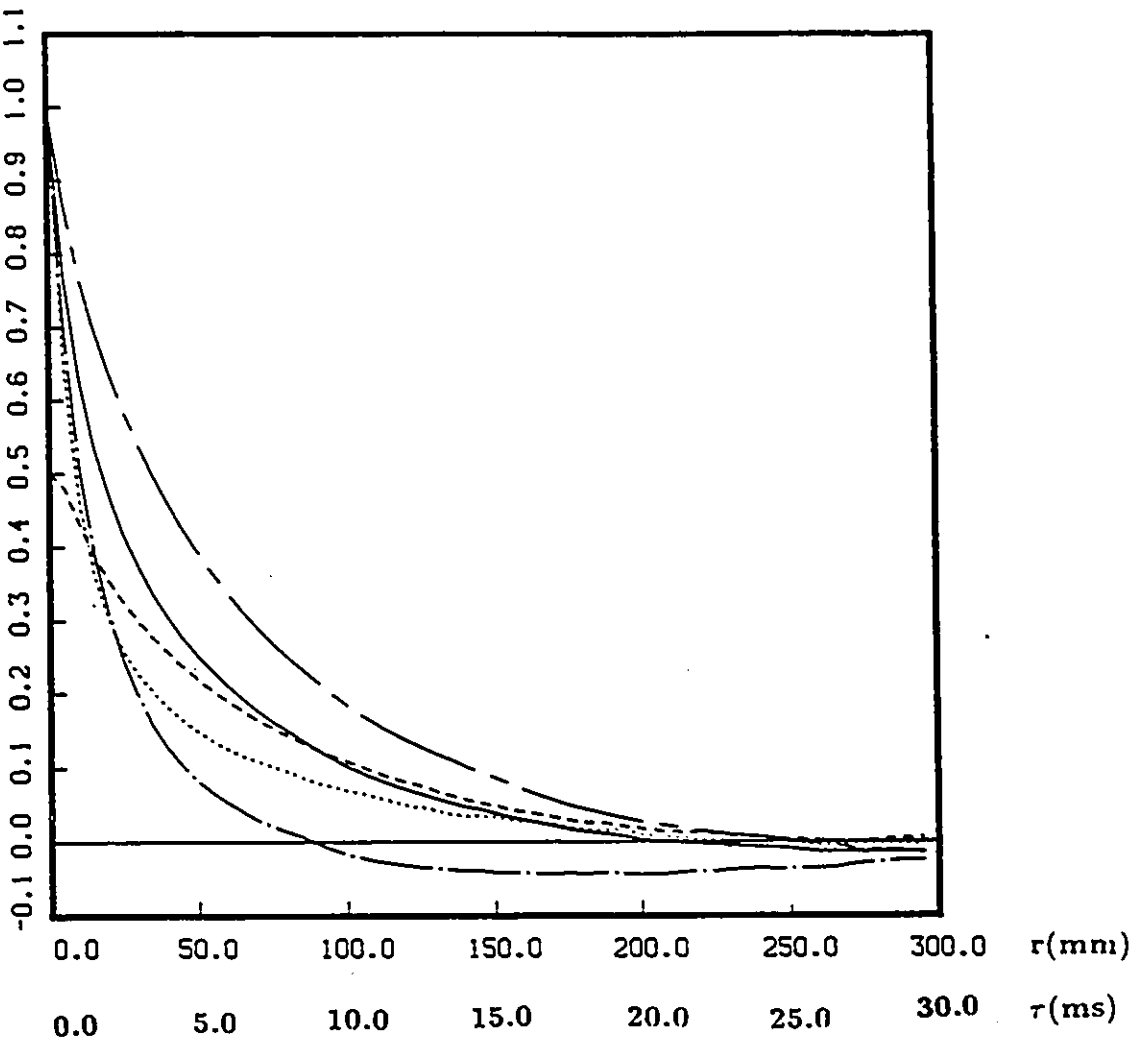

Figure 5.111: Components of the streamwise space-correlation in the strongly curved section, $S = -.10$; — - — B_{uu}, ····· B_{vv}, —·— B_{ww}, — — — B_{uv}, ——— B_{qq}; $\frac{s}{h_c}$=3.01, n=0, z=0.

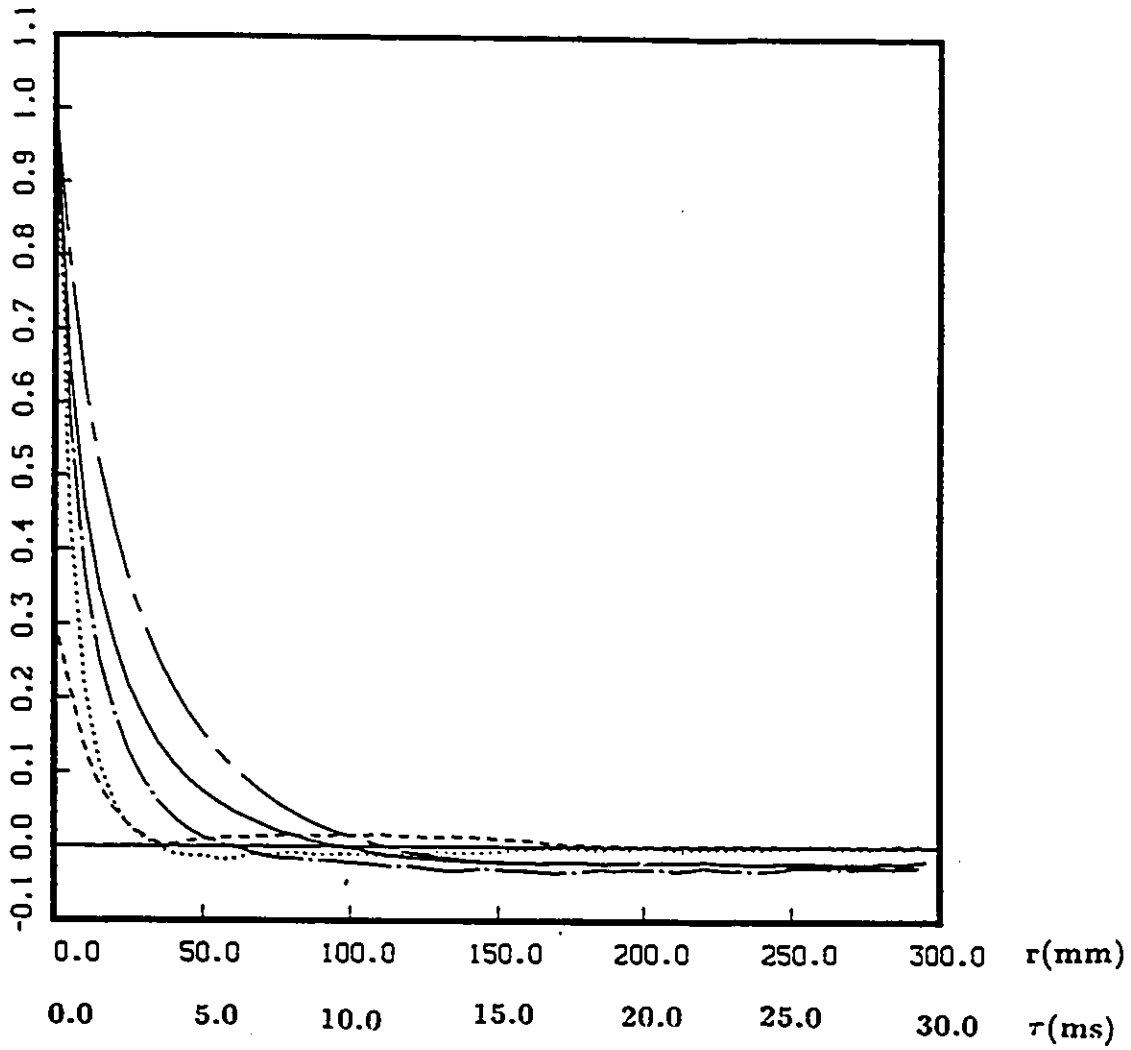

Figure 5.112: Components of the streamwise space-correlation in the strongly curved section, $S = .10$; — — B_{uu}, • • • • • B_{vv}, — • — B_{ww}, - - - - B_{uv}, ——— B_{qq}; $\frac{s}{h_c}$=3.01, n=0, z=0.

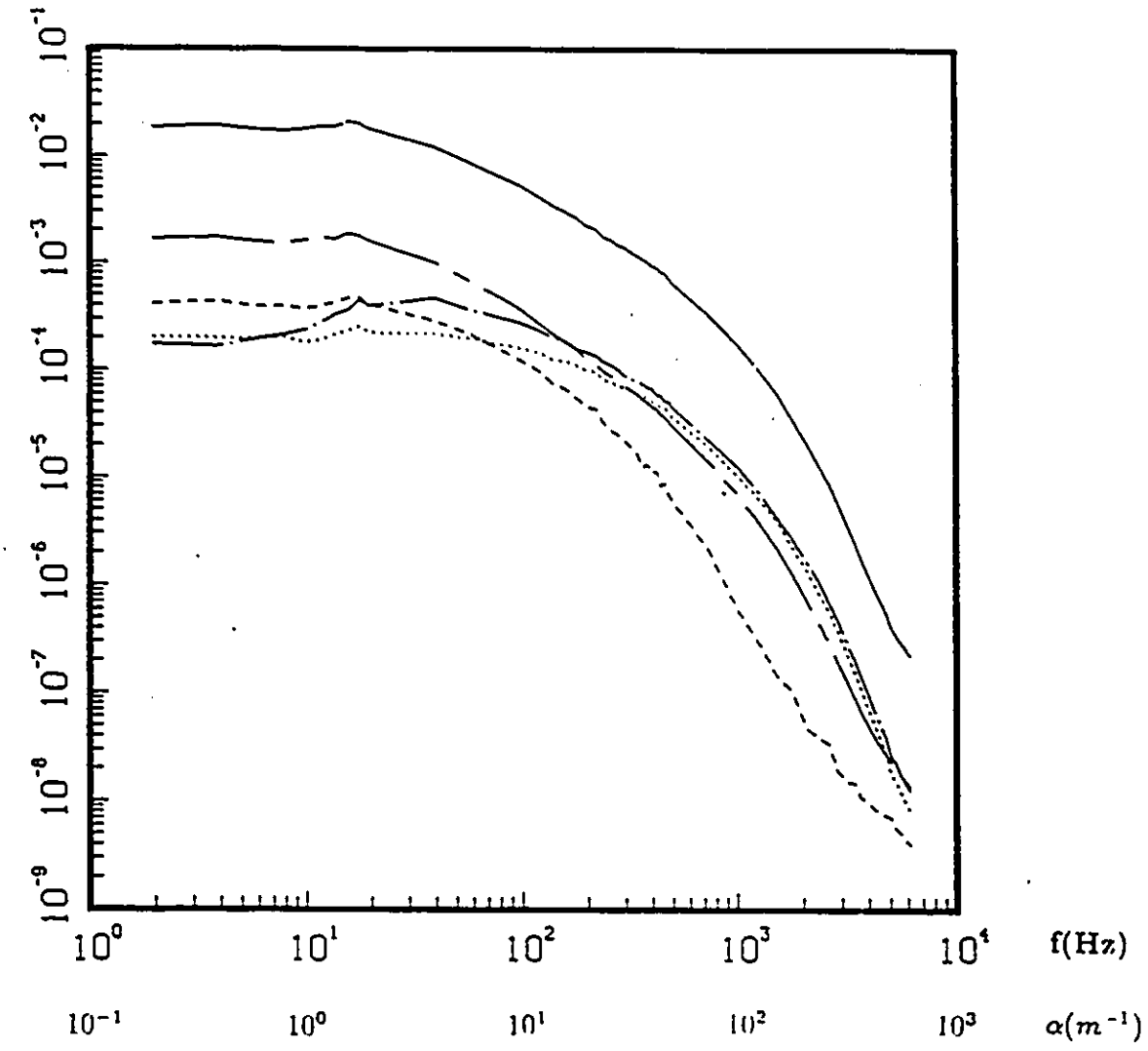

Figure 5.113: Components of the streamwise spectra in the straight section, Case NB; —-—- F_{uu}, · · · · · F_{vv}, —·— F_{ww}, - - - - $|F_{uv}|$, ——— F_{qq} x10 $\frac{x_1}{h_s}$=9.9, x_2=0, x_3=0.

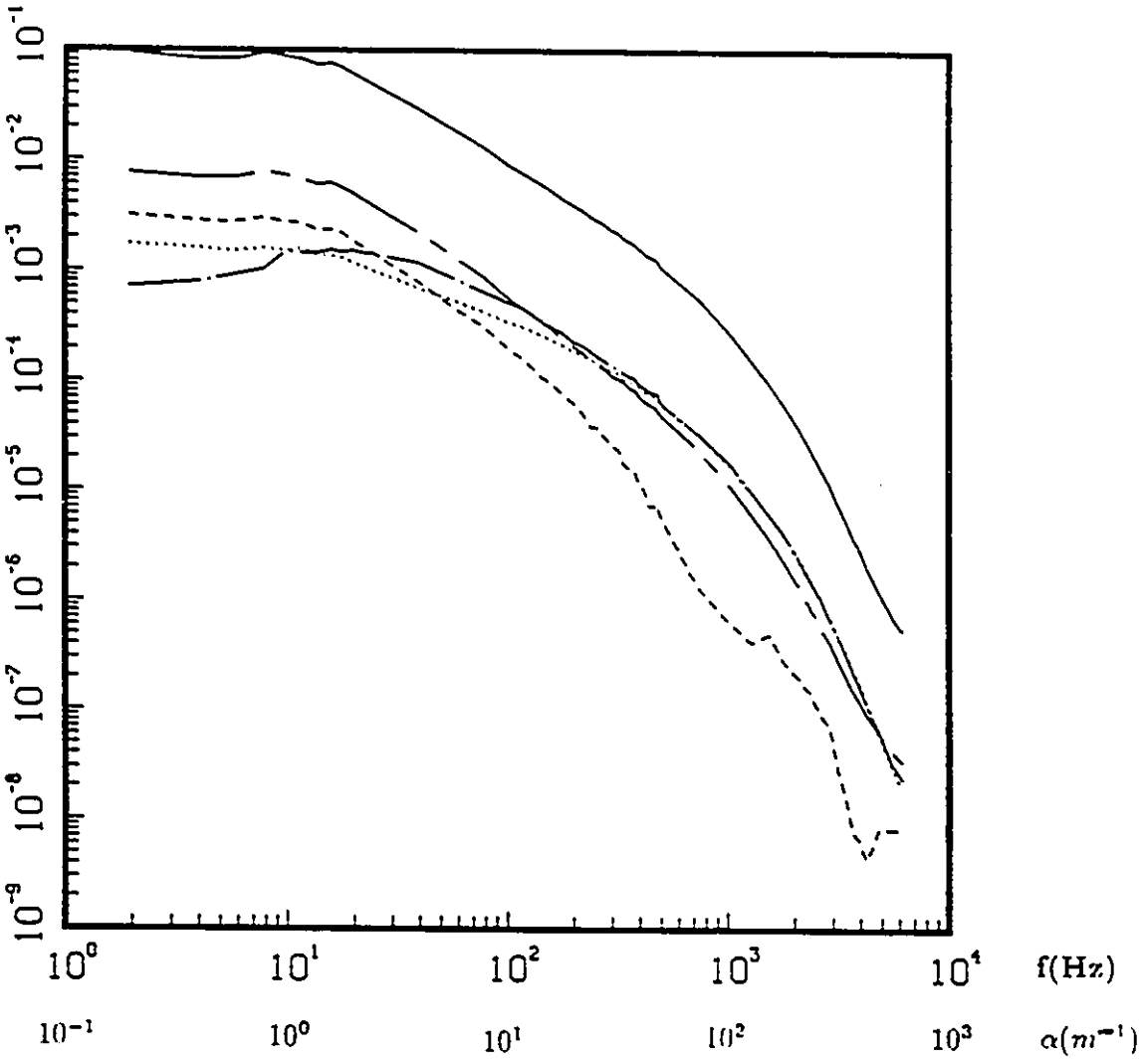

Figure 5.114: Components of the streamwise spectra in the strongly curved section, $S = -.10$; — - — F_{uu}, ····· F_{vv}, —·—·— F_{ww}, - - - - $|F_{uv}|$, ——— 10x F_{qq}; $\frac{s}{h_c}$=3.01, n=0, z=0.

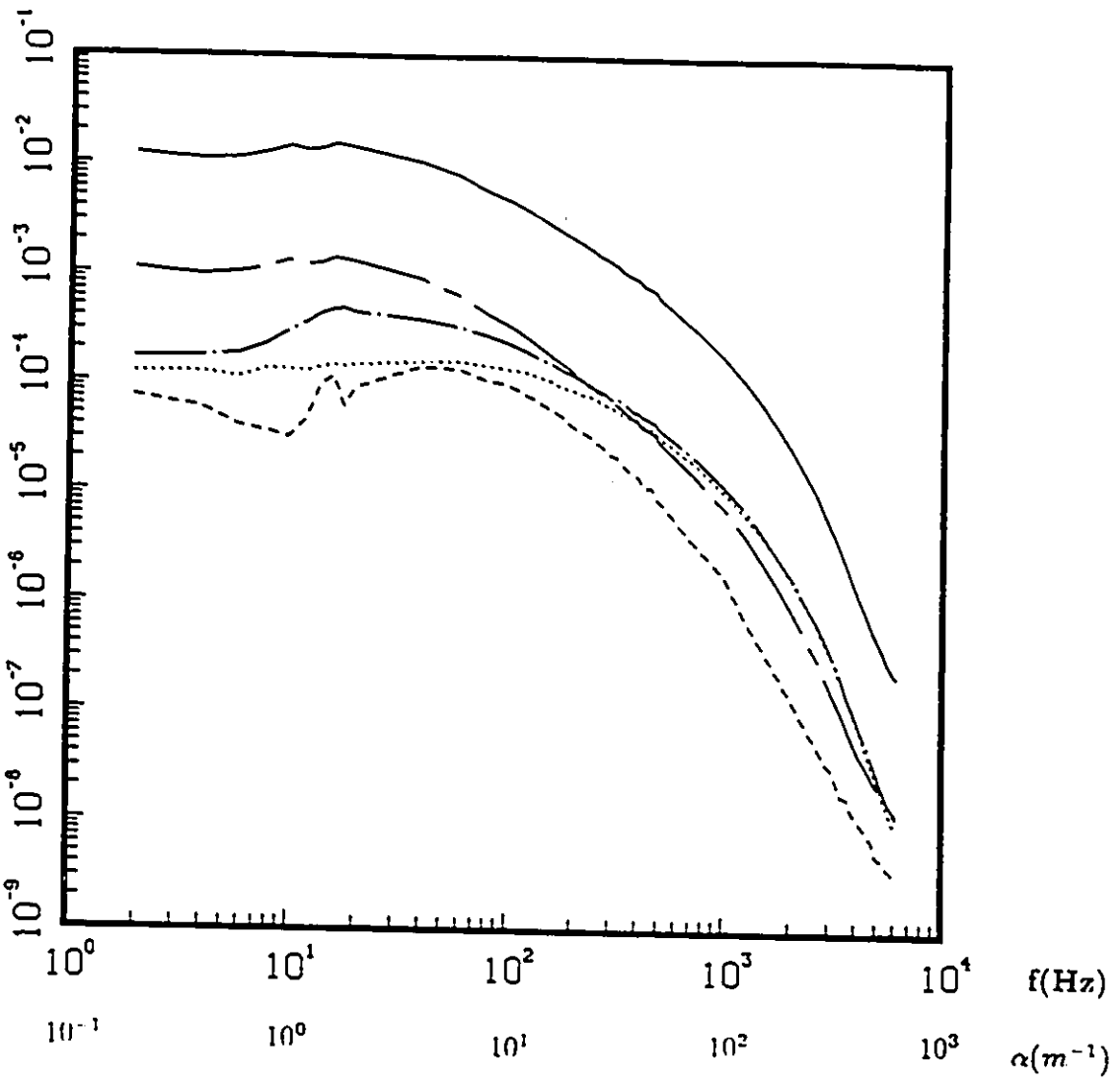

Figure 5.115: Components of the streamwise spectra in the strongly curved section, $S = .10$; — - - — F_{uu}, · · · · · F_{vv}, — · — F_{ww}, - - - - $|F_{uv}|$, ——— 10x F_{qq}; $\frac{s}{h_c}$=3.01, n=0, z=0.

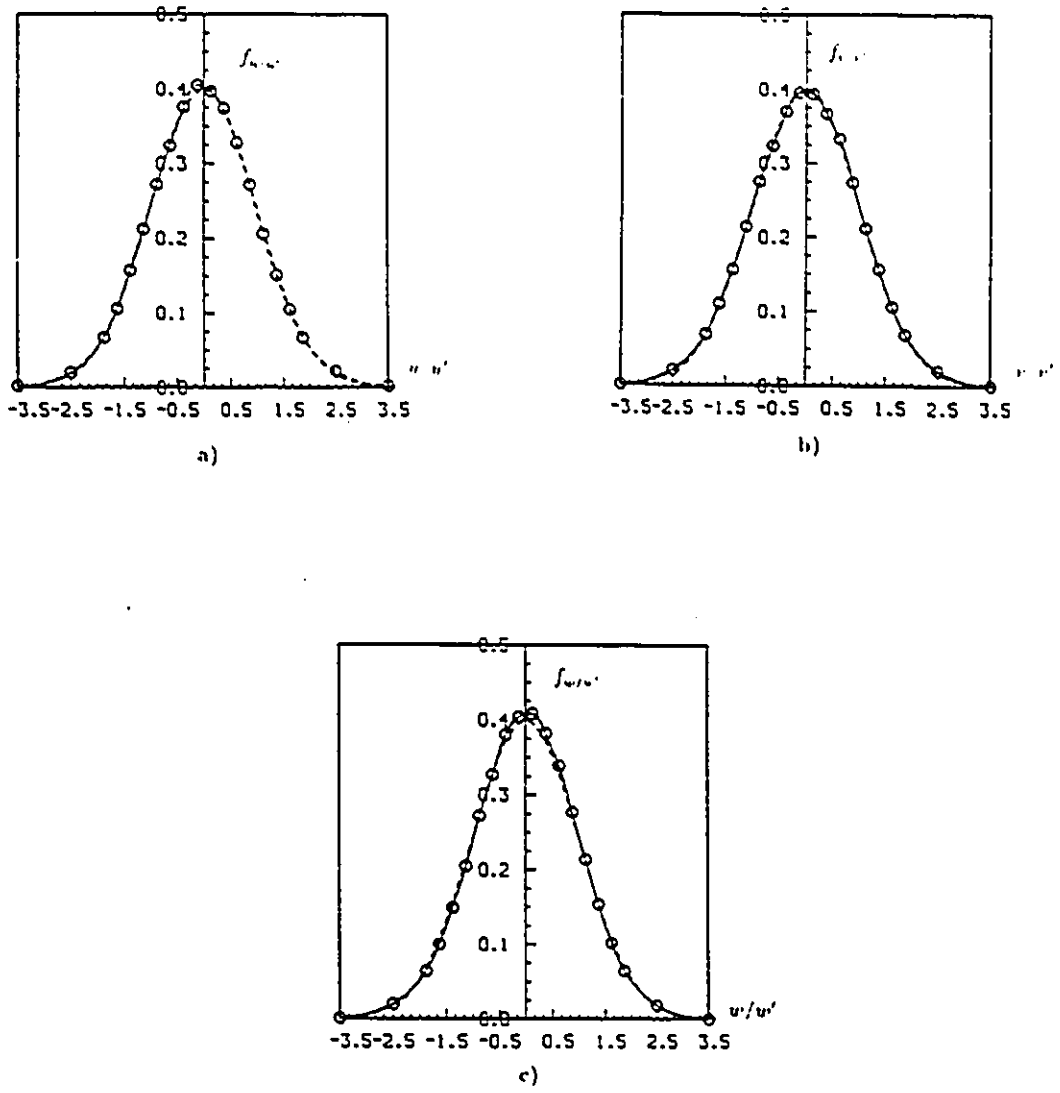

Figure 5.116: Probability density functions of the fluctuating velocities in the straight section, Case NB; - - - - - Gaussian distribution, ——— smooth curve through data; $\frac{x_1}{h_e}$=9.9, x_2=0, x_3=0.

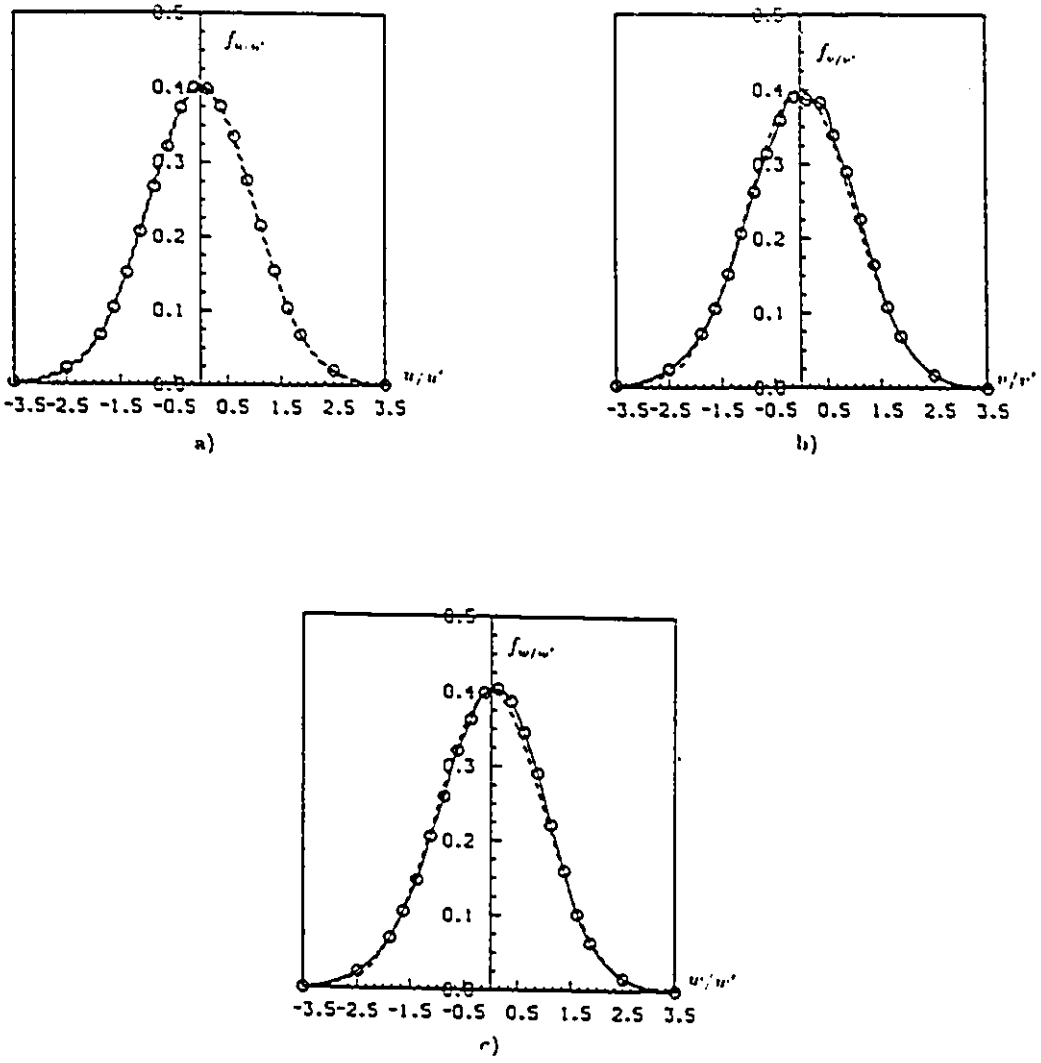

Figure 5.117: Probability density functions of the fluctuating velocities in the strongly curved section, S =-.01; ----- Gaussian distribution,—— smooth curve through data; $\frac{s}{h_c}$=3.01, n=0, z=0.

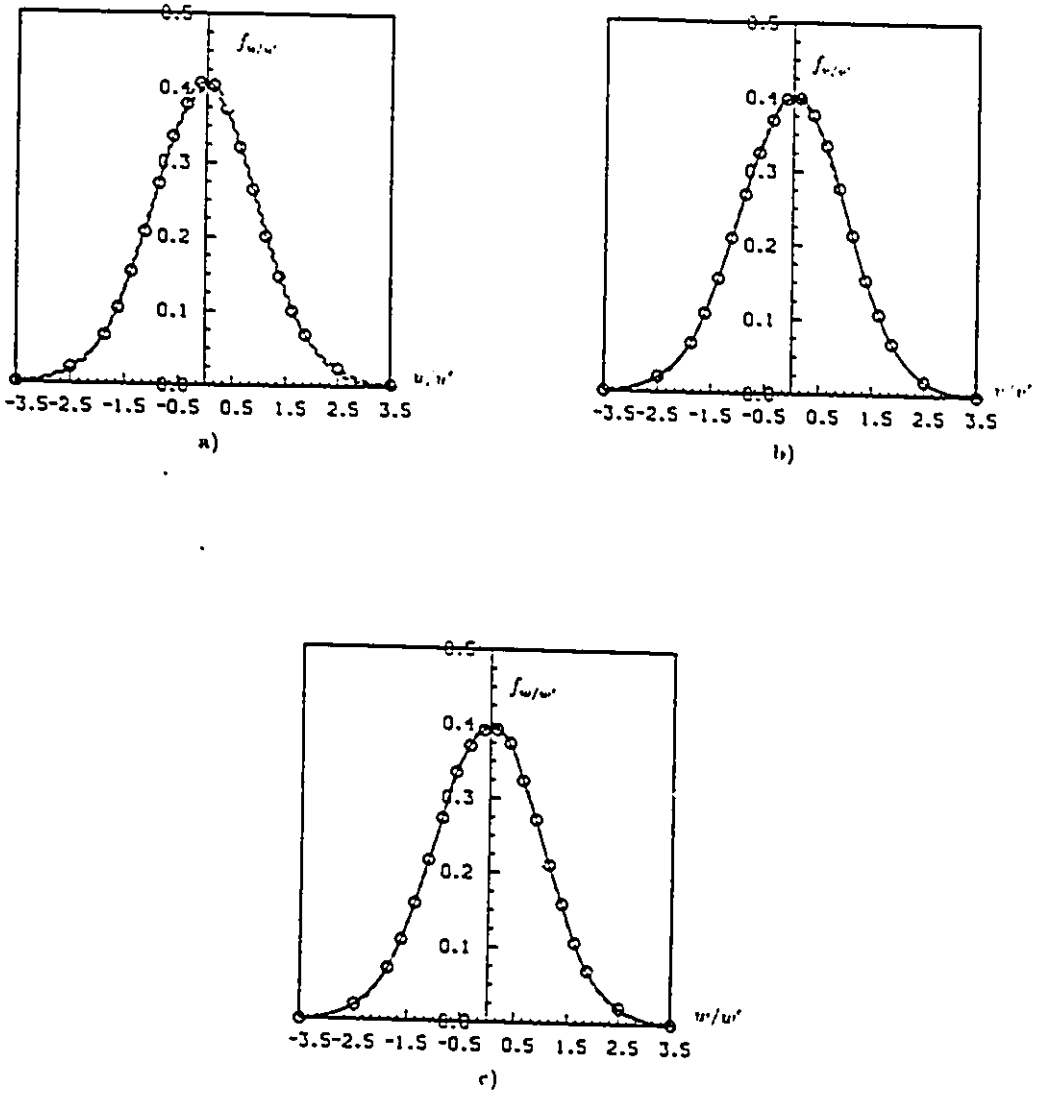

Figure 5.118: Probability density functions of the fluctuating velocities in the strongly curved section, S =.01; – – – – – Gaussian distribution, —— smooth curve through data: $\frac{s}{h_c}$=3.01, n=0, z=0.

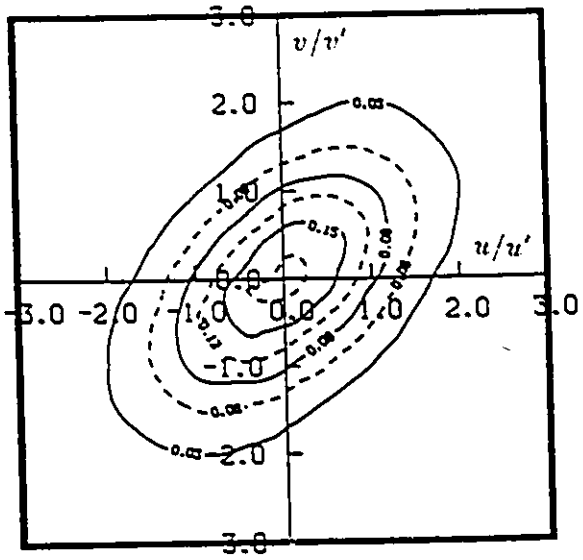

a)

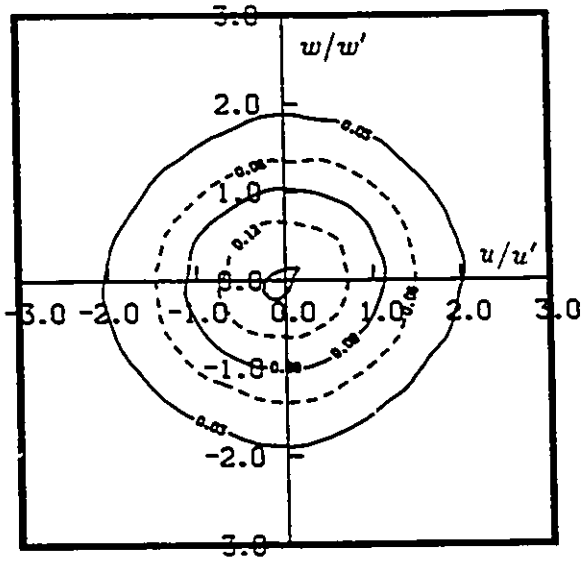

b)

Figure 5.119: Iso-probability contours of the fluctuating velocities in the straight section, Case NB; $\frac{x_1}{h_s}$=9.9. x_2=0, x_3=0.

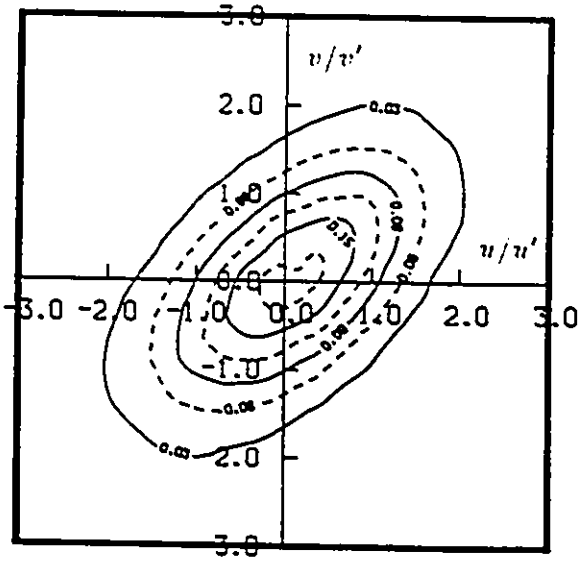

a)

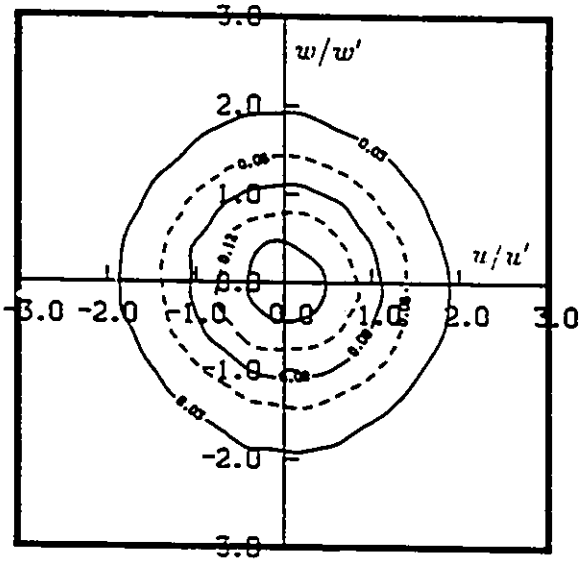

b)

Figure 5.120: Iso-probability contours of the fluctuating velocities in the strongly curved section, S =-.01; $\frac{s}{h_c}$=3.01, n=0, z=0.

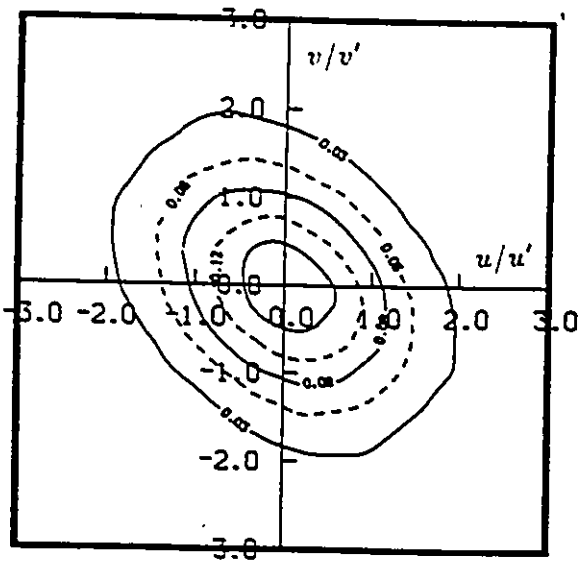

a)

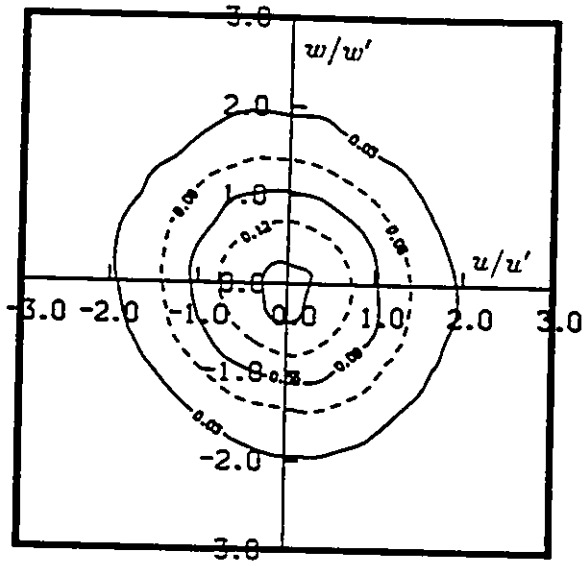

b)

Figure 5.121: Iso-probability countours of the fluctuating velocities in the strongly curved section, S =.01; $\frac{s}{h_c}$=3.01 n=0, z=0.

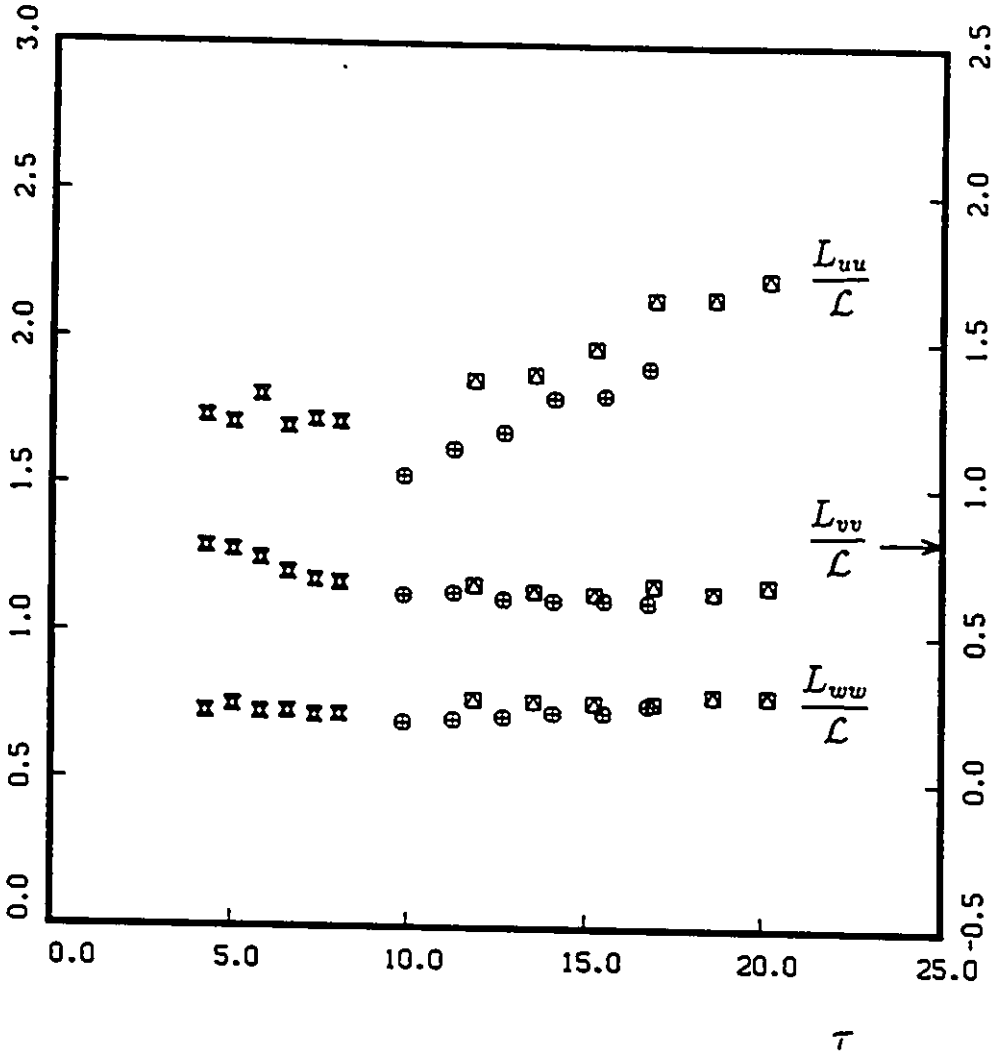

Figure 6.1: Development of the dimensionless integral lengthscales along the wind tunnel centerline in straight shear flow (Cases A, B and C). Symbols as in Table 6.1.

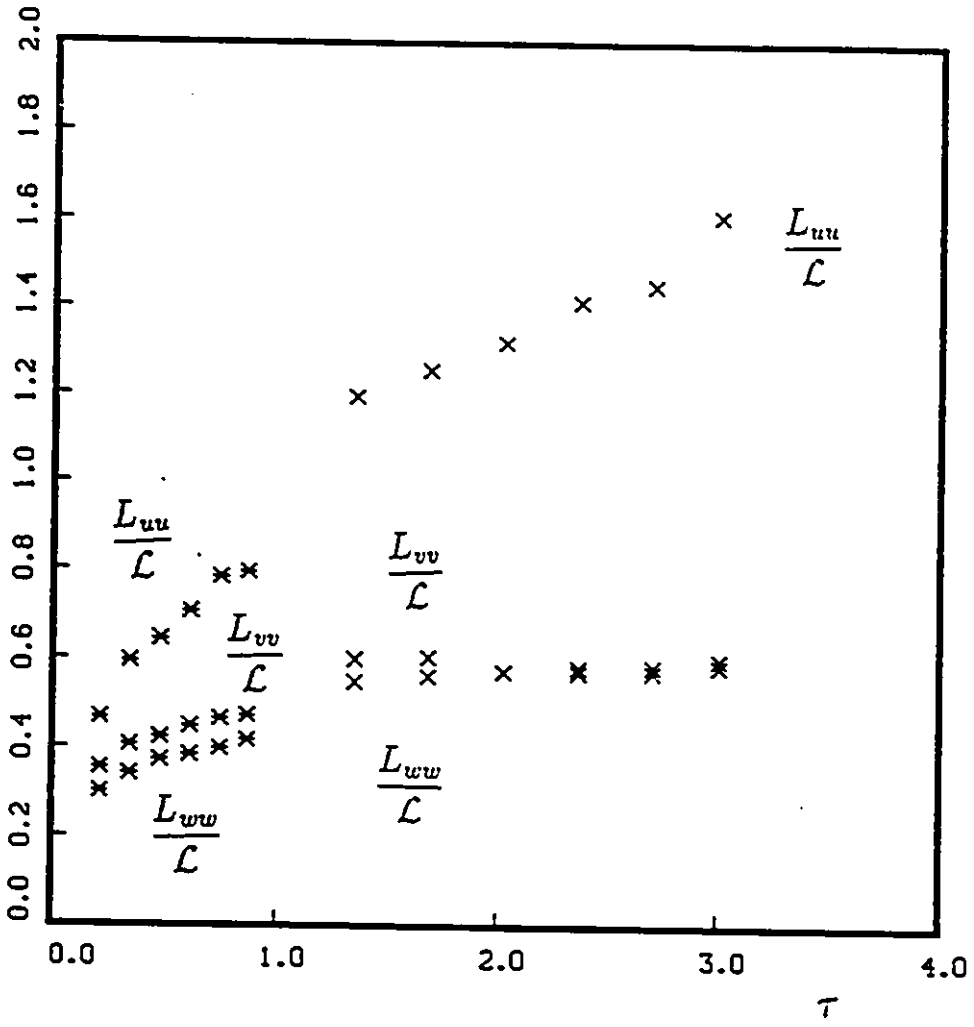

Figure 6.2: Development of the dimensionless integral lengthscales along the wind tunnel centerline in straight shear flow (Cases D and E). Symbols as in Table 6.1.

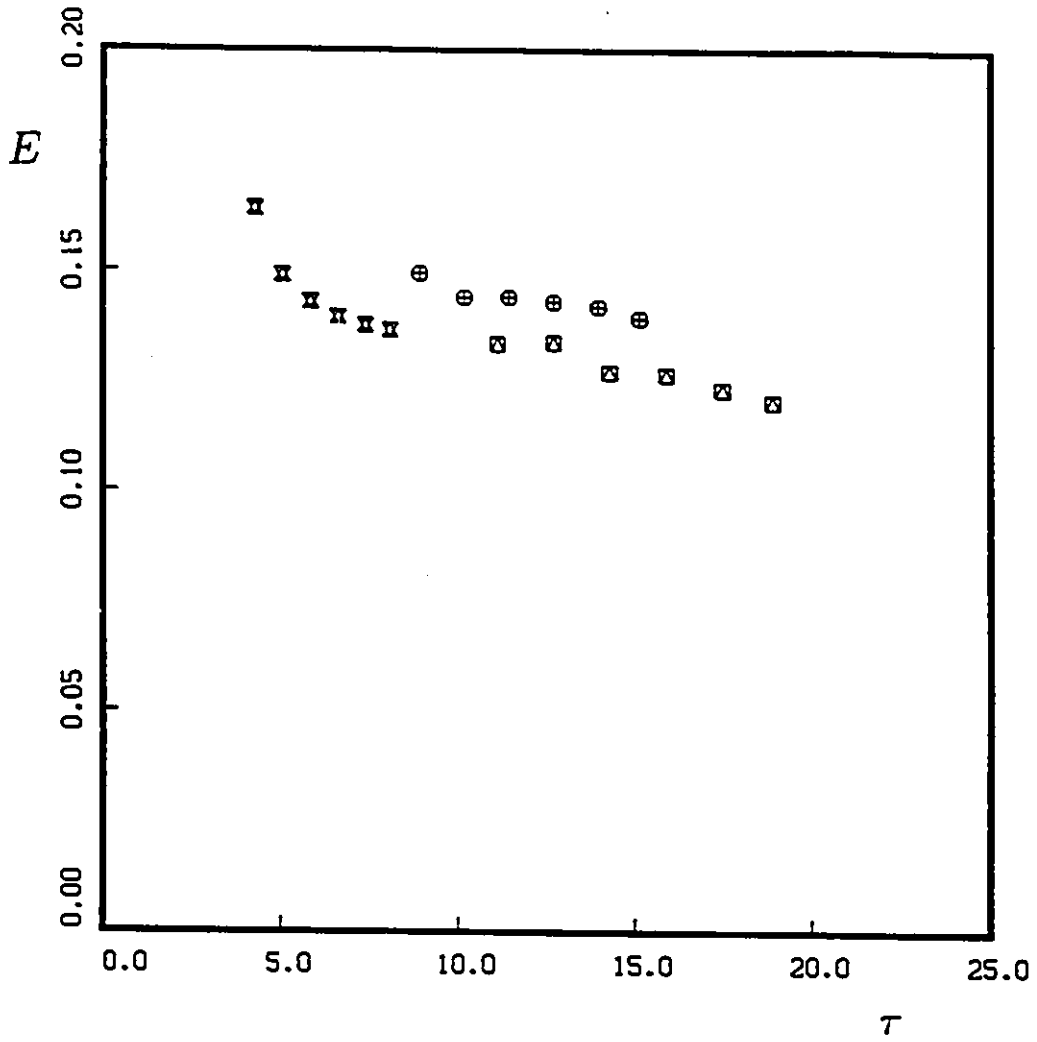

Figure 6.3: Development of E along the wind tunnel centerline in straight shear flow (Cases A, B and C). Symbols as in Table 6.1.

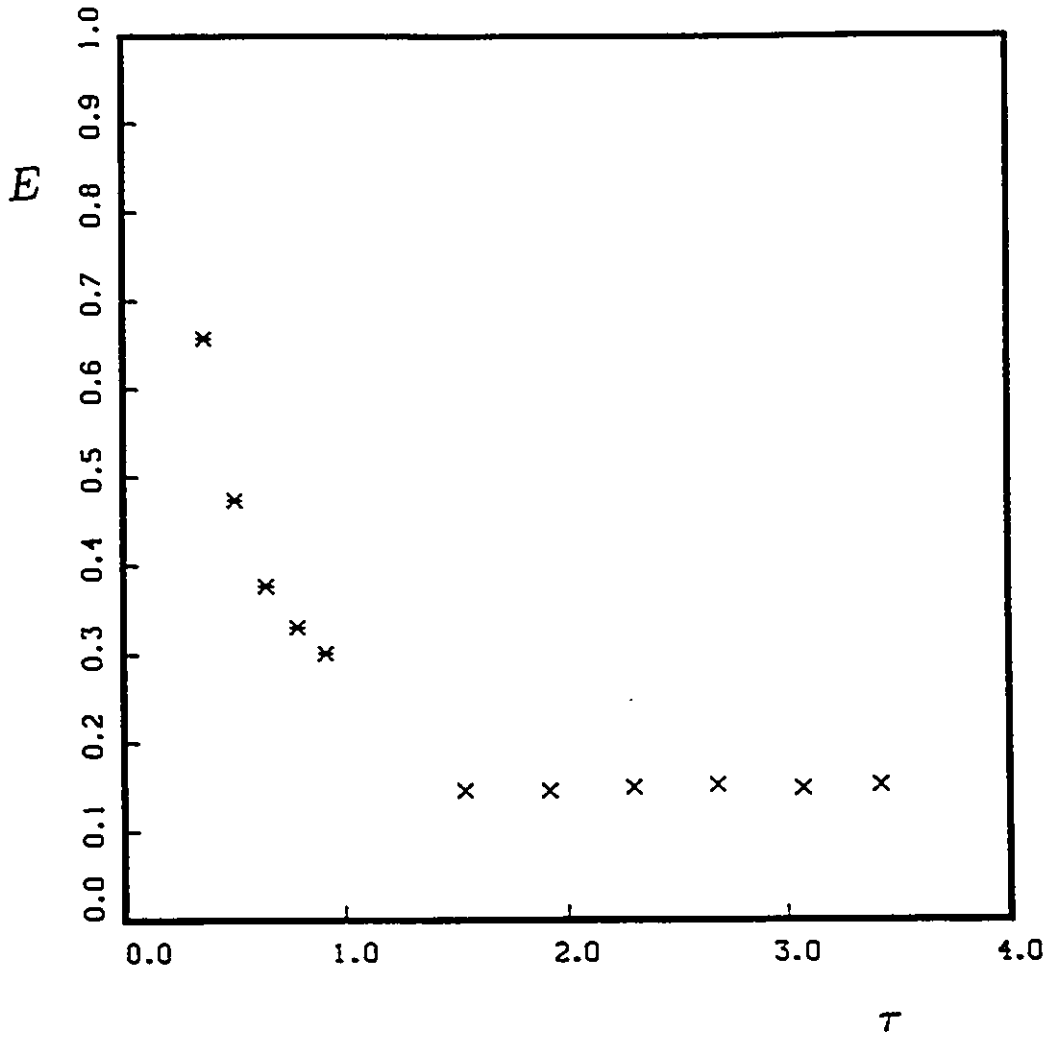

Figure 6.4: Development of E along the wind tunnel centerline in straight shear flow (Cases D and E). Symbols as in Table 6.1.

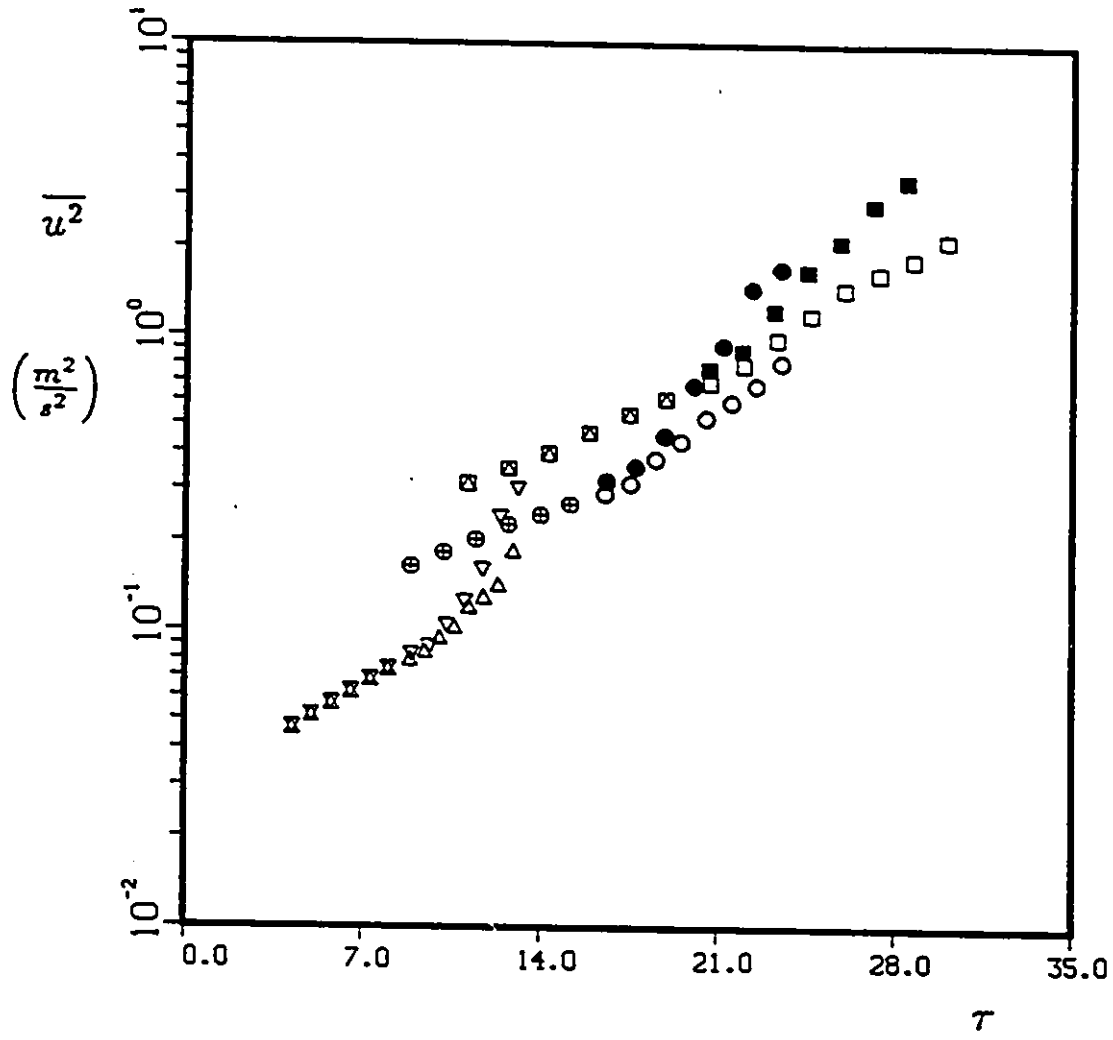

Figure 6.5: Development of $\overline{u^2}$ along the wind tunnel centerline in destabilized shear flow, S <0 (Cases A, B and C). Symbols as in Table 6.1.

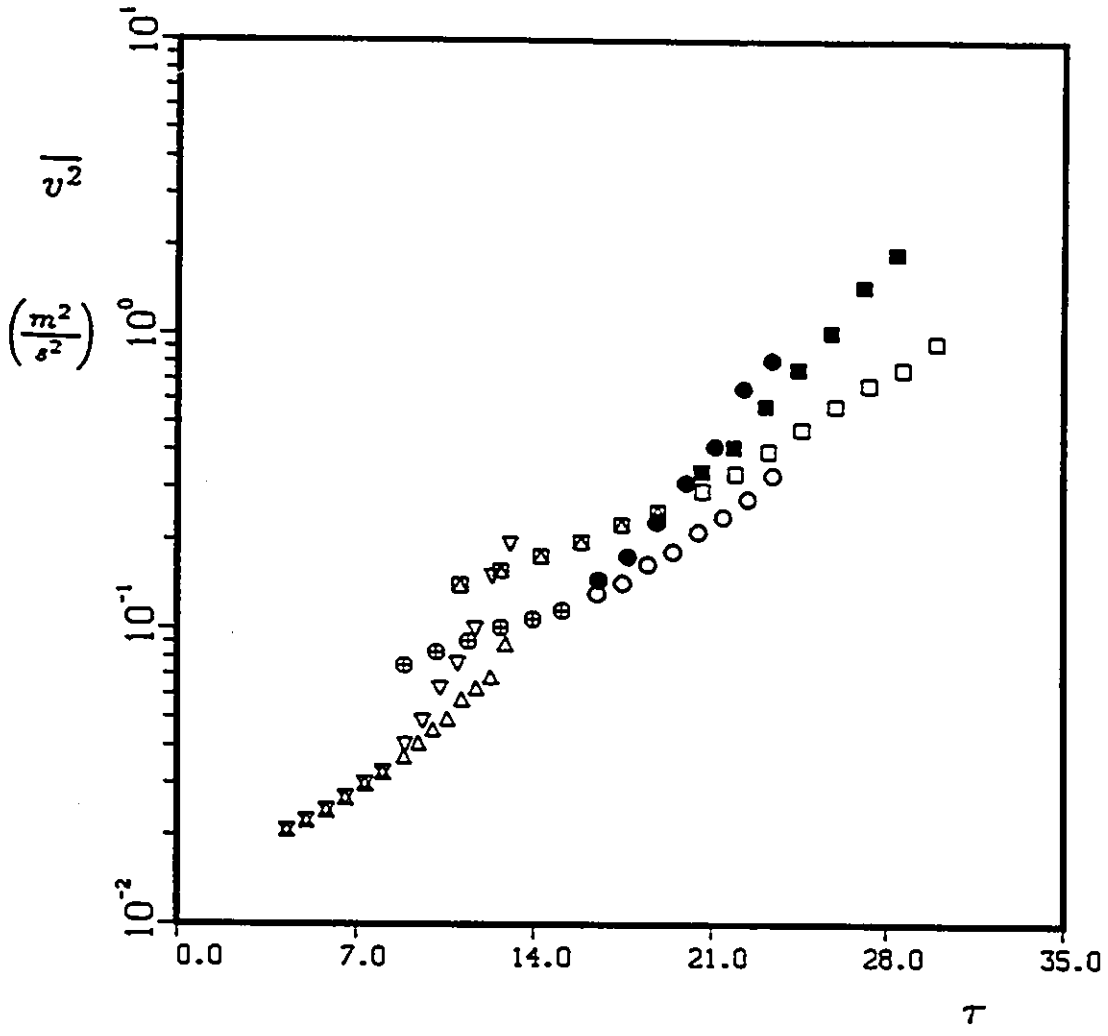

Figure 6.6: Development of $\overline{v^2}$ along the wind tunnel centerline in destabilized shear flow, S <0 (Cases A, B and C). Symbols as in Table 6.1.

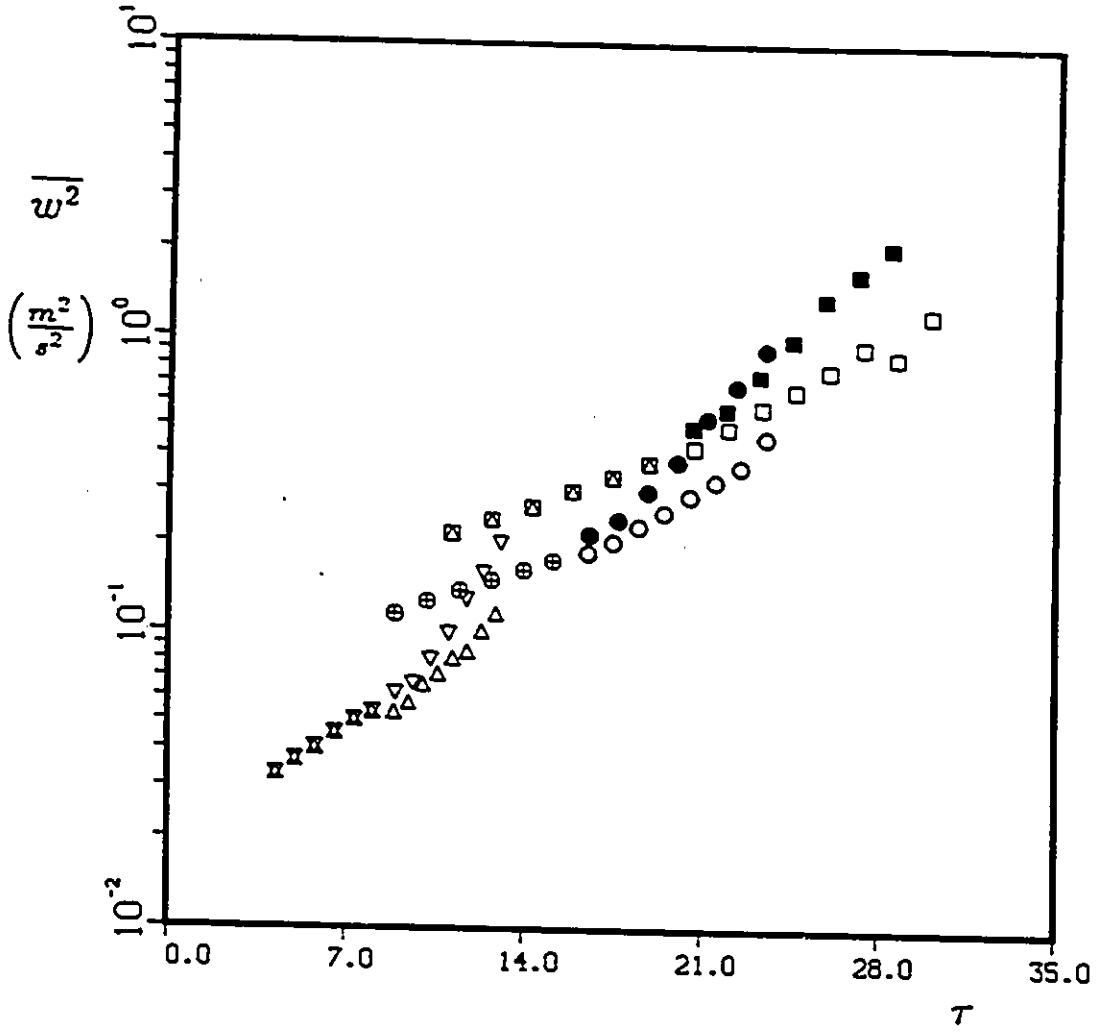

Figure 6.7: Development of $\overline{w^2}$ along the wind tunnel centerline in destabilized shear flow, $S < 0$ (Cases A, B and C). Symbols as in Table 6.1.

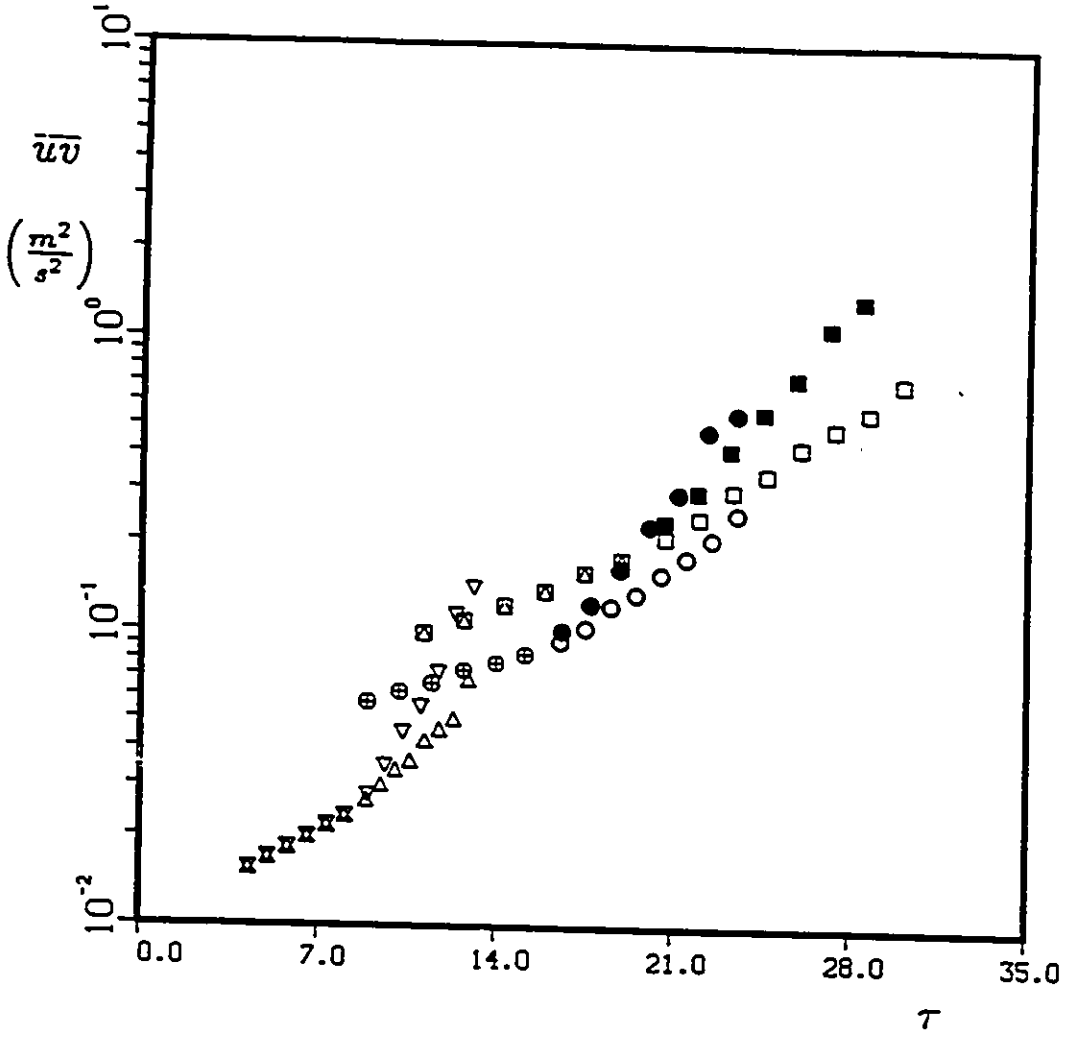

Figure 6.8: Development of $\overline{uv}$ along the wind tunnel centerline in destabilized shear flow, $S < 0$ (Cases A, B and C). Symbols as in Table 6.1.

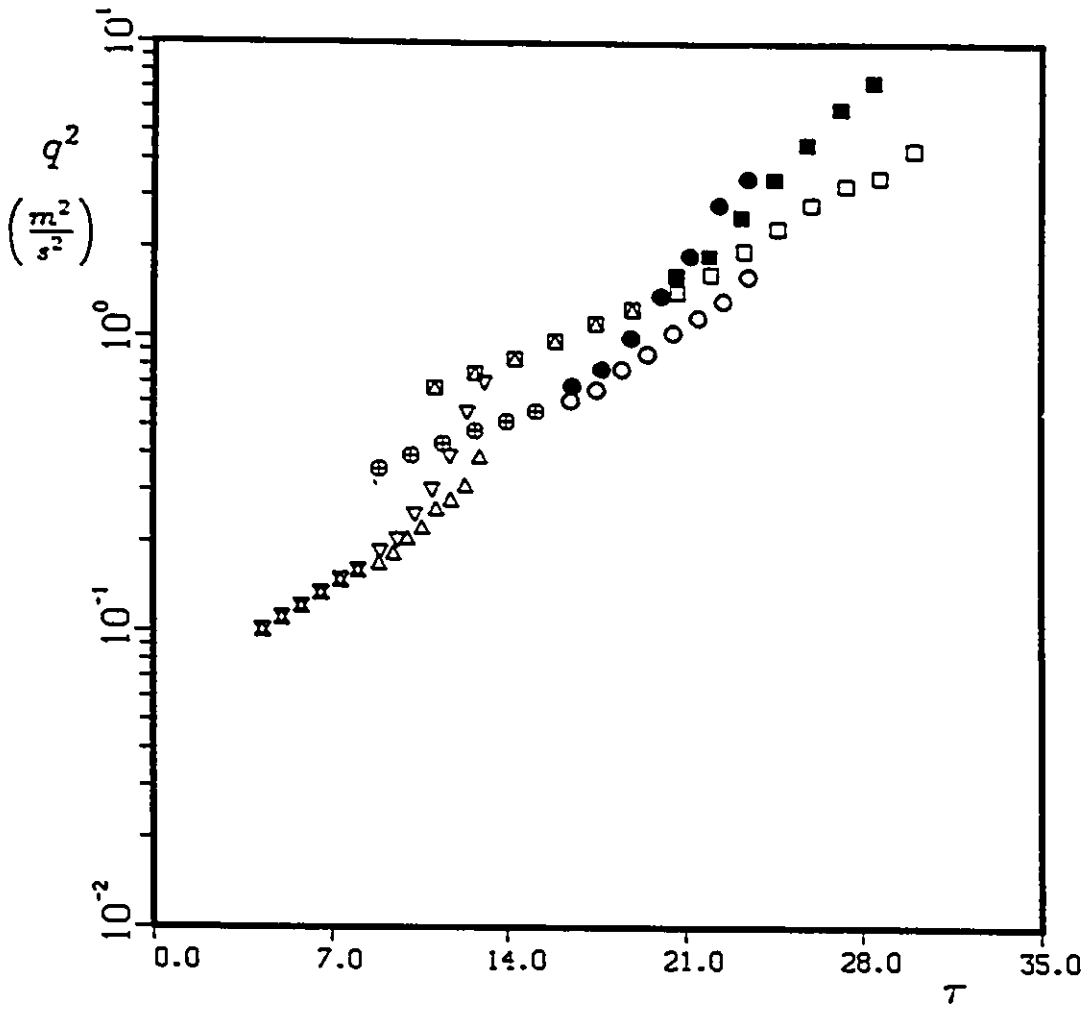

Figure 6.9: Development of q^2 along the wind tunnel centerline in destabilized shear flow, S <0 (Cases A, B and C). Symbols as in Table 6.1.

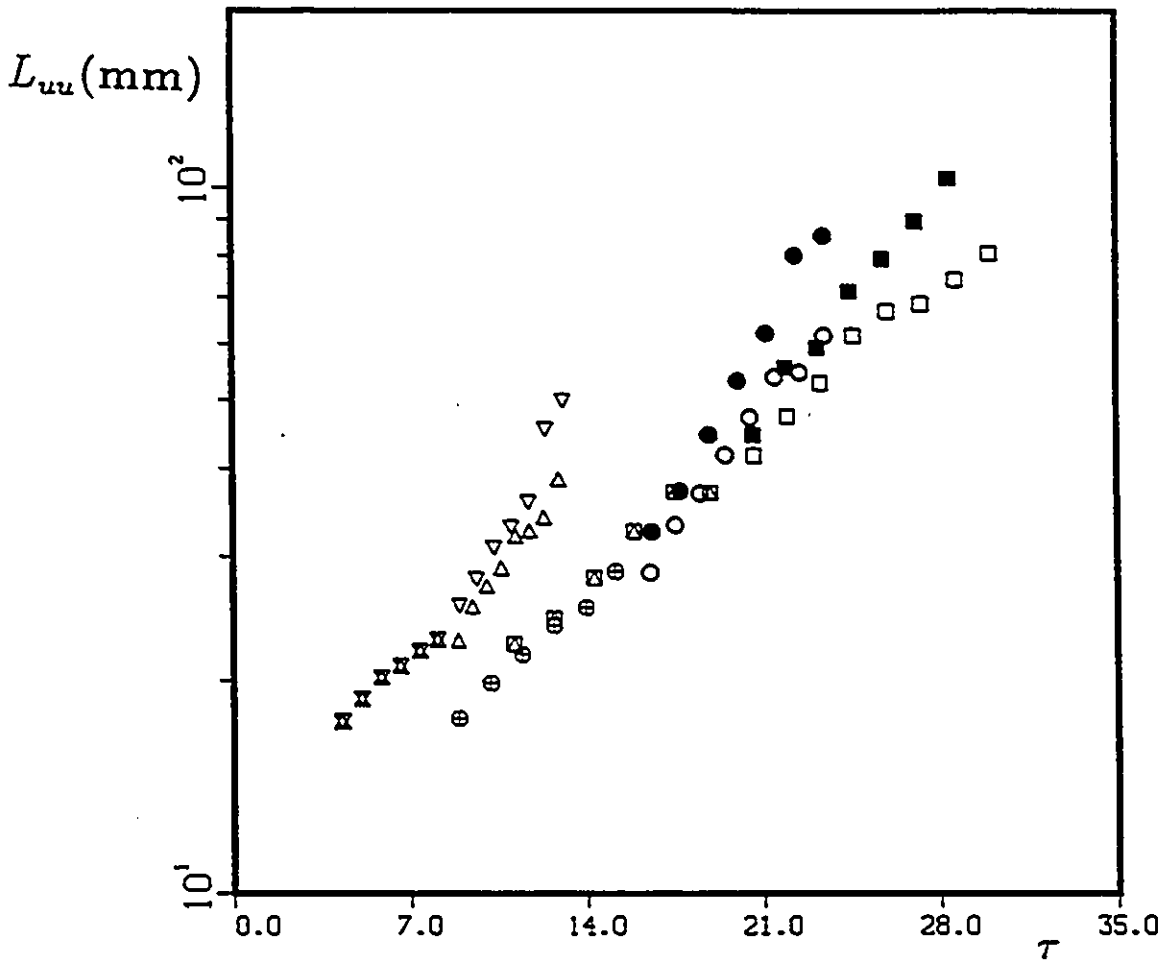

Figure 6.10: Development of L_{uu} along the wind tunnel centerline in destabilized shear flow, S <0 (Cases A, B and C). Symbols as in Table 6.1.

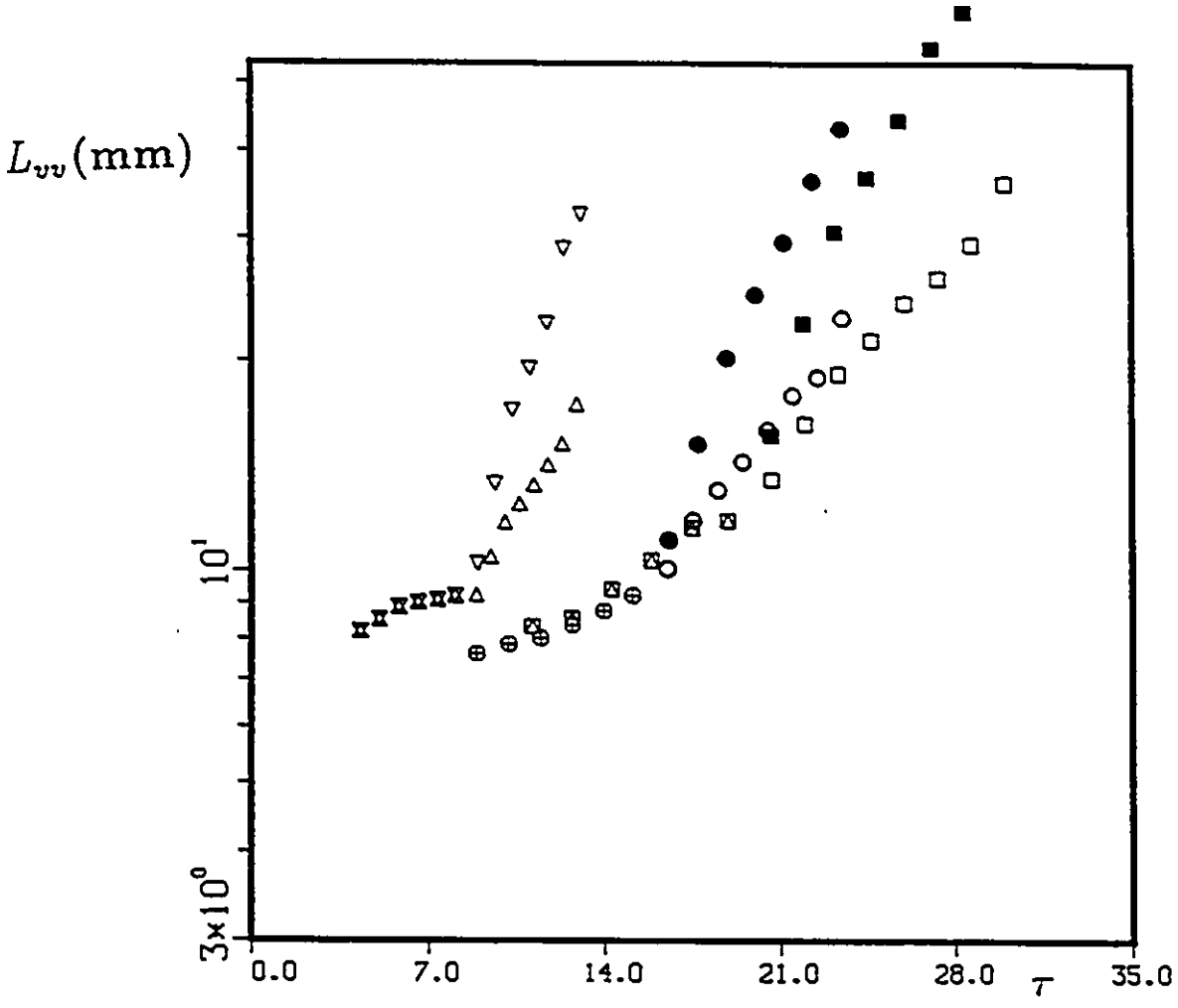

Figure 6.11: Development of L_{vv} along the wind tunnel centerline in destabilized shear flow, S <0 (Cases A, B and C). Symbols as in Table 6.1.

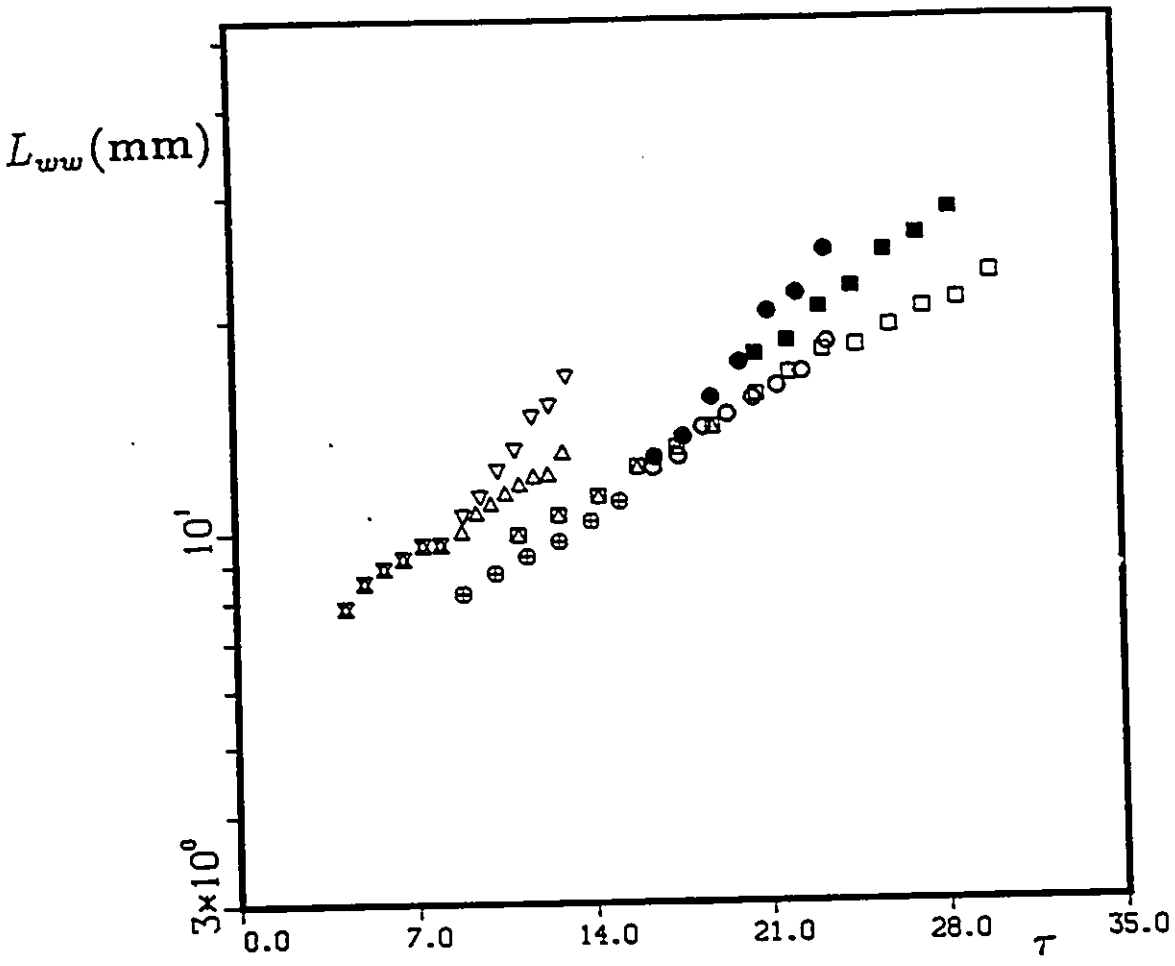

Figure 6.12: Development of L_{ww} along the wind tunnel centerline in destabilized shear flow, S <0 (Cases A, B and C). Symbols as in Table 6.1.

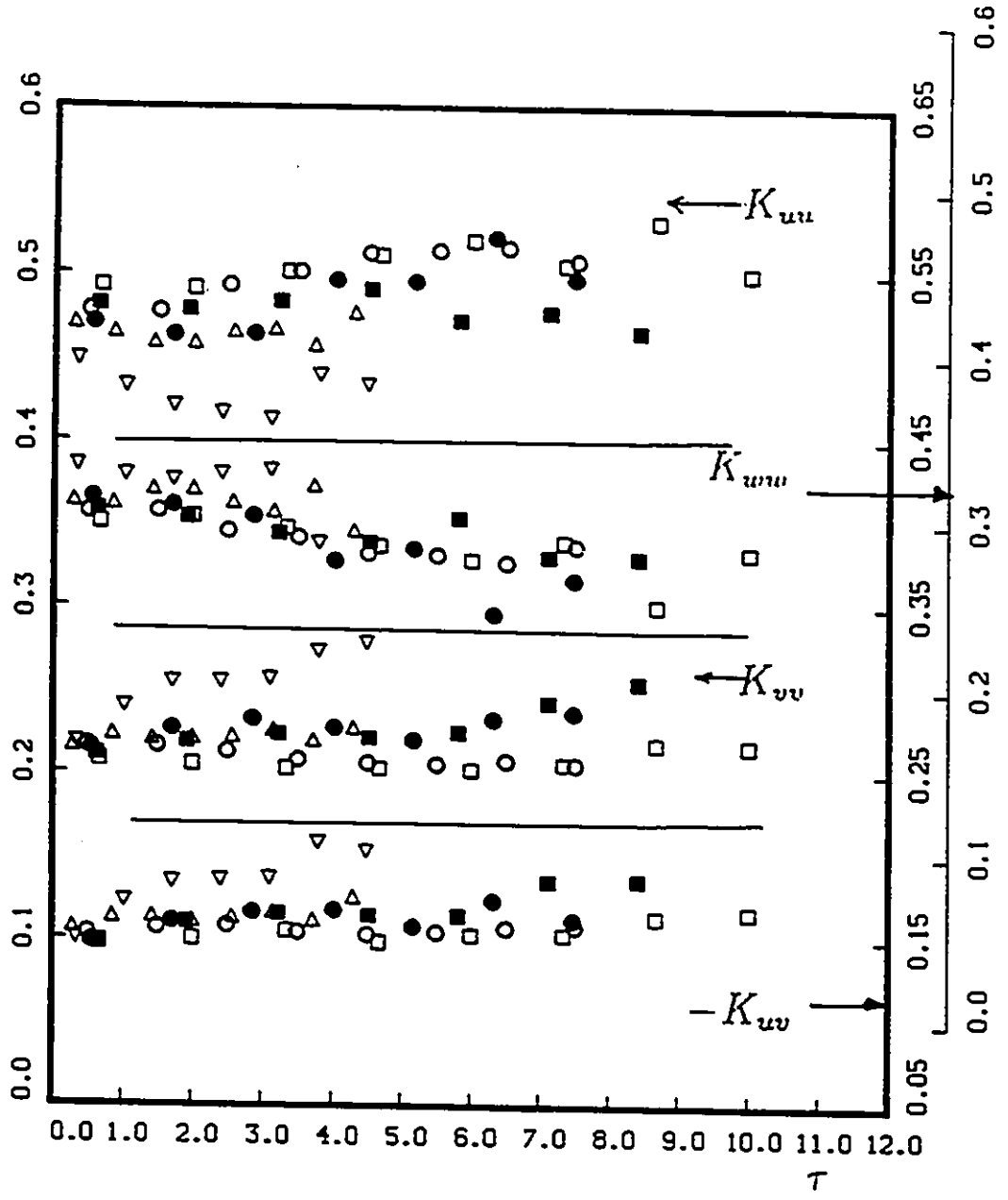

Figure 6.13: Development of the dimensionless stresses along the wind tunnel centerline in destabilized shear flow, S <0 (Cases A, B and C). Symbols as in Table 6.1.

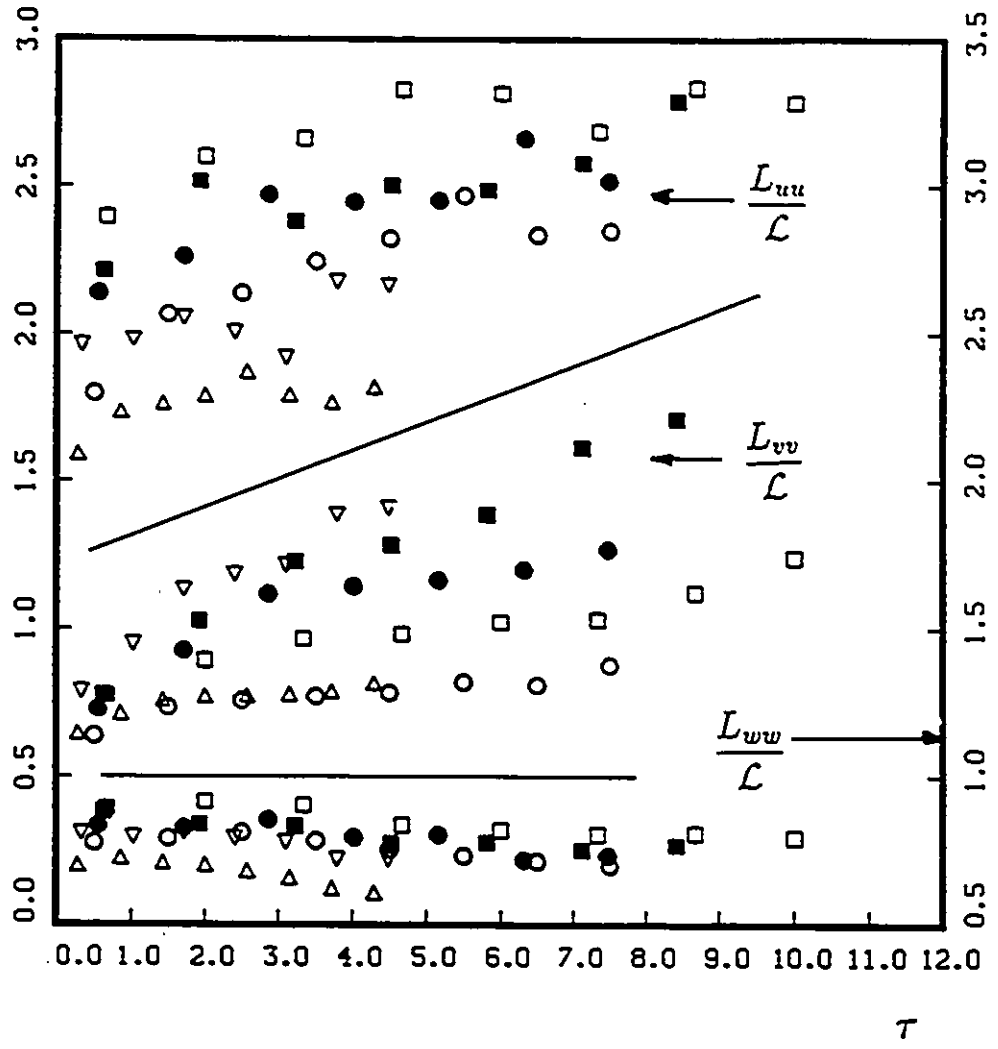

Figure 6.14: Development of the dimensionless integral lengthscales along the wind tunnel centerline in destabilized shear flow. S <0 (Cases A, B and C). Symbols as in Table 6.1.

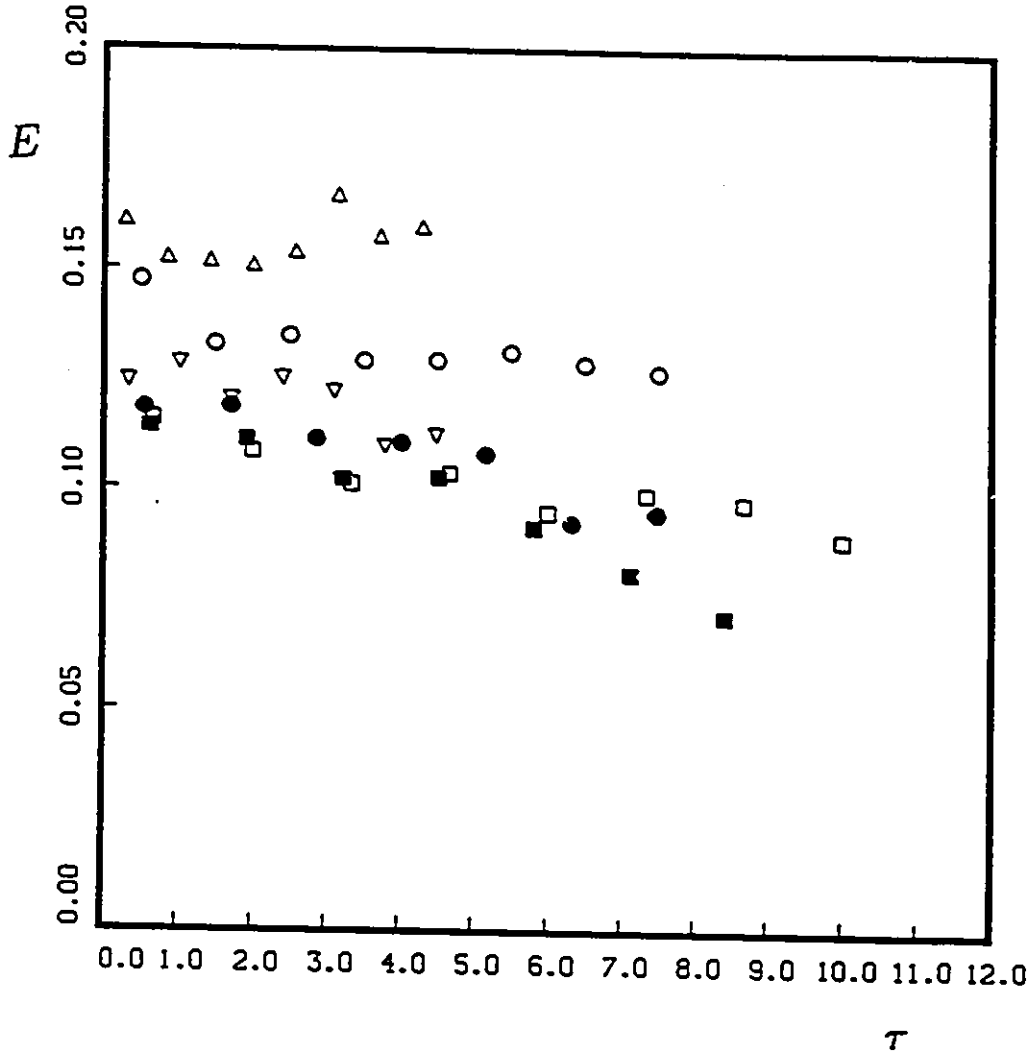

Figure 6.15: Development of E along the wind tunnel centerline in destabilized shear flow, S <0 (Cases A, B and C). Symbols as in Table 6.1.

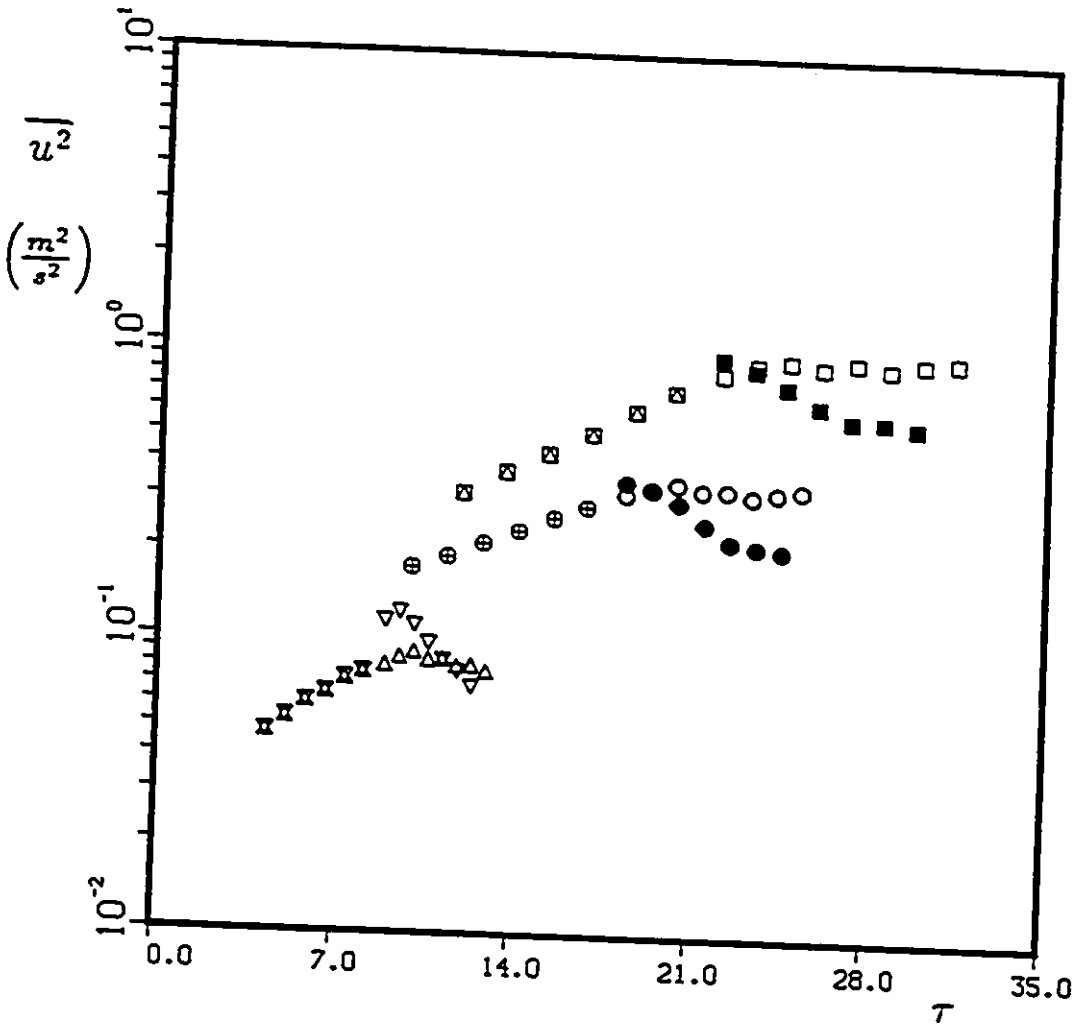

Figure 6.16: Development of $\overline{u^2}$ along the wind tunnel centerline in stabilized shear flow, $S > 0$ (Cases A, B and C). Symbols as in Table 6.1.

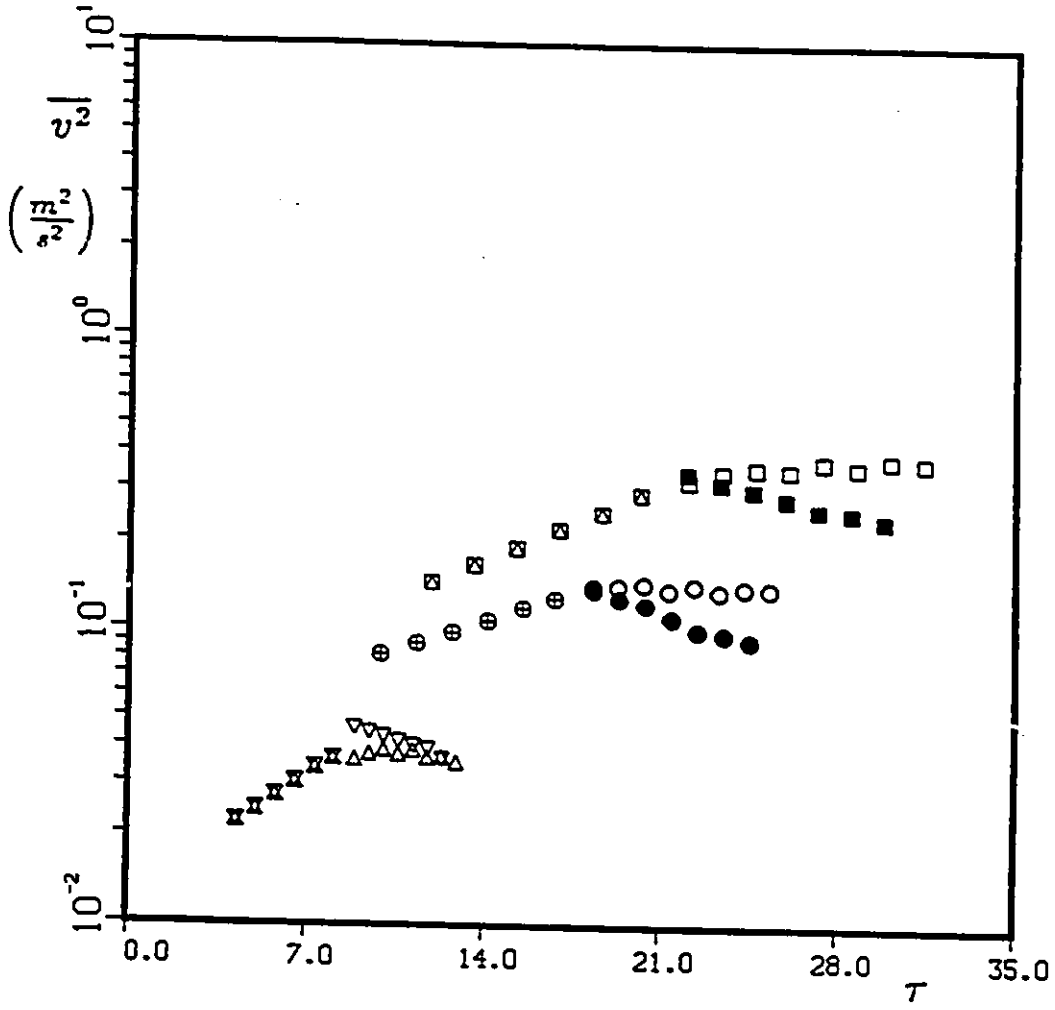

Figure 6.17: Development of $\overline{v^2}$ along the wind tunnel centerline in stabilized shear flow, $S > 0$ (Cases A, B and C). Symbols as in Table 6.1.

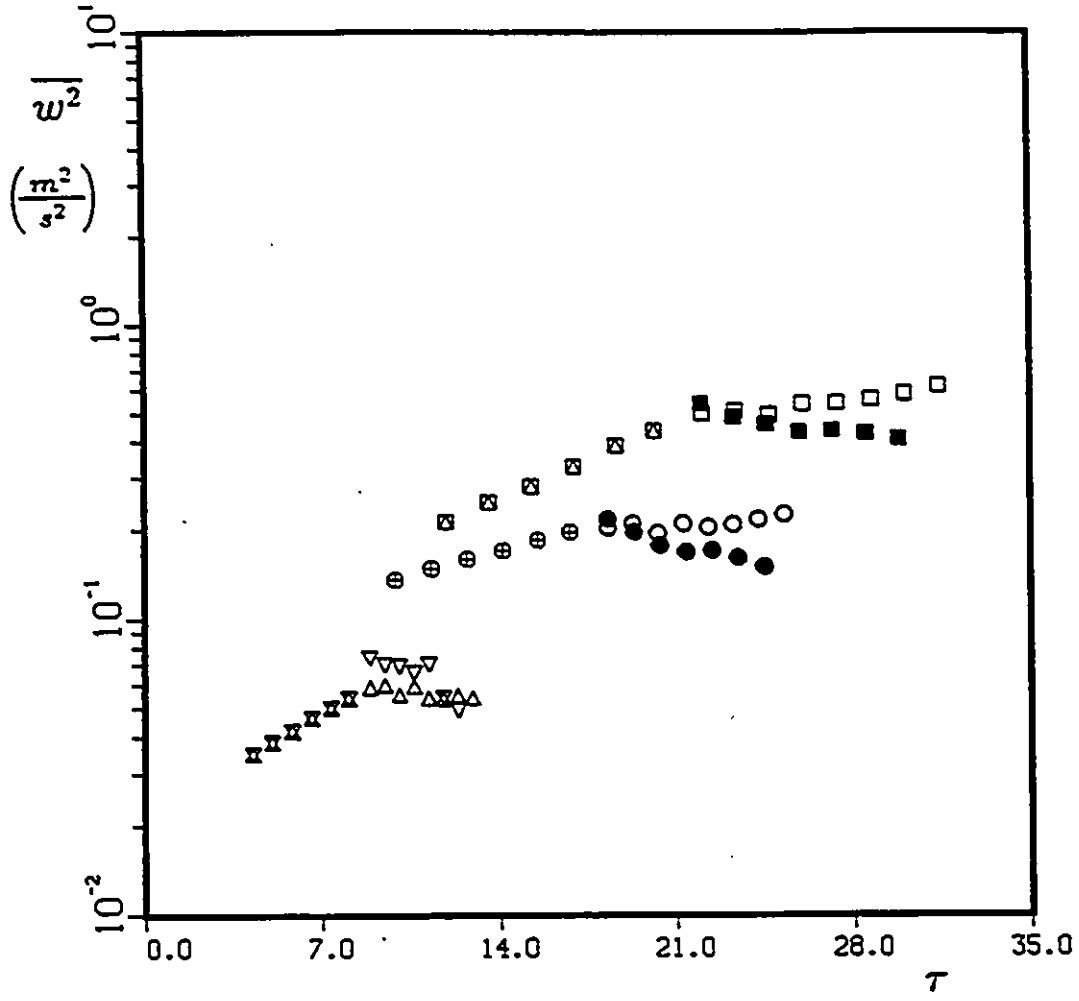

Figure 6.18: Development of $\overline{w^2}$ along the wind tunnel centerline in stabilized shear flow, $S > 0$ (Cases A, B and C). Symbols as in Table 6.1.

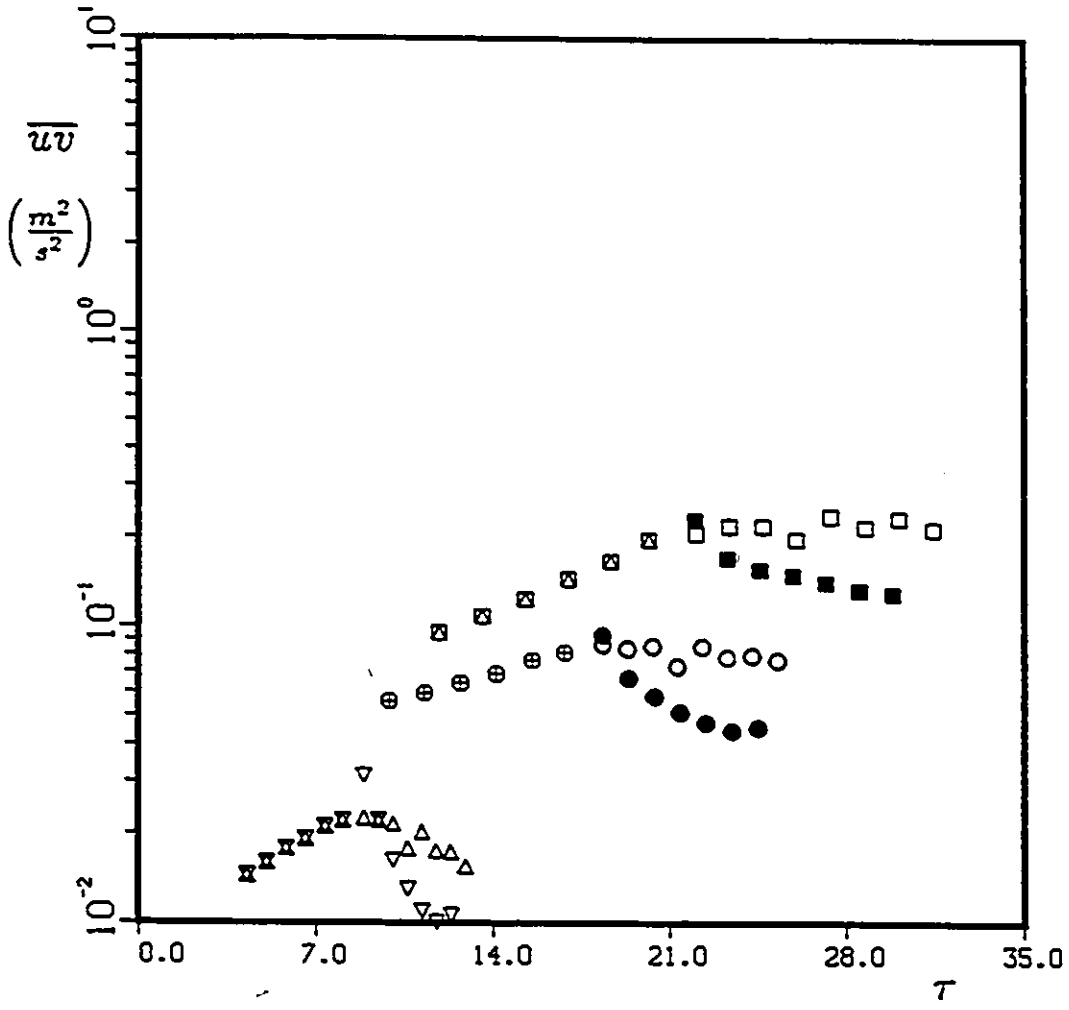

Figure 6.19: Development of $\overline{uv}$ along the wind tunnel centerline in stabilized shear flow, $S > 0$ (Cases A, B and C). Symbols as in Table 6.1.

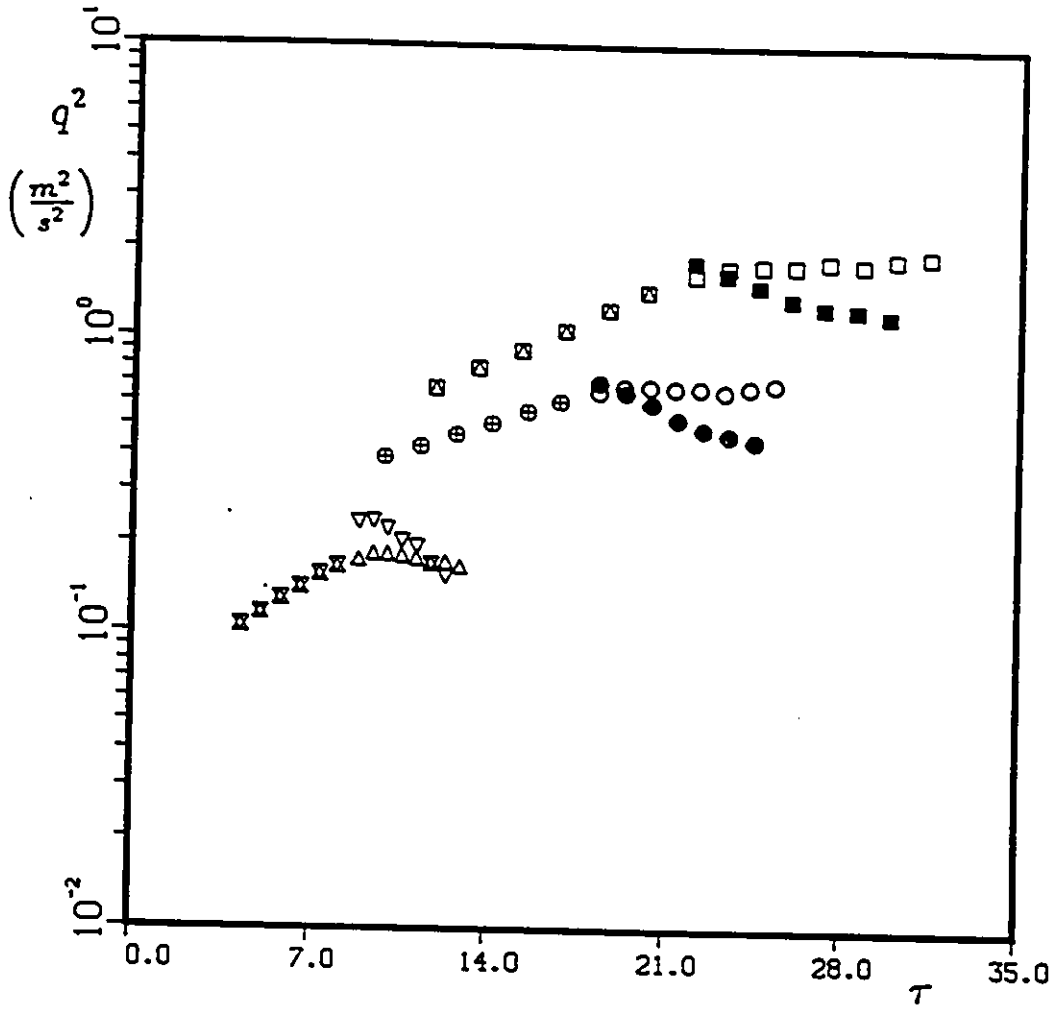

Figure 6.20: Development of q^2 along the wind tunnel centerline in stabilized shear flow, $S > 0$ (Cases A, B and C). Symbols as in Table 6.1.

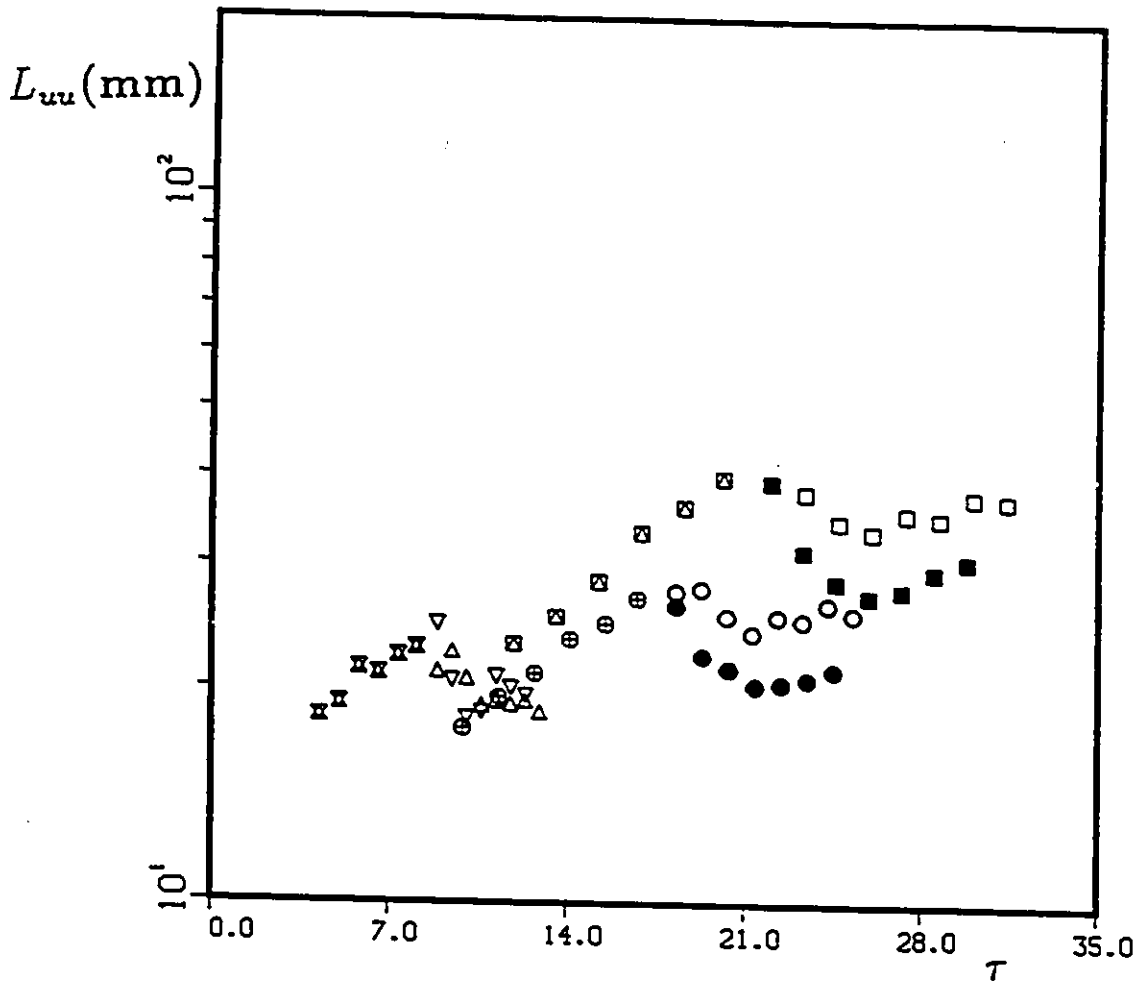

Figure 6.21: Development of L_{uu} along the wind tunnel centerline in stabilized shear flow, $S > 0$ (Cases A, B and C). Symbols as in Table 6.1.

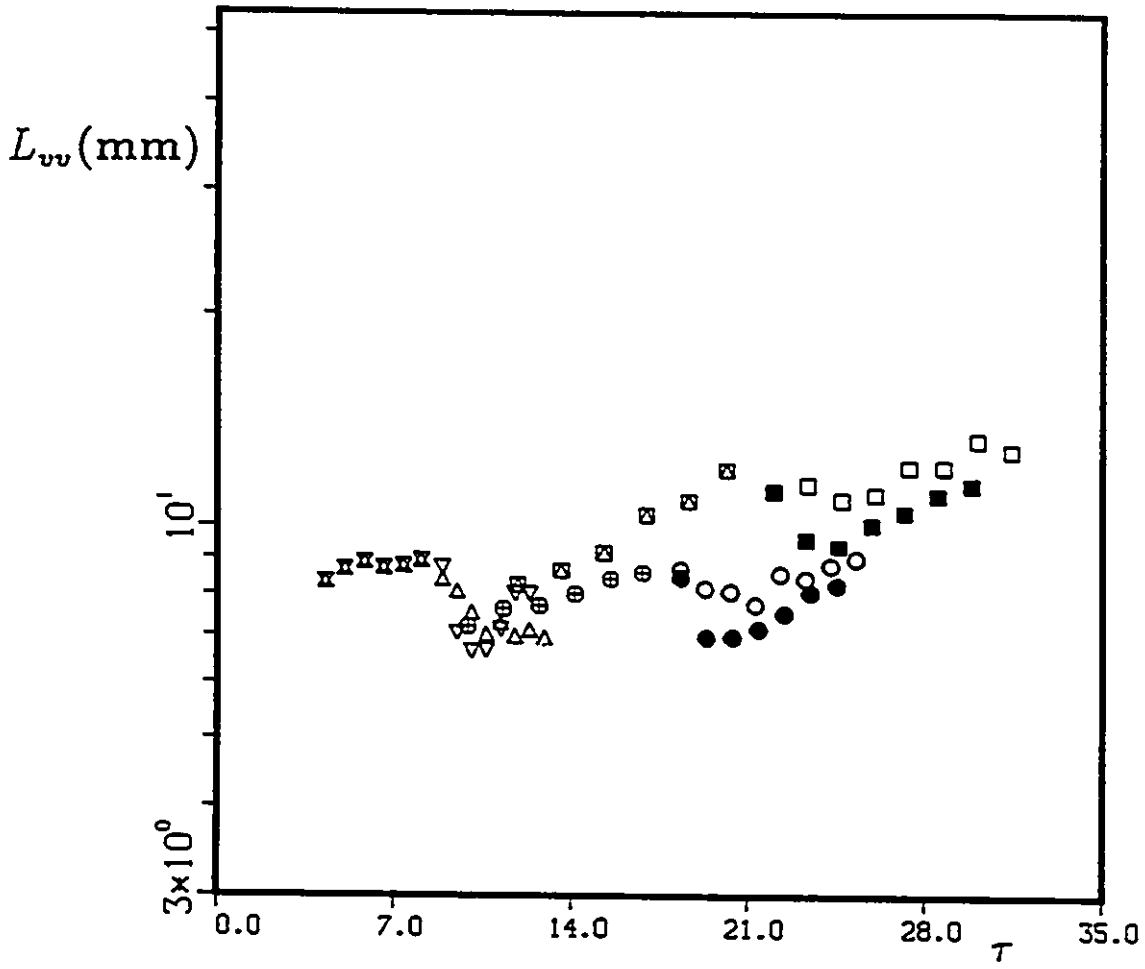

Figure 6.22: Development of L_{vv} along the wind tunnel centerline in stabilized shear flow, $S > 0$ (Cases A, B and C). Symbols as in Table 6.1.

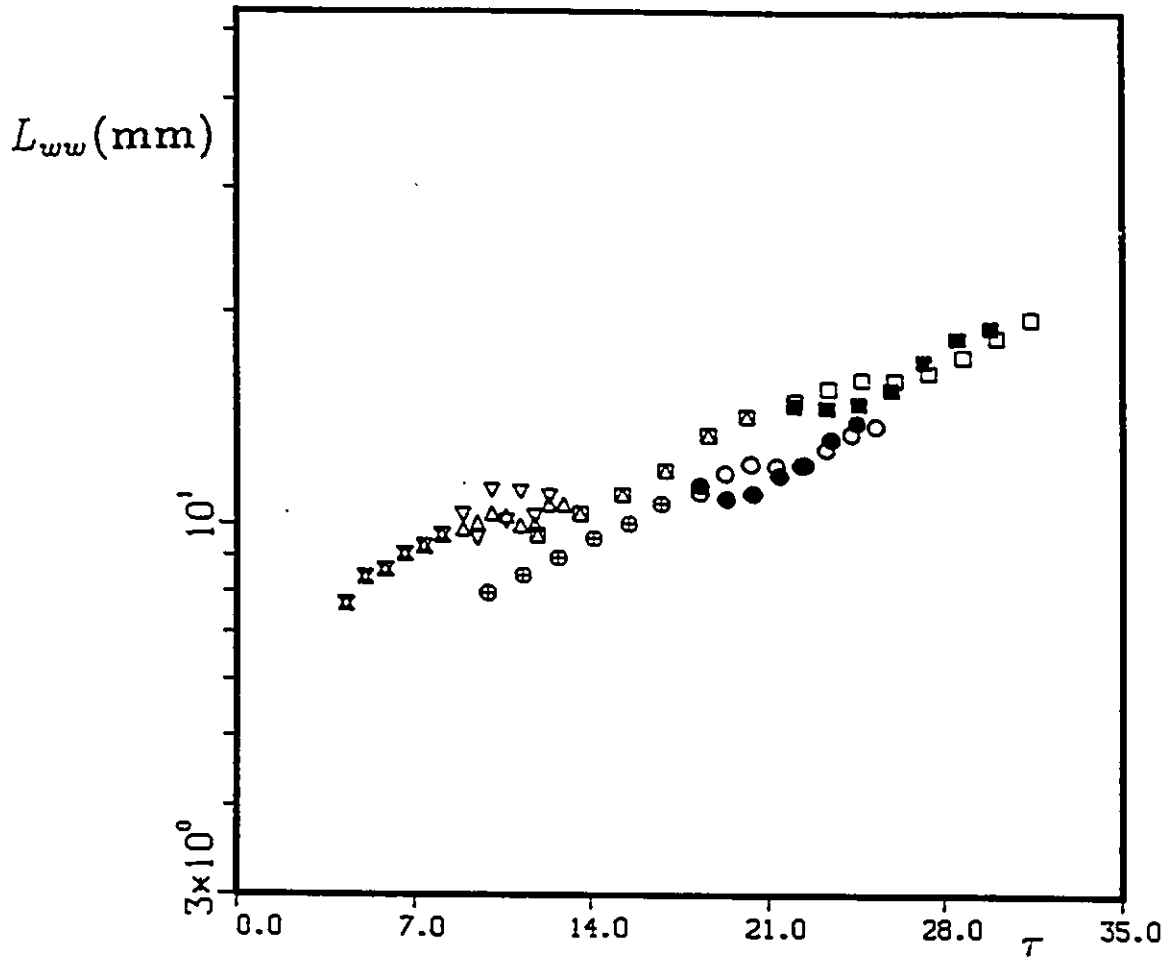

Figure 6.23: Development of L_{uw} along the wind tunnel centerline in stabilized shear flow, $S > 0$ (Cases A, B and C). Symbols as in Table 6.1.

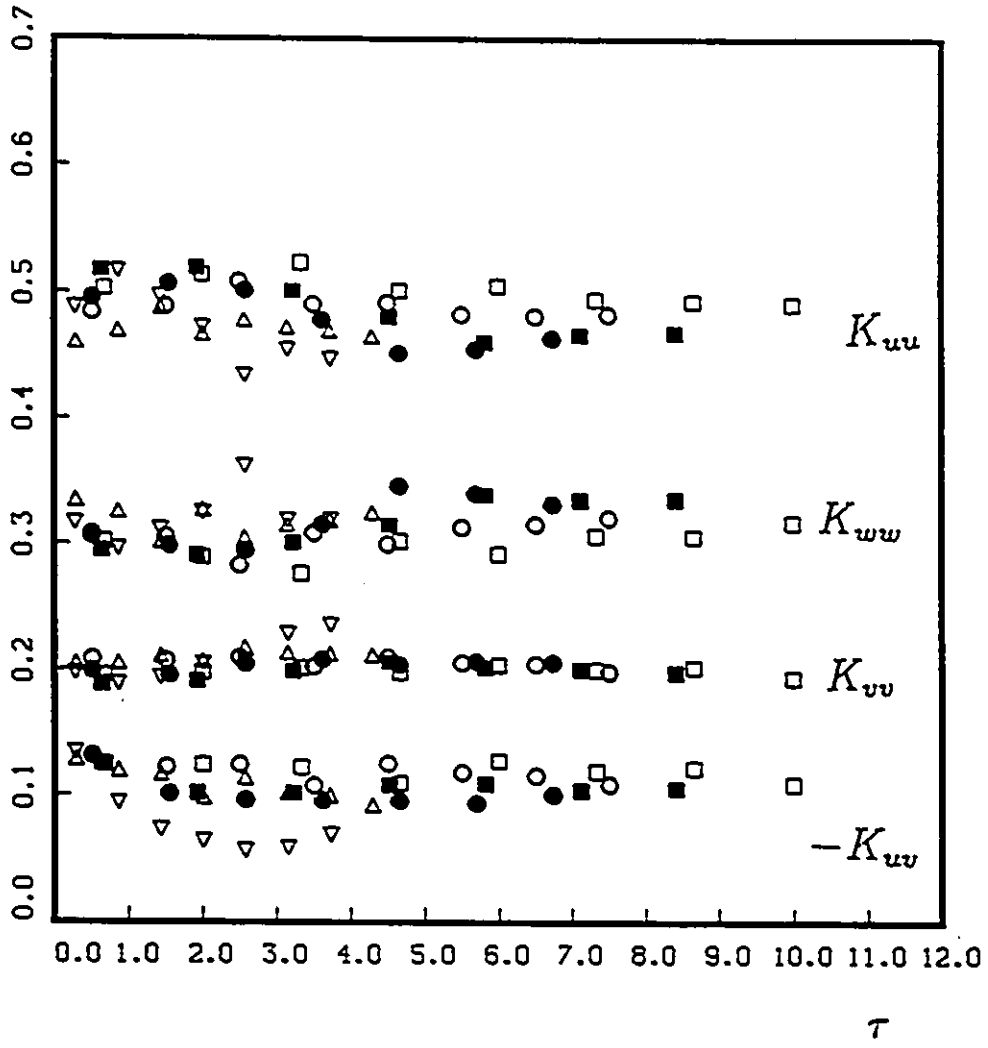

Figure 6.24: Development of the dimensionless stresses along the wind tunnel centerline in stabilized shear flow, S >0 (Cases A, B and C). Symbols as in Table 6.1.

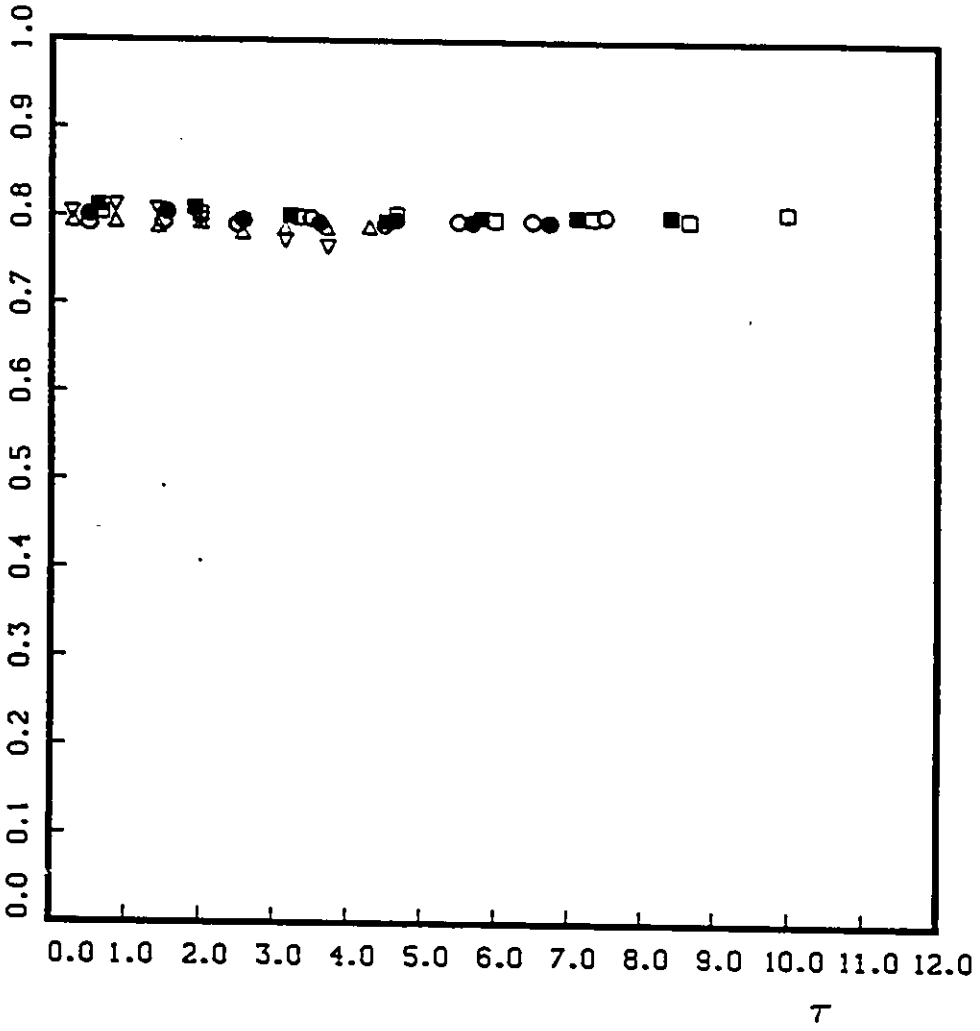

Figure 6.25: Development of $K_{uu} + K_{ww}$ along the wind tunnel centerline in stabilized shear flow, $S > 0$ (Cases A. B and C). Symbols as in Table 6.1.

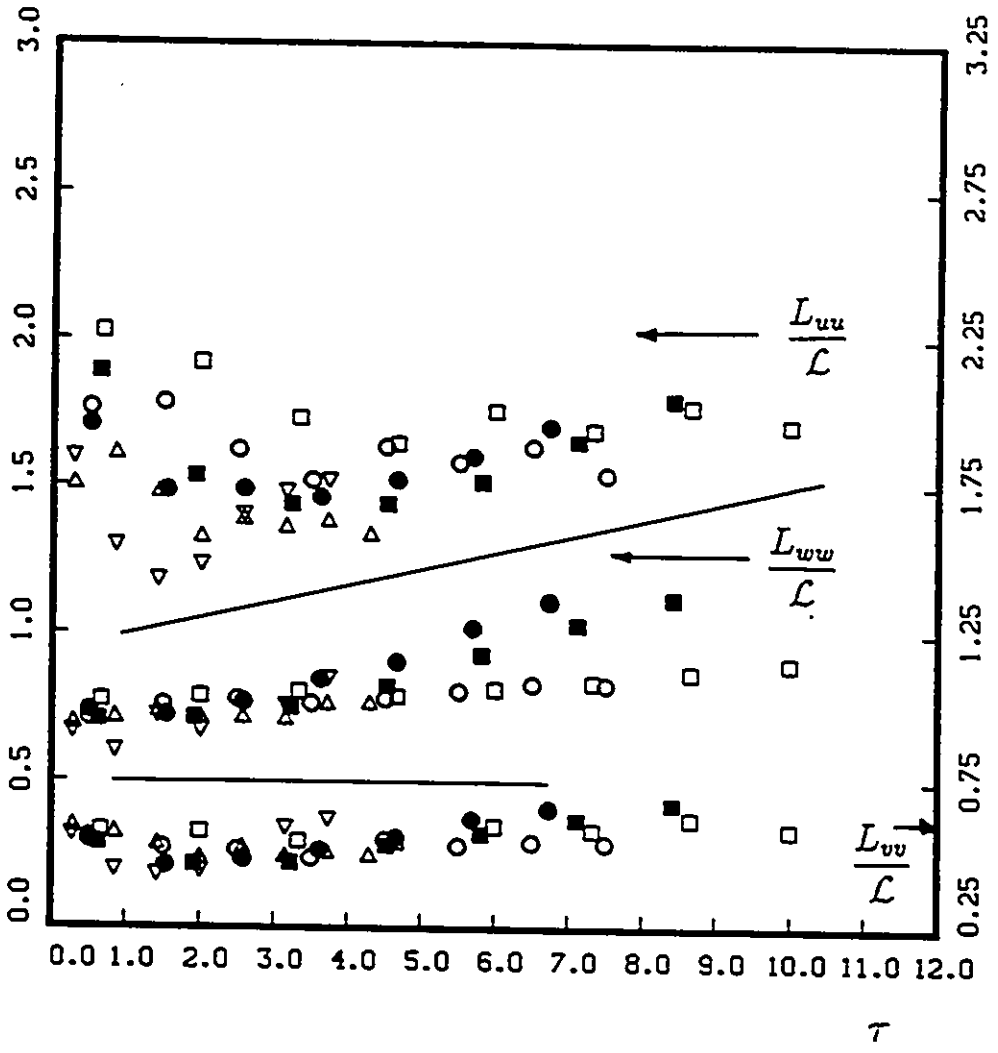

Figure 6.26: Development of the dimensionless integral lengthscales along the wind tunnel centerline in stabilized shear flow, $S > 0$ (Cases A, B and C). Symbols as in Table 6.1.

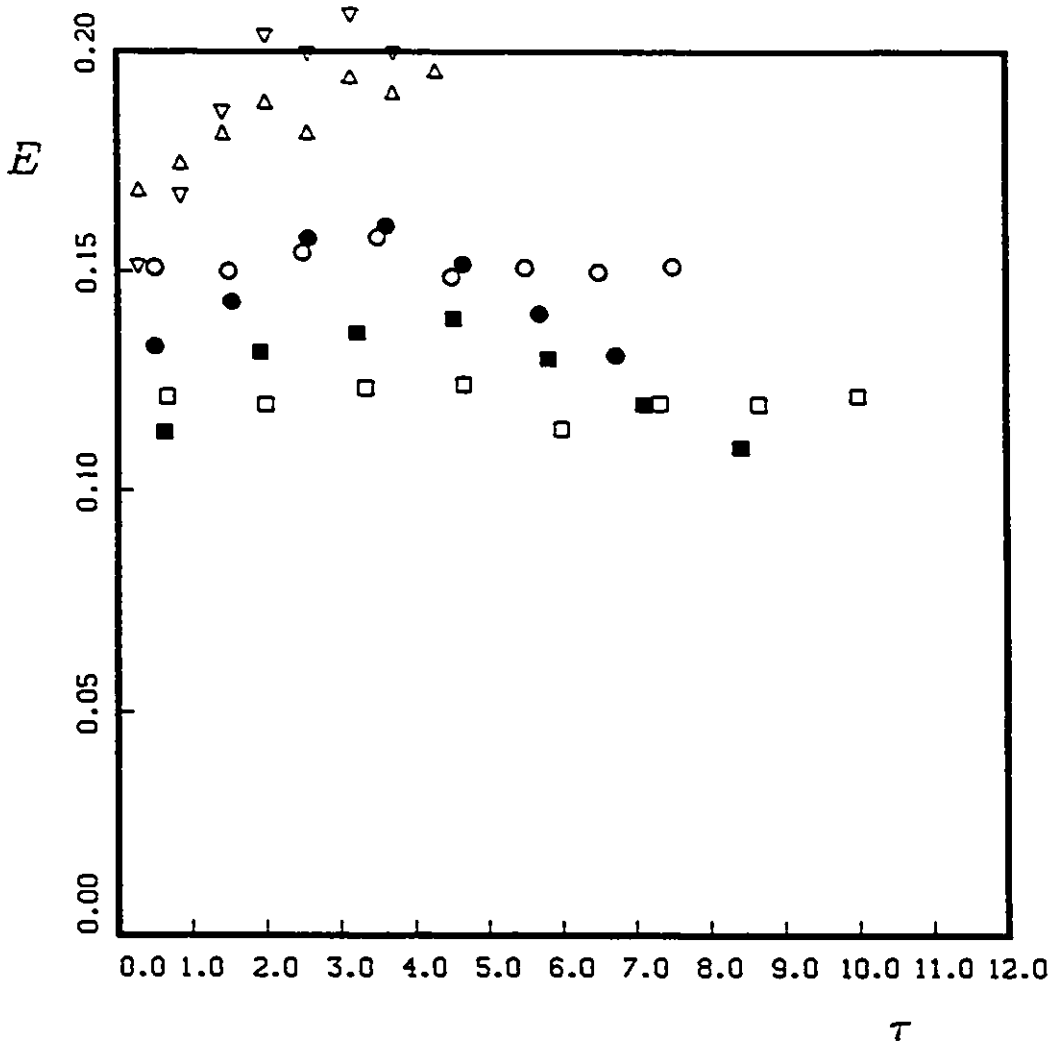

Figure 6.27: Development of E along the wind tunnel centerline in stabilized shear flow, $S > 0$ (Cases A, B and C). Symbols as in Table 6.1.

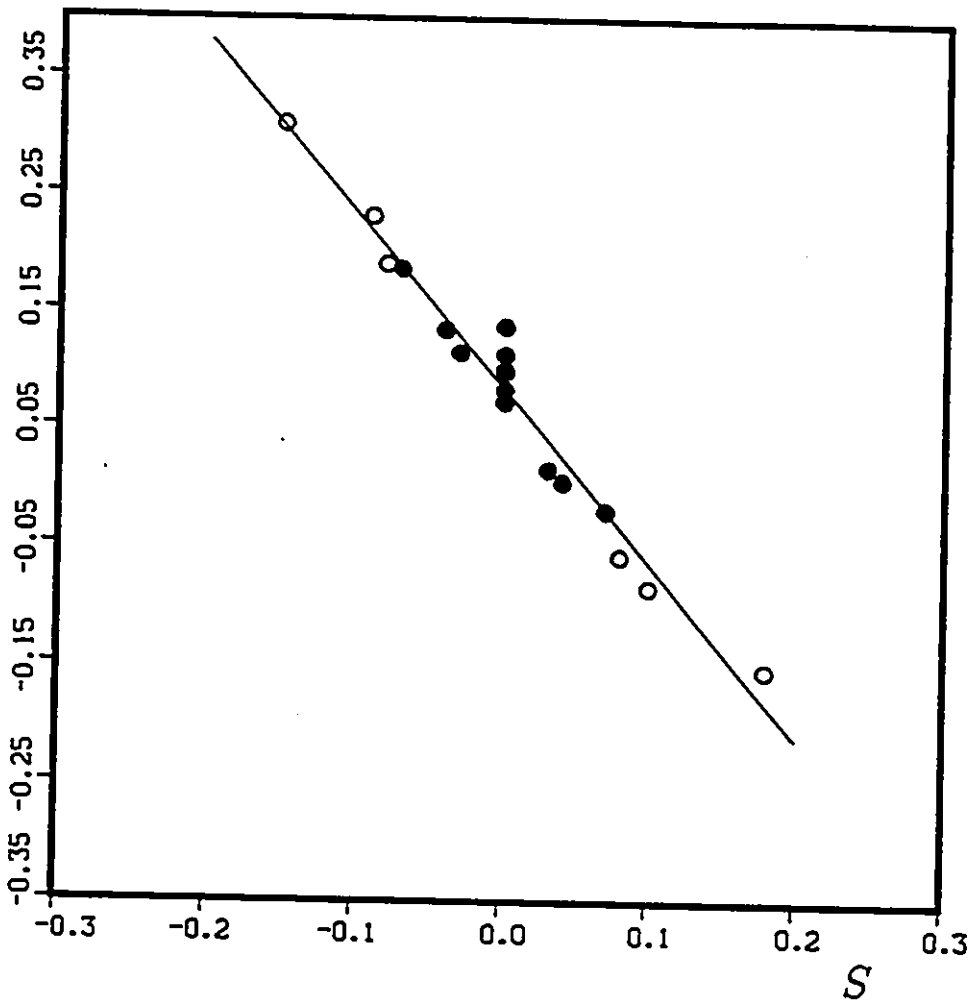

Figure 6.28: The dependence of the exponent of growth of q^2, κ_q, on S, data from cases A, B and C. The solid symbols represent data from the mildly curved section, the open symbols represent data from the strongly curved section and the solid line represents a least squares fit to all the data, equation 6.19.

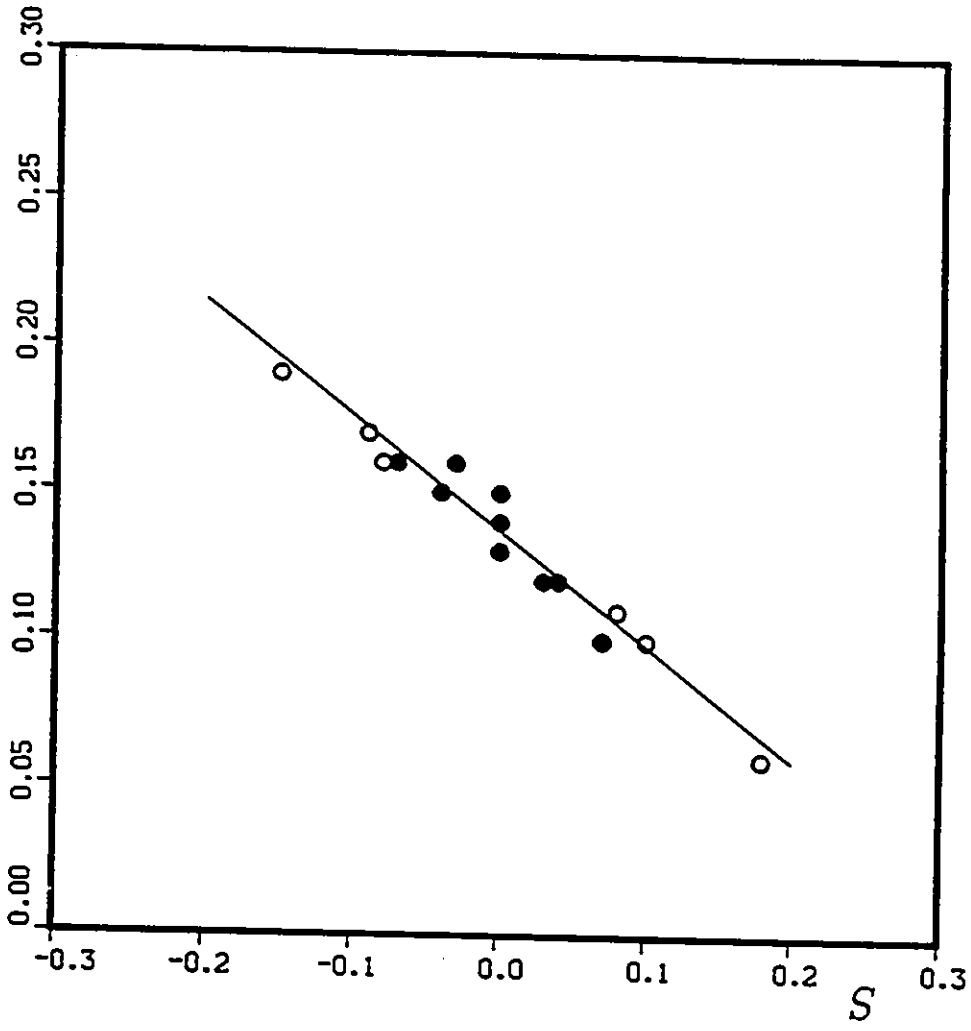

Figure 6.29: The dependence of K_{uv} on S, data from cases A, B and C. The solid symbols represent data from the mildly curved section, the open symbols represent data from the strongly curved section and the solid line represents a least squares fit to all the data, equation 6.20.

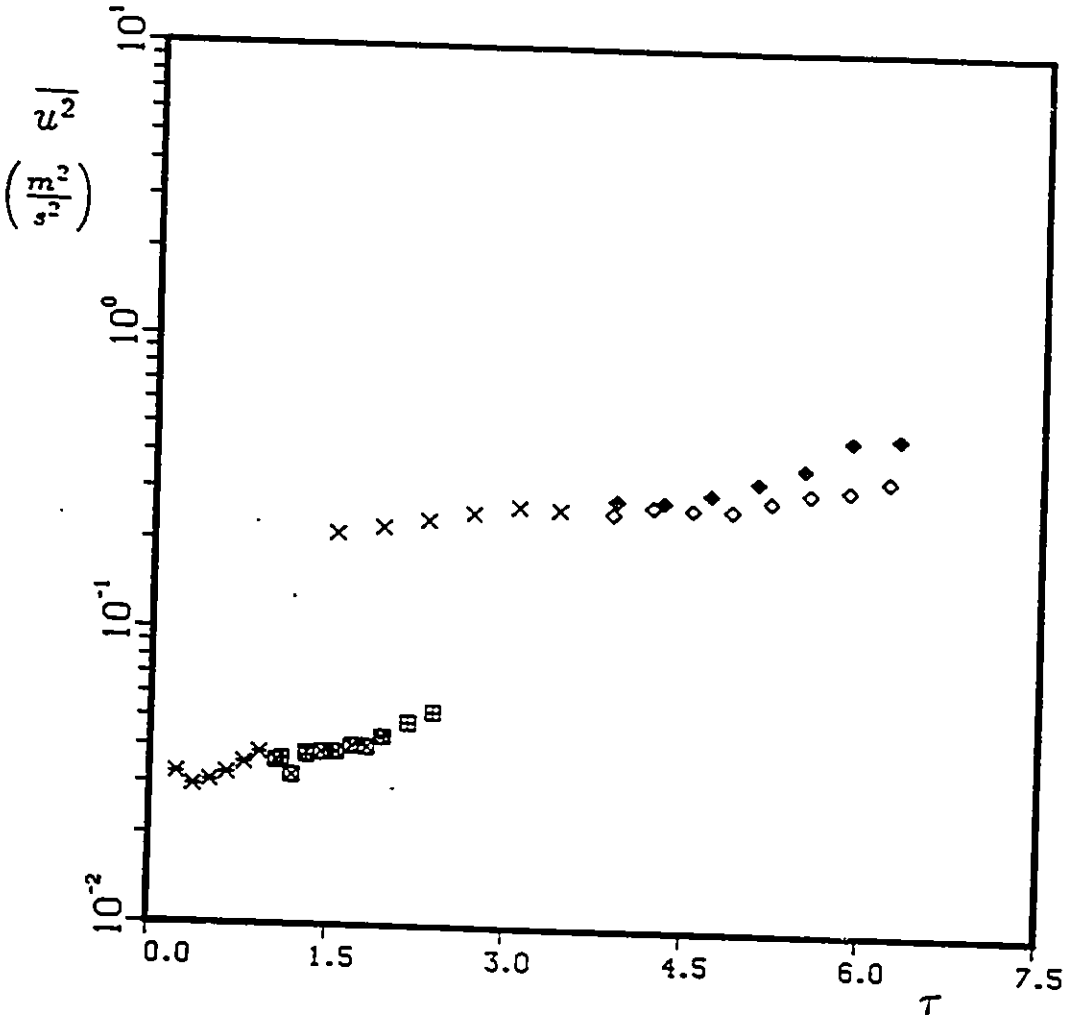

Figure 6.30: Development of $\overline{u^2}$ along the wind tunnel centerline in destabilized shear flow, S <0 (Cases D and E). Symbols as in Table 6.1.

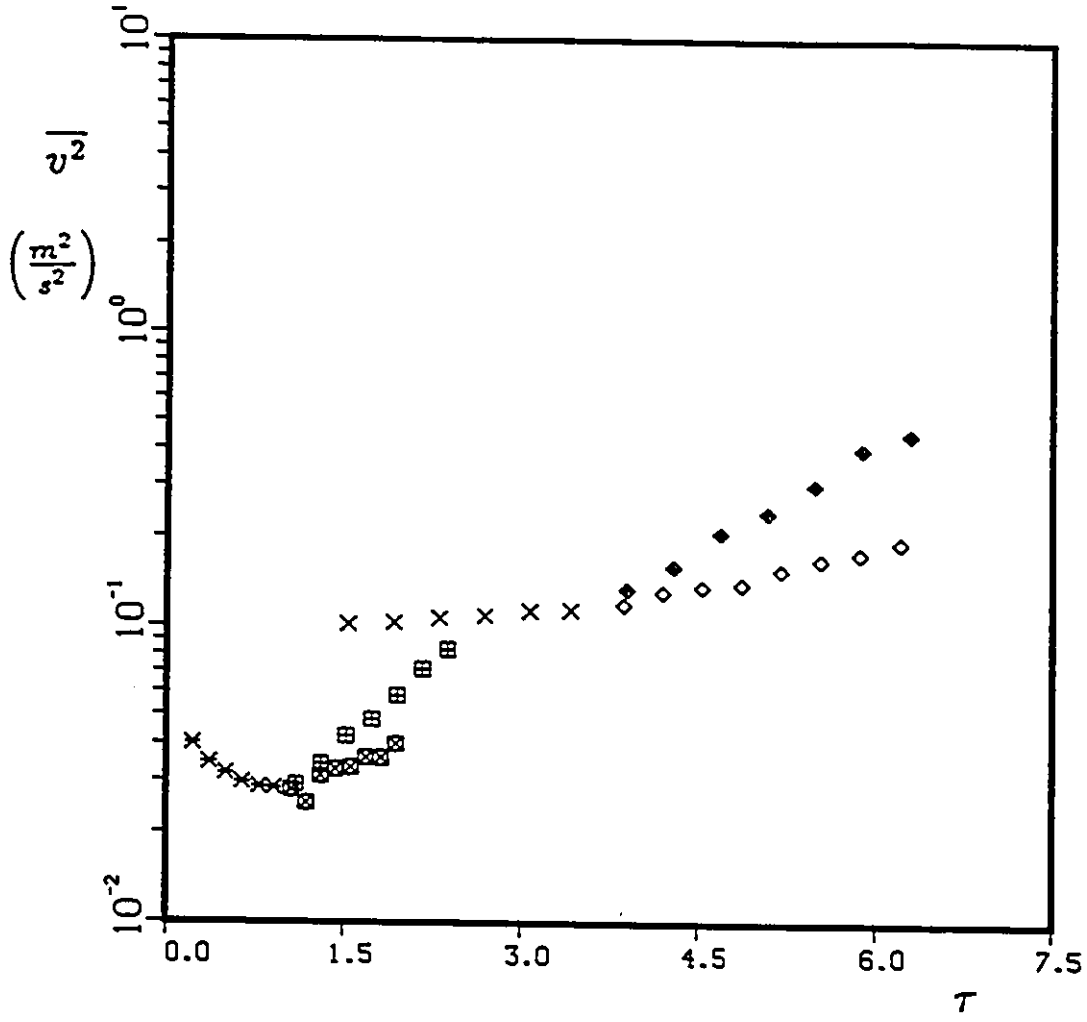

Figure 6.31: Development of $\overline{v^2}$ along the wind tunnel centerline in destabilized shear flow, S <0 (Cases D and E). Symbols as in Table 6.1.

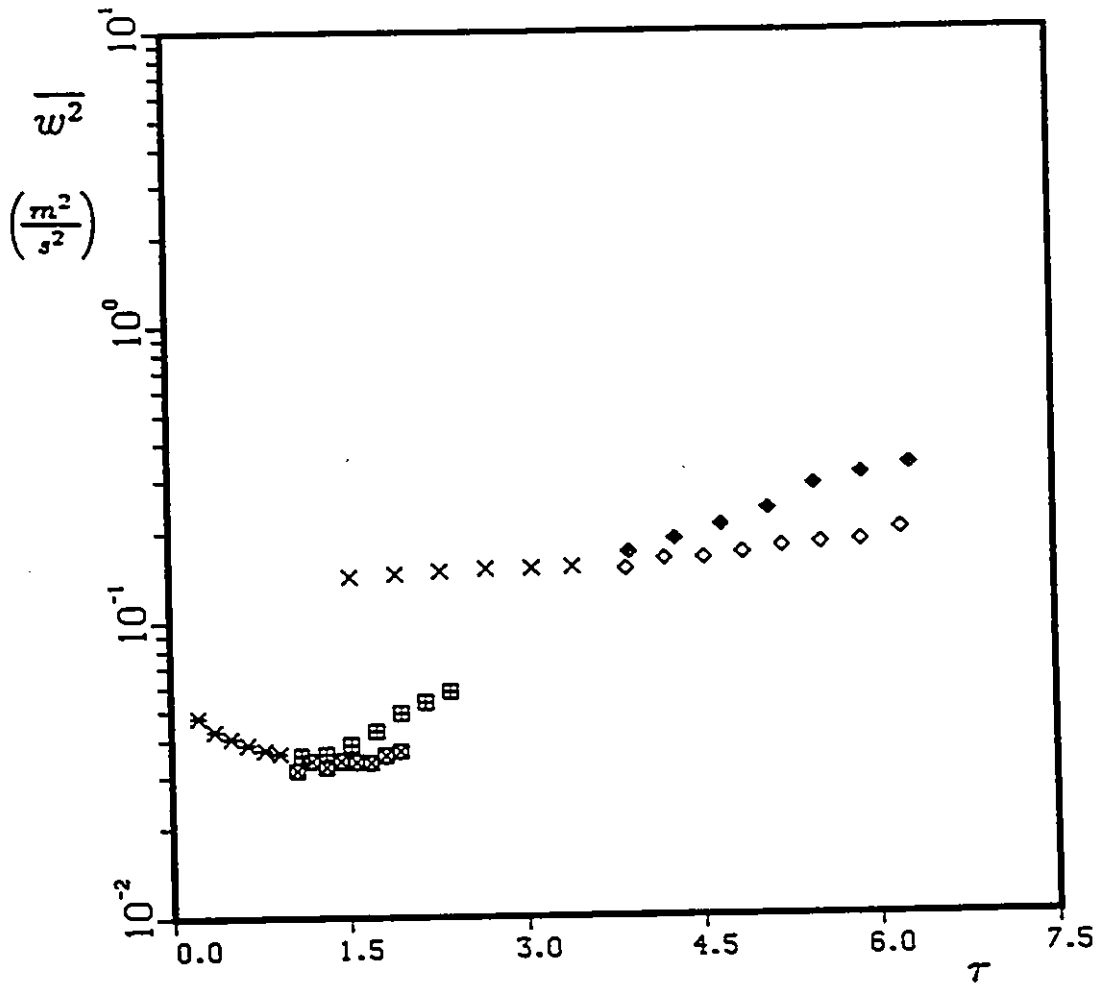

Figure 6.32: Development of $\overline{w^2}$ along the wind tunnel centerline in destabilized shear flow, S <0 (Cases D and E). Symbols as in Table 6.1.

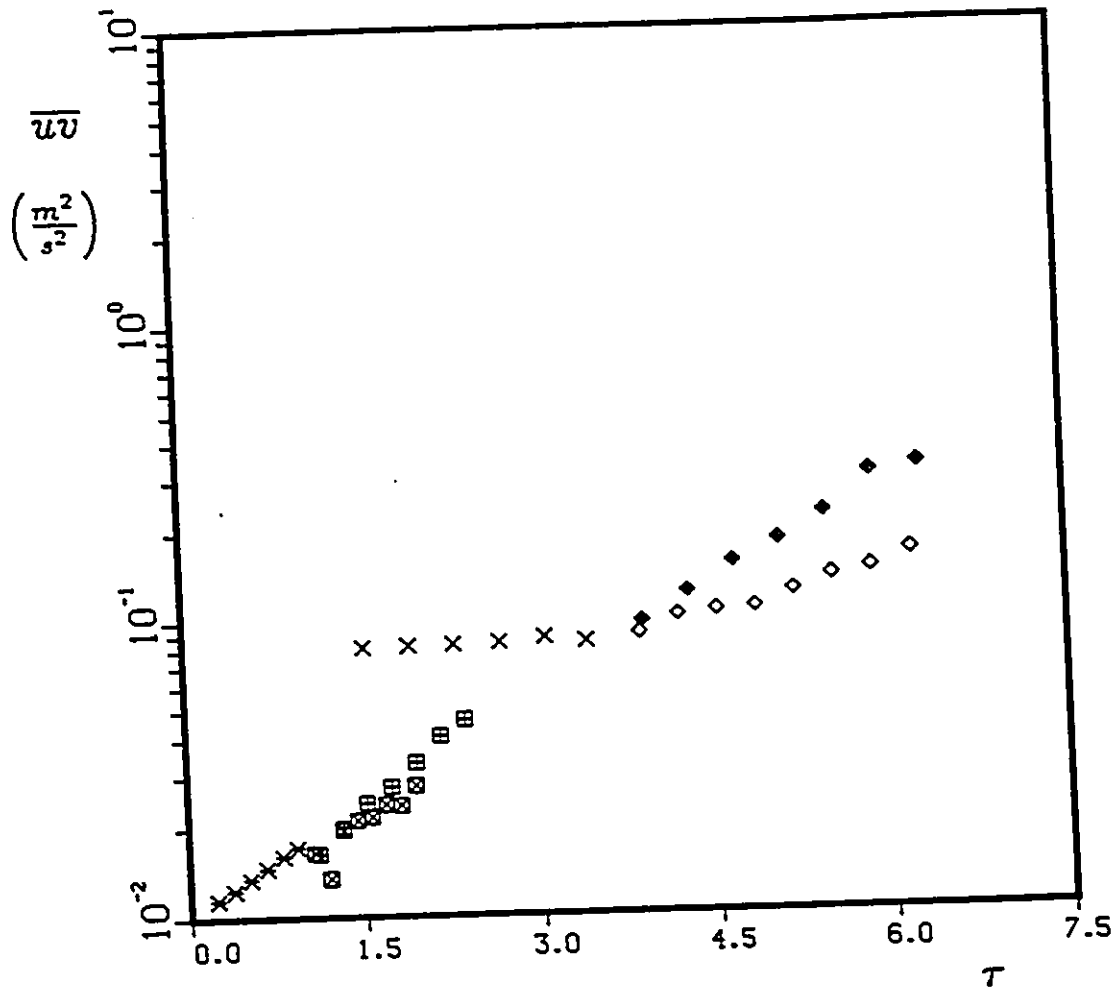

Figure 6.33: Development of $\overline{uv}$ along the wind tunnel centerline in destabilized shear flow, S <0 (Cases D and E). Symbols as in Table 6.1.

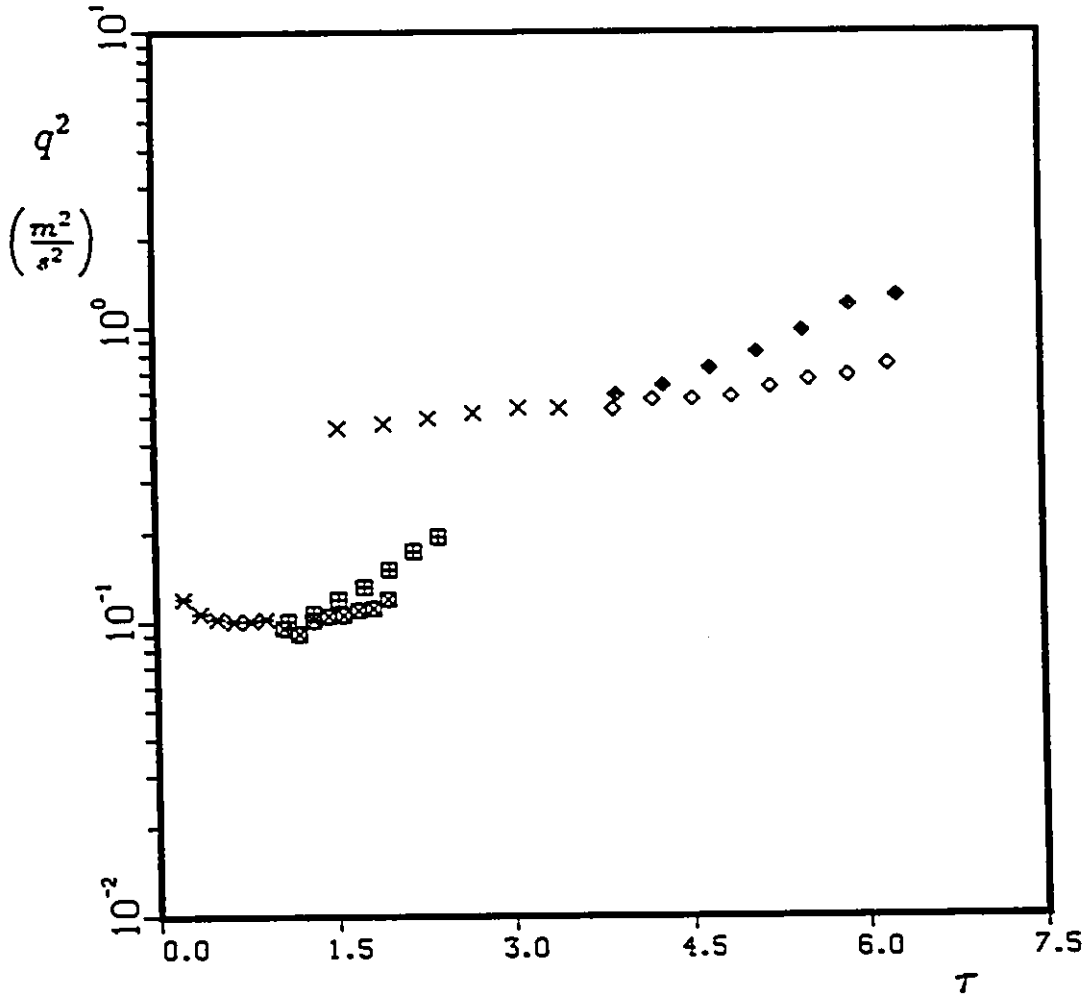

Figure 6.34: Development of q^2 along the wind tunnel centerline in destabilized shear flow, S <0 (Cases D and E). Symbols as in Table 6.1.

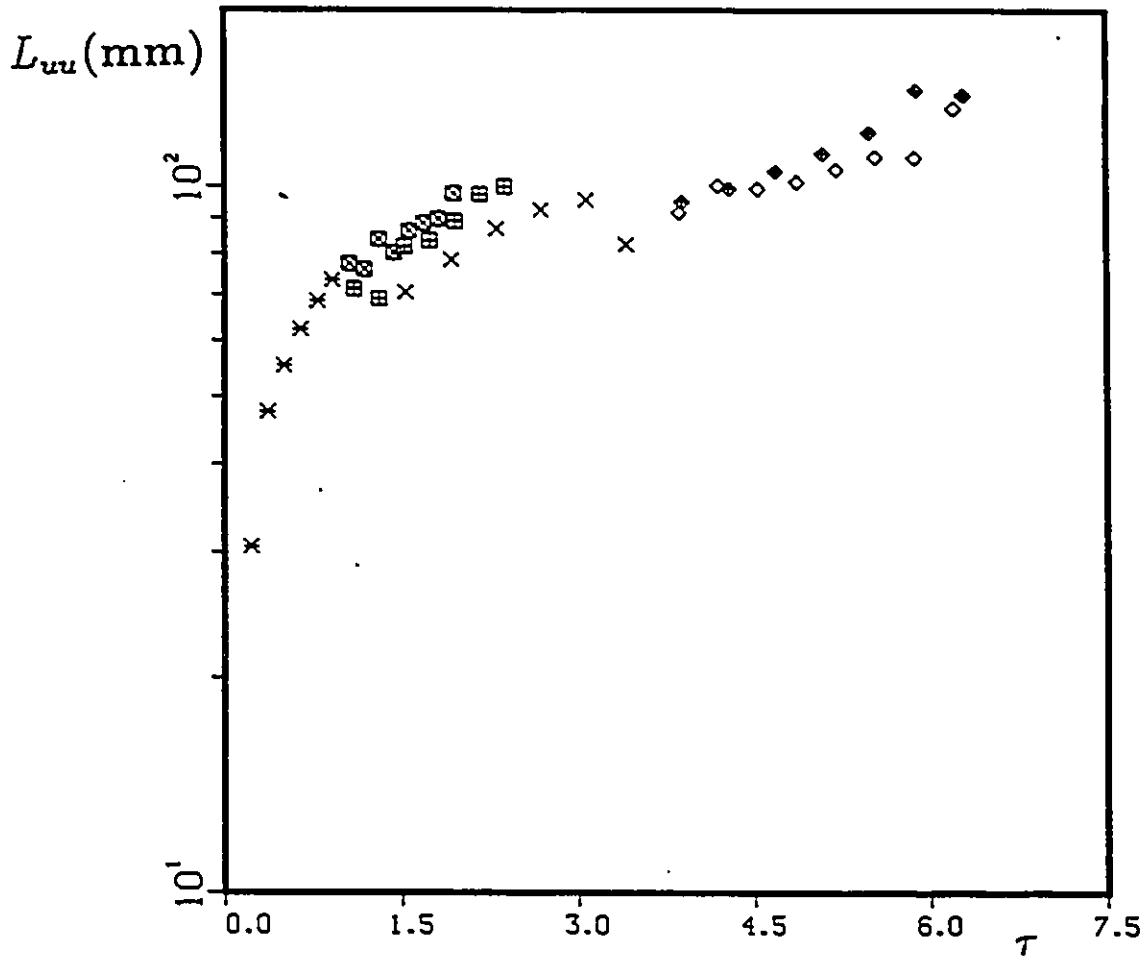

Figure 6.35: Development of L_{uu} along the wind tunnel centerline in destabilized shear flow, S <0 (Cases D and E). Symbols as in Table 6.1.

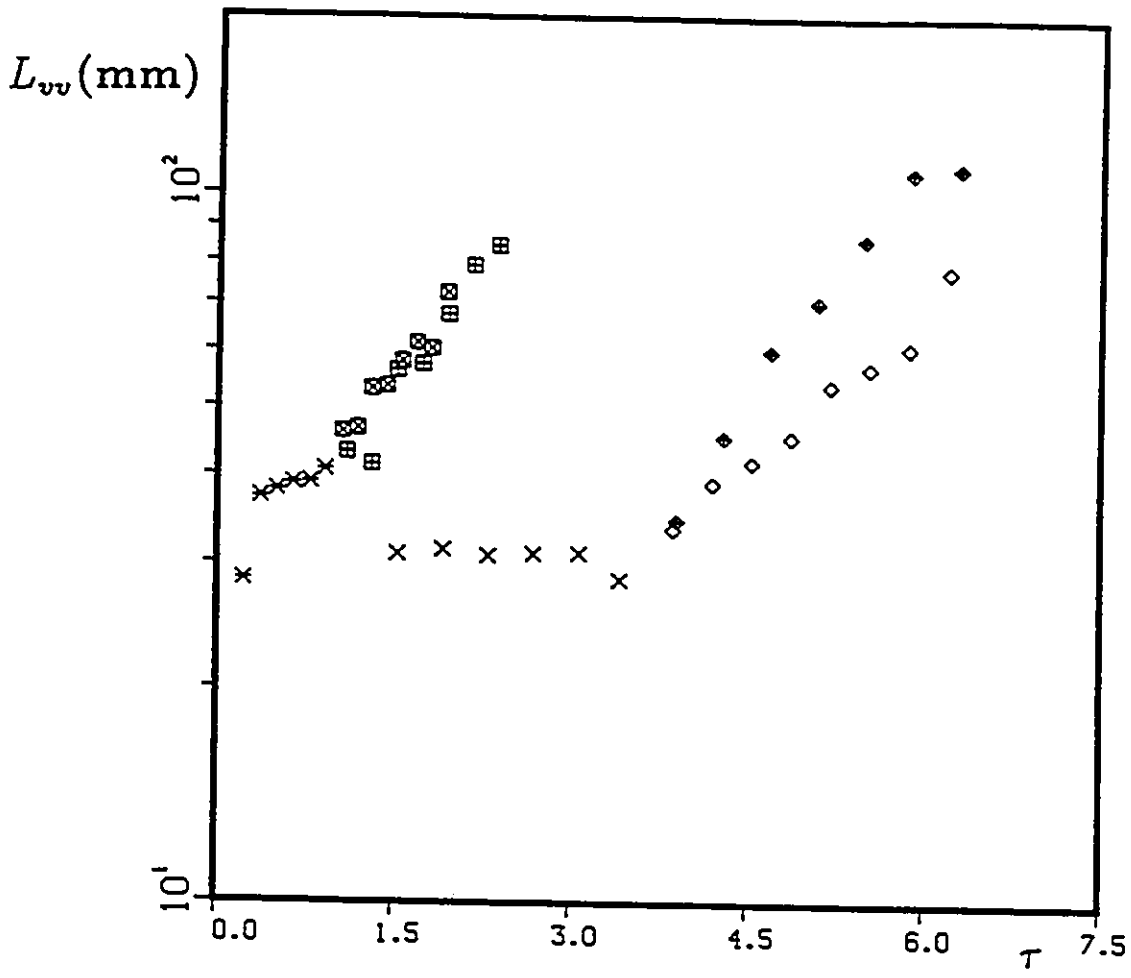

Figure 6.36: Development of L_{vv} along the wind tunnel centerline in destabilized shear flow, S <0 (Cases D and E). Symbols as in Table 6.1.

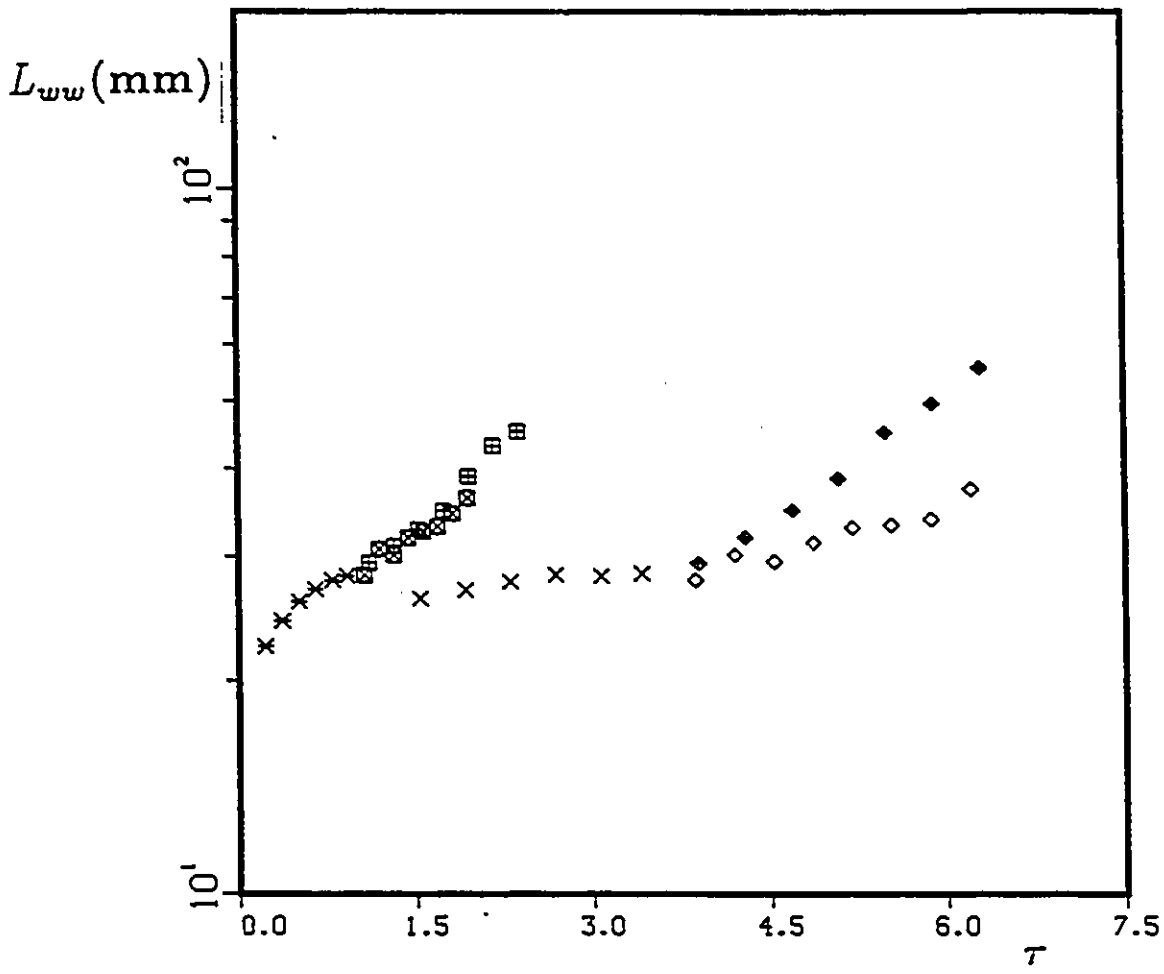

Figure 6.37: Development of L_{ww} along the wind tunnel centerline in destabilized shear flow, S <0 (Cases D and E). Symbols as in Table 6.1.

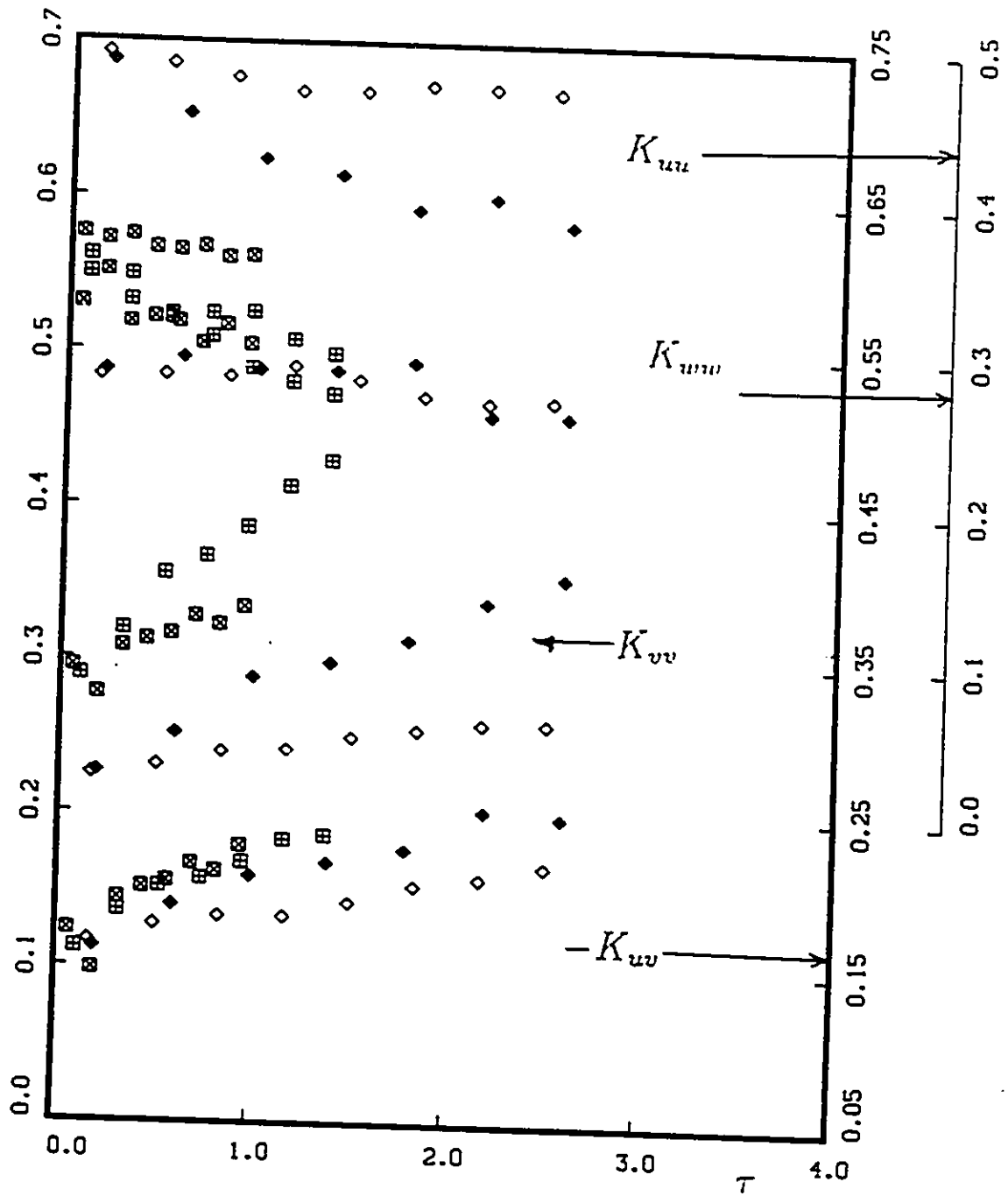

Figure 6.38: Development of the dimensionless stresses along the wind tunnel centerline in destabilized shear flow, S <0 (Cases D and E). Symbols as in Table 6.1.

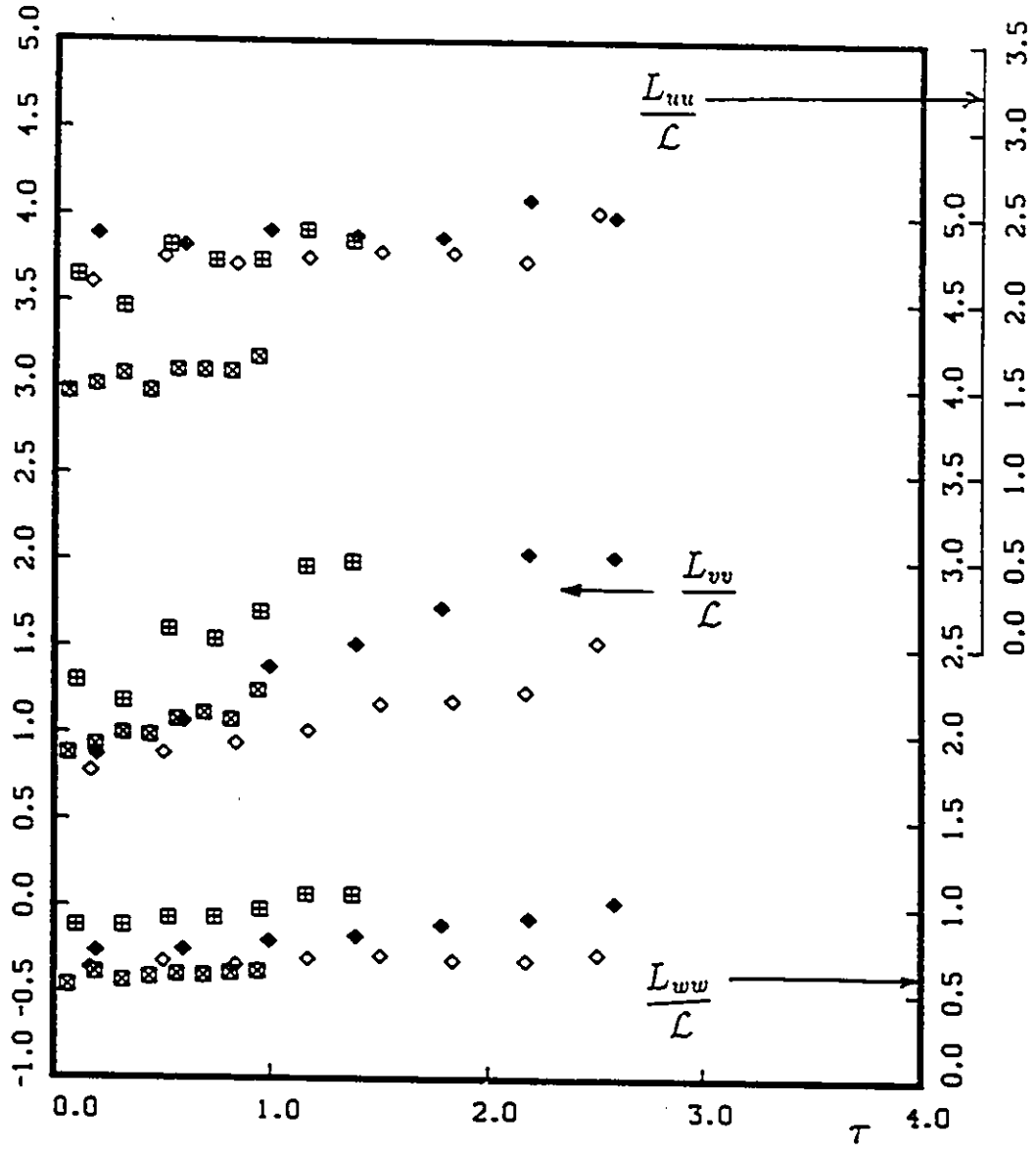

Figure 6.39: Development of the dimensionless integral lengthscales along the wind tunnel centerline in destabilized shear flow, S <0 (Cases D and E). Symbols as in Table 6.1.

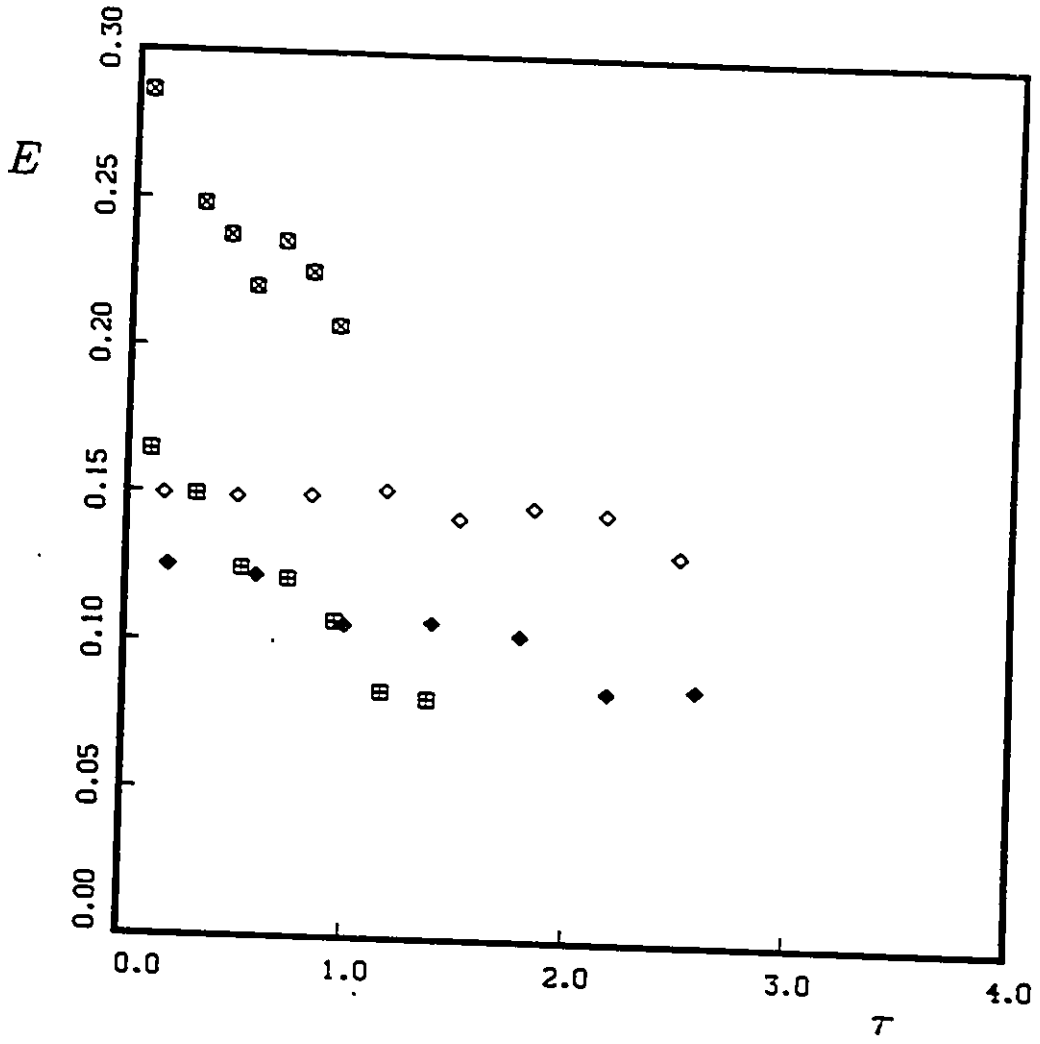

Figure 6.40: Development of E along the wind tunnel centerline in destabilized shear flow, S <0 (Cases D and E). Symbols as in Table 6.1.

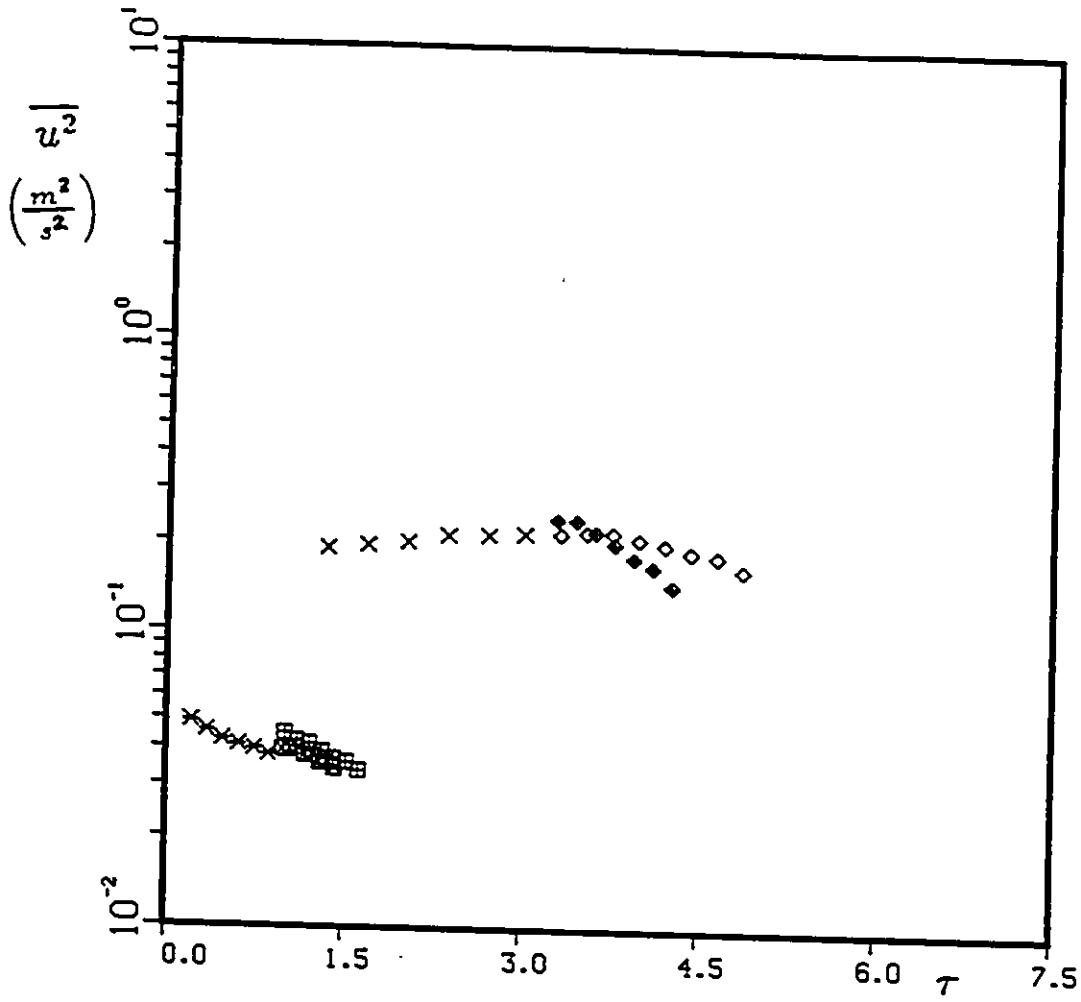

Figure 6.41: Development of $\overline{u^2}$ along the wind tunnel centerline in stabilized shear flow, $S > 0$ (Cases D and E). Symbols as in Table 6.1.

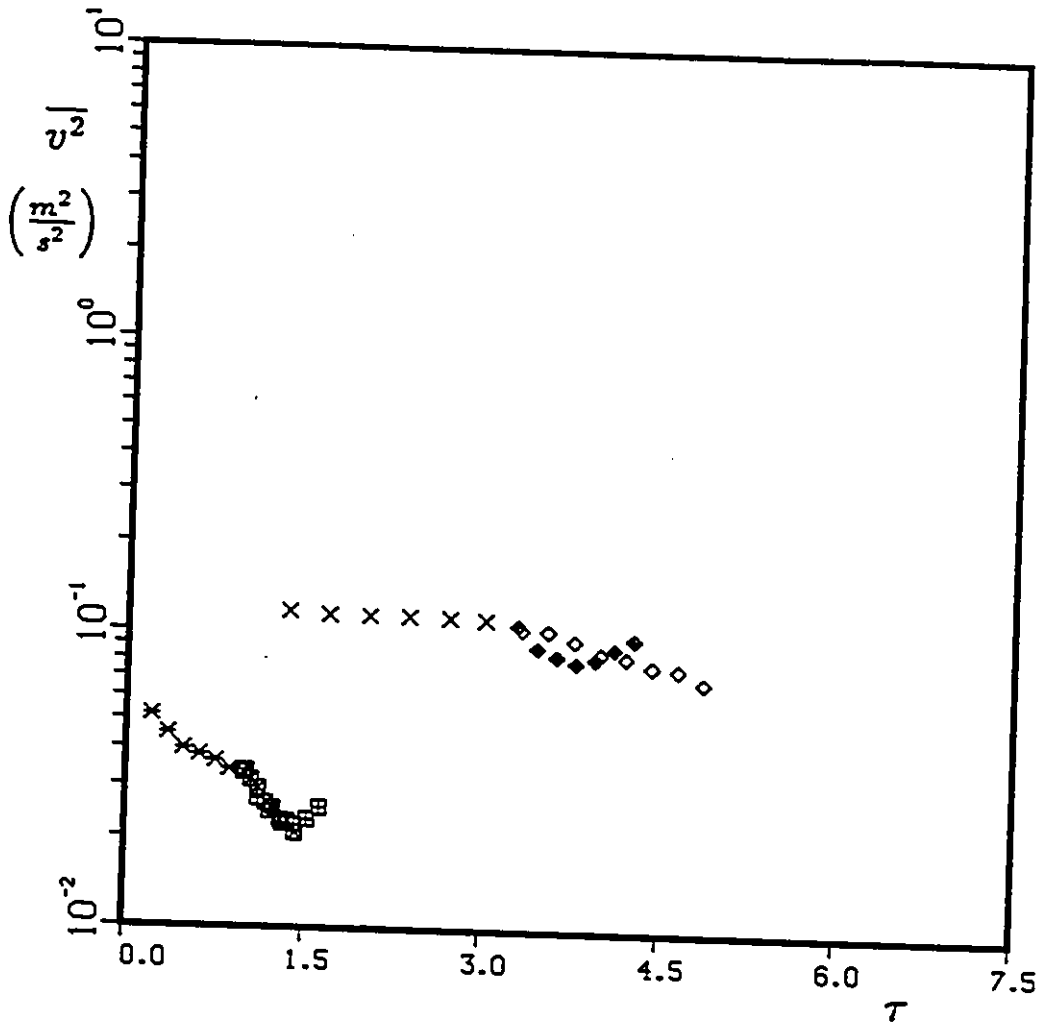

Figure 6.42: Development of $\overline{v^2}$ along the wind tunnel centerline in stabilized shear flow, $S > 0$ (Cases D and E). Symbols as in Table 6.1.

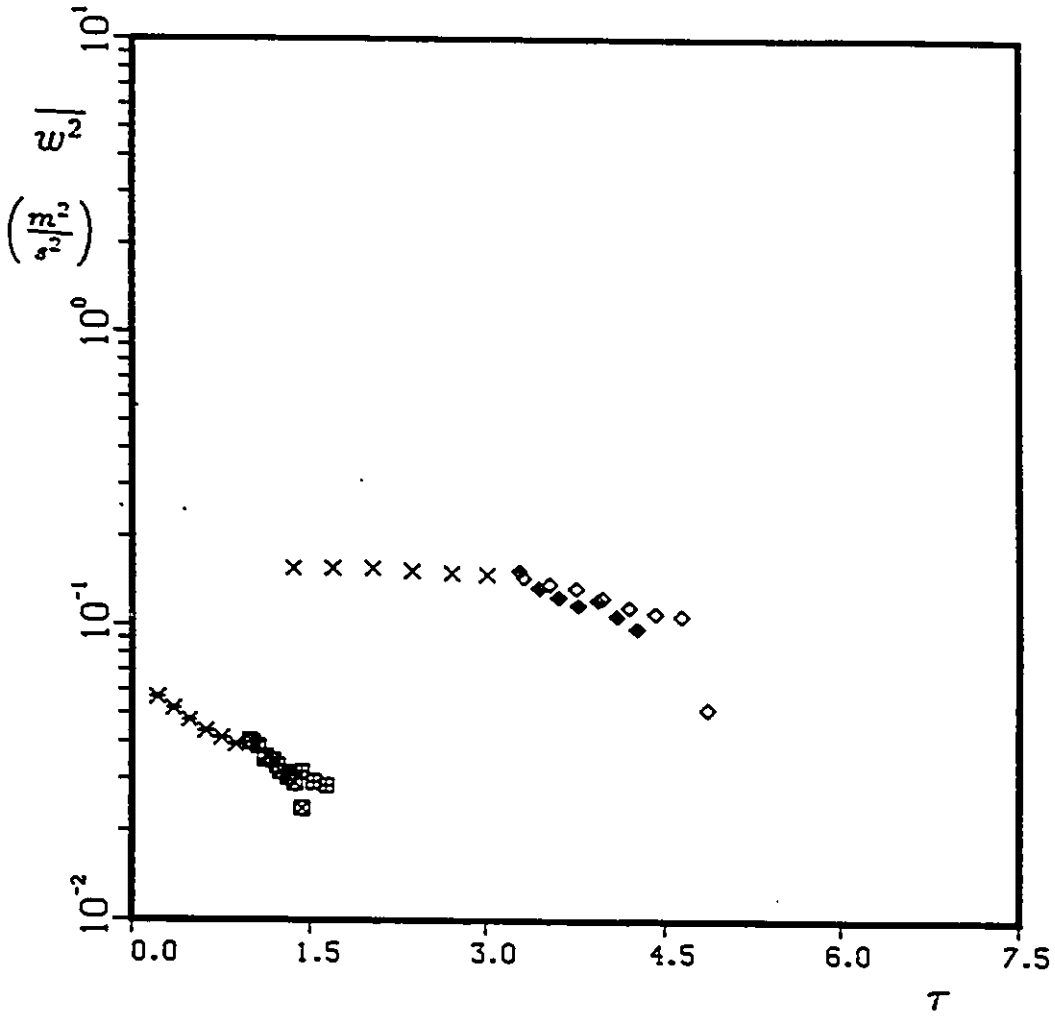

Figure 6.43: Development of $\overline{w^2}$ along the wind tunnel centerline in stabilized shear flow, $S > 0$ (Cases D and E). Symbols as in Table 6.1.

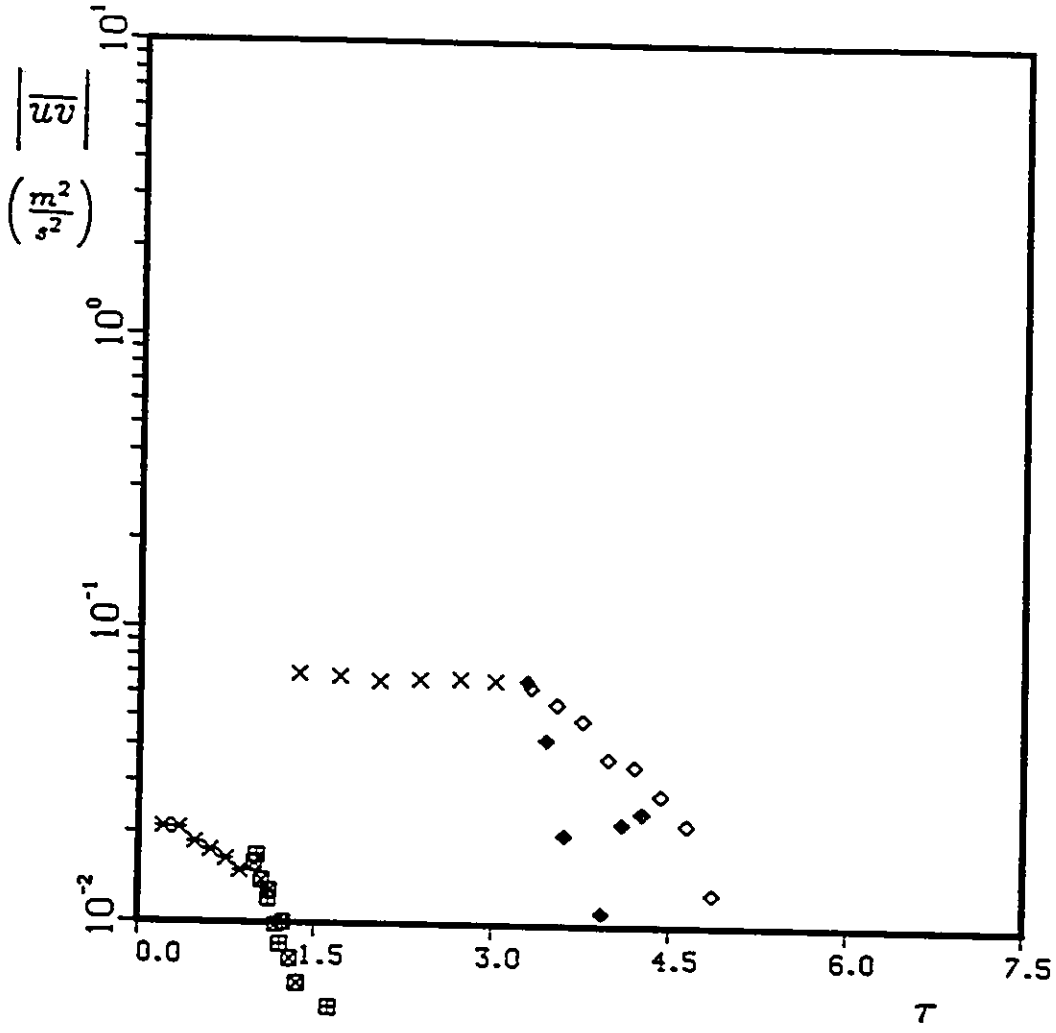

Figure 6.44: Development of $\overline{uv}$ along the wind tunnel centerline in stabilized shear flow, $S > 0$ (Cases D and E). Symbols as in Table 6.1.

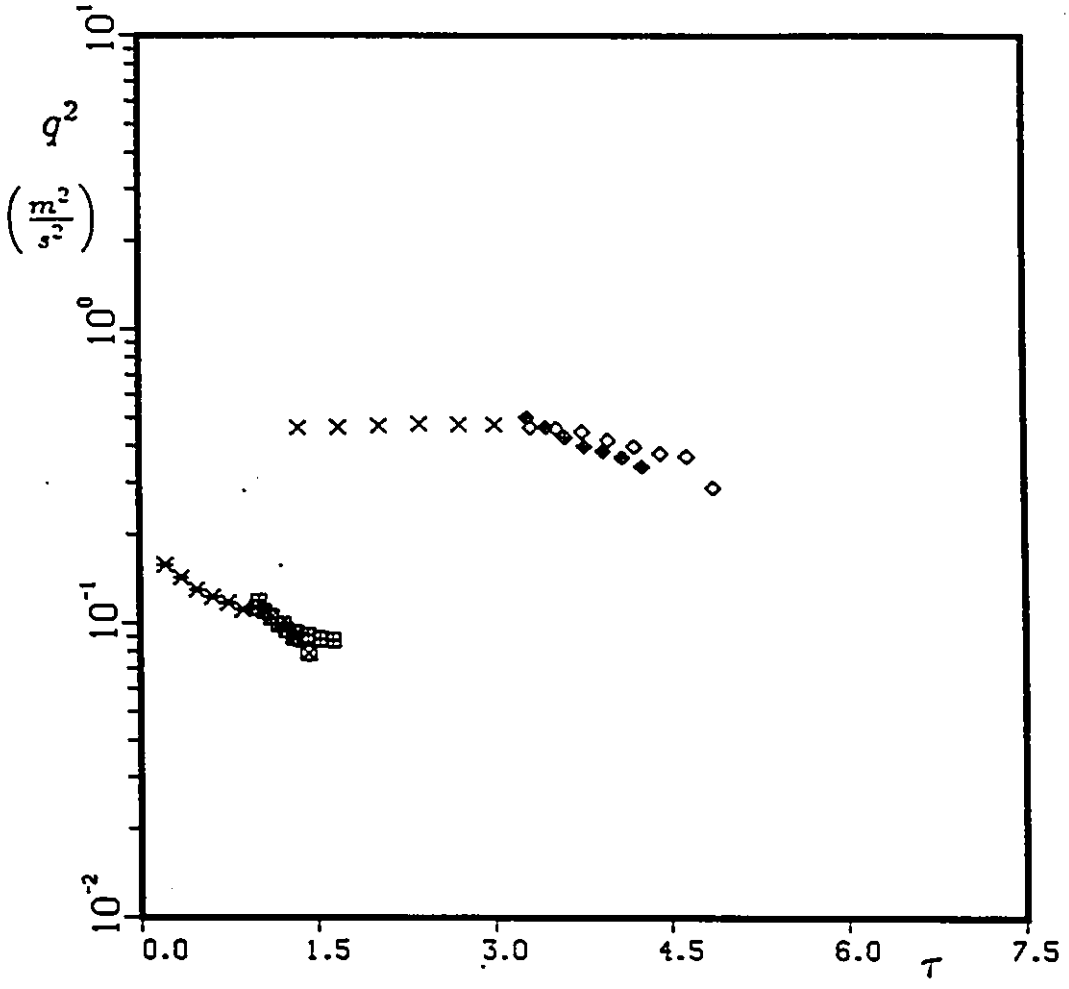

Figure 6.45: Development of q^2 along the wind tunnel centerline in stabilized shear flow, $S > 0$ (Cases D and E). Symbols as in Table 6.1.

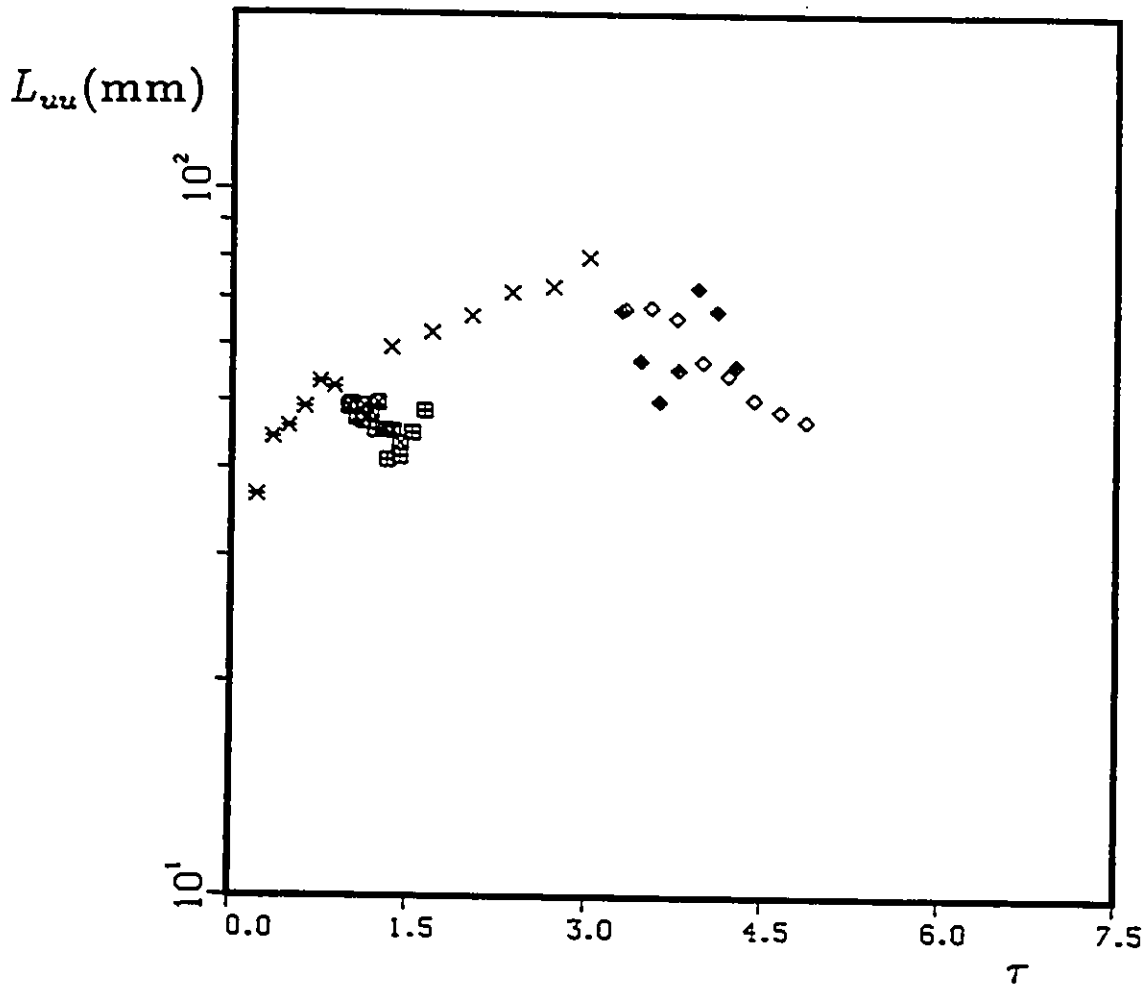

Figure 6.46: Development of L_{uu} along the wind tunnel centerline in stabilized shear flow, $S > 0$ (Cases D and E). Symbols as in Table 6.1.

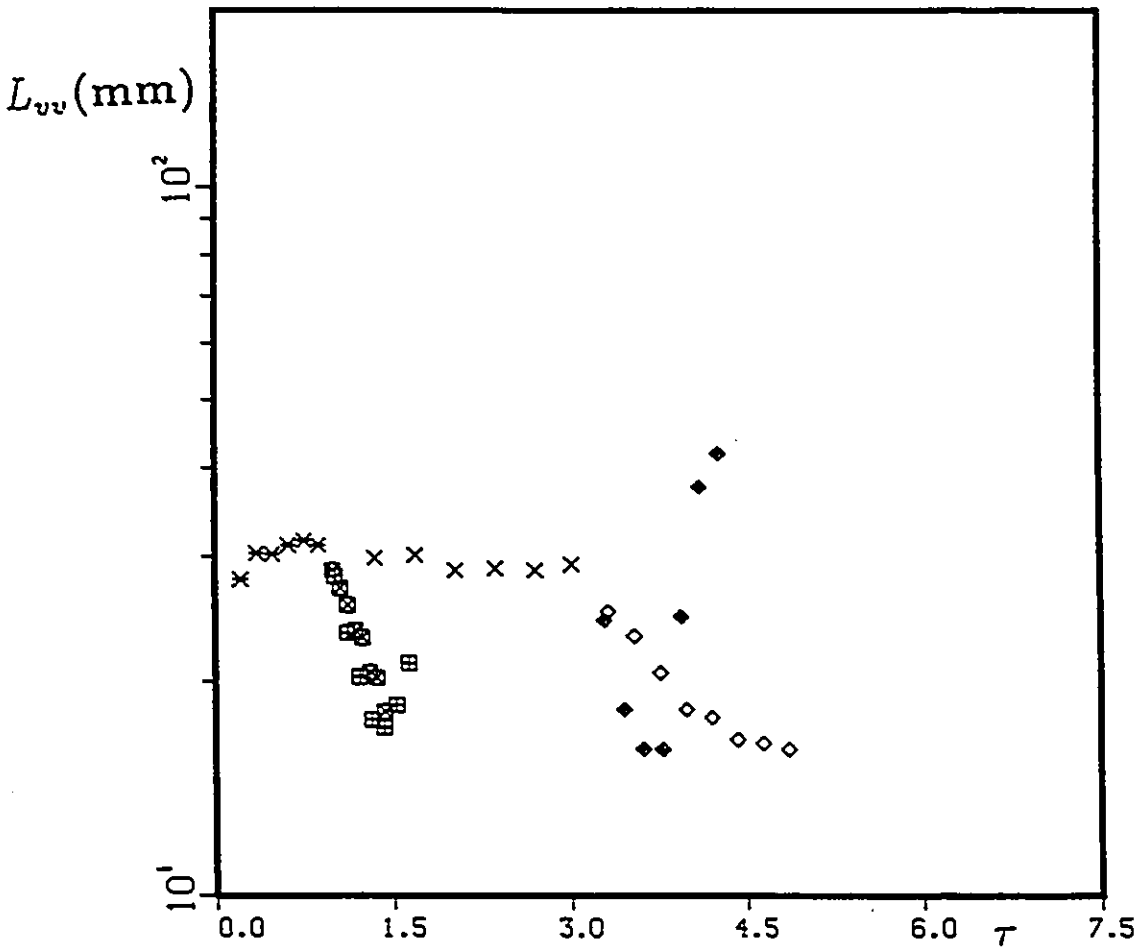

Figure 6.47: Development of L_{vv} along the wind tunnel centerline in stabilized shear flow, S >0 (Cases D and E). Symbols as in Table 6.1.

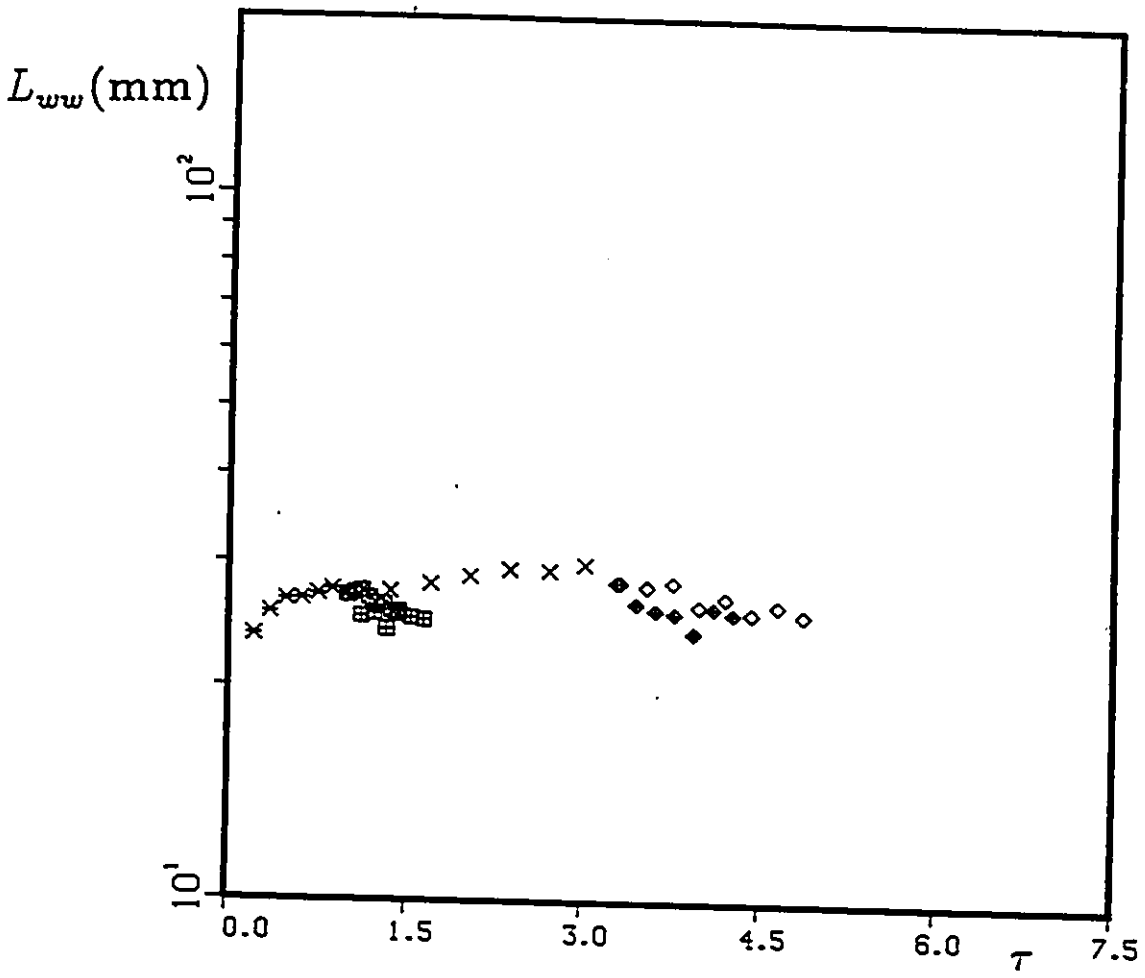

Figure 6.48: Development of L_{ww} along the wind tunnel centerline in stabilized shear flow, $S > 0$ (Cases D and E). Symbols as in Table 6.1.

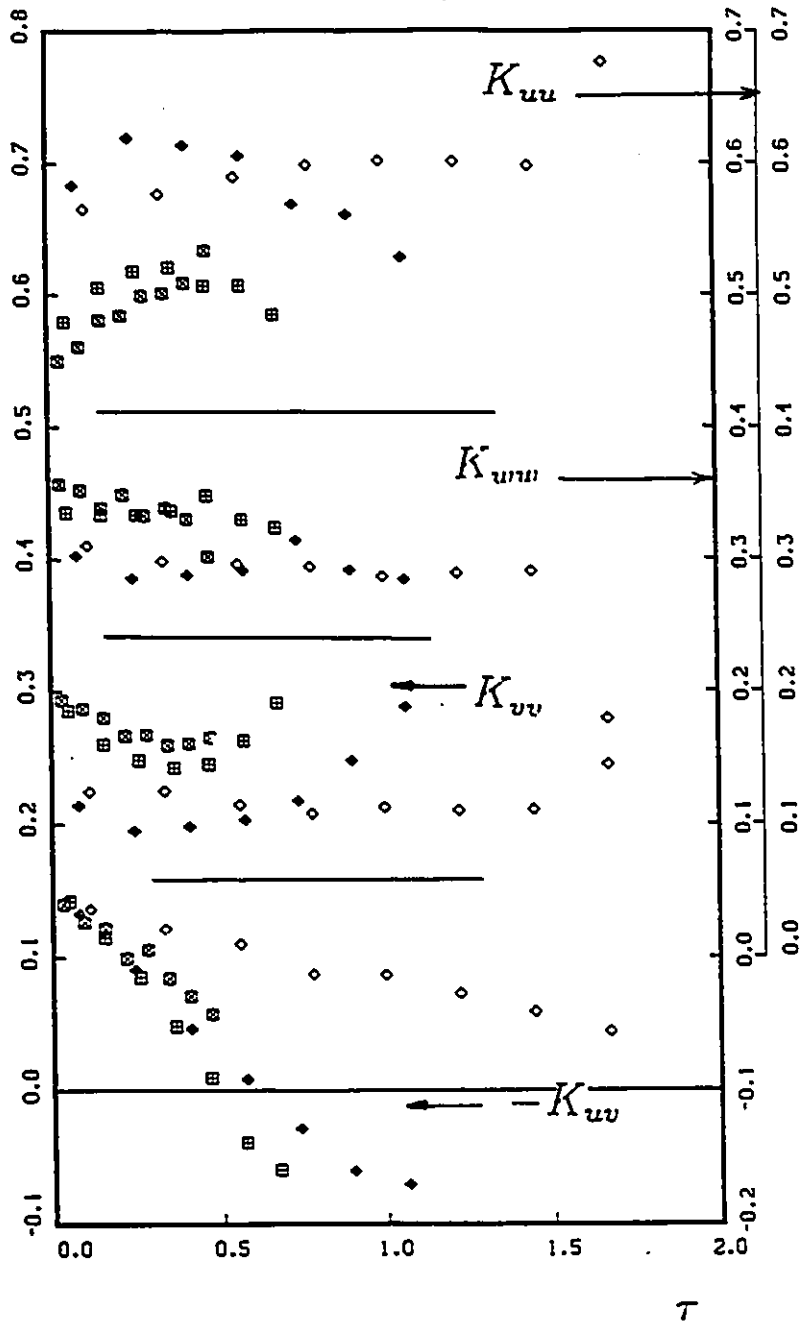

Figure 6.49: Development of the dimensionless stresses along the wind tunnel centerline in stabilized shear flow, $S > 0$ (Cases D and E). Symbols as in Table 6.1.

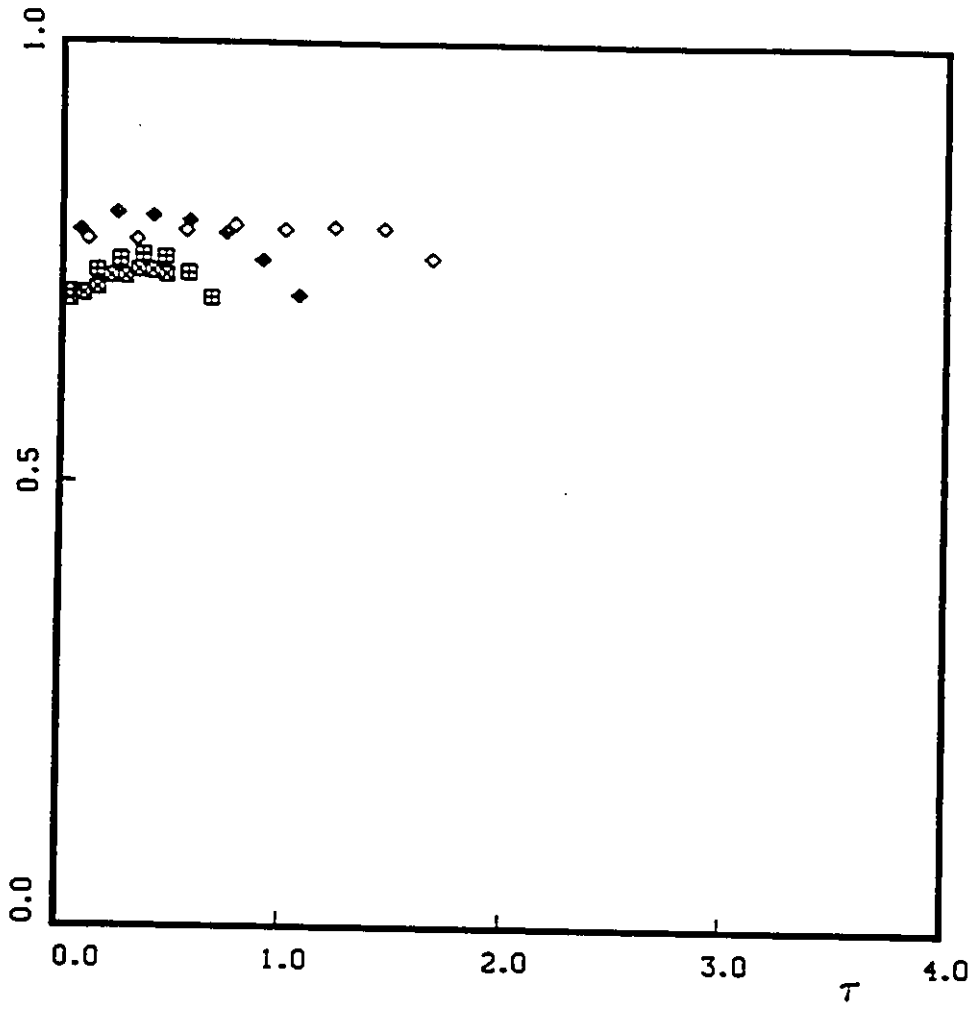

Figure 6.50: Development of $\breve{K}_{uu} + \breve{K}_{ww}$ along the wind tunnel centerline in stabilized shear flow, $S > 0$ (Cases D and E). Symbols as in Table 6.1.

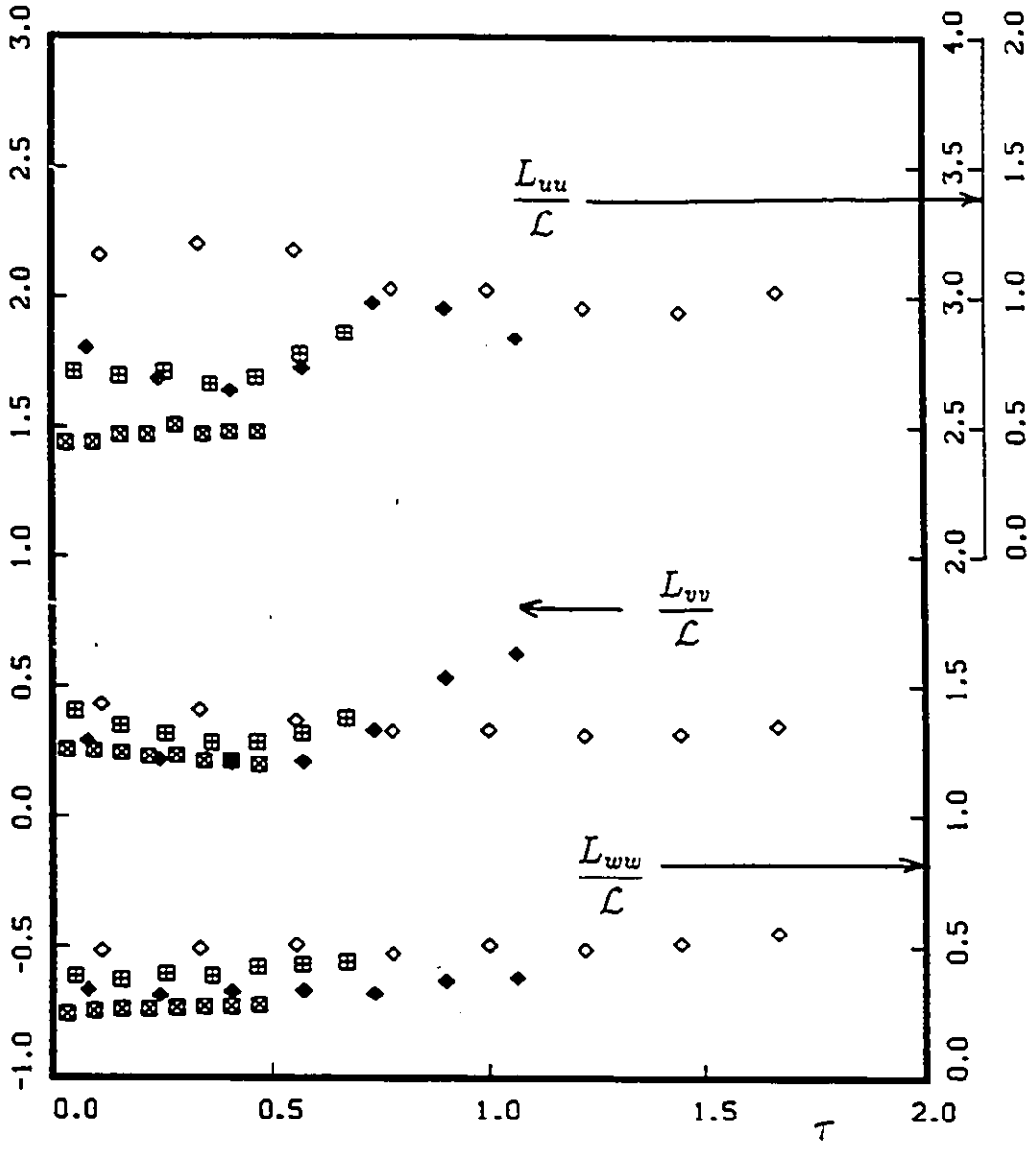

Figure 6.51: Development of the dimensionless integral lengthscales along the wind tunnel centerline in stabilized shear flow, $S > 0$ (Cases D and E). Symbols as in Table 6.1.

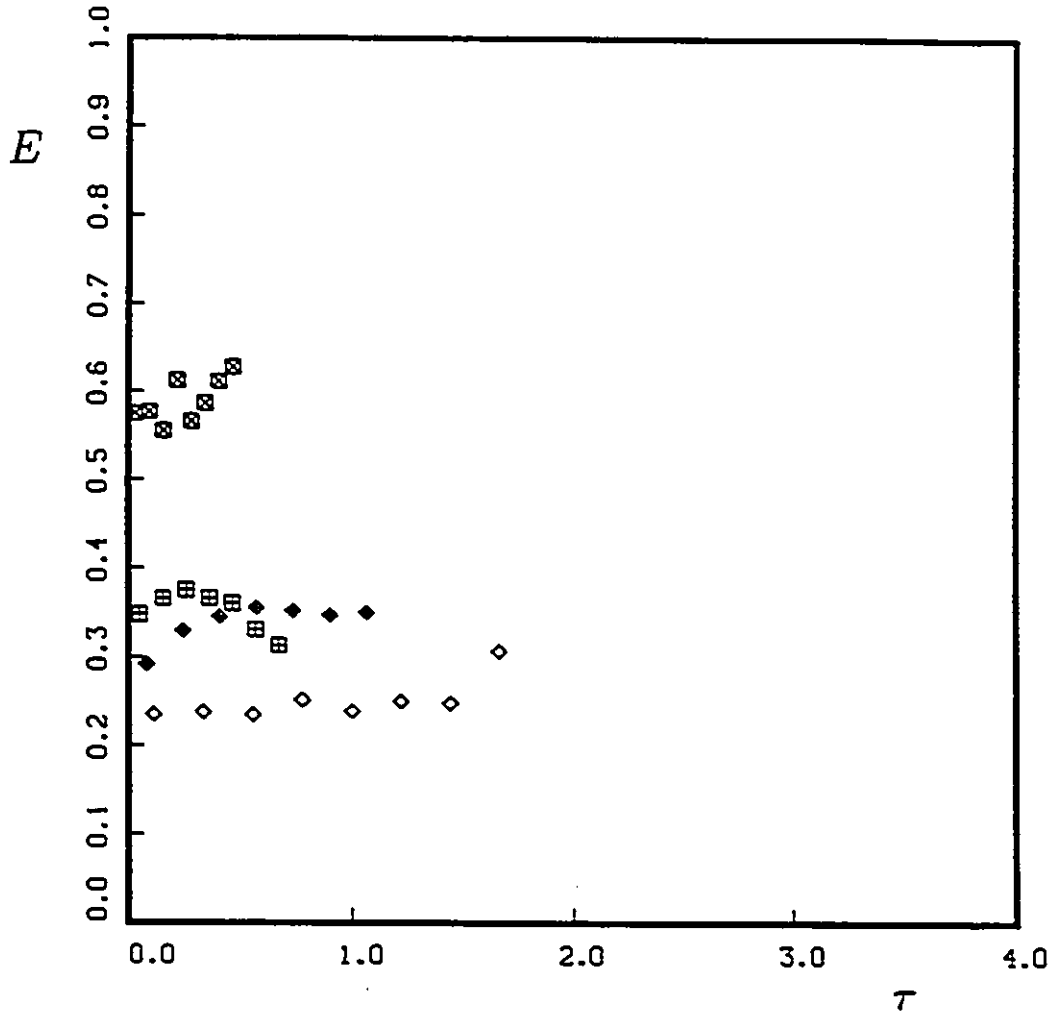

Figure 6.52: Development of E along the wind tunnel centerline in stabilized shear flow, $S > 0$ (Cases D and E). Symbols as in Table 6.1.

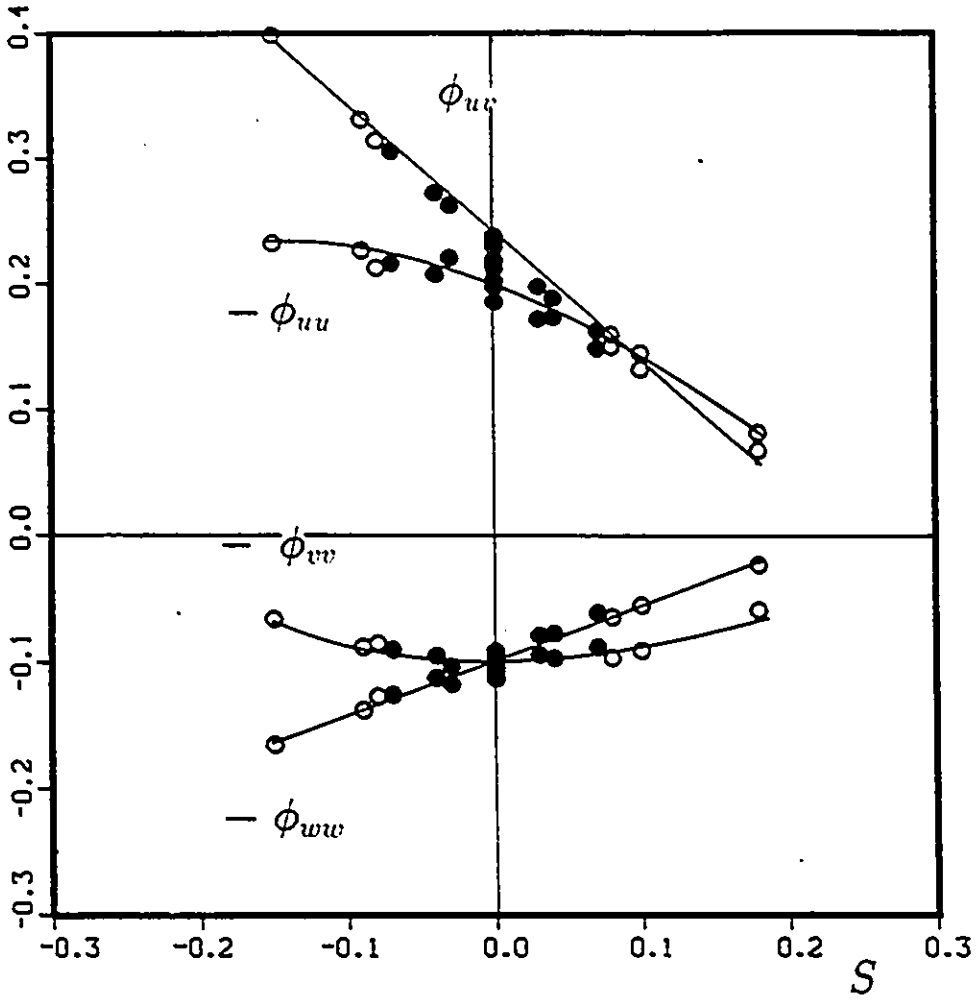

Figure 6.53: The dependence of the pressure-strain rate covariance on S calculated from the balance of the Reynolds stress equations assumming isotropic dissipation. Solid symbols represent data from the mildly curved section, open symbols represent data from the strongly curved section.

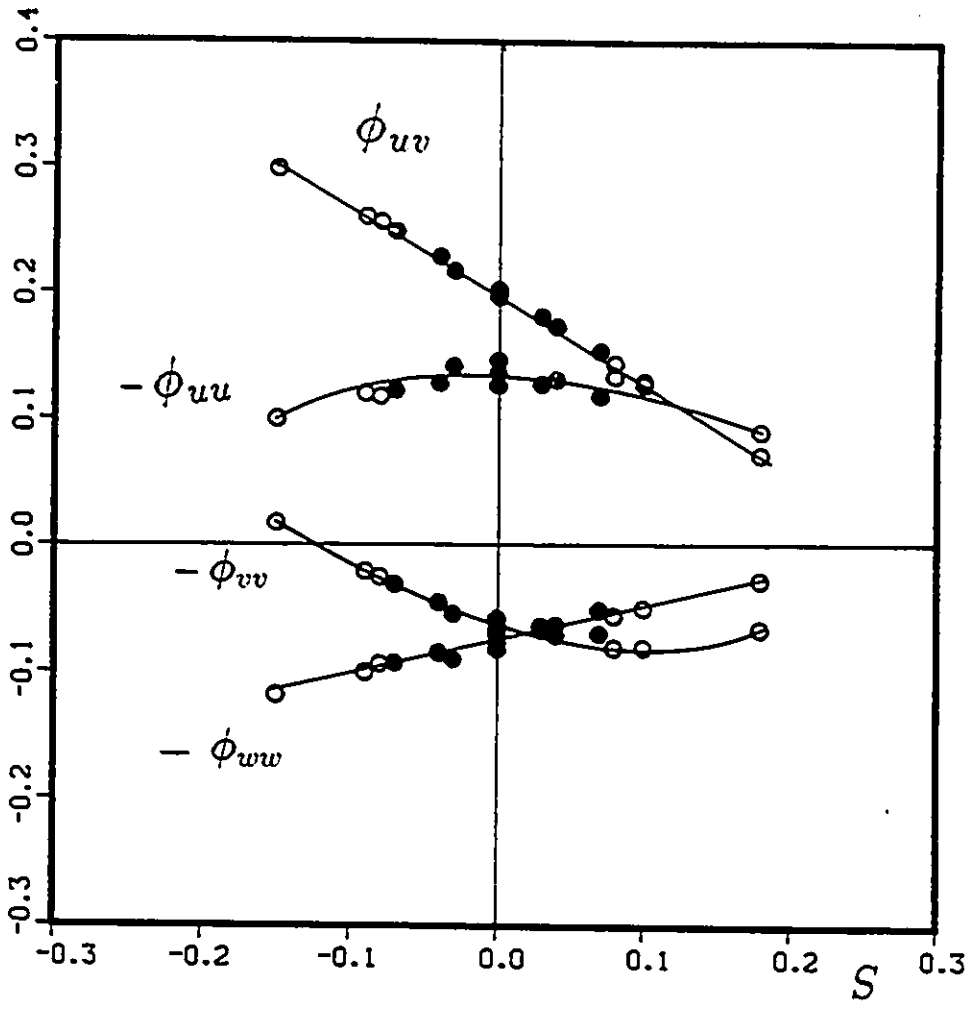

Figure 6.54: The dependence of the pressure-strain rate covariance on S calculated from the balance of the Reynolds stress equations assumming anisotropic dissipation. Solid symbols represent data from the mildly curved section, open symbols represent data from the strongly curved section.

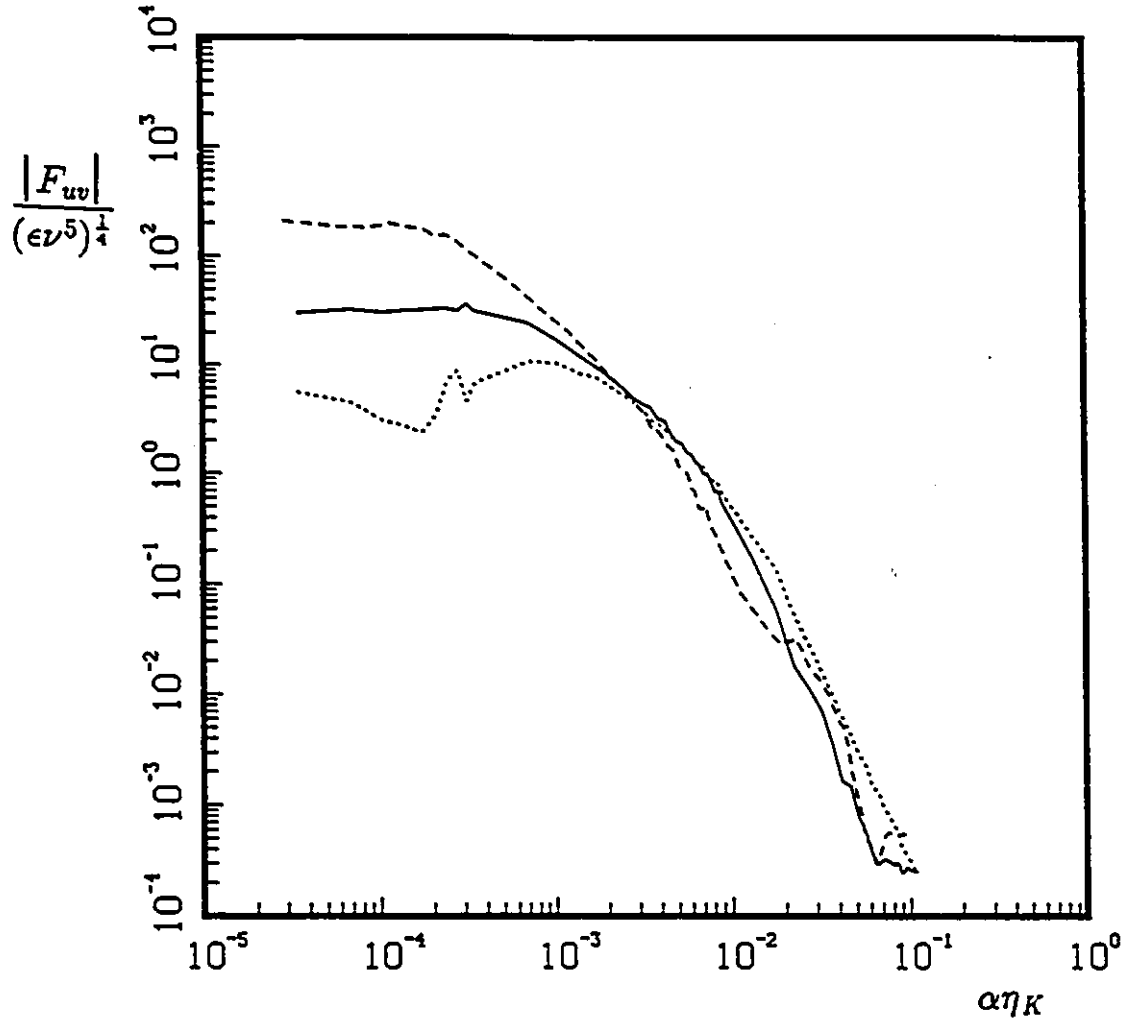

Figure 6.55: The effect of curvature on the cross-spectral density; —— $S = 0$, - - - $S = -.10$, • • • • • $S = .10$, $\frac{s}{h_c}$=3.01, n=0, z=0.

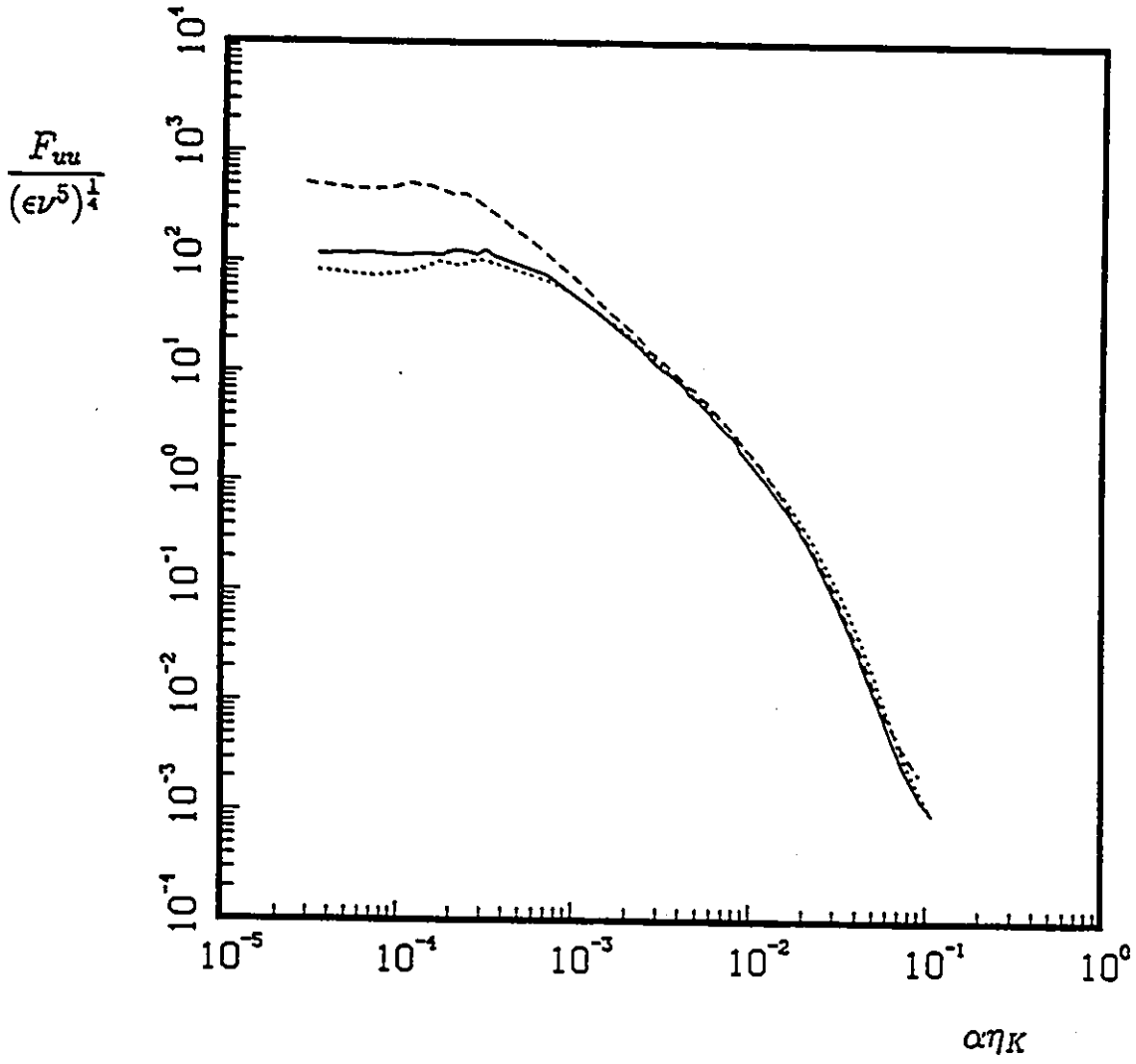

Figure 6.56: The effect of curvature on the $\overline{u^2}$ spectral density; ——— $S = 0$, – – – $S = -.10$, ····· $S = .10$, $\frac{s}{h_c}$=3.01, n=0, z=0.

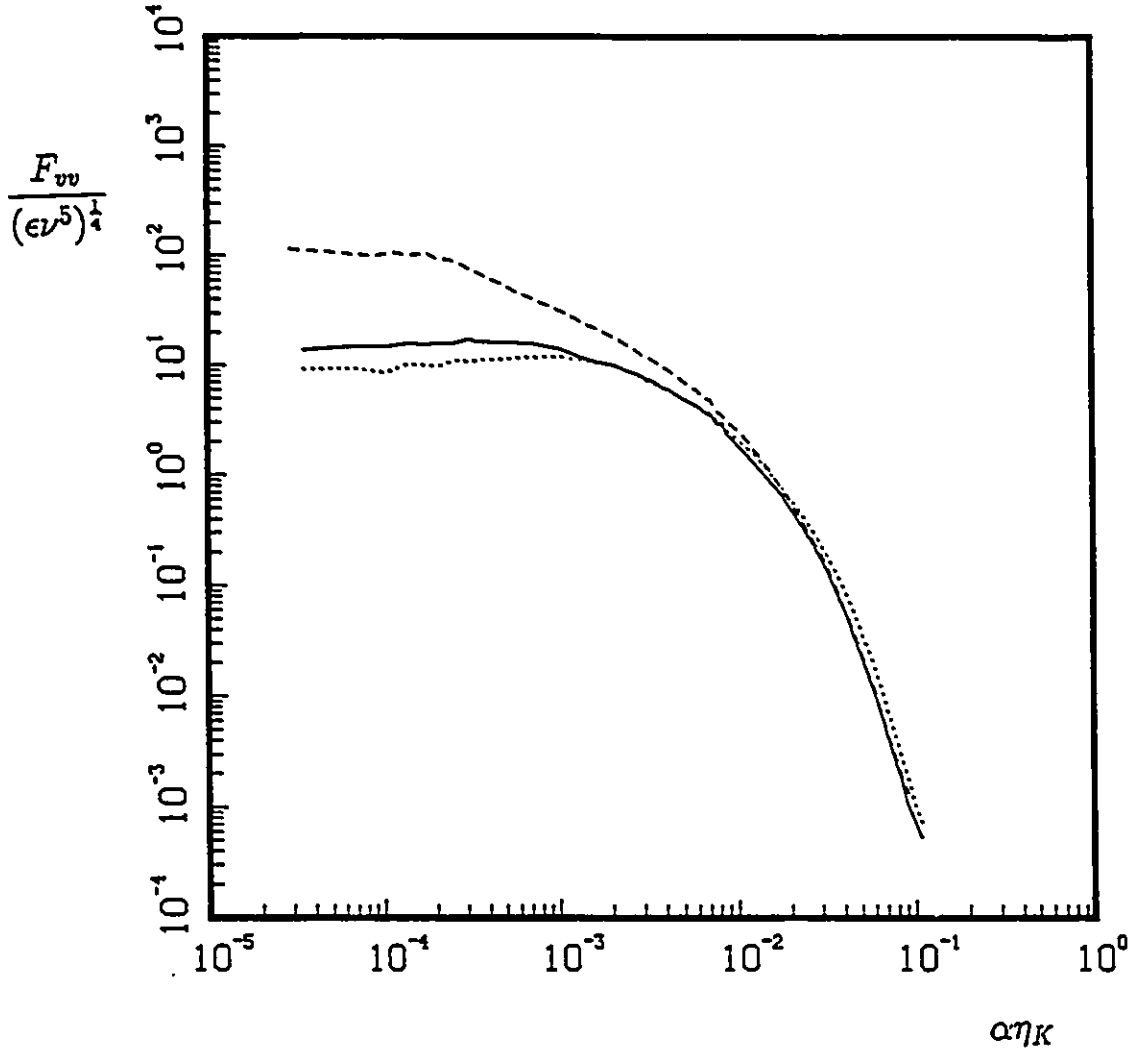

Figure 6.57: The effect of curvature on the $\overline{v^2}$ spectral density; —— $S = 0$, - - - - $S = -.10$, ····· $S = .10$, $\frac{s}{h_c}$=3.01, n=0, z=0.

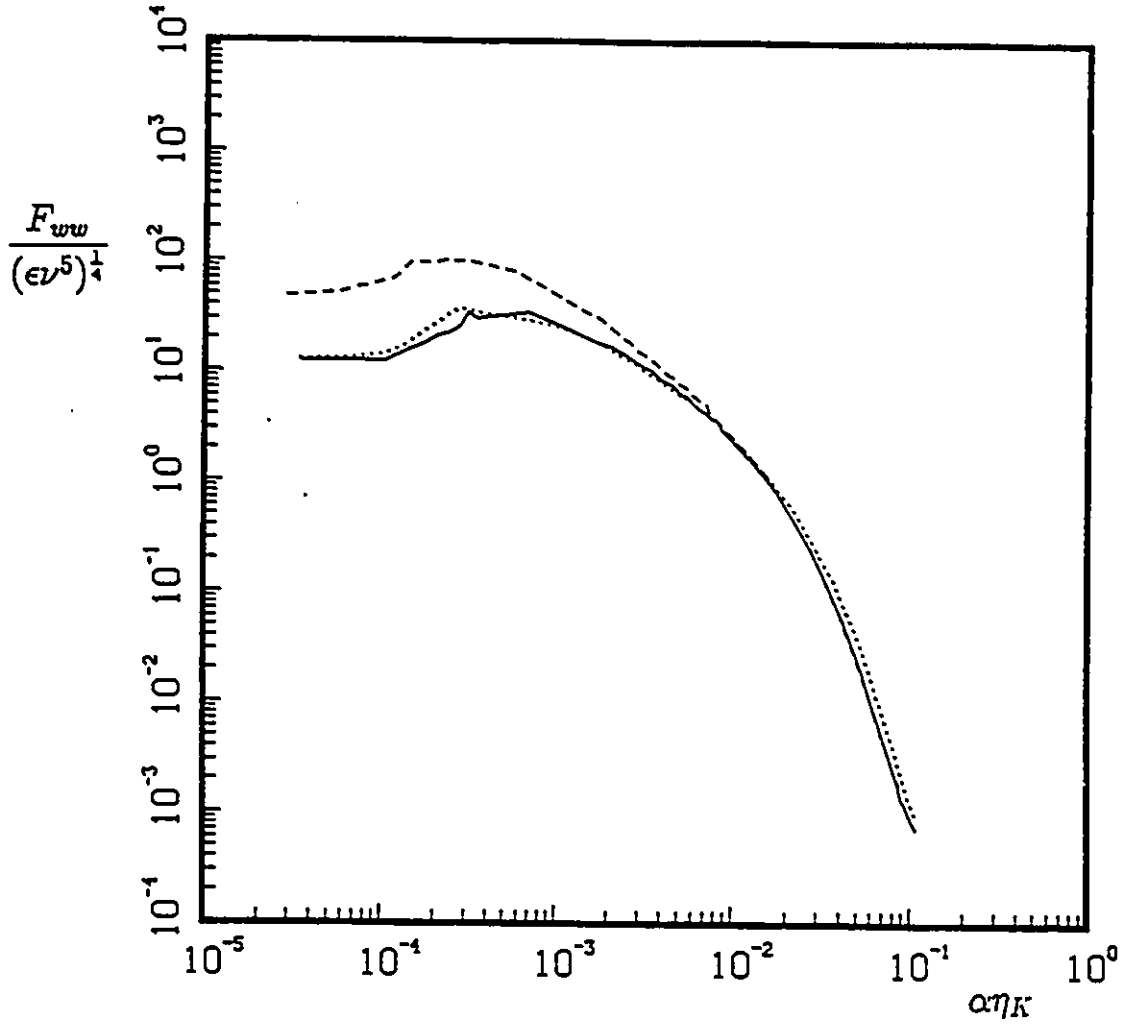

Figure 6.58: The effect of curvature on the $\overline{w^2}$ spectral density; ——— $S = 0$,- - - - $S = -.10$, ····· $S = .10$, $\frac{s}{h_c}$=3.01, n=0, z=0.

Appendix A

TABLES OF RAW DATA

case	$\frac{x_1}{a}$	r	U ($\frac{m}{s}$)	V ($\frac{m}{s}$)	W ($\frac{m}{s}$)	$\frac{\overline{u'u'}}{q^2}$	$\frac{\overline{v'v'}}{q^2}$	$\frac{\overline{w'w'}}{q^2}$	$\frac{\overline{u'v'}}{q^2}$	$\frac{\overline{u'w'}}{q^2}$	q^2 ($\frac{m^2}{s^2}$)
pa	5.83	11.86	9.868	-0.136	0.049	0.469	0.215	0.316	-0.141	0.042	0.673511
pa	6.66	13.55	9.886	-0.148	0.047	0.476	0.211	0.313	-0.136	0.044	0.791447
pa	7.50	15.25	9.905	-0.159	0.045	0.481	0.210	0.309	-0.136	0.049	0.908125
pa	8.33	16.94	9.927	-0.163	0.045	0.483	0.208	0.309	-0.135	0.048	1.064934
pa	9.16	18.64	9.955	-0.169	0.041	0.491	0.201	0.308	-0.132	0.056	1.259192
pa	9.91	20.16	10.012	-0.222	0.044	0.498	0.202	0.300	-0.135	0.055	1.454584
pb	5.83	9.87	9.815	-0.088	-0.011	0.444	0.210	0.346	-0.142	0.005	0.392498
pb	6.66	11.26	9.825	-0.094	0.005	0.445	0.210	0.345	-0.139	0.010	0.428367
pb	7.50	12.69	9.860	-0.106	0.004	0.453	0.208	0.339	-0.137	0.016	0.470007
pb	8.33	14.10	9.867	-0.112	0.002	0.460	0.210	0.331	-0.134	0.018	0.513747
pb	9.16	15.51	9.892	-0.120	0.008	0.464	0.210	0.326	-0.135	0.021	0.566251
pb	9.91	16.78	9.975	-0.168	0.024	0.470	0.210	0.321	-0.133	0.027	0.612386
pc	4.63	4.28	10.117	-0.089	-0.104	0.454	0.213	0.333	-0.138	-0.005	0.104949
pc	5.46	5.05	10.075	-0.089	-0.093	0.460	0.210	0.330	-0.138	0.003	0.116293
pc	6.30	5.82	10.034	-0.097	-0.089	0.467	0.210	0.323	-0.137	0.005	0.129828
pc	7.13	6.59	10.023	-0.100	-0.068	0.459	0.213	0.328	-0.136	0.008	0.142002
pc	7.96	7.36	10.101	-0.111	-0.063	0.464	0.216	0.320	-0.135	0.012	0.157155
pc	8.71	8.05	10.092	-0.145	-0.042	0.459	0.218	0.323	-0.133	0.016	0.167039
pd	3.33	1.35	10.257	-0.131	0.032	0.412	0.252	0.336	-0.150	0.022	0.463502
pd	4.16	1.69	10.269	-0.128	0.028	0.420	0.246	0.334	-0.147	0.027	0.466130
pd	5.00	2.03	10.263	-0.134	-0.039	0.428	0.242	0.331	-0.140	0.026	0.471524
pd	5.83	2.36	10.282	-0.128	0.030	0.444	0.238	0.318	-0.140	0.030	0.478511
pd	6.66	2.70	10.336	-0.142	0.034	0.449	0.237	0.314	-0.142	0.031	0.476650
pd	7.41	3.01	10.387	-0.147	0.040	0.454	0.235	0.311	-0.140	0.029	0.476334
pe	1.33	0.21	9.599	-0.099	0.051	0.312	0.329	0.360	-0.133	-0.067	0.157698
pe	2.16	0.35	9.606	-0.108	0.047	0.321	0.315	0.364	-0.146	-0.034	0.142513
pe	3.00	0.48	9.600	-0.115	0.056	0.328	0.306	0.365	-0.143	-0.014	0.129970
pe	3.83	0.61	9.583	-0.116	0.056	0.335	0.310	0.355	-0.143	-0.006	0.122653
pe	4.66	0.75	9.587	-0.121	0.060	0.339	0.310	0.352	-0.139	-0.000	0.117444
pe	5.41	0.87	9.620	-0.120	0.054	0.342	0.306	0.352	-0.134	0.004	0.111270

Table A.1: Straight section; $x_2 = 0$, $x_3 = 0$.

case	$\frac{x_1}{h_0}$	$\frac{\overline{u^3}}{u'^3}$	$\frac{\overline{v^3}}{v'^3}$	$\frac{\overline{w^3}}{w'^3}$	$\frac{\overline{u^2v}}{u'^2v'}$	$\frac{\overline{uv^2}}{u'v'^2}$	$\frac{\overline{u^2w}}{u'^2w'}$	$\frac{\overline{uw^2}}{u'w'^2}$	u' $(\frac{m}{s})$	v' $(\frac{m}{s})$	w' $(\frac{m}{s})$
pa	5.83	0.21	-0.196	0.009	-0.117	0.138	0.021	0.094	0.562	0.360	0.461
pa	6.66	0.10	-0.116	0.002	-0.061	0.081	0.005	0.065	0.614	0.408	0.498
pa	7.50	0.07	-0.063	0.012	-0.031	0.045	0.011	0.038	0.661	0.437	0.530
pa	8.33	0.01	-0.034	0.005	-0.014	0.024	0.007	0.023	0.717	0.471	0.574
pa	9.16	-0.03	-0.004	-0.047	0.007	-0.004	0.002	-0.003	0.786	0.503	0.623
pa	9.91	-0.05	0.010	-0.009	0.016	-0.014	-0.005	0.013	0.851	0.542	0.661
pb	5.83	0.24	-0.230	-0.012	-0.142	0.170	0.007	0.079	0.418	0.287	0.368
pb	6.66	0.14	-0.158	-0.008	-0.081	0.109	0.002	0.075	0.437	0.300	0.384
pb	7.50	0.07	-0.086	-0.004	-0.037	0.054	0.004	0.063	0.461	0.313	0.399
pb	8.33	0.00	-0.021	0.001	-0.010	0.020	0.007	0.028	0.486	0.328	0.412
pb	9.16	0.00	-0.016	-0.008	-0.005	0.011	-0.003	0.023	0.513	0.345	0.429
pb	9.91	-0.01	0.015	-0.010	0.003	0.000	0.008	0.009	0.536	0.358	0.443
pc	4.63	-0.25	0.204	0.051	0.133	-0.146	0.059	-0.152	0.218	0.149	0.187
pc	5.46	-0.24	0.193	0.031	0.122	-0.139	0.038	-0.141	0.231	0.156	0.196
pc	6.30	-0.23	0.184	0.030	0.130	-0.137	0.023	-0.147	0.246	0.165	0.205
pc	7.13	-0.19	0.166	0.013	0.104	-0.115	0.023	-0.139	0.255	0.174	0.216
pc	7.96	-0.19	0.161	-0.012	0.097	-0.107	0.009	-0.114	0.270	0.184	0.224
pc	8.71	-0.18	0.144	-0.012	0.092	-0.099	0.006	-0.125	0.277	0.191	0.232
pd	3.33	-0.22	0.104	0.001	0.145	-0.115	-0.005	-0.082	0.437	0.342	0.395
pd	4.16	-0.21	0.133	-0.007	0.128	-0.114	0.006	-0.068	0.443	0.338	0.394
pd	5.00	-0.25	0.158	-0.024	0.128	-0.119	-0.009	-0.086	0.449	0.338	0.395
pd	5.83	-0.28	0.167	0.002	0.141	-0.140	-0.013	-0.080	0.461	0.337	0.390
pd	6.66	-0.28	0.209	-0.033	0.137	-0.148	-0.012	-0.087	0.462	0.336	0.387
pd	7.41	-0.31	0.190	-0.033	0.139	-0.144	0.010	-0.097	0.465	0.335	0.385
pe	1.33	-0.09	0.068	-0.004	0.074	-0.077	0.018	-0.117	0.222	0.228	0.238
pe	2.16	-0.09	0.105	0.024	0.067	-0.070	0.005	-0.106	0.214	0.212	0.228
pe	3.00	-0.10	0.084	0.036	0.069	-0.075	0.032	-0.093	0.207	0.200	0.218
pe	3.83	-0.14	0.138	0.012	0.110	-0.121	0.019	-0.097	0.203	0.195	0.209
pe	4.66	-0.16	0.164	-0.001	0.112	-0.118	0.007	-0.098	0.199	0.191	0.203
pe	5.41	-0.18	0.180	-0.034	0.125	-0.130	0.017	-0.098	0.195	0.184	0.198

Table A.2: Straight section; $x_2 = 0$, $x_3 = 0$.

case	$\frac{x_1}{h_0}$	$\frac{u^4}{u'^4}$	$\frac{v^4}{v'^4}$	$\frac{w^4}{w'^4}$	$\frac{u^3v}{u'^3v'}$	$\frac{u^2v^2}{u'^2v'^2}$	$\frac{uv^3}{u'v'^3}$	$\frac{u^3w}{u'^3w'}$	$\frac{u^2w^2}{u'^2w'^2}$	$\frac{uw^3}{u'w'^3}$	u' $(\frac{m}{s})$	v' $(\frac{m}{s})$	w' $(\frac{m}{s})$
pa	5.83	3.012	3.224	3.107	-1.323	1.435	-1.350	0.373	1.148	0.345	0.562	0.380	0.461
pa	6.66	2.995	3.204	3.129	-1.256	1.396	-1.283	0.362	1.133	0.331	0.614	0.408	0.498
pa	7.50	3.014	3.222	3.125	-1.269	1.396	-1.284	0.415	1.152	0.374	0.661	0.437	0.530
pa	8.33	3.016	3.223	3.135	-1.256	1.389	-1.278	0.403	1.176	0.355	0.717	0.471	0.574
pa	9.16	3.034	3.257	3.158	-1.258	1.394	-1.259	0.460	1.181	0.442	0.786	0.503	0.623
pa	9.91	3.079	3.250	3.165	-1.275	1.393	-1.281	0.470	1.169	0.431	0.851	0.542	0.661
pb	5.83	2.898	3.095	2.999	-1.308	1.390	-1.317	0.079	1.172	0.057	0.418	0.287	0.368
pb	6.66	2.859	3.073	3.003	-1.248	1.351	-1.261	0.092	1.199	0.088	0.437	0.300	0.384
pb	7.50	2.865	3.078	3.023	-1.241	1.354	-1.257	0.136	1.165	0.124	0.461	0.313	0.399
pb	8.33	2.901	3.103	3.017	-1.222	1.346	-1.237	0.161	1.132	0.135	0.486	0.328	0.412
pb	9.16	2.959	3.114	3.049	-1.252	1.367	-1.251	0.170	1.157	0.161	0.513	0.345	0.429
pb	9.91	2.925	3.151	3.074	-1.207	1.345	-1.215	0.222	1.140	0.185	0.536	0.358	0.443
pc	4.63	3.069	3.268	3.131	-1.343	1.450	-1.377	-0.088	1.141	-0.066	0.218	0.149	0.187
pc	5.46	3.061	3.234	3.098	-1.333	1.437	-1.351	-0.011	1.111	-0.007	0.231	0.156	0.196
pc	6.30	3.030	3.206	3.116	-1.312	1.418	-1.325	-0.011	1.104	-0.013	0.246	0.165	0.205
pc	7.13	2.976	3.169	3.140	-1.267	1.390	-1.305	0.026	1.141	0.015	0.255	0.174	0.216
pc	7.96	2.969	3.192	3.145	-1.253	1.384	-1.265	0.059	1.111	0.053	0.270	0.184	0.224
pc	8.71	2.966	3.159	3.120	-1.219	1.359	-1.235	0.094	1.129	0.101	0.277	0.191	0.232
pd	3.33	2.886	2.898	3.035	-1.269	1.350	-1.252	0.178	1.068	0.195	0.437	0.342	0.395
pd	4.16	2.890	2.960	3.008	-1.264	1.359	-1.245	0.194	1.053	0.176	0.443	0.338	0.394
pd	5.00	2.922	3.031	3.058	-1.221	1.338	-1.215	0.209	1.070	0.201	0.449	0.338	0.395
pd	5.83	2.966	3.100	3.045	-1.237	1.360	-1.217	0.256	1.053	0.229	0.461	0.337	0.390
pd	6.66	2.972	3.110	3.037	-1.251	1.366	-1.260	0.251	1.048	0.249	0.462	0.336	0.387
pd	7.41	3.035	3.130	3.125	-1.246	1.362	-1.214	0.217	1.106	0.222	0.465	0.335	0.385
pe	1.33	2.828	2.850	2.929	-1.101	1.228	-1.130	-0.477	1.042	-0.342	0.222	0.228	0.238
pe	2.16	2.793	2.857	2.901	-1.200	1.284	-1.221	-0.210	0.996	-0.075	0.214	0.212	0.228
pe	3.00	2.837	2.843	2.911	-1.159	1.231	-1.149	-0.076	1.015	-0.011	0.207	0.200	0.218
pe	3.83	2.838	2.817	2.910	-1.122	1.216	-1.117	-0.017	1.006	0.019	0.203	0.195	0.209
pe	4.66	2.841	2.810	2.921	-1.092	1.206	-1.087	0.011	1.031	0.047	0.199	0.191	0.203
pe	5.41	2.911	2.849	2.942	-1.085	1.234	-1.085	0.031	1.055	0.063	0.195	0.184	0.198

Table A.3: Straight section; $x_2 = 0$, $x_3 = 0$.

case	$\frac{x_1}{h_p}$	L_{uu} (mm)	L_{vv} (mm)	L_{ww} (mm)	λ_u (mm)	λ_v (mm)	λ_w (mm)
pa	5.83	23.2	8.3	9.6	5.0	2.7	3.0
pa	6.66	25.4	8.6	10.4	5.0	2.7	3.0
pa	7.50	28.4	9.2	11.0	5.1	2.7	3.0
pa	8.33	33.5	10.4	11.9	5.1	2.7	3.0
pa	9.16	36.2	10.9	13.4	5.3	2.7	3.1
pa	9.91	39.9	12.0	14.2	5.4	2.8	3.1
pb	5.83	17.6	7.2	8.0	5.2	2.9	3.1
pb	6.66	19.5	7.6	8.5	5.2	2.9	3.2
pb	7.50	21.1	7.7	9.0	5.3	2.9	3.1
pb	8.33	23.6	8.0	9.5	5.2	2.8	3.2
pb	9.16	24.8	8.4	10.0	5.3	2.8	3.2
pb	9.91	26.9	8.6	10.7	5.3	2.8	3.2
pc	4.63	18.3	8.3	7.7	6.5	3.8	3.9
pc	5.46	19.1	8.7	8.4	6.6	3.9	4.0
pc	6.30	21.4	8.9	8.6	6.8	3.9	4.1
pc	7.13	21.1	8.7	9.1	6.8	3.8	4.1
pc	7.96	22.3	8.8	9.3	6.7	3.8	4.0
pc	8.71	22.9	8.9	9.6	6.7	3.8	4.0
pd	3.33	59.5	29.9	27.4	8.8	5.3	5.9
pd	4.16	62.6	30.2	28.1	8.9	5.1	6.0
pd	5.00	66.2	28.7	28.8	9.0	5.2	5.9
pd	5.83	71.4	28.9	29.5	9.2	5.1	5.8
pd	6.66	72.8	28.7	29.4	9.5	5.1	5.7
pd	7.41	80.3	29.2	30.0	9.4	5.0	5.6
pe	1.33	36.7	27.9	23.6	5.1	4.0	4.2
pe	2.16	44.4	30.3	25.5	7.0	5.3	5.6
pe	3.00	46.0	30.2	26.6	8.0	5.8	6.3
pe	3.83	49.0	31.1	26.7	9.1	6.5	6.8
pe	4.66	53.2	31.6	27.1	9.5	6.8	7.1
pe	5.41	52.4	31.1	27.5	9.9	6.9	7.3

Table A.4: Straight section; $x_2 = 0$, $x_3 = 0$.

case	$\frac{x_1}{h_0}$	τ	U $(\frac{m}{s})$	V $(\frac{m}{s})$	W $(\frac{m}{s})$	$\frac{\overline{u_1'u_1'}}{q^2}$	$\frac{\overline{u_2'u_2'}}{q^2}$	$\frac{\overline{u_3'u_3'}}{q^2}$	$\frac{\overline{u_1'u_2'}}{q^2}$	$\frac{\overline{u_2'u_3'}}{q^2}$	q^2 $(\frac{m^2}{s^2})$
na	5.83	11.11	10.048	0.137	0.040	0.469	0.209	0.322	0.147	0.008	-0.669949
na	6.66	12.70	10.111	0.135	0.049	0.471	0.209	0.320	0.145	0.013	0.732754
na	7.50	14.29	10.134	0.127	0.059	0.475	0.209	0.316	0.146	0.009	0.842063
na	8.33	15.87	10.145	0.133	0.059	0.485	0.203	0.312	0.142	0.006	0.970139
na	9.16	17.46	10.179	0.139	0.069	0.492	0.204	0.305	0.144	0.003	1.109514
na	9.91	18.89	10.229	0.185	0.073	0.495	0.201	0.304	0.143	0.002	1.243994
nb	5.83	8.89	9.957	0.088	0.040	0.464	0.212	0.324	0.161	-0.023	0.354307
nb	6.66	10.16	9.989	0.089	0.047	0.466	0.212	0.322	0.158	-0.023	0.393406
nb	7.50	11.43	9.978	0.082	0.051	0.470	0.210	0.320	0.154	-0.024	0.431811
nb	8.33	12.70	9.953	0.084	0.056	0.476	0.211	0.313	0.155	-0.024	0.479166
nb	9.16	13.97	9.961	0.090	0.057	0.477	0.209	0.314	0.152	-0.028	0.516230
nb	9.91	15.11	9.978	0.125	0.065	0.480	0.206	0.314	0.150	-0.024	0.558642
nc	4.63	4.28	10.153	0.104	-0.035	0.465	0.207	0.328	0.154	0.006	0.100672
nc	5.46	5.05	10.142	0.099	-0.016	0.465	0.202	0.333	0.152	0.011	0.110894
nc	6.30	5.82	10.148	0.092	-0.005	0.467	0.200	0.333	0.151	0.014	0.121395
nc	7.13	6.59	10.149	0.094	0.006	0.463	0.200	0.338	0.148	0.017	0.134450
nc	7.96	7.36	10.134	0.092	0.025	0.460	0.201	0.338	0.147	0.024	0.148742
nc	8.71	8.05	10.176	0.115	0.046	0.463	0.203	0.333	0.147	0.021	0.160303
nd	3.33	1.53	9.965	0.084	0.038	0.466	0.223	0.311	0.178	0.000	0.453935
nd	4.16	1.92	9.943	0.066	0.046	0.475	0.219	0.307	0.173	0.003	0.469803
nd	5.00	2.30	9.962	0.057	0.059	0.483	0.217	0.300	0.168	0.008	0.489525
nd	5.83	2.68	9.981	0.056	0.053	0.495	0.212	0.293	0.163	0.005	0.510214
nd	6.66	3.07	10.009	0.051	0.060	0.505	0.212	0.283	0.162	0.006	0.529927
nd	7.41	3.41	10.066	0.064	0.084	0.499	0.215	0.286	0.156	0.007	0.528587
ne	1.33	0.23	9.380	0.062	0.003	0.269	0.334	0.397	0.096	-0.080	0.119991
ne	2.16	0.37	9.376	0.045	0.017	0.275	0.324	0.401	0.116	-0.063	0.106762
ne	3.00	0.51	9.394	0.040	0.029	0.297	0.309	0.394	0.132	-0.053	0.102672
ne	3.83	0.65	9.390	0.036	0.024	0.322	0.295	0.383	0.146	-0.040	0.100538
ne	4.66	0.79	9.373	0.034	0.045	0.349	0.285	0.366	0.160	-0.036	0.100642
ne	5.41	0.92	9.484	0.041	0.045	0.372	0.278	0.350	0.168	-0.030	0.102338

Table A.5: Straight section; $x_2 = 0$, $x_3 = 0$.

case	$\frac{x_1}{h_2}$	$\frac{\overline{u^3}}{u'^3}$	$\frac{\overline{v^3}}{v'^3}$	$\frac{\overline{w^3}}{w'^3}$	$\frac{\overline{u^2v}}{u'^2v'}$	$\frac{\overline{uv^2}}{u'v'^2}$	$\frac{\overline{u^2w}}{u'^2w'}$	$\frac{\overline{uw^2}}{u'w'^2}$	u' $(\frac{m}{s})$	v' $(\frac{m}{s})$	w' $(\frac{m}{s})$
na	5.83	0.12	0.107	0.047	0.067	0.085	0.015	0.030	0.561	0.374	0.464
na	6.66	0.09	0.088	0.050	0.047	0.061	0.024	0.027	0.596	0.397	0.491
na	7.50	0.05	0.059	0.047	0.031	0.041	0.021	0.019	0.632	0.419	0.516
na	8.33	0.04	0.042	0.042	0.024	0.035	0.021	0.013	0.686	0.444	0.550
na	9.16	-0.01	0.029	0.056	-0.002	0.011	0.032	0.008	0.739	0.475	0.582
na	9.91	-0.02	-0.010	0.052	-0.009	-0.004	0.036	-0.003	0.785	0.500	0.615
nb	5.83	0.17	0.173	-0.020	0.101	0.126	-0.016	0.085	0.405	0.274	0.339
nb	6.66	0.11	0.131	-0.002	0.069	0.090	-0.002	0.050	0.428	0.289	0.356
nb	7.50	0.06	0.085	0.004	0.032	0.054	0.004	0.029	0.451	0.301	0.371
nb	8.33	0.03	0.054	0.036	0.019	0.033	0.011	0.021	0.478	0.318	0.387
nb	9.16	0.02	0.029	0.043	0.004	0.010	0.013	0.015	0.496	0.328	0.403
nb	9.91	0.00	0.022	0.038	-0.003	0.008	0.016	0.001	0.518	0.339	0.419
nc	4.63	-0.14	-0.175	0.031	-0.100	-0.129	0.011	-0.087	0.216	0.144	0.182
nc	5.46	-0.12	-0.124	0.022	-0.072	-0.087	0.008	-0.098	0.227	0.150	0.192
nc	6.30	-0.07	-0.085	0.003	-0.054	-0.068	-0.005	-0.079	0.238	0.156	0.201
nc	7.13	-0.04	-0.043	0.006	-0.032	-0.040	-0.004	-0.077	0.249	0.164	0.213
nc	7.96	-0.01	-0.032	0.024	-0.015	-0.029	-0.003	-0.061	0.262	0.173	0.224
nc	8.71	0.00	-0.015	0.028	-0.007	-0.011	0.001	-0.054	0.273	0.181	0.231
nd	3.33	-0.03	0.036	0.003	-0.013	0.009	-0.006	-0.030	0.460	0.318	0.376
nd	4.16	-0.01	0.017	0.008	0.004	0.013	0.002	-0.026	0.472	0.320	0.380
nd	5.00	-0.07	-0.023	-0.002	-0.030	-0.031	0.002	-0.029	0.486	0.326	0.383
nd	5.83	-0.07	-0.048	0.014	-0.034	-0.035	0.008	-0.029	0.502	0.329	0.387
nd	6.66	-0.07	-0.049	0.025	-0.024	-0.030	0.016	-0.012	0.517	0.335	0.387
nd	7.41	-0.09	-0.070	0.025	-0.035	-0.047	0.003	-0.046	0.514	0.337	0.389
ne	1.33	-0.03	-0.036	0.010	-0.013	0.023	0.096	-0.051	0.180	0.200	0.218
ne	2.16	0.09	-0.006	0.006	0.096	0.092	0.046	-0.031	0.171	0.186	0.207
ne	3.00	0.23	0.055	-0.048	0.214	0.165	-0.013	-0.011	0.175	0.178	0.201
ne	3.83	0.29	0.092	-0.020	0.236	0.162	-0.017	-0.015	0.180	0.172	0.196
ne	4.66	0.33	0.127	-0.028	0.242	0.171	-0.023	-0.002	0.188	0.169	0.192
ne	5.41	0.32	0.142	-0.049	0.228	0.160	-0.001	-0.007	0.195	0.169	0.189

Table A.6: Straight section; $x_2 = 0$, $x_3 = 0$.

case	$\frac{x_1}{h_o}$	$\frac{u^4}{u'^4}$	$\frac{v^4}{v'^4}$	$\frac{w^4}{w'^4}$	$\frac{u^3v}{u'^3v'}$	$\frac{u^2v^2}{u'^2v'^2}$	$\frac{uv^3}{u'v'^3}$	$\frac{u^3w}{u'^3w'}$	$\frac{u^2w^2}{u'^2w'^2}$	$\frac{uw^3}{u'w'^3}$	u' $(\frac{m}{s})$	v' $(\frac{m}{s})$	w' $(\frac{m}{s})$
na	5.83	2.944	3.132	3.089	1.337	1.430	1.372	0.024	1.016	0.047	0.561	0.374	0.464
na	6.66	2.956	3.137	3.115	1.353	1.430	1.351	0.082	1.030	0.077	0.596	0.397	0.491
na	7.50	2.960	3.168	3.130	1.354	1.439	1.380	0.064	1.049	0.053	0.632	0.419	0.516
na	8.33	3.017	3.208	3.130	1.338	1.420	1.344	0.055	1.022	0.035	0.686	0.444	0.550
na	9.16	3.030	3.240	3.174	1.335	1.443	1.367	0.013	1.012	0.021	0.739	0.475	0.582
na	9.91	2.997	3.291	3.210	1.334	1.442	1.378	0.002	1.052	0.026	0.785	0.500	0.615
nb	5.83	2.903	3.145	3.043	1.469	1.514	1.517	-0.156	0.996	-0.176	0.405	0.274	0.339
nb	6.66	2.868	3.087	3.026	1.412	1.458	1.449	-0.164	0.991	-0.172	0.428	0.289	0.356
nb	7.50	2.917	3.110	3.020	1.398	1.452	1.420	-0.172	0.992	-0.176	0.451	0.301	0.371
nb	8.33	2.896	3.114	3.043	1.375	1.436	1.413	-0.156	0.979	-0.183	0.478	0.318	0.387
nb	9.16	2.920	3.108	3.067	1.374	1.439	1.394	-0.195	1.023	-0.203	0.496	0.328	0.403
nb	9.91	2.951	3.120	3.021	1.374	1.438	1.385	-0.168	1.030	-0.176	0.518	0.339	0.419
nc	4.63	3.071	3.263	3.106	1.529	1.574	1.573	0.049	1.048	0.057	0.216	0.144	0.182
nc	5.46	3.006	3.200	3.093	1.481	1.532	1.517	0.080	1.052	0.099	0.227	0.150	0.192
nc	6.30	2.995	3.216	3.078	1.470	1.518	1.507	0.110	1.065	0.125	0.238	0.156	0.201
nc	7.13	2.964	3.193	3.061	1.430	1.490	1.472	0.140	1.073	0.146	0.249	0.164	0.213
nc	7.96	2.960	3.162	3.042	1.423	1.483	1.450	0.182	1.077	0.187	0.262	0.173	0.224
nc	8.71	2.943	3.134	3.073	1.384	1.453	1.414	0.156	1.070	0.176	0.273	0.181	0.231
nd	3.33	2.740	2.946	2.999	1.471	1.479	1.498	0.013	0.934	0.019	0.460	0.318	0.376
nd	4.16	2.712	2.965	3.034	1.431	1.456	1.463	0.036	0.948	0.031	0.472	0.320	0.380
nd	5.00	2.760	2.987	3.062	1.384	1.421	1.395	0.072	0.949	0.066	0.486	0.326	0.383
nd	5.83	2.746	3.071	3.004	1.329	1.374	1.360	0.056	0.928	0.072	0.502	0.329	0.387
nd	6.66	2.744	3.013	3.103	1.331	1.393	1.341	0.041	0.907	0.063	0.517	0.335	0.387
nd	7.41	2.766	3.028	3.061	1.285	1.367	1.303	0.048	0.941	0.068	0.514	0.337	0.389
ne	1.33	2.920	2.903	2.923	0.925	1.171	0.907	-0.674	1.066	-0.552	0.180	0.200	0.218
ne	2.16	3.081	2.954	2.868	1.240	1.413	1.232	-0.551	1.027	-0.329	0.171	0.186	0.207
ne	3.00	3.296	3.019	2.879	1.535	1.577	1.416	-0.464	1.009	-0.280	0.175	0.178	0.201
ne	3.83	3.341	3.035	2.819	1.621	1.630	1.510	-0.327	0.990	-0.202	0.180	0.172	0.196
ne	4.66	3.339	3.066	2.869	1.718	1.686	1.606	-0.293	0.960	-0.197	0.188	0.169	0.192
ne	5.41	3.213	3.065	2.868	1.696	1.654	1.614	-0.224	0.947	-0.169	0.195	0.169	0.189

Table A.7: Straight section; $x_2 = 0$, $x_3 = 0$.

case	$\frac{x_1}{h_2}$	L_{uu} (mm)	L_{vv} (mm)	L_{ww} (mm)	λ_u (mm)	λ_v (mm)	λ_w (mm)
na	5.83	22.5	8.3	9.9	5.0	2.7	3.1
na	6.66	24.5	8.6	10.5	5.0	2.7	3.1
na	7.50	28.0	9.4	11.2	5.2	2.7	3.1
na	8.33	32.5	10.4	12.3	5.2	2.7	3.1
na	9.16	37.0	11.5	13.1	5.3	2.8	3.2
na	9.91	37.0	11.8	14.0	5.4	2.8	3.2
nb	5.83	17.7	7.6	8.2	5.3	2.9	3.3
nb	6.66	19.8	7.9	8.7	5.4	2.9	3.3
nb	7.50	21.8	8.0	9.2	5.4	3.0	3.3
nb	8.33	24.0	8.4	9.7	5.5	2.9	3.3
nb	9.16	25.4	8.8	10.3	5.5	2.9	3.3
nb	9.91	28.6	9.2	11.0	5.6	2.9	3.3
nc	4.63	17.5	8.2	7.8	6.4	3.7	4.0
nc	5.46	18.8	8.5	8.5	6.8	3.9	4.2
nc	6.30	20.2	8.9	8.9	6.9	3.8	4.2
nc	7.13	21.0	9.0	9.2	7.0	3.9	4.3
nc	7.96	22.1	9.1	9.6	7.0	3.9	4.3
nc	8.71	22.9	9.2	9.6	7.0	3.9	4.3
nd	3.33	70.4	30.9	26.1	9.8	5.1	5.9
nd	4.16	78.4	31.4	26.9	9.9	5.2	5.9
nd	5.00	86.8	30.8	27.6	9.8	5.0	5.9
nd	5.83	92.4	31.0	28.2	9.9	4.9	5.9
nd	6.66	95.5	31.1	28.1	10.1	4.9	5.6
nd	7.41	82.5	28.5	28.4	9.9	4.9	5.5
ne	1.33	30.6	28.5	22.4	4.4	3.7	3.9
ne	2.16	47.5	37.2	24.3	6.0	4.9	5.2
ne	3.00	55.3	38.1	25.9	7.4	5.7	6.2
ne	3.83	62.3	39.0	26.9	8.6	6.2	6.6
ne	4.66	68.4	39.1	27.7	9.6	6.4	7.1
ne	5.41	73.3	40.7	28.1	10.3	6.6	7.3

Table A.8: Straight section; $x_2 = 0$, $x_3 = 0$.

case	$\frac{h}{R_c}$	r	U ($\frac{m}{s}$)	V ($\frac{m}{s}$)	W ($\frac{m}{s}$)	$\overline{u'u'}$	$\overline{v'v'}$	$\overline{w'w'}$	$\overline{u'v'}$	$\overline{v'w'}$	$\overline{u'w'}$ ($\frac{m^2}{s^2}$)
pa	0.42	0.67	9.961	-0.139	-0.030	0.503	0.195	0.302	-0.124	-0.031	1.658981
pa	1.25	2.00	10.055	-0.170	0.017	0.513	0.198	0.289	-0.124	-0.032	1.766546
pa	2.08	3.33	10.040	-0.159	0.050	0.523	0.201	0.276	-0.122	-0.051	1.793158
pa	2.92	4.66	9.868	-0.003	0.066	0.501	0.198	0.302	-0.110	-0.013	1.794372
pa	3.75	5.99	10.098	-0.151	0.120	0.504	0.204	0.292	-0.127	-0.020	1.857193
pa	4.58	7.33	9.746	-0.075	0.071	0.494	0.200	0.306	-0.119	-0.023	1.817850
pa	5.42	8.66	9.766	-0.064	0.107	0.493	0.202	0.306	-0.122	-0.011	1.906667
pa	6.25	9.99	9.627	0.175	0.067	0.490	0.193	0.317	-0.109	-0.010	1.953402
pb	0.42	0.50	10.413	-0.130	-0.037	0.484	0.208	0.308	-0.131	-0.002	0.662153
pb	1.25	1.50	10.615	-0.170	0.018	0.486	0.207	0.305	-0.122	-0.011	0.688195
pb	2.08	2.50	10.580	-0.155	0.055	0.508	0.209	0.283	-0.124	-0.031	0.690537
pb	2.92	3.50	10.396	-0.004	0.067	0.490	0.202	0.308	-0.107	-0.004	0.682624
pb	3.75	4.50	10.586	-0.140	0.132	0.491	0.210	0.299	-0.125	-0.008	0.683253
pb	4.58	5.50	10.254	-0.058	0.085	0.482	0.205	0.313	-0.118	-0.010	0.666552
pb	5.42	6.50	10.234	-0.028	0.122	0.480	0.204	0.315	-0.116	-0.010	0.669419
pb	6.25	7.50	10.067	0.212	0.084	0.482	0.198	0.320	-0.109	-0.008	0.705739
pc	0.42	0.29	10.436	-0.092	0.005	0.460	0.205	0.334	-0.128	-0.039	0.176035
pc	1.25	0.86	10.705	-0.141	0.039	0.469	0.205	0.325	-0.120	-0.036	0.184203
pc	2.08	1.43	10.731	-0.131	0.074	0.487	0.211	0.302	-0.117	-0.044	0.184717
pc	2.92	2.00	10.435	0.023	0.072	0.466	0.207	0.327	-0.098	-0.027	0.181889
pc	3.75	2.57	10.660	-0.115	0.148	0.478	0.218	0.305	-0.114	-0.004	0.178173
pc	4.58	3.15	10.359	-0.030	0.097	0.472	0.213	0.315	-0.102	-0.013	0.171575
pc	5.42	3.72	10.456	0.008	0.133	0.469	0.213	0.319	-0.100	-0.033	0.173581
pc	6.25	4.29	10.294	0.245	0.095	0.464	0.211	0.324	-0.092	-0.016	0.167614
pd	0.42	0.11	10.525	-0.056	-0.057	0.465	0.224	0.310	-0.137	-0.002	0.465808
pd	1.25	0.33	10.793	-0.114	0.003	0.477	0.225	0.298	-0.121	-0.013	0.461512
pd	2.08	0.55	10.809	-0.112	0.029	0.489	0.214	0.296	-0.110	-0.015	0.449532
pd	2.92	0.78	10.545	0.049	0.053	0.498	0.208	0.294	-0.087	0.001	0.421384
pd	3.75	1.00	10.717	-0.079	0.122	0.501	0.212	0.286	-0.087	-0.008	0.401160
pd	4.58	1.22	10.560	0.018	0.070	0.501	0.210	0.289	-0.073	-0.010	0.379031
pd	5.42	1.44	10.668	0.073	0.113	0.498	0.211	0.291	-0.059	0.000	0.369928
pd	6.25	1.66	10.512	0.320	-0.012	0.576	0.245	0.179	-0.044	-0.160	0.289644
pe	0.42	0.03	9.638	-0.048	-0.063	0.350	0.293	0.357	-0.140	0.019	0.113070
pe	1.25	0.09	9.896	-0.117	-0.018	0.360	0.287	0.353	-0.127	0.013	0.109442
pe	2.08	0.16	9.904	-0.133	0.014	0.380	0.280	0.339	-0.122	0.006	0.105047
pe	2.92	0.22	9.830	0.000	0.014	0.384	0.267	0.349	-0.099	0.007	0.098763
pe	3.75	0.28	10.048	-0.120	0.097	0.399	0.267	0.333	-0.106	0.015	0.094732
pe	4.58	0.34	9.913	-0.035	0.045	0.401	0.260	0.339	-0.085	0.010	0.089205
pe	5.42	0.41	10.067	0.007	0.089	0.409	0.261	0.331	-0.071	0.019	0.087880
pe	6.25	0.47	9.931	0.225	0.054	0.433	0.265	0.302	-0.057	-0.026	0.078918

Table A.9: Mildly curved section; n=0, z=0, R_c=5 m.

case	$\frac{z}{R_c}$	$\frac{\overline{u'^3}}{u'^3}$	$\frac{\overline{v'^3}}{v'^3}$	$\frac{\overline{w'^3}}{w'^3}$	$\frac{\overline{u'^2v'}}{u'^2v'}$	$\frac{\overline{u'v'^2}}{u'v'^2}$	$\frac{\overline{u'^2w'}}{u'^2w'}$	$\frac{\overline{u'w'^2}}{u'w'^2}$	u' $(\frac{m}{s})$	v' $(\frac{m}{s})$	w' $(\frac{m}{s})$
pa	0.42	-0.05	-0.004	0.015	0.017	-0.010	0.009	0.000	0.913	0.569	0.708
pa	1.25	-0.03	-0.013	0.031	0.016	-0.017	0.007	-0.004	0.952	0.591	0.715
pa	2.08	-0.05	0.000	0.006	0.020	-0.021	0.006	-0.011	0.968	0.600	0.704
pa	2.92	-0.03	-0.018	0.033	0.010	-0.004	0.046	-0.019	0.948	0.595	0.736
pa	3.75	-0.06	0.005	0.002	0.021	-0.017	0.006	-0.007	0.968	0.615	0.736
pa	4.58	-0.02	-0.007	0.015	0.013	-0.009	0.011	0.011	0.948	0.603	0.746
pa	5.42	0.00	-0.020	-0.007	0.000	0.003	0.001	0.010	0.969	0.620	0.763
pa	6.25	0.00	-0.039	0.012	0.004	0.005	0.006	0.015	0.979	0.614	0.787
pb	0.42	-0.06	0.049	0.005	0.034	-0.039	-0.019	-0.018	0.566	0.371	0.451
pb	1.25	-0.08	0.063	-0.001	0.041	-0.047	-0.004	-0.027	0.580	0.377	0.458
pb	2.08	-0.06	0.047	0.012	0.041	-0.049	-0.009	-0.027	0.592	0.380	0.442
pb	2.92	-0.11	0.060	-0.005	0.044	-0.051	-0.003	-0.017	0.578	0.371	0.459
pb	3.75	-0.07	0.052	0.002	0.039	-0.046	-0.002	-0.032	0.579	0.379	0.452
pb	4.58	-0.09	0.063	-0.012	0.041	-0.048	-0.005	-0.037	0.567	0.370	0.457
pb	5.42	-0.09	0.046	0.021	0.051	-0.053	-0.007	-0.035	0.576	0.375	0.466
pb	6.25	-0.07	0.043	0.006	0.038	-0.045	-0.011	-0.036	0.583	0.374	0.475
pc	0.42	-0.20	0.166	0.101	0.094	-0.120	0.059	-0.116	0.285	0.190	0.243
pc	1.25	-0.18	0.158	0.089	0.084	-0.116	0.058	-0.106	0.294	0.195	0.245
pc	2.08	-0.14	0.120	0.074	0.070	-0.091	0.036	-0.096	0.300	0.197	0.236
pc	2.92	-0.12	0.112	0.049	0.060	-0.086	0.045	-0.095	0.291	0.194	0.244
pc	3.75	-0.10	0.092	0.006	0.053	-0.064	-0.005	-0.074	0.292	0.197	0.233
pc	4.58	-0.07	0.054	0.012	0.033	-0.045	0.015	-0.065	0.284	0.191	0.232
pc	5.42	-0.08	0.047	0.020	0.033	-0.040	0.021	-0.058	0.285	0.192	0.235
pc	6.25	-0.02	0.013	0.021	0.019	-0.022	0.011	-0.047	0.279	0.188	0.233
pd	0.42	-0.23	0.153	0.025	0.113	-0.127	-0.002	-0.087	0.465	0.323	0.380
pd	1.25	-0.24	0.164	0.043	0.099	-0.127	0.013	-0.095	0.469	0.322	0.371
pd	2.08	-0.26	0.178	0.042	0.095	-0.131	0.022	-0.092	0.469	0.310	0.365
pd	2.92	-0.26	0.159	0.015	0.094	-0.132	-0.003	-0.075	0.458	0.296	0.352
pd	3.75	-0.25	0.133	0.028	0.080	-0.128	0.006	-0.086	0.448	0.292	0.339
pd	4.58	-0.22	0.124	0.020	0.070	-0.120	0.018	-0.089	0.436	0.282	0.331
pd	5.42	-0.17	0.081	0.017	0.056	-0.099	-0.007	-0.068	0.429	0.279	0.328
pd	6.25	-0.20	0.055	0.235	0.062	-0.094	0.084	-0.029	0.408	0.266	0.228
pe	0.42	-0.09	0.130	0.033	0.070	-0.088	-0.014	-0.054	0.199	0.182	0.201
pe	1.25	-0.09	0.116	0.049	0.064	-0.083	-0.009	-0.054	0.199	0.177	0.196
pe	2.08	-0.09	0.131	0.052	0.060	-0.090	0.000	-0.040	0.200	0.172	0.189
pe	2.92	-0.09	0.113	0.055	0.050	-0.067	0.003	-0.037	0.195	0.162	0.186
pe	3.75	-0.10	0.107	0.047	0.054	-0.072	-0.015	-0.046	0.194	0.159	0.178
pe	4.58	-0.09	0.098	0.073	0.044	-0.071	0.003	-0.027	0.189	0.152	0.174
pe	5.42	-0.05	0.072	0.073	0.019	-0.038	0.005	-0.014	0.190	0.151	0.170
pe	6.25	-0.09	0.056	0.073	0.025	-0.055	0.006	-0.018	0.185	0.145	0.154

Table A.10: Mildly curved section; n=0, z=0, R_c=5 m.

case	$\frac{z}{h_c}$	$\frac{u^4}{u'^4}$	$\frac{v^4}{v'^4}$	$\frac{w^4}{w'^4}$	$\frac{u^3v}{u'^3v'}$	$\frac{u^2v^2}{u'^2v'^2}$	$\frac{uv^3}{u'v'^3}$	$\frac{u^3w}{u'^3w'}$	$\frac{u^2w^2}{u'^2w'^2}$	$\frac{uw^3}{u'w'^3}$	u' ($\frac{m}{s}$)	v' ($\frac{m}{s}$)	w' ($\frac{m}{s}$)
pa	0.42	3.016	3.262	3.201	-1.182	1.349	-1.180	-0.256	1.073	-0.232	0.913	0.569	0.708
pa	1.25	3.008	3.262	3.186	-1.147	1.329	-1.157	-0.267	1.060	-0.252	0.952	0.591	0.715
pa	2.08	2.967	3.258	3.174	-1.089	1.301	-1.109	-0.382	1.032	-0.402	0.968	0.600	0.704
pa	2.92	2.953	3.254	3.163	-1.023	1.277	-1.043	-0.082	1.026	-0.099	0.948	0.595	0.736
pa	3.75	2.970	3.249	3.186	-1.140	1.318	-1.169	-0.133	0.998	-0.138	0.968	0.615	0.736
pa	4.58	2.962	3.227	3.170	-1.085	1.302	-1.105	-0.162	1.028	-0.174	0.948	0.603	0.746
pa	5.42	2.936	3.224	3.140	-1.103	1.304	-1.118	-0.054	1.007	-0.067	0.969	0.620	0.763
pa	6.25	2.909	3.201	3.143	-0.994	1.233	-1.006	-0.077	1.034	-0.048	0.979	0.614	0.787
pb	0.42	2.943	3.186	3.116	-1.189	1.333	-1.192	-0.018	1.035	-0.025	0.566	0.371	0.451
pb	1.25	2.939	3.237	3.121	-1.111	1.312	-1.141	-0.072	1.034	-0.102	0.580	0.377	0.458
pb	2.08	2.960	3.217	3.141	-1.106	1.308	-1.127	-0.225	0.963	-0.252	0.592	0.380	0.442
pb	2.92	2.983	3.256	3.156	-1.006	1.264	-1.027	-0.066	1.007	-0.043	0.578	0.371	0.459
pb	3.75	3.000	3.283	3.154	-1.170	1.353	-1.187	-0.052	0.998	-0.062	0.579	0.379	0.452
pb	4.58	3.017	3.279	3.136	-1.123	1.328	-1.142	-0.091	1.051	-0.079	0.567	0.370	0.457
pb	5.42	3.013	3.281	3.141	-1.099	1.311	-1.116	-0.079	1.046	-0.066	0.576	0.375	0.466
pb	6.25	2.999	3.271	3.177	-1.044	1.260	-1.050	-0.053	1.049	-0.064	0.583	0.374	0.475
pc	0.42	2.991	3.239	3.097	-1.229	1.381	-1.264	-0.294	1.114	-0.274	0.285	0.190	0.243
pc	1.25	2.965	3.260	3.074	-1.122	1.325	-1.150	-0.290	1.093	-0.271	0.294	0.195	0.245
pc	2.08	2.945	3.211	3.107	-1.050	1.270	-1.072	-0.291	0.997	-0.335	0.300	0.197	0.236
pc	2.92	2.957	3.257	3.101	-0.913	1.221	-0.946	-0.213	1.067	-0.200	0.291	0.194	0.244
pc	3.75	2.936	3.176	3.113	-1.017	1.244	-1.037	-0.019	0.963	-0.041	0.292	0.197	0.233
pc	4.58	2.929	3.200	3.106	-0.921	1.206	-0.941	-0.099	1.004	-0.100	0.284	0.191	0.232
pc	5.42	2.956	3.195	3.092	-0.913	1.198	-0.924	-0.240	1.027	-0.217	0.285	0.192	0.235
pc	6.25	2.971	3.174	3.100	-0.849	1.182	-0.858	-0.110	1.033	-0.102	0.279	0.188	0.233
pd	0.42	2.980	3.182	3.089	-1.218	1.353	-1.186	0.001	1.002	0.007	0.465	0.323	0.380
pd	1.25	2.942	3.191	3.083	-1.051	1.276	-1.071	-0.071	0.998	-0.085	0.469	0.322	0.371
pd	2.08	2.960	3.247	3.046	-0.962	1.232	-0.974	-0.115	0.977	-0.103	0.469	0.310	0.365
pd	2.92	2.931	3.241	3.057	-0.762	1.144	-0.776	-0.005	0.947	0.033	0.458	0.296	0.352
pd	3.75	2.891	3.235	3.144	-0.718	1.115	-0.746	-0.035	0.944	-0.059	0.448	0.292	0.339
pd	4.58	2.844	3.240	3.107	-0.612	1.083	-0.621	-0.070	0.958	-0.046	0.436	0.282	0.331
pd	5.42	2.844	3.211	3.133	-0.494	1.051	-0.510	0.013	0.964	0.036	0.429	0.279	0.328
pd	6.25	2.903	3.262	3.316	-0.313	1.026	-0.323	-1.152	1.294	-1.410	0.408	0.266	0.228
pe	0.42	2.818	2.842	2.911	-1.108	1.240	-1.125	0.168	0.993	0.162	0.199	0.182	0.201
pe	1.25	2.853	2.887	2.940	-1.024	1.210	-1.025	0.126	0.963	0.127	0.199	0.177	0.196
pe	2.08	2.878	2.907	2.948	-0.957	1.172	-0.957	0.057	0.952	0.090	0.200	0.172	0.189
pe	2.92	2.830	2.935	2.970	-0.785	1.113	-0.786	0.071	1.011	0.095	0.195	0.162	0.186
pe	3.75	2.836	2.928	2.980	-0.811	1.110	-0.807	0.155	0.926	0.140	0.194	0.159	0.178
pe	4.58	2.779	2.956	3.012	-0.638	1.062	-0.639	0.100	0.977	0.127	0.189	0.152	0.174
pe	5.42	2.770	3.020	2.971	-0.502	1.009	-0.516	0.151	0.962	0.206	0.190	0.151	0.170
pe	6.25	2.784	3.006	3.195	-0.381	1.005	-0.383	-0.126	1.023	-0.039	0.185	0.145	0.154

Table A.11: Mildly curved section; n=0, z=0, R_c=5m.

case	$\frac{z}{h_c}$	L_{uu} (mm)	L_{vv} (mm)	L_{ww} (mm)	λ_u (mm)	λ_v (mm)	λ_w (mm)
pa	0.42	39.3	11.2	15.0	5.3	2.6	3.1
pa	1.25	38.1	11.5	15.6	5.4	2.6	3.1
pa	2.08	34.6	10.9	16.1	5.3	2.6	3.9
pa	2.92	33.5	11.1	16.0	5.3	2.7	3.2
pa	3.75	35.6	12.1	16.4	5.4	2.8	3.1
pa	4.58	35.1	12.1	17.3	5.3	2.7	3.2
pa	5.42	37.6	13.2	18.4	5.3	2.8	3.3
pa	6.25	37.3	12.8	19.6	5.3	2.7	3.4
pb	0.42	27.6	8.7	11.1	5.3	2.7	3.1
pb	1.25	27.9	8.2	11.8	5.3	2.7	3.2
pb	2.08	25.5	8.1	12.2	5.3	2.7	3.8
pb	2.92	24.1	7.8	12.1	5.2	2.6	3.2
pb	3.75	25.5	8.6	12.2	5.3	2.7	3.1
pb	4.58	25.2	8.4	12.8	5.3	2.7	3.2
pb	5.42	26.5	8.8	13.4	5.3	2.7	3.3
pb	6.25	25.7	9.0	13.8	5.3	2.7	3.5
pc	0.42	21.2	8.4	9.8	6.4	3.5	4.0
pc	1.25	22.6	8.1	10.0	6.3	3.4	3.9
pc	2.08	20.7	7.5	10.4	6.3	3.4	4.7
pc	2.92	19.9	7.0	10.3	6.1	3.2	3.7
pc	3.75	19.3	7.3	10.0	6.2	3.4	3.7
pc	4.58	19.1	7.0	10.0	6.1	3.3	3.7
pc	5.42	19.3	7.1	10.7	6.1	3.2	3.8
pc	6.25	18.6	7.0	10.7	6.0	3.2	3.8
pd	0.42	67.8	25.1	28.3	8.7	4.6	5.4
pd	1.25	68.2	23.2	27.9	8.7	4.5	5.3
pd	2.08	65.8	20.6	28.4	8.8	4.4	5.2
pd	2.92	57.1	18.3	26.3	8.7	4.2	4.8
pd	3.75	54.6	17.8	27.0	8.9	4.4	5.1
pd	4.58	50.5	16.6	25.7	8.8	4.3	5.0
pd	5.42	48.6	16.4	26.4	8.7	4.2	5.0
pd	6.25	47.0	16.1	25.6	8.5	4.1	4.5
pe	0.42	49.0	28.7	27.0	9.5	6.6	7.0
pe	1.25	47.2	27.1	27.2	9.5	6.4	7.1
pe	2.08	49.2	25.6	27.4	10.0	6.4	7.0
pe	2.92	48.1	23.6	26.7	9.6	6.0	6.9
pe	3.75	49.7	23.0	26.2	10.1	6.1	6.8
pe	4.58	45.5	20.6	26.2	10.0	6.0	6.7
pe	5.42	45.3	20.2	25.6	9.8	5.8	6.8
pe	6.25	43.5	18.2	25.3	10.0	5.8	7.2

Table A.12: Mildly curved section; n=0, z=0, R_c=5 m.

case	$\frac{z}{R_c}$	r	U ($\frac{m}{s}$)	V ($\frac{m}{s}$)	W ($\frac{m}{s}$)	$\frac{u'u'}{U_{max}^2}$	$\frac{v'v'}{U_{max}^2}$	$\frac{w'w'}{U_{max}^2}$	$\frac{u'v'}{U_{max}^2}$	$\frac{u'w'}{U_{max}^2}$	$\frac{e}{(\frac{m^2}{s^2})}$
na	0.42	0.67	10.249	0.230	-0.065	0.492	0.208	0.300	0.148	0 008	1.422473
na	1.25	2.00	10.531	0.142	-0.004	0.491	0.205	0.304	0.150	0.019	1.640954
na	2.08	3.33	10.590	0.118	0.015	0.500	0.203	0.297	0.155	0.016	1.970502
na	2.92	4.67	10.522	0.153	0.064	0.511	0.203	0.287	0.148	0.045	2.345715
na	3.75	6.00	10.615	0.172	0.007	0.520	0.202	0.278	0.153	0.037	2.822464
na	4.58	7.34	10.634	0.284	0.076	0.505	0.206	0.289	0.153	0.019	3.270374
na	5.42	8.67	10.711	0.387	0.196	0.532	0.218	0.251	0.164	0.047	3.480301
na	6.25	10.00	10.742	0.610	0.067	0.501	0.217	0.283	0.167	0.030	4.308477
nb	0.42	0.50	9.864	0.150	-0.081	0.477	0.216	0.307	0.153	0.034	0.609305
nb	1.25	1.50	10.107	0.032	-0.032	0.477	0.216	0.307	0.157	0.043	0.662108
nb	2.08	2.50	10.231	-0.029	-0.035	0.492	0.213	0.295	0.158	0.052	0.779988
nb	2.92	3.50	10.072	-0.003	-0.011	0.501	0.208	0.292	0.154	0.064	0.880595
nb	3.75	4.50	10.012	-0.036	0.018	0.512	0.206	0.282	0.153	0.061	1.037713
nb	4.58	5.50	9.914	0.033	-0.024	0.514	0.205	0.281	0.154	0.070	1.170612
nb	5.42	6.50	9.857	0.076	0.036	0.516	0.208	0.277	0.157	0.073	1.332776
nb	6.25	7.50	9.667	0.224	-0.050	0.508	0.205	0.287	0.158	0.086	1.616497
nc	0.42	0.29	10.084	0.131	-0.042	0.470	0.216	0.314	0.157	-0.046	0.170480
nc	1.25	0.86	10.217	0.021	0.022	0.465	0.223	0.312	0.163	-0.043	0.184130
nc	2.08	1.43	10.287	-0.024	-0.006	0.459	0.221	0.321	0.164	-0.026	0.206967
nc	2.92	2.00	10.269	0.005	0.008	0.459	0.221	0.320	0.161	-0.016	0.224940
nc	3.75	2.57	10.406	0.014	0.104	0.465	0.222	0.313	0.163	-0.021	0.260441
nc	4.58	3.15	10.152	0.047	0.026	0.467	0.226	0.307	0.167	-0.047	0.279297
nc	5.42	3.72	10.138	0.060	0.057	0.457	0.220	0.323	0.162	-0.039	0.312997
nc	6.25	4.29	10.298	0.367	-0.024	0.477	0.227	0.296	0.176	-0.040	0.391356
nd	0.42	0.17	9.963	0.062	-0.067	0.492	0.225	0.283	0.167	0.011	0.524663
nd	1.25	0.50	10.132	-0.030	-0.003	0.485	0.231	0.284	0.178	0.021	0.565330
nd	2.08	0.83	10.077	-0.068	0.206	0.477	0.240	0.283	0.183	0.032	0.568056
nd	2.92	1.17	10.080	-0.022	0.040	0.468	0.242	0.290	0.183	0.036	0.577241
nd	3.75	1.50	10.223	-0.033	0.137	0.468	0.250	0.282	0.193	0.022	0.623364
nd	4.58	1.84	10.087	0.040	0.053	0.473	0.255	0.272	0.204	0.018	0.660242
nd	5.42	2.17	10.048	0.077	0.110	0.472	0.260	0.268	0.209	0.021	0.679740
nd	6.25	2.50	10.047	0.307	0.041	0.470	0.260	0.270	0.218	0.024	0.739272
ne	0.42	0.06	9.401	0.031	-0.068	0.375	0.294	0.330	0.174	0.028	0.095131
ne	1.25	0.19	9.626	-0.025	-0.006	0.351	0.277	0.372	0.148	0.042	0.091065
ne	2.08	0.31	9.572	-0.077	0.166	0.374	0.307	0.318	0.194	0.041	0.101384
ne	2.92	0.44	9.542	-0.044	0.014	0.366	0.312	0.321	0.202	0.029	0.104828
ne	3.75	0.56	9.637	-0.066	0.115	0.365	0.316	0.319	0.206	0.034	0.105270
ne	4.58	0.69	9.575	-0.005	0.042	0.368	0.328	0.305	0.218	0.027	0.109547
ne	5.42	0.81	9.473	0.024	0.089	0.361	0.323	0.317	0.213	0.039	0.111114
ne	6.25	0.94	9.515	0.235	0.040	0.362	0.334	0.304	0.229	0.029	0.119676

Table A.13: Mildly curved section; n=0, z=0, R_c=5 m.

case	$\frac{z}{h_c}$	$\frac{u^3}{u^{*3}}$	$\frac{v^3}{v^{*3}}$	$\frac{w^3}{w^{*3}}$	$\frac{u^2v}{u^{*2}v^*}$	$\frac{uv^2}{u^*v^{*2}}$	$\frac{u^2w}{u^{*2}w^*}$	$\frac{uw^2}{u^*w^{*2}}$	u' $(\frac{m}{s})$	v' $(\frac{m}{s})$	w' $(\frac{m}{s})$
na	0.42	-0.05	-0.019	-0.018	-0.025	-0.021	-0.007	-0.039	0.837	0.543	0.634
na	1.25	-0.07	-0.024	-0.031	-0.025	-0.024	-0.041	-0.037	0.897	0.580	0.707
na	2.08	-0.09	-0.038	-0.018	-0.035	-0.034	-0.022	-0.054	0.993	0.632	0.765
na	2.92	-0.10	-0.047	-0.039	-0.032	-0.030	0.007	-0.084	1.094	0.690	0.820
na	3.75	-0.10	-0.039	-0.015	-0.032	-0.031	-0.007	-0.096	1.211	0.755	0.886
na	4.58	-0.12	-0.068	-0.041	-0.044	-0.049	-0.025	-0.074	1.286	0.820	0.972
na	5.42	-0.13	-0.063	-0.022	-0.054	-0.055	0.041	-0.131	1.360	0.871	0.934
na	6.25	-0.15	-0.076	-0.006	-0.061	-0.059	-0.001	-0.115	1.468	0.966	1.104
nb	0.42	-0.03	-0.007	-0.064	-0.016	-0.018	-0.028	-0.026	0.539	0.363	0.432
nb	1.25	-0.08	-0.041	-0.062	-0.041	-0.038	-0.030	-0.033	0.562	0.378	0.451
nb	2.08	-0.09	-0.036	-0.096	-0.038	-0.040	-0.057	-0.040	0.620	0.407	0.480
nb	2.92	-0.11	-0.052	-0.082	-0.045	-0.052	-0.019	-0.040	0.664	0.428	0.507
nb	3.75	-0.11	-0.044	-0.097	-0.039	-0.046	-0.030	-0.033	0.729	0.462	0.541
nb	4.58	-0.11	-0.052	-0.120	-0.039	-0.050	-0.069	-0.043	0.775	0.490	0.574
nb	5.42	-0.12	-0.057	-0.127	-0.048	-0.058	-0.067	-0.036	0.829	0.526	0.607
nb	6.25	-0.10	-0.028	-0.137	-0.031	-0.039	-0.057	-0.035	0.906	0.576	0.681
nc	0.42	0.01	-0.001	-0.023	0.009	0.007	-0.008	-0.037	0.283	0.192	0.231
nc	1.25	0.03	0.006	-0.017	0.022	0.013	-0.009	-0.020	0.293	0.203	0.240
nc	2.08	0.02	0.015	-0.079	0.016	0.017	-0.009	-0.035	0.308	0.214	0.258
nc	2.92	0.04	0.010	-0.076	0.021	0.017	-0.010	-0.044	0.321	0.223	0.268
nc	3.75	0.07	0.045	-0.107	0.039	0.038	-0.039	-0.026	0.348	0.240	0.285
nc	4.58	0.08	0.016	-0.106	0.039	0.032	-0.051	0.016	0.361	0.251	0.293
nc	5.42	0.06	0.014	-0.104	0.021	0.019	-0.034	-0.025	0.378	0.262	0.318
nc	6.25	0.05	0.035	-0.145	0.030	0.034	-0.051	-0.020	0.432	0.298	0.340
nd	0.42	-0.07	-0.068	0.017	-0.026	-0.042	-0.011	-0.024	0.508	0.344	0.385
nd	1.25	-0.06	-0.051	-0.018	-0.021	-0.032	-0.011	-0.031	0.524	0.361	0.401
nd	2.08	-0.07	-0.049	-0.008	-0.032	-0.033	-0.016	-0.056	0.520	0.369	0.401
nd	2.92	-0.08	-0.077	-0.010	-0.043	-0.050	0.025	-0.052	0.520	0.374	0.409
nd	3.75	-0.11	-0.086	-0.007	-0.047	-0.050	0.004	-0.032	0.540	0.395	0.419
nd	4.58	-0.11	-0.093	-0.013	-0.052	-0.057	-0.008	-0.057	0.559	0.411	0.423
nd	5.42	-0.15	-0.118	-0.012	-0.079	-0.075	-0.002	-0.078	0.566	0.420	0.427
nd	6.25	-0.21	-0.176	-0.054	-0.108	-0.113	-0.017	-0.078	0.589	0.439	0.447
ne	0.42	0.29	0.130	0.012	0.208	0.150	0.000	0.007	0.189	0.167	0.177
ne	1.25	0.27	0.129	0.035	0.194	0.139	0.013	0.013	0.179	0.159	0.184
ne	2.08	0.26	0.157	0.053	0.181	0.145	0.017	0.032	0.195	0.177	0.180
ne	2.92	0.23	0.129	0.037	0.169	0.132	0.012	0.027	0.196	0.181	0.184
ne	3.75	0.25	0.135	0.056	0.176	0.141	0.016	0.023	0.196	0.182	0.183
ne	4.58	0.23	0.175	0.080	0.169	0.149	0.005	0.054	0.201	0.189	0.183
ne	5.42	0.20	0.132	0.061	0.145	0.130	0.004	0.040	0.200	0.189	0.188
ne	6.25	0.16	0.083	0.061	0.112	0.089	0.029	0.041	0.208	0.200	0.191

Table A.14: Mildly curved section; n=0, z=0, R_c=5 m.

case	$\frac{z}{h_c}$	$\frac{u^4}{u'^4}$	$\frac{v^4}{v'^4}$	$\frac{w^4}{w'^4}$	$\frac{u^3v}{u'^3v'}$	$\frac{u^2v^2}{u'^2v'^2}$	$\frac{uv^3}{u'v'^3}$	$\frac{u^3w}{u'^3w'}$	$\frac{u^2w^2}{u'^2w'^2}$	$\frac{uw^3}{u'w'^3}$	u' $(\frac{m}{s})$	v' $(\frac{m}{s})$	w' $(\frac{m}{s})$
na	0.42	3.072	3.229	3.190	1.405	1.492	1.410	0.047	1.047	0.037	0.837	0.543	0.634
na	1.25	3.000	3.214	3.207	1.388	1.465	1.411	0.168	1.116	0.157	0.897	0.560	0.707
na	2.08	2.990	3.176	3.185	1.441	1.502	1.437	0.133	1.117	0.124	0.993	0.632	0.765
na	2.92	2.978	3.191	3.188	1.326	1.433	1.353	0.345	1.029	0.335	1.094	0.690	0.820
na	3.75	2.933	3.167	3.195	1.344	1.437	1.361	0.315	1.004	0.288	1.211	0.755	0.886
na	4.58	2.857	3.144	3.169	1.303	1.394	1.332	0.133	1.074	0.154	1.286	0.820	0.972
na	5.42	2.887	3.077	3.256	1.336	1.406	1.332	0.313	0.886	0.382	1.360	0.871	0.934
na	6.25	2.855	3.039	3.144	1.399	1.439	1.398	0.265	1.036	0.223	1.468	0.966	1.104
nb	0.42	2.954	3.135	3.073	1.390	1.456	1.406	0.255	1.036	0.242	0.539	0.363	0.432
nb	1.25	2.987	3.148	3.050	1.418	1.475	1.435	0.327	1.071	0.314	0.562	0.378	0.451
nb	2.08	2.946	3.140	3.089	1.407	1.470	1.417	0.390	1.064	0.396	0.620	0.407	0.480
nb	2.92	2.968	3.226	3.104	1.392	1.467	1.417	0.458	1.064	0.483	0.664	0.428	0.507
nb	3.75	2.957	3.171	3.083	1.358	1.447	1.370	0.433	1.045	0.477	0.729	0.462	0.541
nb	4.58	2.922	3.126	3.144	1.344	1.426	1.348	0.520	1.074	0.524	0.775	0.490	0.574
nb	5.42	2.940	3.201	3.129	1.381	1.461	1.410	0.523	1.082	0.542	0.829	0.526	0.607
nb	6.25	2.913	3.159	3.126	1.402	1.464	1.407	0.628	1.155	0.629	0.906	0.576	0.681
nc	0.42	2.968	3.136	3.041	1.436	1.487	1.454	-0.352	1.006	-0.338	0.283	0.192	0.231
nc	1.25	3.021	3.114	3.054	1.523	1.541	1.510	-0.303	0.956	-0.320	0.293	0.203	0.240
nc	2.08	2.992	3.122	3.060	1.495	1.527	1.525	-0.184	1.022	-0.193	0.308	0.214	0.258
nc	2.92	2.958	3.102	3.067	1.466	1.513	1.482	-0.104	1.034	-0.111	0.321	0.223	0.268
nc	3.75	3.007	3.138	3.109	1.491	1.533	1.510	-0.150	1.017	-0.158	0.348	0.240	0.285
nc	4.58	3.019	3.124	3.126	1.512	1.545	1.516	-0.365	1.006	-0.368	0.361	0.251	0.293
nc	5.42	2.975	3.115	3.069	1.483	1.527	1.504	-0.301	1.145	-0.275	0.378	0.262	0.318
nc	6.25	2.900	3.031	3.073	1.508	1.527	1.516	-0.281	1.029	-0.279	0.432	0.298	0.340
nd	0.42	2.822	3.031	3.075	1.377	1.420	1.383	0.076	0.958	0.095	0.508	0.344	0.385
nd	1.25	2.759	2.982	3.108	1.420	1.454	1.441	0.149	0.938	0.165	0.524	0.361	0.401
nd	2.08	2.732	2.965	3.132	1.429	1.461	1.475	0.267	0.984	0.268	0.520	0.369	0.401
nd	2.92	2.757	2.930	3.049	1.466	1.483	1.467	0.262	0.986	0.268	0.520	0.374	0.409
nd	3.75	2.749	2.911	3.134	1.495	1.491	1.494	0.178	1.002	0.183	0.540	0.395	0.419
nd	4.58	2.697	2.913	3.110	1.537	1.533	1.575	0.148	0.937	0.170	0.559	0.411	0.423
nd	5.42	2.704	2.847	3.069	1.564	1.553	1.590	0.164	0.957	0.166	0.566	0.420	0.427
nd	6.25	2.662	2.800	3.093	1.584	1.560	1.616	0.191	0.975	0.221	0.589	0.439	0.447
ne	0.42	3.168	3.043	2.871	1.653	1.630	1.607	0.209	0.918	0.205	0.189	0.167	0.177
ne	1.25	3.319	3.439	2.894	1.705	1.793	1.765	0.341	1.122	0.313	0.179	0.159	0.184
ne	2.08	3.037	2.974	2.920	1.685	1.643	1.676	0.298	0.921	0.321	0.195	0.177	0.180
ne	2.92	2.986	2.948	2.903	1.742	1.688	1.724	0.222	0.959	0.227	0.196	0.181	0.184
ne	3.75	2.949	2.960	2.904	1.738	1.691	1.747	0.252	0.978	0.270	0.196	0.182	0.183
ne	4.58	2.920	2.920	2.954	1.764	1.706	1.777	0.213	0.943	0.243	0.201	0.189	0.183
ne	5.42	2.844	2.920	2.957	1.722	1.685	1.759	0.315	1.009	0.322	0.200	0.189	0.188
ne	6.25	2.779	2.768	2.937	1.759	1.692	1.766	0.237	0.980	0.238	0.208	0.200	0.191

Table A.15: Mildly curved section; n=0, z=0, R_c=5 m.

case	$\frac{z}{R_c}$	L_{uu} (mm)	L_{vv} (mm)	L_{ww} (mm)	λ_u (mm)	λ_v (mm)	λ_w (mm)
na	0.42	41.7	13.5	15.5	5.3	2.8	3.2
na	1.25	47.4	16.3	16.7	5.4	2.8	3.3
na	2.08	52.9	19.2	17.9	5.6	2.9	3.3
na	2.92	61.7	21.4	18.2	5.6	2.9	3.4
na	3.75	66.8	24.3	19.4	5.9	3.0	3.4
na	4.58	68.5	26.3	20.5	5.7	3.0	3.5
na	5.42	74.0	29.3	21.1	5.9	3.1	3.5
na	6.25	80.6	35.9	23.0	5.9	3.2	3.7
nb	0.42	28.4	10.1	12.3	5.4	2.9	3.3
nb	1.25	33.2	11.8	12.7	5.7	3.0	3.4
nb	2.08	36.5	13.1	14.0	5.7	2.9	3.4
nb	2.92	41.8	14.3	14.6	5.9	3.0	3.4
nb	3.75	47.2	15.9	15.3	6.0	3.0	3.4
nb	4.58	53.8	17.9	16.0	6.0	3.0	3.4
nb	5.42	54.7	18.9	16.7	6.0	3.0	3.8
nb	6.25	61.8	23.1	18.4	6.1	3.1	3.5
nc	0.42	22.8	9.2	10.0	6.8	3.8	4.2
nc	1.25	25.5	10.5	10.7	6.9	3.9	4.2
nc	2.08	27.3	11.7	11.0	6.8	3.8	4.3
nc	2.92	28.9	12.5	11.4	6.8	3.9	4.1
nc	3.75	32.1	13.3	11.7	6.8	3.8	4.2
nc	4.58	32.6	14.2	12.0	6.6	3.7	4.1
nc	5.42	34.1	15.2	12.1	6.7	3.7	4.5
nc	6.25	38.6	17.3	13.0	6.8	3.6	4.0
nd	0.42	91.6	33.7	27.7	9.4	4.8	5.3
nd	1.25	100.1	39.1	30.1	9.3	4.9	5.3
nd	2.08	99.0	41.9	29.5	9.2	5.0	5.3
nd	2.92	101.4	45.5	31.4	9.1	5.0	5.3
nd	3.75	105.5	54.0	33.0	9.3	5.2	5.4
nd	4.58	110.0	57.1	33.2	9.3	5.2	5.4
nd	5.42	109.8	61.0	33.9	9.3	5.2	6.1
nd	6.25	128.9	78.2	37.3	9.8	5.5	5.6
ne	0.42	77.4	46.1	28.2	10.0	7.0	7.2
ne	1.25	76.0	46.6	30.7	8.4	6.2	7.6
ne	2.08	83.9	53.0	30.1	10.7	7.4	7.5
ne	2.92	80.2	53.4	31.9	10.8	7.7	7.8
ne	3.75	86.2	57.9	32.5	11.1	7.9	7.8
ne	4.58	88.3	61.5	33.1	10.8	7.9	7.7
ne	5.42	89.6	60.4	34.5	11.0	8.0	7.9
ne	6.25	97.4	72.4	36.3	11.5	8.3	8.1

Table A.16: Mildly curved section; n=0, z=0, R_c=5 m.

case	$\frac{r}{R_c}$	r	U ($\frac{m}{s}$)	V ($\frac{m}{s}$)	W ($\frac{m}{s}$)	$\frac{u'^2}{q^2}$	$\frac{v'^2}{q^2}$	$\frac{w'^2}{q^2}$	$\frac{u'v'}{q^2}$	$\frac{u'w'}{q^2}$	q^2 ($\frac{m^2}{s^2}$)
pa	0.42	0.62	10.372	-0.183	-0.050	0.517	0.188	0.295	-0.125	-0.030	1.834792
pa	1.28	1.92	10.082	-0.124	-0.276	0.519	0.191	0.290	-0.102	-0.004	1.674759
pa	2.15	3.22	9.978	-0.139	-0.332	0.500	0.199	0.301	-0.102	-0.013	1.539697
pa	3.01	4.52	9.907	-0.221	-0.343	0.480	0.206	0.314	-0.108	-0.022	1.377271
pa	3.88	5.81	9.911	-0.145	-0.448	0.460	0.201	0.339	-0.109	-0.033	1.292068
pa	4.74	7.11	10.115	-0.018	-0.426	0.466	0.200	0.334	-0.104	-0.037	1.271311
pa	5.61	8.41	10.377	-0.042	-0.480	0.467	0.198	0.335	-0.106	-0.044	1.216584
pb	0.42	0.50	10.921	-0.177	-0.054	0.495	0.199	0.306	-0.131	-0.008	0.710954
pb	1.28	1.54	10.763	-0.091	-0.313	0.506	0.196	0.298	-0.101	-0.014	0.660647
pb	2.15	2.57	10.759	-0.079	-0.358	0.501	0.204	0.295	-0.096	-0.017	0.603307
pb	3.01	3.61	10.503	-0.136	-0.384	0.477	0.208	0.315	-0.096	-0.015	0.535616
pb	3.88	4.65	10.426	-0.036	-0.467	0.451	0.204	0.345	-0.096	-0.032	0.494832
pb	4.74	5.69	10.608	0.083	-0.434	0.454	0.206	0.340	-0.094	-0.019	0.474221
pb	5.61	6.73	10.709	0.084	-0.442	0.463	0.206	0.331	-0.101	-0.018	0.453144
pc	0.42	0.28	11.256	-0.175	-0.092	0.487	0.197	0.316	-0.134	-0.049	0.234052
pc	1.28	0.85	11.040	-0.050	-0.297	0.516	0.188	0.296	-0.094	0.048	0.236580
pc	2.15	1.43	11.003	-0.008	-0.360	0.496	0.193	0.311	-0.073	0.037	0.223049
pc	3.01	2.00	10.805	-0.038	-0.389	0.472	0.204	0.324	-0.064	0.023	0.203793
pc	3.88	2.58	10.722	0.070	-0.499	0.433	0.206	0.361	-0.056	-0.029	0.194750
pc	4.74	3.15	10.986	0.234	-0.478	0.454	0.228	0.318	-0.059	0.004	0.171061
pc	5.61	3.73	10.971	0.234	-0.509	0.446	0.235	0.319	-0.069	-0.009	0.154169
pd	0.42	0.08	10.690	-0.119	-0.091	0.483	0.214	0.303	-0.133	0.001	0.503108
pd	1.28	0.24	10.326	-0.034	-0.286	0.519	0.195	0.286	-0.091	-0.039	0.466535
pd	2.15	0.41	10.569	-0.016	-0.350	0.514	0.198	0.288	-0.047	-0.041	0.431364
pd	3.01	0.57	10.462	-0.063	-0.358	0.506	0.203	0.291	-0.009	-0.043	0.400326
pd	3.88	0.73	10.581	0.052	-0.450	0.469	0.217	0.314	0.029	-0.067	0.386510
pd	4.74	0.90	10.910	0.241	-0.422	0.461	0.248	0.292	0.060	-0.047	0.368118
pd	5.61	1.06	11.056	0.246	-0.459	0.428	0.288	0.284	0.070	-0.035	0.342408
pe	0.42	0.05	9.911	-0.112	-0.091	0.379	0.285	0.335	-0.142	0.010	0.118481
pe	1.28	0.15	9.647	-0.061	-0.275	0.405	0.260	0.334	-0.115	-0.034	0.104470
pe	2.15	0.26	9.875	-0.074	-0.332	0.418	0.248	0.334	-0.085	-0.039	0.099193
pe	3.01	0.36	9.823	-0.137	-0.344	0.421	0.242	0.337	-0.048	-0.040	0.092695
pe	3.88	0.46	9.995	-0.108	-0.364	0.407	0.245	0.348	-0.010	-0.046	0.090768
pe	4.74	0.57	10.263	0.104	-0.401	0.407	0.263	0.330	0.039	-0.042	0.088391
pe	5.61	0.67	10.539	0.090	-0.454	0.385	0.291	0.324	0.059	-0.043	0.087647

Table A.17: Strongly curved section; n=0, z=0, R_c=2 m.

case	$\frac{z}{h_c}$	$\frac{\overline{u'^3}}{u'^3}$	$\frac{\overline{v'^3}}{v'^3}$	$\frac{\overline{w'^3}}{w'^3}$	$\frac{\overline{u'^2v'}}{u'^2v'}$	$\frac{\overline{u'v'^2}}{u'v'^2}$	$\frac{\overline{u'^2w'}}{u'^2w'}$	$\frac{\overline{u'w'^2}}{u'w'^2}$	u' ($\frac{m}{s}$)	v' ($\frac{m}{s}$)	w' ($\frac{m}{s}$)
pa	0.42	-0.05	-0.024	0.030	0.010	-0.004	0.001	-0.003	0.974	0.588	0.735
pa	1.28	-0.03	0.002	-0.029	0.028	-0.025	0.004	0.017	0.932	0.565	0.697
pa	2.15	-0.02	-0.005	-0.035	0.007	-0.002	-0.011	0.001	0.875	0.552	0.679
pa	3.01	-0.02	0.017	-0.022	0.019	-0.020	-0.014	0.006	0.813	0.532	0.658
pa	3.88	-0.00	-0.012	0.001	0.014	-0.009	-0.001	0.007	0.771	0.510	0.662
pa	4.74	-0.01	-0.006	0.002	0.001	-0.002	0.012	0.001	0.769	0.504	0.652
pa	5.61	-0.01	-0.021	0.010	0.007	0.001	0.009	0.004	0.754	0.490	0.638
pb	0.42	-0.10	0.074	0.010	0.042	-0.048	-0.021	-0.013	0.594	0.378	0.466
pb	1.28	-0.08	0.034	-0.004	0.032	-0.044	0.010	-0.023	0.578	0.359	0.444
pb	2.15	-0.04	0.044	-0.013	0.026	-0.044	0.001	-0.027	0.550	0.351	0.422
pb	3.01	-0.05	0.050	-0.003	0.037	-0.037	0.002	-0.021	0.506	0.334	0.411
pb	3.88	-0.06	0.041	-0.015	0.035	-0.036	-0.012	-0.014	0.472	0.317	0.413
pb	4.74	-0.06	0.029	-0.014	0.036	-0.025	0.000	-0.022	0.464	0.313	0.401
pb	5.61	-0.07	0.023	0.002	0.036	-0.032	0.011	-0.023	0.458	0.305	0.388
pc	0.42	-0.07	0.027	0.069	0.026	-0.025	0.032	-0.055	0.338	0.215	0.272
pc	1.28	-0.06	0.019	-0.049	0.014	-0.032	-0.023	-0.032	0.349	0.211	0.264
pc	2.15	-0.06	0.010	-0.041	0.011	-0.034	-0.015	-0.017	0.333	0.208	0.263
pc	3.01	-0.06	0.005	-0.032	0.008	-0.029	-0.004	-0.010	0.310	0.204	0.257
pc	3.88	-0.02	0.007	-0.027	0.011	-0.018	-0.010	0.010	0.291	0.200	0.265
pc	4.74	0.00	0.000	-0.002	0.009	-0.012	0.002	0.000	0.279	0.198	0.233
pc	5.61	-0.01	0.005	0.013	0.008	-0.006	0.005	-0.013	0.262	0.190	0.222
pd	0.42	-0.23	0.169	0.035	0.102	-0.136	0.001	-0.097	0.493	0.328	0.390
pd	1.28	-0.25	0.152	-0.026	0.081	-0.133	0.022	-0.069	0.492	0.302	0.365
pd	2.15	-0.23	0.076	-0.036	0.047	-0.117	0.009	-0.071	0.471	0.292	0.352
pd	3.01	-0.22	0.051	-0.046	0.017	-0.104	0.011	-0.057	0.450	0.285	0.341
pd	3.88	-0.20	0.005	-0.064	0.009	-0.088	-0.011	-0.028	0.426	0.290	0.348
pd	4.74	-0.14	-0.033	-0.043	0.005	-0.051	-0.003	-0.044	0.412	0.302	0.328
pd	5.61	-0.10	-0.028	-0.081	0.007	-0.031	-0.014	-0.024	0.383	0.314	0.312
pe	0.42	-0.13	0.142	-0.014	0.080	-0.097	-0.020	-0.072	0.212	0.184	0.199
pe	1.28	-0.15	0.148	0.010	0.081	-0.106	0.025	-0.072	0.206	0.165	0.187
pe	2.15	-0.14	0.122	0.000	0.062	-0.091	0.022	-0.058	0.204	0.157	0.182
pe	3.01	-0.08	0.076	-0.013	0.032	-0.074	0.008	-0.038	0.197	0.150	0.177
pe	3.88	-0.11	0.063	-0.042	0.029	-0.050	-0.007	-0.011	0.192	0.149	0.178
pe	4.74	-0.11	0.045	-0.036	-0.006	-0.047	0.003	-0.032	0.190	0.152	0.171
pe	5.61	-0.07	0.018	-0.055	0.028	-0.015	0.006	-0.015	0.184	0.160	0.169

Table A.18: Strongly curved section; n=0, z=0, R_c=2 m.

case	$\frac{r}{R_c}$	$\frac{u^4}{u'^4}$	$\frac{v^4}{v'^4}$	$\frac{w^4}{w'^4}$	$\frac{u^3v}{u'^3v'}$	$\frac{u^2v^2}{u'^2v'^2}$	$\frac{uv^3}{u'v'^3}$	$\frac{u^3w}{u'^3w'}$	$\frac{u^2w^2}{u'^2w'^2}$	$\frac{uw^3}{u'w'^3}$	u' $(\frac{m}{s})$	v' $(\frac{m}{s})$	w' $(\frac{m}{s})$
pa	0.42	2.988	3.295	3.186	-1.175	1.348	-1.202	-0.250	1.067	-0.227	0.974	0.588	0.735
pa	1.28	3.015	3.339	3.214	-0.963	1.251	-0.993	-0.025	1.022	-0.052	0.932	0.565	0.697
pa	2.15	2.996	3.306	3.167	-0.945	1.227	-0.978	-0.088	1.004	-0.113	0.875	0.552	0.679
pa	3.01	3.025	3.280	3.153	-1.030	1.273	-1.040	-0.176	1.020	-0.167	0.813	0.532	0.658
pa	3.88	3.005	3.296	3.174	-1.063	1.309	-1.098	-0.262	1.095	-0.239	0.771	0.510	0.662
pa	4.74	3.012	3.297	3.191	-1.006	1.265	-1.040	-0.267	1.023	-0.291	0.769	0.504	0.652
pa	5.61	2.976	3.288	3.128	-1.034	1.265	-1.061	-0.304	0.982	-0.332	0.734	0.490	0.638
pb	0.42	2.975	3.187	3.081	-1.216	1.349	-1.226	-0.046	1.036	-0.054	0.594	0.376	0.466
pb	1.28	2.980	3.300	3.135	-0.953	1.233	-0.976	-0.122	0.992	-0.105	0.578	0.359	0.444
pb	2.15	2.987	3.294	3.175	-0.892	1.215	-0.937	-0.127	0.965	-0.134	0.550	0.351	0.422
pb	3.01	2.990	3.285	3.167	-0.911	1.222	-0.945	-0.128	0.999	-0.128	0.506	0.334	0.411
pb	3.88	3.056	3.269	3.159	-0.972	1.257	-0.988	-0.264	1.108	-0.251	0.472	0.317	0.413
pb	4.74	3.014	3.290	3.124	-0.923	1.230	-0.950	-0.150	1.041	-0.148	0.464	0.313	0.401
pb	5.61	3.053	3.254	3.181	-0.976	1.247	-0.997	-0.136	0.969	-0.157	0.458	0.305	0.388
pc	0.42	3.111	3.325	3.088	-1.342	1.461	-1.377	-0.357	1.076	-0.389	0.338	0.215	0.272
pc	1.28	2.983	3.345	3.052	-0.889	1.234	-0.936	0.316	0.985	0.352	0.349	0.211	0.264
pc	2.15	3.019	3.351	3.048	-0.721	1.172	-0.753	0.281	1.024	0.255	0.333	0.208	0.263
pc	3.01	3.015	3.324	3.045	-0.630	1.132	-0.668	0.161	1.067	0.149	0.310	0.204	0.257
pc	3.88	3.014	3.237	3.011	-0.588	1.111	-0.603	-0.247	1.157	-0.211	0.291	0.200	0.265
pc	4.74	3.010	3.205	3.075	-0.558	1.101	-0.579	0.022	0.964	0.011	0.279	0.198	0.233
pc	5.61	3.008	3.219	3.090	-0.643	1.131	-0.666	-0.069	0.941	-0.095	0.262	0.190	0.222
pd	0.42	2.929	3.154	3.156	-1.178	1.340	-1.198	-0.012	1.005	0.004	0.493	0.328	0.390
pd	1.28	2.908	3.269	3.109	-0.795	1.164	-0.822	-0.303	0.991	-0.293	0.492	0.302	0.365
pd	2.15	2.888	3.399	3.129	-0.405	1.050	-0.395	-0.269	0.990	-0.321	0.471	0.292	0.352
pd	3.01	2.907	3.305	3.100	-0.055	1.008	-0.087	-0.315	1.010	-0.323	0.450	0.285	0.341
pd	3.88	2.905	3.253	3.046	0.250	1.026	0.246	-0.564	1.130	-0.500	0.426	0.290	0.348
pd	4.74	2.852	3.167	3.092	0.502	1.049	0.495	-0.391	1.053	-0.379	0.412	0.302	0.328
pd	5.61	2.947	3.082	3.065	0.584	1.072	0.584	-0.277	0.996	-0.283	0.383	0.314	0.312
pe	0.42	2.856	2.926	2.963	-1.145	1.282	-1.173	0.083	0.939	0.075	0.212	0.184	0.199
pe	1.28	2.809	2.941	3.001	-0.901	1.147	-0.903	-0.262	0.946	-0.303	0.206	0.165	0.187
pe	2.15	2.785	2.970	3.072	-0.647	1.062	-0.664	-0.316	0.969	-0.352	0.204	0.157	0.182
pe	3.01	2.759	3.102	3.067	-0.329	0.991	-0.347	-0.320	0.995	-0.395	0.197	0.150	0.177
pe	3.88	2.781	3.176	3.067	-0.014	0.975	-0.007	-0.400	1.072	-0.441	0.192	0.149	0.178
pe	4.74	2.785	3.176	3.082	0.402	1.015	0.405	-0.344	1.018	-0.406	0.190	0.152	0.171
pe	5.61	2.792	3.160	3.138	0.545	1.041	0.538	-0.393	1.035	-0.442	0.184	0.160	0.169

Table A.19: Strongly curved section; n=0, z=0, R_c=2 m.

case	$\frac{z}{h_c}$	L_{uu} (mm)	L_{vv} (mm)	L_{ww} (mm)	λ_u (mm)	λ_v (mm)	λ_w (mm)
pa	0.42	39.4	11.2	14.8	5.6	2.7	3.2
pa	1.28	31.5	9.6	14.7	5.3	2.6	3.1
pa	2.15	28.5	9.4	14.8	5.2	2.6	3.1
pa	3.01	27.3	10.1	15.6	5.0	2.6	3.1
pa	3.88	27.8	10.5	17.0	5.1	2.7	3.3
pa	4.74	29.5	11.1	18.4	5.3	2.8	3.5
pa	5.61	30.5	11.4	19.0	5.4	2.8	3.5
pb	0.42	26.3	8.5	11.4	5.5	2.8	3.3
pb	1.28	22.4	7.0	10.9	5.4	2.7	3.1
pb	2.15	21.5	7.0	11.1	5.2	2.6	3.1
pb	3.01	20.4	7.2	11.8	5.1	2.6	3.1
pb	3.88	20.5	7.5	12.2	5.1	2.7	3.3
pb	4.74	20.8	8.1	13.2	5.2	2.8	3.4
pb	5.61	21.4	8.3	14.0	5.5	2.9	3.5
pc	0.42	24.7	8.7	10.3	6.8	3.5	4.0
pc	1.28	20.6	7.1	9.5	6.7	3.3	3.8
pc	2.15	18.2	6.6	11.2	6.3	3.2	3.7
pc	3.01	18.6	6.7	10.1	5.9	3.1	3.7
pc	3.88	20.8	7.1	11.1	5.7	3.1	3.7
pc	4.74	20.1	8.0	10.2	5.7	3.2	3.6
pc	5.61	19.6	8.0	10.9	5.8	3.3	3.7
pd	0.42	67.4	24.4	28.3	9.4	4.7	5.5
pd	1.28	57.3	18.3	26.4	9.3	4.4	5.3
pd	2.15	50.1	16.1	25.9	9.0	4.2	5.2
pd	3.01	55.6	16.1	25.6	8.8	4.2	5.0
pd	3.88	72.6	24.7	24.1	8.5	4.3	5.0
pd	4.74	67.4	37.6	26.1	8.3	4.6	5.1
pd	5.61	56.4	42.0	25.7	7.9	4.9	5.0
pe	0.42	49.5	28.1	26.9	10.0	6.4	7.1
pe	1.28	46.7	23.4	25.2	10.2	6.1	6.8
pe	2.15	45.5	20.3	25.4	10.1	5.8	6.6
pe	3.01	41.2	17.7	24.1	10.3	5.8	6.8
pe	3.88	41.6	17.3	25.6	10.1	5.7	7.1
pe	4.74	45.0	18.6	25.1	10.4	6.1	7.0
pe	5.61	48.5	21.2	24.9	10.2	6.4	6.9

Table A.20: Strongly curved section; n=0, z=0, R_c=2 m.

case	$\frac{h}{h_c}$	r	U ($\frac{m}{s}$)	V ($\frac{m}{s}$)	W ($\frac{m}{s}$)	$\sqrt{\overline{u'^2}}$	$\sqrt{\overline{v'^2}}$	$\sqrt{\overline{w'^2}}$	$\overline{u'v'}$	$\overline{u'w'}$	$\sqrt{k}$ ($\frac{m^2}{s^2}$)
na	0.42	0.62	10.092	0.138	-0.104	0.481	0.211	0.308	0.148	0.008	1.620561
na	1.28	1.92	9.949	0.211	-0.276	0.478	0.219	0.303	0.160	-0.034	1.588343
na	2.15	3.22	10.271	0.230	-0.245	0.483	0.223	0.294	0.166	-0.026	2.561214
na	3.01	4.52	10.408	0.234	-0.357	0.490	0.221	0.289	0.164	-0.029	3.448072
na	3.88	5.81	10.662	0.388	-0.352	0.472	0.225	0.303	0.164	-0.030	4.523287
na	4.74	7.11	11.247	0.753	-0.380	0.477	0.243	0.280	0.185	-0.031	5.971560
na	5.61	8.41	11.764	0.892	-0.368	0.466	0.255	0.280	0.186	-0.031	7.384706
nb	0.42	0.55	9.786	0.063	-0.129	0.470	0.214	0.315	0.148	0.032	0.683149
nb	1.28	1.71	9.667	0.069	-0.215	0.463	0.226	0.311	0.161	-0.066	0.778695
nb	2.15	2.86	9.939	0.040	-0.234	0.464	0.232	0.304	0.166	-0.074	0.994446
nb	3.01	4.01	9.738	-0.103	-0.211	0.496	0.227	0.277	0.167	-0.080	1.383002
nb	3.88	5.16	9.763	-0.064	-0.186	0.495	0.220	0.285	0.158	-0.114	1.892124
nb	4.74	6.32	10.030	0.049	-0.160	0.522	0.233	0.246	0.174	-0.108	2.817016
nb	5.61	7.47	9.876	0.007	-0.151	0.497	0.236	0.266	0.162	-0.136	3.465825
nc	0.42	0.33	9.919	0.052	-0.093	0.448	0.218	0.334	0.150	-0.008	0.184891
nc	1.28	1.03	9.608	0.022	-0.279	0.432	0.239	0.329	0.172	0.025	0.202486
nc	2.15	1.71	9.930	-0.001	-0.302	0.420	0.254	0.326	0.184	0.029	0.246620
nc	3.01	2.41	9.974	-0.054	-0.285	0.416	0.254	0.330	0.185	0.033	0.299075
nc	3.88	3.10	10.051	-0.043	-0.293	0.412	0.256	0.332	0.186	0.025	0.389095
nc	4.74	3.79	10.675	0.205	-0.275	0.439	0.273	0.288	0.208	0.018	0.550771
nc	5.61	4.48	10.900	0.291	-0.260	0.433	0.278	0.289	0.203	0.009	0.596258
nd	0.42	0.19	10.036	0.006	-0.143	0.487	0.227	0.287	0.163	-0.005	0.589145
nd	1.28	0.59	9.691	0.071	-0.206	0.453	0.252	0.295	0.190	-0.043	0.631355
nd	2.15	0.99	10.130	0.082	-0.253	0.424	0.288	0.288	0.210	-0.047	0.721438
nd	3.01	1.39	10.052	0.031	-0.252	0.415	0.298	0.287	0.219	-0.036	0.818516
nd	3.88	1.79	10.172	0.079	-0.257	0.393	0.313	0.293	0.228	-0.052	0.967513
nd	4.74	2.18	10.711	0.320	-0.285	0.401	0.339	0.260	0.253	-0.044	1.183986
nd	5.61	2.58	10.836	0.373	-0.354	0.385	0.355	0.260	0.250	-0.047	1.266211
ne	0.42	0.10	9.375	-0.029	-0.136	0.361	0.289	0.350	0.162	0.024	0.100680
ne	1.28	0.31	9.151	0.018	-0.212	0.349	0.319	0.332	0.186	-0.056	0.107112
ne	2.15	0.53	9.601	0.015	-0.262	0.324	0.355	0.321	0.202	-0.049	0.119282
ne	3.01	0.74	9.504	-0.068	-0.275	0.309	0.367	0.324	0.208	-0.043	0.131273
ne	3.88	0.95	9.559	-0.020	-0.295	0.289	0.386	0.325	0.219	-0.049	0.150447
ne	4.74	1.16	10.105	0.160	-0.331	0.280	0.412	0.308	0.234	-0.051	0.172995
ne	5.61	1.37	10.161	0.160	-0.387	0.272	0.429	0.298	0.236	-0.042	0.193376

Table A.21: Strongly curved section; n=0, z=0, R_c =2 m.

case	$\frac{z}{R_c}$	$\frac{u^3}{u'^3}$	$\frac{v^3}{v'^3}$	$\frac{w^3}{w'^3}$	$\frac{u^2v}{u'^2v'}$	$\frac{uv^2}{u'v'^2}$	$\frac{u^2w}{u'^2w'}$	$\frac{uw^2}{u'w'^2}$	u' $(\frac{m}{s})$	v' $(\frac{m}{s})$	w' $(\frac{m}{s})$
na	0.42	-0.07	-0.028	-0.052	-0.024	-0.022	-0.028	-0.038	0.883	0.584	0.707
na	1.28	-0.10	-0.034	0.056	-0.047	-0.035	0.024	-0.045	0.950	0.643	0.757
na	2.15	-0.12	-0.024	0.006	-0.040	-0.024	0.024	-0.051	1.112	0.756	0.867
na	3.01	-0.14	-0.050	0.013	-0.046	-0.034	0.034	-0.065	1.300	0.873	0.998
na	3.88	-0.15	-0.065	0.027	-0.050	-0.045	0.020	-0.094	1.461	1.008	1.171
na	4.74	-0.16	-0.087	0.062	-0.067	-0.057	0.034	-0.112	1.688	1.204	1.294
na	5.61	-0.23	-0.137	0.043	-0.120	-0.098	0.053	-0.108	1.854	1.371	1.437
nb	0.42	-0.04	-0.005	-0.049	-0.025	-0.018	-0.019	-0.007	0.567	0.383	0.464
nb	1.28	-0.09	-0.030	0.072	-0.042	-0.032	0.057	-0.038	0.601	0.420	0.492
nb	2.15	-0.17	-0.069	0.078	-0.073	-0.065	0.058	-0.054	0.679	0.481	0.550
nb	3.01	-0.14	-0.063	0.100	-0.051	-0.060	0.071	-0.062	0.828	0.560	0.619
nb	3.88	-0.19	-0.073	0.142	-0.059	-0.070	0.112	-0.099	0.968	0.645	0.734
nb	4.74	-0.13	-0.039	0.113	-0.045	-0.052	0.061	-0.050	1.212	0.809	0.832
nb	5.61	-0.06	0.012	0.099	0.008	-0.002	0.037	-0.009	1.313	0.905	0.961
nc	0.42	-0.01	0.007	-0.064	-0.009	-0.004	-0.027	-0.064	0.288	0.201	0.249
nc	1.28	-0.01	-0.015	0.035	-0.006	-0.006	0.014	-0.018	0.296	0.220	0.258
nc	2.15	-0.01	0.003	0.029	-0.007	-0.001	0.030	0.004	0.322	0.250	0.283
nc	3.01	-0.02	-0.005	0.062	-0.011	-0.008	0.023	-0.014	0.353	0.276	0.314
nc	3.88	0.00	0.010	0.038	0.005	0.014	0.061	0.001	0.401	0.316	0.359
nc	4.74	0.01	0.011	0.131	0.005	0.018	0.059	-0.026	0.492	0.388	0.398
nc	5.61	0.00	0.026	0.128	0.006	0.020	0.082	-0.045	0.549	0.440	0.448
nd	0.42	-0.07	-0.046	-0.019	-0.028	-0.036	-0.015	-0.024	0.535	0.365	0.411
nd	1.28	-0.11	-0.071	0.010	-0.049	-0.045	0.014	-0.042	0.535	0.399	0.432
nd	2.15	-0.07	-0.029	0.000	-0.021	-0.019	0.034	-0.078	0.553	0.456	0.455
nd	3.01	-0.15	-0.103	0.021	-0.077	-0.074	0.014	-0.086	0.583	0.494	0.485
nd	3.88	-0.22	-0.123	0.032	-0.122	-0.097	0.050	-0.117	0.617	0.551	0.533
nd	4.74	-0.25	-0.168	0.042	-0.151	-0.131	0.024	-0.137	0.689	0.633	0.555
nd	5.61	-0.36	-0.259	0.062	-0.226	-0.202	0.059	-0.194	0.698	0.671	0.574
ne	0.42	0.27	0.119	0.069	0.184	0.126	0.007	0.023	0.191	0.171	0.188
ne	1.28	0.27	0.165	-0.057	0.199	0.163	-0.044	0.023	0.193	0.185	0.189
ne	2.15	0.26	0.170	-0.032	0.199	0.169	-0.010	0.019	0.196	0.206	0.196
ne	3.01	0.20	0.127	-0.033	0.145	0.126	-0.008	0.024	0.201	0.219	0.206
ne	3.88	0.16	0.105	-0.034	0.123	0.108	-0.025	0.020	0.208	0.241	0.221
ne	4.74	0.14	0.097	-0.038	0.104	0.094	-0.021	0.004	0.220	0.267	0.231
ne	5.61	0.05	0.048	-0.018	0.036	0.039	0.003	0.004	0.229	0.288	0.240

Table A.22: Strongly curved section; n=0, z=0, R_c=2 m.

case	$\frac{x^2}{R_c^2}$	$\frac{\mu x^4}{\omega^2 z^2}$	$\frac{\mu x^4}{\omega^2 z^2}$	$\frac{\mu x^4}{\omega^2 z^2}$	$\frac{\mu^3 x^3}{\omega^3 z^3}$	$\frac{\mu^2 x^2}{\omega^2 z^2}$	$\frac{\mu^3 x^3}{\omega^3 z^3}$	$\frac{\mu^3 x^3}{\omega^3 z^3}$	$\frac{\mu^2 x^2}{\omega^2 z^2}$	$\frac{\mu^3 x^3}{\omega^3 z^3}$	u' $(\frac{m}{s})$	v' $(\frac{m}{s})$	w' $(\frac{m}{s})$
na	0.42	3.057	3.225	3.153	1.388	1.461	1.378	0.059	1.119	0.051	0.883	0.584	0.707
na	1.28	3.024	3.169	3.162	1.457	1.511	1.462	-0.279	1.133	-0.263	0.950	0.643	0.757
na	2.15	2.997	3.106	3.195	1.452	1.494	1.440	-0.217	1.120	-0.203	1.112	0.756	0.867
na	3.01	2.934	3.100	3.163	1.411	1.481	1.428	-0.223	1.066	-0.224	1.300	0.873	0.998
na	3.88	2.887	3.074	3.186	1.388	1.449	1.396	-0.230	1.201	-0.240	1.461	1.008	1.171
na	4.74	2.795	2.958	3.131	1.450	1.475	1.473	-0.259	1.082	-0.268	1.686	1.204	1.294
na	5.61	2.744	2.915	3.099	1.412	1.438	1.418	-0.287	1.099	-0.272	1.854	1.371	1.437
nb	0.42	2.999	3.158	3.077	1.376	1.447	1.373	0.237	1.078	0.218	0.567	0.383	0.464
nb	1.28	3.019	3.123	3.072	1.463	1.508	1.455	-0.548	1.131	-0.516	0.601	0.420	0.492
nb	2.15	3.028	3.128	3.101	1.469	1.519	1.480	-0.622	1.189	-0.605	0.679	0.481	0.550
nb	3.01	2.945	3.135	3.126	1.420	1.490	1.441	-0.595	1.063	-0.638	0.828	0.560	0.619
nb	3.88	2.943	3.123	3.081	1.350	1.439	1.352	-0.899	1.252	-0.900	0.968	0.645	0.734
nb	4.74	2.776	3.023	3.053	1.347	1.422	1.351	-0.727	1.049	-0.829	1.212	0.809	0.832
nb	5.61	2.710	3.001	2.962	1.246	1.351	1.255	-1.007	1.235	-0.971	1.313	0.905	0.961
nc	0.42	3.003	3.100	3.045	1.409	1.461	1.412	-0.066	1.093	-0.046	0.288	0.201	0.249
nc	1.28	2.962	3.068	3.065	1.547	1.566	1.575	0.155	1.039	0.161	0.296	0.220	0.258
nc	2.15	2.995	3.039	3.067	1.636	1.624	1.645	0.227	1.069	0.196	0.322	0.250	0.283
nc	3.01	2.986	3.069	3.083	1.644	1.641	1.676	0.257	1.135	0.232	0.353	0.276	0.314
nc	3.88	2.970	3.052	3.094	1.649	1.638	1.673	0.188	1.082	0.154	0.401	0.316	0.359
nc	4.74	3.000	3.043	3.086	1.755	1.724	1.768	0.111	0.977	0.113	0.492	0.388	0.398
nc	5.61	2.900	2.971	3.064	1.638	1.632	1.660	0.024	1.012	0.039	0.549	0.440	0.448
nd	0.42	2.753	3.032	3.088	1.316	1.390	1.345	-0.036	0.991	-0.034	0.535	0.365	0.411
nd	1.28	2.750	2.914	3.066	1.500	1.499	1.510	-0.328	1.061	-0.345	0.535	0.399	0.432
nd	2.15	2.762	2.868	3.111	1.587	1.575	1.617	-0.402	1.111	-0.374	0.553	0.456	0.455
nd	3.01	2.675	2.809	3.094	1.596	1.583	1.638	-0.284	1.072	-0.300	0.583	0.494	0.485
nd	3.88	2.708	2.743	3.132	1.664	1.620	1.679	-0.493	1.170	-0.433	0.617	0.551	0.533
nd	4.74	2.670	2.720	3.118	1.746	1.685	1.772	-0.350	1.036	-0.383	0.689	0.633	0.555
nd	5.61	2.763	2.758	3.196	1.763	1.703	1.778	-0.418	1.119	-0.429	0.698	0.671	0.574
ne	0.42	3.224	3.101	2.875	1.632	1.636	1.577	0.198	1.038	0.158	0.191	0.171	0.188
ne	1.28	3.057	2.980	2.922	1.691	1.647	1.648	-0.518	1.090	-0.450	0.193	0.185	0.189
ne	2.15	3.060	2.970	2.915	1.763	1.706	1.747	-0.457	1.124	-0.422	0.196	0.206	0.196
ne	3.01	2.906	2.877	2.964	1.707	1.661	1.725	-0.422	1.106	-0.373	0.201	0.219	0.206
ne	3.88	2.783	2.724	2.980	1.716	1.652	1.729	-0.518	1.197	-0.452	0.208	0.241	0.221
ne	4.74	2.844	2.776	2.930	1.859	1.779	1.872	-0.522	1.135	-0.485	0.220	0.267	0.231
ne	5.61	2.736	2.726	2.907	1.772	1.710	1.821	-0.442	1.116	-0.411	0.229	0.288	0.240

Table A.23: Strongly curved section; n=0, z=0, R_c=2 m.

case	$\frac{\delta}{h_c}$	L_{uu} (mm)	L_{vv} (mm)	L_{ww} (mm)	λ_u (mm)	λ_v (mm)	λ_w (mm)
na	0.42	44.7	15.7	17.7	5.5	2.9	3.4
na	1.26	55.6	22.7	18.5	5.6	3.0	3.4
na	2.15	59.3	30.6	20.7	5.8	3.1	3.5
na	3.01	71.4	36.6	22.1	5.7	3.1	3.6
na	3.88	79.4	44.3	24.8	5.9	3.3	3.8
na	4.74	89.6	56.1	26.1	6.1	3.6	3.9
na	5.61	103.1	63.3	28.4	6.3	3.9	4.1
nb	0.42	32.5	11.1	12.7	5.7	3.1	3.4
nb	1.26	37.2	15.2	13.6	5.7	3.1	3.5
nb	2.15	44.6	20.2	15.4	5.8	3.3	3.6
nb	3.01	53.2	24.9	17.3	6.1	3.2	3.6
nb	3.88	62.2	29.6	20.4	6.2	3.3	3.7
nb	4.74	80.2	36.2	21.7	6.8	3.6	3.7
nb	5.61	85.5	43.1	24.9	6.6	3.6	3.8
nc	0.42	25.5	10.2	10.5	7.0	4.0	4.3
nc	1.26	27.8	13.3	11.2	6.9	4.1	4.3
nc	2.15	30.8	17.0	12.2	6.9	4.3	4.4
nc	3.01	33.0	19.5	13.0	6.7	4.2	4.4
nc	3.88	35.8	22.6	14.5	6.7	4.2	4.5
nc	4.74	45.4	26.9	15.0	7.1	4.4	4.2
nc	5.61	49.7	32.4	16.5	6.9	4.3	4.2
nd	0.42	94.9	34.6	29.3	9.5	5.0	5.6
nd	1.26	99.1	45.5	31.9	9.5	5.3	5.6
nd	2.15	104.9	60.2	34.9	9.6	6.1	5.8
nd	3.01	111.3	70.8	38.7	9.5	6.1	5.9
nd	3.88	119.3	86.8	45.1	9.4	6.3	6.3
nd	4.74	136.9	107.9	49.4	10.2	7.1	6.3
nd	5.61	134.7	109.5	55.6	9.8	7.0	6.2
ne	0.42	71.2	43.1	29.3	10.2	6.8	7.5
ne	1.26	69.0	41.5	31.0	10.6	7.7	7.7
ne	2.15	81.8	56.2	32.8	10.9	8.6	8.1
ne	3.01	83.4	57.4	34.8	10.9	8.9	8.5
ne	3.88	88.9	67.4	38.9	11.2	9.6	9.2
ne	4.74	97.1	79.1	43.1	12.1	11.2	9.1
ne	5.61	99.6	84.4	45.2	12.1	11.5	9.3

Table A.24: Strongly curved section; n=0, z=0, R_c=2 m.